CENTER FOR NUCLEAR WASTE REGULATORY ANALYSES

TRIP REPORT

SUBJECT: OECD/NEA Workshop

DATE/PLACE: October 15–21, 2002; Istanbul, Turkey (06002.01.061)

AUTHOR: John A. Stamatakos

DISTRIBUTION:

CNWRA	NRC	SwRI Contracts
W. Patrick	J. Linehan	T. Nagy (Contracts)
CNWRA Directors	W. Reamer	
CNWRA Element Managers	J. Schlueter	
	D. DeMarco	
	E. Whitt	
	B. Meehan	
	J. Greeves	
	A. Campbell	
	P. Justus	
	J. Trapp	
	A.-B. Ibrahim	
	M. Shah	
	M. Delligatti	
	J. Hall	
	A. Persinko	
	C. Munson (NRR)	

CENTER FOR NUCLEAR WASTE REGULATORY ANALYSES

TRIP REPORT

Subject

This report summarized Dr. John A. Stamatakos's participation at the recent Organization for Economic Cooperation and Development (OECD)/ Nuclear Energy Agency (NEA) workshop on the relations between seismological data and seismic engineering analyses.

Dates of Travel and Countries/Organizations Visited

Dr. Stamatakos traveled to Istanbul, Turkey on October 15, 2002. He participated in a one-day field trip to visit some of the sites around Izmit Bay that were damaged by the two large earthquakes that struck Turkey in 1999. On October 16 and 17, Dr. Stamatakos attended the two-day workshop on seismological data and seismic engineering. The workshop was sponsored by Turkish Atonim Energy Authority and was held at Best Wester President Hotel in Istanbul. The workshop was organized by the working group on Integrity of Components and Structures, which is part of the Committee on the Safety of Nuclear Installations (CSNI). The CSNI is one of many committees within the Nuclear Energy Agency (NEA) of the Organization of Economic Cooperation and Development (OECD). Participants at the workshop were from OECD member countries, including Japan, China, Taiwan, Canada, Germany, England, France, Italy, Spain, Czechoslovakia, Austria, Finland, Turkey, and the United States. Dr. Stamatakos returned to the United States on October 21.

Author, Title, and Agency Affiliation

The author of this report is Dr. John A. Stamatakos from the Center for Nuclear Waste Regulatory Analyses in San Antonio, Texas.

Sensitivity

N/A

Background/Purpose

The OECD/NEA workshop on the relations between seismological data and seismic engineering was a direct outgrowth of a similar workshop held several years ago at the Brookhaven National Laboratory on Long Island, New York. At the Brookhaven meeting, the OECD/NEA recommended that the seismologists and seismic engineers work together to better integrate earthquake information used to characterize seismicity and information needed for design. The meeting at Brookhaven was organized by NRC.

NRC has traditionally played an important role in these meetings, which foster critical dialogues between scientists, engineers, and regulators. Information from these workshops provides regulators with information that they need to continually improve regulations, improvements that simultaneously maintain public health and safety while reducing unnecessary regulatory burden.

Abstract: Summary of Pertinent Points/Issues

The first day of the workshop (October 16, 2002) was devoted to an all-day field trip to visit regions east of Istanbul that were affected by two large-magnitude earthquakes that struck Turkey in 1999. These two earthquakes destroyed more than 25,000 housing units (mostly multi-story apartment buildings) and killed more than 19,000 people. Large facilities were also extensively damaged by the earthquakes, including a petro-chemical plant, Ford motor factory, and a Turkish naval base. The field trip was very informative because it highlighted the role local site conditions play in earthquake damage. We saw many examples where a building was largely destroyed while nearby and similar structures remained intact simply because of the variable site conditions.

Many of the presentations were of NRC interest. Of note were the series of talks that examined those ground motion parameters that are the most reliable indicators of potential earthquake damage. Most presenters agreed that ground motion acceleration is appropriate for relatively high spectral frequencies of ground motion (5 to 30 Hz), but for lower spectral frequencies, velocity or a combination of velocity and displacement appear to be better indicator of earthquake damage. Also of note were a series of talks that examined the role of probabilistic and deterministic methodologies and related developments in the regulatory procedures in Europe and Japan.

Discussion

The field trip departed Istanbul by bus early in the morning. We drove east along the northern coastline of Izmit Bay, stopping to see damage to many buildings in Gebze and Kocaeli. We also saw the remnants of the fault trace at Izmit, which seismologists refer to as the mole tracks. It was interesting to note how rapidly the mole track has been degraded by erosion during the last 3 years, compared to photographs of the track taken just after the earthquakes in 1999.

From Izmit we then drove west along the southern coast of Izmit Bay. This coast line was much closer to the fault and epicenter and thus suffered extensive damage. We stopped at Gõlcük, near a Turkey naval base, where we saw a stone fence line offset horizontally by more than 3 m. The naval base apparently suffered considerable damage from the earthquake, including the loss of many sailors who were killed when the Commissary collapsed.

From there we went to the small town of Derirmendere, where the town's mayor told us of the earthquake damage in his community. This damage included a submarine landslide that destroyed a two-story shopping mall and hotel complex, both now under 17 m of water. Finally, we drove west to Yalova, viewing more earthquake damage along the way.

The most interesting observation on the trip was the significance of local site conditions to damage. Structures built on soft soil were completely destroyed whereas identical structures, built nearby but on bedrock, remained intact. The observation points to the need for reliable site response and soil-structure interaction analyses in order to adequately evaluate damage potential of systems, structures, and components to earthquake damage.

The next two days of the meeting were devoted to presentations on seismology and seismic engineering. The presentations were focused around three main sessions: (i) Damage Capacity of Seismic Motions; (ii) Seismic Input Motions for Design Purposes; and (iii) Regulatory Aspects. The meeting agenda also included a final session for discussion of conclusions and recommendations

for future study and follow-up workshops. The organizers tentatively proposed that the next workshop will be held in two years in Japan.

The meeting focused on a number of issues related to seismological data and seismic engineering, but there appears to be three topics most pertinent to NRC.

(1) Several of the papers (e.g., Ghobarah and Elgohary) focused on what types of ground motion data are most appropriate to assessing potential earthquake response of critical systems, structures, and components. The theme of these papers was to assess the appropriate earthquake parameters for sites that could experience near-field earthquakes with a long-duration and large-amplitude velocity pulses (*i.e.*, forward directivity). The traditional measure in earthquake design and regulatory practice has been to use peak ground acceleration (PGA) or spectral acceleration. Many response spectral shapes such as those in NUREG 1.60 are based on acceleration. Several of the papers at the meeting showed how velocity or a combination of velocity and displacement information are better parameters for developing design requirements and regulatory guidance for sites that might experience near-field earthquakes.

(2) A second set of papers addressed problems of the variability of local site response. Presentations by Professor Gulkan and Dr. Çelbi reinforced what we had seen on the field trip—that damage to buildings varies significantly at the local scale simply because of small differences in site conditions. This observation makes application of the few strong motion records (*e.g.*, time histories) from large earthquakes problematic, because these records have to be properly scaled to account for the local site response. Dr. Anderson presented a paper in which he showed how theoretical considerations (*i.e.*, source models and vibration theory) are being used to develop synthetic strong motion records that take into account site specific conditions.

(3) A third set of papers examined the role of probabilistic methods and risk information in Regulatory practice and design. Based on many of the papers presented on this topic, it appears that regulations and regulatory guidance in the United States is well ahead of other nuclear safety agencies in implementing a risk-informed and performance based approach. Of note is the application of these methods in the revised IAEA safety guide, which was summarized in a presentation by Dr. Gürpinar.

<u>Pending Actions/Planned Next Steps for NRC</u>

(1) A final meeting report and proceedings will be published by the OECD/NEA sometime next summer (2003). NRC and CNWRA staff should obtain a copy of the final report.

(2) The OECD/NEA has proposed a follow up meeting to discuss further developments in the relationship between seismological data and seismic engineering. In particular, preliminary recommendations for the next meeting include (i) how to establish the scenario earthquake for design analysis; (ii) methods to simulate strong earthquake ground motions at a site taking into account near-source faults; (iii) validity of probabilistic seismic hazard assessments of ground motions at small exceedence probabilities (less than 10^{-4}/yr); (iv) appropriate strong ground motion instrumentation; and (v) appropriate ways to relate vibratory ground motion to damage potential of important systems, structures, and

components. This follow-on meeting is tentatively planned to be held in Japan in 2004. NRC and CNWRA should be prepared to attend and contribute to the meeting.

Points for Commission Consideration/Items of Interest

No Commission action is requested, the information is considered of interest to the Commission.

Many of the presentations indicated that performance-based and risk informed concepts are being considered by nuclear safety agencies around the world. Performance-based engineering analyses integrates information about the demand earthquakes place on critical systems, structures, and components (the vibratory ground motion) and the capacity of those systems, structures, and components to maintain their intended safety functions. In the areas of earthquake safety and earthquake engineering, performance-based and risk-informed regulations often incorporate probabilistic information about earthquakes and SSC fragility.

To keep abreast of newest developments in earthquake predictions and earthquake engineering, NRC and CNWRA staffs should continue to participate in meetings and discussions with other nuclear safety agencies around the world. In particular NRC and CNWRA staffs should monitor technological and scientific developments in (i) the application of probabilistic seismic hazard results, especially as results from probabilistic seismic hazard assessments are extrapolated to small annual exceedence probabilities (less than 10^{-4}/yr); (ii) appropriate ways that seismologists and seismic engineers can most effectively express earthquake information in terms of damage potential to critical systems, structures, and components; (iii) site-specific effects that can greatly influence the type of damage sustained by critical systems, structures, and components during an earthquake; and (iv) near-source effects such as directivity which can lead to short-duration but large amplitude pulses of seismic energy. Scientific and technological advances in these areas could influence the future course of seismic-related regulations and regulatory guidance.

Attachments

Attachment 1: Meeting Agenda
Attachment 2: Copy of Papers Submitted to the Workshop

"On the Margins"

N/A

SIGNATURES:

John A. Stamatakos
Principal Research Scientist

11/20/02
Date

CONCURRENCE:

H. Lawrence McKague, Manager
Geology and Geophysics

11/21/02
Date

Budhi Sagar
Technical Director

11/20/02
Date

rae
Attachments
D:\GLGP Group\Stamatakos\Trip Reports\TR-10-15-to-21-2002-Istanbul-JS.wpd

OECD/NEA Workshop on the Relations Between Seismological Data and Seismic Engineering

Istanbul, 16-18 October 2002

Tentative Agenda

Wednesday, October 16, 2002

8H30 – 17H30 Site Visit to Kocaeli Earthquake Region – Lunch will be served as sandwiches and soft drinks

19H00 Welcoming Cocktail at Pool Bar

Thursday, October 17, 2002

Opening session		**TAEK official**
9H00	Opening	TAEK official
9H10	OECD	Mr. Mathet
9H20	IAGE WG Presentation	Prof. Labbe
9H40	Introductory paper	Prof. Gulkan (Chairman)
10H10	Quantification of the effect of low magnitude near field earthquakes	Mr. Sollogoub (Chairman of the IAGE Seismic WG)
10H30	*Coffee Break*	

Session 1 topic 1		**Prof. Shibata**
11H	Sucuoglu	The effect of near-field ground motions on degrading systems.
11H15	Elgohary	Seismic response of structures to near fault ground motion
11H30	Brun	Damaging effects of near-field and far-field earthquake on reinforced concrete shear walls evaluated by a simplified model taking into account stiffness degradation
11H45	Mollaioli	Analysis of the response behaviour of structures subjected to damaging pulse-type ground motions
12H00	Discussion	
12H30	*Lunch break*	

Session 2 topic 2		**Dr Murphy**
14H	Kudo	Estimation of the near-source strong ground motion during the Kocaeli, Turkey earthquakes of August 17, 1999 at damaged areas with regards of site effects
14H20	Çelebi	Absence of actual main-shock records, recorded aftershocks & estimated main-shock motions at south izmit bay during the august 17, 1999 izmit (turkey) earthquake
14H40	Kikuchi	The study for the evaluation methods for the design basis earthquake ground motions
15H00	Discussion	
15H15	*Coffee break*	

Session 3 topic 3		**To Be Determined**
15H45	Gürpinar	The new IAEA safety guide on seismic hazard analysis (with emphasis on considerations for zones of diffuse seismicity)
16H00	Procházková	Seismic hazard determination of nuclear facilities in the czech republic
16H15	Konno	A developing risk-informed design basis earthquake ground motion methodology for nuclear power facilities in Japan
16H30	Jiménez Juan	Nuclear power plants seismic instrumentation: Spanish practice.
16H45	Takashima	Discussions on Improving Japanese "Examination Guide for Seismic Design of Nuclear Power Reactor Facilities"
17H00	Discussion	
17H15	*Adjourn*	

19H30 Dinner at Orient House

Friday, October 18, 2002

Session 4 topic 2		**Dr Gürpinar**
9H00	Panza	Seismic ground motion modelling and damage earthquake scenarios – a bridge between seismologists and seismic engineers
9H15	Anderson	Generation of synthetic strong earthquake ground motions using a composite source model and synthetic green's functions
9H30	Lee J-R	Inversion of Stochastic Earthquake Model Parameters in Korea using the Modified Levenberg-Marquardt's method
9H45	Ohtani	Characteristics of three-dimensional Strong Ground Motions along Principal Axes
10H00	Kitada	On A Test To Resolve Issues Related To Earthquake Response of Nuclear Structures And The Ground Motions Used for The Test
10H15	Discussion	
10H30	*Coffee break*	
Session 5 topics 1 and 3		**Dr Anderson**
11H00	Sollogoub	Seismic behaviour of masonry in-filled frames - Local and global modelling for the seismic assessment of existing structures
11H15	Mollaioli	The use of simplified multi-story models in characterising damage potential of earthquake ground motions
11H30	Sano	Notes on ground motions defined by EUROCODES
11H45	Shibata	Proof of Seismic Design Code and its Probabilistic Evaluation - Role of Damage Reports Including Shaking Table Tests
12H00	Discussion	
12H30	*Lunch break*	
Session 6 topic 2		
14H00	Wenzel	Design Input based on Ground Motion Analysis for the Taiwan High Speed Rail Project
14H15	Mills	Seismic Input Motions for Structure, Plant and Equipment Design
14H30	Noda	Response Spectra for Design Purpose of Stiff Structures on Rock Sites
14H45	Leydecker	Long term seismological hazard assessment: Deterministic and probabilistic approach
15H00	Costantino	Methodology to produce hazard consistent free-field And in-structure design response spectra
15H15	Discussion	
15H30	*Coffee break*	
Final Session		**Mr. Sollogoub**
16h00	Final Session	
17h30	*Closure*	

OECD

OECD/NEA WORKSHOP

ON THE RELATIONS BETWEEN SEISMOLOGICAL DATA AND SEISMIC ENGINEERING ANALYSES

PAPERS SUBMITTED

16-18 October 2002, The President Hotel
Istanbul, TURKEY

Turkish Atomic Energy Authority

THE EFFECT OF NEAR-FIELD GROUND MOTIONS ON DEGRADING SYSTEMS

Haluk Sucuoğlu and Altuğ Erberik
Middle East Technical University, Turkey

Abstract

The damage which occurs in degrading systems under-near field ground motions is evaluated by employing energy based hysteresis and damage models. Low-cycle fatigue principle forms the basis of both models where damage is expressed as the reduction in the effective stiffness. The results indicate that both displacement demands and damage in degrading systems increase significantly due to the degradation of stiffness and strength under near-field ground motions of large magnitude earthquakes which cause a significant number of inelastic displacement cycles.

Introduction

Near-field ground motions have two important characteristics regarding their effects on engineering structures. The first one is well identified in the past, which is the presence of a long acceleration pulse leading to a large peak ground velocity, usually exceeding 50 cm/s, sometimes approaching 1 m/s or larger. Such a dominant pulse produces excessive displacement and inter-storey drift demands from structures subjected to the near field ground motions. These demands usually dominate damage in structures.

Another important aspect of near-field ground motions is the presence of a significant number of large amplitude acceleration cycles during their effective duration. This is a result of the fault rupture process during a large magnitude event, where the fault rupture characteristics are directly reflected into the near-field ground motions. Although the amplitudes of these cycles may be less than the dominant pulse, their compound effect is detrimental, especially on systems which degrade under repeated significant excitation cycles.

An energy-based low-cycle fatigue model is proposed for degrading systems in this study, and energy-based hysteresis and damage models are developed for SDOF systems. These models are employed for evaluating the damageability of near field ground motions for assessing their effects on existing structures whose structural properties deteriorate under severe repeated excitation cycles. Damage is expressed in two parts. The first part is related to the maximum response displacement whereas the second part is related to low-cycle fatigue. The objective of the paper is to evaluate the comparative damage in degrading and non-degrading systems, both subjected to samples of near field ground motions from large magnitude earthquakes.

Degrading Systems

Deterioration in the mechanical properties of concrete, masonry and steel structures and soils are usually observed under repeated cyclic loading in the inelastic response range. It is possible to classify deteriorating systems into two groups: a) Only stiffness deteriorating systems (SD), and b) Both stiffness and strength deteriorating systems (SSD). Under imposed

constant-amplitude inelastic displacement cycles, the first group displays stable hysteresis loops with constant energy dissipation at each cycle. However the second group can not maintain stable cyclic energy dissipation under the same type of loading (Fig.1.a). Although they may attain their initial strength at larger displacements, they exhibit reduced cyclic energy dissipation capacity under constant-amplitude cycles (Fig.1.b). Therefore cyclic energy dissipation capacity can be employed as a convenient measure in differentiating between SD and SSD systems. In this study, SD and SSD systems are described as non-deteriorating and deteriorating inelastic systems respectively, regarding their energy dissipation characteristics. The reduction in the energy dissipation capacity with the number of constant amplitude cycles, normalized with respect to the first cycle dissipation, is expressed by the low-cycle fatigue model shown in Figure 2 for non-degrading and several degrading systems.

Energy-Based Hysteresis Model

A simple piece-wise linear hysteresis model is developed in this study for representing the force-deformation response of single degree of freedom deteriorating systems. It is based primarily on the stiffness degrading model (Clough and Johnston, 1966), extended with an energy-based memory for simulating strength deterioration. An energy-based low cycle fatigue model is developed for calculating the reduction in the energy dissipation capacity under repeated inelastic displacement cycles (Figure 2). The fatigue model in Figure 2 is expressed by

$$\bar{E}_{h,n} = \alpha + (1-\alpha)e^{\beta(1-n)} \qquad (1)$$

where $\bar{E}_{h,n}$ is the normalized energy dissipation at the n'th cycle, α and β are two characteristic fatigue parameters. Once the reduced energy dissipation capacity at an equivalent cycle number is predicted by this model, the force-displacement path in the hysteresis model is determined by reducing the strength capacity of the degrading system accordingly (Erberik and Sucuoğlu, 2001).

Figure 1 demonstrates that the hysteresis model simulates the observed energy dissipation reasonably well in a test specimen under low-cycle fatigue loading. The same model can also predict the energy dissipation characteristics under variable-amplitude loading as shown in Figure 3.

Energy-Based Damage Model

Dissipated energy represents the complete response of a system throughout its entire response duration. Therefore deterioration of structural characteristics can be expressed in terms of the loss in energy dissipation capacity if appropriate physical links can be established.

A hybrid damage model is developed here for degrading systems which takes into account the combined effects of maximum displacement response and strength deterioration due to low-cycle fatigue. Displacement response and strength deterioration under seismic excitations are both expressed in terms of dissipated energy as explained in the previous section.

The damage model is adopted to a system which exhibit both stiffness and strength degradation, subjected to low-cycle fatigue cycles as illustrated in Figure 4 where the first and

n'th cycles are shown. The projection of the intercept of the equivalent stiffness k_e with the initial yield level F_y on the displacement axis indicates that the same amount of damage would be experienced if the system was pushed to the displacement u_e. Accordingly, damage is expressed in two parts constituting u_e. One is due to the observed maximum displacement u_m, and the other is due to the additional displacement Δu_e arising from strength loss. Both displacement components are transformed into damage through normalizing them with the plastic displacement capacity of the system.

$$D_e = \frac{u_m - u_y}{u_u - u_y} + \frac{\Delta u_e}{u_u - u_y} \qquad (2)$$

Damage Estimation Under Near-Field Ground Motions

The energy-based hysteresis and damage models developed in this study are employed for estimating the seismic performance of inelastic SDOF systems under different strong ground excitations. This may provide an insight on the performance assessment of degrading systems during future earthquakes.

Two different ground motions are used for response analysis. These are the El Centro 1940 NS component (ELC), which is a benchmark record in earthquake engineering, and Yarımca NS component from the 17 August Kocaeli earthquake (YPT). Their acceleration traces are shown in Figure 5. Peak ground accelerations were 340, 314 cm/s^2, and peak ground velocities were 35, 73 and 70 cm/s for ELC and YPT, respectively. Both ground motions were recorded in the near fields of their respective sources, during strong earthquakes with magnitudes above 7.

Dynamic responses of degrading systems are calculated under the selected ground excitations. Three different sets of low-cycle fatigue parameters are assigned to the energy-based hysteresis model for comparative assessment. There is no strength deterioration in the first set, accordingly α=1 and β=0. This is identical to the Clough-Johnston model, and identified as the non-deteriorating system (ND). The second set represents a moderately deteriorating system (MD) with α=0.5 and β=1, and the third set is a severely deteriorating system (SD) with α=0.22 and β=0.82. This third set of values represent the CH family of specimens tested within the scope of this study, and presented in the companion paper. The low-cycle fatigue models of the three systems are presented in Figure 2 in the normalized cyclic energy dissipation capacity format.

The displacement responses of degrading SDOF systems with 5% critical damping and a yield strength to weight ratio (η) of 0.2 are calculated under the two ground excitations, for vibration periods T between 0 and 2 seconds. A sample of displacement response histories for T=0.5 second under the YPT record is shown in Figure 6. It is evident from this figure that both the maximum displacement response amplitude and the number of large-amplitude displacement cycles increase significantly with the level of deterioration under a strong ground excitation.

The spectral displacement responses of the elastic, stiffness deteriorating (ND), and both stiffness and strength deteriorating (MD and SD) systems under ELC and YPT are presented in Figure 7 in the form of inelastic to elastic spectral displacement ratios. Although the number of large- amplitude displacement cycles cannot be compared from this figure, it is clearly observed

that spectral displacements of deteriorating systems increase notably in the short and medium period ranges. Further, the well-accepted equal displacement rule, which is based on assuming equal elastic and inelastic spectral displacements in the moderate and long period ranges, does not hold for deteriorating systems in the moderate period range between 0.5 and 1.5 seconds. This range widens with the intensity of ground motion. Similar observations were also reported by Song and Pincheira (2000).

Seismic damage accumulation with time for degrading systems introduced above is calculated under the selected ground motions by using Eq.(2) for SDOF systems in the 0-2 second periods range. Then the maximum damage obtained at the end of each seismic excitation is expressed in spectral form, presented in Figures 8 and 9 for ELC and YPT records respectively. In these figures, two components of the damage function D_e in Eq.(2) are also shown seperately. The first component is the damage resulting from the maximum response displacement or ductility, and the second component is the accumulated damage due to low-cycle fatigue. The second component only exists for the systems that exhibit strength deterioration (MD and SD), hence it is zero for the systems with no strength deterioration (ND).

Both figures reveal that the level of deterioration influences the fatigue-based component of damage function much more than it influences the displacement-based component. Although the displacement-based component is effected from the level of deterioration only in the short period range, total damage is sensitive to deterioration over a wider range including both short and medium periods.

The ELC record may be considered weaker in intensity compared to the YPT record in view of the peak ground velocities. However its long duration has a significant influence on the fatigue-based component of damage for degrading systems. Hence spectral distribution of damage for degrading systems under ELC is comparable to the damage distribution under the other ground motion with higher peak ground velocity. Damage spectrum offers a broader definition for the intensity, or damage potential of ground motions since it contains the effect of the number of large-amplitude response cycles, or the effective response duration, which increases damage in degrading systems considerably.

Damage spectra for inelastic systems with constant strength ratio η are obtained as smooth curves, decaying inversely with the vibration period under the selected ground motion components as shown in Figures 8-9. In order to obtain a uniform spectral damage distribution over the entire period range, larger design strength ratios are assigned to shorter period systems in seismic design codes. Accordingly, damage spectra such as these shown in Figures 8-9 reflect the expected shape of the strength spectra for obtaining a uniform damage distribution. Therefore, if strength deterioration under repeated displacement cycles is inherent under long duration seismic excitations, its effect on damage can only be compensated by a larger yield strength.

Conclusions

An energy-based hysteresis model is developed in this study for predicting the seismic response of degrading SDOF systems deteriorating in strength and energy dissipation capacity. Further, a damage model is proposed for measuring the seismic performance of degrading systems. Both models are verified by the test results. Finally, these models are employed for calculating the dynamic performance of degrading systems under strong ground motions. The following conclusions are obtained from the results of the presented study:

1. A hysteresis model which captures the variation of cyclic energy dissipation capacity predicts the response of degrading systems reasonably well.

2. Spectral displacements of deteriorating systems increase significantly with the level of deterioration in the short and medium period ranges, exceeding the elastic displacements by far.

3. Seismic performance of degrading systems reduce remarkably in the short and medium period ranges under long duration strong excitations which produce a number of significant response cycles. This reduction manifested by the fatigue component of damage function has to be considered realistically in seismic performance evaluation of existing structures.

References

Clough, R.W. and Johnston, S.B., 1966. "Effect of Stiffness Degradation on Earthquake Ductility Requirements", Proceedings, Second Japan National Conference on Earthquake Engineering, pp.227-232.

Erberik, A. and Sucuoğlu, H., 2002. "Energy-Bassed Seismic Evaluation of Degrading Systems". Report No: METU/EERC 01-02, Middle East Technical University, Earthquake Engineering Research Center, Ankara.

Song, J-K and Pincheira, J.A., 2000. "Spectral Displacement Demands of Stiffness and Strength Degrading Systems", Earthquake Spectra, Vol.16, No.4, pp.817-851.

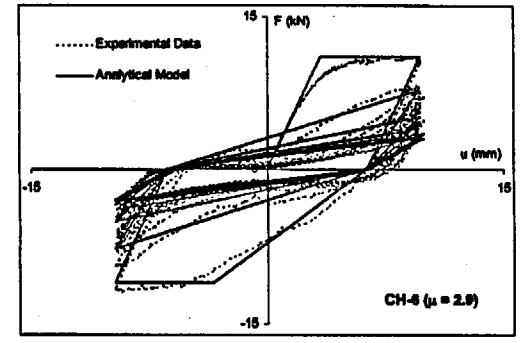

Figure 1.a Observed response and analytical simulation of a degrading system under low-cycle fatigue

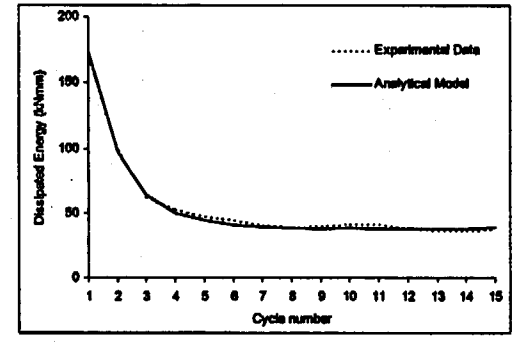

Figure 1.b Observed and predicted energy dissipation of a degrading system under low-cycle fatigue

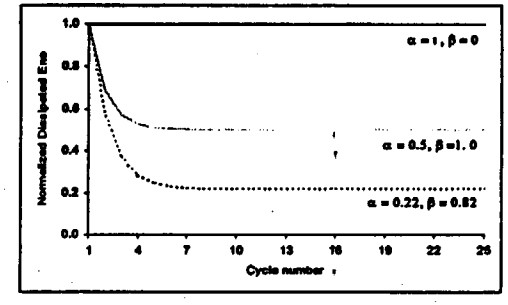

Figure 2. Energy-based fatigue model for non-degrading and degrading systems

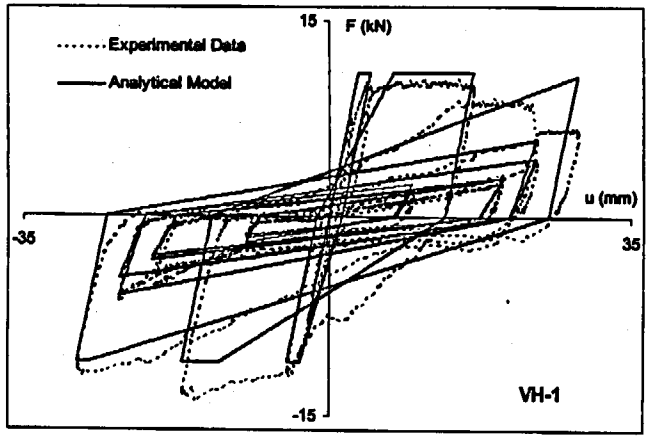

Figure 3.a Observed and predicted hysteresis relations of a degrading system under variable amplitude displacements

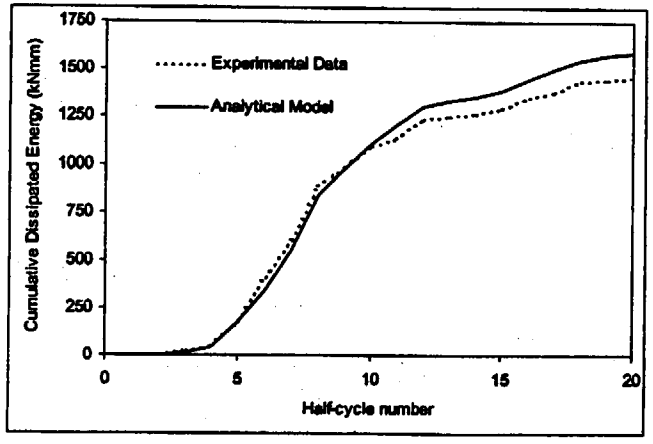

Figure 3.b Comparison of observed and predicted cumulative energy dissipation of a degrading system under variable amplitude displacements

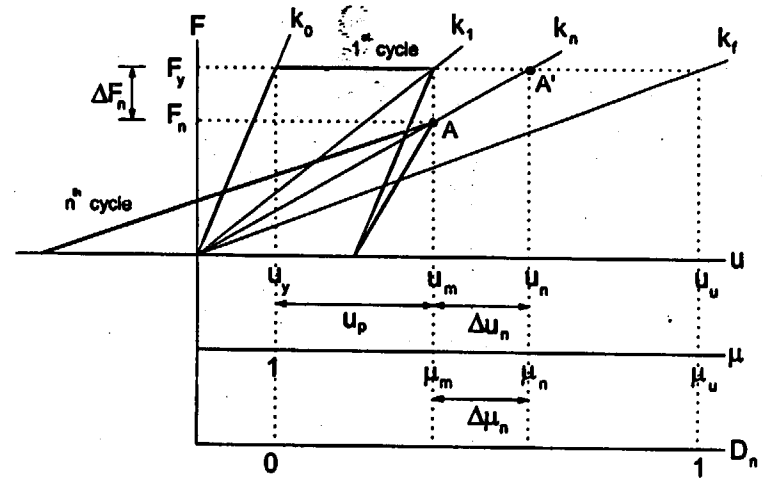

Figure 4. Geometric description of the damage model

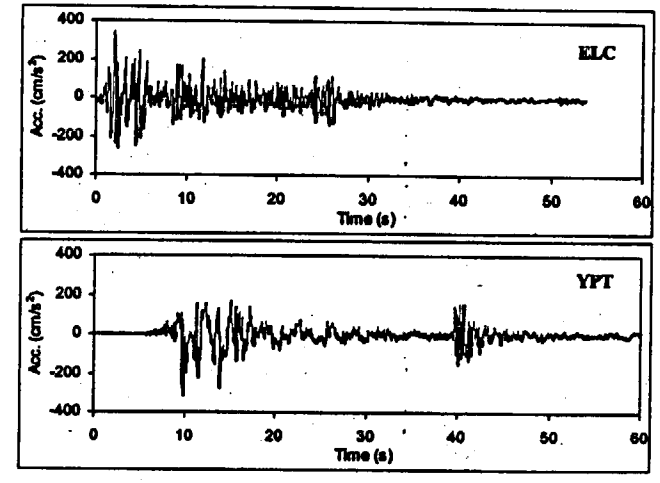

Figure 5. The ground motions used in response analysis.
a) El Centro 1940 NS, b) Yarimca 1999 NS

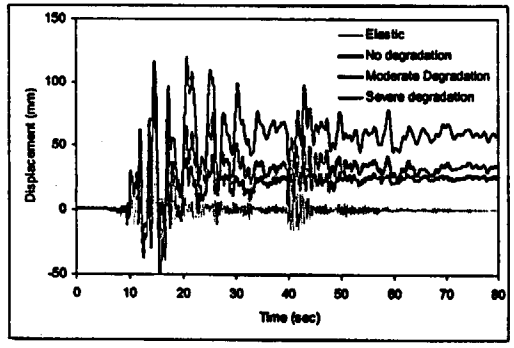

Figure 6. Displacement responses of elastic and inelastic deteriorating SDOF systems under the YPT ground acceleration (T=0.5 second, ξ=0.05, η=0.2)

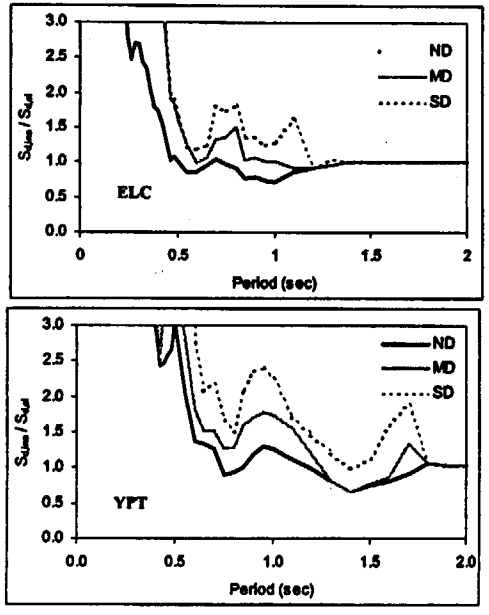

Figure 7. Inelastic to elastic spectral displacement ratios under El Centro (ELC) and Yarimca(YPT) ground accelerations

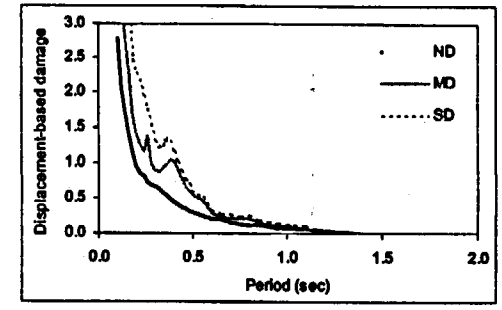

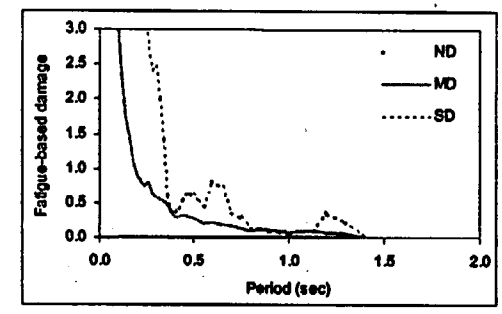

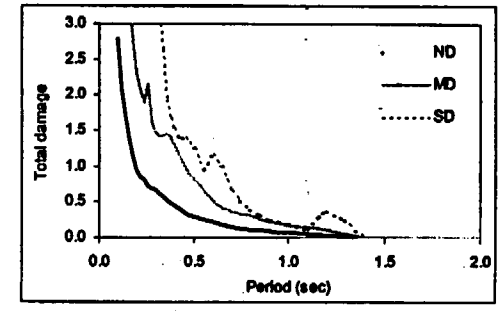

Figure 8. Spectral variation of total damage and its components under El Centro for degrading systems

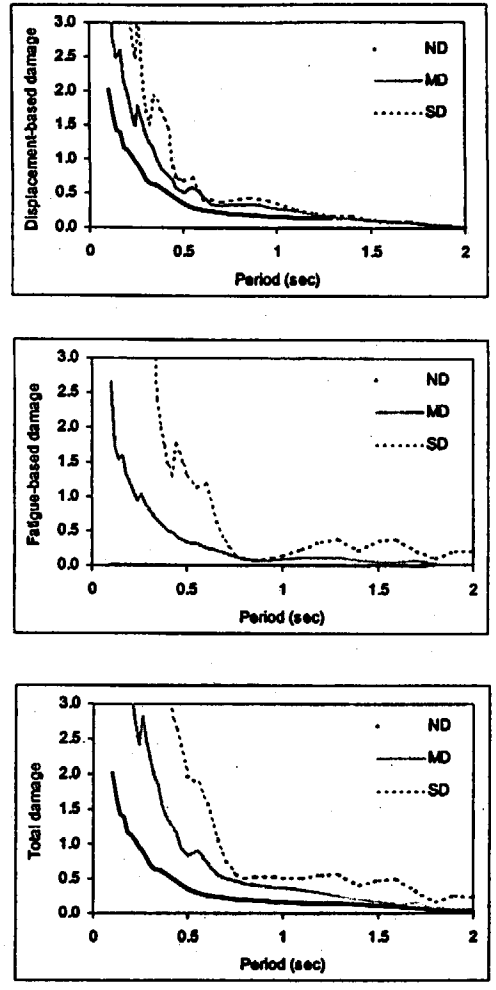

Figure 9. Spectral variation of total damage and its components under Yarimca for degrading systems

SEISMIC RESPONSE OF STRUCTURES TO NEAR FAULT GROUND MOTION

Ahmed Ghobarah[1] and Medhat Elgohary[2]
[1] Department of Civil Engineering, McMaster University, Hamilton, Ontario, Canada
[2] Atomic Energy of Canada Limited AECL, Sheridan Park, Ontario, Canada

Abstract

Near fault ground motion in the forward directivity zone is characterized by large-amplitude velocity pulses of long duration with superimposed high frequency component. The response of structures to near field records is expected to be different from the response to far field records, which were the basis for current design codes. The objective of this study is to evaluate the response of structures to near fault earthquakes (NFE) and compare the response to the standard spectra used in nuclear design. The response spectra of a set of NFE records from recent events were compared to the standard spectra used in the design of nuclear structures. It is concluded that near fault earthquake records affect the response of long period structures. Although the response spectra used in nuclear design codes can be modified to account for the special characteristics of near fault motion. This approach may not be adequate to represent the different states of damage and failure modes of the structure subjected to NFE.

Introduction

Although the special characteristics of near-fault ground motion were known for some time, their importance in earthquake design of civil engineering structures was not fully realized until several failures occurred during the 1994 Northridge and 1995 Kobe earthquake events. Near-fault earthquake (NFE) records in the forward directivity zone are characterized by large amplitude velocity pulses of long duration.

Available research on the response of structures to near-fault records is fairly limited. Anderson and Beretero (1987) studied the nonlinear dynamic response of ten-storey, three-bay steel frame to near-fault records from the October 1979 Imperial Valley earthquake. They remarked that the peak ground acceleration (PGA) might not be the appropriate parameter for classifying the severity of strong ground motion with regard to structural damage potential. Iwan et al. (2000) studied the response of inelastic structures to near-fault ground motion using simplified SDOF and MDOF structural models. A shear-building model was used to analyze building response to NFE ground motions. It was concluded that the single-mode analysis provides misleading results for long period structures subjected to pulse-type ground motions.

Alavi and Krawinkler (2001) studied the elastic and inelastic response of SDOF systems and MDOF frame structures subjected to NFE. They showed that for structures with long period T in comparison to the pulse period T_p ($T > T_p$), the distribution of elastic storey shear forces over the height is sensitive to the ratio of natural period of the structure to the pulse duration. It was observed that the shear forces in upper storeys might exceed the base shear. It was shown that the traveling wave effect causes highly non-uniform distribution of ductility demands over the height.

Liao et al. (2001) studied the nonlinear response characteristics of reinforced concrete frames subjected to NFE. Five and twelve-storey moment resisting frames were designed according to the Taiwan building code. Four near-fault records during the 1999 Chi-Chi (Taiwan) earthquake were used as well as another set of earthquake records at the same sites recorded from past events representing far-field ground motions. All records were scaled to the same PGA of 3 m/s^2. It was concluded that storey drift induced by the near-fault ground motion for both 5 and 12-storey frames was much higher than that due to far-field ground motion.

The limited number of the structures and near-fault records used in the published research emphasize the need for a comprehensive study of near-fault ground motions and their effect on a wide range of actual structures designed according to current codes. As a first step, it is important to compare the response spectra of identified near fault records with the design spectra recommended by codes. This analysis will give an indication as to whether the code design spectra are representative of the near fault earthquake effect. The objective of this study is to evaluate the response of structures to near fault ground motion and compare the response to the standard spectra used in nuclear design.

Characteristics of NFE records

Strong ground motion recorded near fault during major earthquakes showed significant variation between records even between those stations located in the same general area. Some of these records contain high PGA with short-duration pulses that are known as acceleration spikes. In other cases, the pulses are of longer duration but lower PGA (Anderson and Bertero, 1987). Most of the variability of the ground motion in the far field region is attributed to distance to fault, the path and the local site effects. While in the near-fault zone the variability in time histories is mainly due to rupture directivity effect, type of faulting and hanging wall effects for thrust faults.

In the near fault zone, the propagation of rupture towards a site at a velocity very close to the shear wave velocity causes most of the seismic energy from the rupturing process to arrive in a single large pulse of motion. These pulses occur at the beginning of the record and represent the cumulative effect of almost all of the seismic radiation from the fault. The radiation pattern of the shear dislocation on the fault causes this large pulse of motion to be oriented in the direction perpendicular to the fault (Somerville et al., 1997). The ground motion in the forward rupture sites are characterized by the large pulses in the direction perpendicular to the fault while the backward sites have low amplitude long duration motion.

The fault type affects the tectonic deformation and produces the fling effects. For blind thrust fault type, permanent deformation effects occur over a large region above or near the rupture and does not change significantly between two close points. However, for strike-slip and dip-slip faults permanent displacement differs drastically across the fault, which affects structures located directly on the surface of the fault. This permanent displacement is combined with a velocity pulse in the direction of the fault for strike-slip faults and in the direction normal to the fault of the dip-slip faults.

Records from the 1994 Northridge earthquake show that ground accelerations on the hanging wall of thrust faults in the range of 10 to 20 km from the fault are as much as 50% higher than the average value for all site locations (Bardet et al., 1997). The hanging wall effect is most dominant for short periods while at long periods ground motions are more strongly influenced by rupture directivity effects.

Selected NFE records

A set of 30 near-fault records from ten major earthquake events was selected for use in this study (PEER, 2002). Table 1 summarizes the properties of the selected ground motion records. All the records were selected from free field or in building basement in order to minimize the effect of the structure response on the recorded ground motion. The selection of the earthquakes was based on major events with moment magnitude larger than 6. The records were from stations at horizontal distance to the surface projection of the rupture not more than 15 km. The peak ground acceleration (PGA), peak ground velocity (PGV) and peak ground displacement (PGD) of the records are listed in Table 1.

Effect of NFE ground motion on the response of structures

In the far field, damage to structures is caused by several cycles of inelastic deformation where hysteretic mechanisms contribute to the dissipation of input energy. On the other hand, damage to structures in the near field is due to one or two cycles of large deformation that correspond to large amplitude velocity pulse. In this case, the energy dissipation mechanisms in the structure may not have time to be mobilized and the structure may fail abruptly.

The current seismic codes and design procedures are based on the far field earthquake ground motion records that were available at the time of code development. Recently, near fault hazards have been recognized and NFE records are becoming available. An attempt was made to account for near fault hazards by introducing scale up coefficients to design spectra to represent increased demands. However, this approach may not be appropriate given that the response of structures to near fault and far field ground motions may be significantly different.

Table 1 Properties of selected NFE records.

Earthquake	Date	M_w	Station	Fault Dist. km	Component Deg	PGA g	PGV cm/s	PGD cm	ID
Superstition Hills	11/24/87	6.7	286 Superstition Mountain	4.3	45	0.68	32.50	4.70	SH1
					135	0.89	42.20	7.30	SH2
			5051 Parachute Test Site	0.7	225	0.46	112.00	52.80	SH3
					315	0.38	43.90	15.20	SH4
Cape Mendocino	4/25/92	7.1	89005 Cape Mendocino	8.5	0	1.50	127.40	41.01	CM1
					90	1.04	42.00	12.39	CM2
Erzincan, Turkey	3/13/92	6.9	95 Erzincan	2.0	EW	0.50	64.30	22.78	ER1
					NS	0.52	83.90	27.35	ER2
Imperial Valley	10/15/79	6.5	5054 Bonds Corner	2.5	140	0.59	45.20	16.78	IV1
					230	0.78	45.90	14.89	IV2
			5155 EC Meloland	0.5	0	0.31	71.70	25.53	IV3
					270	0.30	90.50	31.71	IV4
Kobe	1/16/95	6.9	KJMA	0.6	0	0.82	81.30	17.68	KB1
					90	0.60	74.30	19.95	KB2
Nahanni, Canada	12/23/85	6.8	6097 Site 1	6.0	10	0.98	46.00	9.67	NA1
					280	1.10	46.10	14.58	NA2
Northridge	1/17/94	6.7	77 Rinaldi	7.1	228	0.84	166.10	28.78	NR1
					318	0.47	73.00	19.76	NR2
			75 Sylmar Converter	6.1	18	0.83	117.50	34.22	NR3
					288	0.49	74.60	28.69	NR4
			24514 Sylmar Olive	3.6	90	0.61	78.20	16.05	NR5
					360	0.84	129.60	32.68	NR6
Tabas, Iran	9/16/78	7.4	9101 Tabas	3.0	LN	0.84	97.80	36.92	TB1
					TR	0.85	121.40	94.58	TB2
Landers	6/28/92	7.	Joshua Tree	11.6	0	0.27	27.50	9.82	LA1
					90	0.28	43.20	14.51	LA2
			24 Lucerne	1.1	0	0.79	32.40	69.78	LA3
					275	0.73	146.50	262.7	LA4
San Fernando	2/9/71	6.6	Pacoima Dam	2.8	164	1.23	112.50	35.50	SF1
					254	1.16	54.30	11.73	SF2

In order to investigate the effect of near fault ground motion on the response of various structures, a frequency digital filtering procedure was applied. The procedure separates low frequency pulses by filtering out the superimposed high frequencies in the record. The cut off filter frequency is determined as the end frequency of the constant amplitude segment of the Fourier amplitude velocity spectrum. Figures 1 and 2 show the velocity power spectrum, ground acceleration, velocity and displacement time histories of earthquake records SH3 and TB2, respectively. The two figures also show a comparison between recorded and filtered time histories for the two earthquakes.

The Fourier amplitude is a measure of the input energy of the ground motion at various frequencies. The broad velocity spectrum shown in Figure 1 indicates motion with large range of frequencies, which represent a random record in the time domain. The narrow spectrum shown in Figure 2 implies that the motion has a dominant frequency, which can be interpreted as a smooth pulse in the time domain. Figures 1 and 2 show that as a result of filtering the velocity record, the acceleration time history is changed especially if it contains high frequency spikes.

Record SH3 shown in Figure 1, contains several peaks in the velocity power spectrum but they all correspond to low frequency pulses. In general, this record has low frequency pulses in both the acceleration and velocity time histories. As the filter is applied to the record, no significant change in the PGV and minor changes to the PGA result. These changes correspond to high frequency spikes. Earthquake record TB2 shown in Figure 2, has completely different characteristics than SH3 record. High frequencies are superimposed on the near-fault velocity pulse but with low input energy as shown in the power spectrum plot. The comparison between recorded and filtered time histories from TB2 record shows small variations in the PGV before and after applying the filter but the PGA of filtered time history is significantly smaller than the recorded one. It is believed that the near-fault low frequency pulse is responsible for most of the damage in flexible structures even when it may have relatively low PGA.

The peak acceleration, the peak velocity or the peak displacement of the pulse can be used to describe ground records in the near-fault. Usually the PGA is the parameter most associated with severity of ground motion. Unfortunately, this parameter cannot be related to the damage potential of the earthquake. Near-fault records may contain acceleration spikes or long duration pulses of low frequency. In case of record SH3, the recorded high peak acceleration is of short duration, which may be out of the range of the natural frequencies of most structures. Therefore, large values of PGA alone can seldom initiate either resonance or be responsible for damage in the inelastic range. However, in case of record TB2, significant deformation of the structure even with lower PGA can occur. For this reason, modifying the code design procedure by increasing the acceleration for design is not a good indicator of damage and is not representative of NFE effects. Anderson and Bertero (1987) suggested the use of maximum incremental velocity and maximum incremental displacement for characterizing the damage potential of earthquake motion instead of PGA. Incremental velocity represents the area under an acceleration pulse and the area under the velocity pulse equals the incremental displacement.

Since the PGA is inadequate for quantifying the near-fault effects, the focus is on the velocity and displacement pulses. The velocity pulses correspond to the integration of relatively large pulses in the acceleration time history. The displacement time history may also contains large pulse, which can be used to quantify near-fault records. However, most recording systems do not adequately record the complete permanent displacements, which are filtered out of the records during processing. This leaves the velocity pulses as the most representative parameter for quantifying the characteristic of near-fault records based on the damage potential of these records.

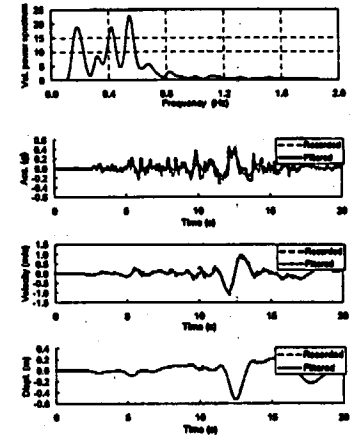

Figure 1 Velocity power spectrum, ground acceleration, velocity and displacement time histories for SH3 earthquake record

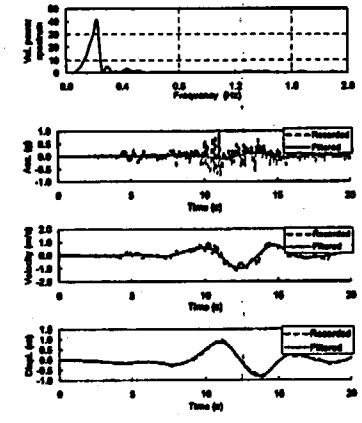

Figure 2 Velocity power spectrum, ground acceleration, velocity and displacement time histories for TB2 earthquake record

Response and design spectra

The response spectrum is used extensively in earthquake engineering practice in the design and evaluation processes. The response spectrum describes the maximum elastic response of SDOF to a particular input ground motion as a function of the natural period and damping ratio of the system. The acceleration response spectra for 5% damping are plotted in Figure 3 for the unfiltered NFE time histories listed in Table 1.

The PGA, PGV, PGD, the Canadian (CSA N289.3, 1992) and the US (REG 1.60, 1978) nuclear design spectra calculated for 5% damping ratio are plotted in Figure 4. The Canadian nuclear design spectrum is based on ground motion of 0.1 g peak acceleration, 71 mm/s peak velocity and 30.5 mm peak displacement. The US nuclear design spectrum plotted in Figure 4 is scaled to 0.1 g. To compare the response spectra of NFE records with the nuclear design spectra, scaling of the NFE to PGA of 0.1 g or PGV of 71 mm/s is necessary. The mean and the mean plus one standard deviation of all the NFE records listed in Table 1 scaled to PGA of 0.1 g, are plotted in Figure 5. The 5% damping spectra of the nuclear design guides scaled to 0.1 g are also plotted in Figure 5. The design spectra envelope the mean and mean plus one standard deviation curves in the high frequency range. However, the spectra are below the other curves in the long period range. The fundamental frequencies of major nuclear structures are normally in the range of 2 to 10 Hz.

The mean and the mean plus one standard deviation of all the NFE records listed in Table 1 scaled to PGV of 71 mm/s are plotted in Figure 6. The 5% damping nuclear design spectra are plotted on the same graph for comparison. It is found that on the basis of PGV scaling, the design spectra are higher than the mean and the mean plus one standard deviation curves in the high frequency range. However, the seismic demands for long period structures are higher than the nuclear design spectra. The spectra of all the NFE records are presented on tripartite plots in Figures 7 and 8. In Figure 7 the NFE were scaled to PGA of 0.1 g.

When the uniform hazard spectrum was introduced in seismic design, concern was expressed by practicing designers that it appears to underestimate the seismic demand in the long period range. The high demands of NFE records in the long period range may finally offer a logical resolution of the controversy.

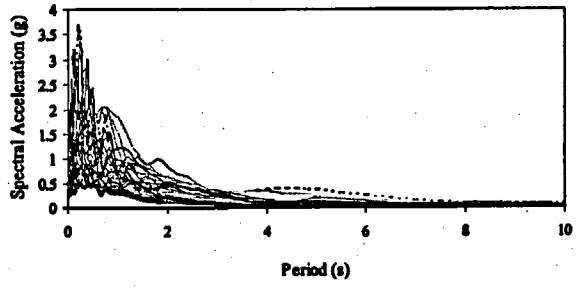

Figure 3 Absolute spectral accelerations of NFE records

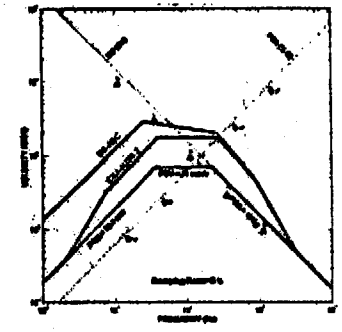

Figure 4 Canada and US (scaled to 0.1 g) design spectra calculated for 5% damping ratio

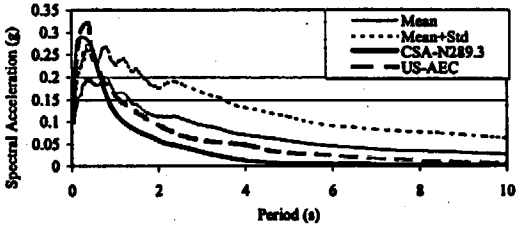

Figure 5 Comparison between the mean and mean plus one standard deviation of NFE records scaled to PGA of 0.1 g and Canada and US nuclear spectra

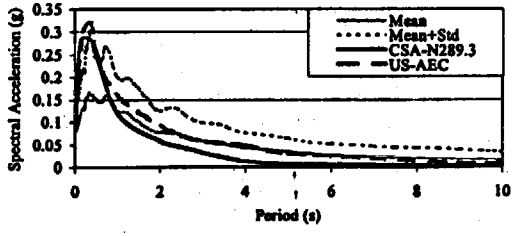

Figure 6 Comparison between the mean and mean plus one standard deviation of NFE records scaled to PGV of 71 mm/s and Canada and US design spectra

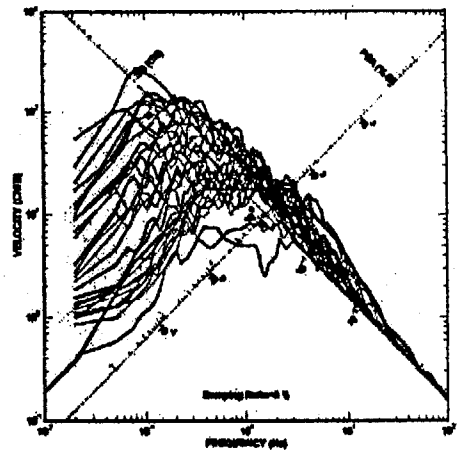

Figure 7 Comparison between the spectra of NFE records scaled to PGA of 0.1 g and the CSA N289.3 Canadian nuclear design spectrum

Conclusions

From the study of the characteristics of the NFE records and the comparison between NFE, the Canadian (CSA N289.3, 1992) and the US (REG 1.60, 1978) nuclear design spectra, the following conclusions are arrived at:

1. The separation of the low frequency component of near-fault record from the high frequency content by applying digital signal filters seems to be a realistic method for identifying the near-fault pulse parameters. This procedure provides some basis to justify and clarify when idealized pulses can substitute the complete near-fault record in structural analysis.

2. NFE affect the response of long period structures. However, major nuclear structures are normally in the high frequency range. The most important parameters of the near fault ground motion are the velocity pulse magnitude and pulse duration. The site-specific seismological prediction of these parameters is required for designing structures that may be subjected to near fault ground motion.

3. Long period structures designed to meet the minimum Canadian and US nuclear design requirements (CSA N289.3, 199) and US (REG 1.60, 1978) may be subjected to severe seismic demands and damage in the near fault zone. The design requirement should address the near-fault motion explicitly in a time history form. It is recommended to define pulse parameter by the velocity pulse magnitude and duration and not by an implicit form of increasing the ordinates of the design response spectra.

Acknowledgement

This research was conducted under a research grant from Atomic Energy of Canada Limited. The support of AECL is gratefully acknowledged.

References

1. Alavi, B. and Krawinkler, H., 2001 'Effects of near-field ground motion on building structures', Consortium of Universities for Research in Earthquake Engineering, CUREE Publication No. CKIII-02, CA.
2. Anderson, J.C. and Bertero, V.V., 1987 'Uncertainties in establishing design earthquakes', Journal of Structural Engineering, ASCE, Vol. 113, No. 8, 1709-1724.
3. Bardet, J. P., Idriss I. M., O'Rourke T. D., Adachi T., Hamada M., and Ishihara K., 1997 'North America - Japan Workshop on the Geotechnical Aspects of the Kobe, Loma Prieta and Northridge Earthquakes", Report to National Science Foundation, Air Force Office of Scientific Research, and the Japanese Geotechnical Society, January 1996, Osaka, Japan.126 pages.
4. CSA N289.3, 1992 'Design procedures for seismic qualification of CANDU Nuclear Power Plants' Canadian Standards Association, Rexdale, Ontario.
5. Iwan, W.D., Huang, C. and Guyader, A.C., 2000 'Important features of the response of inelastic structures to near-field ground motion', 12th World Conference on Earthquake Engineering [Proceedings on CD], New Zealand Society for Earthquake Engineering, New Zealand, Paper No. 1740.
6. Liao, W.I., Loh, C.H. and Wan, S., 2001 'Earthquake responses of RC moment frames subjected to near-fault ground motions', Structural Design of Tall Buildings, 10, n 3, 219-229.
7. PEER 2002 'Strong Motion Database'. Available form the Pacific Earthquake Engineering Research Center and the University of California, Retrieved July 2002, from http://peer.berkeley.edu/smcat/
8. REG 1.60, 1978 Design response spectra for seismic design of nuclear power plants. US Atomic Energy Commission (US AEC), Regulatory Guide REG 1.60, Washington, DC.
9. Somerville, P.G., Smith, N. F., Graves, R.W., Abrahamson, N. A., 1997 'Modification of empirical strong ground motion attenuation relations to include the amplitude and duration effects of rupture directivity', Seismological Research Letters, 68, 199-222.

Damaging effects of near-field and far-field earthquake on reinforced concrete shear walls evaluated by a simplified model taking into account stiffness degradation

M. Brun*, J.M. Reynouard[1], L.Jezequel[2], C. Duval and S. Goubet
URGC-Structures, Institut National des Sciences Appliquées de Lyon, 69621, Villeurbanne, France.

Abstract :

The study intends to compare the damaging effects of a great variety of seismic ground motions included in a large data base. In particular, the purpose is to question the grade of conservatism of engineering rules in case of low-magnitude near-field earthquake, coming partly from the fact that the design of a civil engineering structure at its initial fundamental frequency does not take into account the degradation of the fundamental frequency for an increasing damage. For this purpose, an important step is to set up a simplified model of a reinforced structure, capable of reproducing at a global level the damage incurred. First of all, a low-rise shear wall, which has been previously pseudodynamically, is modelled by means of local models of concrete and steel materials. After verifying their relevance for predicting global response values such as top displacements and stiffness degradation, a simplified model, based on the fundamental frequency decrease as a function of a simple non-cumulative damage variable, is derived. The simplified model is validated by comparing the time-history damage prediction with the experimental one.
Owing to drastic reduction of computation times, the simplified model allows to assess the damage undergone by the reinforced concrete shear wall submitted to a large data base, composed of 2125 horizontal accelerograms. The simplified model constructed for a particular shear wall with a given initial fundamental frequency, is adapted to others shear walls, with initial fundamental frequencies covering an appropriate range for the civil engineering structures. Then, the interdependency between the seismic acceleration parameters proposed in the literature (PGA, PGV, Arias Intensity, CAV, ...) and the damage is explored. A spectral intensity, taking into account the degradation of the fundamental frequency, is proposed. Its correlation with the damage is significantly improved. Finally, the damage is connected to seismological parameters, i.e. the magnitude and the focal distance. For a deterministic structure, the grade of conservatism from engineering rules related to low-magnitude near-field earthquakes in comparison to the one related to further distance and greater magnitude earthquakes, is underlined. The spectral intensity proposed in this study, provides a homogeneous and relevant tool for estimating the damage potential of low-magnitude near-field earthquakes as well as greater and further ones.

* Ph.D Student, corresponding author.
Tel : 04-72-43-89-72 / From abroad (+33) 4-72
Fax : 04-72-43-85-23
E-mail : michael.brun@insa-lyon.fr
[1] Professor, URGC-Structures, Institut National des Sciences Appliquées de Lyon, 69621, Villeurbanne, France.
[2] Professor, LTDS, , Ecole Centrale de Lyon, 69000, Ecully, France.

1. Introduction

The aim of this study is to investigate the grade of conservatism issued from the engineering practice by taking into account the seismic input as a spectral value at the initial frequency of the structure in particular case of low-magnitude near-field earthquake. Indeed, owing to the decrease of the dynamic characteristics of the damaged structure, the pseudo-acceleration value corresponding to the initial frequency can be a misleading parameter for the characterisation of the seismic damage potential. It is well recognised that, as the damage increases within the reinforced concrete structure, the alteration of the mechanical characteristics yields modal characteristics changes. In this way, Chen and al. ([1]) investigated the structural damage by means of the identification method of modal changes. At a critical damage level, they indicated that a decrease of the fundamental frequency up to 10% can be expected for steel beams. For reinforced concrete structures, the fundamental frequency reduction, related to the structural damage can be significantly greater. Actually, pseudodynamic tests on a low-rise shear wall, carried out at the European Laboratory for Structural Assessment (JRC-Ispra), showed fundamental frequency reductions of more than 60% (Pegon and al. [2]). In this study, this simple structure, which will be briefly presented in the following, is adopted. Such a fundamental frequency decrease strongly influences the dynamic response of the structure subjected to a seismic excitation. A reliable global model should reproduce in the best way this feature.
The first step concerns with the construction of a simplified based on the decrease of the fundamental frequency as a function of a damage variable. The used concept lies in coupling during time the dynamic characteristics of the structure with a non cumulative damage variable relevant for the structure under consideration. The decrease of the fundamental frequency as a function of damage, identified by the help of predictive local behaviour models of concrete and steel materials, represents the only parameter curve of the non linear simplified model. The first validation of the simplified model is undertaken by comparing numerical results with experimental results. Then, for a set of 501 strong motions belonging to a large strong motions data base, the damages issued from the simplified analysis and from a more refined analysis using local models, are compared.
As the computation times are drastically reduced, the second step of this paper aims to determine the characteristics of the accelerograms that exhibit the strongest influence on damage. The purpose is to explore the interdependency between several seismic acceleration parameters and the damage variable predicted by the previously set up simplified model. The grade of interdependency is deemed by means of a linear correlation coefficient. By changing the effective mass of the uniaxial simplified model, the ability of the explored parameters to reproduce the seismic damage potential is investigated for a set of shear wall structures, each one being defined by a given initial fundamental frequency. A spectral parameter, which is based on spectral displacements and takes into account the degradation of the fundamental frequency, is put forward. The new parameter exhibit a good correlation with the damage variable for the whole range of initial fundamental frequencies. Then, the grade of conservatism issued form the use of the pseudo-acceleration value at the initial frequency of the considered structure as input seismic characterisation, is highlighted in particular case of low-magnitude near-field earthquake. The proposed spectral parameter turns out to be very efficient for reducing the grade of the previously exhibited conservatism concerning the low-magnitude near-field earthquakes.

2. Experimental programme

2.1 Presentation of the structure

In this work, the chosen structure is a heavily reinforced concrete shear wall which has been tested during the SAFE research programme at the European Laboratory for Structural Assessment (JRC-Ispra) in Italy. The SAFE programme included 13 pseudodynamic tests on low-rise reinforced concrete shear walls with different reinforcement ratios. The geometry of the selected wall T5 is depicted in Fig. 1. The wall is surrounded by a top and a base slab. The two heavily reinforced flanges are 20 cm thick. The web wall is 20 cm thick. The aspect ratio of the shear wall is equal to 0.4 indicating that the response is essentially controlled by shearing action. The horizontal and vertical reinforcement ratios of specimen T5 are equal to 0.8%.
The design frequency of the shear wall T5 is equal to 8 Hz. No vertical loading is applied to the specimen. In order to submit the structure to a pure shear loading, the rotation of the top slab is prevented by means of hydraulic pistons.

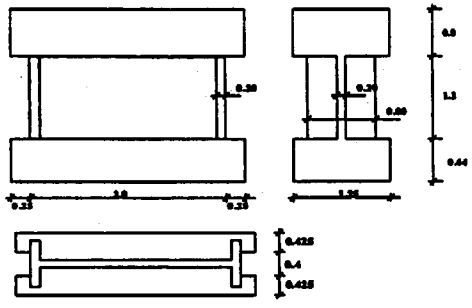

Fig. 1. Geometry of the wall T5 in m

2.2 Pseudodynamic tests

The input excitation used during the SAFE tests is a synthetic accelerogram having as target elastic spectrum a standard spectrum employed in the nuclear construction field. The spectral peak value of this standard spectrum is at about 4 Hz. The specimen is subjected to a series of pseudodynamic tests with increasing level up to the failure.
The measured initial fundamental frequency is equal to 6.7 Hz. In the first RUN, a relatively important cracking is observed, which is confirmed by a large drop of the fundamental frequency. The damage increases progressively during the two following RUNs to become very important in the fourth RUN. The failure of the specimen occurred at the beginning of the fifth RUN, by concrete crushing in the compressive zones of the wall, without fracture of reinforcement steels.

3. Simplified model

3.1 Coupling damage variable and degradation of the fundamental frequency

The purpose of the simplified model is to provide a reliable and efficient tool for the evaluation of the damage on the wall generated by strong motions contained in a large data base. First of all, the attention is focussed on the appropriate way to quantify the structural damage sustained by the low-rise shear wall. The maximum displacement at the top of the wall seems to be a good parameter to evaluate the damage. Park and Ang [3] proposed to complete this damage variable with a second term taking into account the dissipation under loading cycles. Among several authors, Fardis [4] concluded the relevance of this variable to reproduce the failure of the structure subjected to flexural forces. However, one can notice that the weighting coefficient associated with the energetic term appeared very low. Therefore, the contribution of the energetic term in the Park&Ang's indicator becomes negligible in comparison to the displacement term. This consideration leads to the idea of adopting the simple maximum top displacement (denoted X) as the damage variable.
The kinematics of the low-rise shear wall is essentially the one of a one degree of freedom system. It is crucial to reproduce in the best way the strong decrease of the structural frequency observed in the experimental programme. The concept of the simplified model is to couple the fundamental frequency decrease with the damage variable X, by updating during time the frequency according to the damage variable X. The changes of the fundamental frequency during time is controlled explicitly by the damage variable X, which keep in memory the maximum of the prior response.
It is interesting to compare this simplified model with global hysteretic models commonly used in earthquake engineering. In accordance with the design philosophy of plastic hinges, hysteretic models are concerned with predicting in the most realistic way the energy dissipation corresponding to hysteretic loops area. The fundamental frequency decrease is implicitly taken into account through the stiffness loss. The model proposed in this work takes into account explicitly the changes in the fundamental frequency due to damage. Due to the relative stability of the viscous damping ratio computed from experimental results, the damping is modelled in a rough manner through an equivalent constant viscous damping ratio.
Owing to the fact that the shear wall can be considered to a one degree of freedom system, the top-displacement response x(t) during time follows the equation of motion given as:

$$\ddot{x}(t)+2\xi\omega(t)\dot{x}(t)+[\omega(t)]^2 x(t)=-a(t) \qquad (1)$$

with $\omega(X)=2\pi f(X)$ and $X(t)=\max_{0\le t'\le t}|x(t')|$

where $x(t)$, $\dot{x}(t)$, $\ddot{x}(t)$ are the relative displacement, relative velocity and relative acceleration, respectively;
a(t) is the imposed acceleration at the base of the wall;
f(X) is the fundamental frequency depending on the damage variable X.
Since the damping ratio computed from experimental data was in the vicinity of 5 %, this mean value is adopted.
The decrease of the fundamental frequency f(X) is identified by using a local approach.

3.2 Identification of the coupling relation

The identification of the fundamental frequency is carried out by means of local behaviour models of concrete and steel materials. The concrete model, which makes use of the smeared fixed crack concept, has been already validated during previous research programmes (Ile, [5], [6]). The ability of the model to reproduce the main phenomena which take place within the wall, is evaluated by comparing numerical results issued from a refined finite element modelling with local models and experimental results for the pseudodynamic tests on the wall T5. Then, the finite element modelling is kept and submitted to a variety of ideal sinusoidal excitations with different frequency and amplitude in order to derive the relationship between damage variable and fundamental frequency degradation. After applying one given ideal excitation, the final damage variable X is computed as the maximum of the top displacement of the wall during excitation. The final fundamental frequency is directly derived from the secant stiffness by the relation:

$$f=\frac{1}{2\pi}\sqrt{\frac{K}{M}} \qquad (2)$$

where K is the final secant stiffness and M is the effective mass.
Fig. 2 shows the numerical values of the fundamental frequency related to the damage variable X.

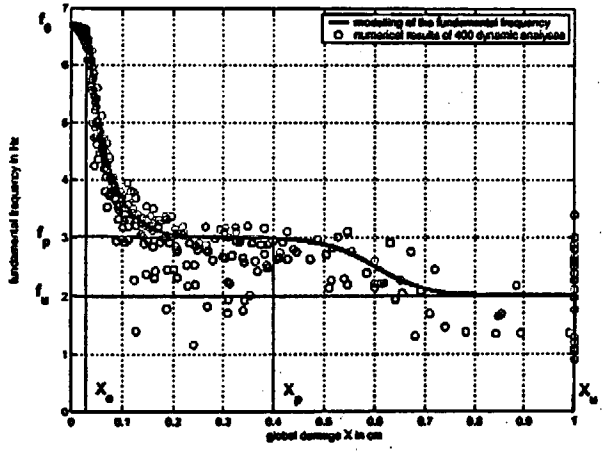

Fig. 2. Fundamental frequency against global damage X: numerical results and modelling

As a general trend, it can be seen that, from a certain threshold of the maximum top displacement X, the decrease of the fundamental frequency is very abrupt, to become softer in a second stage. The first stage of the fundamental frequency decrease from a threshold value X_e is essentially due to the sudden concrete cracking. By inspiring to local formulations in traction proposed in the literature, which expressed the degradation of the Young modulus E as a negative exponential law depending on the plastic strain (Nechnech [7], Laborderie [8]), the strong decrease of the fundamental frequency is modelled by an exponential law with a negative coefficient c_1, charged to reflect the high kinetic of the cracking phenomenon. The second stage of the fundamental frequency decrease is essentially controlled by compressive non linear concrete behaviour, steel yielding and softening concrete. Due to the scarcity of the numerical results, this stage is modelled in a approximate way by an hyperbolic law with a lower kinetic constant c_2 than the one associated with the first stage decrease. Finally, the function f(X) identified from numerical results is given as :

$$\begin{aligned} &f = f_0 && \text{for } X \le X_e \\ &\frac{f-f_p}{f_0-f_p}=\exp[-c_1(X-X_e)] && \text{for } X_e \le X \le X_p \\ &\frac{2f-(f_u+f_p)}{f_p-f_u}=th[-c_2(X-0.6)] && \text{for } X_p \le X \le X_u \end{aligned} \qquad (3)$$

The parameters f_0, f_p, f_u, X_e, X_p and X_u involved are identified from numerical results, so that the fundamental frequency curve fits them in the best possible way. In Fig. 2, the modelling of the fundamental frequency is compared with the numerical results.

3.3 Discussion

The formulation of the simplified model of a shear wall is based on the explicit decrease of the fundamental frequency as a function of the non cumulative damage variable X. We assume that the degradation of the fundamental frequency is dependent on the only damage variable X, without considering cumulative effects. The good results obtain under this assumption lead to the idea that the damage cumulative effect is not significant for the selected low-rise shear wall. Obviously, this assumption is more questionable for a slender wall.
A limitation of the simplified model lies in the fact that it is valid for one degree of freedom system. Furthermmore, the dissipation under cyclic seismic loading has been taken into account through a constant viscous damping ratio, what is a rough manner to describe the complex phenomena under cyclic loading.

4. Validations

4.1 Experimental results

The first validation of the simplified model concerns with the pseudodynamic tests. The simplified model of the shear wall is employed to predict the top-displacement response. The top displacement history is computed by resolving the previous equations (1) and (3). The damage variable time-history, corresponding to the maximum top-displacement, is deduced. The numerical prediction is compared, on the one hand, with experimental results, and on the other hand, with numerical results obtained with local models. The prediction shown in Fig. 3 seems quite good in comparison to the experimental results and the numerical results issued from a refined approach. We can notice a slight underestimation of the simplified model

during the RUN2. This can be attributed to a slight error of the modelled decrease of the fundamental frequency in comparison to the real one. It can also results from a higher value of the modelled viscous damping ratio than the experimental one, which has been experimentally estimated at about 4 % during the RUN2.

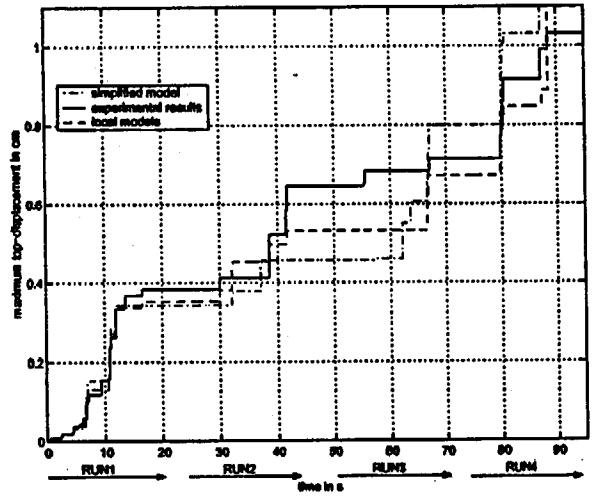

Fig. 3. Time-history maximum top displacement X for the first four RUNs

4.2 Data base

A large data base containing 2125 horizontal strong motions is employed to verify the relevance of the damage prediction from the simplified analysis, by comparing those from a finite element approach. This data base is the input data of our study concerning the characterisation of the seismic damage potential. Therefore, it is of great importance, because all results remain closely associated with it. It comes from the work of European Council, Environment and Climate Research Programme, which has been collected european strong motions, and gathered together in an available CD-ROM (Ambraseys, [9]). The magnitude, the epicentral distance and the focal depth are provided for each accelerogram. In this study, the focal distance is employed, directly deduced form the epicentral distance and the focal depth. The strong motions are shown in terms of focal distance-magnitude in the Fig. 4.

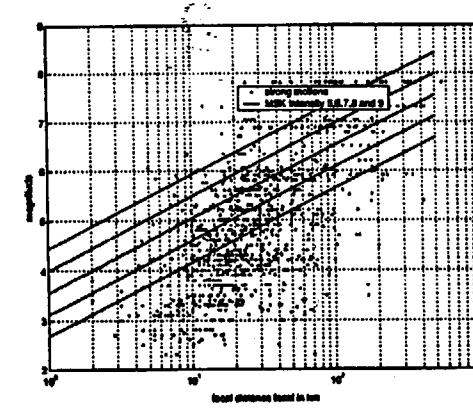

Fig. 4. Strong motion data base (2125 accelerograms)

Given the computation time required by the finite element approach, only 501 strong motions are applied to the finite element modelling of the shear wall in order to verify the ability of the simplified model to reproduce the damage. The two numerical predictions are compared in the Fig. 5. As we can see, the results issued from the simplified analysis are close to the finite element modelling predictions. For a few strong motions, the simplified model underestimate the damage in comparison to local models. This can be attributed to the sensitivity of the threshold value X_s involved in the definition of the parameter curve f(X) of the simplified model. For these strong motions, the damage X remain lower than this threshold value and the structure does not suffer any degradations under cyclic loading, while local models predict a progressive damage.

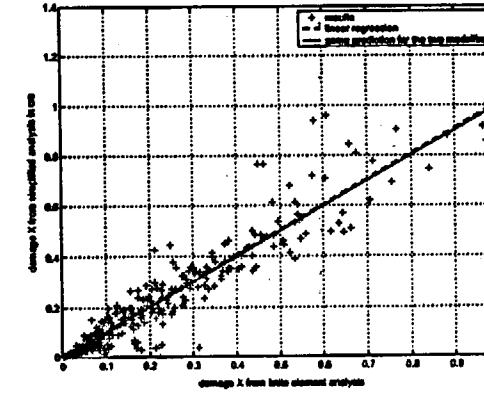

Fig. 5. Damage predicted by simplified model and local models for 501 strong motions

5. Conclusion

The coupling concept of the fundamental frequency decrease with the non cumulative damage variable X, appears to be capable of reproducing the global damage sustained by the studied low-rise shear wall under seismic excitations. Thanks to the drastic reduction of the required computation times in comparison to a refined finite element approach, a statistical study based on the large data base is carried out in the following. The ability for reflecting the seismic damage potential of the investigated acceleration parameters will be scrutinised by the help of the simplified model, reproducing the decrease of the dynamic properties of the structure during seismic excitation.

Acknowledgements

The support of Electricity of France and grant from the Region Rhône-Alpes are gratefully acknowledged.

References

1. Chen H.L. and al. Evaluating Structural deterioration by dynamic response.
Journal of structural engineering, Vol.121, No. 8, August, 1995.
2. Pegon P. et al. Programme SAFE : Rapport du Test T5.
Technical Note, Joint Research Center, 1998.
3. Park Y.J. & Ang AH.S. Mechanistic seismic damage model for reinforced concrete.
Journal of Structural Engineering (ASCE), 111(4): 722-739, 1985.
4. Fardis M.N. Damage measures and failure criteria for reinforced concrete members.
Proceedings 10th European Conference on Earthquake Engineering, Vienna, Austria, August-September ,1994. Vol.2, Rotterdam, Balkema, 1995: 1377-1382.
5. Ile N. Contribution à la compréhension du fonctionnement des voiles en Béton Armé sous sollicitation dynamique.
Thèse de Génie Civil, INSA de Lyon, 2000.
6. Ile N. et al. Nonlinear analysis of reinforced concrete shear wall under cyclic and dynamic loading.
Journal of Earthquake Engineering, Vol.4, No.2, 2000.
7. Nechnech W. Contribution à l'étude numérique du comportement du béton et des structures en béton armé soumises à des sollicitations thermiques et mécaniques couplées: une approche thermo-élasto-plastique endommageable.
Thèse de Génie Civil, INSA de Lyon, 2000.
8. La Borderie C. Phénomènes unilatéraux dans un matériau endommageable - Modélisation et application à l'analyse des structures en béton armé.
Thèse de Génie Civil, Université de Paris 6, ENS de Cachan, 1991.
9. Ambraseys N., Smit P., Berardi R., Rinaldis D., Cotton F., Berge-Thierry C. Dissemination of European Strong-Motion Data. CD-ROM collection. European Council, Environment and Climate Research Programme, 2000.

ANALISYS OF THE RESPONSE OF STRUCTURES TO DAMAGING PULSE-TYPE GROUND MOTIONS

Luis D. Decanini, Silvia Bruno, Fabrizio Mollaioli
Dipartimento di Ingegneria Strutturale e Geotecnica - Università di Roma "La Sapienza", Italy
luis.decanini@uniroma1.it, silvia.bruno2002@virgilio.it, fabrizio.mollaioli@uniroma1.it

Giuliano F. Panza
Dipartimento di Scienze della Terra - Università di Trieste
The Abdus Salam International Center for Theoretical Physics - Miramar, Trieste
panza@dst.univ.trieste.it

Abstract

The presence of long period pulses in near-fault records can be considered as an important factor in causing damage due to the transmission of large energy amounts to the structures in a very short time. Under such circumstances high energy dissipation demands usually occur, which are likely to concentrate in the weakest parts of the structure. From the study of the response of nonlinear oscillators, the effects of these distinctive long period pulses, derived from records obtained during recent earthquakes, have been assessed by means of: i) synthetic parameters directly derived from the strong ground motion records, such as peak ground acceleration, peak ground velocity, incremental velocity, and ii) elastic and inelastic spectra of input energy, hysteretic energy, displacement, strength. The results indicate that long duration pulses strongly affects the inelastic response, with very high energy and drift demands which may be several times larger than the limit values specified by the majority of codes.

Introduction

The recently increased availability of recorded near-fault ground motions suggests that the dynamic characteristics of ground shaking can vary significantly as a function of the location of the recording station with respect to the fault and the evolution of the rupture process. It has been known for a long time that under certain conditions earthquake ground motions can consist of a limited number of distinct velocity and displacement long duration pulses. Typically, these pulses are the result of a particular phenomenon, known as forward directivity effect, attributable to the earthquake rupture moving toward the site. In the case of backward directivity, occurring when the rupture propagates away from the site, the corresponding motion is generally characterized by lower amplitudes and longer duration. The directivity itself is a well-known phenomenon in seismology [1-5], however only recently the impact of the directivity pulse has been considered in a limited number of seismic codes. In a document included in the 1983 Argentinian seismic code [6] it was suggested to utilize in the near-field area accelerograms including long duration pulses. However, the first seismic code including factors to account for near-field directivity effects on spectral ordinates is the 1997 version of the Uniform Building Code [7].

The presence of long duration pulses in near-field ground motions implies the transmission of large amounts of energy into the structure which should be dissipated in a short time. This behavior is characterized by one or two large inelastic excursions with few reversals, usually concentrated in the weakest parts of the structure, such as soft stories and any other zone where sharp changes in strength or stiffness occur. On the other hand high frequency, harmonic motions, typical of far-field records, generally require a continual dissipation of energy over a relatively long time, with numerous yield reversals. Therefore, while the total input energy corresponding to long duration ground motion pulses (i.e., of low to medium frequency) can reach considerable values, even though the seismic intensity is not particularly significant, high frequency motions do not produce severe damage, since their high spectral acceleration are not consistent with the corresponding moderate energy effectively imparted to structures.

Recent concern about the damage potential of near-field ground motion has led to considerable interest in the nature of these motions and their impact on structural performance. As long ago as the end of the fifties it was suggested [8] that the presence of a single pulse of energy was responsible of the exceptional damage inflicted on structures by the Port Hueneme Earthquake of March 18, 1957, in spite of its small magnitude ($M_L = 4.7$) and low peak ground acceleration (0.08g). However, the recognition of the effects of ground motions near the causative fault is significantly connected with the study of two other strong motion records, namely those known as Station 2 in the 1966 Parkfield, California Earthquake and Pacoima Dam Station in the 1971 San Fernando, California Earthquake. Though both records were obtained a few kilometers from the source, relatively little damage was caused by the former, characterized by pulses of very short duration, whereas the latter almost immediately awakened the interest of the scientific community, being the first destructive seismic event in the USA with a recorded accelerogram containing severe long duration acceleration pulses which resulted in large ground velocity increments. In particular in [9], in the analysis of the damage suffered by the Olive View Hospital, a few kilometers down the rupture surface of the 1971 San Fernando Earthquake, it was suggested that the significant nonlinear structural behavior would probably have occurred during the response to the relatively long duration pulse highlighted by the Pacoima Dam record. This dynamic demand would have forced the structure beyond its elastic capacity, with consequent destructive damage to the supporting columns of the lower floors. Subsequent to the pulse, the strong ground motion was dominated by higher frequencies than that of the pulse. However such later motion, though containing the overall peak acceleration, appeared to have shaken the damaged building about its newly deformed configuration. The misleading notion of scaling the earthquake intensity near to a fault by a peak ground acceleration value, since it is normally associated to waves of relatively high frequency, had been previously demonstrated in [3], as recalled in [5]. Actually, in near-fault records the most energetic velocity and displacement pulses are not even in phase with the peak acceleration; yet dynamic considerations suggest that the former might produce more profound structural response consequences than the latter.

After the 1979 Imperial Valley, California Earthquake, the incremental velocity was indicated as one of the most important parameters influencing the maximum inelastic response of structures subject to near-fault ground motions; moreover, it was pointed out that long duration acceleration pulses are especially damaging if the width of the pulse is large compared with the natural period of the structure [10]. These concepts were reasserted in [11, 12]. More recently several studies have focused on the dynamic response of MDOF systems subject to pulse-like ground motions. Simplified modelling techniques were used to highlight the effect of such pulses on multi-storey frames [13-16].

The importance of assessing near-fault effects has led several authors [17-20] to demonstrate that near-fault records with forward directivity can be represented by equivalent pulses defined on the basis of a limited number of ground motion parameters. On recognizing that the intensity and distribution of the seismic energy demand depend upon the duration of the pulses, in [21] the significance of energy-based parameters in the characterization of the seismic demand of structures subject to near-fault pulses was emphasized, and some relationships between energy and displacement demands were suggested. Finally, starting from an energy-based characterization of the damage potential, a series of parameters, namely the incremental velocity, the area enclosed by the input energy spectra and the pulse duration, were identified in order to set the equivalence between idealized and ground motion pulses [20].

In this research, from the study of the response of oscillators having nonlinear behavior, the effect of such distinctive long period pulses derived from records obtained during recent earthquakes has been analyzed by means of: i) synthetic parameters directly derived from the strong ground motion records,

such as peak ground acceleration, peak ground velocity, incremental velocity, and ii) elastic and inelastic spectra of input energy, hysteretic energy, displacement and seismic strength. The results indicate that long duration pulses strongly affects the inelastic response, with very high energy and drift demands which may be several times larger than the limit values specified by the majority of codes.

Structural implications of long duration pulses

As a general rule, the current linear elastic response spectra do not provide sufficient information to account for the energy transmission mechanisms attributable to the presence of long duration pulses in near-field ground motions. In this context, even the opportunity of adopting inelastic response spectra derived from the elastic response spectra is questionable, since the excitations that induce the maximum response in elastic and inelastic systems are different in kind. It is therefore necessary that such information should be complemented with data on the duration of strong ground motion and the number, sequence and characteristics of intense, relatively long acceleration pulses associated with large velocity increments.

A comparison of the different effects produced by impulsive and harmonic excitations has been illustrated in [22, 23] by a series of analyses on SDOF elastic and inelastic systems subject to simple idealized ground motion. Again in the present research the study of the mechanical behavior of SDOF elastic and inelastic systems has been carried out in order to highlight the importance of considering, in the assessment of the effective damage potential of earthquakes, the mutual relations between different types of ground motion and the structural performance . The effects of both high frequency and long period pulses have been investigated by computing strength, energy and displacement demand quantities, underlining the significance of energy-based parameters in the characterization of the seismic demand of structural systems subject to such pulses.

Two simple idealized ground motions have been considered, both made up of sinusoidal motions of different frequency and duration, with null initial acceleration, velocity and displacement, and consisting in a single pulse of duration equal to 1.0 s, followed by a harmonic motion with duration equal to 2.0 s and period equal to 0.2 s. The first, denoted as Type 1, is characterized by the fact that both the single pulse and the harmonic motion have values of the relative acceleration maxima equal to $0.35g$, while in the second, denoted as Type 2, the relative acceleration maximum of the single pulse is two thirds of that of the harmonic motion.

The response of SDOF systems in terms of displacement (δ) time histories, has been analyzed with reference to a linear elastic and an elasto-plastic model. The results presented herein refer to oscillators with damping coefficient, ξ, equal to 5 percent, yield strength, C_y, equal to $0.15g$ and $0.2g$. The natural period, T, is equal to 0.2 s, i.e., coincides with the period of the harmonic excitation, and to 0.4 s, i.e., greater than that of the harmonic excitation but still far from the duration of the single pulse. From the inspection of the curves reported in Figure 1, the effects of long duration pulses on the response of oscillators beyond the elastic threshold are clearly visible and it appears that, for a given system, the definition of a critical ground motion strongly depends on the constitutive law adopted for that system.

As expected, for linear-elastic systems, the critical dynamic excitation is that of periodic type with frequency equal to that of the system (i.e., the harmonic part of both types 1 and 2 idealized motions, with period equal to 2.0 s), since it induces a resonance phenomenon in the oscillators with natural period T equal to 2.0 s (Figures 1a and 1b, top). On the contrary, long duration pulses may become critical for inelastic system, especially in the case of oscillators with yielding resistance, R_y, equal or less than the inertial force corresponding to the effective ground acceleration of the pulse, i.e., $R_y \le m\ddot{u}_g$, where m is the mass of the system, or $C_y \le \ddot{u}/g$. Moreover, the displacement demand increases as the natural period of the oscillators approaches the duration of the single pulse (Figures 1a and 1b, bottom). In the case of elasto-plastic systems, the presence of periodic, high frequency acceleration pulses in the ground motion only contributes to building the response of the system up to its yielding threshold. Once the system begins to yield, the phenomenon of response amplification due to resonance is mitigated, since the energy dissipated through even small inelastic deformations is associated to large values of ξ [22]. Therefore, large inelastic deformations do not occur during yielding reversal induced by periodic short pulses. Actually, the number and amplitude of these reversals are not sufficient to give rise to low cycle fatigue phenomena, since the amount of inelastic strain, developed in each excursion during an earthquake, is usually so small that the number of cycles necessary to cause collapse would exceed the number which can possibly occur even in the longest strong motions. The high displacement demands, imposed by the long duration pulse, suggest that the effective acceleration values of long duration pulses, generally coincident with the peak ground acceleration, *PGA*, are greater than those relevant to high frequency excitations, even when the former are characterized by lower values of *PGA* than the latter.

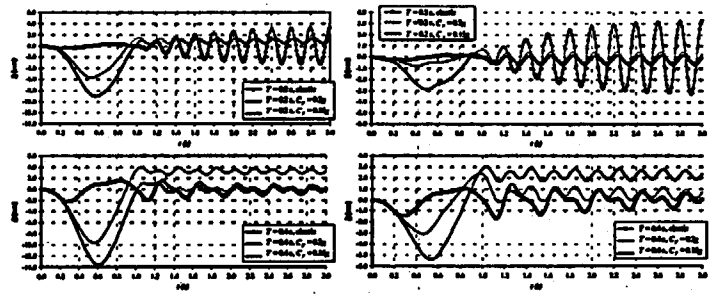

a) Type 1 b) Type 2

Fig. 1 Displacement demand for SDOF systems subject to idealized ground motions

The results presented above confirm that, while the maximum linear-elastic response of a structural system is usually controlled by the resonance phenomenon, considerably larger deformations can be induced by the presence of just one, long pulse with an effective acceleration even slightly greater than that corresponding to the yielding strength of the structure. It is also evident from Figure 1 that, the larger the intensity of the effective acceleration of a pulse with respect to the yielding strength of the system, the larger the amount of inelastic deformations that will develop; furthermore, while high frequency motions are critical essentially for elastic systems with fundamental period close to the resonance period, long duration pulses appear to be critical for structures with fundamental periods laying within a significantly wider interval. Actually, according to [22], the presence of repeated severe long acceleration pulses can produce a sufficient amount of cumulative damage to give raise to one or a combination of two types of failure, respectively known as low cycle fatigue and incremental collapse or crawling. In [22] it is emphasized the advise to design structures against that type of incremental collapse, between the two listed above, which appears to constitute the critical failure. Similar conclusions may be drawn from Figure 2, that shows, for SDOF systems with $\xi = 5\%$, $T = 0.4$ s, and C_y equal to $0.15g$ and $0.2g$, the demand in terms of input energy, E_i, and hysteretic energy, E_h, according to the definition given in [24].

The totality of the energy demand is concentrated in the time interval corresponding to the long duration pulse. This time interval is not long enough for the structure to efficiently utilize the structural damping; consequently, most of the energy is dissipated through hysteresis, which implies the development of structural damage.

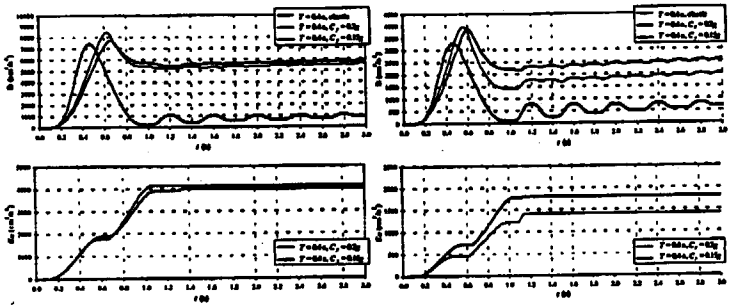

a) Type 1 b) Type 2

Fig. 2 Energy demand for SDOF systems subject to idealized ground motions

Analysis of the response to near-fault records

Near-fault records obtained during the 1979 Imperial Valley Earthquake contain severe velocity and displacement pulses. In Figure 3a the location of the recording stations considered in the present study with respect to the causative fault is shown. Since the strike-slip fault rupture progressed toward the El Centro Array, #7 Imperial Valley College Station (IVC) and #6 Houston Road Station (HOU) can be considered in forward directivity conditions, while Agrarias Station (AGR) results in backward directivity conditions. Due to the proximity to the epicenter, Bonds Corner Station (BCR) can be regarded as in neutral position. Records from Calexico Station (CXO), which are not affected by directivity effects, were also considered for mere comparison purposes.

The velocity, v_g, time histories shown in Figures 3b, c, d, e for the fault-normal (FN) components of the four stations affected by directivity indicate the presence of long duration pulses, particularly in forward directivity conditions. In fact, at the beginning of the velocity time histories of Imperial Valley College Station and Houston Road Station, pulses of duration, T_p, equal to approximately 3.7 s are detected. The elastic spectra of input energy, E_I, and seismic coefficient, C_I, are illustrated in Figure 4. The spectral E_I ordinates are maximum for periods T close to the value of T_p. Since the energy demand attains largest values in the in the long-period region, i.e., for $1.0 \le T \le 4.0$ s approximately, on reckoning that the seismic coefficient spectral ordinates keep equal to approximately $0.5g$ in the same period region, it can be affirmed that critical conditions may develop for a wide class of structures, actually designed to ensure lower values of the seismic coefficient. In fact, a general feature making near-fault signals in forward directivity conditions particularly critical for structures is that the periods range where the energy demand is maximum is wider than that encountered for other type of signals, such as those recorded at Calexico, Bonds Corner and Agrarias stations; moreover, the strength demand keeps considerably high in the same period range.

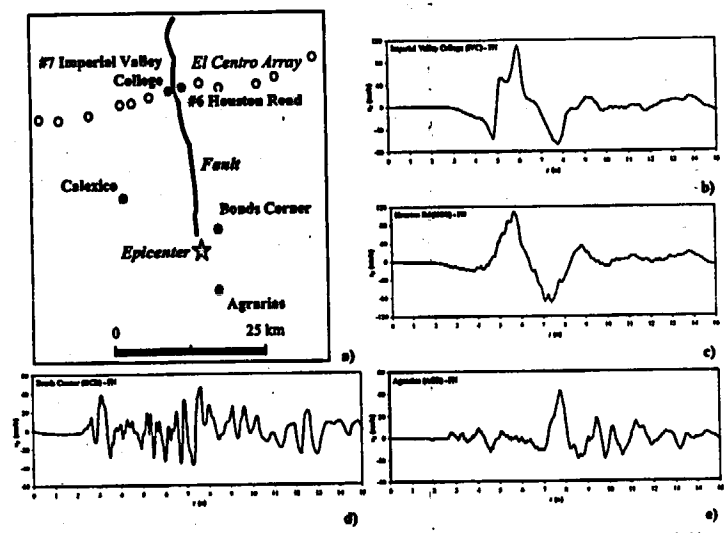

Fig. 3 1979 Imperial Valley Earthquake: recording stations (a); ground velocity time histories recorded in directivity conditions (b, c, d, e)

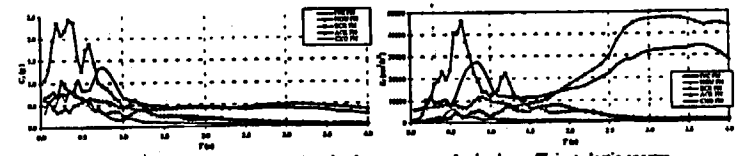

Fig. 4 1979 Imperial Valley Earthquake: input energy and seismic coefficient elastic spectra

In Table 1 the values of peak ground acceleration, *PGA*, peak ground velocity, *PGV*, incremental velocity, *IV*, seismic hazard energy factor, AE_h, and peak energy spectral ordinate, $E_{I,max}$, relevant to the fault-normal, FN, and fault-parallel, FP, components of the ground motions considered are reported. The quantity AE_h, introduced in [25], is defined as the area enclosed by the elastic input energy spectrum in the interval of periods between 0.05 s and 4.0 s. As anticipated, in the records IVC and HOU, velocity and energy parameters appear to be more indicative quantities of the effects of forward directivity on the FN components than the *PGA*. In fact, while the ratios of the values relevant to the FN component to those relevant to the FP component are about 2-3 for the former, they are close to the unity for the latter. This

result can also be observed in the inelastic case, for values of the ductility ratio, μ, equal to 2 and 4. Such circumstances do not occur for the remaining signals considered, recorded in backward directivity conditions or outside the near-field. We like to stress the significant differences in terms of energy and velocity demands between the NF components of HOU and IVC, and the other records.

TABLE 1
1979 IMPERIAL VALLEY EARTHQUAKE: STRONG GROUND MOTIONS PARAMETERS

	#6 HOUSTON Rd			#7 IVC			BONDS CORNER			AGRARIAS			CALEXICO		
	NF	PF	NF/PF	NF	PF	NF/PF	NF	PF	NF/PF	NF	PF	NF/PF	NF	PF	NF/PF
PGA (cm/s²)	431	403	1.1	454	331	1.4	760	577	1.3	216	363	0.6	270	197	1.4
PGV (cm/s)	110	65	1.7	109	48	2.3	46	45	1.0	42	35	1.2	18	16	1.1
IV (cm/s)	199	62	3.2	177	65	2.7	84	77	1.1	53	44	1.2	29	23	1.3
$AE_{L,elastic}$ (cm²/s)	100935	44250	2.3	83952	25882	3.2	33406	24216	1.4	13305	7888	1.7	4667	4875	1.0
$AE_{L,\mu=2}$ (cm²/s)	83902	36316	2.3	63589	20630	3.1	30285	21592	1.4	11221	8538	1.3	4469	4528	1.0
$AE_{L,\mu=4}$ (cm²/s)	66882	27646	2.4	54444	16239	3.4	25876	18349	1.4	8912	6748	1.3	3873	4199	0.9
$E_{L,max,elastic}$ (cm²/s²)	50557	23477	2.2	36342	13589	2.7	45462	29706	1.5	10115	6030	1.7	6151	3326	1.8
$E_{L,max,\mu=2}$ (cm²/s²)	36007	16449	2.2	21383	10893	2.0	36596	24618	1.5	7236	4955	1.5	5489	2834	1.9
$E_{L,max,\mu=4}$ (cm²/s²)	31710	12029	2.6	17300	7907	2.2	26436	20162	1.3	6300	3789	1.7	4260	2274	1.9

Near-fault records obtained during the 1992 Landers, California Earthquake offer another clear example of forward and backward directivity effects. This event, one of the largest in California since 1952 with magnitude $M_w = 7.3$, was caused by a right-lateral strike-slip fault with a slip length of about 70 km. The near-fault stations activated during the earthquake were located in different position with respect to the fault rupture directivity. In particular, the Lucerne Valley Station (LV) was within a distance of 2 km from the fault trace, near the end of the fault segment that ruptured, in a forward directivity position, while the Joshua Tree Station (JT) was located also in the near-field but at a distance of about 8 km from the surface projection of the rupture, in a backward directivity position. Even though both stations were close to the fault, the damage potential exhibited by the corresponding records is very different. The fault normal component of Lucerne Valley record presents a severe long duration pulse in the velocity trace of about 4.5÷4.8 s (Figure 5), which is not easily visible in the acceleration trace. This pulse, characterized by an incremental velocity equal to 200 cm/s, contains most of the seismic energy radiating in the direction of the rupture. As shown in Figure 6c, the maximum of the input energy spectrum occurs at a period of approximately 4.5 s, close to the pulse duration.

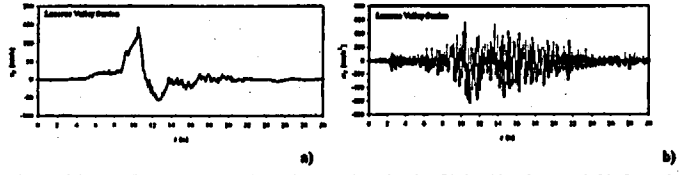

Fig. 5 1992 Landers Earthquake: ground velocity (a) and acceleration (b) time histories recorded in forward directivity conditions (fault normal components)

In Table 2 the strong ground motion parameters relevant to the FN and FP components of the records considered are reported. Also in this case, the effects of the presence of long-duration pulses in the NF component obtained at Lucerne Valley Station are essentially revealed by velocity and energy parameters. In fact, the ratio of the values relevant to the FN component to those relevant to the FP component is much greater than unity for these parameters, while the PGA values are comparable in the FN and FP components of both Lucerne Valley and Joshua Tree. It is interesting to remark that the ratio of the values relevant to the FN components of the two records examined is close to the unity only in the case of the maximum input energy, $E_{L,max}$ (Table 2, last column).

However, as shown in Figures 6c, d, while the input energy relevant to JT reaches an isolated peak value, rapidly decreasing outside a very narrow band of periods, the values spectral ordinate relevant to LV remain considerably high within a large band of periods. Therefore, it can be concluded that the effects of forward directivity conditions are, in this case, more effectively accounted for by the high values of the parameter $AE_{L,max}$. Finally in the periods range corresponding to the maximum demand in energy terms for Lucerne Valley, i.e., 3 ÷ 5 s, the values of the seismic coefficient spectral ordinates remain close to 0.4g, and considerably greater than those observed for Joshua Tree within the same range of periods (Figures 6a, b).

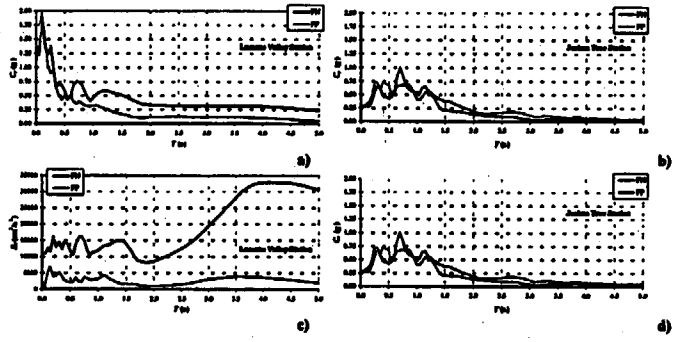

Fig. 6 1992 Landers Earthquake: elastic seismic coefficient (a, b) and input energy (c, d) spectra

TABLE 2
1992 LANDERS EARTHQUAKE: STRONG GROUND MOTIONS PARAMETERS

	LUCERNE VALLEY (LV)			JOSHUA TREE (JT)			NF_{LV}/NF_{JT}
	NF	PF	NF/PF	NF	PF	NF/PF	
PGA (cm/s²)	713	774	0.9	278	268	1.0	2.6
PGV (cm/s)	146	33	4.4	42.7	27.1	1.6	3.4
IV (cm/s)	200	31	6.5	62	44	1.4	3.2
$AE_{L,elastic}$ (cm²/s)	64963	10736	6.1	36809	19579	1.9	1.8
$AE_{L,\mu=2}$ (cm²/s)	63542	9225	6.9	32861	18344	1.8	1.9
$AE_{L,\mu=4}$ (cm²/s)	64802	7424	8.7	28922	16236	1.8	2.2
$E_{L,max,elastic}$ (cm²/s²)	32934	7175	4.6	31826	19631	1.6	1.0
$E_{L,max,\mu=2}$ (cm²/s²)	28990	7367	3.9	26393	16333	1.6	1.1
$E_{L,max,\mu=4}$ (cm²/s²)	26803	6622	4.0	18935	14634	1.3	1.4

Conditions required for forward directivity are also met in dip slip faulting, including both reverse and normal faults. During the 1994 Northridge earthquake, which occurred on a blind thrust fault, several stations recorded motions affected by rupture directivity effects. The record obtained at Rinaldi Receiving Station (RRS) exhibits significant damage potential due to the presence of a pulse occurring after about 2 s

in the velocity FN component, with incremental velocity equal to 255 cm/s and duration of 1.2 s. The peak input energy is attained at a period value approximately equal to the pulse duration value (Figure 7b). As in the cases examined previously, the energy values keep considerably high over a large interval of periods; correspondingly, high values of the seismic coefficient are observed (Figure 7a). In Figure 8 the time histories of the energy dissipated by hysteresis, E_H, and the displacement, δ, are reported for elasto-plastic SDOF systems of different natural periods (0.5 s, 0.7 s and 1.3 s), characterized by a seismic coefficient $C_y = 0.35g$ and 5% of the critical damping. Due to the high strength demand, all oscillators yield; furthermore, both hysteretic energy and displacement demands do not differ significantly from one oscillator to another, turning out to be critical for a broad class of structures.

a) b)

Fig. 7 1994 Northridge Earthquake: elastic seismic coefficient (a) and input energy (b) spectra (RRS, FN)

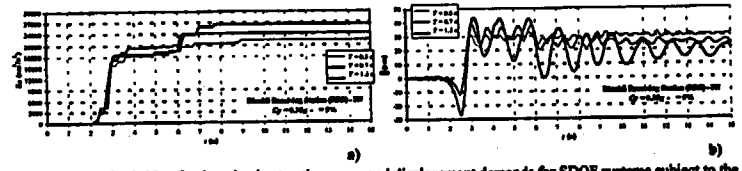

a) b)

Fig. 8 1994 Northridge Earthquake; hysteretic energy and displacement demands for SDOF systems subject to the Rinaldi Receiving Station FN component

Conclusion

The present research is focused on the characterization of the damage potential of long period pulses recorded, during recent earthquakes, by near-fault instruments . It is particularly important to develop and improve their representation using synthetic parameters, which take into account simultaneously the amplitude, duration and number of cycles of the near-fault pulse, in addition to the conventional response spectra. In this context, velocity, displacement and energy parameters appear to be appropriate indicators of the effects of the presence of near-fault pulses, particularly in forward directivity conditions. Long period pulses, due to near-fault rupture directivity are produced by the superposition of waves radiated from asperities of the fault. The degree of the superposition depends on the station location with respect to the fault, and it is affected by disturbances in the propagation media. The limited number of records from the near-fault region do not allow to characterize the influence of the seismotectonic environment completely, therefore reliance should be placed on realistic seismological simulations in order to quantify the pulse effects adequately.

References

1. Aki, K. 1968. Seismic displacements near a fault. *J. Geophys. Res.* 73(16): 5359-5376.
2. Archuleta, R.J. & Hartzell, S.H. 1981. Effects of fault finiteness on near-source ground motion. *Bulletin of the Seismological Society of America*, 71: 939-957.
3. Bolt, B.A. 1983. *The contribution of directivity focusing to earthquake intensities*. Report 20, U.S. Army Corps of Engineers, Waterways Experiment Station, Vicksburg.
4. Panza, G. F. & Suhadolc, P. 1987. Complete strong motion synthetics. In B. Bolt (ed), *Seismic Strong Motion Synthetics*: 153-204, Academic Press, New York.
5. Bolt, B.A. 1996. *From earthquake acceleration to seismic displacement*. The Fifth Mallet-Milne Lecture, SECED, John Wiley & Sons.
6. Decanini, L.D. & Prato C.A. 1980. *Proyecto de Reglamento CIRSOC 103: Accion de los sismos sobre las construcciones*. Centro de Investigacion de los Reglamentos Nacionales de Seguridad para las Obras Civiles, Argentina.
7. UBC 1997. *Uniform Building Code*. International Conference of Building Officials, Whittier, Ca.
8. Housner, G.W. & Hudson, D.E. 1958. The Port Hueneme Earthquake of March 18, 1957. *Bulletin of the Seismological Society of America*, 48(2): 163-168.
9. Bertero, V. V. , Herrera, R. A. & Mahin, S. A. 1978. Aseismic design implications of near-fault San Fernando Earthquake records. *Earthquake Engng Struct. Dyn.*, 6: 31-42.
10. Anderson, J.C. & Bertero, V.V. 1987. Uncertainties in establishing design earthquakes. *ASCE Journal of Structural Engineering*, 113(8): 1709-1724.
11. Nasim, F. 1995. On seismic design implications of the 1994 Northridge earthquake records. *Earthquake Spectra*, 11(1): 91-109.
12. Decanini, L.D. & Mollaioli, F. 1998. Parameters to be considered in the establishment of the design earthquake based on energy concepts. In *Proc. of the Structural Engineers World Congress*, San Francisco, 1998.
13. Hall, J.F., Heston, T.H., Halling, M.W. & Wald, D.J. 1995. Near-source ground motion and its effects on flexible buildings. *Earthquake Spectra*, 11(4): 569-605.
14. Iwan, W.D. 1997. Drift spectrum: measure of demand for earthquake ground motions. *ASCE Journal of Structural Engineering*, 123(4): 397-404.
15. Chopra, A.K. & Chintanapakdee, C. 2001. Comparing response of SDF systems to near-fault and far-fault earthquake motions in the context of spectral regions. *Earthquake Engng Struct. Dyn.*, 30: 1769-1789.
16. Decanini, L., Mollaioli, F. & Mura, A. 2002. Shear-beam model for the prediction of the response of MDOF systems subjected to severe earthquake ground shaking. To appear in *Proc. of the 12th European Conference on Earthquake Engineering, London, September 2002*, paper no. 055.
17. Makris, N. 1997. Rigidity-plasticity-viscosity: can electrorheological dampers protect base-isolated structures from near-source ground motions? *Earthquake Engng Struct. Dyn.*, 26: 571-591.
18. Anderson, J.C., Bertero, V.V. & Bertero, R.D. 1999. *Performance improvement of long period building structures subjected to severe pulse-type ground motions*. PEER Report 1999/09, Pacific Earthquake Engineering Research Center, College of Engineering, University of California, Berkeley, October 1999.
19. Jennings, P.C. 2000. Ground motion pulses and structural response. In *Proc. of the China-U.S. Millenium Symposium on Earthquake Engineering, Beijing, China, November 8-11, 2000.*
20. Mollaioli, F., Decanini, L.D. & Bruno, S. 2002. Damage potential of severe long duration acceleration pulses in near-fault records. To appear in *Proc. of the 12th European Conference on Earthquake Engineering, London September 2002*, paper no. 155.
21. Decanini, L.D., Mollaioli, F. & Saragoni, R. 2000 Energy and displacement demands imposed by near-source ground motions. In: *Proceedings of the 12th World Conference on Earthquake Engineering Auckland, New Zealand*, Paper no. 1136, New Zealand Society for Earthquake Engineering, Silverstream, Upper Hutt.
22. Bertero, V.V., Herrera, R.A. & Mahin, S.A. 1976. Establishment of Design Earthquake - Evaluation of Present Methods. In *Proc. of the International Symposium on Earthquake Structural Engineering. St.Louis, Missouri, Usa, August 1976*: 551-580.
23. Mollaioli, F. & Decanini, L. 1997. Influenza delle pulsazioni accelerometriche di lunga durata sui danneggiamenti osservati in recenti terremoti. In *Proc. of the VIII Convegno Nazionale ANIDIS "L'Ingegneria sismica in Italia", Taormina, 21-24 september 1997.*
24. Uang, C.M., & Bertero, V.V. 1990. Evaluation of seismic energy in structures. *Earthquake Engng Struct. Dyn.*, 19: 77-90.
25. Decanini, L. D. & Mollaioli, F. 1998. Formulation of Elastic Earthquake Input Energy Spectra, *Earthquake Engng Struct. Dyn.*, 27: 1503-1522.

ESTIMATION OF THE NEAR-SOURCE STRONG GROUND MOTION DURING THE KOCAELI, TURKEY EARTHQUAKES OF AUGUST 17, 1999 AT DAMAGED AREAS WITH REGARDS FOR SITE EFFECTS

Kazuyoshi Kudo and Tatsuo Kanno
Earthquake Research Institute, University of Tokyo, Japan (K. K.)
National Research Institute for Earth Science and Disaster Prevention, Japan (T. K.)

Abstract

The estimation of strong ground motions at downtown Adapazari and Golcuk, where heavy damage was observed, is inevitable to understand the relation between ground motion severity and damage to buildings. For this purpose, we adopted an empirical Green's function method for ground motion synthesis using observed aftershock recordings. First, we estimated the bedrock motion and then convolved the effects of surface sediments taking into account of nonlinear behaviors of soil by an equivalent linear method. We selected five large asperities from the heterogeneous source model determined by Sekiguchi and Iwata (2002) for synthesizing the ground motion from the mainshock. The validity of this simulation was confirmed by the comparison of the strong motion records and the synthetics at several stations near the fault.

Introduction

Major damage to buildings and loss of life during the Kocaeli (Izmit), Turkey earthquake, were concentrated near the surface earthquake fault, therefore, the primary reasons for the damage are attributed to near earthquake source effects, leaving aside the quality of buildings. The strong motion records from the Kocaeli earthquake near the fault were successfully recovered by the Earthquake Research Department (ERD, 1999), and the Kandilli Observatory (KOERI, 1999). However, because of a sparse network in Turkey (Celebi et al., 2000), no strong motion record was obtained at severely damaged areas, except Duzce (DZC). The strong contrast of damage ratios between the strong motion observation site, Sakarya (SKR) and downtown Adapazari, and the wide variation of the damage ratios even in the relatively small area of Golcuk (Architectural Institute of Japan Reconnaissance Team et al., 2000) are also similar issues. It is our concerns to estimate the severity of the ground motions at damaged areas.

The shallow and intermediate-depth S-wave velocity structures in Adapazari and Golcuk areas were determined by the array observation of microtremors (Kudo et al., 2002). In addition, we also conducted temporal array observations of aftershocks to understand the relative differences of site effects on strong motion or damage in and around Golcuk, near the surface fault. It is our concerns to estimate the strong ground motions at the severely damaged areas, especially at downtown Adapazari and Golcuk. In case of Adapazari, the ground motion at SKR is able to use as an input motion to sediment sites, or bedrock motion, for roughly estimating the ground motions in downtown Adapazari (e.g. Kudo et al, 2002; Bakir, et al., 2002), since the S-wave velocity near the surface at SKR is approximately 1,000 m/sec or higher and the distance between SKR and downtown sites is not large. However, there still exist uncertainties, which are the NS motion, near source radiation effects, nonlinear effects of surface soils, and so on. The case of Golcuk is much difficult task, because we have no record near by the sites and the damaged areas in Golcuk, where surface soils are very soft, was very close to the surface earthquake fault.

Nevertheless very limited data and these difficulties, this paper is an attempt to estimate strong ground motions at damaged areas using the empirical Green's function method with regards for source complexities (asperities) and nonlinear amplification of seismic waves in sedimentary basins.

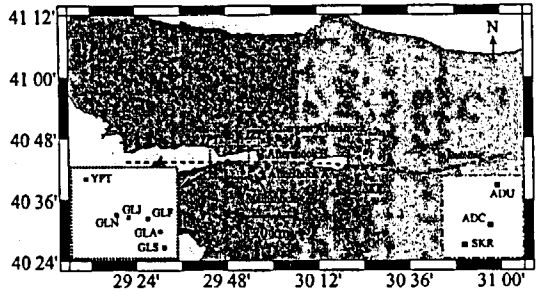

Figure 1. Studied area that showing locations of epicenters of the mainshock, the aftershocks, and observation sites.

Site characteristics of studied area

Studied areas that we made temporal aftershock observations and array observations of microtremors are shown in Figure 1, with permanent strong motion observation sites SKR, YPT, and IZT and the surface earthquake fault (e.g. Barka et al., 2002). A temporary aftershock observation, which was very short period (three days), was conducted at GLS, GLA, GLF, GLJ, and GLN in the Izmit bay area including YPT (Figure.1). The array observations of microtremors were carried out at SKR, ADC, ADU, YPT, GLF, and GLN and the S-wave velocity structures of sedimentary layers are estimated. The estimated S-wave velocity structures are shown in Table 1, which are mostly reproduced from Table 3 in Kudo et al. (2002) with slight modifications. Underground structures at GLA and GLJ, where only aftershock observations were carried out, were estimated using the following procedures. At first, we computed spectral ratios of the aftershock motions at GLA and GLJ to those at GLF. Next we estimated the S-wave velocity structures so as that the 1D theoretical spectral ratios match with the observed spectral ratios using the genetic algorithm (GA) (e.g., Yamanaka and Ishida, 1996). Figure 2 shows the comparison of the theoretical spectral ratios with the observed ones. We assume further that common seismic basements (bedrock) among sites in Golcuk and Adapazari are the layers of which S-wave velocities are 950 m/sec and 1,500 m/sec, respectively. It is also assumed that the seismic basement of similar S-wave velocity outcrops at GLS and IZT.

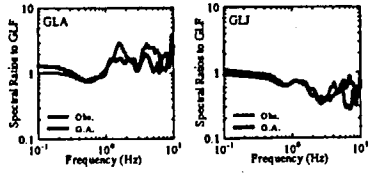

Figure 2. Comparison of the spectral ratios to GLF estimated by the genetic algorithm with observed ones.

The studied areas are very close to the surface earthquake fault, especially the observation sites GLN, GLJ, and GLF are located within a distance of a few hundreds meters from the fault. While the distance of ADC and ADU in Adapazari area from the fault are 6 km and 10 km, respectively.

Table 1. The S-wave velocity structure model estimated by the array observations of microtremors (Kudo et al., 2002) and the inversion analysis of spectral ratios of the aftershock records using the GA.

SKR		ADC		ADU		YPT	
Vs (m/s)	Thickness (m)	Vs (m/s)	Thickness (m)	Vs (m/s)	Thickness (m)	Vs (m/s)	Thickness (m)
1050	72	234	38	166	44	344	42
1500	—	441	97	351	88	445	94
		728	242	500	281	591	90
		1500	—	878	63	727	290
				1050	100	950	—
				1500	—		

GLN		GLF		GLA		GLJ	
Vs (m/s)	Thickness (m)	Vs (m/s)	Thickness (m)	Vs (m/s)	Thickness (m)	Vs (m/s)	Thickness (m)
283	19	150	14	52	4	90	1
512	52	259	70	108	10	281	47
694	97	531	270	269	245	400	101
752	61	950	—	530	33	600	253
950	—			950	—	950	—

—: infinity

Estimation of strong ground motion during the mainshock at downtown Adapazari

1) Preliminary estimation (Linear soil response)

In a previous paper (Kudo, et al., 2002), we estimated the ground motions at ADC and ADU during the mainshock. The EW component of the ground motion at SKR deconvolved by the response of the surface layer, although the surface effects are only for very high frequency, is used for the input motion at ADC and ADU. The synthetic motions at ADC and ADU are estimated by convolving the response of sedimentary layers determined by microtremors. The velocity models used in the computation are shown in Table 1, and constant Q factors are assumed associated with the S-wave velocity, ranging from 15 to 80 in the sedimentary layers. The synthetic ground accelerations and the velocities at ADC and ADU were estimated, assuming 1D propagation of S-wave without any corrections to distance and non-linearity (Figure 8). The synthetic motions are only valuable as an upper band of estimations at the sites. The distances at SKR, ADC, and ADU from the nearest surface fault-line were 3.4, 6.4, and 9.6 km, respectively. The peak acceleration (582 cm/sec^2) and the velocity (108 cm/sec) at ADC are reduced to 488 cm/sec^2 and 74 cm/sec, respectively, using the relative distance relation with the help of the empirical formula (Joyner and Boore, 1982). In the case of ADU, they become to 368 cm/sec^2 and 61 cm/sec, respectively.

Next our concerns are to estimate the effects of nonlinear behaviors of surface soils, NS motion at those sites, and geometrical effects of source radiation for these sites.

2) Estimation by the equivalent linear method for soil response.

We estimated the strong ground motions during the mainshock in the Adapazari sites similarly to the previous case, but taking into nonlinearity of soils. First, we estimated the incident wave at ADC and ADU by deconvolving the responses of the surface layers estimated by microtremors at SKR from the mainshock record based on the equivalent linear method (Schnabel et al, 1975), while the computer code developed by Yoshida and Suetomi (1995) was used. Next, the estimated input motion is convolved with the response due to the velocity structure models at ADC and ADU, assuming a common seismic bedrock of which S-wave velocity is 1,500 m/sec. Distances form the surface earthquake fault to SKR, ADC, and ADU are 3.4 km, 6.4 km, and 9.6 km, respectively, therefore, a distance correction would be necessary, when we use the ground motion at SKR for input motions to ADC and ADU. As mentioned before, we assumed that the contribution of source to strong ground motion were only five large asperities as shown in Figure 6 (discuss later). We evaluated the distances of those sites using the method of equivalent hypocentral distance (Ohno et al., 1990) by only taking into account the number 3 asperity (see Figure 6), which was closest to the Adapazari area.

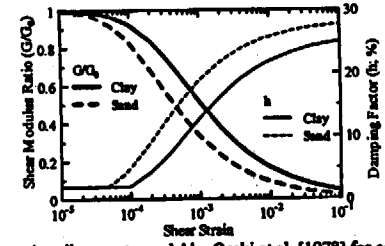

Figure 3. A dynamic soil property model by Osaki et al. [1978] for equivalent linear method.

As we have not enough data on soil properties at those sites, we used the representative dynamic model of soil property proposed by Osaki et al. (1978) for equivalent linear analyses, as shown in Figure 5. While, we used the effective strain proposed by Sugito et al. (1995), , for taking into account damping factors, in which the strain of each layer depends on frequency as equation 1. .

$$\gamma_{ef}(\omega) = \alpha\, \gamma_{max}\, F(\omega) / F_{max}, \qquad (1)$$

where ω is angular frequency, $\gamma_{ef}(\omega)$ and $F(\omega)$ effective strain and Fourier spectra of ground motion strain at ω, respectively. γ_{max} and F_{max} are the maximum strain and the maximum value of their spectra, respectively. α is the coefficient (0.65) for the equivalent linear method. In addition, we assumed that the soft layers of which S-wave velocity is lower than 400 m/sec were taken as sand, because of less information of soil properties. Analysis was made for only EW component because of lack of record of NS motion at SKR during the mainshock and the frequency ranges between 0.1 Hz to 10Hz was used following processing.

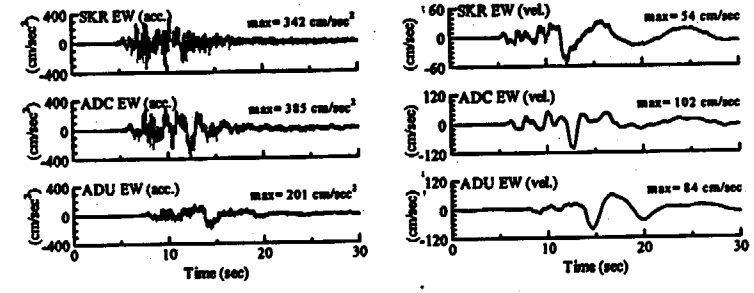

Figure 4 Estimated strong ground motion during the mainshock in downtown Adpazari by and the equivalent linear method using the observed earthquake records at SKR that were corrected for distances and responses of surface layers .

Figure 4 shows thus estimated ground motions in terms of acceleration and velocity. The equivalent hypocentral distances of SKR, ADC, and ADU are 10.1 km, 11.4 km, and 14.1 km, then correction factors become 0.89 and 0.72 at ADC and ADU, respectively. The estimated peak acceleration at ADC is not so high relative to SKR (factor of 1.1), may due to large damping at high frequency range, while the peak velocity is a factor of approximately 2 that would be significant to damage of building. This is the case that we assumed the surface layers of both sites to be sand. However, we have not enough information on soil properties of the individual sites. We also computed the ground motion in case of clay at ADC and compared the case of sand. The difference of acceleration is considerable, but the ground velocity is almost identical, as shown in Figure 5. Hereafter we will discuss mostly in terms of ground velocity, therefore, we assumed the surface layers for all the sites to be sand and the ground velocities have no significant difference of soil property.

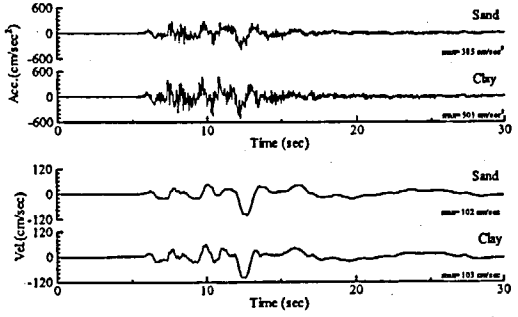

Figure 5 Comparisons of ground accelerations and velocities for the cases of surface layers to be sand and clay.

Source model and synthetic motions by the empirical Green's function method

Near source effects on ground motion are not only distance but also source geometry and fault rupture processes. In order to consider the effects, we employed the empirical Green's function (EGF) method developed by Irikura (1986), Irikura et al (1997), and Kamae et al. (1990). The method postulate the omega square model (Aki, 1967; Brune, 1970), synthetics are constructed as followings;

$$
\begin{aligned}
&U(t) = \sum_{i=1}^{N^3} (r/r_i) \cdot F(t) * (C \cdot u(t)) \\
&F(t) = \delta(t - t_i) + \{1/n'(1 - \exp(-1))\} \\
&\sum_{k=1}^{(N-1)n'} [\exp\{-(k-1)/(N-1)n'\}\delta\{t - t_i - (k-1)T/(N-1)n'\}] \\
&t_i = (r_i - r_0)/V_r + \xi_i/V_r + \varepsilon_i
\end{aligned}
\qquad (2)
$$

where, $U(t)$ is the synthetic motion, $u(t)$ is the small event, N is ratio of fault length between the large and the small events, and r and r_i are hypocentral distance of the small earthquake that is used as a Green's function, and from the i-th element to the site, respectively. C is the ratio of stress parameter between the large and the small event, $F(t)$ is function for correcting source time function, and * means convolution. T is rise time of the target event, n' is an appropriate integer number to shift the fictitious periodicity $T/(N-1)$ into a high frequency beyond the interest (here $n' = 100$ is used), Vs is the S-wave velocity and Vr is the rapture velocity of the fault. ε_i is random number to prevent artificial periodicity generated by the relation between a interval of subfaults and rapture velocity. In this study, we used the empirical relation of T proposed by Gellar (1976); $T=16S\,0.5 / 7\pi 1.5\ Vs$, where S is the fault area of the target event.

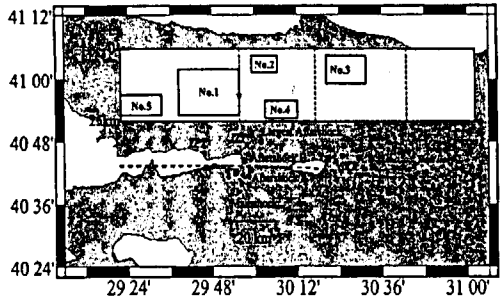

Figure 6. Complex fault model, which have five asperities referring to Sekiguchi and Iwata (2002) and Kamae and Irikura (2000). Locations of earthquakes and observation sites are also plotted.

1) Empirical Green' function

We used the records from the largest aftershock (M5.8) of September 13, 1999, at SKR, IZT, and YPT as EGF. At first, we deconvolved the responses of the surface layers from strong motion records based on the above-mentioned equivalent linear method. The effects of nonlinear behavior of soils at SKR and IZT are negligibly small but we processed to keep uniformity of the analyses. We used the deconvolved baserock motions from the largest aftershock, thus obtained, as Green's functions for those sites. The synthetic motion was first constructed as a bedrock motion at each site and then it was convolved the response of surface layers by the equivalent linear method as mentioned above.

2) Asperity model

Investigations on the complex fault process for the Kocaeli earthquake have been conducted using strong motion records by Sekiguchi and Iwata (2002) and Bouchon (2002), as well jointly with the other data by Yagi and Kikuchi (2000), Li et al. (2002), and Delouis (2002). We only intend to estimate strong ground motion of relatively high frequency, say from 0.3 to 10 Hz, therefore, the constraint by static or long-period motion are not necessary required. We selected five asperities, as shown in Figure 6, referring mostly to the source inversion results by Sekiguchi and Iwata (2002). We, in addition, assumed that the strong motion was generated by only these asperities. In order to confirm the validity of our procedures, we obtained the synthetic motions for the mainshock at SKR, IZT, and YPT. Figure 6 compares the synthetic strong motion with the observations with velocity waveforms and Fourier spectra. Minor modifications, like forward modeling, from the model by Sekiguchi and Iwata (2002) were made, so as to obtain good match between synthetics and observations. The final characterized asperity model is shown Table 2. The frequency ranges in the analyses were restricted to 0.1-10 Hz for SKR and YPT, and to 0.4-10 Hz for IZT, due to the S/N ratios of the aftershock records. A somewhat disagreement in the synthesized strong motion for IZT at high frequency, however, generally the synthetics are in good agreement with the observations. Therefore, we inferred that these procedures and the fault model represented by five asperities would be valid. The numbers of subfaults

Figure 4 shows thus estimated ground motions in terms of acceleration and velocity. The equivalent hypocentral distances of SKR, ADC, and ADU are 10.1 km, 11.4 km, and 14.1 km, then correction factors become 0.89 and 0.72 at ADC and ADU, respectively. The estimated peak acceleration at ADC is not so high relative to SKR (factor of 1.1), may due to large damping at high frequency range, while the peak velocity is a factor of approximately 2 that would be significant to damage of building. This is the case that we assumed the surface layers of both sites to be sand. However, we have not enough information on soil properties of the individual sites. We also computed the ground motion in case of clay at ADC and compared the case of sand. The difference of acceleration is considerable, but the ground velocity is almost identical, as shown in Figure 5. Hereafter we will discuss mostly in terms of ground velocity, therefore, we assumed the surface layers for all the sites to be sand and the ground velocities have no significant difference of soil property.

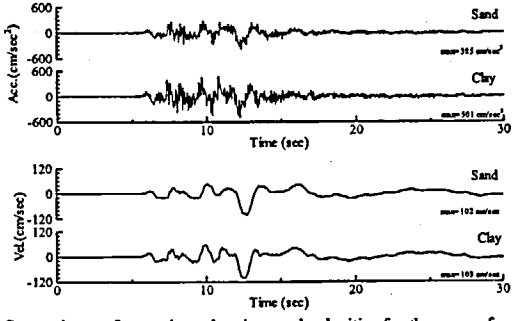

Figure 5 Comparisons of ground accelerations and velocities for the cases of surface layers to be sand and clay.

Source model and synthetic motions by the empirical Green's function method

Near source effects on ground motion are not only distance but also source geometry and fault rupture processes. In order to consider the effects, we employed the empirical Green's function (EGF) method developed by Irikura (1986), Irikura et al (1997), and Kamae et al. (1990). The method postulate the omega square model (Aki, 1967; Brune, 1970), synthetics are constructed as followings;

$$U(t) = \sum_{i=1}^{N^2} (r/r_i) \cdot F(t) * (C \cdot u(t))$$

$$F(t) = \delta(t - t_i) + \{1/n'(1 - \exp(-1))\} \qquad (2)$$

$$\sum_{k=1}^{(N-1)n'} [\exp\{-(k-1)/(N-1)n'\}\delta\{t - t_i - (k-1)T/(N-1)n'\}]$$

$$t_i = (r_i - r_0)/V_r + \xi_i/V_s + \varepsilon_i$$

where, $U(t)$ is the synthetic motion, $u(t)$ is the small event, N is ratio of fault length between the large and the small events, and r and r_i are hypocentral distance of the small earthquake that is used as a Green's function, and from the i-th element to the site, respectively. C is the ratio of stress parameter between the large and the small event, $F(t)$ is function for correcting source time function, and * means convolution. T is rise time of the target event, n' is an appropriate integer number to shift the fictitious periodicity $T/(N-1)$ into a high frequency beyond the interest (here $n' = 100$ is used), Vs is the S-wave velocity and Vr is the rapture velocity of the fault. ε_i is random number to prevent artificial periodicity generated by the relation between a interval of subfaults and rapture velocity. In this study, we used the empirical relation of T proposed by Gellar (1976); $T=16S\,0.5 / 7\pi 1.5\ Vs$, where S is the fault area of the target event.

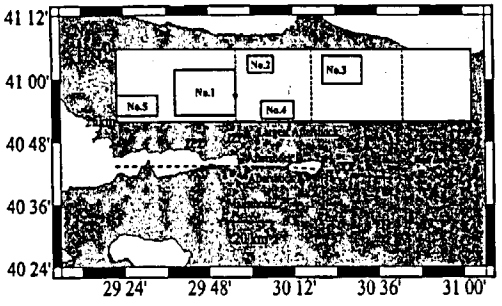

Figure 6. Complex fault model, which have five asperities referring to Sekiguchi and Iwata (2002) and Kamae and Irikura (2000). Locations of earthquakes and observation sites are also plotted.

1) Empirical Green' function

We used the records from the largest aftershock (M5.8) of September 13, 1999, at SKR, IZT, and YPT as EGF. At first, we deconvolved the responses of the surface layers from strong motion records based on the above-mentioned equivalent linear method. The effects of nonlinear behavior of soils at SKR and IZT are negligibly small but we processed to keep uniformity of the analyses. We used the deconvolved baserock motions from the largest aftershock, thus obtained, as Green's functions for those sites. The synthetic motion was first constructed as a bedrock motion at each site and then it was convolved the response of surface layers by the equivalent linear method as mentioned above.

2) Asperity model

Investigations on the complex fault process for the Kocaeli earthquake have been conducted using strong motion records by Sekiguchi and Iwata (2002) and Bouchon (2002), as well jointly with the other data by Yagi and Kikuchi (2000), Li et al. (2002), and Delouis (2002). We only intend to estimate strong ground motion of relatively high frequency, say from 0.3 to 10 Hz, therefore, the constraint by static or long-period motion are not necessary required. We selected five asperities, as shown in Figure 6, referring mostly to the source inversion results by Sekiguchi and Iwata (2002). We, in addition, assumed that the strong motion was generated by only these asperities. In order to confirm the validity of our procedures, we obtained the synthetic motions for the mainshock at SKR, IZT, and YPT. Figure 6 compares the synthetic strong motion with the observations with velocity waveforms and Fourier spectra. Minor modifications, like forward modeling, from the model by Sekiguchi and Iwata (2002) were made, so as to obtain good match between synthetics and observations. The final characterized asperity model is shown Table 2. The frequency ranges in the analyses were restricted to 0.1-10 Hz for SKR and YPT, and to 0.4-10 Hz for IZT, due to the S/N ratios of the aftershock records. A somewhat disagreement in the synthesized strong motion for IZT at high frequency, however, generally the synthetics are in good agreement with the observations. Therefore, we inferred that these procedures and the fault model represented by five asperities would be valid. The numbers of subfaults

The studied areas are very close to the surface earthquake fault, especially the observation sites GLN, GLJ, and GLF are located within a distance of a few hundreds meters from the fault. While the distance of ADC and ADU in Adapazari area from the fault are 6 km and 10 km, respectively.

Table 1. The S-wave velocity structure model estimated by the array observations of microtremors (Kudo et al., 2002) and the inversion analysis of spectral ratios of the aftershock records using the GA.

SKR		ADC		ADU		YPT	
Vs (m/s)	Thickness (m)	Vs (m/s)	Thickness (m)	Vs (m/s)	Thickness (m)	Vs (m/s)	Thickness (m)
1050	72	234	38	166	44	344	42
1500	---	441	97	331	88	445	94
		728	242	500	281	591	90
		1500	---	878	63	727	290
				1050	100	950	---
				1500	---		

GLN		GLF		GLA		GLJ	
Vs (m/s)	Thickness (m)	Vs (m/s)	Thickness (m)	Vs (m/s)	Thickness (m)	Vs (m/s)	Thickness (m)
283	19	150	14	52	4	90	1
512	52	259	70	108	10	281	47
694	97	531	270	269	245	400	101
752	61	950	---	530	33	600	253
950	---			950	---	950	---

---: infinity

Estimation of strong ground motion during the mainshock at downtown Adapazari

1) Preliminary estimation (Linear soil response)

In a previous paper (Kudo, et al., 2002), we estimated the ground motions at ADC and ADU during the mainshock. The EW component of the ground motion at SKR deconvolved by the response of the surface layer, although the surface effects are only for very high frequency, is used for the input motion at ADC and ADU. The synthetic motions at ADC and ADU are estimated by convolving the response of sedimentary layers determined by microtremors. The velocity models used in the computation are shown in Table 1, and constant Q factors are assumed associated with the S-wave velocity, ranging from 15 to 80 in the sedimentary layers. The synthetic ground accelerations and the velocities at ADC and ADU were estimated, assuming 1D propagation of S-wave without any corrections to distance and non-linearity (Figure 8). The synthetic motions are only valuable as an upper band of estimations at the sites. The distances at SKR, ADC, and ADU from the nearest surface fault-line were 3.4, 6.4, and 9.6 km, respectively. The peak acceleration (582 cm/sec^2) and the velocity (108 cm/sec) at ADC are reduced to 488 cm/sec^2 and 74 cm/sec, respectively, using the relative distance relation with the help of the empirical formula (Joyner and Boore, 1982). In the case of ADU, they become to 368 cm/sec^2 and 61 cm/sec, respectively.

Next our concerns are to estimate the effects of nonlinear behaviors of surface soils, NS motion at those sites, and geometrical effects of source radiation for these sites.

2) Estimation by the equivalent linear method for soil response.

We estimated the strong ground motions during the mainshock in the Adapazari sites similarly to the previous case, but taking into nonlinearity of soils. First, we estimated the incident wave at ADC and ADU by deconvolving the responses of the surface layers estimated by microtremors at SKR from the mainshock record based on the equivalent linear method (Schnabel et al, 1975), while the computer code developed by Yoshida and Suetomi (1995) was used. Next, the estimated input motion is convolved with the response due to the velocity structure models at ADC and ADU, assuming a common seismic bedrock of which S-wave velocity is 1,500 m/sec. Distances form the surface earthquake fault to SKR, ADC, and ADU are 3.4 km, 6.4 km, and 9.6 km, respectively, therefore, a distance correction would be necessary, when we use the ground motion at SKR for input motions to ADC and ADU. As mentioned before, we assumed that the contribution of source to strong ground motion were only five large asperities as shown in Figure 6 (discuss later). We evaluated the distances of those sites using the method of equivalent hypocentral distance (Ohno et al., 1990) by only taking into account the number 3 asperity (see Figure 6), which was closest to the Adapazari area.

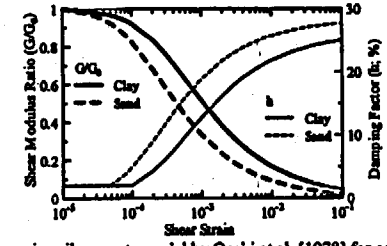

Figure 3. A dynamic soil property model by Osaki et al. [1978] for equivalent linear method.

As we have not enough data on soil properties at those sites, we used the representative dynamic model of soil property proposed by Osaki et al. (1978) for equivalent linear analyses, as shown in Figure 5. While, we used the effective strain proposed by Sugito et al. (1995), , for taking into account damping factors, in which the strain of each layer depends on frequency as equation 1. .

$$\gamma_{ef}(\omega) = \alpha \, \gamma_{max} \, F(\omega) / F_{max} \qquad (1)$$

where ω is angular frequency, $\gamma_{ef}(\omega)$ and $F(\omega)$ effective strain and Fourier spectra of ground motion strain at ω, respectively. γ_{max} and F_{max} are the maximum strain and the maximum value of their spectra, respectively. α is the coefficient (0.65) for the equivalent linear method. In addition, we assumed that the soft layers of which S-wave velocity is lower than 400 m/sec were taken as sand, because of less information of soil properties. Analysis was made for only EW component because of lack of record of NS motion at SKR during the mainshock and the frequency ranges between 0.1 Hz to 10Hz was used following processing.

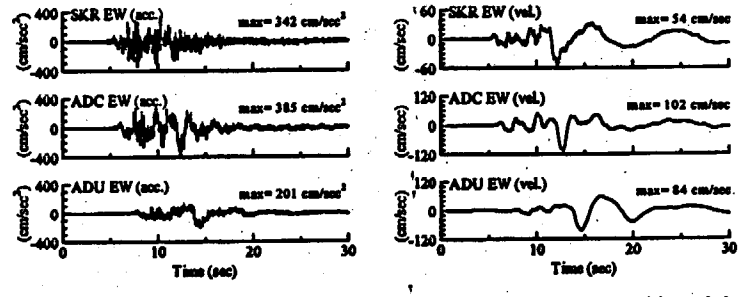

Figure 4 Estimated strong ground motion during the mainshock in downtown Adpazari by and the equivalent linear method using the observed earthquake records at SKR that were corrected for distances and responses of surface layers .

are 6x4, 2x1, 4x3, 3x2, and 2x2 for the asperities from No.1 to No. 5, respectively, and the ratios of stress parameters are 1.5, 1.0, 1.5, 3.0, and 1.0 for the asperities from No.1 to No.5, respectively, as shown in Table 3.

3) Effects of radiation pattern

Radiation pattern effects are sometimes ambiguous or frequency dependent. Kamae et al (1990) suggested a method to consider the frequency dependency of source radiation pattern that the observed radiation pattern in a longer period range has a tendency to follow the theoretical one, however, it tends to uniform for all directions in short period range. We assumed the low frequency to be 0.2 Hz and the high frequency to be 2 Hz, and the weights between two frequency were given following Kamae et al. (1990). In order to include the source radiation pattern effects, because of the differences of strike and dip of a fault between the main- and the aftershock (EGF) and the geometry of the extended fault (asperities) of the mainshock, we first rotated the axis of the bedrock horizontal (NS and EW) motions into radial and transverse motions. Next, the rotated waveforms of the small event are corrected concerning to the radiation pattern, source time function, and time shift for including rapture propagation and then they are summed. Thus obtained synthetic baserock motions were convolved the response of surface layers by the equivalent linear method as described before and they rotated again to NS and EW directions, and they compared in Figure 7.

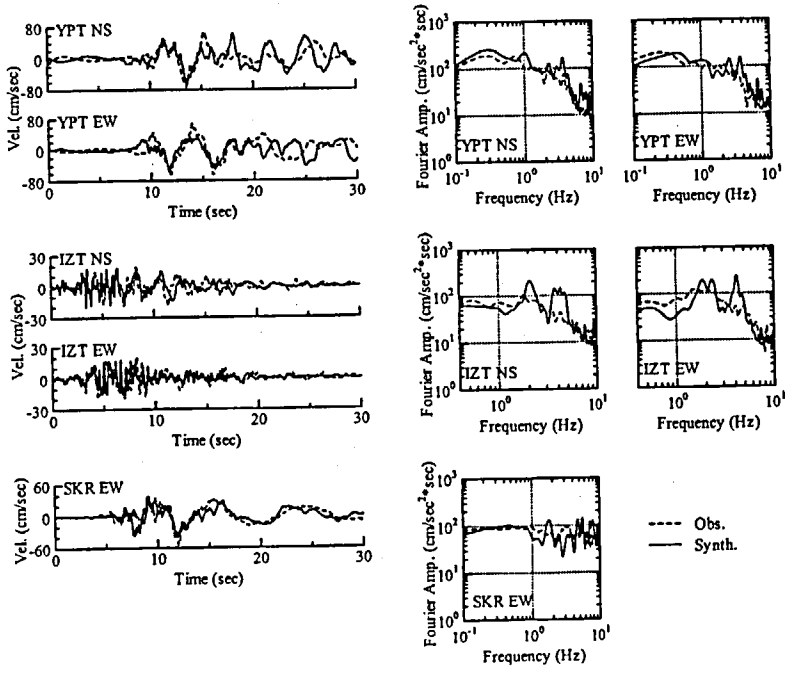

Figure 6. Comparison of the synthetic waveforms during the mainshock from strong motion records during the largest aftershock with the observed earthquake motions during the mainshock.

Table 2. The source parameters of each asperity.

Asperity	Rapture starting point			Mechanism			Size		Vs (km/s)	Vr (km/s)	Stress Drop (bar)
	Lat.	Long.	Depth (km)	Dip	Strike	Slip	L (km)	W (km)			
1	40.700	29.910	15.9	80	89	180	30.00	20.00	3.6	2.5	120
2	40.699	29.999	4.5	80	91	180	10.00	5.00	3.6	2.5	80
3	40.692	30.301	13.0	80	95	180	20.00	15.00	3.6	2.8	120
4	40.701	30.017	15.9	80	91	180	15.00	10.00	3.6	3.0	240
5	40.695	29.483	15.9	80	89	180	15.00	10.00	3.6	3.0	80

Table 3. The source parameters of the largest aftershock and parameters for synthesis from the largest aftershock records to strong motion during the mainshock.

		Largest aftershock
Hypocenter	Lat.	40.80
	Long.	30.03
	Depth (km)	4.3
Size	L (km)	5.00
	W (km)	5.00
number of div.	Asperity 1	6X4
	Asperity 2	2X1
	Asperity 3	4X3
	Asperity 4	3X2
	Asperity 5	3X2
Stress Drop (bar)		80

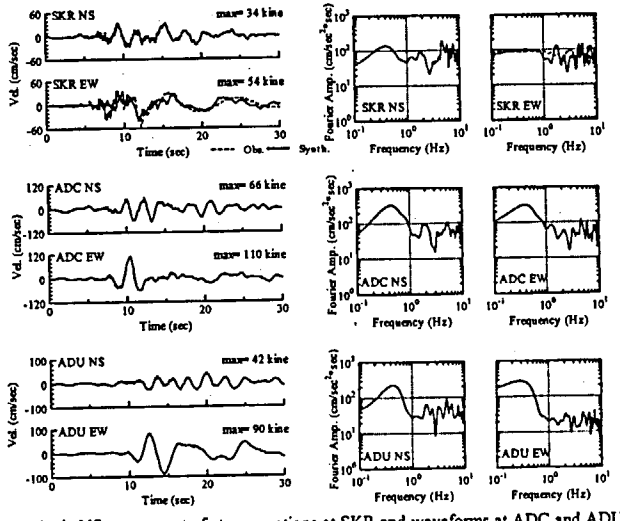

Figure 7. Synthetic NS component of strong motions at SKR and waveforms at ADC and ADU during the mainshock using the empirical Green's function method.

Estimation of ground motion in downtown Adapazari based on EGF

A lack of the NS component of strong ground motion at SKR during the mainshock brought large ambiguity on estimating the severity of ground motion in downtown Adapazari. A forward directivity effect (e. g. Somerville et al., 1997) on NS motion is the one plausible suggestion. EGF method enables us to estimate the NS motion at SKR and at downtown Adapazari using both horizontal motions from the largest aftershock. Figure 7 shows the estimated ground motions at SKR, ADC, and ADU. The EW motion at SKR is only compared with the observation. The NS component of strong motion at SKR is estimated to be 126 percent in the peak ground acceleration, however, the peak ground velocity is 87 percent of the EW motion, which is rather small than we expected. Estimated strong motions are prominent in long period, 3 to 4 seconds. The peak ground velocities at ADC and ADU are factors of 2.8 and 1.2 to that at SKR.

We estimated the ground motion at ADC downtown Adapazari using three different methods. Their acceleration response spectra of 5 percents damping are compared in Figure 8. An estimation with linear method will be understand as an upper bound in short period range. There exit a considerable difference of factor 2 between 'OBS.+non-linear' and 'EGF+non-linear' at longer period than 1 sec., however, no significant difference is found in the peak velocity.

In this study, we used two methods for estimating of the incident wave at damaged area. We compare results by two methods as shown in Figure 8. The waveforms in Figure 8 are not the surface motions but the incident waves on the bedrock. They are in agreement in time domain comparably, however, the Fourier amplitude of bedrock motion at damaged area estimated by the observed motion at SKR is smaller than that by the empirical Green's function method in longer period range than 1 second. This reason is attributed to difference of the radiation pattern and the dynamic source process of the fault even though distance between two observation sites is close because objective area is located near the fault. Therefore, though strong motion data are obtained at rock site near sedimentary site, in case that their sites are located near the fault, it is necessary to pay attention for use of rock site data as incident wave at sedimentary site.

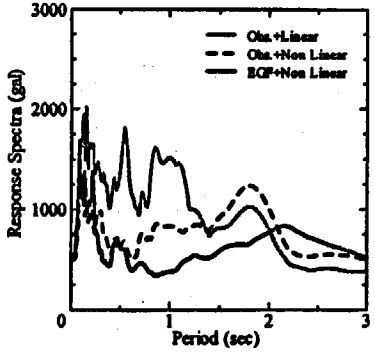

Figure 8 Comparison of acceleration response spectra for the synthetics by three different methods

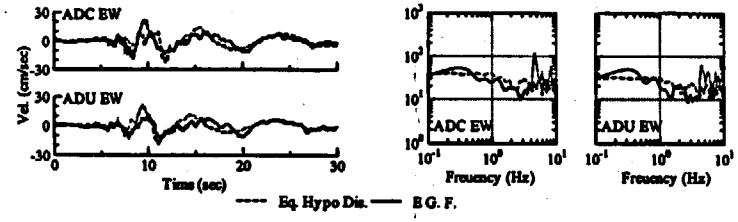

Figure 9. Comparison of the synthetic strong motions at ADC and ADU using between the observed strong motion at SKR during the mainshock and the empirical Green's function method.

Estimation of strong ground motion in Golcuk area

We examined that we were possible to synthesize the strong ground motion during the mainshock near Izmit Bay area and Adapazari, using the largest aftershock motion. This would be applicable for Golcuk area, however, unfortunately no strong motion records from the largest aftershock was available in Golcuk area. Therefore, we have to estimate the largest aftershock motion in order to synthesize strong ground motion during the mainshock. We will apply a two-step estimation, that is, we first simulate the ground motion in Golcuk area during the largest aftershock using two small aftershock data, and next we estimate the ground motion during the mainshock using the simulated aftershock motion as EGF.

1) Synthesis of the largest aftershock motion using small (M3) aftershocks.

Quite temporal aftershock observations were carried out in Golcuk area (Kudo et a., 2002), however, a sparse of instruments, we were obliged to separate observations into 2 groups. The aftershock data of September 13, 1999, (event A) were obtained at GLS, GLA, GLF, and YPT (Group A). Those of September 15, 1999, (event B) were acquired at GLF, GLJ, and GLN (Group B). We estimate earthquake motion during the largest aftershock in Golcuk area using these small events as EGF, similar to the study in Adapazari area.

At first, we use the site YPT as a constraint for determining the source parameters, because both records form the largest and small (event A) aftershocks were obtained. We assumed the small event had the isotropic radiation pattern of 0.63 (Boore and Boatwright, 1984), and used the bedrock motions, which the response of surface soil were deconvolved, as the empirical Green's functions at those sites. As a result of forward modeling, we obtained the synthetic parameters that a number of subfaults and ratio of stress parameter were 9x9 and 20, respectively, as shown in Table 4.

Figure 10(a) shows a comparison of the synthetic waveform for the largest aftershock with the observed one at YPT. The synthetic waveform matches well with the observations, and then we synthesized the largest aftershock motions at the Group-A sites (Figure 10(b)). Next, we determine necessary parameters for synthesizing the largest aftershock motions at other sites using the small event B. Both A and B events were recovered at GLF, therefore, the parameters were determined so as to match the synthetic motions of the largest aftershock at GLF by comparing their waveforms. Figure 11(a) shows comparison of synthetics for the largest aftershock at GLF using the small event A and B. They are in good agreement, therefore, it is possible to synthesize earthquake motions for GLJ and GLN during the largest aftershock using records from the small event B. The determined parameters for the synthetics are subfaults of 9x7 and the stress parameter ratio of 12 and the others are shown in Table 4(b). Figure 11(b) shows the synthetic waveforms during the largest aftershock at Group B

stations.

Table 4. The source parameters of the aftershock A and B and parameters for synthesis from earthquake motions during the aftershock A and B to strong motion during the largest aftershock.

		Aftershock A	Aftershock B
Hypocenter	Lat.	40.71	40.74
	Long.	29.98	29.95
	Depth (km)	15.9	11.5
Size	L (km)	0.56	0.56
	W (km)	0.56	0.71
number of div.		9X9	9X7
Stress Drop (bar)		4	7

The estimated bedrock motions at individual sites during the largest aftershock synthesized from small events have differences of a factor 2 in amplitude, however, the phase characteristics are similar among the sites in Golcuk area. Therefore, we postulated that the incident waves or the bedrock motions during the largest aftershock in Golcuk area is identical, because the Golcuk area is relatively narrow and comparatively far from the largest aftershock, therefore, bedrock motions should be almost identical in the area. We computed the average among four sites except for GLS in time domain. At first, we obtain shift time of earthquake motion at each site, which has the best correlation, referring to GLF synthesized from the event A. Next, we estimated the common input motion by stacking with high correlation time shift. The reason why we exclude only GLS is that Vs near the surface at GLS is higher than that of the common bedrock at the other sites. Figure 12 shows the averaged bedrock motion during the largest aftershock in sedimentary area of Golcuk.

2) Synthesis of strong ground motion during the mainshock using the estimated largest aftershock motion

We apply the parameters for synthesizing the mainshock motion in Golcuk area used in the previous section. The common synthetic motion is used as EGF at bedrock for the individual sites. Figure 13 shows the NS component of synthesized strong ground motion during the mainshock. The strong ground motion at GLS is wealthy with short period motions. The PGA is larger than the other sites (649 cm/sec^2), while the PGV is the smallest (47 cm/sec) among others. The PGA and PGV at GLA are estimated to be 197 cm/sec^2 and 68 cm/sec, respectively, however, their precision will be very low, because the strain of soil sometimes exceeds 10 percent, which strain level would not be applicable of the equivalent linear method. The PGA and PGV at GLF are estimated to be 363 cm/sec^2 and 68 cm/sec, at GLJ 385 cm/sec^2 and 76 cm/sec, and at GLN 622 cm/sec^2 and 101 cm/sec, respectively. The underground structure at GLN estimated by the array observations of microtremors is rather stiff than that at GLF; therefore, the site amplification factor computed using the structure at GLN based on 1D propagation theory is predominated with short period motion. Nevertheless, the amplification factor at GLN is smaller than that of GLF, the ground motion at GLN is much larger than GLF. By comparison of bedrock motions at GLF and GLN, a directivity effect is suggested. As noted before, although we have to carefully survey the significant level of strain applicable to the equivalent linear method for soil behavior during strong shaking, the reason of the difference between GLN and GLF will be attributed to that GLF was affected larger damping by nonlinear effects of soil behavior.

The severity of ground motion cannot be evaluated by only peak acceleration or velocity, however, ground motion level in Golcuk, nevertheless the distance to the fault is much closer than that of Adapazari, seems to be low compared with that of Adapazari. One possible reason is that the period range of the analysis in case of Golcuk was restricted in shorter period than 2.5 sec., due to the limitation of reliable period range of small events.

Comparison of estimated strong ground motion with the significant earthquake records

We verify strong motion level at damaged area compared with the significant earthquake using acceleration response spectra of 5 percent damping computed from vectorial summation for two horizontal components of the time history of response.

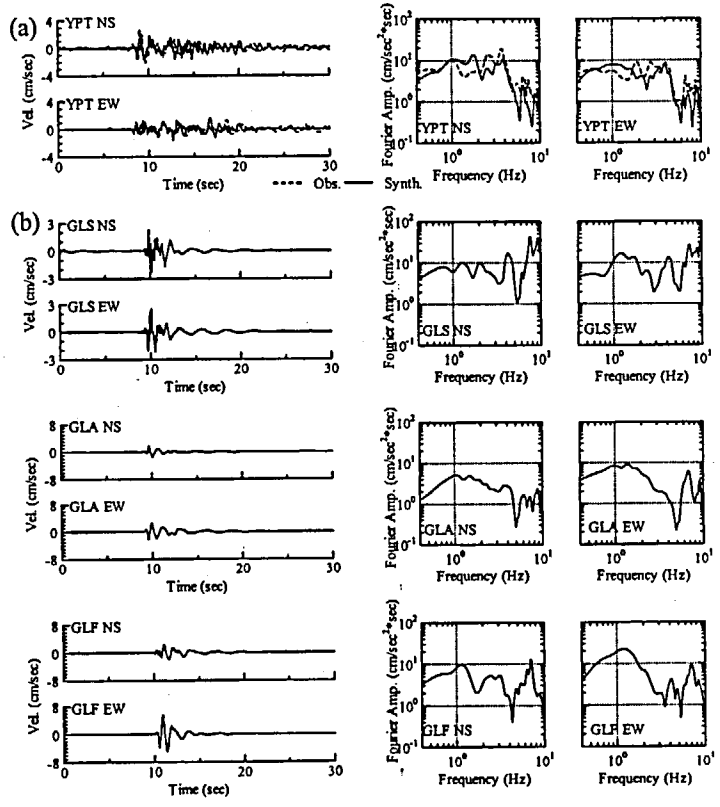

Figure 10. (a): Comparison of strong motions at YPT during the largest aftershock synthesized from the earthquake records of the aftershock A with the observed earthquake motions. (b): The earthquake motions during the largest aftershock at GLS, GLA, and GLF synthesized by using the aftershock A.

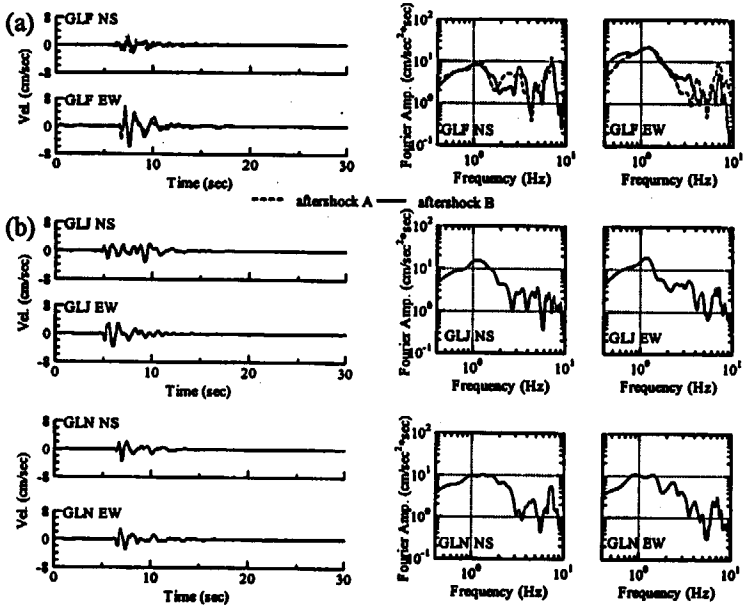

Figure 11. (a): Comparison of the earthquake motions at GLF during the largest aftershock synthesized from the earthquake records of the aftershock A with those of the aftershock B. (b): The earthquake motions at GLJ and GLN during the largest aftershock synthesized from the earthquake records of the aftershock B

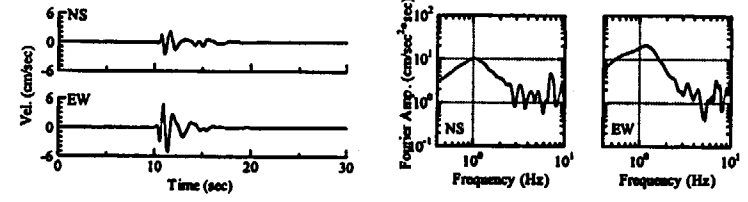

Figure 12. The Averaged velocity waveforms and the Fourier spectra during the largest aftershock on the bedrock in Golcuk area.

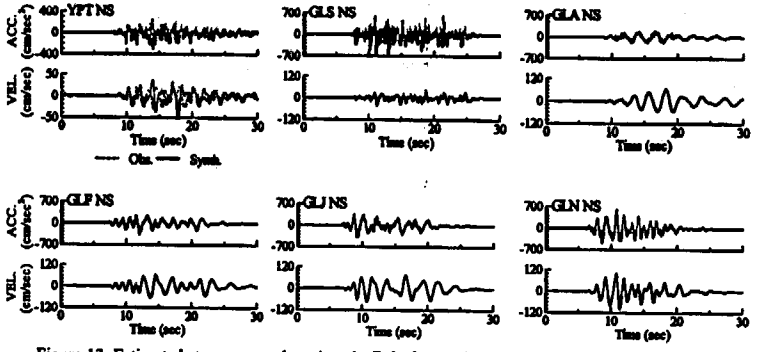

Figure 13. Estimated strong ground motions in Golcuk area during the mainshock.

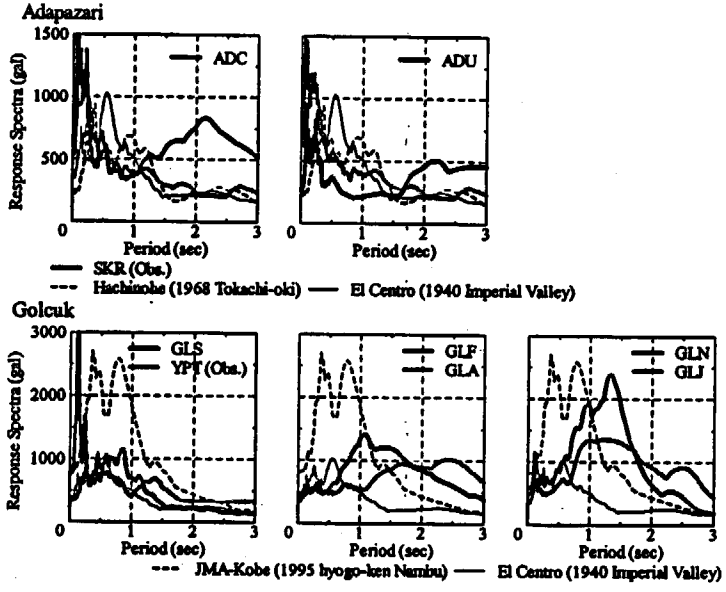

Figure 14. Comparison of the acceleration response spectra with damping of 5percent of estimated strong ground motion during the mainshock with those of some significant earthquakes.

Figure 14 shows acceleration response spectra of strong ground motion estimated using the EGF method at Adapazari and Golcuk areas together with those of some historical recordings. Response spectra at SKR in shorter period range than 0.5 seconds are larger than ones at Hachinohe from the Tokachi-oki earthquake of 1968 and El Centro from the Imperial Valley earthquake of 1940, on the other hand, those are similar in longer period range. The strong ground motion level at ADC, severely damaged area in Adapazari area, is larger in longer period range than 1 second, especially at a period of about 2 sec., it becomes factor of 3 to those of Hachinohe and El Centro. This is qualitatively consistent with the severe damage to medium-rise buildings. While, the acceleration response at ADU, where the buildings were mostly one or two stories and scarcely damaged, is smaller than that at SKR and Hachinohe in shorter period range than 1.5 seconds. This is also correlate with less damage to low-rise buildings near ADU.

Response spectra in Golcuk area, except at GLS, show very high level in the longer period range than 1.0 seconds, exceeding to that of JMA Kobe from Hyougo-ken numbu earthquake of 1995. Although we are required to find quantitative relation between ground motion and damage to buildings, however, heavy damage to medium-rise buildings in Golcuk area is much easier to quantitatively understand.

Concluding remarks

We estimated strong ground motion during the Kocaeli, Turkey earthquake of 1999 at damaged area based on underground structures estimated by array observations of microtremors, the empirical Green's function method, and the equivalent linear method.

We employed EGF method for bedrock motion as a first stage of simulation for the surface strong motion. This is applied because it is inevitable for the strong ground motion in sedimentary basins to include the effects of nonlinear of basin response. For simplicity, nonlinear behavior of soil layers is evaluated by an equivalent linear method, however, the strain level in Golcuk sometimes exceed the applicable level of strain in the method. Therefore, reliability of our results will not be high and it should be carefully taken into account for quantitative evaluation to find relation between ground motion severity and damage ratio. This is due to sparse of available data, however, our approach has a possibility to extend the application for estimating strong ground motion that was not recorded.

As results, the ground motion at a period of 1-2 seconds in downtown Adapazari (ADC) during the mainshock is estimated to be two or three times larger than that of Hachinohe from the Tokachi-oki earthquake of 1968. The estimated strong ground motion at ADU is smaller than that at SKR in shorter period range than 1 second, and this is qualitatively in consistency with damage level.

We have not investigated into details, however, ground motion due to synergetic effects of surface soils and source would be very important. Directivity effects were not distinct in the results of Adapazari, however, the ground motion near Golcuk would be influenced by not only site condition but also source process or rupture propagation of a fault. The ground motion in a longer period than 1 second at damaged area in Golcuk during the mainshock is estimated to be larger than that of JMA-Kobe from Hyogo-ken Nambu earthquake of 1995.

Acknowledgements

We thank the organizations that provide us the strong motion data through their web pages; the Earthquake Research Department, Directorate for Disaster Affairs of the Ministry of Public Works and Settlement and the Kandilli Observatory, Earthquake Research Institute. We thank Prof. A. Ito who provided us the aftershock hypocenter data. The computer code developed by Drs. N. Yoshida and I. Suetomi was used. We are also grateful to Dr. H. Sekiguchi who provided important information on the fault model and Prof. K. Kamae and Prof. K. Irikura who gave us useful advise on the method of analysis.

References

Aki, K. (1967). Scaling law of seismic spectrum, *J. Geophys. Res.*, **72**, 1217-1231.

Architectural Institute of Japan Reconnaissance Team with Bogazici University, Istanbul Technical University, and Middle East Technical University (2000). Progress report on damage investigation after Kocaeli earthquake by Architectural Institute of Japan, *Int. J. for Housing Sci. and Its Applications*, **24**, 97-126.

Bakir, B. S., H. Sucuoglu, and T. Yilmaz (2002). An overview of local site effects and the associated building damage in Adapazari during the 17 August 1999 Izmit earthquake, *Bull. Seism. Soc. Am.*, 92, 509-526.

Barka, A., et al. (2002). The surface rupture and slip distribution of the 17 August 1999 Izmit earthquake (M7.4), North Anatolian fault, *Bull. Seism. Soc. Am.*, 92, 43-60.

Bouchon, M. et al. (2002). Space and time function of rupture and faulting during the 1999 Izmit (Turkey) earthquake, *Bull. Seism. Soc. Am.*, 92, 256-266.

Celebi, M., S. Toprak, and T. Holzer (2000). Strong-motion, site-effects and Hazard Issues in rebuilding Turkey: in light of the 17 August 1999 earthquake and its aftershocks, *Int. J. for Housing Sci. and Its Applications*, **24**, 21-38.

Delouis, B., D. Giardini, P. Lundgren, and J. Salichon (2002). Joint inversion of InSAR, GPS, telseismic, and strong-motion data for spatial and temporal distribution of earthqaue slip: application to the 1999 Izmit mainshock, *Bull. Seism. Soc. Am.*, 92, 278-299.

Irikura, K. (1986). Prediction of strong acceleration motions using empirical Green's functions, *Proc. 7th Japan Earthq. Eng. Symp.*, 151-156.

Irikura, K., T. Kagawa, and H. Sekiguchi (1997). Revision of the empirical Green's function method by Irikura (1986), *Proc. Seismological Society of Japan*, **2**, B25 *in Japanese.*

Kamae, K., K. Irikura, and Y. Fukuchi (1990). Prediction of strong ground motion for M7 earthquake using regional scaling relations of source parameters, *J. of Struct. Constr. Engng, AIJ*, **416**, 57-70, *in Japanese with English abstract.*

Kamae, K. and K. Irikura, 2000, Simulation of broad-band strong motions from recent large earthquakes, *WPGM2000, AGU*, S52C-02.

Kudo, K., T. Kanno, H. Okada, O.Ozel, M. Erdik, T. Sasatani, S. Higashi, M. Takahashi, and K. Yoshida (2002). Site specific issues for strong ground motions during the Kocaeli, Turkey earthquake of August 17, 1999, as inferred from array observations of microtremors and aftershocks, *Bull. Seism, Soc. Am.* 92, 448-465.

Li, X., V.F. Cormier, and M.N. Toksoz (2002). Complex source process of the 17 August 1999 Izmit, Turkey earthquake, *Bull. Seism. Soc. Am.*, 92, 267-277.

Ohno, S., T. Ohta, T. Ikeura, and M. Takemura (1990). Estimation of strong-motion spectrum by regression analysis on near-field records, *Proc. 8th Japan Earthq. Eng. Symp.*, 295-300 *in Japanese with English abstract*

Ohsaki, Y., A. Hara, and Y. Kiyota (1978). Stress-strain model of soils for seismic analysis, *Proc. 5th Japan Earthq. Eng. Symp.*, 697-704 *in Japanese with English abstract.*

Schnabel, P. B., J. Lysmer, H. B. Seed (1972). SHAKE A computer program for earthquake response analysis of horizontally layered sites, *Earthq. Eng. Res. Cent. Univ. California, Berekeley,* Rep. No. 72-12, p. 88.

Sekiguchi, H. and T. Iwata, 2000, Rapture process of the 1999 Kocaeli Turkey earthquake estimated from strong motion waveforms, *Bull. Seism. Soc. Am.* , 91, 300-311.

Somerville, P. G., N. F. Smith, R.W. Graves, and N.A. Abrahamson (1997). Modification of empirical strong ground motion attenuation relations to include the amplitude and duration effects of rupture directivity, Seim. Res. Lett., 68, 199-222.

Sugito, M. (1995), Frequency-dependent equivalent strain for equi-linearized technique, *Proc. IS-Tokyo '95, The First International Conference on Earthquake Geotechnical Engineering,*

655-660.
Yagi, Y., and M. Kikuchi (2000). Source rupture process of the Kocaeli, Turkey, earthquake of August 17, 1999, obtained by joint inversion of near-field data and tele-seismic data, *Geophys. Res. Lett.* 27, 1969-1972.
Yamanaka, H. and H. Ishida (1996). Application of genetic algorithms to an inversion of surface-wave dispersion data, *Bull. Seism. Soc. Am.*, 86, 436-444.
Yoshida, N. and I. Suetomi (1996). DYNEQ: A computer program for dynamic response analysis of level ground by equivalent linear method, *Bull. Sato Kogyo Co.,Ltd.*, 61-70 *in Japanese*.

IN ABSENCE OF ACTUAL MAINSHOCK RECORDS, RECORDED AFTERSHOCKS & ESTIMATED MAINSHOCK MOTIONS AT SOUTH IZMIT BAY DURING THE AUGUST 17, 1999 IZMIT (TURKEY) EARTHQUAKE

Mehmet Çelebi
USGS, MS977, 345 Middlefield Rd., Menlo Park, Ca. 94025, celebi@usgs.gov
and
Haruko Sekiguchi
Geological Survay of Japan, Tsukuba, Japan

Abstract

The August 17, 1999 Izmit (Turkey) earthquake (M_w=7.4) will be remembered as one of the largest earthquakes of recent times that affected a large urban environment (U.S. Geological Survey, 1999). The shaking that caused the widespread damage and destruction was recorded by a handful of accelerographs in the earthquake area operated by different networks. Within the epicentral area and particularly in South Izmit Bay there were no strong-motion stations. However, following the main shock, temporary dense arrays were deployed at two main regions of South Izmit Bay: in Gölcük and in and around Yalova, 50 km to the west of Gölcük. Recorded aftershocks are analyzed using spectral ratio techniques. Aftershocks are also used to estimate the motions at the time of the main event of 17 August 1999. These estimates provide insight as to the extent of damage as well as what might be expected during future earthquakes.

Introduction

It is now well known that improper design and construction practices played an important role in detrimental performance of more than 20,000 structures during the August 17, 1999 (M_w=7.4) Izmit earthquake. This being a given, the main goal must be to improve design and construction practices. During this process, it is important to assess the recorded ground motions, site effects and other earthquake related hazard issues, which need to be considered during rebuilding efforts.

On-scale recordings of ground shaking during earthquakes are important for understanding causes of earthquake damage and the physics of fault rupture, and for advancing design codes. Approximately 38 strong-motion mainshock ground records were retrieved by different institutions in Turkey that operate strong motion networks.

The purposes of this paper are to (a) discuss the characteristics and engineering implications of the strong-motion records of the Izmit, Turkey earthquake, and (b) deduce from aftershock recordings, the site response characteristics and estimated mainshock motions at select locations where there were no stations to record the mainshock.

Strong-Motion Records

The Networks and Recorded Accelerations

The National Strong-Motion Network of the Earthquake Research Department of the Ministry of Public works (NSMN-ERD), the largest strong-motion network operator in Turkey, has aimed to

deploy one strong-motion instrument in every major town within the earthquake zones of Turkey. This systematic effort on part of NSMN-ERD, supplemented by strong motion stations deployed by Kandilli Observatory and Earthquake Research Institute (KOERI) and Istanbul Technical University (ITU) in Istanbul and Marmara Region, produced very significant and important records that will be useful for studying the earthquake and establishing important and necessary criteria in rebuilding efforts. These organizations recorded the main shock at 38 stations within the epicentral region. Peak accelerations of the records from some of the stations are plotted on the map in Figure 1. To date, detailed site characterizations of these stations have not been documented.

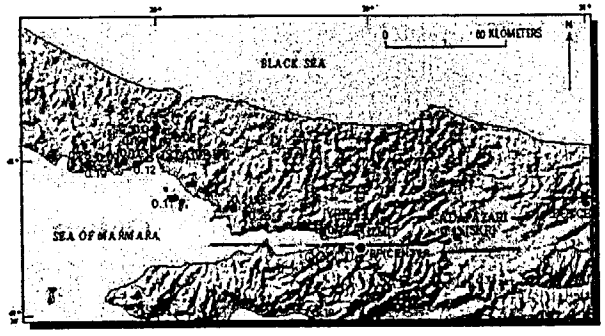

Figure 1. Map showing significant peak accelerations (g) in the earthquake affected area, plotted at relative locations of significant strong-motion stations within and in close proximity to the epicentral area (Base map courtesy of BKS Surveys Ltd., N. Ireland). Approximate fault rupture trace is also shown. Stations YPT and SKR are two significant stations referenced in the paper.

At the time of the earthquake, the strong-motion network in the epicentral area, as well as in other segments of the North Anatolian Fault and elsewhere in Turkey, was quite sparse[1]. Therefore, it is important to consider that recording of larger peak accelerations was possibly missed. For example, no record of the mainshock was obtained in Gölcük and vicinity in the immediate epicentral area where there was extensive damage. Hence, absence of strong-shaking records inhibits reliable evaluation of the effect of the shaking and consequential damage on the typical structures in the area. In addition, only one record (minus a component due to malfunction) was retrieved from Adapazari, at station SKR, which was on stiff soil in the undamaged part of Adapazari. There were no permanent stations in the fast-growing urban/industrial areas of the Adapazari basin. The peak accelerations in the basin almost certainly were amplified compared to that recorded at the stiff soil site. Records of the shaking in the basin would have likely revealed different characteristics such as amplification due to softer layered media, basin effects, and in certain areas, the effect of liquefaction that occurred.

Therefore, during the main shock of the August 17, 1999 earthquake, the largest recorded peak accelerations (SKR, 0.41 g horizontal and Düzce, 0.48 g vertical) were most likely not the largest that actually occurred. This possibility is strengthened by the fact that accelerations with larger peaks were recorded during events of smaller magnitude. This is illustrated in Figure 2 which shows three

[1] Since 1999, new strong-motion networks have been deployed in the epicentral areas of 1999 earthquakes to facilitate better and more widespread recording of strong shaking during future events.

acceleration time-histories recorded during: (a) the SKR record cited above, (b) the M_s=5.7 aftershock on 13 September 1999 at Tepetarla (a temporary station near Izmit) with peak ~ 0.6 g, and (c) the November 12, 1999 (Ms=7.2) Duzce event, station (Bolu) with peak ~ 0.8 g (EW).

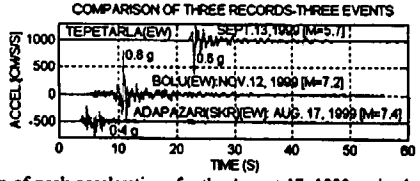

Figure 2. Comparison of peak accelerations for the August 17, 1999 main shock (station SKR) and two aftershocks, each recorded at a different location.

Two samples of recorded main shock motions presented in Figure 3a shows the acceleration time-histories recorded at SKR (Adapazari in Sakarya Province) on stiff soil. The records exhibit more than three different shocks. Figure 3b shows re-plotted SKR record for 40 seconds and time variant sum of square of acceleration to depict relative cumulative significant shaking (representative of energy). As depicted in Figure 3c, the duration of strong shaking is determined as approximately 5 seconds, using the time span between 5%-95% of the normalized sums (Novikava and Trifunac, 1994). The main shock contributes to approximately 70% of the total significant shaking of the two shocks within the 40 seconds of the record.

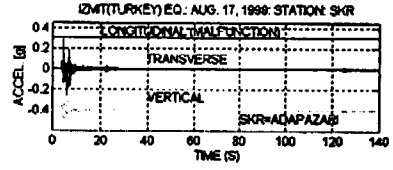

Figure 3 (a): Time-history of SKR record (Longitudinal component malfunctioned). The plot shows several events, including two significant aftershocks about 20 and 100 s following the mainshock.

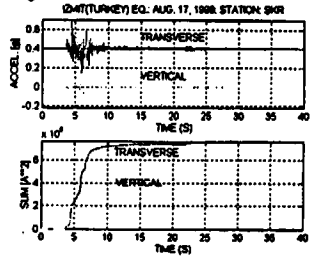

Figure 3(b) Initial 40-second window of the SKR acceleration record (top) and cumulative sum of squared amplitude (bottom) to show the significant strong shaking, almost all by the first shock, and indicating the duration of strong shaking as 5-6 s (bottom).

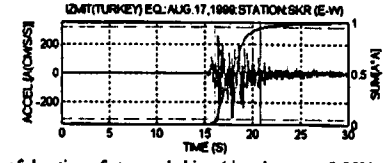

Figure 3(c) Definition of duration of strong shaking (time between 5-95% of the relative cumulative squared acceleration) [Reference: Novikava and Trifunac, 1994].

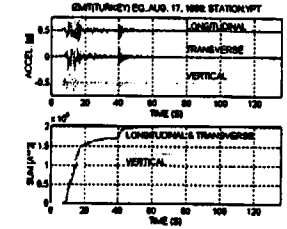

Figure 3d. Time-history of YPT. The plots show the second event approximately 30-seconds after the first (top) and that the significant strong shaking of the mainshock contributes approximately 70 % of the total and the strong shaking duration is 5-6 s (bottom).

In Figure 3d, the acceleration time-history of YPT (an alluvial site at Petro-Chemical Plant in Körfez) is shown. The figure exhibits two distinctive earthquakes. The figure also shows the relative cumulative significant shaking as calculated by summing the square of the acceleration over time. This figure exhibits that the strong shaking of the earthquake lasted approximately 5-6 seconds.

Near-Fault Issues and Pulses

One of the main reasons why near-fault motions are important is the presence of long-duration pulses that result in large displacements, which are detrimental to the performance of long-period structures. Somerville (1998) explains the long-period pulse characteristics of near-fault motions as follows:

- "the propagation of fault rupture toward a site at a velocity close the shear wave velocity causes most of the seismic energy from the rupture to arrive in a single large long-period pulse of motion,"
- "the pulse of motion represents the cumulative effect of almost all of the seismic radiation from the fault," and
- "the radiation pattern of the shear dislocation on the fault causes this large pulse of motion to be oriented in the direction perpendicular to the fault, causing the fault-normal peak velocity to be larger than strike-parallel peak velocity."

Abrahamson recently (2000) noted that, worldwide, for M>7 earthquakes between 1940 and 1999, there were only 8 records within <20 km of a fault rupture. The Turkey earthquakes of 1999 and the Chi-Chi, Taiwan earthquake of September 21, 1999, respectively added 5 and 60 more records for a total of 73.

Since long-duration pulses translate into large displacements, a simple explanation using vibrational physics of pulse action is useful for quick assessment of such actions. Consider four undamped, single-cyle sinusoidal accelerations with equal amplitudes, $\ddot{Y}$, but having different pulse durations. Figure 4 shows that corresponding displacements, y, are increased with increase in pulse duration, T_p, by virtue of the relationship : $y = -\ddot{Y}/(2\pi/T_p)^2$. It should be remembered that the amplitude to be considered in this simplified estimation process is the amplitude of the pulse with the longest cyclic period and not necessarily the peak amplitude of the time-history of a record which possibly may occur at higher frequency. Also, in using the simple process for integration, it is assumed that the accelerogram is a continuous sinusoid and not a truncated sinusoid.

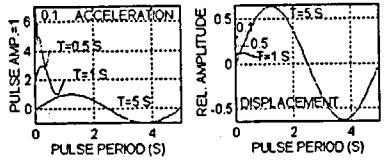

Figure 4. Single-cycle sinusoidal accelerations with constant amplitude but varying periods and corresponding displacements.

This grossly simplified visualization of the effect of long-period pulses in generating large pulse displacements are quantified and verified for two different earthquake records. The YPT record seen in Figure 3d is re-plotted in Figure 5a to better exhibit the long-period pulses and the amplitude spectra with a pulse period (T_p) of about 5 seconds (0.2 Hz) for the horizontal components. With peak acceleration of 0.22g for the EW component, the calculated pulse displacement, $y = 0.22(981)/(2\pi/5)^2 \sim 137$cm compares reasonably well with the displacement obtained by double-integration (Figure 5b). Figure 6a shows three components of accelerations recorded at Station TCU068 during the (M=7.3) September 21, 1999 Chi-chi (Taiwan) earthquake and their amplitude spectra that exhibit the lowest dominant frequency of approximately 0.11 Hz ($T_p \approx 9.09$ s). With peak acceleration of 0.37g for the east-west component, the peak pulse displacement of 757 cm is calculated. This compares well with the displacement of 707 cm (Figure 6b) obtained by double integration of the acceleration record (Tsai, 2000). These results are summarized in Table 1. Thus, since long-period pulses result in larger velocities and displacements, it is important to assess how the large displacements affect the response and performance of long-period structures such as tall buildings, long-span bridges, viaducts, overpasses, and base-isolated structures.

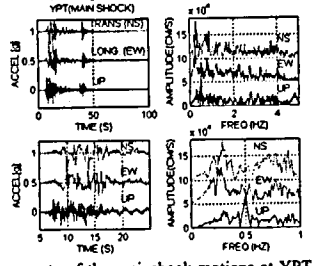

Figure 5a. The three components of the mainshock motions at YPT (Yarimca) recorded during the 19 August Izmit earthquake, along with the amplitude spectra of the motions, are shown for the entire record (upper) and for a 20-second window ending prior the first large aftershock.

Consequently, to compensate for the additional demand in design strength caused by such large displacements, recent codes in the United States adopted the Near Fault Factors (UBC, 1997). Thus, the seismic zoning factors are effectively increased by a factor, $1<N<2$ for seismic zone 4 (the highest seismic risk zones in the United States) within 10 km of those fault zones that are capable of generating (a) M≥7 earthquakes with slip rates exceeding 5 mm/year or (b) M≥6.5 earthquakes with slip rates smaller than 5 mm/year[2]. The North Anatolian Fault (NAF) is tectonically similar to the San Andreas Fault in California; therefore, such factors should also be considered in selective zones along the NAF. The recorded responses clearly show long period pulses (e.g. ~5 sec in case of YPT record – Figure 5b).

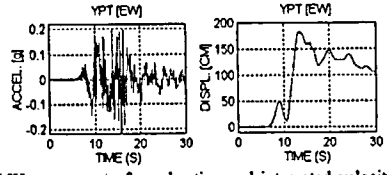

Figure 5b. Recorded E-W component of acceleration and integrated velocity and double-integrated displacements at YPT.

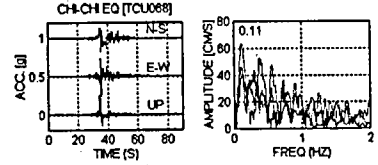

Figure 6a. Accelerations recorded at the TCU068 Station during the Chi-Chi (Taiwan) earthquake and the amplitude spectra [data from Lee, W, Shin, T., Kuo, K. and Chen, K., 1999).

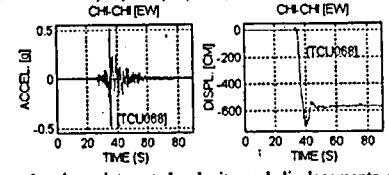

Figure 6b. Recorded accelerations, integrated velocity and displacements of TCU068 Station EW Component (from Boore, 2000).

[2] In the Uniform Building Code, the total design base shear in a given direction is determined from the following formula: $V = [C_v I / R T] W$, where C_v is is the seismic coefficient (for zone 4, is given by $0.32N_v$, $0.40N_v$, $0.56N_v$, $0.64N_v$ $0.96N_v$ for soil profile types S_A [shear wave velocity, V_s>1500 m/s] , S_B [760< V_s <1500 m/s], S_C [360< V_s <1500 m/s], S_D[180< V_s <360 m/s] and S_E[V_s<180 m/s] respectively), I is the importance factor, R is the ductility factor, T is the fundamental period of the design structure and W is the weight of the structure. The total design base shear is not to exceed $V=[2.5C_a I/R]W$ but is not to be less than $V=[0.11C_a I W]$ where C_a is the seismic coefficient and similarly ranges as $0.32 N_a$, $0.40N_a$,$0.40N_a$, $0.44N_a$ and $0.36N_a$ for the soil profiles S_A, S_B,S_C, S_D and S_E respectively. Furthermore, for Seismic Zone 4, the total base shear shall also not be less than the following: $V=[0.8ZN_vI/R]W$. Z is the seismic zone factor and is 0.4 for zone 4. In the above, $1<N_v<2$ and $1<N_a<1.5$] and are interpolated from tables according to different type of soil profiles and distance from fault. The highest factors are for sites less than 2 km from the faults (Uniform Building Code, 1997).

Table 1. Evaluation of Peak Displacements Using Sinusoidal Pulse Analogy versus Double Integration of Recorded Acceleration.

Earthquake	Mag. M_w	Station	Peak Acc.[g]	Pulse		Sinusoidal Pulse Displ.[cm]	Integrated Displ (cm)
				f(Hz)	T_p(s)		
Izmit [Turkey] 1999	7.4	YPT [EW]	0.22	0.2	5.0	137	~175
Chi-chi [Taiwan] (1999	7.6	TCU068 [EW]	0.37	0.11	9.09	757	707

Response Spectra

Figures 7a,b and c show the response spectra and the normalized response spectra (all calculated for 5 % damping), for north-south and east-west directions, respectively, for five stations, including SKR and YPT for which the time-history plots have been presented (Figures 2-3). These five stations cover the epicentral area (stations IZT and YPT) and locations that are heavily damaged east of the epicentral area (SKR and DZC) and a location in Istanbul (MCK). IZT, YPT and DZC are on alluvial sites whereas SKR and MCK are on stiff soil and rock, respectively. The response spectra show that at different stations, the resonant periods change drastically. Furthermore, the normalized response spectra indicate that both YPT and DZC have long periods (low frequencies). For comparison of response spectra shapes, Figure 7c also shows the current Turkish Code response spectra for stiff soil and alluvial site conditions (Specifications for structures to be built in disaster areas, English translation by Aydinoglu, 1998). The figure indicates that for periods between 0.1-1, the design response spectra, similar to those used in the United States, are exceeded for this earthquake.

Taller buildings on rocky hills of Istanbul, and the two suspension bridges in Istanbul were not adversely affected by the long-period motions of this earthquake – most likely due to attenuated ground motions. However, the important lifeline structures need to be reviewed for an earthquake that might occur closer to Istanbul.

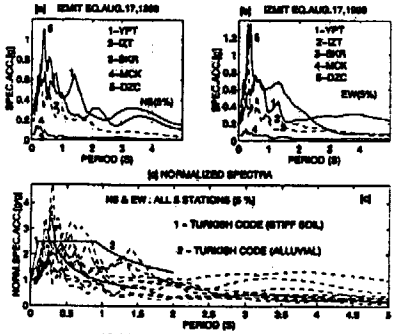

Figure 7. (a and b) Response spectra (5 % damped) for 5 stations and (c) Normalized response spectra of 5 stations compared with design response spectra of Turkish Code (1998).

Aftershock Deployments & Site Response Issues

Since, at the time of 1999 earthquakes, the strong-motion network in the epicentral area of the Izmit earthquake was not dense enough to define ground shaking at all damaged areas, a limited number of temporary arrays were deployed to obtain aftershock records to explain site effects at various locations. USGS deployed a number of acceleration and velocity transducers at the South Izmit Bay including Gölcük. Data from these and other deployments are compiled and made public (Çelebi and others, 2001). Figure 8a shows the deployment of the temporary array in Gölcük and a set of seismograms of an aftershock obtained from both sides of the observed normal fault scarp that developed during the main event. Stations FOC and GEM are on the hanging wall and LOJ and GYM are on the footwall of the normal fault. The figure exhibits the variation of ground motion at locations that are short distances apart (<1 km) (Çelebi and Sekiguichi, 2000, 2002) as well as the motions on both sides of the normal fault scarp. The differences of motions on either side of the normal fault are also observed in Figure 8b. The amplitude spectra and the relative cumulative energy plots further reinforce the larger energy at FOC and GEM, on the hanging wall as compared to LOJ and GYM, on the footwall.

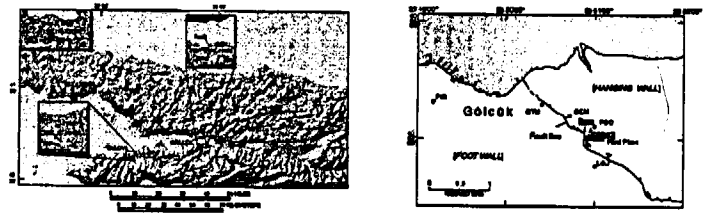

Figure 8a. Aftershock deployment map in South Izmit Bay (left) and specifically in Gölcük (right).

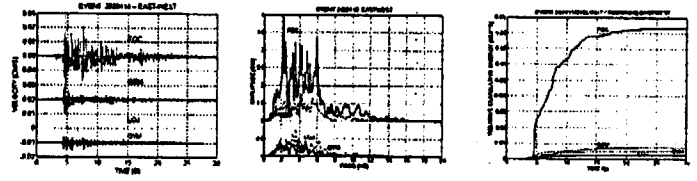

Figure 8b. Seismograms from an aftershock recorded at Gölcük temporary array (left). The seismograms show relative amplitudes of velocity records at close distances (<1km). The stations FOC, GEM and LOJ are within the Ford Plant Grounds near Gölcük. Station GYM is within <1 km of these stations. Amplitude spectra (center) and relative cumulative energy plots (right) of one event exhibiting significant differences of energy on either side of the vertical faulting.

Figure 9 shows the mean transfer functions of 11 events for FOC and LOJ, calculated using Nakamura's Method (1989, 2000) which, in absence of reference rock sites, facilitates calculation of the transfer function as the ratio of amplitude spectra of horizontal to vertical components of motion at a station [R=A(horizontal)/A(vertical)]. For frequencies less than 2 Hz, the north-south components

exhibit almost twice the amplification at FOC when compared to LOJ. This implies that in the hanging wall, alluvial deposits are deeper. This is consistent with the fact that, historically, there have been similar earthquakes in the area approximately every 250 years (e.g. two prior earthquakes, now confirmed by geological trenching and carbon dating, have occurred in 1719 and 1509 AD, respectively [Barka, *pers. comm.*, 2000, Sieh, *pers. comm.*, 2000]. Thus, over centuries, repetitive hanging walls have been filled over with alluvial material. Identification and recognition of such fault locations with associated historical events is necessary for siting purposes of facilities and important infrastructures in such areas.

The aftershock data is also used to estimate the strong-motions during the main event. Figure 10 shows the estimated motions for FOC and LOJ using aftershock data at both FOC, LOJ and YP1 (same as YPT) and the recorded mainshock data at YPT (Çelebi and Sekiguchi, 2002). The particular hybrid process uses (a) simulated ground motion in lower frequency range (0.1-1.5Hz) by theoretical Green's functions for laterally homogeneous structure model and a source process model obtained by Sekiguchi and Iwata (2002), (b) stochastic Green's function (Boore, 1983) for higher frequency range (1.5-10Hz). Details of the hybrid model are provided in Appendix A. The NS components, the fault-normal direction, of the estimated motions are highly polarized. These characteristics have been observed at stations in source regions of the past earthquakes. Therefore, it is important to consider directivity effects of near-fault ground motions, as also stated by Somerville (1998).

In the case of Yalova, approximately 50 km from the epicenter, the estimated motions (Figure 11) are again larger and polarized in the fault normal direction. This is also attributable to the fault rupture forward directivity, remarkably as it is at that distance from the epicenter but along the extension of the fault.

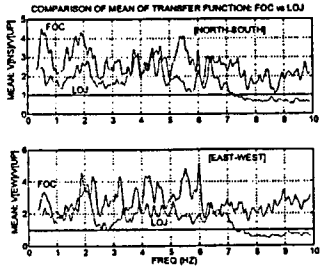

Figure 9. Mean transfer function of 11 events showing the amplification differences on both sides of vertical faulting.

Implications for the future

Finally, an issue that needs to be addressed is the forecasting of the future earthquakes following the 17 August 1999 earthquake. Parsons and others (2000) calculated that the August 1999 event increased the stress in the Marmara Sea close to Istanbul, the largest city of Turkey (Figure 12). They forecast that the stress increase results in a probability of 62 ± 15 % for a M>7 earthquake to occur in the next 30 years. Thus, there is an urgent need to be ready.

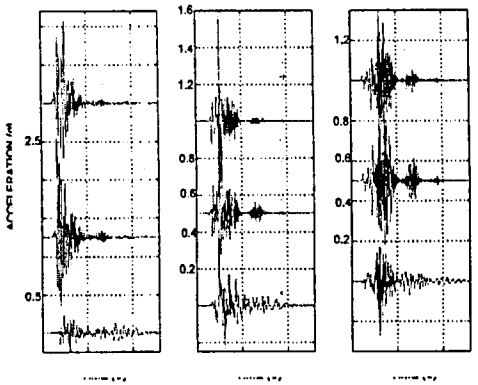

Figure 10. Estimated (mainshock) ground motions at FOC, LOJ and YPT using inversion technique with aftershock recordings at FOC, LOJ and YP1 (from Çelebi and Sekiguchi, 2002). Note differences in scales for different components, and that the fault-normal (NS) motions are larger for both FOC, LOJ and YP1.

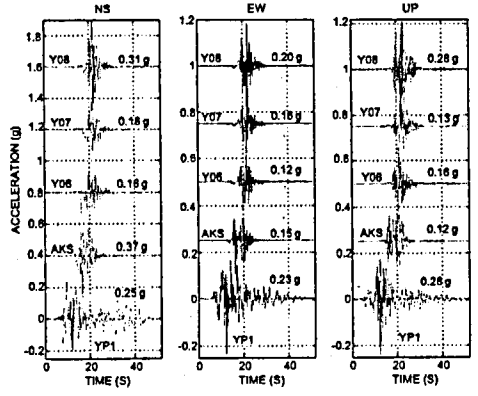

Figure 11. Estimated (mainshock) ground motions at Y06, Y07, Y08, AKS, and YP1 using inversion technique with aftershock recordings at Y06, Y07, Y08 and YP1 (from Çelebi and Sekiguchi, 2002). Note the fault-normal motions are somewhat larger.

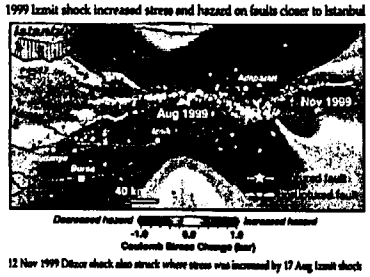

Figure 12. [courtesy of R. Stein] Change in Stress pattern triggered by the Izmit earthquake on 17 August 1999. Yellow to red colors indicate the area where stress increased whereas green to purple colors show the area where the stress decreased in the wake of the Izmit event (Parsons and others, 2000).

Conclusions

1. At the time of 1999 earthquakes, the strong-motion network on the North Anatolian Fault was very sparse. Denser arrays have now been added. The arrays should be supplemented with downhole accelerographs and piezometer arrays in liquefaction susceptible areas. It is important to increase the number of accelerographs in urban environments to cover different geological settings so that the actual motions in the basins and heavily damaged areas can be recorded.
2. Detailed site-characterization of the stations are not known. A systematic effort should be embarked upon to characterize the sites.
3. In absence of strong-motion records, aftershock motions have been used to estimate the strong-shaking during the main event. The estimated motions are very strong in the epicentral area, and in particular show stronger shaking in the fault-normal direction. The differences caused by site effects among sites closely located to each other are particularly noted. The motions are somewhat strong at distances of approximately 50 km from the epicenter due to a combination of distance and site effects.
4. Furthermore, on either side of a vertical fault, the amplification is observed to be larger on the hanging wall and is likely due to greater thickness of softer sediments. Therefore, it is essential to better identify existing normal faults for siting of important infrastructure and facilities.
5. The long-period pulses from near-fault motions must be accounted for in assessing the performance of structures. One possible way is to establish, in selected zones of the NAF, near-fault factors that increase the seismic coefficients in the codes.
6. Whenever applicable (e.g. in Adapazari basin), special site-specific design response spectra should be developed.

References

Abrahamson, N., 2000, seminar talk at USGS.

Ambraseys, N. N., 1988, Engineering seismology: Earthquake Engineering and Structural Dynamics,v. 17, no. 1, 1-105.

Barka, A., personal communication, 2000.

Boore, D. M.,1999, *Bull. Seism. Soc. Am.*, 73, 1865-1894.

Boore, D., 2000, effect of Baseline Corrections on Displacements and Response Spectra for Four Recordings of the 1999 Chi-Chi, Taiwan ,earthquake, BSAA, Chi-Chi Special Issue, v1.1.

Çelebi, M., and Sekiguichi, H., 2000, Estimation of Ground Motions at Gölcük during the 1999 Kocaeli, Turkey, Earthquake, AGU Abstract, San Francisco, Ca. Dec. 2000.

Çelebi, M., and Sekiguichi, H., 2002, Estimation of Ground Motions at South Izmit Bay during the 1999 Kocaeli, Turkey, Earthquake, *paper in preparation.*

Çelebi,M., Toprak, S., and Holzer,T., 1999, Strong-Motion, Site-Effects and Hazard Issues in Rebuilding Turkey: in Light of the 17 august 1999 earthquake and its aftershocks , invited paper, PROC. ITU Conference on Marmara Earthquake of August 17, 1999: Scientific Assessments and Recommendations for Rebuilding, Istanbul Technical University, Istanbul, Turkey, 2-5 December 1999.

Çelebi, M. (Scientific Editor), Akkar, S., Gulerce, U., Sanli, A., Bundock, H., Salkin, A., 2001, Main Shock and Aftershock Records of the 1999 Izmit and Duzce, Turkey earthquakes, USGS OFR-01-163 (CD-ROM). [also in, http://geopubs.wr.usgs.gov/open-file/of01-163/].

Irikura, K. (1986). *Proc. of 7th Japan Earthq. Eng. Symp.*, 151-156.

Lee, W., Shin, T., Kuo, K., and Chen, K., 1999, CWD Free-Field Strong-Motion Data from the 9-21_1999 Chi-Chi earthquake, V. 1: Digital Acceleration Files on CD.

Motosaka, M., A. Niousha and M. Nishihara (2000). *Proceedings of general conference, AIJ*, 37-38 (in Japanese).

Nakamura, Y. , 1989, A Method for Dynamic Characteristics Estimation of Subsurface using Microtremor on the Ground surface, QR of RTRI, February 1989, vol. 30, no. 1, 25-33.

Nakamura, Y., 2000, Clear Identification of Fundamental Idea of Nakamura's Technique and its Applications, CD-ROM Proceedings,12th World Conference on Earthquake Engineering, Auckland, New Zealand.

Novikava, E. I., and Trifunac, M. D., 1994, Duration of ground motion in terms of earthquake magnitude, epicentral distance, site conditions and site geometry, Journal of Earthquake Engineering and Structural Dynamics, 23, 1023-1043.

Parsons, T., Toda, S., Stein, R., Barka, A. and Dieterich, J., 2000, Heightened odds of large earthquakes near Istanbul: An interaction-based probability calculation, Science, v. 288, 28 April 2000.

Sekiguchi, H. and T. Iwata , 2002, Rupture process of the 1999 Kocaeli, Turkey, earthquake estimated from strong motion waveforms, submitted to *Bull. Seismol. Soc. Am.(in press).*

Sieh, K., personal communication, 2000.

Somerville, P.G., K. Irikura, R. Graves, S. Sawada, D. J. Wald, N. Abrahamson, Y. Iwasaki, T. Kagawa, N. Smith, and A. Kowada , 1999, *Seism. Res. Lett.*, 70, 59-80.

Somerville, P., 1998, Development of an improved representation of near-fault ground motions, SMIP98 Seminar on Utilization of Strong-Motion Data, Dept. of Conservation, Div. of Mines and Geology, Calif. Strong Motion Instrumentation Program, Sept. 15, 1998.

Specification for Structures to be Built in Disaster Areas , Ministry of Public Works and Settlement Government of Republic of Turkey, *Issued on: 2.9.1997, Official Gazette No.23098, Effective from: 1.1.1998, Amended on: 2.7.1998, Official Gazette No.23390 (English translation by N.* Aydinoglu, 1998).

Tsai, Y-B, (no date), Some Observations about the Chi-Chi, Taiwan earthquake of September 21, 1999, Technical report, National Taiwan University (Taiwan), 29p.

U. S. Geological Survey, 1999, Implications for earthquake risk reduction in the United States from the Kocaeli, Turkey, earthquake of August 17, 1999: U.S. Geological Circular 1193, *in press.*

Uniform Building Code, 1997, International Conference of Building Officials, Whittier, Ca.

Appendix A: Estimation of ground motion during the mainshock at sites without observation

In order to estimate ground motions in a wide frequency range at sites without mainshock recordings but with aftershock observations, we adopted a hybrid method. Ground motions in the lower frequency range (0.1-1.5Hz) were simulated using theoretical Green's functions and a source process model obtained by waveform inversion (Sekiguchi and Iwata, 2000, hereafter, SI model). The higher frequency (1.5-10Hz) ground motions were simulated using the stochastic Green's function method (Boore, 1983) from asperities extracted from the SI model. The bounding frequency of the two ranges nearly corresponds to the frequency at which the radiation pattern in observed seismic motions is submerged (Somerville et al., 1997).

Lower frequency range (0.1-1.5Hz):

Theoretical Green's functions were calculated for a laterally homogeneous velocity structure model using the discrete wave-number method (Bouchon, 1981) together with the reflection transmission method (Kennett and Kerry, 1979) [in laterally homogeneous (1-D) velocity structure models]. Assumed velocity structure models are based on Mindevalli and Mitchel (1989) for the deeper part and Kudo et al. (2000) for the subsurface part. The slip time functions and the rupture propagation correction functions inside each subfault from the SI model were convolved with the Green's functions. Then they are summed up taking into account the rupture propagation over the fault plane.

Higher frequency range (1.5-10Hz):

Based on Boore (1983), we generated ground motions from small earthquakes with the subfault size. Thus, the acceleration spectra of a small earthquake is given by:

$$A(f) = C\,S(f)R^{-1}\exp\left[\frac{-\pi f R}{Q(f)\beta}\right]g(f), \qquad (A.1)$$

where $S(f) = Mo(2\pi f)^2 / \left[1+(f/fc)^2\right]$ is an ω^{-2} type source acceleration spectra (Aki, 1967), R is a ray path length between a subfault and a observation station, $R^{-1}\exp\left[\frac{-\pi f R}{Q(f)\beta}\right]$ is the propagation path effect (geometrical spreading and attenuation), $g(f)$ is a site amplification factor, and C is a constant including free surface effects and radiation patterns etc. M_0 and f_c are seismic moment and corner frequency. Corner frequency was assumed to be 0.35 Hz by Madariaga's (1976) equation for a circular crack. Frequency dependent Q was based on Akinci et al. (1995). The site amplification factor was obtained through modeling aftershock ground motion spectra using equation (A.1).

To generate ground motion from a large earthquake from those of small earthquakes, we used the method of Irikura (1986), who proposed a filtering function which consists of a delta function and a boxcar function with duration of large earthquake's rise time to adjust the difference in slip time function between a large earthquake and a small one. For high frequency, the correction function is approximated by a delta function.

The source for the higher frequency motions were confined to asperities extracted by Miyakoshi (personal communication) from the SI model following the criterion by Somerville et al. (1999). This assumption is based on the results by Miyakoshi et al. (2000) and Miyake et al. (2000). The strong motion generation area found by Miyake et al. (2000) for a M_w=6.3 earthquake in 2.0-10Hz range is consistent with the asperity region extracted from the source model in lower frequency range (0.1-0.5Hz) for the same earthquake determined by Miyakoshi et al. (2000) and the contribution of the off-asperity area in the lower frequency source model is necessary for lower frequency ground motions but negligible for higher frequency ground motions.

Acknowledgements for Appendix A

We acknowledge the help and work of Tomotaka Iwata, Hiroe Miyake, Ken Miyakoshi, Masato Tsurugi.

References for Appendix A

Aki, K., 1967, Scaling relations of seismic spectrum, *J. Geophys. Res.*, 72,1217-1231.

Akinci, A., E. D. Pezzo and J. M. Ibanez , 1995, Separation of scattering and intrinsic attenuation in southern Spain and western Anatolia (Turkey), *Geophys. J. Int.*, 121, 337-353.

Boore, D. M., 1983, Stochastic simulation of high frequency ground motion based on seismological models of radiated spectra, *Bull. Seism. Soc. Am.*, 73, 1865-1894.

Bouchon, M., 1981, A simple method to calculate Green's function for elastic layered media, *Bull. Seism. Soc. Am.*, 71, 959-971.

Irikura, K. , 1986, Prediction of strong acceleration motion using empirical Green's function, *Proc. of 7th Japan Earthq. Eng. Symp.*, 151-156.

Kamae, K., K. Irikura, and A. Pitarka ,1998, A technique for simulating strong ground motion using hybrid Green's function, *Bull. Seismol. Soc. Am.*, 88, 2, 357-367.

Kennett, B. L. and N. J. Kerry ,1983, Seismic waves in a stratified half space, *Geophys. J. R. astr. Soc.*, 57, 557-583.

Kudo, K., T. Kanno, H. Okada, O. Ozel and M. Erdik ,2000, Site effects on strong ground motions during the Kocaeli, Turkey, earthquake of August 17, 1999, as inferred from array microtremors observations and aftershock data, *Proceedings of 3rd Japan-Turkey Workshop.*

Madariaga, R ,1976,. Dynamics of an expanding circular fault, *Bull. Seism. Soc. Am.*, 66, 639-667.

Mindevalli, O. Y. and B. J. Mitchell ,1989, Crustal structure and possible anisotropy in Turkey from seismic surface wave dispersion, *Geophys. J. Int.*, 98, 93-106.

Miyake, H., T. Iwata, and K. Irikura , 2000, Source characterization of inland crustal earthquakes for near-source ground motion, *Proceedings of 6th International Conference on Seismic Zonation.*

Miyakoshi, K., T. Kagawa, H. Sekiguchi, T. Iwata and K. Irikura, 2000, Source characterization of inland earthquakes in Japan using source inversion results, Proc. 12th World Conf. Earthq. Eng., Auckland, New-Zealand, 1850, 8pp (CDROM).

Sekiguchi, H. and T. Iwata ,2000, Rupture process of the 1999 Kocaeli, Turkey, earthquake estimated from strong motion waveforms, submitted to *Bull. Seismol. Soc. Am.*

Somerville, P.G., K. Irikura, R. Graves, S. Sawada, D. J. Wald, N. Abrahamson, Y. Iwasaki, T. Kagawa, N. Smith, and A. Kowada ,1999, Characterizing earthquake slip models for the prediction of strong ground motion, *Seism. Res. Lett.*, 70, 59-80.

THE STUDY FOR THE EVALUATION METHODS FOR THE DESIGN BASIS EARTHQUAKE GROUND MOTIONS

Rikiro Kikuchi
Seismic Engineering Center, Nuclear Power Engineering Corporation, Japan

Abstract

NUPEC (Nuclear Power Engineering Corporation, Japan) has been carrying out a series of Sitting Reliability Studies relating to seismic design for nuclear power plants. We are currently conducting two studies under commission by METI (Ministry of Economy, Trade and Industry, Japan).

One of these studies, entitled "Evaluation Methods for Seismic Wave Propagation Characteristics",has been in progress since the 1994 FY. In this study, NUPEC carried out earthquake observations using a down-hole array of 1670m depth in the Kobe area. This vertical array observation system is equipped with eight seismometers from deep seismic bedrock to the surface stratum. We have observed 144 earthquake events in the period of 1999-2002. The major objective of the study is to verify current methods for evaluating design earthquake ground motions based on detailed investigations of observed seismic wave propagation data. In order to enhance the study, NUPEC is installing an additional earthquake observation system comprising a 1300m-depth down-hole array in the Narita aria.

The other study, entitled "Evaluation Methods for Strong Ground Motion in the Near-field Region", has been in progress since the 1998 FY. In this study, NUPEC collected and studied near-field strong earthquake ground motion data mainly from California. We also carried out a peer review on current seismological views relating to near-field strong motion characteristics. Up to the 2002 FY, we will verify the current methodologies for evaluating design earthquake ground motion especially in the near-field region.

Introduction

In Japan , all new nuclear power plants have been designed in accordance the Regulatory Guide for Aseismic Design of Nuclear Reactor Facilities in Power Plants (latest version July 20 , 1981 , by the Nuclear Safety Commission) , the design basis earthquake ground motion have been defined on the rock outcrop*[1] (free surface of the base stratum) .

This Regulatory Guide was established about twenty years ago, but it currently considered desirable the design basis earthquake ground motion to be defined on seismic bedrock obtained from analysis using observation records. Thus, NUPEC has been carrying out observations of seismic ground motions at vertical array stations equipped with seismometers from the seismic bedrock to the surface. We are also carrying out detailed geological investigations. We have been carrying out observations in the Kobe area from 1999 to March 2002, and in the Narita area since September 2002.

NUPEC has also been carrying out investigations to more precisely evaluate the seismic ground motion in the near-field region. This study has used observation records obtained mainly in California. Because each seismometer was only installed on the surface, we have calculated seismic ground motions on the rock outcrop. We researched detailed geological conditions for the selected observatory stations in California using a drilling survey and a micro-tremor array survey.

Evaluation Methods for Seismic Wave Propagation Characteristics

This study was undertaken to investigate seismic wave propagation characteristics from the seismic bedrock to the the rock outcrop defined as the design basis earthquake ground motion. It is outlined as follows.

(1) Investigation of the soil/rock profiles and properties from the surface to the seismic bedrock by drilling, sampling and laboratory tests
(2) Installation of accelerometers at the various depths in the boreholes to carry out the vertical array observation
(3) Observation of the seismic ground motions and data acquisition
(4) Study of the evaluation methods considering the seismic wave propagation characteristics from the seismic bedrock to the rock outcrop

The Kobe vertical array station (KHG) is located in the land reclaimed for the Higashinada Gas Turbine Power Plant of the Kansai Electric Power Company, as shown in Figure 1. Eight vertical array accelerometers were installed in December 1998. The depths at which the accelerometers are installed are GL-2m, GL-10m, GL-25m, GL-50m, GL-110m, GL-200m, GL-750m and GL-1,670m from the surface. The shear wave velocity of this seismic bedrock (GL-1,670m) is about Vs=3,200m/s.

The Narita vertical array station (NTY) is located on the Kanto Plain, in the Toyozumi industrial development complex of Narita City, as shown in Figure 2. NIED (National Research Institute for Earth Science and Disaster Prevention, Japan) had primarily installed two vertical array accelerometers in this area, and NUPEC installed four vertical array accelerometers adjoining them. When both accelerometers are put together, this vertical array observation system is composed of six accelerometers. The depths at which the accelerometers are installed are GL-2m, GL-10m, GL-25m, GL-65m, GL-300m and GL-1,300m from the surface. The shear wave velocity of this seismic bedrock (-1,300m) is not clear. The primary wave velocity is about Vp=6,000m/s. This observation system was just installed completely in this September.

This study is outlined in Figure 3. In Kobe, the bedrock forms a basin-edge structure and has a slope beneath KHB site, although it is almost horizontal in Narita. We will estimate the effect on the differences of seismic bedrock slopes. Records at only two stations are considered insufficient to evaluate the seismic ground motions. Thus, it precedes to the examination with other observation records (KiK-net data) that NIED open to the public via Internet in seismic bedrock as well recently in Japan.

The observation record, which it could get more for this study, and a part of that result of an examination, are introduced. Though the space from 1999 until 2002 could get 144 records, the biggest record was the Western Tottori Earthquake (October 6, 2000, JMA magnitude Mj =7.3, Epicentral distance Δ=187km). This acceleration records in the NS direction at Kobe vertical array station is shown in Figure 4. Moreover, the result that velocity response spectra were calculated by using these observation records with two-dimensional FEM on each position of the rock outcrop and seismic bedrock is shown in Figure 5.

Evaluation Methods for Strong Ground Motion in the Near-field Region

This study was undertaken to evaluate the characteristics of strong ground motion in the near-field region by using observation records from California earthquakes. Figure 6 shows the distribution of epicenters of seven earthquakes in California. For the investigation, we selected observatory stations within 20 km of the fault rupture for those earthquakes. There are not so many observatory stations, except for the Imperial Valley Earthquake in 1979 and the Northridge Earthquake in 1994.

Because each seismometer was only installed on the surface, we predicted the seismic ground motion on the rock outcrop. We investigated the detailed geological conditions for the selected observatory stations in California using a drilling survey, a micro-tremor array survey, and laboratory tests. The seismic ground motion on the rock outcrop was estimated by a non-linear analysis method based on those data. In the analysis, the horizontal components of the observation records were transformed to a fault-normal component and a fault-parallel component.

In the earthquakes in California and in the Hyogo-ken Nanbu Earthquake in 1995, Japan, the dominance of the fault-normal component with periods from one to a few seconds was seen in the near-field region. It is said to have an NFRD (Near Fault Rupture Directivity) effect in the near-field region. Figure 7 shows the ratio of response spectral amplitude of the fault-normal component to that of the fault-parallel component based on the predicted seismic motion on the rock outcrop. This shows that the fault-normal component tends to be greater than the fault-parallel component for periods greater than 1.0 second, while dispersion is recognized in those results.

Period of the Study

1. Study of Evaluation Methods for Seismic Wave Propagation Characteristics
   This study was planned for the 1994 FY to the 2004 FY.
2. Study of Evaluation Methods for Strong Ground Motion in the Near-field Region
   This study was planned for the 1998 FY to the 2002 FY.

Acknowledgement

These two studies have just been started under the sponsorship of the Ministry of Economy, Trade and Industry (METI). NUPEC has established an executive committee for both studies. The Study of Evaluation Methods for Seismic Wave Propagation Characteristics is chaired by Professor Emeritus H.Kobayashi, and the Study of Evaluation Methods for Strong Ground Motion in the Near-field Region is chaired by Professor K.Kudo. The author wishes to express his deep appreciation to the responsible officials of METI and the members of both committees.

Note

*1 : "the rock outcrop"

The rock outcrop is a nearly flat surface of the base stratum extending over a considerable area, and above which neither surface layers nor structures are assumed to be present. The base stratum is firm bedrock which was formed in general in the Tertiary or earlier era and which is not significantly weathered.

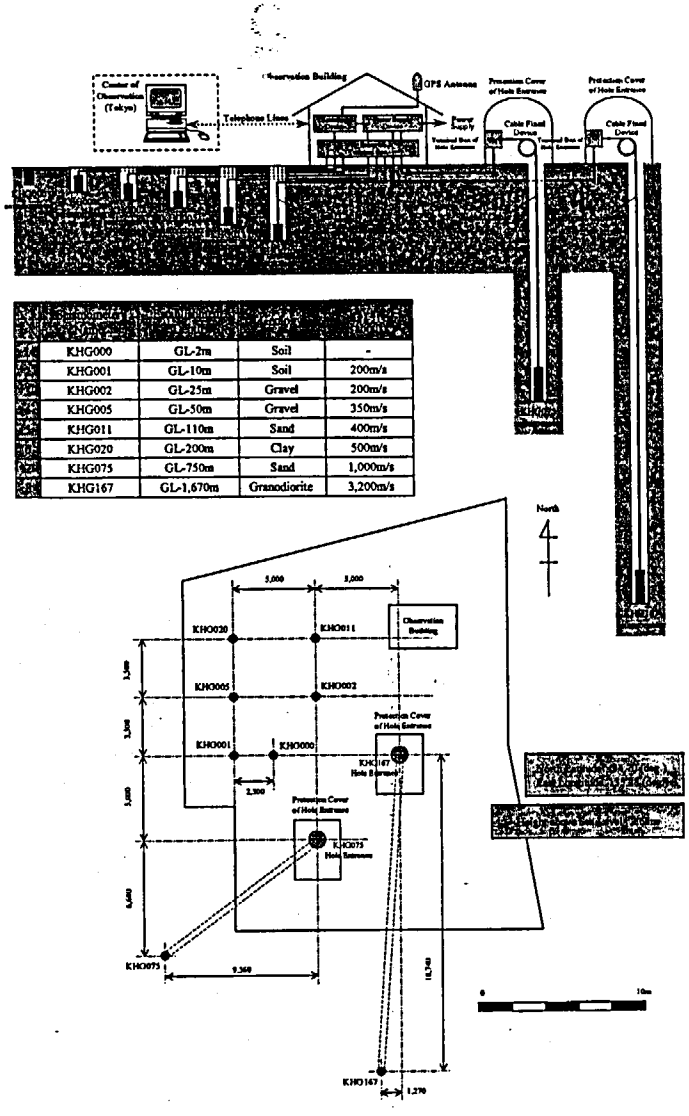

KHG000	GL-2m	Soil	-
KHG001	GL-10m	Soil	200m/s
KHG002	GL-25m	Gravel	200m/s
KHG005	GL-50m	Gravel	350m/s
KHG011	GL-110m	Sand	400m/s
KHG020	GL-200m	Clay	500m/s
KHG075	GL-750m	Sand	1,000m/s
KHG167	GL-1,670m	Granodiorite	3,200m/s

Figure-1 Outline explanation of Kobe vertical array station

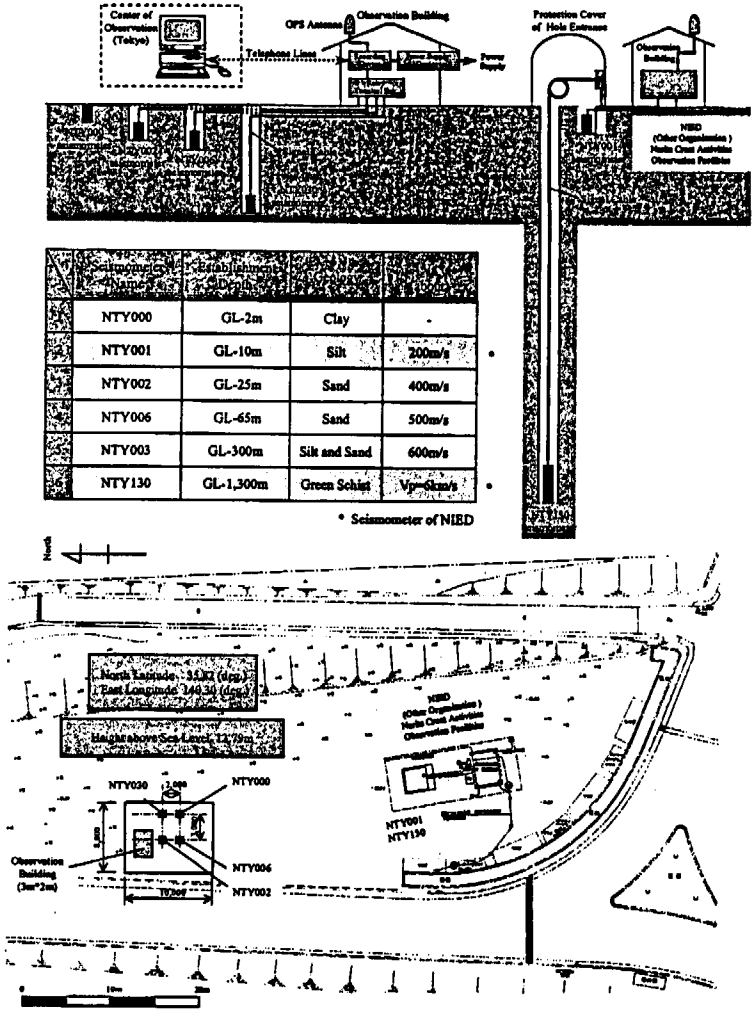

Figure-2 Outline explanation of Narita vertical array station

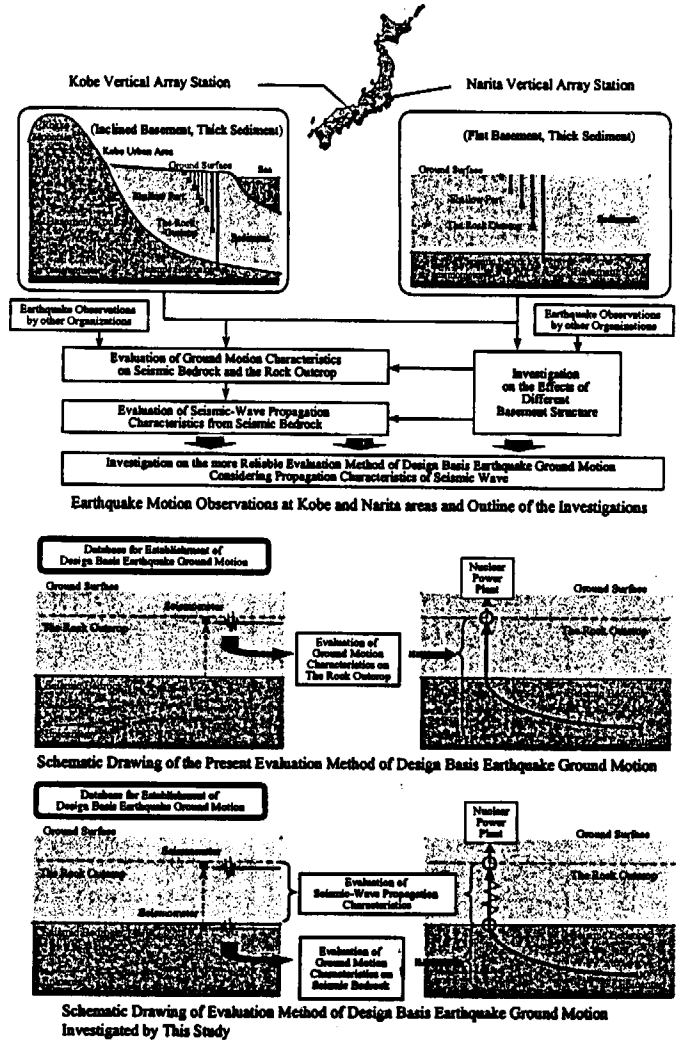

Figure-3 Outline of the Study for the Evaluation Methods for the Design Basis Earthquake Ground Motions

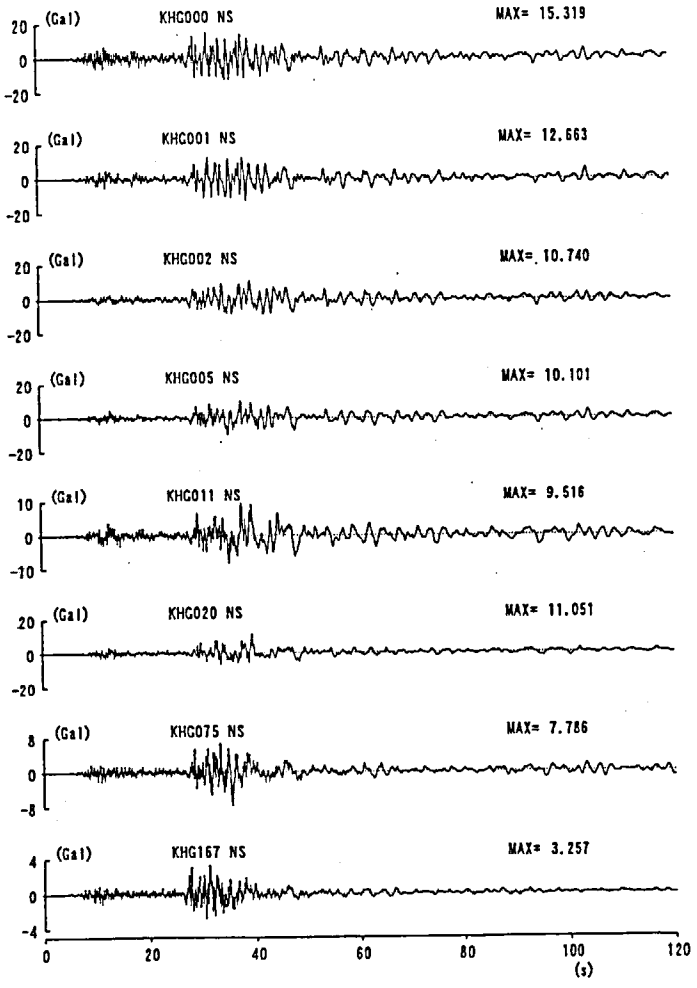

Figure-4 Acceleration time history of Western Tottori Earthquake in 2000 at Kobe observation station (NS direction)

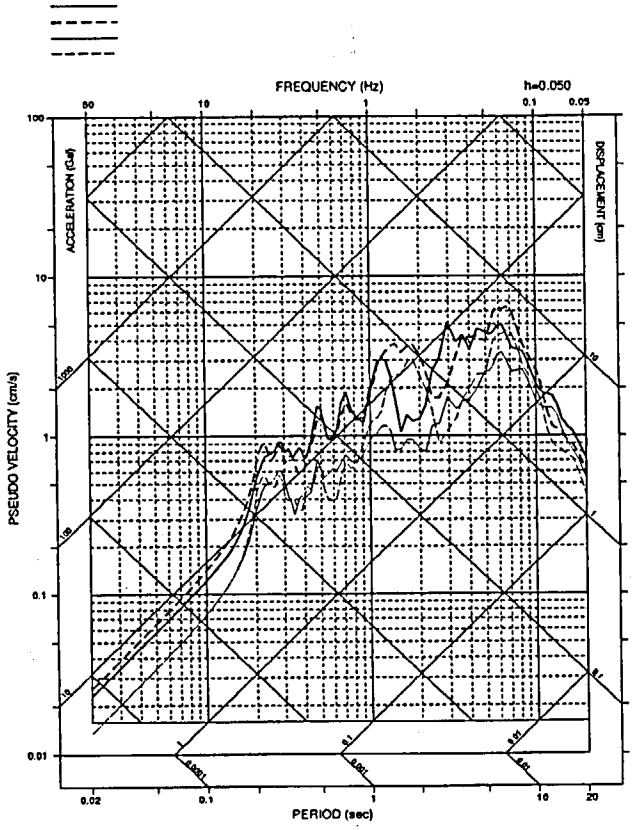

Figure-5 Velocity response spectra calculated Western Tottori Earthquake in 2000 at Kobe observation station

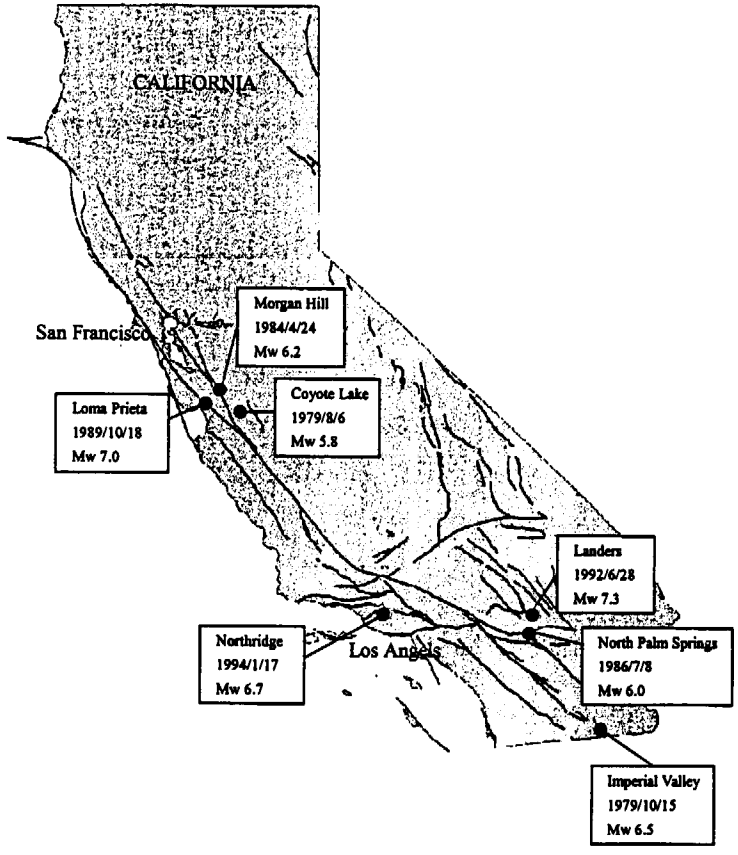

Figure-6 Distribution of epicenters of investigating earthquakes in California

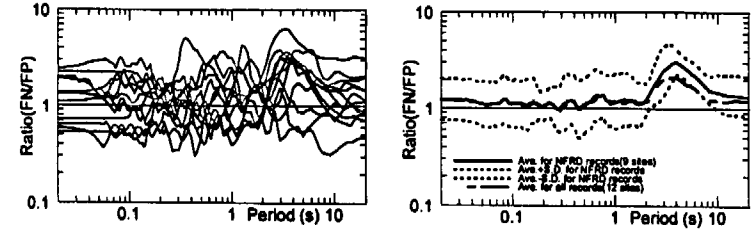

(a) All records

(b) Average and standard deviations of records in which the NFRD effect is predominant

(1) Near-source records in which the NFRD effect is predominant in the 1994 Northridge earthquake

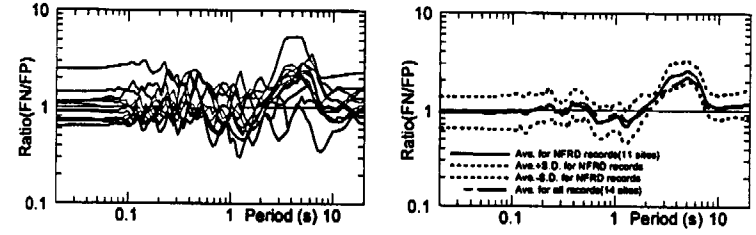

(a) All records

(b) Average and standard deviations of records in which the NFRD effect is predominant

(2) Near-source records in which the NFRD effect is predominant in the 1979 Imperial Valley earthquake

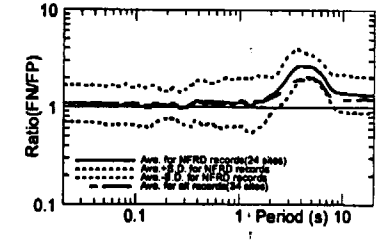

(3) Near-source records in which the NFRD effect is predominant in 7 California earthquakes

Figure-7 Fault-normal to fault-parallel response spectral ratios of predicted horizontal seismic ground motion on the rock outcrop

Seismic Hazard Determination of Nuclear Facilities in the Czech Republic

Dana Prochazkova
Emergency Planning Department, Fire and rescue Service
Praha, Czech Republic

Seismic safety management and seismic risk management strategies

Seismic safety management strategy and seismic risk management strategy [22] are in the Czech Republic based on the real seismic hazard knowledge and on the use of preventive measures (technological and organisational) that at a strong earthquake occurrence mitigate or even avert severe earthquake impacts. To be able to reduce a seismic risk we must know site seismic hazard, site, facility and technology seismic vulnerabilities.

By legal rules and seismic design code in force we require:

- determining the real site seismic hazard corresponding to time periods 100 and 10 000 years,
- determining the NPP seismic risk in dependence on NPP type and local conditions,
- adhering the defined professional principles and procedures at site evaluation, designing, construction and operation,
- using the construction procedures, technical measures (materials, structural elements, equipment etc.) and operation procedures that reduce seismic vulnerability during construction and operation,
- preparing the set of organisational measures for the case of strong earthquake occurrence.

Legal rules in force

To guarantee the NPPs seismic protection against earthquakes the legal rules [1 - 5] in force are used, i.e. Civil Construction Act, Nuclear Safety State Supervision Act, Special decrees and technical standards. These regulations are in keeping with the current used international rules and the IAEA recommendations [6,7].

By legal rules in force we require:

- to determine the real site seismic hazard corresponding to time periods 100 and 10 000 years,
- to adhere the defined professional principles and procedures at site evaluation, designing, construction and operation,
- to use the construction procedures, technical measures (materials, structural elements, equipment etc.) and operation procedures that reduce seismic vulnerability during construction and operation,
- to prepare set of organisational measures for the case of strong earthquake occurrence.

Data sets used

The seismic database contains the earthquake catalogues (macroseismic and instrumental) for Central Europe and for its individual parts, atlas of isoseismal maps of earthquakes macroseismically felt on the territory of Central Europe, maps of maximum observed intensities, investigations of individual earthquakes or earthquake sequences (e.g. swarms), description and characteristics of seismic regime of Central Europe and of individual focal zones being found there and analysis of seismotectonic relations. Data on earthquakes considered are for the last 1000 years.

The geological database contains the geological maps, hydro-geological maps, tectonic maps, maps of vertical crustal movements, gravimetrical, geomagnetic and geothermal maps for Central Europe and for individual regions in several different scales, tables and professional analysis and synthesis of data. Data for geological structure and tectonic movements considered are for the last 200 Ma.

To obtain realistic seismic hazard assessment the following ground-works were compiled for Central Europe:

- neotectonic movements chronological model for the last 40 Ma [9],
- neotectonic regional units and their present movements [9],
- earthquake occurrence scenarios [8,10],
- seismogenic movements determination [9, 20].

Methodology of investigation and evaluation of earthquakes

For the seismic hazard determination we use the methodology specified in the IAEA safety guide [6]. Seismic, geological and tectonic histories of Central Europe and its parts were evaluated by several independent methods. Revealed basic trends are generally coincident, only in evaluation of some partial events some differences from time to time occur.

A seismic hazard of any site depends on:

- a model of earthquake occurrence used,
- input data that calibrate the model used as:
  - the boundaries of focal regions or the boundaries of seismoactive parts of faults (i.e. fault parts that can produce an earthquake),
  - the values of maximum earthquakes that can be generated.

The assumptions and demands for the seismic hazard determination are given in the papers [11,18]. The assumptions are:

- earthquake may origin at any place of a focal zone or a seismoactive part of a fault,
- attenuation in the direction „focal zone - given locality" is the least favourable (from the safety reasons) of all empirical relations known,
- M_{max} value must be determined by the following way:
  - in a focal zone as a magnitude equal to the magnitude of maximum observed earthquakes in the history (ca last 1000 years) plus 0.5 - 1° MSK-64,

- as a result of expert assessment of symptoms of fault ability to generate earthquakes.

Taking into account the results of seismotectonic and statistical studies there are for given site determined: the safe shutdown earthquake (corresponding to SL-2 according to the IAEA recommendation), the design basis earthquake (corresponding to SL-1 according to the IAEA recommendation), the hazard curves for different return periods, the ground motion parameters of the site (site accelerograms or site specific spectral shape scaling to the ground motion level). If accelerograms are calculated from the response spectra the maximum probable estimation of duration of maximum phase of acceleration for real site is considered. The design response spectra, the zero period peak ground acceleration, the accelerograms and the duration of the maximum phase of acceleration are passed to the NPP designers and operators.

The used determination of site accelerograms, site response spectra, duration of maximum phase of acceleration in given site and the used evaluation of influence of local soil conditions on seismic waves are in the agreement with the IAEA recommendations [6,7]. Because the response spectra predicted from the ground acceleration time histories, the amplitudes and the amplification effects vary over the period range and are strongly affected by the subsoil, the magnitude of earthquake and the distance of NPP structure to the source rupture, their determination is very careful. They are determined in agreement with the IAEA materials [6,7,12,15].

Taking into account the real data [8-10,20] the seismic hazards of NPPs sites are less than 0.1 g for Dukovany NPP and Temelin NPP, 0.1 g for Mochovce NPP and 0.25 g for Jaslovské Bohunice NPP [21].

Taking into account the models of constructions of individual plant buildings of the category I of seismic resistance (the finite element method is used), the site dependent ground accelerograms and the site dependent design ground response spectra the set of floor design response spectra for individual constructions and floors are calculated considering the site specific soil conditions. The floor response spectra are generated by help of ground accelerograms and of the individual buildings models for several places on the floor and the results are obtained by the technique „median plus σ (standard deviation)". The combination of seismic stresses with other stresses resulted from dead load, live load, thermal load, pressure load, etc. in the total stress determination is considered for generation of floor response spectra for design and qualification of mechanical and electrical equipment and piping systems [17,19].

For the important equipment that are ranked in the category I of seismic resistance, the bounding spectra are determined taking into account the corresponding floor accelerograms, floor response spectra, floor model and the load combinations corresponding to the normal operating conditions [13] using the expert system [14].

Seismic terms of references

On the basis of real data we determine:

Maximum Calculated (safe shutdown) Earthquake - the greatest earthquake, defined as an extreme natural event of this type, which may potentially occur at the location of the given nuclear power plant. In conformity to the IAEA recommendation (SL-2) [6] it is required that its minimum value be chosen as 0.1 g.

Design (basis) earthquake - the greatest earthquake, defined as a standard external event, whose occurrence may reasonably be expected at the locality of the given nuclear power plant in the course of its technical service life. In the IAEA recommendation [6] the denotation (SL-1) is used. It is the earthquake, which produces the vibratory ground motion for which those features of the NPP necessary for continued operation without undue risk to the health and safety of the public are designed to remain functional.

Control Earthquake - an earthquake that the nuclear power plant will withstand without problems as far as of nuclear safety and functionality are concerned. It is usually considered to be equal to design basis earthquake and it is important for the correct setting of the nuclear power plant seismometric instrumentation.

Ground Motion Accelerogram - accelerogram representing the time dependent acceleration at the building's foundation or at ground level.

Floor accelerogram - accelerogram representing the time dependent acceleration of a selected point on the floor.

Ground Response Spectrum - response spectrum designed for the given free field accelerogram, or for the accelerogram at ground level.

Floor Response Spectrum - response spectrum designed for the given floor accelerogram.

Real seismic terms of references depend on site seismic parameters and on a NPP model and type [11,17,19]. They consist of safe shutdown earthquake, design basis earthquake, control earthquake, set of ground motion accelerograms, set of floor accelerograms, ground response spectra, floor response spectra, bounding spectra for important equipment, ranking the constructions, systems and components of the NPP into seismic categories.

The seismic categories [17,18] are defined in agreement with the IAEA guide [7] as follows:

Category I of Seismic Resistance - contains those safety systems and selected systems linked to nuclear safety including all works of civil engineering connected therewith and individual facilities components that are necessary for the fulfilment of the main safety functions of the unit in case of earthquake and must be seismically resistant up to the safe shutdown earthquake level and also in case of aircraft impact or external pressure wave on the reactor building and on other selected civil structures of the Nuclear Power Plant, as well as systems, structures and components, whose disturbance or failure during earthquakes up to the safe shutdown earthquake level inclusive, or in the case of aircraft impact or external pressure wave, could as a secondary consequence threaten other systems, structures or components in their vicinity that are important for nuclear safety in the case of an earthquake, or in the case of an airplane crash or impact of an external pressure wave. Included in the mentioned category are:

- civil structures, systems and individual components, whose failure could directly or indirectly cause the occurrence of emergency conditions,
- civil structures, systems and components that are necessary for safety shutdown of the reactor, monitoring critical parameters, for maintaining the reactor under safe shutdown conditions, and the remove of the reactor's residual heat for a sufficiently long period of time,

- civil structures, systems and individual components that are essential of preventing the spread of radioactive substances and ionising radiation into the vicinity, or for the maintenance of the respective leakage under the limits that apply to emergency conditions.

Conservatively, the category I of seismic resistance also includes selected civil structures, systems and components that are designed for the mitigation of the consequences of design accidents, postulated for the primary circuit, regardless of the fact that the primary circuit is in and of itself designed as being seismically resistant up to the safe shutdown level inclusively. Note: The category I of seismic resistance is further operatively divided to three sub-categories:

- sub-category Ia - seismic resistance is required in the sense of preserving full functionality,
- sub-category Ib - seismic resistance is required in the sense of preserving mechanical rigidity and hermetic sealing in accordance with the respective rigidity standards and regulations; partial violations of functionality are possible,
- sub-category Ic - seismic resistance is required only in the sense of possible seismic interactions with other civil structures, systems or components, most often in the sense of preserving the stability of the position, partial disturbance of functionality, mechanical rigidity or hermetic sealing being possible. This concerns such civil structures, systems and components that could, due to their location, forced motion and in particular their eventual loss of stability, impact civil structures, systems and components included in the seismic sub-categories Ia and Ib.

Category II of Seismic Resistance - means that there is not requirement to do seismic assessment of structures, components and systems.

Mitigation of earthquake impacts on NPP

The nuclear power plant seismic resistance is defined as the ability of the nuclear power plant civil structures, systems and components to maintain their functionality, mechanical rigidity and hermetic sealing, or only to prevent their being disturbed as a result of seismic interactions. Seismic interactions denote events occurring in the course of an earthquake and similar phenomena that may cause damage to systems, structures, technical systems or individual components as the result of a mechanical interaction with civil structures, system or components in their vicinity [17,19].

The evaluation of the seismic resistance of civil structures, systems and components of the nuclear power plant's facilities of the category I of seismic resistance must be carried out by calculations and tests, the details are in report [17].

In conjunction with the impact of a seismic alarm on the functionality of the regulating devices of the concrete reactor, it must be demonstrated by calculations or by experiment that the duration of their emergency outage from the full level of operational functioning, with the electromagnets switched off, even in the case of safe shutdown earthquake will be within allowable limits given by the manufacturer, i.e., less than 4 seconds [17].

In conjunction with the installation of viscous pipe dampers on the primary circuit, condenser circuit and other piping systems, the requirements of the respective technical conditions stipulated for their delivery must be met, including the requirement for an attestation of these dampers for use at a nuclear power plant.

To proof the resistance against earthquakes only verified, generally accessible and reliable methods, models, codes and standards are acceptable [3].

The NPP protection against to earthquakes is provided by:

- aseismic design of civil structures, systems and components that belong to the category I of seismic resistance (they must be resistant to predicted impacts of design basis earthquake and of safe shutdown earthquake, respectively),
- selection of systems and technological components that belong to the category I of seismic resistance (they must be resistant to predicted impacts of design basis earthquake and of safe shutdown earthquake, respectively),
- the use of different types of supports, dampers, anchoring, etc.

[2,3,7,15,16].

Aseismic design

Facilities that are important for nuclear safety must be designed in such a way that in the case of natural events that may realistically be expected to occur (earthquakes, hurricanes, flooding, etc.) or events caused by human activity outside of the nuclear energy facility (airplane crashes, explosion in the nuclear power plant's vicinity, etc.) it should be possible:

- to safety shutdown the reactor and maintain it in a sub-critical condition,
- to remove the residual output of the reactor for a sufficiently extensive period of time,
- to maintain any radioactive leakage under the limiting values stipulated for the given locality of the nuclear energy facility

[3,15] in agreement with the IAEA recommendations [6,7,16].

Seismometric instrumentation

The seismometric instrumentation (SMS) must be designed in conformity with the IAEA requirements [7, 17, 19]. It is considered acceptable if control earthquake is equal to design earthquake for the nuclear power plant [17, 19]. In conformity with the IAEA instructions [7] the following is applied:

- SMS is seismically resistant up to the safe shutdown earthquake level, including the respective electrical supply,
- SMS is dependent on the primary circuit diagnostic systems and the probability of its failure is smaller than once in 105 years,
- SMS is automatically activated if the measured absolute acceleration in any direction and at any arbitrary location of the sensors exceeds the value of 0.01 g,
- SMS meets the minimum requirements on the number and location of the accelerometers based on IAEA 50-SG-D15 instruction [7] and the signalling equipment is connected to the unit control room, with a link to the NPP computer information system.

Inspections and walkdowns

Systematic investigation of NPP seismic resistance is provided by regular inspections of the State Office for Nuclear Safety [2] and by professional walkdowns either after stronger earthquakes (greater or equal to design basis earthquake) or after important inspector's findings (e.g. effects caused by ageing) [18].

References

[1] Act No. 50/1976 Sb. Civil construction act. Czechoslovak law collection, Praha 1976.

[2] Act No28 /1984 Sb. State supervision of nuclear safety of nuclear facilities. Czechoslovak law collection, Praha 1984.

[3] Regulation No 2 of Czechoslovak Atomic Energy Commission on nuclear safety assurance during designing, permission or licence issuance and construction of nuclear power facilities. Czechoslovak law collection, Praha 1978.

[4] Regulation No 4 of Czechoslovak Atomic Energy Commission on general criteria for sitting NPPs with regard to nuclear safety. Czechoslovak law collection, Praha 1979.

[5] Technical standard CSN 73 0036, 1973, Revision 1990. Seismic loads and response of technical structures. Praha: UNM.

[6] IAEA, 50-SG-S1 (1991). Earthquakes and associated topics in relation to nuclear power plant sitting. Vienna: IAEA.

[7] IAEA, 50-SG-D15 (1992). Seismic design and qualification of nuclear power plants. Vienna: IAEA.

[8] Prochazkova, D. (1984). Analysis of earthquakes in Central Europe (in Czech). Doctor's Thesis. Praha: Geoph. Inst. Czechosl Acad. Sci.

[9] Prochazkova, D. & Z. Roth (1993). Complex investigation of earthquakes in Central Europe. In: Environmental monitoring and adjacent problems: 287-349. Praha: Czech Ecol. Inst. and Ministry of Environment.

[10] Prochazkova, D. (1993). Earthquake pattern in Central Europe. Acta Universitatis Carolinae - Mathematica et Physica. 34: 3-66.

[11] Prochazkova, D. (1996) Seismic terms of references of site with nuclear equipment (for conditions in the Czech Republic) (in Czech). Bezpecnost jaderne energie. 42: 486-498.

[12] Gürpinar, A., ed. (1995). Co-ordinated research programme on Benchmark study for the seismic analysis and testing of WWER-type nuclear power plants. Vienna: IAEA, 7 Volumes.

[13] Masopust, R. (1995). Demands for seismic calculations and seismic resistance assessments of constructions and equipment of NPPs and rules for their execution (in Czech). Report. Plzen: Stevenson and Associates.

[14] Expert system SUG-GIP for assessment of seismic resistance of NPP equipment. Plzen: Stevenson and Associates, 1995.

[15] IAEA, 50-C-D (1988). Code on the safety of nuclear power plants: Design. Vienna: IAEA.

[16] IAEA, 50-SG-D11 (1986). General design safety principles for nuclear power plants. Vienna: IAEA.

[17] Masopust, R. (1996). Directions for evaluating the ETE safety documentation. 3rd volume. Civil engineering, assembly of technical systems and facility components (in Czech). 131p. Praha: 3E Praha Engineering, a.s.

[18] Prochazkova, D. (1996). Consideration of earthquakes in the nuclear domain (Czech Republic). In: Report of the task group on the seismic behaviour of structures. Paris: OECD/NEA: 106-118.

[19] Prochazkova, D. (1996). Guidelines for evaluating ETE safety Documentation. Internal directive. Praha: SUJB.

[20] Simunek, P. (1989). Seismotectonic evaluation of region of Tetov NPP (in Czech). Report. Praha: Archives in Energoprojekt.

[21] Seismic Hazard Assessments of NPP Sites. Praha: Archives in Energoprojekt.

[22] Gürpinar, A. (1997). A review of seismic safety considerations in the life cycle of critical facilities. JEE, 1, 57-76.

A developing risk-informed design basis earthquake ground motion methodology for nuclear power facilities in Japan

Takaaki Konno,
Secretariat of Nuclear Safety Commission, Japan

ABSTRACT

Design basis earthquake ground motions for nuclear installations in Japan should be determined to assure the design purpose of reactor safety: that reactors should be built and operated to pose no undue risk to public health and safety from earthquake and other hazards. Regarding the influence of seismic hazard to a site, large numbers of earthquake ground motions can be predicted considering possible variability among the source, path, and site parameters. However, seismic safety design using all predicted ground motions is practically impossible. In the determination of design basis earthquake ground motions it is therefore important to represent the influences of the large numbers of earthquake ground motions derived from the seismic ground motion prediction methods for the surrounding seismic sources. Viewing the relations between current design basis earthquake ground motion determination and modern earthquake ground motion estimation, a development of risk-informed design basis earthquake ground motion methodology is discussed for insight into the on going modernization of the Examination Guide for Seismic Design on NPP's in the Nuclear Safety Commission (NSC) of Japan.

INTRODUCTION

The seismic safety of reactor facilities is required to assure the reactor safety and radiation protection to the public health and safety by defense-in-depth philosophy for any supposed seismic load occurrences during the reactor operation. The Examination Guide for Seismic Design by the NSC requires that the safety-related structures, systems and components (SSCs) shall be designed to withstand the effects of earthquakes without loss of capability to perform their safety functions in accordance with the classification of seismic importance.

Two types of design basis earthquake ground motions for seismic design are defined. One is derived as the design basis maximum earthquake S1 specified from the past earthquake records and active faults. The other one is derived as the design basis extreme earthquake S2 that exceeds the S1 and would have the greatest effect at a proposed site. However, the sufficiency of the intensity of the current S2 earthquake determination became a controversial problem after the recent inland earthquake experiences such as 1995 Hyogo-ken Nanbu Earthquake Mj=7.2 or 2000 Tottori-ken Seibu Earthquake Mj=7.3. The disasters in the damage belt of the 1995 Hyogo-ken Nanbu earthquake Mj=7.2 that struck the densely populated city of Kobe demonstrated to the public the dangerous power of the near-fault inland earthquakes. The 2000 Tottori-ken Seibu earthquake Mj=7.3 occurred at a previously unknown active fault for which the epicenter was located approximately 45 km southeast from an existing NPP. This caused discussion about the sufficiency of the blind fault earthquake magnitude that is required in the S2 earthquake; commonly a magnitude 6.5 earthquake at the hypocenter distance of 10 km is currently used for seismic design of every exiting NPP. These recent earthquake experiences awoke public concern about the seismic safety of NPPs that the current examination guide considers necessary for review based on the state of the art knowledge of seismology, geology, and earthquake engineering to ensure the seismic safety performance of NPPs from the point of risk managements.

The method to numerically handle the total earthquake effects to the site as probabilistic events is recently evolving in seismic probabilistic safety assessments (seismic PSAs). These systematic examinations are beneficial in identifying plant-specific vulnerabilities to severe accidents to evaluate the risk involved in the seismic safety design of the reactor facilities. Previous results of seismic PSAs for Japanese NPP's by JAERI [1] or NUPEC [2] showed that the reactor core damage occurrence frequency curve has the peak close to the design earthquake levels rather than excessively extreme earthquake level. This suggests the importance of not only the seismic safety assessment for the total earthquake hazard in identifying plant-specific vulnerabilities but also the importance of seismic design for design basis earthquakes including the risk-dominant earthquake level informed by seismic PSAs. The seismic design based on the risk-informed should confirm the integrity of structures and safety functions of the safety-related SSCs by

the dynamic response analyses using design basis earthquake ground motions defined including the risk dominant level earthquake that is important to ensure the seismic safety reliability on the seismic design in the face of significant uncertainties.

The seismic safety performances should be confirmed in accordance with the multiple levels of safety conditions complying with the risk information from seismic PSAs to meet the defense-in-depth philosophy. The safety levels that should be assured are: normal operation during high frequency occurrence earthquakes; transient incident of moderate frequency occurrence earthquakes; accidental incident of low frequency occurrence earthquakes. Based on these considerations, severe accident management should be planned for the probabilistic seismic risk. However current deterministic design practice to meet this seismic design requirement is not suitable for thoroughly explaining the relationship between the reactor safety performance and the integrities of structures, systems and components (SSCs). This is because uncertainties both of the seismic hazard among earthquake magnitude, occurrence, ground motion attenuation and of the seismic safety performance within the complex functional structures of reactor facilities.

A probabilistic approach to seismic safety assessment is important from the point of view of "How safe is safe enough." Such an approach takes into account the ground motion from the full range of earthquake magnitudes, allowing explanation of the relationship between the reactor safety performance and the strengths of safety-related SSCs considering the uncertainties within the seismic hazard and the safety performance system. The probabilistic approach to seismic hazard characterization is very compatible with current trends in earthquake engineering and the development of building codes, which have embraced the concept of performance-based design. The objective of the performance-based design is to clarify how reactor safety performance is degrading with the increasing magnitude of earthquakes. Earthquake occurrences are probabilistic events. Design basis earthquakes (DBEs) should consider the effects of every seismic event by occurrence probability to confirm the seismic safety of reactor facilities. Earthquake ground motions are made complex by the effects of the source, path, and site conditions, that is, it can be said the same ground motion will not again.

As experienced the disasters by the near-fault earthquake ground motions of the 1995 Hyogo-ken Nanbu Earthquake, the estimation of the effects of earthquakes to structures is difficult only from the response spectra of earthquake ground motions. The seismic impacts to structures should be evaluated by time domain dynamic response analyses. The adequacy of design basis earthquake ground motions to assure the seismic safety of the complex facilities of NPPs does not suitably explained only by the envelopment response spectrum or a uniform hazard spectrum of seismic sources. The current Examination Guide is under reviewed reflecting the risk insights informed by recent study results of seismic PSAs. The task group on seismic design guide was organized on July 10, 2001 under the Special Committee on Safety Standard in the NSC.

In this paper, a methodology of development the risk-informed design basis earthquake ground motions of NPPs is discussed based on the risk information by seismic PSAs compared with the risk insights by the current deterministic design basis earthquake ground motions.

SEISMIC SAFETY BY DEFENSE -IN-DEPTH PHILOSOPHY

Seismic classification comply the defense-in-depth philosophy

The seismic safety of NPPs by defense-in-depth philosophy is usually explained in Japan that 1) prevention of abnormal event occurrence, 2) early detection of abnormal event occurrence and mitigation to reduce the influence of the event before it become the accident, and 3) at the accident occurrence, prevent the accident progress and mitigate the accident to reduce the influence by the multiple preparation with diversity and redundancy of the various safety functions of prevention and mitigation systems. If any accident is induced it will be detected quickly and managed to the safety conditions by the safety functions, which hold high reliability due to diversity and redundancy the integrity of safety functions of safe shutdown, safe cooling and containment should be maintained assuming the combination with a random failure of prevention functions and a unit failure of mitigation functions. The seismic design basis requirements defined the performance criterion for the protection against earthquakes that safety related SSCs that are important to assure reactor safety and radiation protection shall be designed to withstand the effects of any supposed earthquakes without loss of capability to perform their safety functions in the seismic design examination guide by the NSC.

The examination guide classified the seismic grades of reactor facilities in accordance with the importance of the safety functions into four classes from high important to low important facilities as called seismic grades As, A, B, and C from the point of the magnitudes of radiation release impacts to environments and public health. The corresponding design basis earthquake ground motions are categorized into four classes from extreme to small earthquake magnitudes considering probability of occurrence frequencies, that are, extreme design earthquake (S2), maximum design earthquake (S1), 1.5 times a non-nuclear facilities design earthquake as the S_B, and non-nuclear facilities design earthquake as the Sc so that the integrity of safety-related SSCs required should be maintained, respectively. Each seismic grade facilities are designed to maintain the structural and functional integrities for corresponding earthquakes. Each seismic grade facilities should not be damaged to loss the safety functions by the failure of lower class facilities. The maximum design earthquake S1 is determined based on past earthquakes, earthquakes due to active faults with high activity whose recurrence interval is shorter than 10,000 years. The extreme design earthquake S2 is determined based on the both of seismo-tectonic structures and active faults of high to less activity faults whose recurrence interval is shorter than 50,000 years considering the seismological possibilities of excess the S1 event occurrence based on the characteristics of past earthquakes, active faults and possible blind faults. Current seismic design employed deterministically the seismic source of magnitude M6.5, hypocenter distance X=10 km, to represent the unknown blind faults assuming that could take place at any inland location in Japan. This seismic design requirement is intended to consider sufficient range of earthquakes to assure reactor safety for any potential earthquake shaking.

Plant safety levels related with seismic events

In general, earthquake occurrence frequency is higher in the small seismic. As shown in the Figure 1, generally speaking, plant safety conditions might be induced into from slightly abnormal conditions to highly abnormal conditions along with the intensity of earthquake events increased. These abnormal conditions induced by earthquake events should be detected quickly and settled to safety conditions by various safety functions of mitigation. Assuming the combination with a low occurrence frequency/large accident event by random failure, the safety conditions can be induced to severe condition even in a small earthquake. How much the severe earthquake events should be considered and also how much severe event combinations should be considered is therefore become important point in the deterministic seismic design relied on the risk insights. To obtain the quantitative answer to this problem, seismic PSAs might be a useful method to provide adequate solution based on the risk information. The design basis earthquakes also should be defined explicitly the relations with the probability of annual exceedance occurrence frequencies so that the event combinations considering random failures and human factors can be rationally employed for the safety managements in reactor operations.

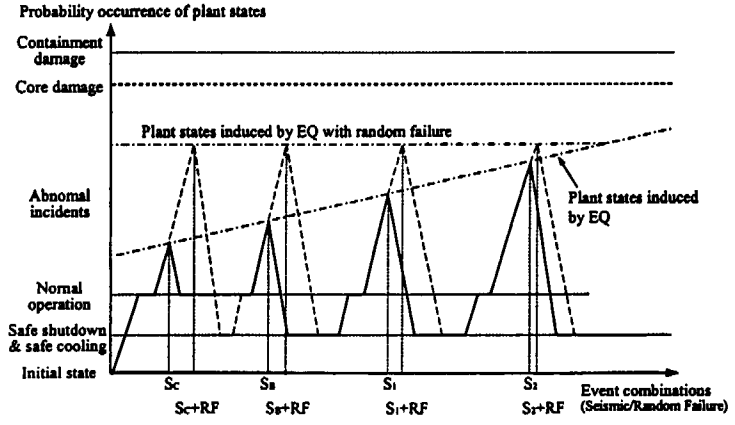

Figure 1 Plant safety levels related with earthquake events. The safety level is higher when the plant states closer to the normal operation.

UNCERTAINTY IN CURRENT SEISMIC DESIGN

Considering the uncertainty of variables, the seismic load and the seismic capacity of a plant can generally be represented by lognormal density functions. The design basis seismic loads and seismic capacity are determined considering the standard deviations, respectively, so that the loads exceedance capacity rates become negligibly small. The seismic loads of structures are derived from the collaborations both of the earthquake ground motions and structure responses. The earthquake ground motions from a seismic source can be predicted many numbers of different ground motions. In the current seismic design, plant-specific safety margin is secured deterministically between the design basis seismic load and seismic capacity based on the engineering judge in the face of risk insights that the safety might not be compromised by uncertainties as shown in the Figure 2. In the deterministic approach, the earthquake ground motion is generally determined as the most likely ground motion of occurrence at a site, such as the mean value derived from the most significant seismic source to a site. On the other hand, the earthquake ground motions might be considered all variations related with the occurrence frequency in the probabilistic approach. The variable range of seismic loads will become larger than deterministic one corresponding the earthquake ground motion variations. The risk of the probability of the seismic loads excess the seismic capacity becomes larger in the case of considering the variation of earthquake ground motions. The design basis seismic loads derived from the earthquake ground motion variations should not exceed the design basis seismic capacity at least in the reliable range of the ground motion variation from the seismological point due to the safety margin included in the seismic design. Current seismic design addresses this qualitatively but does not explicitly perform the quantitative confirmations. The determination of the reliable variation range of the extreme design earthquake ground motion S2 is necessary to explain rationally based on the risk information considering the influences of the uncertainty concerning the seismic safety assured by current seismic design. The accumulation of many strong earthquake ground motion records by the recent densely installed earthquake observations and disastrous earthquake experiences are developing the knowledge on the effects of source rapture process, source and site location relations, and deep soil structures to the earthquake ground motions.

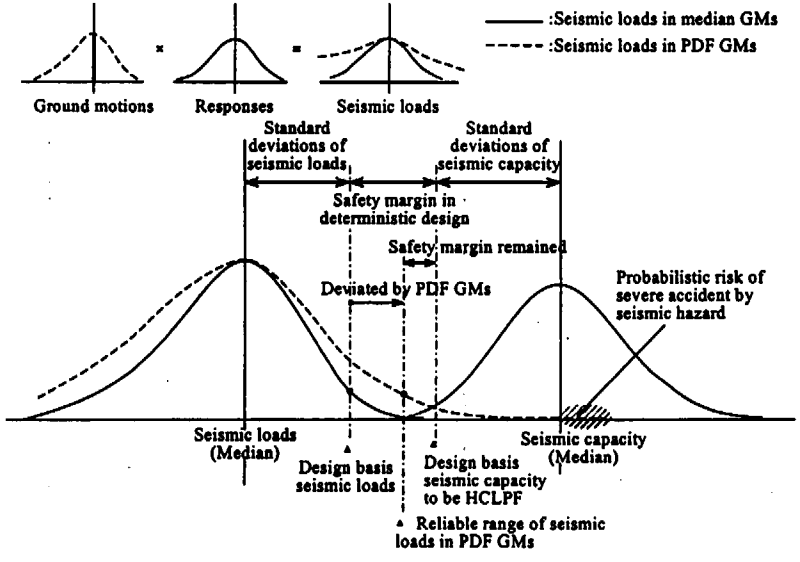

Figure 2 Concept of seismic safety margin in deterministic design. The safety margin should be remained in considerations of the ground motion variability in seismically reliable range.

EARTHQUAKE GROUND MOTION DERIVED FROM SOURCE

Seismic hazard and source characterization

The earthquake ground motions derived from a seismic source can be predicted many variety of different ground motions. The investigation to identify the characteristics of the sources existing around a site region is important to provide a systematic and comprehensive evaluation of the seismic hazard and its effects on the safe operation of nuclear power plants. Many seismic sources might exist, from the small to large magnitudes and from known active faults to unknown blind faults around a site region. These seismic sources should be characterized based on the past earthquake records, geological and geophysical surveys, and micro earthquake observations. Some of the blind seismic sources might be still remained unknown even after the investigations. As one of the way to represent the effects of seismic sources to a site, a seismic hazard curve is made by defining the annual frequency of exceedance in terms of levels of a ground motion intensity, such as peak ground accelerations, which can be correlated with the damage of critical structures, systems, and components (SSCs) into beyond the current design basis earthquake by the probabilistic seismic hazard analysis. From the site-specific hazard curves, a set of Uniform Hazard Spectrum as recommended in US NRC, may be obtained as the seismic design spectra. One of the objectives in developing seismic design spectra is to achieve approximate uniformity of seismic risk for the safety-related SSCs designed to those spectra, across a range of seismic environments, annual probabilities, and structural frequencies.

As shown in Figure 3, a seismic hazard curve is obtained by the contribution of many sources and the contribution rate of the sources to the annual exceedance of earthquake occurrence frequency is different by each source. The seismic safety assurance into the non-linear range of nuclear power plants consisted with the multiple dimensions and complex systems is essentially required that should be performed based on the dynamic response analyses using time domain earthquake ground motions. However, the determination of the earthquake ground motions from the seismic design spectra such as an envelope spectrum or a uniform hazard spectrum of seismic sources brings up another problem regarding the disconnection with the individual source characteristics. These should also accommodate uncertainty in the site-specific dynamic material properties as well as local and regional seismicity and attenuation characteristics.

The determination of an earthquake ground motion to envelop all the prediction is almost impossible. But, development of design basis earthquake ground motions to represent the effective earthquake ground motions could be possible. In order to include the influences of surrounding source effects in to the design basis earthquake ground motions, determination methods using envelope response spectra or uniform hazard spectra of multiple sources are usually employed. In current seismic design it is generally assumed that the DBEs represent the effects of earthquake ground motions by surrounding earthquake sources at proposed site using envelope response spectrum of influential earthquake ground motions with certain margin instead of using all earthquake ground motions predicted. However, the potential variations of ground motion deriver from the envelope response spectrum of the design basis ground motion are not explicitly explained.

The relationship between individual sources and the ground motions is not clear in this method. It is not sufficient to represent the earthquake influences only by the spectrum and maximum amplitude of ground motions. The earthquake influences to structures represented by the frequency contents of the amplitudes and phase of acceleration, velocity, displacement, impact force, etc., can be changed by the dynamic characteristics of structures. The seismic capacities of structures are also influenced by the accumulation of fatigue depending on the cycles and intensities of earthquake ground motions. Therefore, earthquake ground motions should be determined to represent the varied amplitude, frequency, and phase characteristics. This can only be done by sufficient numbers of time domain earthquake ground motions.

On the Relations Between
Seismological Data And Seismic Engineering Analyses
Istanbul, Turkey, 17 & 18 October 2002

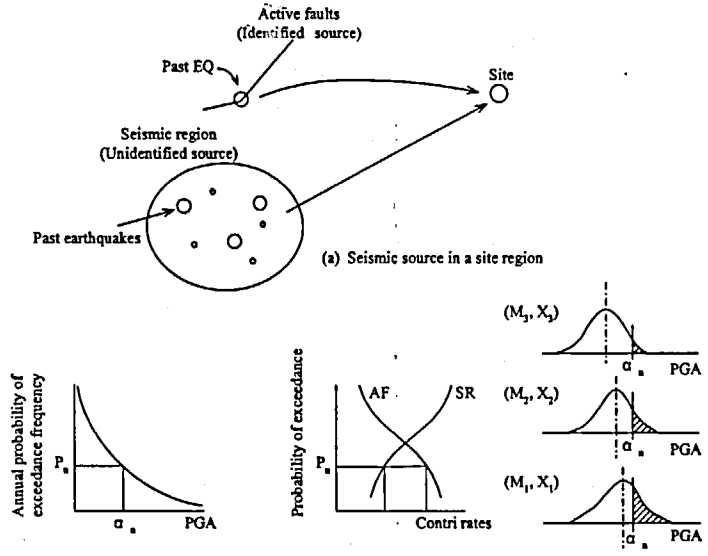

Figure 3 Source contributions to seismic hazard at a site. The each source contribution rates are changed according with the probability of exceedance frequency changing.

DBE for evaluation seismic impact on safety requirements

Nuclear power stations generally have several reactor units in a site. The earthquake ground motions in a site could vary at the each unit depend on the deep soil structures even though the up coming incident waves are same at the seismic base-rock at a site. The seismic impacts to multiple units in a site regarding the reactor safety and the radiation protection should be assured by the estimation based on the all units in a site. The design basis earthquake ground motions of the each unit are usually determined on the free field rock surface supposed depend on the location of the unit layout basically considering the incident upcoming waves could be defined on the seismic base-rock surface at a site. The reactor safety can be confirmed by the response analyses of each unit. The safety for the radiation protection should be confirmed based on the radiation dose rate by the total release of radiations from the all units in the site. As shown in the Figure 4, the evaluation of the seismic safety on multiple units is preferable to be performed in detail by response analyses using the earthquake ground motions on the seismic base-rock at a site considering the deep soil structures and the unit layout. The seismic response evaluation of a unit using earthquake ground motions defined on the rock surface at a site can be acceptable when the design basis earthquake ground motions at the rock surface is determined conservatively as the representative earthquake by selecting most severe condition for the unit in a site. The evaluation of the seismic safety for radiation protection regarding multiple units is also possible to estimate conservatively based on the summation of the each unit evaluations by the design basis earthquake ground motions defined on the rock surface. However, the estimation method might be too conservative and could be resulted to have excessive dose rate estimation to the public. In order to assure the reasonable radiation protection to the public by the evaluation more detailed, it is preferable to perform the seismic response analyses of the multiple units considering the plant layout using the earthquake ground motions defined on the seismic base-rock surface at a site. The wave reflection and refraction survey to investigate the seismic-base rock in the site can be presents useful information to the determination of the magnitude and location of blind faults.

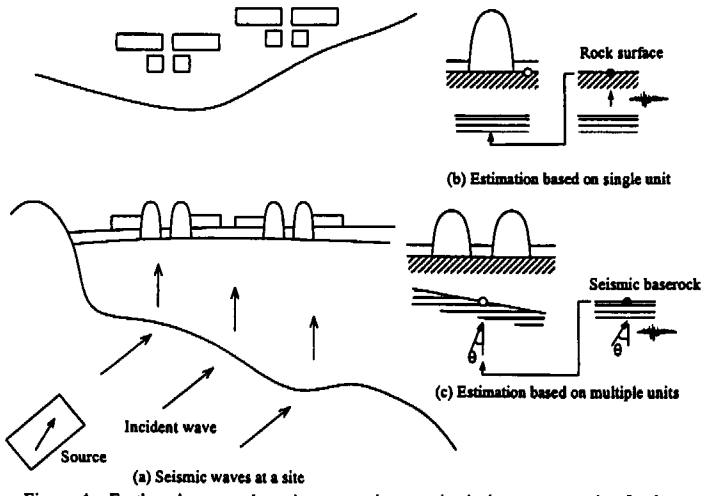

Figure 4 Earthquake ground motions to estimate seismic impacts at a site. In the estimation of seismic impacts, site responses due to deep structure have a major role.

RISK-INFORMED DESIGN BASIS EARTHQUAKE GROUND MOTIONS

Risk dominant earthquake informed by seismic PSA

The design basis earthquake ground motions should be risk-informed by the seismic PSA on the proposed site. This is so that the necessity of assuming the extremely large earthquake beyond the design basis earthquakes that could cause the damage of reactor core by the failure of the seismic capacity of almost all safety-related SSCs, is negligible from the point of the risk. The earthquake ground motions should be derived on the source of most significant contribution rate for the risk-dominant earthquake. Identification of dominant seismic risk contributors considering the uncertainties involved are an important process in a seismic design to enhance the reliability of the seismic safety assurance. The current results of seismic PSAs for existing nuclear power plants shows a tendency that the risk of core damage frequency caused by earthquakes are largely contributed by less severe initiating events. The large contribution rate of initiating events are, in the order from larger rate: loss of the offsite power accident (LOSP); small break loss of coolant accident (S.LOCA); medium break loss of coolant accident (M.LOCA); large break loss of coolant accident (L.LOCA); and reactor pressure vessel failure as shown in the Figure 5. The result shows the seismic risk is rather dominated by the failures of less important SSCs than high important SSCs according with the relations of the seismic hazard and fragility curves. The conditional core damage frequency by the each initiating event is shown to become larger along with the seismic load increasing until to show maximum peak at the certain earthquake level and then decreasing the risk curve. It indicates the risk-dominant earthquake is derived in the range of the initiating event of loss of offsite power accident (LOSP).

Current seismic PSA can confirm the necessary conditions of reactor safety by secure the success path of safety-related SSCs, but are not yet sufficient to confirm the design basis criteria of reactor safety performances that can be confirmed based on the time domain analyses of reactor behaviors on abnormal operation in seismic events. In order to assure the seismic safety of reactor facilities to the dominant earthquake events, integrities of structures and safety functions of the safety-related SSCs that are necessary to maintain reactor safety conditions in the seismic events should be evaluated by the dynamic response analyses using time domain earthquake ground motions. This is essential to confirm the reactor safety and also the safety for radiation to the public based on the estimation of radiation release derived from the failures of the SSCs.

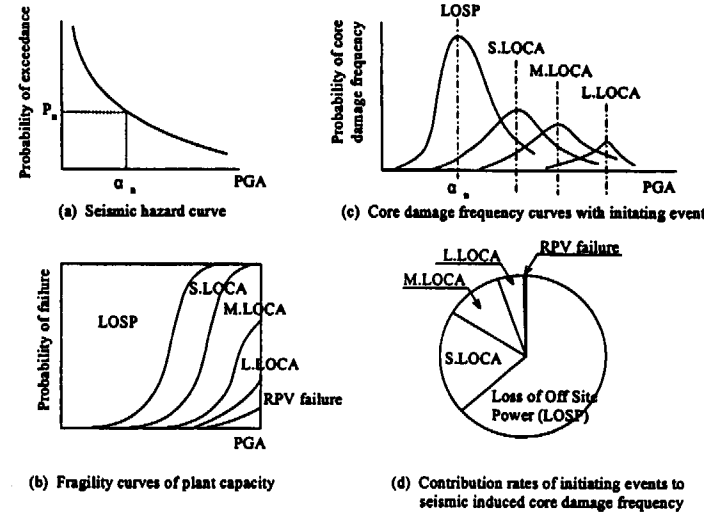

Figure 5 Risk information by seismic PSA

Development risk-informed DBE ground motions

When the risk-dominant earthquake ground motion intensity is obtained from the peak of the core damage frequency curve estimate, the probability of annual exceedance earthquake occurrence frequency of the dominant level earthquake is decided by the seismic hazard curve estimate. Then the seismic sources contributing the risk-dominant earthquake ground motion intensity are identified as shown in the Figure 6. The method to identify the seismic sources consistent with the occurrence frequency of the risk-dominant earthquake level is available by the studies of Ishikawa and Kameda (1995) [3] or JAERI [4]. The probability occurrence of the earthquake ground motions generated by the sources is distributed as a lognormal density function and the exceedance probability of the risk dominant earthquake level correspond at some deviations apart from the median to low occurrence rate depend on the each source contributions. The design basis ground motions by the risk-dominant seismic source should be derived the two types of ground motions, that are, the most likely earthquake ground motion for the extreme design earthquake S2 by the median exceedance probability and the ground motion by the low exceedance probability to be the risk-dominant earthquake.

The risk-dominant earthquake ground motion could be defined newly as the site evaluation earthquake Ss that could be used for the evaluation of the reactor safety by the plant seismic capacity with the criterion of high confidence low probability of failure (HCLPF), and also, for the evaluation of radiation safety to the public based on the radiation release by the failure of safety related SSCs on the multiple units in a site. The studies to obtain the time history of such low occurrence rate earthquake ground motions that is likely large deviated from the median were not much performed and the evaluation method to be acceptable is not yet established. The evaluation methods of such earthquake ground motions should be developed based on the numerical method considering the variation of the source rapture process parameters using seismic fault model. The new, high-quality data recorded in the near-fault region of recent large earthquakes are useful to source characterization such as spatial variations of slip, slip velocity, or rupture velocity for accomplish precise strong motion prediction by modern earthquake ground motion evaluation technology. In the numerical simulation methods to estimate the ground motions, a recipe for prediction of scenario earthquake strong ground motion caused by active fault by means of numerical analysis considering the spatial distribution of fault slip and the time function of slip on the fault has been proposed (Irikura, 2000)[5]. The influences by the factor of the earthquake such as acceleration, velocity, displacement, impact force etc. to the structures are different the significance depend on the dynamic response

characteristics of the objectives. The earthquake ground motions to be used in the evaluation of the seismic safety of the reactor facilities are necessary to be derived enough numbers of ground motions to represent the seismic impacts considering the many aspects required for the ground motions depend on the characteristics of objectives.

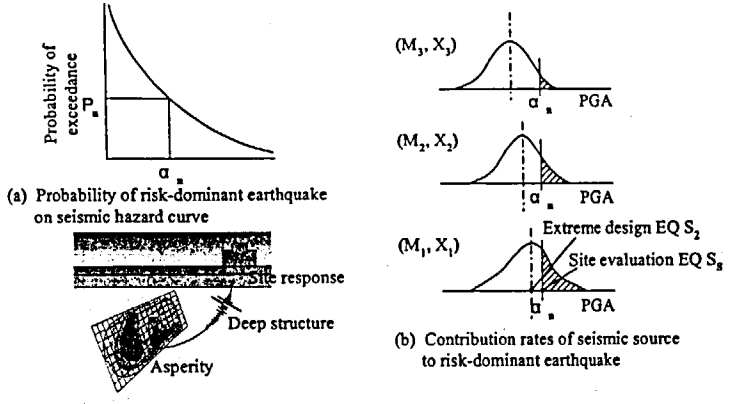

(a) Probability of risk-dominant earthquake on seismic hazard curve

(b) Contribution rates of seismic source to risk-dominant earthquake

(c) Risk-dominant earthquake ground motion prediction by numerical methods

Figure 6 Risk-dominant earthquake ground motion methodology.

Improvement comply with risk information

The other aspects to utilize the risk information by the seismic PSA are the improvements of the risk contribution rate distributions to be uniformed if it is inclined too much to the less important event, and also, if the risk-dominant earthquake level is smaller than the extreme design earthquake S2 it should be improved the seismic vulnerability to be beyond the S2. The contribution rate of the initiating events for the core damage frequency is generally inclined to the events induced by the failures of not much important facilities for reactor safety such as the LOSP. This tendency of the risk contribution rate could be improved to be uniformed the distribution by grade up of the seismic integrity of the mitigation systems of safety-related SSCs to mitigate the influences of the LOSP accident that are usually considered un-important as shown in Figure 7.

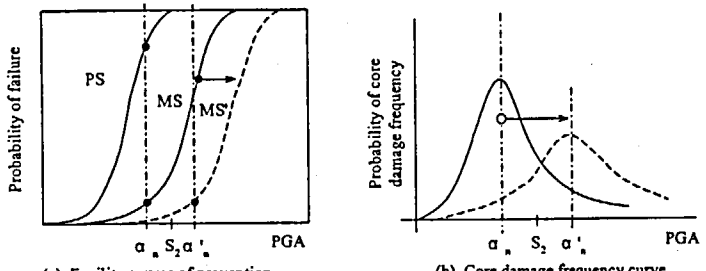

(a) Fagility curves of prevention and mitigation systems

(b) Core damage frequency curve

Figure 7 Improvement of seismic vulnerability to uniform risk contribution rate of controlling events.

CONCLUSION

The seismic design of nuclear power plants should evolve by considering quantitatively the risk induced by earthquakes to be more consistent with the nuclear safety philosophy. Concerning the risk information in a seismic PSA, seismic design should be performed including the risk dominant level earthquake. A development of the risk-informed design basis earthquake ground motions methodology was discussed and summarized here.

First of all, the risk-dominant earthquake level should be identified by the preliminary seismic PSA at the proposed site in the site-licensing phase. If the dominant earthquake level is smaller than the extreme design earthquake the seismic vulnerability should be improved to be beyond the S2.

The extreme design earthquake S2 is not enough to explain the safety beyond DBEs. The DBE ground motions by the risk-dominant seismic source should be used to derive the two types of ground motions that are the most likely earthquake ground motion for the extreme design earthquake S2 by the median exceedance probability and the ground motion by the low exceedance probability to be the risk-dominant earthquake in order to assure the safety beyond DBEs.

The risk-dominant earthquake ground motion could be defined newly as the site evaluation earthquake Ss that could be used for the evaluation of the reactor safety by the plant seismic capacity with the criterion of high confidence low probability of failure (HCLPF), and also, for the evaluation of radiation safety to the public based on the radiation release by the failure of safety-related SSCs on the multiple units in a site.

The numerical evaluation methods are useful for determination the time domain ground motions of the site evaluation earthquake Ss consistent with the probability of exceedance occurrence rate of risk-dominant earthquake by the seismic source of most significant contribution. The time domain earthquake ground motions should be employed, with several different time histories needed to represent sufficiently the seismic impact to the safety-related SSCs.

The seismic performance confirmations by the other design basis earthquakes such as Sc, Sb, and S1 defined by the current examination guide are also important for the safety management. The DBEs should be defined explicitly the relations with the probability of annual exceedance occurrence frequencies so that the event combinations considering random failures and human factors can be rationally employed for the safety managements in reactor operations.

ACKNOWLEDGEMENTS

The on going discussions for modernization of the current Examination Guide for Seismic Design on NPPs under the Special Committee on Safety Standard in the NSC inspired the author's view that is greatly appreciated.

DISCLAIMER

The views expressed in this paper are those of author and should not be construed to reflect the official Japanese NSC position.

REFERENCES

1. Oikawa, T., Kondo, M., Watanabe, Y., Shiraishi, I., Hirose, J. and Muramatsu, K., "Sensitivity Analyses for the Effects of Uncertainty Issues on Risk Contributors in a Seismic PSA of the BWR Model Plant at JAERI," Proceedings of the OECD/NEA Workshop on Seismic Risk, Tokyo, August 1999
2. Sakagami, M. and Hirano, M., "Comparison of Trial Seismic PSA and Seismic Margin Analysis for a BWR" Proc. of PSAM5, Osaka, 2000
3. Ishikawa, Y. and Kameda, H., "Hazard-consistent Magnitude and Distance for Extended Seismic Risk Analysis," Proc. of 9th WCEE, Vol. II, pp.89-94, 1995
4. Takada, T., Okumura, T., Hirose, J., Muramatsu, K., Taki, S. and Ishii, K., "Probabilistic Scenario Earthquake for Seismic Design – Comparison of Two Identification Procedures" Proceedings of the OECD/NEA Workshop on Seismic Risk, Tokyo, August 1999
5. Irikura, K., "Prediction of Strong Motion From Future Earthquakes Caused by Active Faults-Case of the Osaka Basin," Proc. Of the 12WCEE, Auckland, 2000

DISCUSSIONS ON IMPROVING JAPANESE "EXAMINATION GUIDE FOR ASEISMIC DESIGN OF NUCLEAR POWER REACTOR FACILITIES"

Kenji Takashima and Shuji Kawahara
Nuclear and Industrial Safety Agency,
Ministry of Economy, Trade and Industry (METI), Japan

Abstract

Various technologies related to seismic design have been advanced, since "Examination Guide for Seismic Design of Nuclear Power Reactor Facilities" was established 20 years ago. Through the experiences of big earthquakes including the Hyogo-ken Nanbu Earthquake (Kobe Earthquake), the latest knowledge related to earthquakes and earthquake ground motions has been accumulated. By taking into account these circumstances, it is commonly recognized by Japanese experts on seismology and seismic engineering that some improvement in the Examination Guide for Nuclear Power Plants is necessary to enhance the reliability of seismic safety of nuclear facilities based on the latest knowledge. In this paper we introduce the state-of-the-arts of the study on improving Japanese "Examination Guide" and some key points of the discussions on the improvement.

Introduction

The current Japanese "Examination Guide for Seismic Design of Nuclear Power Reactor Facilities" (Examination Guide) was established 20 years ago [1]. Since then various knowledge and technologies related to seismic engineering have been advanced through the experiences of big earthquakes including the Hyogo-ken Nanbu Earthquake (Kobe Earthquake) [2]. During this period, METI has also contributed the advancement of the knowledge and technologies as a regulating agency by undertaking numerous projects to enhance seismic reliability and to improve seismic design methodology of Nuclear Power Plants (NPPs). These projects have also contributed to upgrading the rationalization of seismic design of NPPs. In addition, knowledge concerning earthquakes has progressed greatly and a large number of earthquake ground motion records have been accumulated. By taking these facts into account, it is commonly recognized by Japanese experts on seismology and seismic engineering that some improvement in the Examination Guide for Nuclear Power Plants is necessary to enhance the reliability of seismic safety of nuclear facilities based on the latest knowledge.

The basic items to be discussed among the experts in regards to improving the Examination guide are roughly grouped into the following three categories:

Items related to the logical structure of seismic design evaluation criteria:
- Definition and framework of seismic safety,
- Relationship between deterministic and probabilistic approaches,
- Review of SSC (System, Structures, and Components) classification on the basis of their seismic safety importance,
- Performance regulation for advanced technologies including new siting methodologies.

Items related to the criteria for determining the design basis ground motion:
- Identification and characterization of seismic sources to be considered,
- Methodology to estimate design basis earthquake including fault model,
- Introduction of probabilistic approach,
- Requirements for geological, seismological, and geophysical investigation of plant region,
- Evaluation of seismically induced hazard sources including tsunami and eruption.

Items related to the criteria for assuring integrity of systems, structure, and components:
- Determination of design basis earthquake motion (method, single or multiple, horizontal and vertical components),
- Methodologies for earthquake response analysis of SSC,
- Method for stress analysis of SSC,
- Load combination,
- Allowable limit for assurance of functionality of SSC,
- Allocation of safety margin, consideration of reliability based structural design approach.

To date, the discussion is being focused on the following items as:
1. Evaluation of near field earthquakes (how to determine design earthquake ground motion),
2. Clarification of the concept for securing seismic safety:
   How to introduce Seismic Safety Goals,
   How to evaluate seismic safety quantitatively (e.g., application of seismic PSA).

In this paper, we firstly introduce the activities of METI as a regulating agency relating to the examination guide mostly aiming at proving and confirming the procedure of the current design practice as well as upgrading the design methodologies.

Then we describe our recent activities to study how to introduce probabilistic approaches to seismic design examination processes.

Activities of METI in The Seismic Engineering Field

METI has been carrying out many projects covering the whole area of seismic engineering to comprehend and resolve the various issues from the viewpoint of a regulation agency as follows;
- earthquake ground motion (near field earthquake and the ground motion propagation)
- earthquake response of structures and equipment (shaking table test and field test)
- upgrading of seismic design engineering (new siting issue and study of vertical motion).

Besides the above, we are studying probabilistic methodologies to handle the uncertainties relating to seismic design of NPPs. However handling of the uncertainty becomes big argument in the discussion of revising the guidelines. Therefore we introduce the studies in the next chapter together with the discussion. And here we introduce the projects described above carried out to briefly elucidate the phenomenon relating to seismic issues [3].

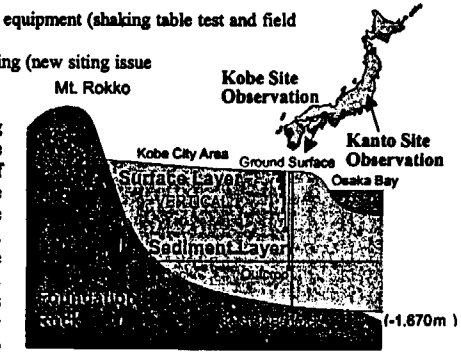

Fig.1 The Earthquake Observation Well at Kobe Site.

Earthquake ground motion

Seismic Wave Propagation in The Vertical Direction (FY1994-2004)

The major objective of the project is to study the characteristics of seismic wave propagation from seismic bedrock to the current seismic design ground motion definition outcrop level. The study is being carried out using earthquake observation data collected by seismometers set at depth of from the surface to seismic bedrock since 1998 and will be terminated by 2002.

Figure 1 shows a cross sectional outline of the earthquake observation well at the Kobe site. The depths of earthquake observation wells are 1,700m at the Kobe site and 1,200m at Kanto Plane site.

Strong Ground Motion Study in the Near Field (FY1998-2002)

The major objectives of the project are to study strong ground motions by near field earthquakes and to advance evaluating methodology of near field earthquake ground motion. Figure 2 shows earthquake ground motion data caused by near field active faults being used in this project. The data are used to study the relationship between fault parameters and strong ground motion characteristics. The study is being carried out using recent fault models. We have performed simulation analyses to check, and modified the fault model. Then the results are reflected to advancing the fault models and evaluation methodologies for the near field strong ground motion.

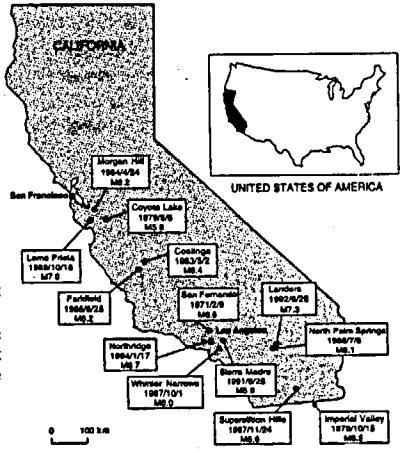

Fig.2 Near Field Earthquake Ground Motion Data Being used in this project

Earthquake Response of Structures and Equipment

The earthquake response of structures and equipment of NPP has been a big concern of METI. Thus, we have carried out many test projects. In the following section we briefly introduce the outlines of the projects.

Structural Response Study

Our efforts have been mainly toward structures, more specifically, the soil-structure interaction (SSI) and the nonlinear characteristics of reinforced concrete (RC) shear walls. Figure 3 shows a snap-shot of an SSI test project.

In the SSI test, we have accumulated a large volume of earthquake observation data. The test data have been used to check the applicability and to confirm the appropriateness of analytical methodologies of SSI.

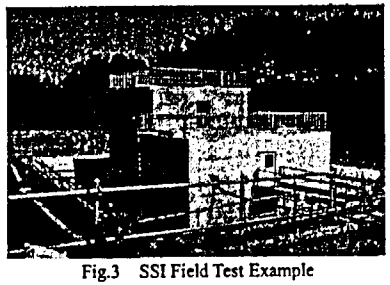

Fig.3 SSI Field Test Example (Reactor and Turbine Building Modes)

Also in the RC shear wall test, we have accumulated various data to predict dynamic nonlinear behavior of RC buildings during earthquakes up to their failure, including under the multi-axis loading condition. The test data have been used to evaluate seismic design margins of RC building to the design earthquake ground motions.

Equipment Response Study

We have been carrying out equipment response studies as the seismic proving tests of NPP installations for over 20 years. Up to the present, fourteen projects have been completed and three projects are on going. The seismic proving tests have been conducted in the four stages, i.e., (1) demonstration of structural integrity of massive and heavy components, (2) proving of functional integrity of safety systems, (3) demonstration of newly developed equipment, and (4) confirming seismic margins of equipments.

Figure 4 shows an example of item (2), the proving test of the reactor shutdown cooling system.

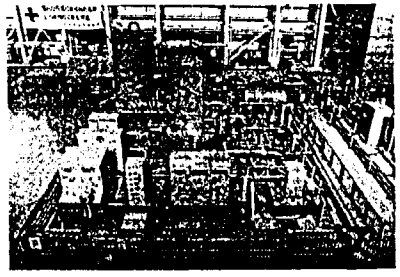

Fig. 4 The Seismic Proving Test of Reactor Shutdown Cooling System

The mission of the seismic proving test has been changed gradually over these 20 years from item (1), demonstration of seismic integrity of major components, to item (4), check of functional integrity and/or seismic margins of equipment.

Figure 5 shows conceptual drawing of a new test project started this year (2002-2004). The test applying sub shaking table on the Tadotsu Shaking Table that amplifies input motion to the specimen up to 6g of maximum acceleration to confirm functional integrity of electric panels and horizontal pumps.

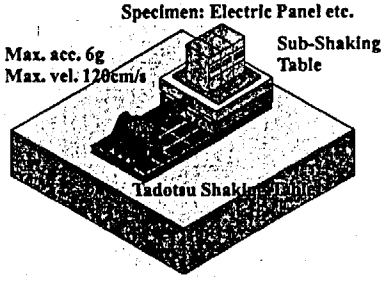

Fig.5 Conceptual Drawing of Functional Integrity Test (Using Vibration Amplification Device)

Upgrading of Seismic Design Engineering

The purpose of the study is to upgrade seismic design engineering from the viewpoint of a regulatory agency. Belonging to these technical issues are new siting technologies and handling of vertical motion in seismic design.

The study of new siting technologies has been carried out with the aim of expanding the possibility of future NPP construction sites because current standards for NPP siting require that NPP should be constructed on bedrock.

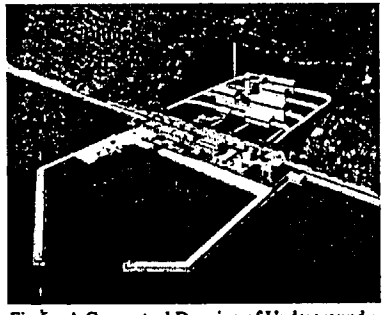

Fig.6 A Conceptual Drawing of Underground Siting of NPP

The new siting technologies we have investigated are quaternary deposit siting, underground siting and artificial island siting. Figure 6 shows a conceptual drawing of an NPP sited underground. Our major mission in this new siting study is to develop a preliminary version of evaluated guidelines for future NPP site applications.

Beside this, the study of upgrading seismic design engineering has been undertaken to improve the methodologies of handling vertical earthquake ground motion, to create analytical building models and components for evaluating the earthquake response to vertical motion, and to handle nonlinear analysis of piping systems.

Study on Seismic Probabilistic Safety Assessment

METI has carried out a study on Seismic Probabilistic Safety Assessment (SPSA) as a part of the probabilistic safety assessment study to understand its scheme and applicability to Japanese NPPs. Figure 7 shows an outline of the SPSA used in the study. The SPSA methodology used is based on the precedent studies in US [4].

In order to do the SPSA, realistic responses of buildings and components to earthquake ground motion are calculated using the Monte Carlo response analysis method considering modeling uncertainties directly or using the response factor method that deals the uncertainties indirectly. In the latter method, the response factor is defined as the ratio of design response to realistic response excluding all conservatism introduced in the seismic design.

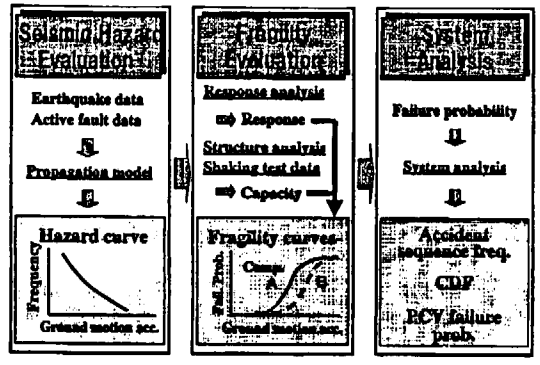

Fig.7 An Outline of The SPSA Used in The Study

The response factors obtained for each component group in advance are applied to obtain the realistic responses. Then probabilistic distribution of capacity of components, which is the intensity of earthquake motion leading to its malfunction or failure, is evaluated realistically based on design information, literature surveys for an existing evaluation or test data. The probability distributions of the capacity and realistic response are used to calculate the component failure probability for each level of earthquake motion.

System vulnerability is evaluated by applying the component failure probability to a fault tree model to obtain the conditional core damage probability as a function of, for example, the maximum acceleration at the bedrock. The core damage frequency due to earthquakes is calculated by integrating the conditional core damage probability over the whole range of the ground motion with the seismic hazard curve.

Discussion on Improving Examination Guide

As described in the previous section, current deliberation to revise the Examination Guide in the Nuclear Safety Commission (NSC) of Japan is focused on the issues of clarification of the concept for securing seismic safety and of the evaluation methodologies of design earthquake ground motions.

Concerning the clarification of the concept for securing NPP seismic safety, there are some expectations for introducing probabilistic approaches to the Examination Guide to resolve seismic issues relating to uncertainties in determining design earthquake ground motion and in evaluating earthquake response of structures and components. However at the same time, there are also experts of the opinion that the committee should not have too many expectations for the probabilistic approaches for seismic design evaluation.

For the other issue, the discussion is being carried out as to how to consider the design earthquakes. Current design earthquake ground motions for an NPP in Japan are typically defined by the so-called Ohsaki Spectra. An earthquake ground motion defined at an NPP site based on the Ohsaki Spectra by taking into account the earthquake magnitude and focal distance of probable big earthquakes, that would affect the NPP site, has been considered as the biggest ground motion on the bedrock in that condition.

In this chapter, we firstly describe the issues related to the discussions on design earthquake ground motion then we describe the probabilistic approaches that are expected to be introduced in the framework of the revised examination guide.

Definition of Design Earthquake Ground Motion

In the preliminary discussion we are talking on both deterministic and probabilistic methodologies as to how to apply them to the revised design guide.

Deterministic Approach

In these past 20 years we have accumulated many records of earthquakes that have occurred in Japan and surveys of active faults in land and submarine areas have been unveiled. In accordance with the development of such research, studies on the relationship between active faults and the maximum magnitude of an earthquake that is supposed to occur in the future at the site in concern have been conducted.

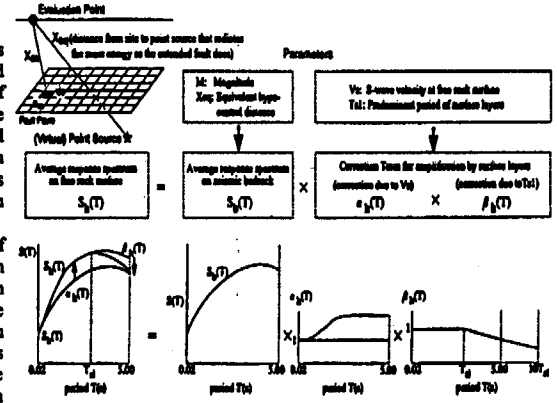

Fig. 8 The Outline of The Proposed Empirical Method for Evaluating Design Response Spectra for an NPP Site [5]

Based on the results of these studies, an empirical method for evaluating response spectra for an NPP design earthquake ground motion has been proposed. Figure 8 shows the outline of the proposed method. In this method, averaged response spectra of horizontal and vertical ground motions between the periods of 0.02 and 5 seconds at a site on rock surfaces are evaluated by the product of those earthquake ground motion spectra on seismic bedrock and the correction terms which take in the amplifications effect of horizontal and vertical motion due to surface layers.

The introduction of the vertical motion can makes the vertical seismic load rationalize, because the vertical load is taken as a static load (based on the half the level of the horizontal peak acceleration) in the current seismic design practice. The features of the proposed design earthquake ground motions point out that it takes diverse tectonics into account and is defined based on averaged levels of observed earthquake ground motions. Therefore in applying the ground motion to an NPP design, we have to consider the effect of the variations from the average levels [5].

In order to cope with this issue, we can propose a measure that introduces a seismic margin earthquake, having a maximum acceleration level exceeding that of the design earthquake, e.g., by one standard deviation on the averaged level. However, this methodology might lead to an overly pessimistic result for existing NPPs and result in excessively conservative designs for new NPPs. Therefore cautious consideration based on statistics of earthquake records is required in introducing the seismic margin earthquake.

Other concerns of the NPP design earthquake ground motions are the issues on near-field earthquake ground motions. Damaging ground motions due to earthquakes in far and intermediate fields were caused by strong magnitude earthquakes (typically larger than Mw6.5). These earthquakes had generated some traces (faults) on the ground surface, thus we can evaluate the potential earthquake occurrence in the near future with considerable high reliability by taking into account the results of detailed field surveys of faults around an NPP site. On the other hand, a near field earthquake has a severely damaging potential even for weak magnitude earthquakes. This kind of earthquake in the past might have left no traces on the ground surface. In such a case, we cannot identify any evidence of the earthquakes having happened whereas there might be a possibility that some weak magnitude potentially destructive earthquakes had occurred near the site in concern. Therefore the seismic design system should be formulated to take into account the risk e.g., introduction of seismic margins in the design ground motion, structures and equipment.

Probabilistic Approach

In order to take into consideration the possibility of unidentified near field earthquake ground motion in the seismic design of NPPs, we are facing the needs to introduce some probabilistic approach for determining the design earthquakes.

For this purposes, the seismic hazard evaluation methodology is promising. There are several precedents that propose the application of the seismic hazard evaluation in the

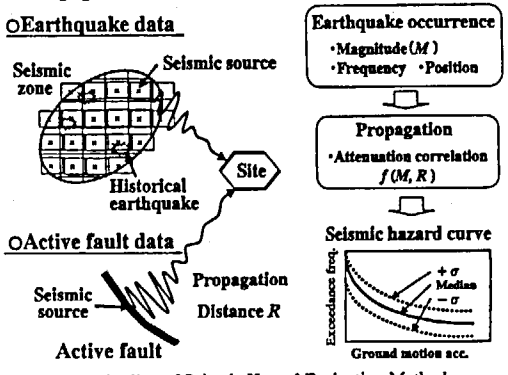

Fig.9 Outline of Seismic Hazard Evaluation Method

establishment of seismic the design review guide, including that of USNRC [6] and [7].

The seismic hazard curve defined as a relation between intensity of ground motion at a specific site expressed in terms of the maximum or spectral acceleration of the bedrock of the site, a, versus annual frequency that the intensity of ground motion exceeds a is estimated based on the data of seismic activity around the site and attenuation model for seismic ground motion as shown in Fig.9.

In the seismic hazard analysis we propose to use both historical records of earthquakes and active fault data for the evaluation of the seismic hazard at the site as follows:

1) Grids having historical records of sources of earthquakes in Fig.9 are set as earthquake regions around a site. The occurrence frequency of a ground motions at each ground motion level at the site is calculated for each grid, considering the statistical distributions of the magnitude and frequency of earthquakes expected to occur at the grid and the attenuation of the ground motion propagating to the site. The relationship between the frequency and the magnitude of earthquakes in a grid is expressed as a simple correlation between the magnitude and the number of occurrences obtained from the historical earthquake records.
2) The occurrence frequency of ground motions at each ground motion level at the site is calculated for each active fault around the site. The earthquake magnitude is determined with an empirical equation, which relates it with the length of the active fault and the occurrence frequency estimated from the observation of fault dislocation and the displacement velocity at the active fault.
3) The seismic hazard for the site is obtained by summing up the above two occurrence frequencies.

One of the issues in this process of seismic hazard evaluation is the existence of a large uncertainty in the attenuation models, resulting in a large uncertain range of seismic hazard level at a given frequency of exceedance. To reduce this uncertainty, JAERI developed a procedure for mechanistic prediction of seismic ground motion under the guidance [8] based on the "fault model". The model is defined by parameters that describe the characteristics of hypocenter, propagation pass and site, as illustrated in Fig.10. We (NUPEC/METI) have developed a methodology to evaluate ground motion due to diffusive earthquakes from unidentified faults near and/or/ around the site more precisely than ever, by treating the timing, location and magnitude of earthquakes statistically, together with the revised b-value model [9].

We also propose to utilize the solicitation of expert judgments in the processes to characterize both seismic sources and ground motion propagation and quantify the uncertainty in the hazard curve at the site. The task is to determine a design basis ground motion based on the analysis of seismic hazard at the site in concern. An issue of the deliberation was how to deal with uncertainties in the identification of seismic sources around an NPP site and in the prediction of the frequency of earthquakes expected to occur at the sources [10].

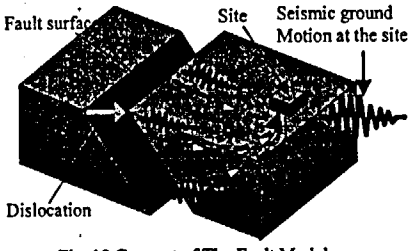

Fig. 10 Concept of The Fault Model

Application of SPSA

It is widely recognized in Japan that a lot of proof tests and tests-to-failure have been conducted to ensure that there is substantial margin in the capacity of the SSC in the framework of the current seismic design evaluation criteria. Nevertheless, many opinions have arisen that require quantitative seismic margins of the SSC.

Furthermore, a quick review of the basic items being deliberated among the experts for improving the Examination Guide described in the introduction of this paper suggested to us that important common issues of the deliberation are closely related to the uncertainty in the identification of seismic sources, earthquake response of the SSC of NPPs and seismic margins of the SSC. These uncertainties are already taken into consideration in the current seismic design evaluation criteria independently in the determination of both design base seismic loads and the acceptance criteria for responses of the SSC. However, some experts insist that it is important to evaluate the seismic safety of a plant under the existence of these uncertainties as transparently as possible. From this viewpoint, the experts require the evaluation of the seismic risk of NPPs by taking those uncertainties into account as rationally as possible [10].

For that reason, application of the SPSA methodology is now under discussion as for a tool for evaluating the seismic safety of the NPPs that have been designed. Some experts propose introducing SPSA more positively together with a probabilistic safety goal such as defined in the IAEA Safety Guide to the seismic safety evaluation of NPPs at the occasion of the revision of the seismic design evaluation criteria of the Nuclear Safety Commission of Japan.

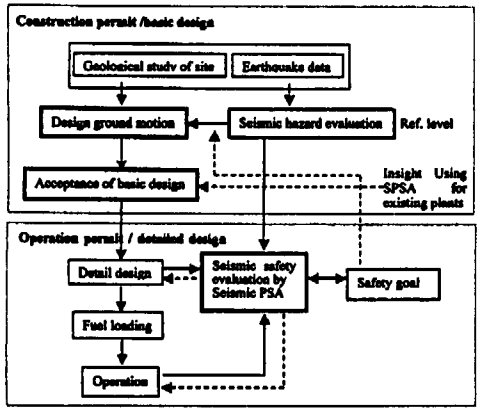

Fig.11: Schematic Diagram of The Proposed Framework of Seismic Design Safety Evaluation

The schematic diagram of the proposed framework for seismic safety evaluation is shown in Fig.11, which is composed of design basis earthquake (DBE) determination based on the seismic hazard evaluation, acceptance criteria for the responses of safety-related SSC to the DBE at the basic design review, and acceptance criteria of seismic risk of the NPP obtained by SPSA at the detailed design review.

Discussion on Application of the Probabilistic Approach to The Examination Guide

As described in the previous sections, the trend of the discussions on the revision of the examination guide is toward the introduction and/or application of a probabilistic approach. Therefore discussions among the experts are naturally focused on the application of probabilistic approaches. In this section, we will introduce some of the discussion points.

Application of the probabilistic method on the determination of DBE

One point for discussion on determining the DBE is whether the DBE based on seismic hazard analysis is sufficiently reliable as compared with the conventional determining of the DBE. Some experts in seismology point out that even though the phenomena related to the occurrence of earthquakes are gradually being unveiled, understanding is still very limited. Therefore the evaluation of parameters related to the probability of the failure of the future occurrence is still difficult.

Acceptance criteria for the responses of buildings and components

Many experts support the opinion that the SPSA will play an important role in evaluating existing plants under the revised examination criteria. Furthermore the SPSA should have a proper position in the revised criteria, as for the measurement of an integral check of the validity of seismic design.

Issues Related to Uncertainties in SPSA

It is recognized that there are uncertainties in the risk estimation by SPSAs not only that due to the uncertainty of input data such as common cause failure rates but also due to variations in the success criteria of safety systems functions. However, as PSAs include efforts to quantify these uncertainties as transparently as possible, even by explicitly and systematically requiring expert judgments, the results can be used to rank safety systems and to make decisions that have an impact on plant safety that take risk and uncertainty into account.

Issues in Application of Safety Goals

The opinion, of introducing SPSA into the examination guide, simultaneously aims at introducing seismic safety goals, such as that the core damage frequency for any given year should be below the value of, for example, 10^{-5}. In this framework of the seismic design, the result of the SPSA can be used in the detailed examination of the seismic safety evaluation, including a check as to whether the plant design is consistent with the safety goals. If the safety goals were not being met, modifications in plant design would be required.

However, as for the discussion on the safety goals, some experts are worrying about the evaluation results. This is because as it has been described in relation to uncertainty issues, the results of SPSA contain a large degree of uncertainty, thus the determination of the safety goals without deep consideration might be a cause of confusion in the design and/or operation of NPPs.

CONCLUDING REMARKS

Modification of the Japanese NPP design evaluation criteria has been under investigation since 2001 by the Nuclear Safety Commission (NSC) of Japan. As for the background of this revision, there is a common recognition that the knowledge and technology related to seismic design for NPPs has advanced significantly in the past 20 years. In this paper, at first we introduced the activities the Ministry of Economy, Trade and Industry of Japan (METI) toward improving NPP seismic design technology, and then we introduced the major discussion issues in the deliberations by the committee organized by NSC, i.e., the definition of design basis earthquake ground motion and the application of probabilistic approaches to the examination guide. Although the discussions are now underway and no concrete conclusion has yet been reached, there are apparent trends toward introducing some probabilistic approaches into the framework of the revised examination guide. However, at the same time, there are wide discrepancies among the opinions of experts regarding their expectations from these probabilistic approaches. From now on, from our perspective as a regulatory agency, we will watch and listen to the opinions cautiously, and these opinions will play an important role in developing the new examination Guide.

REFERENCES

[1] Government of Japan: "Convention on Nuclear Safety National Report of Japan for Second Review Meeting", October 2001.

[2] Kenji Takashima, Kunihiro Yoshimura: "Conception des centrales nucleaires pour les evenements externes naturels au Japon", Controle, La protection contre les risques externes, pp.53-55, Sep. 2001. (in French)

[3] NUPEC: "ANNUAL REPORT 2001" – OUR ACTIVITIES IN FISCAL 2000), Nuclear Power Engineering Corporation. <URL>http://www.nupec.co.jp.

[4] USNRC: "PRA PROCEDURE GUIDE", NUREG/CR-2300 Vol.2, January 1983, U.S. NRC.

[5] Isao Nishimura, Shizuo Noda, Katsuya Takahashi, Masayuki Takemura, Susumu Ohno, Masanobu Tohdo, and Takahide Watanabe.: "Response Spectra for Design Purpose of Stiff Structure on Rock Sites", *Trans. SMiRT 16, Washington DC,USA, August 2001, Paper#1133, CD-ROM.*

[6] Murphy A.J., Chokshi N.C., McMullen R., Kenneally R., Shao L.C. and Rothman R.: Revision of Seismic and Geologic Siting Criteria, *Trans. of SMiRT 14, Lyon, France, Aug. 17-22 1997.*

[7] IAEA Safety Guide 50-SG-S1: Earthquakes and Associated Topics in Relation to Nuclear Power Plant Siting, 1991; IAEA Safety Standards Series DS-302 (Draft) Seismic Hazard Evaluation for Nuclear Power Plants, 2001.

[8] Kameda H., Hagio K. and Sakagami M.: Study on Methodology of Seismic Hazard Evaluation in Japan, *Proc. of OECD/NEA Workshop on Seismic Risk, Tokyo, Japan, Aug.10-12 1999.*

[9] Utsu T.: A Three-Parameter Formula for Magnitude Distribution of Earthquakes, *J. Phys. Earth*, 22, pp.71-85, 1974.

[10] S. Kondo, M. Sakagami, K. Ebisawa and M. Hirano: "A PROBABILISTIC APPROACH FOR SEISMIC SAFETY EVALUATION OF NUCLEAR POWER PLANTS", *Proc. PSAM 6, Probabilistic Safety Assessment & Management 6, San Juan, Puerto Rico, USA, June 23-28 2002, CD-ROM.*

SEISMIC GROUND MOTION MODELLING AND DAMAGE EARTHQUAKE SCENARIOS A BRIDGE BETWEEN SEISMOLOGISTS AND SEISMIC ENGINEERS

G.F. Panza[1,2], F. Romanelli[1]
[1]Dipartimento di Scienze della Terra - Universita' di Trieste
[2]The Abdus Salam International Center for Theoretical Physics – Miramar, Trieste
panza@dst.univ.trieste.it, romanel@dst.univ.trieste.it

F. Vaccari
INGV - Oss. Vesuviano, c/o Dipartimento di Scienze della Terra - Universita' di Trieste
vaccari@dst.univ.trieste.it

L. Decanini, F. Mollaioli
Dipartimento di Ingegneria Strutturale e Geotecnica - Universita' di Roma "La Sapienza"
Luis.Decanini@uniroma1.it, Fabrizio.Mollaioli@uniroma1.it

Abstract

The input for the seismic risk analysis can be expressed with a description of "groundshaking scenarios", or with probabilistic maps of perhaps relevant parameters.

The probabilistic approach, unavoidably based upon rough assumptions and models (e.g. recurrence and attenuation laws), can be misleading, as it cannot take into account, with satisfactory accuracy, some of the most important aspects like rupture process, directivity and site effects. This is evidenced by the comparison of recent recordings with the values predicted by the probabilistic methods.

We prefer a scenario-based, deterministic approach in view of the limited seismological data, of the local irregularity of the occurrence of strong earthquakes, and of the multiscale seismicity model, that is capable to reconcile two apparently conflicting ideas: the Characteristic Earthquake concept and the Self Organized Criticality paradigm.

Where the numerical modeling is successfully compared with records, the synthetic seismograms permit the microzoning, based upon a set of possible scenario earthquakes. Where no recordings are available the synthetic signals can be used to estimate the ground motion without having to wait for a strong earthquake to occur (pre-disaster microzonation). In both cases the use of modeling is necessary since the so-called local site effects can be strongly dependent upon the properties of the seismic source and can be properly defined only by means of envelopes.

The joint use of reliable synthetic signals and observations permits the computation of advanced hazard indicators (e.g. damaging potential) that take into account local soil properties. The envelope of synthetic elastic energy spectra reproduces the distribution of the energy demand in the most relevant frequency range for seismic engineering. The synthetic accelerograms can be fruitfully used for design and strengthening of structures, also when innovative techniques, like seismic isolation, are employed.

For these reasons the skill of seismology to estimate realistic ground motions at a particular site should be fully exploited by seismic engineers. In fact, even if recently strong motion records in near-fault, soft soil, or basin conditions have been obtained, their number is still very limited to be statistically significant for seismic engineering applications.

1. Introduction

Earthquakes, as many other natural disasters, have both immediate and long-term economic effects. Within a fraction of a minute, single earthquakes can inflict damage to houses, business, government buildings, and infrastructures. A single earthquake may trigger a global ecological catastrophe, cause up to thousands of casualties and global economic depression: the disruption of commerce will affect the rate of economic growth, inflation, productivity and trade balance.

Case studies of seismic hazard assessment techniques indicate the limits of the currently used methodologies, deeply rooted in engineering practice, based on a probabilistic approach. The probabilistic analysis supplies indications that can be useful but-not sufficiently reliable to characterize the seismic hazard.

The mathematical modelling, with different degrees of complexity, based on probabilistic concepts cannot fill in the gap due to the lack of knowledge about the physical process behind an earthquake, at the most it can supply some guidelines. Moreover, it may loose validity in dealing with uncertainties that are so large that may not be quantifiable in a meaningful sense (Chandler et al., 2001) as it happens in low to moderate seismicity regions, or regions lacking historical and instrumental earthquake data.

For a given zone, the mathematical modelling of the occurrence of seismic events and of the related values of probability are derived from empirical data that may fail to describe adequately the reality.

When constructing appropriate earthquake-resistant structures, design and construction should not be such that in extreme event no damage occurs but rather that an acceptable level of damage takes place as a function of the corresponding performance expectations (operational, safe-life, etc.).

Therefore the realistic definition of hazard in scenario-like format should be accompanied by the determination of advanced hazard indicators as, for instance, damaging potential. Such a determination, due to the limitation of the available strong ground motion records, requires resorting to broad band synthetic seismograms that allow us to perform realistic waveform modelling for different seismotectonic environments. The modelling takes into account source properties, like dimensions, directivity, duration, lateral heterogeneity's along the path and local site features. Such a procedure is a must since it has been proven both experimentally (e.g. Wang and Nisimura, 1999) and theoretically (Romanelli and Vaccari 1999; Field et al., 2000; Panza et al, 2001) that the so-called local site effects can be strongly dependent upon the characteristics of the seismic source generating the seismic input. At present, only from a careful performance of modelling experiments it is possible to realistically account for effects such as long duration pulses, shaking duration, temporal distribution of pulses, amplitude and, connected to them, the linear and nonlinear structural response in terms of strength, energy and displacement.

2. General problems in seismic hazard assessment

The typical seismic hazard problem lies in the determination of the ground motion characteristics associated to future earthquakes, both on regional and on local scale. The input for the subsequent seismic risk analysis can be expressed in various ways, e.g. with a description of the groundshaking severity due to an earthquake of a given distance and magnitude ("groundshaking scenario"), or with probabilistic maps of relevant parameters describing the ground motion. For example, the historically

most used parameter in the engineering analysis for the characterization of the seismic hazard is the PGA (Peak Ground Acceleration), which is a single-value indicator commonly used in seismic hazard assessment. Actually, it is recognized that the PGA alone can not describe adequately all the effects associated to the ground shaking, since the frequency content and the duration of a seismic wavetrain can play a decisive role. Although it has been understood that the characteristics of the ground motion such as its amplitude, frequency content and duration are relevant to estimate its damaging potential, some of these characteristics have been often ignored.

A more adequate definition of the seismic ground motion due to an earthquake with a given magnitude and source-to-site distance, can be done following two main approaches. The first one (denoted as engineering approach) is based on the analysis of the available strong motion databases, collected by existing seismic networks, and on the grouping of those accelerograms that contain similar source, path, and site effects (e.g. Decanini and Mollaioli, 1998). A fundamental step in this approach involves the estimation of realistic source-to-site transfer functions.

The second approach (seismological approach) is based on modeling techniques, developed from the knowledge of the seismic source process and of the propagation of seismic waves, that can realistically simulate the ground motion associated with the given earthquake scenario (Panza et al., 1996; Field et al., 2000). The ideal procedure is to follow the two complementary ways, in order to validate, for the different areas to be investigated, the numerical modeling with the available recordings (e.g. Decanini et al., 1999; Panza et al., 2000a,b). In the last decades the number of the recorded strong motions has considerably increased, especially for North America, Japan and Taiwan, but the installation and maintenance costs make the deployment of a dense seismic network in each earthquake prone area a too expensive operation. For most of the European seismic zones strong motion data are very scarce and most of the available data for destructive events are only the macroseismic intensities. In these cases synthetic signals, to be used as seismic input in a subsequent engineering analysis, must be produced (immediately and at a very low cost/benefit ratio) taking into account the source characteristics, the path and the local geological and geotechnical conditions and must be validated against observed intensities.

As a result, we suggests a scenario-based, deterministic approach in view of the limited seismological data and of the multiscale seismicity model formulated by Molchan et al. (1997). Accordingly to this model only the ensemble of events that are geometrically small, compared with the elements of the seismotectonic regionalization, can be described by a log-linear FM relation. This condition, largely fulfilled by the early global investigation by Gutenberg and Richter (e.g. see Fig. 49 of Båth, 1973), it has been subsequently violated in many investigations. This violation has given rise to the Characteristic Earthquake (CE) concept (Schwartz and Coppersmith, 1984) in opposition to the Self-Organized Criticality (SOC) paradigm (Bak and Tang, 1989). The multiscale model implies that, in order to apply the probabilistic approach the seismic zonation must be made at several scales, depending upon the self-similarity conditions of the seismic events and the linearity of the log FM relation, in the magnitude range of interest.

Moreover, the macroseismic observations made in correspondence of the destructive events of the last century have clearly evidenced the influence of other two fundamental aspects in the characterization of the damage distribution: the near-surface geological and topographical conditions. This observation highlights the large spatial variability of the destructive potential of earthquake ground motion. Since most of the anthropised areas are settled in correspondence of sedimentary basins (e.g. river valleys), a realistic definition of the seismic input that takes into account the site response has become one of the most relevant tasks in the seismic engineering analysis. The soft surface layering often controls local amplification of the ground motion. The impedance contrast between the soft surface soils and the underlying bedrock leads to the trapping of the seismic energy,

and the relatively simple onset of vertical resonance can be transformed into a complex resonance's pattern, strongly dependent on the characteristics of the sub-surface layers and the bedrock configuration.

The most traditional empirical techniques for the estimation of site effects are based on the computation of the spectral ratio between the signal (or a portion of it, e.g. a single phase) recorded at the sedimentary site and a reference one, preferably recorded at a nearby bedrock site (Borcherdt, 1970). Quite often a signal recorded on bedrock is not available close to the investigated sites, so that directional effects due to the source could become relevant. Even in the favorable condition that such a reference site exists, unless well isolated single phases are used, the spectral ratios are not completely free from source influences (e.g. Romanelli and Vaccari, 1999). Some techniques have been proposed that are non-reference-site dependent (e.g. Boatwright et al., 1991).

An alternative approach, originally applied by Langston (1979) for crustal and upper mantle studies, is based on the measurement of the spectral ratio between the horizontal and vertical components of motion. The method is based on the assumption, not always fulfilled, that the propagation of the vertical component of motion (in general only S-waves are considered) is not perturbed by the uppermost surface layers, and can therefore be used to remove source and path effects from the horizontal components. Anyway, this method produced unsatisfactory results, as verified in recent severe earthquakes.

As a matter of fact, local site effects can be strongly dependent upon the characteristics of the seismic source (e.g. Romanelli and Vaccari, 1999). Therefore, the use of synthetic seismograms is fundamental even when relevant observational data are available, in order to explore the local responses that may correspond to sources that are different from the known ones.

The wide use of synthetic signals allows us to easily construct scenarios based on ground motion descriptors, strictly linked with energy and displacement demands (Decanini and Mollaioli, 2001).

3. Shortcomings of the probabilistic approach

The probabilistic analysis of the seismic hazard determines the probability rate of exceeding, over a specified period of time, various levels of ground motion. It is basically conditioned by the definition of the seismogenic zones, which is affected by serious uncertainties. Within each of them the seismogenic process is frequently assumed to be rather uniform, however the uncritical assumption of homogeneity can introduce significant errors in the estimate of the seismic hazard in a given site. For a recent extreme example concerning the Italian territory reference can be made to the 17 July 2001 (M_b=4.9; M_s=4.0, NEIC), event occurred in NorthEast Italy outside the defined seismogenic zones (Meletti et al., 2000), thus in a region not considered for hazard analysis.

The multiscale seismicity model supplies a formal framework that describes the intrinsic difficulty of the probabilistic evaluation of the occurrence of earthquakes (Molchan et al., 1997). The problem is chiefly due to the difficulty to properly choose the size of the region to analyze, so that it is large enough to guarantee the applicability of the Gutenberg-Richter law and related concepts. In order to apply the probabilistic approach, the seismic zonation must be made at several scales, depending upon the self-similarity conditions of the seismic events and the linearity of the log frequency-magnitude (FM) relation, in the magnitude range of interest.

The difficulty to evaluate the occurrence of the earthquakes (log FM relations) and the propagation of their effects (attenuation laws), as well as the parameters characterizing the destructive

potential of the ground motion leads to a probabilistic estimate of the seismic hazard that could represent a gross approximation of the reality. When the multiscale seismicity model is applied to analyze the seismicity, the time dependence of seismicity becomes unimportant. In fact, the classical Poisson hypothesis (seismic events are time independent) can hardly be accepted if the considered seismic events are those associated to a specific source (where there are processes of storage and release of energy). The Poisson hypothesis can be physically acceptable when the considered area is large enough to contain a great number of sources.

To deal with the time dependence of seismicity, that is relevant only if we consider a very small number of seismic sources, the concept of renewal process has been introduced (Esteva, 1970; Araya and Der Kiureghian, 1988; Hagiwara, 1974; Savy et al., 1980). Accordingly with the renewal process models a memory is introduced so that each event, with some probability, depends from the previous one. In these models the intercurrence time between two events does not follow an exponential distribution, thus the probability of occurrence of an earthquake is not constant with time. Assuming that the seismic crisis is over or during a seismic sequence, the occurrence of the events is interpreted using mixed functions of the density of probability, obtained with the combination of two different functions. These functions depend upon the seismogenetic properties of the sources and upon the time evolution of the sequences; therefore they differ from place to place. Such models rely upon several assumptions that to be verified require the availability of observations that often are not available or insufficient, and this makes it difficult, if not impossible, the calibration of the distribution functions. The application of the renewal process model requires the evaluation of the time elapsed from the last event. Such an evaluation can be impossible if the length of the catalogue is smaller than the storage and release time interval and palaeoseismological data are not available, or when a linear source does not correspond to a single fault but to a system of several faults almost parallel. In the latter a case the occurrence of severe seismic events, within close epicentral zones and during short time intervals, could not be analyzed resorting to criteria based on the existence of seismic gaps.

Further shortcomings of the probabilistic approach are connected with (1) the choice of the parameters characterizing the destructiveness potential of earthquake ground motion, and (2) the attenuation relationships for the estimation of the ground motion at a site for a given earthquake.

3.1 Characterization of earthquake destructiveness potential

The characterization of seismic motion in earthquake prone areas requires the identification of adequate parameters that characterize accurately the earthquake destructiveness potential. The specification of these parameters in general requires the selection of significant signals for the design of new structures or the seismic safety assessment of existing ones. To define, in general, a design earthquake represents a fundamental step in a seismic hazard analysis. The adoption of inadequate parameters can lead to the definition of a non-realistic design earthquake and, consequently, to the unreliable evaluation of the seismic risk. Recent earthquakes (e.g. Imperial Valley 1979, Loma Prieta 1989, Landers 1992, Northridge 1994, Kobe 1995, Turkey 1999, Taiwan 1999, Greece 1999, Gujarat, 2001) have demonstrated that the seismic hazard evaluation, based prevalently on a probabilistic approach, has underestimated considerably these demands, particularly in near-fault regions.

The quite large number of near-fault records from recent earthquakes indicate that, for a given soil condition, the characteristics of strong ground motion and consequently of the damage potential can vary significantly as a function of the location of the site with respect to the propagation of the rupture. Particularly, in the case of *forward rupture directivity* most of the energy arrives in a single large pulse of motion which may give rise to an amplification of the ground motion at sites toward which fracture propagation progresses (e.g. Bolt, 1983; Panza and Suhadolc, 1987; Heaton et al.,

1995). The long-period parts of the signals in forward directivity locations can be energetic due to the development of one or more, unidirectional, long-period pulses. The dynamic response of a structure depends simultaneously on its mechanical properties and on the characteristics of the induced excitation. Therefore it is necessary to investigate if certain properties which are efficient to mitigate the structure response when subjected to certain inputs might have an undesirable effect during other seismic inputs. Moreover, the presence of long duration accelerometric pulses in the ground motion constitutes an important factor in causing damage, as it involves the transmission of large energy amounts to the structures in a very short time, with high energy dissipation and displacement demands.

The quantification of the ground motion expected at a particular site, that would drive the structure to its critical response, resulting in the highest damage potential, requires: (a) the identification of the ground motion parameters that characterize the severity and the damage potential of the earthquake ground motion (for a more complete discussion on this topic see Appendix), and (b) the seismological, geological, and topographic factors that affect them. In this context, energy-based and displacement demand parameters constitute an adequate approach to highlight the damaging potential of these kind of signals (Decanini and Mollaioli, 1998; Decanini et al., 2000). This necessity is confirmed by the analysis performed by Panza et al. (1999) when seeking for a correlation between maximum observed macroseismic intensity, I, (MCS) and computed peak values of ground motion, like Design Ground Acceleration (DGA), Peak Ground Velocities (PGV) and Peak Ground Displacements (PGD). They do not show any significant improvement in the regression scatter when going from DGA to PGV and PGD. The slope value is always close to 0.3, a value that corresponds to the relation DGA(I-1)/DGA(I)=PGV(I-1)/PGV(I)=PGD(I-1)/PGD(I)=2. Such a value is not contradicted by the numerous empirical relations (see Shteinberg et al., 1993 and references therein) found when considering peak values of ground acceleration.

The large energy demand in the near-field region ($D_f \leq 5$ km), with respect to larger distance ranges, is clearly evidenced in Tab. 1. In the table, a comparison between maximum input energy $E_{I(max)}$ and a Seismic Hazard Energy Factor AE_I (Decanini and Mollaioli, 1998) is given for sites located on a soil of intermediate mechanical properties, S2; for different values of interval of magnitude (M) and source-to-site distance (D_f) classes. D_f is defined as the closest distance from the intersection with the free surface of the fault plane, or of its extension to the surface for blind faults.

SOIL S2 $5.4 \leq M \leq 6.2$			
D_f (km)	$AE_{I(design)}$ cm²/s	$E_{I(max)}$ cm²/s²	$AE_{I(max)}$ cm²/s
$D_f \leq 5$	45000	39000	34568
$5 < D_f \leq 12$	18000	13000	8960
$12 < D_f \leq 30$	10000	7600	5828
$D_f > 30$	3000	480	420
SOIL S2 $6.5 \leq M \leq 7.1$			
D_f (km)	$AE_{I(design)}$ cm²/s	$E_{I(max)}$ cm²/s²	$AE_{I(max)}$ cm²/s
$D_f \leq 5$	110000	90000	98446
$5 < D_f \leq 12$	75000	41000	31320
$12 < D_f \leq 30$	50000	31000	42683
$D_f > 30$	15000	9400	9836

Table 1. Comparison between AE_I (design and maximum observed) and E_I (maximum observed). Soil S2 (intermediate).

The input energy per unit of mass, $\frac{E_I}{m} = \int \ddot{u}_t du_g = \int \ddot{u}_t \dot{u}_g dt$, has been extensively used for the evaluation of the damage potential of earthquake ground motion (Akiyama, 1985; Uang and Bertero, 1988; Fajfar and Fishinger, 1990; Uang and Bertero, 1990; Bertero and Uang, 1992; Krawinkler 1997; Decanini and Mollaioli, 1998; Decanini and Mollaioli, 2001). The parameter $AE_I = \int_{0.05}^{4.0} E_I(x = 5\%, T)\, dT$, which represents the area enclosed by the elastic input energy spectrum in the interval of periods between 0.05 and 4.0 seconds, may be considered a global hazard index in energy terms (Decanini and Mollaioli, 1998). In fact it considers the influence of the energy demand in the whole period range. The proposed values of E_I and AE_I were determined from a database of 300 acceleration time histories taken from 37 different seismic events with magnitude ranging from 4 to 8.1 and distance, from the horizontal projection of the causative fault, from 0 to 390 km.

The large difference among the energy parameters in the near-fault ($D_f \leq 5$ km) and at other locations ($5 < D_f \leq 12$ km; $12 < D_f \leq 30$ km; $D_f > 30$ km) has been found for the displacement demand too, as shown in Fig. 1. The largest displacements can be observed on soft soil sites (S3), in the same distance and magnitude range (Fig. 2), as the amplification of ground motions may be significantly affected by the combined effect of the source and of the soil stiffness and thickness.

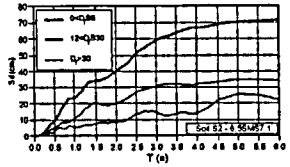

Fig. 1. Mean Displacement Spectra for different source-to-site distance ranges. Intermediate soil class (S2). $6.5 \leq M \leq 7.1$.

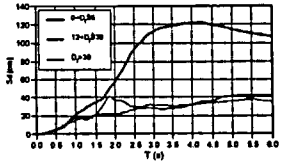

Fig. 2. Mean Displacement Spectra for different source-to-site distance ranges; soft soil (S3); $6.5 \leq M \leq 7.1$.

Each recorded strong ground motion history is a useful addition to the time record database, which increases our choices in selecting acceleration histories for various analyses. The growing database for near-field and soft soil strong motion records, gives the opportunity to enhance the state of knowledge in damage potential evaluation. Anyway, it has been noted that other seismological characteristics, such as the different styles of faulting, the radiation pattern, the orientation of the seismic source, etc., should inevitably be taken into account. These issues may be clearly understood resorting to seismological modeling techniques. For example, due to the lack of data, the nature of near-fault ground motions from larger magnitude earthquakes should be examined using seismologically based ground motion simulation methods.

3.2 Attenuation relationships

The other factor which influences a seismic-hazard estimate is represented by the assessment of the attenuation relationships of the ground motion parameters. These relationships can differ in the assumed functional form, the number and definition of independent variables, the data selection criteria, and the statistical treatment of the data. Anyway, in general, attenuation laws assume the same propagation model for all the size and type of events, but such a hypothesis is not very realistic. The

most frequently used attenuation models of ground motion parameters, like PGA, PGV, etc., have the form:

$$\log y = a + b\,M + c\,\log r_f + d\,D_f + e\,S \qquad (1)$$

where y is the ground motion parameter, a, b, c, d, and e are coefficients empirically determined, r_f is derived from D_f by considering a conventional depth h_0, with $r_f = \sqrt{D_f^2 + h_0^2}$, and S is a binary variable (0, 1) which depends on the soil type. Generally, the coefficients are determined empirically by means of regression analyses and they turn out to be quite sensitive to the data set utilized. Usually regional data sets are statistically not significant, while the national or global data sets, even if statistically significant, they can represent very different seismotectonic styles that therefore are not mixable. Quite often the coefficients are obtained in such a way that they turn out to be (almost) independent from magnitude, distance and soil type. A nice example of the strong dependence of attenuation laws on the procedure followed in the data processing is given by Parvez et al. (2001) for the Himalayas. Moreover, typically the standard deviation associated with the predictions of the attenuation relationships ranges between 50% and 100% of the mean value.

Introducing the relative decay

$$R_y = y_{rf}/y_{source} \qquad (2)$$

where the suffix "source" indicates the values at the closest instrument to the source (typically D_{source} may be about 2 km), we obtain

$$\log R_y = c(\log r_f - \log r_{source}) + d(D_f - D_{source}) \qquad (3)$$

Thus the relative decay does not depend upon the magnitude (size of the event) and the type of soils (local soil conditions). In general, r_f is different for PGA and PGV because a different conventional depth h_0 is assumed: usually $3 \leq h_0 \leq 10$ km for PGA and PGV. The parameter h_0 has a strong influence on the relative decay, conditioning the reliability of the results.

In the particular case of Sabetta and Pugliese (1987) relations (SP87) c=-1, d=0 thus

$$\log R_y = \log r_{source} - \log r_f \qquad (4)$$

and h_0 is 5.8 km for PGA and 3.6 km for PGV.

The attenuation relationships utilized by Ambraseys et al. (1996) for the evaluation of peak ground acceleration (PGA), with h_0 equal to 3.5 km, results (AMB96):

$$\log R_y = 0.922\,(\log r_{source} - \log r_f) \qquad (5)$$

Finally, the attenuation law for PGA suggested for the South East Sicily (ASI) by the Authors (Decanini et al., 2001), for h_0=10 km, is:

$$\log R_y = 0.92\,(\log r_{source} - \log r_f) + 0.0005\,(D_{source} - D_f) \qquad (6)$$

These results seem to be in contrast with the physical phenomenon, often observed. For example, it has been found that the PGV and PGD (and consequently energy) attenuate differently with distance than accelerations, depending on the magnitude range and soil type.

The analysis of selected events and of a set of strong motion records, classified accordingly to magnitude intervals and soil conditions, indicates that the trend of the relative decay of AE_I energy hazard parameter (Decanini and Mollaioli, 1998) is not constant. It depends on magnitude and soil type (see Tab. 2 to 6).

If we consider that the energetic parameter AE_I is a good and relatively stable indicator of the global damaging potential of ground motion, it is natural to assume that PGA and PGV cannot follow

	S1			S2		S3
D_f(km)	M (6.5-7.1)	M (5.4-6.2)	M (4.2-5.2)	M (6.5-7.1)	M (5.4-6.2)	M (6.5-7.1)
2.5	1.00	1.00	1.00	1.00	1.00	1.00
8.5	0.34	0.35	0.70	0.49	0.33	0.59
21	0.15	0.18	0.19	0.27	0.12	0.39
30	0.11	0.15	0.07	0.21	0.08	0.32
50	0.07	0.13	0.01	0.13	0.03	0.24

Table 2. Relative attenuation of AE_I as determined from the regression analysis of about 300 recordings worldwide, classified by magnitude (M) and soil type (S1, S2, S3)

	R(PGA)				R(PGV)		$R(AE_I)$	$R(AE_I)^{0.5}$
D_f(km)	Observ.	SP87	AMB96	ASI	Observ.	SP87	Observ.	Observ.
4.5	1.00	1.00	1.00	1.00	1.00	1.00	1.00	1.00
15	0.88	0.46	0.40	0.62	0.54	0.37	0.52	0.72
19	0.54	0.37	0.33	0.53	0.34	0.30	0.29	0.54
24	0.67	0.30	0.26	0.44	0.28	0.24	0.08	0.28
31.5	0.55	0.23	0.21	0.35	0.27	0.18	0.18	0.42

Table 3. Kobe (1995 event), soft soil (S3), relative attenuation, R, of PGA, PGV and AE_I. Comparison between observed and predicted values.

	R(PGA)				R(PGV)		$R(AE_I)$	$R(AE_I)^{0.5}$
D_f(km)	Observ.	SP87	AMB96	ASI	Observ.	SP87	Observ.	Observ.
1.0	1.00	1.00	1.00	1.00	1.00	1.00	1.00	1.00
27.5	0.18	0.21	0.15	0.36	0.18	0.14	0.13	0.36
34	0.35	0.17	0.13	0.30	0.25	0.11	0.12	0.35
106	0.17	0.06	0.05	0.10	0.17	0.04	0.05	0.23

Table 4. Kobe (1995 event), soil S2, relative attenuation, R, of PGA, PGV and AE_I. Comparison between observed and predicted values.

	R(PGA)				R(PGV)		$R(AE_I)$	$R(AE_I)^{0.5}$
D_f(km)	Observ.	SP87	AMB96	ASI	Observ.	SP87	Observ.	Observ.
19.0(*)	1.00	1.00	1.00	1.00	1.00	1.00	1.00	1.00
20.5	0.58	0.93	0.93	0.94	0.45	0.93	0.44	0.66
33	0.46	0.59	0.61	0.64	0.17	0.58	0.34	0.58
36	0.32	0.55	0.56	0.59	0.18	0.53	0.17	0.41

(*)The closest station is as far as 19 km, therefore these data are only indicative (far fault reference)
Table 5. Irpinia (1980 event), soil S2, relative attenuation, R, of PGA, PGV and AE_I. Comparison between observed and predicted values.

	R(PGA)				R(PGV)		$R(AE_I)$	$R(AE_I)^{0.5}$
D_f(km)	Observ.	SP87	AMB96	ASI	Observ.	SP87	Observ.	Observ.
0.2(*)	1.00	1.00	1.00	1.00	1.00	1.00	1.00	1.00
3.2	1.51	0.88	0.76	0.95	0.48	0.75	0.34	0.58
4.8	0.58	0.77	0.62	0.90	0.68	0.60	0.32	0.57
7.3	0.41	0.62	0.46	0.82	0.39	0.44	0.19	0.43
9.0	0.58	0.54	0.39	0.75	0.44	0.37	0.22	0.47
10.2	0.56	0.50	0.36	0.71	0.22	0.33	0.10	0.32

(*)The closest station is at 0.2 km from the surface projection of the source, therefore this is a good example of near fault reference.

Table 6. Imperial Valley (1979 event), soil S2, relative attenuation, R, of PGA, PGV and AE_I. Comparison between observed and predicted values.

the same law of relative attenuation. This is a clear example of the difficulty, which is intrinsic when using attenuation laws. The introduction of the parameter $(AE_I)^{0.5}$ allows a better comparison of therelative decay of destructive potential of earthquake ground motion than peak ground values (PGA and PGV).For the events herein illustrated, and considering the relative decay of PGA, the average values of the ratio Observed/Predicted are: 1.4 for SP87, 1.7 for AMB96, and about 1 for ASI. The ratio corresponding to PGV is about 1.3 for the SP87 relationship.

By considering the specific cases illustrated in Tables 3 to 6, it can be seen that the predictions of the relative attenuation of PGA and PGV are generally in disagreement with the observed values and between the predicted themselves. This aspect evidences the great uncertainties deriving from the existing attenuation functional forms relative to the adopted hazard parameter.

4. Deterministic seismic zoning, hazard assessment and damaging seismic energy

While waiting for the accumulation of new strong motion data, a very useful approach to perform immediate microzonation is the development and use of modeling tools. These tools are based, on one hand, on the theoretical knowledge of the physics of the seismic source and of wave propagation and, on the other hand, exploit the rich database, already available, that can be used for the definition of the source and structural properties. Actually, the realistic modeling of ground motion requires the simultaneous knowledge of the geotechnical, lithological, geophysical parameters and topography of the medium, on one side, and tectonic, historical, palaeoseismological, seismotectonic models, on the other, for the best possible definition of the probable seismic source. The initial stage for the realistic ground motion modeling is thus devoted to the collection of all available data concerning the shallow geology, and the construction of a three-dimensional structural model to be used in the numerical simulation of ground motion.

With these input data, we model the ground motion using two approaches based on the modal-summation technique (Panza, 1985; Panza and Suhadolc, 1987; Florsch et al., 1991; Panza et al., 2001). The hybrid technique (e.g. Fäh et al., 1993), which combines the modal-summation and the finite-difference scheme, and the mode-coupling analytical technique for laterally heterogeneous models (e.g. Vaccari et al., 1989; Romanelli et al., 1996; 1997; Panza et al., 2001).

To minimize the number of free parameters we account for source finiteness by properly weighting the double-couple point source spectrum using the scaling laws of Gusev (1983), as

reported in Aki (1987). Even if this is a rough approximation of the physical source process, when a large earthquake is considered in the calculation of synthetic seismograms at distances of the same order of the fault dimensions, the adoption of a spectral scaling law ensures to obtain reliable spectral scenarios. The adoption of a spectral scaling law corresponds to averaging on the directivity function and on the regional variations due to different tectonic regimes. This limitation is therefore much less severe if spectral or PGA amplification is the main topic of interest instead of actual time-histories, and small- to medium-magnitude events are considered.

However, also kinematics models for a spatially extended source (e.g. Panza and Suhadolc, 1987) can be tackled by our approach. In such a case the generation of seismic waves due to an extended source is obtained by approximating the source with a rectangular plane surface corresponding to the fault plane on which the main rupture process is assumed to occur. Effects of directivity and of the energy release on the fault can be easily modeled, simulating the wide-band radiation process from a finite earthquake source/fault. The source is represented as a grid of point subsources, and their seismic moment rate time functions are generated considering each of them as realizations (sample functions) of a non-stationary random process. Specifying in a realistic way the source length and width, as well as the rupture velocity, one can obtain realistic far-field source time functions. Furthermore, assuming a realistic kinematic description of the rupture process, the stochastic structure of the accelerograms can be reproduced, including the general envelope shape and peak factors.

The methods have been applied, for the purpose of seismic microzoning, to several urban areas like Augusta (e.g. Panza et al., 2000b), Beijing (Sun et al., 1998), Benevento (e.g. Marrara and Suhadolc, 1998a), Bucharest (e.g. Moldoveanu et al., 2000), Catania (e.g. Romanelli and Vaccari, 1999), Mexico City (e.g. Fäh et al., 1994), Naples (e.g. Nunziata et al., 2000a,b), Rome (e.g. Fäh et al., 1993) and Thessaloniki (e.g. Marrara and Suhadolc, 1998b) in the framework of the UNESCO/IUGS/IGCP project "Realistic Modelling of Seismic Input for Megacities and Large Urban Areas" (Panza et al., 1999a). For urban areas where the realistic numerical modeling has been compared with recorded data (like Beijng, Benevento, Bucharest, Mexico City, Naples, Thessaloniki), the results of such comparison is fully satisfactory for engineering purposes and no data fitting is required. For events with magnitude in the range 6.5-7.1 and distances in the range 10-30 km, these pilot studies show that, distances from the causative fault, D_f, being equal, the elastic energy spectra computed from synthetic signals are comparable with those computed from real records (e.g. see Fig. 3)

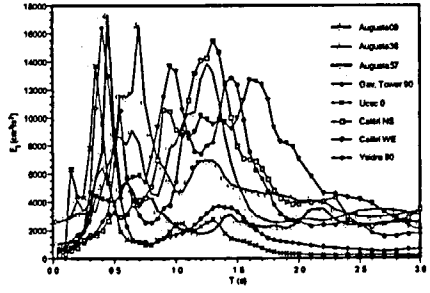

Fig. 3. Elastic energy E_I (cm^2/s^2) spectra. Comparison between Augusta synthetic signals and strong motion records of Irpinia 1980 (Calitri station) and Loma Prieta 1989 (Gav. Tower, Ucsc and Ysidro stations) earthquakes (from Decanini et al., 2001).

Thus, where recordings are absent or very limited, the synthetic time series can be reasonably used to estimate the expected ground motion, including ground velocity and displacement time series, before the next strong earthquake will occur. These time series can be readily used for the estimation of the damaging potential in energetic terms (Fig. 3).

4.1 Umbria-Marche (Central Italy) sequence

The Umbria-Marche earthquake sequence started on September 26, 1997 and took place in a complex deforming zone, along a normal fault system in the Central Apennines. The seismic sequence left significant ground effects, which were mainly concentrated in the Colfiorito intermountain basin.

The crustal events generated extensive ground motion and caused great damage in several urban areas. The extent of macroseismic data and the abundance of recorded ground motions permits a good knowledge of the source and structural parameters to better understand the nature of the ground shaking and the resulting damage patterns.

Predicting the intensity of shaking due to an earthquake before it occurs can prevent damage. Doing this rapidly after an earthquake can be useful for emergency rescue.

These objectives all belong to the overall objective of understanding and predicting the ground motion, therefore reducing the seismic risk.

Before the seismic sequence, started on September 1997, probabilistic (Fig 4) and deterministic maps were available for the Italian territory. The probabilistic map (Fig 4) indicates, for the Umbria-Marche region, peak ground accelerations (PGA) not exceeding 0.4g, for 475 years return period, and 0.24g, for 100 years return period (Corsanego et al. 1997). A first-order deterministic seismic zoning of Italy (Fig. 5), obtained by the application of the method developed by Costa et al. (1993) and its extensions (Panza et al., 1996) lead to theoretical peak values (Panza et al., 1996; 1997; 1999b) well in agreement with the representative EPA (effective peak acceleration) values observed ~ 0.3g. The EPA is defined as the average spectral acceleration in the period interval from 0.1 s to 0.5 s divided by 2.5, therefore it is equivalent to the DGA calculated by Panza et al. (1996) using design response spectra.

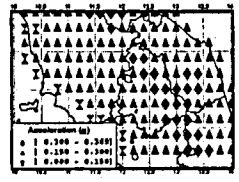

Fig. 4. Probabilistic estimation of maximum acceleration for 475 years return period (from Corsanego et al., 1997).

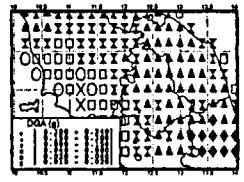

Fig. 5. Deterministic design ground acceleration focussed on the Umbria-Marche region (modified from Panza et al., 1996).

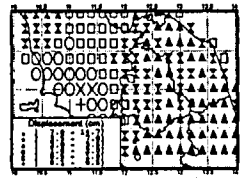

Fig. 6. Computed peak ground displacements, consistent with the acceleration values given in Fig. 5.

The information about ground displacement can be of great importance, but such information is difficult to be extracted from analog recordings, thus the available experimental database is very scarce. The realistic ground motion modelling we have developed represents an efficient way to

minimize the problem arising from the lack of statistically significant observations about ground displacement. In fact, the good agreement obtained between modeled and observed acceleration and velocities makes it reasonable to use the modeled displacements (Fig. 6), as boundary conditions in the design.

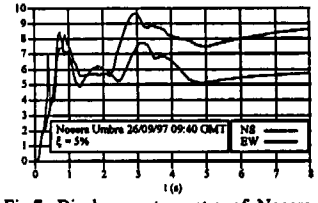

Fig.7. Displacement spectra of Nocera Umbra strong motion records (rock site). 5% damping. Event of September26, 1997, 09:40 GMT, $M_L = 5.8$, $M_W = 6.0$.

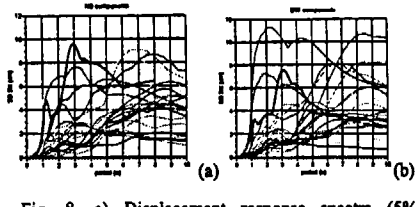

Fig. 8. a) Displacement response spectra (5% damping) computed at the grid point close to Nocera Umbra for 23 sources located in the surroundings at distances between 13 and 90 km. Thick black line corresponds to the spectrum of the signal, NS component of motion, recorded at Nocera Umbra (R1168), filtered at 1 Hz. b) Same as a) but for the EW component of motion.

The displacement response spectra (5% damping) of the observed signals are shown in Fig. 7 for the NS and EW components of motion recorded at Nocera Umbra during the main shock of the sequence. The same kind of response spectra, but obtained with the observed signals filtered with the cut off frequency used in our modeling (1 Hz), are compared (Fig. 8) with the displacement response spectra obtained from all the synthetic signals computed in the grid point (43.2°N, 12.8°E), i.e. the grid point closer to Nocera Umbra. The predictive capabilities of our modeling, made in 1996, are quite evident and indicate that future events may generate even larger seismic input.

4.2 Bovec event of Easter 1998

For Bovec, Slovenia, event (12 April 1998) the only available strong motion records belong to the Rete Accelerometrica of Friuli Venezia Giulia (RAF) (minimum epicentral distance >30 km), therefore the only relevant comparison is with the epicentral macroseismic intensity, which has been observed equal to IX (MCS).

From the deterministic maps shown in Fig. 9 and considering the conversion tables between peak values of ground motion and macroseismic intensity (MCS), proposed by Panza et al. (1999), the epicentral macroseismic values observed, IX (MSC), are in perfect agreement with the values predicted by our modelling.

5. Conclusions

Case studies of seismic hazard assessment techniques indicate the limits of the currently used methodologies, deeply rooted in engineering practice, based prevalently on a probabilistic approach,

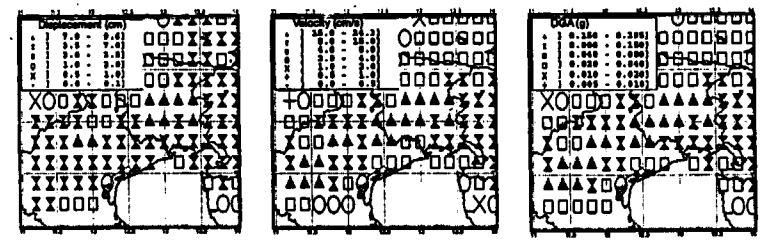

Fig. 9. Deterministic peak ground displacement, velocity and EPA=DGA, computed by Panza et al. (1996; 1997; 1999b).

and show that the related analyses are not sufficiently reliable to characterize seismic hazard. The probabilistic analysis of the seismic hazard is basically conditioned by the definition of the seismogenic zones. Within each of them the seismogenic process is assumed to be rather uniform, however the uncritical assumption of homogeneity can introduce severe errors in the estimate of the seismic hazard in a given site. Further shortcomings are connected with the choice of the other components needed for the calculation of the rate of probability of exceeding various levels of ground motion, over a specified period of time, i.e. the parameters characteristic of the damage potential of earthquake ground motion, and the attenuation relationships for the estimation of the ground motion at a site for a given earthquake.

The quantification of the critical ground motion expected at a particular site, requires the identification of the parameters that characterize the severity and the damage potential. Such critical ground motion can be identified in terms of energy and displacement demands which should be evaluated by considering the seismological, geological, and topographic factors that affect them.

In view of the limited seismological data, it seems more appropriate to resort to a scenario-based deterministic approach, as it allows us the realistic definition of hazard in scenario-like format to be accompanied by the determination of advanced hazard indicators as, for instance, damaging potential in terms of energy. Such a determination, due to the limitation of the number of strong motion records, requires to resort to broad band synthetic seismograms, that allow us to perform realistic waveform modeling for different seismotectonic environments, taking into account source properties (e.g. dimensions, directivity, duration, etc.), lateral heterogeneities, and path effects.

Each synthetic strong ground motion history, characterized as a function of its damage potential, constitutes a useful addition to the records database which increases our choices in selecting acceleration histories for various analyses. The growing database for near-field and soft soil strong motion signals (recorded and modeled), which can be considered as limit conditions, gives the opportunity to enhance the state of knowledge in damage potential evaluation.

The results we have reported are the outcome of a rather unusual but very fruitful close collaboration between seismologists and seismic engineers, that we consider a prerequisite for the achievement of significant step forward in the future.

Appendix: Parameters used to describe the severity of an earthquake

A fundamental need for the definition of the seismic hazard of a given site or, in general, a region, is to select a parameter descriptive of the earthquake severity. A large number of parameters has been proposed for measuring the capacity of earthquakes to damage structures. However, recently observed damage distribution and strong motion acceleration records indicate the need for a more comprehensive definition of the existing parameters and for the introduction of new ones to account for the complex characteristics of earthquake induced strong ground motions in the engineering analysis and design. The adoption of inadequate parameters can lead to the definition of unrealistic design earthquakes and consequently to the unreliable evaluation of the seismic risk for the existing built environment, or to the insufficient protection of new one.

The parameters fundamentally involved in the evaluation of the level of severity associated with strong motion are, for engineering purposes, the frequency content, the amplitude and the effective duration. Because of the complexity of the earthquake ground motions, generally more than one parameter is required to describe the most important ground motion characteristics.

In general, these parameters can be obtained either directly or with some simple calculation from the digitized and corrected records, from the parametric integration of the equation of motion of elastic and inelastic single-degree-of-freedom (SDOF) systems, and considering the energy balance equation for elastic and inelastic systems. Application of the Duhamel (convolution) integral to a linear elastic SDOF system gives the expressions for the displacement response time history u(t) and allows to define a pseudo-velocity, $v(t)= \omega\, u(t)$, and a pseudo-acceleration, $a(t)= \omega^2\, u(t)$ (Clough & Penzien 1993, Chopra, 1995). They get their names from the fact that they have units of velocity and acceleration, respectively, but they are not equal to instantaneous velocity, and acceleration, respectively, of the system, since earthquake time histories are far from being purely harmonic motions. In terms of peak values, one can define the displacement, pseudo-velocity and pseudo-acceleration response spectra:

$$S_d(x,\omega)=|u|_{max}; \qquad S_d(x,\omega)=\frac{1}{\omega}S_{pv}(x,\omega); \qquad S_{pa}(x,\omega)=\omega S_{pv}(x,\omega)$$

where ω is the natural frequency (spectral variable) of the SDOF, u is the displacement, $S_d(\xi,\omega)$ is the spectral displacement $S_{pv}(\xi,\omega)$ is the pseudo-spectral velocity, and $S_{pa}(\xi,\omega)$ is the pseudo-spectral acceleration. Accordingly with the following equation, the pseudo-velocity $S_{pv}(\xi,\omega)$ can be related to the maximum energy stored in the SDOF during the earthquake ground motions:

$$E=\frac{kS_d^2(x,\omega)}{2}=\frac{k\,S_{pv}^2(x,\omega)/\omega^2}{2}=\frac{mS_{pv}^2(x,\omega)}{2}$$

where k and m are the stiffness and the mass of the SDOF systems. Note that a SDOF system of zero natural period (infinite natural frequency) would be rigid, and its spectral acceleration would be equal to the peak ground acceleration.

PGA, PGV, PGD, EPA and EPV

The most commonly used measure of amplitude of a particular ground motion is the peak ground acceleration, PGA, which corresponds to the largest value of acceleration obtained from the recorded accelerogram. As the inertia forces depend directly on acceleration, PGA is one of the parameters widely used to describe the intensity and damage potential of an earthquake at a given site. However, PGA is a poor indicator of damage, since it has been observed that time histories with the same PGA

could be very different in frequency content, strong motion duration, and energy level, thus causing varying amounts of damage. In fact, PGA may be associated with high frequency pulses which do not produce significant damage to the buildings as most of the impulse is absorbed by the inertia of the structure with little deformation. On the other hand, a more moderate acceleration may be associated with a long-duration pulse of low-frequency (acceleration pulse) which gives rise to a significant deformation of the structure.

For example, after the 1971 Ancona earthquake (M_L = 4.7) a large PGA value (716 cm/s^2) was recorded at the Rocca station, located at a distance of about 7 km from the surface projection of the fault rupture. This high PGA value is associated with a short duration pulse of high frequency, as indicated in Fig. A1 where the acceleration time histories is shown, and generated a limited damage. A peak ground acceleration quite close (827 cm/s^2) to the above mentioned one, was recorded at the Sylmar station (Fig. A2), sited at about 2 km from the surface projection of the fault rupture, after the destructive 1994 Northridge earthquake (M_w=6.7). In this case, the peak ground acceleration is associated with a long duration pulse of low frequency. The moderate difference between these two PGA values seems to disagree with the large difference between the magnitude of the two seismic events. In other words, analyses of strong motion data have shown clearly that even small earthquakes can produce high accelerations and that these accelerations are not necessarily damaging.

The peak ground velocity PGV (shown in Fig. A3) is another useful parameter for the characterization of ground motion amplitude. Since the velocity is less sensitive to the higher-frequency components of the ground motion, the PGV, more likely than the PGA, should characterize the damaging potential of ground motion.

Peak ground displacement PGD is generally associated with the lower-frequency components of an earthquake ground motion. It is, however, difficult to determine accurately PGD, due to signal processing errors in the filtering and integration of accelerograms and due to long-period noise. The situation will certainly improve with the dissemination of good quality digital instruments.

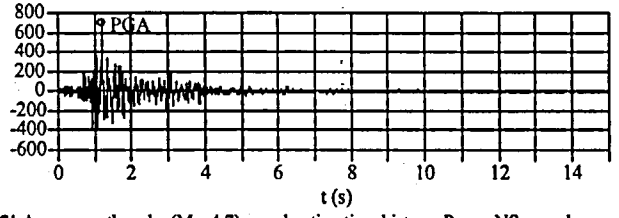

Fig. A1. 1971 Ancona earthquake (M_L=4.7); acceleration time history: Rocca NS record.

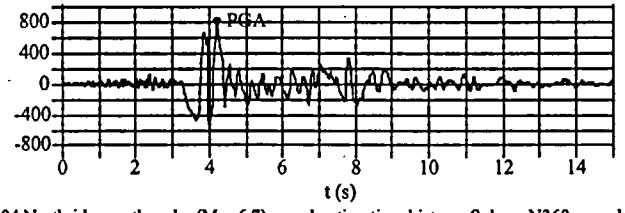

Fig. A2. 1994 Northridge earthquake (M_w=6.7); acceleration time history: Sylmar N360 record.

From the point of view of damage potential, the area under the largest acceleration pulse, which represents the incremental velocity (IV), makes many earthquake strong motion records particularly damaging. As indicated in Fig.A3, the maximum incremental velocity represents the distance between two consecutive peaks. The larger is the change in velocity, the larger is the acceleration pulse. In the case of the Takatori record obtained after the 1995 Kobe earthquake (Fig.3), the PGV is equal to 127 cm/s, while the IV is equal to 227 cm/s).

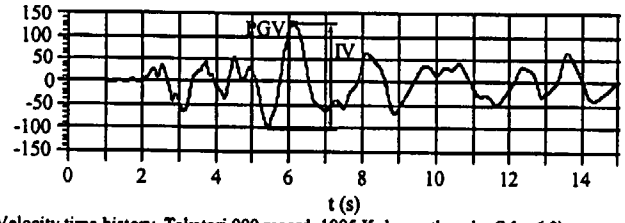

Fig. A3 – Velocity time history. Takatori 000 record. 1995 Kobe earthquake (M_w=6.9)

Realizing the limitation of using peak instrumental values, since damage can not be related only to the peak values, but it may require the occurrence of several repeated cycles, Applied Technology Council (1978) ATC introduced the concept of effective peak acceleration, EPA. The effective peak acceleration EPA is defined as the average spectral acceleration over the period range 0.1 to 0.5 s divided by 2.5 (the standard amplification factor for a 5% damping spectrum), as follows:

$$EPA = \frac{\overline{S}_{pa}}{2.5}$$

where $\overline{S}_{pa}$ is the mean pseudo-acceleration value. The empirical constant 2.5 is essentially an amplification factor of the response spectrum obtained from real peak value records. Thus EPA is correlated with the real peak value, but not equal to nor even proportional to it. If the ground motion consists of high frequency components, EPA will be obviously smaller than the real peak value. It represents the acceleration which is most closely related to the structural response and to the damage potential of an earthquake. The EPA values for the two records of Ancona and Sylmar stations are 205 cm/s^2 and 774 cm/s^2 respectively, and describe in a more appropriate way, than PGA values, the damage caused by the two earthquakes.

The effective peak velocity EPV is defined as the average spectral velocity at a period of 1 s divided by 2.5. The process of averaging the spectral accelerations and velocities over a range of periods minimizes the influence on the EPA and EPV of local spikes in the response spectrum. EPA and EPV can be thought of as normalizing factors for the development of smooth response spectra. Although effective peak acceleration is a conceptually sound parameter for the damage potential characterization of earthquake ground motion, at present there is no clear and standardized definition of this parameter.

Other ground motion parameters

Several observations derived from analyses of strong motion records of recent earthquakes indicate the considerable influence of the duration on the cumulative damage of the structures. For example, time histories with high amplitudes but short duration can be associated to moderate damages compared to ground motion with lowest amplitude but with longest duration. Moreover, it is

well known that the major drawback in the use of elastic response spectra, S_{pa}, is the neglecting of the duration. Different approaches have been taken to the problem of evaluating the duration of strong motion in an accelerogram. The bracketed duration (Bolt, 1973) is defined as the time between the first and the last exceedances of a threshold acceleration (usually 0.05g). Among the different duration definitions that can be found in the literature, one commonly used is that proposed by Trifunac and Brady (1975), $t_D = t_{0.95} - t_{0.05}$, where $t_{0.05}$ and $t_{0.95}$ are the time at which respectively the 5% and 95%, of the time integral of the history of squared accelerations are reached, which corresponds to the time interval between the points at which 5% and 95% of the total energy has been recorded.
The Arias Intensity (Arias, 1969), I_A, is defined as:

$$I_A = \frac{p}{2g}\int_0^{t_t} a_g^2(t)dt,$$

where t_t and a_g are the total duration and ground acceleration of a ground motion record, respectively. The Arias intensity has units of velocity. I_A represents the sum of the total energies, per unit mass, stored, at the end of the earthquake ground motion, in a population of undamped linear oscillators. Arias Intensity, which is a measure of the global energy transmitted to an elastic system, tends to overestimate the intensity of an earthquake with long duration, high acceleration and broad band frequency content. Since it is obtained by integration over the entire duration rather than over the duration of strong motion, its value is independent of the method used to define the duration of strong motion.

Housner (1952) defined a measure expressing the relative severity of earthquakes in terms of the area under the pseudo-velocity spectrum between 0.1 and 2.5 seconds. Housner's spectral intensity I_H is defined as:

$$I_H = \int_{0.1}^{2.5} S_{pv}(T,\xi)\,dT = \frac{1}{2\pi}\int_{0.1}^{2.5} S_{pa}(T,\xi)\,T dT,$$

where S_{pv} is the pseudo-velocity at the undamped natural period T and damping ratio ξ, and S_{pa} is the pseudo-acceleration at the undamped natural period T and damping ratio ξ. Thus, Housner's spectral intensity is the first moment of the area of S_{pa} ($0.1<T<2.5$) about the S_{pa} axis, implying that the Housner spectral intensity is larger for ground motions with a significant amount of low frequency content. The I_H parameter captures important aspects of the amplitude and frequency content in a single parameter, however, it does not provide information on the strong motion duration which is important for a structural system experiencing inelastic behaviour and yielding reversals. Housner (1956) gave also a definition of the maximum input energy of an elastic SDOF system on the basis of the pseudo-velocity spectrum S_{pv}. In fact, the pseudo-velocity spectrum S_{pv} reflects the energy demand of an elastic SDOF system as follows:

$$E_v = \frac{1}{2}m\left(S_{pv}\right)^2$$

This parameter can be utilized for the estimation of earthquake damage potential from an energy perspective. The pseudo-velocity spectrum constitutes approximately the lower bound of the hysteretic energy spectrum adjusted in terms of equivalent velocity (Decanini & Mollaioli 1998, Uang & Bertero, 1988).

Araya & Saragoni (1984) proposed the destructiveness potential factor, P_D, that considers both the Arias Intensity and the rate of zero crossings, ν_0 and agrees with the observed damage better than other parameters. The destructiveness potential factor, which simultaneously considers the effect of the ground motion amplitude, strong motion duration, and frequency content on the relative destructiveness of different ground motion records, is defined as:

$$P_D = \frac{\pi}{2g}\frac{\int_0^{t_0} a_g^2(t)dt}{v_0^2} = \frac{I_A}{v_0^2} \qquad v_0 = \frac{N_0}{t_0}$$

where t is the time, a_g is the ground acceleration, $v_0 = N_0/t_0$ is the number of zero crossings of the acceleration time history per unit of time (Fig. A4), N_0 is the number of the crossings with the time axis, t_0 is the total duration of the examined record (sometimes it could be a particular time-window), and I_A is the Arias intensity.

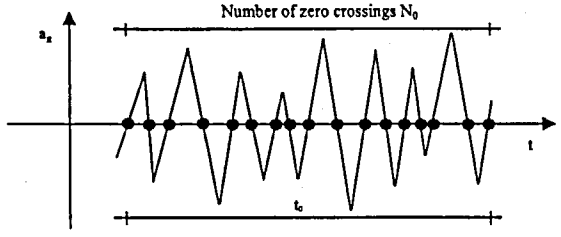

Fig. A4. Evaluation of the parameter v_0.

The amplitudes of ground motion acceleration and strong motion duration are incorporated in the Arias intensity, while v_0 [sec-1] results an average index of the frequency content of the time history. Araya and Saragoni (1984) and Saragoni et al. (1989) have shown that the horizontal earthquake destructiveness potential factor PDH (sum of the PD values corresponding to the two horizontal components, PDH=PDx+PDy) correlates well with the Modified Mercalli macroseismic Intensity I_{MM} values. However, it is possible that two different time histories have similar destructiveness potential factors but very different values of the zero crossings rate and Arias intensity. A time history with a small zero-crossing rate would cause less damage to short period structures than a time history with a larger zero-crossing rate close to the fundamental period of the structures, although both time histories have the same destructiveness potential factor.

In designing structures to perform satisfactorily under earthquake excitations the concept of response spectrum was introduced as a practical mean of characterizing ground motions and their effects on structures. The response spectrum, a concept that has been recognized for many years in the literature (e.g., Newmark & Hall 1982), describes the maximum response of a SDOF system to a particular input motion as a function of its natural frequency (or period) and damping ratio. The response may be expressed in terms of acceleration, velocity, or displacement. The importance of the response spectra in earthquake engineering has led to the development of methods for predicting them directly as a function of soil conditions, magnitude and source-to-site conditions. Response spectra are often used to represent seismic loading in terms of design spectra, which are the result of the smoothing, averaging or enveloping of the response spectra of multiple motions.

Although the response spectrum provides the basis for the specification of design ground motions in all current design guidelines and code provisions, there is a growing recognition that the response spectrum alone does not provide an adequate characterization of the earthquake ground motion. In order to give a major conceptual improvement, methods using ground motion spectra based on EPA and EPV have been suggested.

Energy based parameters

Linear elastic response spectra or linear elastic design response spectra recommended by seismic codes have been proved to be inadequate by recent seismic events, as they are not directly related to structural damage. Extremely important factors such as the duration of the strong ground motion and the sequence of acceleration pulses are not taken into account adequately. Therefore response parameters based on the inelastic behaviour of a structure should be considered with the ground motion characteristics.

In current seismic regulations, the displacement ductility ratio μ is generally used to reduce the elastic design forces to a level which implicitly considers the possibility that a certain degree of inelastic deformations could occur. To this purpose, employing numerical methods, constant ductility response spectra were derived through non-linear dynamic analyses of viscously damped SDOF systems by defining the following two parameters:

$$C_y = \frac{R_y}{mg}$$

$$\eta = \frac{R_y}{m\ddot{u}_{g(max)}} = \frac{C_y}{\ddot{u}_{g(max)}/g}$$

where R_y is the yielding resistance, m is the mass of the system, and $\ddot{u}_{g(max)}$ is the maximum ground acceleration. The parameter C_y represents the structure's yielding seismic resistance coefficient and η expresses a system's yield strength relative to the maximum inertia force of an infinitely rigid system and reveals the strength of the system as a fraction of its weight relative to the peak ground acceleration expressed as a fraction of gravity. Traditionally, displacement ductility was used as the main parameter to measure the degree of damage sustained by a structure.

One significant disadvantage of seismic resistance (C_y) spectra is that the effect of strong motion duration is not considered. An example of constant ductility C_y spectra, corresponding to the 1986 San Salvador earthquake (CIG record) and 1985 Chile earthquake (Llolleo record) is reported in Fig. A5 a,b, respectively. By comparing these spectra it seems that the damage potential of these ground motions is quite similar, even though the CIG and Llolleo are records of two earthquakes with very different magnitude, 5.4 and 7.8, respectively.

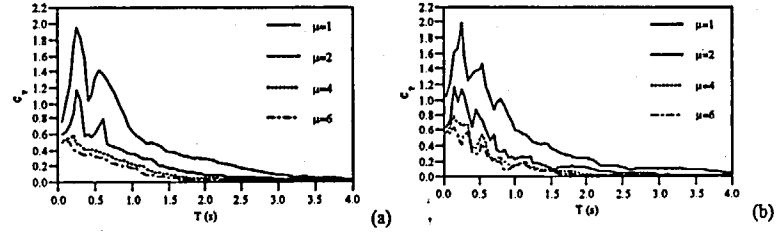

Fig. A5. Comparison between constant ductility C_y spectra. (a) 1986 San Salvador earthquake (CIG record); 1985 Chile earthquake (Llolleo record)

In other words, the elastic and inelastic (in terms of displacement ductility) response spectra are not sufficient for the estimation of the damage potential of the earthquake ground motion because they do not give a precise description of the quantity of the energy that will be dissipated through hysteretic behaviour; in the inelastic case they give only the value of the maximum ductility requirement. To overcome this problem other ductility definitions, e.g. hysteretic or cyclic ductility, were introduced.

However, in this context, the introduction of appropriate parameters defined in terms of energy can lead to more reliable estimates, since, more than others, the concept of energy provides tools which allow to account rationally for the mechanisms of generation, transmission and destructiveness of seismic actions. Moreover, energy-based parameters could provide more insight into the ultimate cyclic seismic performance than traditional design methods do, and could be considered as effective tools for a comprehensive interpretation of the behaviour observed during recent destructive events. In fact, energy-based parameters, allowing us to characterize properly the different types of time histories (impulsive, periodic with long durations pulses, etc.) which may correspond to an earthquake, could provide more insight into the seismic performance.

Among all the different parameters proposed for defining the damage potential, perhaps the most promising is the Earthquake Input Energy (E_I) and associate parameters (the damping energy E_ξ and the plastic hysteretic energy E_H) introduced by Uang & Bertero (1990). This parameter considers the inelastic behavior of a structural system and depends on the dynamic features of both the strong motion and the structure. The formulation of the energy parameters derives from the following balance energy equation (Uang & Bertero, 1990), $E_I = E_k + E_\xi + E_s + E_H$, where ($E_I$) is the input energy, ($E_k$) is the kinetic energy, (E_ξ) is the damping energy, (E_s) is the elastic strain energy, and (E_H) is the hysteretic energy.

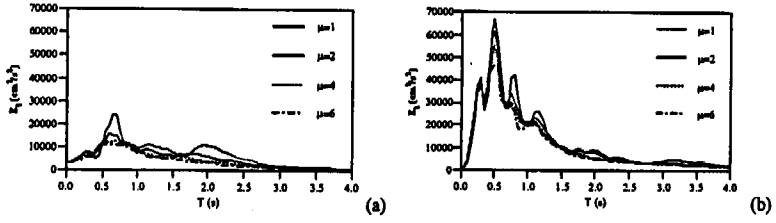

Fig. A6 – Comparison between constant ductility input energy E_I spectra. (a) 1986 San Salvador earthquake (CIG record); 1985 Chile earthquake (Llolleo record)

The absolute input energy, according to the definition of Uang & Bertero (1990), which seems suitable for the estimation of the energy terms in the range of periods of interest for the majority of structures, has the advantage to point to the physical input energy. In fact, E_I represents the work done by the total base shear at the foundation displacement. The input energy can be expressed by:

$$\frac{E_I}{m} = \int \ddot{u}_t du_g = \int \ddot{u}_t \dot{u}_g dt$$

where m is the mass, $u_t = u + u_g$ is the absolute displacement of the mass, and u_g is the earthquake ground displacement. Usually the input energy per unit mass, i.e. E_I/m, is simply denoted as E_I.

Re-examining the comparison of the damage potential of the CIG and Llolleo records in terms of input energy (Fig. A6), a completely different picture is obtained. In fact, the E_I of the Llolleo record is considerably higher than that of the CIG record, both in the elastic and inelastic cases.

A similar picture is obtained using another energy-based parameter, recently introduced (Decanini et al. 1994, Decanini & Mollaioli 1998) and denoted as *seismic hazard energy factor*, AE_I, which represents the area enclosed by the elastic input energy spectrum according to different intervals of periods:

$$AE_I = \int_{T_1}^{T_2} E_I(\xi = 5\%, T)\, dT$$

In their procedure for the evaluation of the design earthquake Decanini and Mollaioli (1998) consider the interval of periods between T_1=0.05 and T_2=4.0 seconds.

The advantage of using AE_I derives from the fact that, unlike the peak energy spectral value, which generally corresponds to a narrow band of frequencies, it takes into account the global energy structural response amount, and therefore it is the most stable parameter in energetic analysis. AE_I can be seen as the energy version of the Housner Intensity I_H, with the difference that the pseudo-velocity spectrum constitutes the lower bound of the input energy spectrum (Uang & Bertero, 1988), as illustrated in Fig. A7.

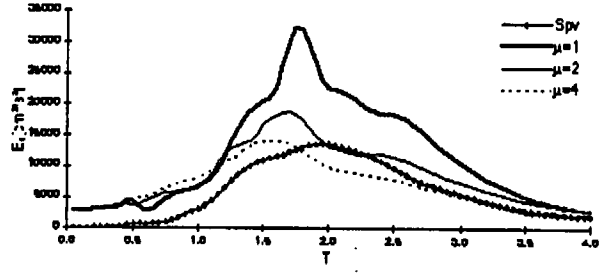

Fig. A7 – Comparison between input energy E_I and pseudo-velocity S_{pv} spectra. 1977 Bucarest earthquake

In conclusion, for a reliable estimation of the destructiveness potential of earthquake ground motions it seems appropriate to perform a comparison of their input and hysteretic energy spectra and associated seismic hazard energy factors, taking also into account the influence of the factors that may be considered external to the structural systems (magnitude, local soil conditions, source-to-site distance, etc.).

References

Aki, K, 1987, *"Strong motion seismology"*. In: Strong ground motion seismology. M. Erdik and M. Toksöz (Editors), NATO ASI Series, Series C: Mathematical and Physical Sciences, D. Reidel Publishing Company, Dordrecht, 204, 3-39.

Akiyama, H., 1985, *"Earthquake-Resistant Limit-State Design for Buildings"*. University of Tokyo Press.

Ambraseys N.N., Simpson K.A., Bommer J.J. (1996), *"Prediction of horizontal response spectra in Europe"*. Earthquake Engineering and Structural Dynamics, 25, 371-400.

Applied Technology Council,1978, *"Tentative Provisions for the Development of Seismic Regulations for Buildings"*. U.S. National Bureau of Standards, Special Publication 510, 1978.

Araya, R., Der Kiureghian, A., 1988, *"Seismic Hazard Analysis: Improved Models, Uncertainties and Sensitivities"*. Report No. UCB/EERC-90/11, Earthquake Engineering Research Center, University of California at Berkeley, March 1988.

Araya, R. and Saragoni, R., 1984, *"Earthquake accelerogram destructiveness potential factor"*. Proc. 8th WCEE, San Francisco, USA, 1984, vol.2, 835-841.

Arias A., 1969, *"A Measure of Earthquake Intensity"*. Massachusetts Institute of Technology, Cambridge, Massachusetts.

Bak, P., Tang, C., 1989, *"Earthquakes as a self-organized critical phenomenon"*. J. Geophys. Res., 94, 15635-15637.

Båth, M., 1973, *"Introduction to Seismology"*. Birkhauser, Basel.

Bertero, V. V., 1989, *"Lesson learned from recent catastrophic earthquake and associated research"*. First Torroja International Lecture, 1989 ICCET.

Bertero, V. V., Uang, C. M., 1992, *"Issues and future directions in the use of energy approach for seismic-resistant design of structures"*. In: Nonlinear Seismic Analysis of RC Buildings, 3-22, Elsevier.

Boatwright, J., Fletcher, J.B., Fumal, T., 1991, *"A general inversion scheme for source, site and propagation characteristics using multiply recorded sets of moderate size earthquakes"*. Bull. Seism. Soc. Am., 81, 1754-1782.

Bolt, B.A., 1973, *"Duration of strong ground motion"*, Proceedings 5th World Conference on Earthquake Engineering, Rome, Italy, Vol.1, 1304-1313.

Bolt, B.A., 1983, *"The contribution of directivity focusing to earthquake intensities"*, Report 20, U.S. Army Corps of Engineers, Waterways Experiment Station, Vicksburg.

Borcherdt, R.D., 1970, *"Effects of local geology on ground motion near San Francisco Bay"*. Bull. Seism. Soc. Am., 60, 29-61.

Chandler, A.M., Lam, N.T.K., Wilson, J.L., Hutchinson, G.L., 2001, *"Response spectrum for regions lacking earthquake records"*. Electronic Journal of Structural Engineering, 1, 60-73.

Chopra A.K., 1995, *"Dynamics of Structure. Theory and Applications to Earthquake Engineering"*, Prentice Hall, Upper Saddle River, New Jersey.

Clough R.W., Penzien J. 1993, *"Dynamics of Structures"*, McGraw-Hill Inc., Second edition, Singapore.

Corsanego, A., Faccioli, E., Gavarini, C., Scandone, P., Slejko, D., Stucchi, M., 1997, *"L'attivita' nel triennio 1993-1995"*. CNR – Gruppo Nazionale per la Difesa dai Terremoti, Rome.

Costa, G., Panza, G.F., Suhadolc, P., Vaccari, F., 1993, *"Zoning of the Italian territory in terms of expected peak ground acceleration derived from complete synthetic seismograms"*. J. Appl. Geophys., 30, 149-160.

Decanini, L., Mollaioli, F., 1998, *"Formulation of Elastic Earthquake Input Energy Spectra"*. Earthquake Engineering and Structural Dynamics, 27, 1503-1522.

Decanini, L., Mollaioli, F., 2001, *"An energy-based methodology for the assessment of the seismic demand"*. Soil Dynamics and Earthquake Engineering, 21, 113-137.

Decanini, L., Mollaioli, F., Panza, G. F., Romanelli, F., 1999, *"The realistic definition of the seismic input: an application to the Catania area"*. Earthquake Resistant Engineering Structures II (G. Oliveto and C.A. Brebbia eds.), WIT press, Boston, 425-434.

Decanini, L., Mollaioli, F., Panza, G. F., Romanelli, F., Vaccari, F., 2001, *"Pericolosità sismica della Sicilia sud orientale. Terremoti di scenario per Augusta, Siracusa e Noto"*. In Scenari di pericolosità sismica ad Augusta, Siracusa e Noto (A cura di L. Decanini e G.F. Panza), CNR-Gruppo Nazionale per la Difesa dai Terremoti, Roma, 80-151.

Decanini, L., Mollaioli, F., Saragoni, R., 2000, *"Energy and Displacement Demands Imposed by Near-Source Ground Motions"*. 12th World Conference on Earthquake Engineering, Auckland, New Zealand, 30 January-4 February 2000.

Decanini, L., Mollaioli, F., Oliveto, G., 1994, "Observations and lessons learned from the earthquake of 13th December 1990 in South-East Sicily. Proc. of the 10th European Conference on Earthquake Engineering, Duma ed. 1995 Balkema, Wien, 1935-1943.

Esteva, L., 1970, *"Seismicity Risk and Seismic Design Decisions"*. Seismic Design for Nuclear Power Plants, ed. R.J. Hansen, M.I.T. Press, Cambridge, Mass.

Fäh, D., Iodice, C., Suhadolc, P., Panza, G.F, 1993, *"A new method for the realistic estimation of seismic ground motion in megacities: the case of Rome"*. Earthquake Spectra, 9, 643-668.

Fäh, D., Suhadolc, P., Mueller, St., Panza, G.F., 1994, *"A hybrid method for the estimation of ground motion in sedimentary basins: quantitative modelling for Mexico City"*. Bull. Seism. Soc. Am., 84, 383–399.

Fajfar, P., Fishinger, M., 1990, *"A seismic design procedure including energy concept"*. Proc. 9th ECEE, Moscow, 2, 312-321.

Field, E.H., the SCEC Phase III Working Group, 2000, *"Accounting for site effects in probabilistic seismic hazard analyses of Southern California: overview of the SCEC Phase III report"*. Bull. Seism. Soc. Am., 90, 6B, S1-S31.

Florsch, N., Fäh, D., Suhadolc, P., Panza, G.F., 1991, *"Complete Synthetic Seismograms for High-Frequency Multimode SH-Waves"*. PAGEOPH , 136, 529-560.

Gusev, A. A., 1983, *"Descriptive statistical model of earthquake source radiation and its application to an estimation of short period strong motion"*. Geophys. J. R. Astron. Soc. 74, 787-800.

Hagiwara, Y., 1974, *"Probability of Earthquake Occurrence as obtained from a Weibull Distribution Analysis of Crustal Strain"*. Tectonophysics, 23, 313-318.

Heaton, T. H., Hall, J. F., Wald, D. J., Halling, M. W., 1995, *"Response of High Rise and Base Isolated Buildings to Hypothetical M_w 7.0 Blind Thrust Earthquake"*. Science Magazine, 267, 206-211.

Housner, G.W., 1952, *"Spectrum Intensities of Strong Motion Earthquakes*. Proc. Symposium of Earthquake and Blast Effects on Structures, EERI, Los Angeles, California, 1952, 21-36.

Housner, G. W., 1956,"Limit design of structures to resist earthquakes. *Proc. of the 1st World Conference on Earthquake Engineering, Berkeley, California*, 5.1-5.13.

Krawinkler, H., 1997, *"Impact of Duration/Energy in Design"*. Proceedings of the FHWA/NCEER Workshop on the National Representation of Seismic Ground Motion for New and Existing Highway Facilities (Friedland, Power, Mayes Eds.), Technical Report NCEER-97-0010.

Langston, C.A., 1979, *"Structure under Mount Rainier, Washington, inferred from teleseismic body waves"*. J. Geophys. Res., 84, 4749-4762.

Marrara, F., Suhadolc, P., 1998a, *"Site amplifications in the city of Benevento (Italy): comparison of observed and estimated ground motion from explosive sources"*. J. Seism., 2, 125-143.

Marrara, F., Suhadolc, P., 1998b, *"Observation and modelling of site effects in the Volvi basin, Greece"*. In: The effects of surface geology on Seismic Motion. K. Irikura, K. Kudo, H. Okada and T. Sasatani (Editors), Balkema, Rotterdam, The Netherlands, 973-980.

Meletti, C., Patacca, E., Scandone, P., 2000, *"Construction of a seismotectonic model"*. PAGEOPH., 157, 11-35.

Molchan, G., Kronrod, T., Panza, G. F., 1997, *"Multi-scale seismicity model for seismic risk"*. Bull. Seism. Soc. Am., 87, 1220-1229.

Moldoveanu, C.L., Marmureanu G., Panza, G.F., Vaccari, F., 2000, *"Estimation of site effects in Bucharest caused by the May 30-31 1990, Vrancea seismic events"*. PAGEOPH., 157, 249-267.

Newmark N.M., Hall W.J., 1982, *"Earthquake spectra and design"*, Monograph Series, Earthquake Engineering Research Institute.

Nunziata, C., Costa G., Marrara F., Panza, G. F., 2000a, *"Calibrated estimation of the response spectra for the 1980 Irpinia earthquake in the eastern area of Naples"*. Earthquake Spectra, 16, 643-660.

Nunziata, C., Luongo, G., Panza, G.F., 2000b, *"Mitigation of seismic hazard in Naples and the protection of cultural heritage"*. Proceedings of the Second EuroConference on Global Change and Catastrophe Risk Management: Earthquake Risks in Europe, IIASA, Laxenburg, Austria, 6–9 July 2000.

Panza, G.F., 1985, *"Synthetic Seismograms: the Rayleigh Waves Modal Summation"*. J. Geophys., 58, 125-145.

Panza, G.F., Cazzaro, R., Vaccari, F., 1997, *"Correlation between macroseismic intensities and seismic ground motion parameters"*. Annali di Geofisica, 40, 1371-1382.

Panza, G.F., Romanelli, F., Vaccari, F., 2000a, *"Realistic modelling of waveforms in laterally heterogeneous anelastic media by modal summation"*. Geophys. J. Int., 143, 1-20.

Panza, G.F., Romanelli, F., Vaccari, F., 2001, *"Seismic wave propagation in laterally heterogeneous anelastic media: theory and applications to the seismic zonation"*. Advances in Geophysics, Academic press, 43, p. 1-95.

Panza, G.F., Romanelli, F., Vaccari, F., Decanini, L., Mollaioli, F., 2000b, *"Contribution of the deterministic approach to the characterization of seismic input"*. OECD-NEA Workshop on Engineering characterization of Seismic Input, BNL, Upton, New York, 15-17 November, 1999, NEA/CSNI/R(2000)2.

Panza, G.F., Suhadolc, P., 1987, *"Complete strong motion synthetics"*. In: Computational techniques, Vol. 4, Seismic strong motion synthetics, B.A. Bolt (Editor), Academic Press, 153-204.

Panza, G.F., Vaccari, F., Cazzaro, R., 1999b, *"Deterministic seismic hazard assessment"*. Vrancea Earthquakes: Tectonics, Hazard and Risk Mitigation. F.Wenzel et al (eds.), Kluwer Academy Publishers, 269-286.

Panza, G.F., Vaccari, F., Costa, G., Suhadolc, P., Fäh, D., 1996, *"Seismic input modelling for Zoning and microzoning"*. Earthquake Spectra, 12, 529-566.

Panza, G.F., Vaccari, F., Romanelli, F., 1999a, *"The IUGS-UNESCO IGCP Project 414: Realistic modelling of Seismic Input for Megacities and Large Urban Areas"*. Episodes, 22, 26-32.

Parvez, A. I. , Gusev, A.A., Panza, G.F., Petukhin, A.G., 2001, *"Preliminary determination of interdependence among strong motion amplitude, earthquake magnitude and hypocentral distance for the Hymalayan region"*. Geophys. J. Int., 144, 577-596.

Romanelli F., Bekkevold J., Panza, G.F., 1997, *"Analytical computation of coupling coefficients in non-poissonian media"*. Geophys. J. Int., 129, 205-208.

Romanelli, F. Bing, Z., Vaccari, F., Panza, G.F., 1996, *"Analytical computation of reflection and transmission coupling coefficients for Love waves"*. Geophys. J. Int., 125, 132-138.

Romanelli, F., Saraò, A., Suhadolc, P., Vaccari, F., 2001, *"Seismic input estimate at Fabriano from scaled and extended sources"*. Italian Geotechnical Journal, in press.##Fabio:aggiornare##

Romanelli, F., Vaccari, F., 1999, *"Site response estimation and ground motion spectral scenario in the Catania Area"*. J. of Seism., 3, 311-326.

Sabetta, F. Pugliese, A., 1987, *"Attenuation of Peak Horizontal Acceleration and Velocity from Italian Strong-Motion Records"*. Bull. Seism. Soc. Am., 77, 1491-1511.

Saragoni, R. Holmberg, A. Saez, A., 1989, *"Potencial Destructivo y Destructividad del Terremoto de Chile de 1985"*. Proceed. Sas. Jorn. Chilenas de Sismologia e Ing Antisismica, August 1989,Vol.1, 369-378.

Savy, J.B., Shah, H.C., Boore, D.M., 1980, *"Nonstationary Risk Model with Geophysical Input"*. J. Struct. Div., ASCE, 106, n. ST1, 145-164.

Schwartz, D.P., Coppersmith, K.J., 1984, *"Fault behaviour and characteristic earthquakes: examples from the Wasatch and San Andres fault zones"*. J. Geophys. Res., 89, 5681-5698.

Shteinberg, V., Saks, M., Aptikaev, F., Alkaz, V., Gusev, A., Erokhin, L., Zagradnik, I., Kendzera, A., Kogan, L., Lutikov, A., Popova, E., Rautian, T., Chernov, Yu., 1993, *"Methods of seismic ground motions estimation (Handbook)"*. Seismic ground motions prediction (Engineering seismology problems; Issue 34), Moscow, Nauka, 5-94. (in Russian)

Sun, R., Vaccari, F., Marrara, F., Panza, G.F., 1998, *"The main features of the local geological conditions can explain the macroseismic intensity caused in Xiji-Langfu (Beijing) by the Ms=7.7 Tangshan 1976 earthquake"*. PAGEOPH, 152, 507-521.

Trifunac, M.D., Brady A.G., 1975, *"A Study on the Duration of Strong Earthquake Ground Motion."* Bulletin of Seismological Society of America, 65, 581-626.

Uang, C.M., Bertero, V.V., 1990, *"Evaluation of seismic energy in structures"*. Earthquake Engineering and Structural Dynamics, 19, 77-90.

Uang, C. M., Bertero, V.V., 1988, *"Implications of Recorded Earthquake Ground Motions on Seismic Design of Buildings Structures". Report No. UCB/EERC-88/13*, Earthquake Engineering Research Center, University of California at Berkeley.

Vaccari, F., Gregersen, S., Furlan, M., Panza G.F., 1989, *"Synthetic seismograms in laterally heterogeneous, anelastic media by modal summation of P-SV waves"*. Geophys. J. Int., 99, 285-295.

Wang, H., Nisimura, A., 1999, *"On the behaviour of near-source strong ground motion from the seismic records in down-hole array at Hyogoken-Nanbu earthquake"*. Earthquake Resistant Engineering Structures II, G.Oliveto and C.A. Brebbia (Editors), WIT Press, Southampton, 363-372.

Wells, D.L., Coppersmith, K.J., 1994, *"New empirical relationships among magnitude, rupture length, rupture width, rupture area, and surface displacement"*. Bull. Seism. Soc. Am., 84, 974-1002.

GENERATION OF SYNTHETIC STRONG EARTHQUAKE GROUND MOTIONS USING A COMPOSITE SOURCE MODEL AND SYNTHETIC GREEN'S FUNCTIONS[1]

John G. Anderson[2], Haluk Sucuoglu[3], Yuehua Zeng[2], Feng Su[2]

Abstract

We describe a model that generates realistic synthetic records of plausible strong ground motions, specific to the fault – station geometry. We model the slip as a superposition of randomly located subevents. Since this source includes random parameters, we generate multiple realizations to investigate the uncertainties. In the context of the Representation Theorem, the motion is transferred to the site using synthetic Green's functions generated for a flat-layered Earth model. The Green's functions are generated using the regional velocity model, and can be modified with shallow layers to match the local site conditions. Source parameters are related energy and effective stress. Thus the parameters in the model are mostly constrained by either geological or geophysical observations. This paper also reviews several applications.

Introduction

Over the past years, we have focused efforts to develop and improve a numerical simulation procedure to compute synthetic strong motion seismogram using a composite source model described by Zeng et al. (1994), and first tested by Yu (1994). The method has been successful in generating realistic strong motion seismograms. The realism is demonstrated by comparing synthetic strong motions with observations from the recent California earthquakes at Landers, Loma Prieta (Su et al., 1994a,b) and Northridge (Zeng and Anderson, 1996; Anderson and Yu, 1996; Su et al., 1998), earthquakes in the eastern US (Ni et al., 1999) and earthquakes in Guerrero, Mexico (Zeng et al., 1994; Johnson, 1999), Turkey (Anderson et al., 1997, 2001; Sucuoglu et al, 2002) and India (Khattri et al, 1994; Zeng et al, 1995; Yu et al, 1995). Anderson and Chen (1995) suggested that the composite source model correctly models the rate of buildup of the seismogram energy for a range of earthquake sizes. We have also applied the method for earthquake engineering applications to compute the ground motion of scenario earthquakes. During the process of continuing development, we have included scattering waves from small scale heterogeneity structure of the earth, site specific ground motion prediction using weak motion site amplification, and nonlinear soil response using the geotechnical engineering model. We have evaluated the numerical procedure for simulating near-fault long-period ground motions and rupture directivity, revisiting some of the Loma Prieta, Landers and Northridge earthquakes, and adding the 1979 Imperial Valley, California earthquake and the 1995 Kobe event (Zeng and Anderson, 2000).

Our motivation is to understand the physics of wave propagation and the earthquake source. Successful predictive models demonstrate understanding. The composite source model procedure provides a framework for improving and testing physical models for the two main problems that must be solved to predict strong earthquake ground motion: source description and wave propagation. Of course, a goal of strong-motion seismology is to generate generating synthetic strong ground motion seismograms that are sufficiently realistic that they can be used in engineering applications. Our intent is to achieve this, but only in the context of continuous improvements of the physical models of the processed that are involved, combined in a rigorous mathematical framework. We measure how closely we can model historical accelerograms so that when we change the model we can measure the consequent improvement.

In our view, adequate synthetic seismograms must satisfy several criteria:

1. They must be broadband seismograms, i.e. including energy in the entire seismic frequency range, from DC to about 30Hz.
2. They should explicitly incorporate the fault geometry and focal mechanism.
3. They should be able to model earthquakes from magnitude 0 to 8+.
4. They should contain P-waves, S-waves, Love waves and Rayleigh waves.
5. They should satisfy the wave equation. This implies, among other criteria, that amplitudes on horizontal and vertical components should be realistic, that surface waves will show appropriate dispersion, and that adjacent sites will show motions with physically realistic amounts of correlation and phase lags.
6. They should have realistic envelopes in the time domain. This implies that seismic scattering must be incorporated.
7. They should have realistic amplitudes in the time domain.
8. They should have realistic spectral amplitudes in the frequency domain. Thus the source must radiate energy at appropriate levels across the entire frequency band of interest.
9. They should have a random component, and a way to obtain multiple realizations that will have a realistic amount of aleatory variability.

The purpose of this paper is to review the method that we have been using to generate the synthetic seismograms, illustrate some applications, and discuss future directions for these studies.

Method

Mathematical Framework

The mathematical framework for this, as for most ground motion simulations, is the representation theorem. After Aki and Richards (1980), one form for the representation theorem is:

$$u_n(\bar{x},t) = \int_{-\infty}^{\infty} d\tau \iint_{\Sigma} \left[u_i(\bar{\xi},\tau)\right] c_{ijpq} \nu_j \frac{\partial G_{np}(\bar{x},t-\tau;\bar{\xi},0)}{\partial \xi_q} d\Sigma \qquad (1)$$

In this equation, $u_n(\bar{x},t)$ gives the n^{th} component of the displacement of the ground at location $\bar{x}$ and at time t. The vector $\bar{\nu}$ is normal to the fault. The i^{th} component of the discontinuity in the slip across the fault is given by $\left[u_i(\bar{\xi},\tau)\right] = u_i^+(\bar{\xi},\tau) - u_i^-(\bar{\xi},\tau)$ where $\bar{\xi}$ represents a location on the fault surface Σ and τ is the time that this displacement occurs. Since the fault is represented by the surface Σ, $d\Sigma$ represents two spatial dimensions. The Green's function is given by $G_{np}(\bar{x},t;\bar{\xi},\tau)$.

---

[1] Paper for Organization for Economic Co-operation and Development-Nuclear Energy Agency Workshop on the Relations between Seismological Data and Seismic Engineering Analysis. October 17-18, 2002, Istanbul, Turkey.

2 Seismological Laboratory, University of Nevada, Reno, Nevada 89557; jga@unr.edu; 775-784-4265

[3] Earthquake Engineering Research Center, Middle East Technical Univerisity, 06531 Ankara, Turkey a06074@metu.edu.tr

This gives the motion in the n direction at location $\bar{x}$ and time t caused by a point force acting in the p direction at location $\bar{\xi}$ and time τ. Finally, c_{ijpq} gives the elastic constants of the medium. For an isotropic medium, $c_{ijpq} = \lambda\delta_{ij}\delta_{kl} + \mu\left(\delta_{ik}\delta_{jl} + \delta_{il}\delta_{jk}\right)$, where λ and μ are the Lame constants. The constant μ is the shear modulus. In Equation (1) summation takes place over repeated indices.

Equation (1) represents the ground motion at the site as the linear combination, through the integral over space, of the contributions from each point on the fault surface. The convolution over time incorporates the effect of the rupture at each point taking a finite amount of time. Through the representation theorem, the problem of predicting ground motions requires specification of the offset on the fault as a function of location and time, which incorporates earthquake source physics, and a specification of the Green's function, which incorporates wave propagation. Next we discuss how the composite source model handles each of these two components.

Composite Source

The composite source that we use is a kinematic model for the slip on the fault. Our models, at this time, are not consistent with dynamic models in which initial stress, rock properties, and friction laws are specified and the rupture is allowed to proceed based on only the laws of physics. While such models improving, they are limited to low frequencies and are based on highly uncertain assumptions about the input. On the other hand, the various versions of the composite source that we have developed so far are able to generate seismograms that satisfy, with measurable misfit and uncertainty, all of the criteria set forth in the introduction.

The source is a superposition of circular subevents with constant stress drop. They are taken to be a realization of a random process, controlled by a density function with a power law dependence:

$$N(R) = \frac{p}{D}\left(R^{-D} - R_{max}^{-D}\right) \tag{2}$$

where N is the number of subevents of radius R or greater, and p is a constant of proportionality. D is the fractal dimension that, according to Frankel (1991), equals twice the b-value, so is typically set at D=2. It is mandatory that $D<3$, for otherwise the majority of the seismic moment is released in small subevents. The maximum subevent size, R_{max}, can be taken by default to have a radius of half the narrower fault dimension, although it may be smaller. The model is motivated by a model of the source proposed by Frankel (1991). The random nature of the heterogeneities on a complex fault is simulated by distributing the subevents randomly. Figure 1 shows a realization of the spatial distribution of subevents. Normally, the locations of subevents are constrained such that the outer limit of the subevent does not overlap the boundary of the fault.

Final slip on each subevent is given by Eschelby's (1957) static solution for the shear offset of a circular crack in the presence of a shear stress:

$$u(r) = \frac{24}{7\pi}\left(\frac{\Delta\sigma}{\mu}\right)\left(R^2 - r^2\right)^{\frac{1}{2}} \tag{3}$$

Equation (3) introduces a stress drop parameter, $\Delta\sigma$, which is the static stress drop of the individual subevents. The seismic moment of each subevent is given by:

$$M_0(R) = \frac{16}{7}R^3\Delta\sigma \tag{4}$$

After selecting a subevent stress drop, integrating the number of subevents (Equation 2) and their moments determins the parameter p:

$$p = \frac{7M_0^E}{16\Delta\sigma}\frac{3-D}{\left(R_{max}^{3-D} - R_{min}^{3-D}\right)} \tag{5}$$

where M_0^E is the seismic moment of the earthquake. In the numerical realizations of the model, R_{min} can be taken to be small enough that it has no significance. The heterogeneous nature of the composite earthquake faulting is thus characterized by the maximum subevent size and the subevent stress drop. It is uncommon for a particular realization to have a subevent with radius more than about 0.75 R_{max}. Figure 2 gives a perspective view of a some realizations of the slip for a magnitude 6 earthquake on a 6 km x 10 km fault, where each subevent is represented with the slip of an Eschelby (1957) crack. The top shows two realizations with a subevent stress drop of 100 bars. The bottom shows the effect of changing the subevent stress drop. A smaller subevent stress drop results in more subevents which, in their accumulated effect, tend to cause the slip function to be smoother, and the associated high-frequency radiation to be reduced in amplitude. The subevent stress drop can also be constrained by other independent geophysical data. Anderson (1997) concludes that the subevent stress drop is proportional to the radiated energy, the effective dynamic stress, and the apparent stress.

To represent the kinematic behavior (the time history of the slip) a hypocenter is chosen at some location on the fault, typically near the bottom. Rupture propagates from the hypocenter at a constant rupture velocity, v, typically taken to be between 2.5 km/s and 3.0 km/s, as given by inverse studies of past earthquakes. Each subevent initiates its radiation when the rupture front reaches it's center.

As part of our continuing efforts to increase the realism, we have used four different models for the displacement pulse radiated from each subevent. At first, we modeled it as a Brune (1970) pulse (Zeng et al., 1994; Yu, 1994). The time function for this case for a subevent with moment M_{0s} is:

$$\Omega(t) = \left(2\pi\ f_c\right)^2 M_{0s}\, t \exp\left(-2\pi\ f_c t\right) H(t) \tag{6}$$

The corner frequency was taken after Brune to be $f_c = 2.34\beta/2\pi\ R$ in which β is the shear velocity. While this time function is sufficient to generate realistic seismograms in most cases, it fails some characteristics that are believed to be true of dynamic ruptures, such as the initial motion beginning proportional to t^2. To make the results somewhat more physical, Zeng and Anderson (1996) modified the source time function to be the radiation, given by Sato and Hirasawa (1973), from a growing circular crack, where the crack at all times has the shape of the Eschelby's (1957) solution. This time function introduces another parameter, v_c, which is the expansion rate of the subevent. A higher subevent rupture expansion rate results in a shorter subevent rupture time and thus a higher corner frequency. This replaces the fixed relationship between the corner frequency and the subevent radius (Eqn. 6). We normally set v_c=v, but for some earthquakes, that does not work.

While the Brune (1970) and Sato and Hirasawa (1973) models were mostly satisfactory for stations relatively far from the fault, additional modification is necessary to match accelerograms from very near to the fault. Thus, Zeng (2002) introduced two asymmetric circular rupture models to improve the subevent source radiation. The first is an asymmetric circular rupture that again matches the Eshelby's (1957) static solution at every successive instant of rupture, where the center moves at a given velocity v_c that must be less than v_r, the velocity at which the crack expands. As a result, the rupture velocity at any point on the crack depends on the azimuth angle from the rupture nucleation to the point. When v_c=0, we have Sato and Hirasawa's model. When the velocity is equal to the growing crack velocity, we have Dong and Papageorgiou's (2002) model. The second modification has the crack rupture velocity accelerating during the rupture. This procedure gives about the right amount of rupture directivity on both the fault normal and fault parallel components, at least in the sense that it approximately agrees with the near-fault directivity model of Somerville et al. (1997).

Green's Functions

This method uses synthetic Green's functions, which characterize wave propagation in a flat-layered medium, in the representation theorem (Equation 1). They are calculated as described by Luco and Apsel (1982). The effect of attenuation (Q) is efficiently incorporated into this model. The synthetic Green's function has been modified to consider the effect of the random lateral heterogeneity of the earth by adding scattered waves into the Green's function (Zeng, 1995; Zeng et al, 1995). The solution is also convolved with a plane wave propagation function through a near surface 1-D velocity layering as complex as that suggested by sonic well logs. Recognizing that the radiation pattern at high frequencies does not represent a double-couple mechanism, presumably due to scattering near the source, we introduce a correction for that effect. Thus the complex high-frequency waveform is generated from a combination of a heterogeneous source , wave reverberation in a stratified crustal structure and scattering from lateral inhomogeneity. Figure 3 is designed to represent major elements of the composite source model. Frames show the effects of the source complexity (upper left), the layered medium (upper right), random scattering (lower left), scattering destroying the radiation pattern (lower middle), and directivity in the pulses radiated from the subevents (lower right).

Representative Results

This section selects figures from some of our papers showing applications of the composite source model. Figure 4, from Zeng et al (1994), shows a comparison of synthetic and actual seismograms for the 19 September, 1985 Michoacan, Mexico earthquake. This result shows that the synthetics are capable of matching the statistical characteristics of actual seismograms over the entire frequency band of interest to strong motion seismology.

Figures 5-7 are from the Anderson and Yu (1996) modeling of the 1994 Northridge, California, earthquake. This was a "semi-blind" experiment, as we generated the synthetic seismograms at 14 sites after the earthquake had occurred, with knowledge of the fault location, focal mechanism, and velocity model, but nothing was modified to improve the fit to the seismograms after we established the parameters that we would use. Figure 5 shows seismograms and Fourier spectra for the station nearest the epicenter. Figure 6 shows the misfit as a function of diatance for peak acceleration, velocity and displacement. Figure 7 shows the misfit as a function of distance for the Fourier amplitude spectrum. The misfit was obtained by finding, for instance, the peak acceleration at a station based on 50 synthetic realizations of the source model. Anderson and Yu (1996) concluded that in this form, the model is capable of performing nearly as well as regression models. Subsequent tests, extending to statiosn nearer the fault and farther from the fault, and computing the seismograms to higher frequencies, demonstrated the need to continue to improve the model.

Zeng and Anderson (1996) found a specific composite source model that fits the accelerograms at low frequencies for the Northridge earthquake (Figs. 8, 9). They used a genetic algorithm inversion to obtain the specific composite source model. Figure 8 shows the slip function, and Figure 9 shows the match to the seismograms. We consider this an important conclusion, since it shows that the low-frequency ground motion from actual earthquake slip functions is within the space spanned by the composite source models. This supports the idea that the composite source model has enough realism to be used to develop scenario accelerograms for future earthquakes.

Anderson et al (2001) and Sucuoglu et al (2002) studied the M=6.2 Dinar, Turkey, earthquake of October 1, 1995. This earthquake had a normal-faulting focal mechanism. Figure 10 shows the location of Dinar, and Figure 11 shows the locations of the nearby strong motions stations. Figure 12 shows the slip function, determined using the genetic algorithm of Zeng and Anderson (1996), and Figure 13 shows the low-frequency match between synthetic and observed seismograms. The composite source model was used to extrapolate the ground motions to additional sites within Dinar. Figure 14 (left) shows Dinar relative to the fault rupture. Figure 15 from Sucuoglu et al (2002) shows the broadband fit between the composite source model seismograms and the data from the Dinar accelerograph. Figure 14 (right) shows the locations of the stations used by Sucuoglu et al to generate synthetic broadband seismograms utilizing near surface geological information. Figure 16 shows a selection of the seismograms. Sucuoglu et al compiled damage data from Dinar according to the city boroughs shown in Figure 14. Figure 17 shows profiles of the damage parameter and various measures of the strength of the ground motions from the synthetics, showing that they have a common form. Figure 18 is one of several figures from Sucuoglu et al (2002) correlating damage parameters with a ground motion parameter (in this case, the spectral energy between 0 and 1 Hz) within a zone of common surficial geology. The positive correlation, which is as good as could be hoped for considering uncertainties, indicates that the composite source model has added information on the nature of ground motions even within the small lateral dimensions of the city of Dinar.

Conclusions and Future Directions

The composite source model seems to be an adequate model for engineering applications. However, our overall goal is to make it more consistent with the physics of earthquake rupture and wave propagation. At low frequencies, future steps could involve merging the computations based on the layered models with finite difference computations of the response of a basin.

Since the model uses exact Green's functions for a layered half space, the seismograms for nearby locations reflect strain in the Earth model, when the random scattering is not used. The correlation of adjacent points is something that can be adjusted to match observations through calibration of the random scattering component of the Green's functions. Thus a future application is to study strains or input motions at separated bridge piers, for instance.

At high frequencies, the physics that generate the high frequency radiation are not well understood (Anderson et al, 2002). More study is needed, for instance, to explain why peak accelerations were unexpectedly low in the 1999 Turkey and Taiwan earthquakes, and then to incorporate these results into the calibration of the model.

Acknowldegements

This material is based upon work supported by the National Science Foundation under Grant Nos. 0000033 and 0000050. This research was also supported by the Southern California Earthquake Center. SCEC is funded by NSF Cooperative Agreement EAR-8920136 and USGS Cooperative Agreements 14-08-0001-A0899 and 1434-HQ-97AG01718. The SCEC contribution number for this paper is 700.

References

Aki, K. and P.G. Richards (1980). Quantitative seismology, W. H. Freeman, New York.

Anderson, J. G. (1997). Seismic energy and stress drop parameters for a composite source model, *Bull. Seism. Soc. Am.* 87, 85-96.

Anderson, J. G. and Q. Chen (1995). Beginnings of earthquakes in the Mexican subduction zoen on strong motion accelerograms, *Bull. Seism. Soc. Am.* 85, 1107-1115.

Anderson, J. G. and G. Yu (1996). Predictability of strong motions from the Northridge, California, earthquake, *Bull. Seism. Soc. Am. No.* 86, 1B, S100-S114.

Anderson, J. G., Y. Zeng, H. Sucuoglu (1997). Analysis accelerations from the Dinar, Turkey earthquake, presented at the Eighth International Conference on Soil Dynamics and Earthquake Engineering at Istanbul, Turkey.

Anderson, J. G., Y. Zeng, H. Sucuoglu (2001). Analysis accelerations from the 1 October 1995 Dinar, Turkey earthquake, *Bull. Seism. Soc. Am.* 91, 1433-1445.

Anderson, J. G., J. N. Brune, S. G. Wesnousky (2002). Physical phenomena controlling high-frequency seismic wave generation in earthquakes, Proceedings, 7th US National Conference on Earthquake Engineering, Boston, July.

Brune, J. N. (1970). Tectonic stress and spectra of seismic shear waves from earthquakes, *J. Geophys. Res.* 76, 5002.

Dong, G. and A. S. Papageorgiou (2002). Seismic radiation from a unidirectional assymetrical circular crack model, Par I: constant rupture velocity, *Bull. Seism. Soc. Am.* 92, 945-961.

Eschelby, J. D. (1957). The determination of the elastic field of an ellipsoidal inclusion, and related problems, Proceedings of the Royal Society of London, A241, 376-396.

Frankel, A. (1991). High frequency spectral falloff for earthquakes, fractal dimension of complex rupture, b-value, and the scaling of strength on faults, *J. Geophys. Res.* 96, 6291-6302.

Johnson, M. (1999). Composite source model parameters for large earthquakes (M>5.0) in the Mexican subduction zone, M. S. thesis, University of Nevada, Reno.

Luco, J.E. and R.J. Apsel (1982). On the Green's functions for a layered half space. Part I. *Bull. Seism. Soc. Am.* 73, 909-929.

Khattri, K. N., Y. Guang, J. G. Anderson, J. N. Brune and Y. Zeng (1994). Seismic hazard estimation using modelling of earthquake strong ground motions: A brief analysis of 1991 Uttarkashi earthquake, Himalaya and prognostication for a great earthquake in the region, *Current Science*, 67, 343-353

Ni., S.-D., J. G. Anderson, Y. Zeng (1999). Comparison of strong ground motions from the 1988 Seguenay earthquake with the synthetic simulations using the composite source model, in preparation.

Sato, T. and T. Hirasawa (1973). Body wave spectra from propagating shear waves, J. Phys. Earth 21, 415-431.

Somerville, P. G., N. F. Smith, R. W. Graves, and N. A. Abrahamson (1997). Modification of empirical strong ground motion attenuation relations to include the amplitude and duration effects of rupture Directivity, Seism. Res. Lett., 68, 199-222.

Su, Feng, Y. Zeng and J. G. Anderson (1994a). Simulation of the Loma Prieta earthquake strong ground motion using a composite source model, EOS, Trans. A.G.U., 75, 44, p448.

Su, F., Y. Zeng and J. G. Anderson (1994b). Simulation of Landers earthquake strong ground motion using a composite source model, Seism. Res. Lett., 65, p52.

Su, F., J. G. Anderson and Y. Zeng (1998). Study of weak and strong motion including nonlinearity in the Northridge, California, earthquake sequence, submitted to *Bull. Seis. Soc. Am.* 88, 1411-1425.

Sucuoglu, H., Anderson, J. G., Y. Zeng, (2002). Predicting intensity and damage distribution during the 1995 Dinar, Turkey, earthquake with generated strong motion accelerograms, BSSA submitted.

Yu, G. (1994). *Ph.D. Thesis*, University of Nevada, Reno.

Yu, G., K. N. Khattri, J. G. Anderson, J. N. Brune, and Y. Zeng (1995). Strong ground motion from the Uttarkashi, Himalaya, India earthquake: comparison of observations with synthetics using the composite source model, *Bull. Seism. Soc. Am.*, 85, 31-50.

Zeng, Y. (1995). A realistic synthetic Green's function calculation using a combined deterministic and stochastic modeling approach, EOS, Trans. A.G.U., 76, F357.

Zeng, Y. (2002). Final Technical Report on Validation of 1-D Numerical Simulation Procedures, Final Technical Report, PEER Project 1C02, Task 1: Earthquake ground motion, Seismological Lab, University of Nevada – Reno.

Zeng, Y., J. G. Anderson and G. Yu (1994). A composite source model for computing realistic synthetic strong ground motions, *Geophys. Res. Lett.*, 21, 725-728.

Zeng, Y., J. G. Anderson and Feng Su (1995). Subevent rake and scattering effects in realistic strong ground motion simulation, *Geophy. Res. Lett*, 22, 17-20.

Zeng, Y. and J. G. Anderson (1996). A composite source modeling of the 1994 North-ridge earthquake using Genetic Algorithm, *Bull. Seism. Soc. Am.* 86, No. 1B, 71-83.

Zeng, Y. and J. G. Anderson (2000). Earthquake source and near-field directivity modeling of several large earthquakes, EERI Proceedings for the Sixth International Conference on Seismic Zonation.

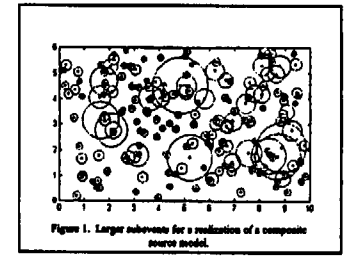

Figure 1. Larger subevents for a realization of a composite source model.

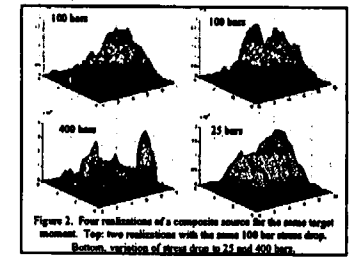

Figure 2. Four realizations of a composite source for the same target moment. Top: two realizations with the same 100 bar stress drop. Bottom, variation of stress drops to 25 and 400 bars.

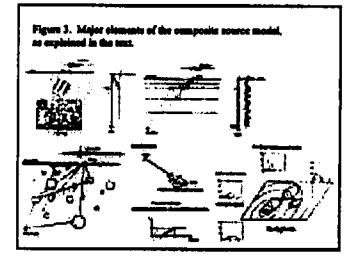

Figure 3. Major elements of the composite source model, as explained in the text.

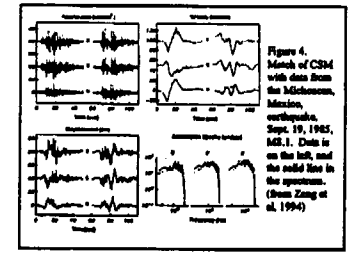

Figure 4. Match of CSM with data from the Michoacan, Mexico, earthquake, Sept. 19, 1985, M8.1. Data is on the left, and the solid line in the spectrum. (from Zeng et al. 1994)

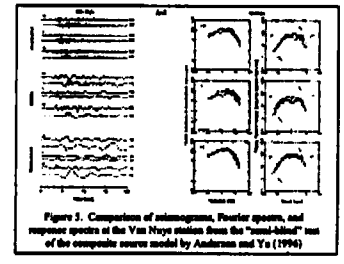

Figure 5. Comparison of seismograms, Fourier spectra, and response spectra at the Van Nuys station from the "hand-blind" test of the composite source model by Anderson and Yu (1994)

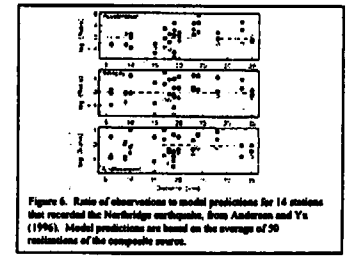

Figure 6. Ratio of observations to model predictions for 14 stations that recorded the Northridge earthquake, from Anderson and Yu (1996). Model predictions are based on the average of 50 realizations of the composite source.

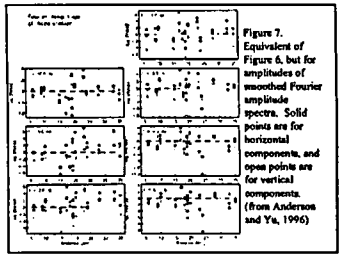

Figure 7. Equivalent of Figure 6, but for amplitudes of smoothed Fourier amplitude spectra. Solid points are for horizontal components, and open points are for vertical components. (from Anderson and Yu, 1996)

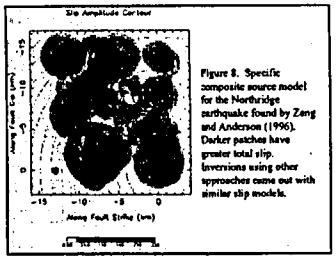

Figure 8. Specific composite source model for the Northridge earthquake found by Zeng and Anderson (1996). Darker patches have greater total slip. Inversions using other approaches came out with similar slip models.

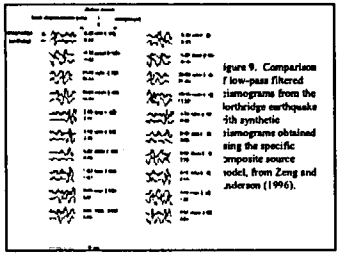

igure 9. Comparison f low-pass filtered ismograms from the lorthridge earthquake ith synthetic ismograms obtained sing the specific omposite source odel, from Zeng and nderson (1996).

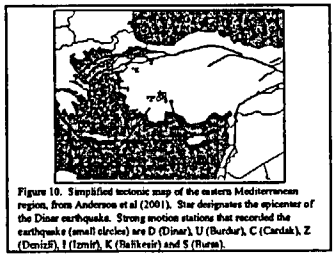

Figure 10. Simplified tectonic map of the eastern Mediterranean region, from Anderson et al (2001). Star designates the epicenter of the Dinar earthquake. Strong motion stations that recorded the earthquake (small circles) are D (Dinar), U (Burdur), C (Cardak), Z (Denizli), I (Izmir), K (Balikesir) and S (Bursa).

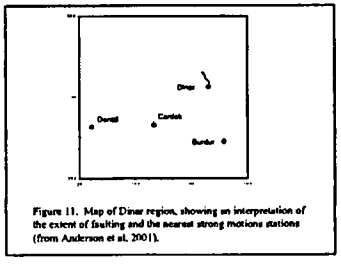

Figure 11. Map of Dinar region, showing an interpretation of the extent of faulting and the nearest strong motions stations (from Anderson et al, 2001).

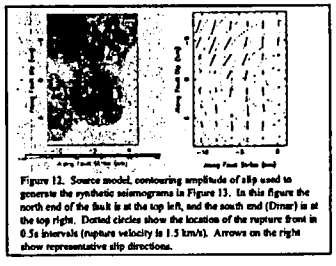

Figure 12. Source model, contouring amplitude of slip used to generate the synthetic seismograms in Figure 13. In this figure the north end of the fault is at the top left, and the south end (Dinar) is at the top right. Dotted circles show the location of the rupture front in 0.5s intervals (rupture velocity is 1.5 km/s). Arrows on the right show representative slip directions.

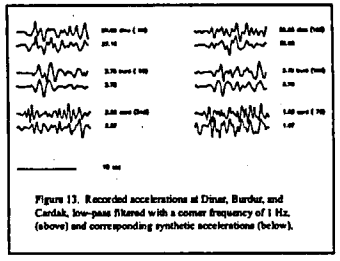

Figure 13. Recorded accelerations at Dinar, Burdur, and Cardak, low-pass filtered with a corner frequency of 1 Hz. (above) and corresponding synthetic accelerations (below).

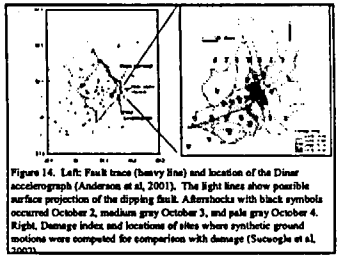

Figure 14. Left: Fault trace (heavy line) and location of the Dinar accelerograph (Anderson et al, 2001). The light lines show possible surface projection of the dipping fault. Aftershocks with black symbols occurred October 2, medium gray October 3, and pale gray October 4. Right, Damage index and locations of sites where synthetic ground motions were computed for comparison with damage (Sucuoglu et al, 2002).

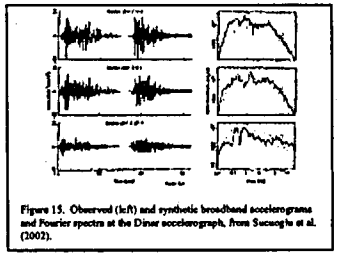

Figure 15. Observed (left) and synthetic broadband accelerograms and Fourier spectra at the Dinar accelerograph, from Sucuoglu et al. (2002).

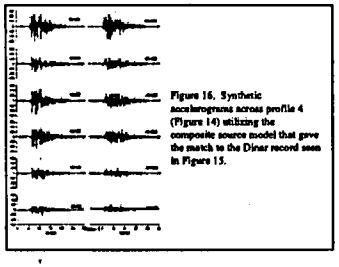

Figure 16. Synthetic accelerograms across profile 4 (Figure 14) utilizing the composite source model that gave the match to the Dinar record seen in Figure 15.

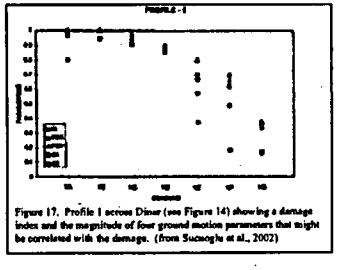

Figure 17. Profile 1 across Dinar (see Figure 14) showing a damage index and the magnitude of four ground motion parameters that might be correlated with the damage. (from Sucuoglu et al., 2002)

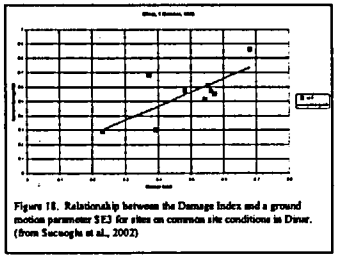

Figure 18. Relationship between the Damage Index and a ground motion parameter SE3 for sites on common site conditions in Dinar. (from Sucuoglu et al., 2002)

INVERSION OF STOCHASTIC EARTHQUAKE MODEL PARAMETERS IN KOREA USING THE MODIFIED LEVENBERG-MARQUARDT'S METHOD

Kwan-Hee Yun[1)], Walter Silva[2)], Jong-Rim Lee[1)]
1) Korea Electric Power Research Institute, Korea 2) Pacific Engineering and Analysis, USA

Abstract

Parameters of stochastic point-source ground motion model were inverted based on extensive digital records from dense seismic networks for small-to-moderate earthquakes in and around the Korea. Modified Levenberg-Marquardt's nonlinear inversion method was employed for stable inversion which considers the second derivatives of the Hessian matrix. After trying various cases with regard to seismic source types, frequency dependency of crustal attenuation, and crustal amplification, the best estimates for earthquake simulation are determined to be $348f^{0.53}$ for crustal attenuation, 20~30 bars for stress drop, 0.02 for site anelastic attenuation (kappa), and 50 km for crossover distance. In addition, detailed features of crustal attenuation such as anisotropy and localized Q were evaluated, which contributes to providing scientific bases for developing site-specific ground motion attenuation relations and interpreting the geological and geophysical characteristics of the Korean Peninsula.

Introduction

In the region where strong ground motion data are scarce such as in Korea, it becomes engineering practice to employ well-founded, validated, and simple stochastic point-source ground motion earthquake model to predict strong ground motion. The parameters for stochastic point-source ground motion model are stress drop for sources, frequency dependent quality factor (Q) for crustal attenuation, and kappa (κ) for site effects.

In this study, these model parameters were inverted based on extensive earthquake dataset at the first step and more detailed features of crustal attenuation were investigated at the second step. For stable inversion of these parameters under various cases, conventional Levenberg-Marquardt's nonlinear inversion method is simply modified by taking into account the second derivatives of the Hessian matrix.

As a result of the first step, it turned out that crustal attenuation with frequency dependent model, $348 \cdot f^{0.53}$ (f means frequency) is calculated to be the best estimate for simulating almost all of the earthquake records in and around the South Korea with amplification ratio of 1.67 at high frequencies (> 5Hz) for crustal amplification and stress drop ranging from 20 to 30 bars. However by analyzing the fitting results from the inversion, it seems that some misfit can not be fully accounted for by site characteristics only, which suggests that the crustal attenuation is different over the region. Also unsatisfactorily the inverted Q is significantly higher than the previous crustal attenuation values determined by using the S coda wave for a specific region ([2,3,4,5,6,7]). This would have serious implication in developing site-specific ground motion attenuation relations. In addition if the lateral variation of crustal attenuation is fully identified, this would contribute to reducing the uncertainties inherent in developing ground motion attenuation relations. Especially considering the fact that earthquakes with moderate size and above could occur far from the seismic observation networks, it is necessary to take into account the lateral variation of crustal attenuation to accurately estimate the source characteristics. Also the study on crustal attenuation provides the scientific data to help interpret the earth interior beneath the Korean Peninsula, since the Q is known to be well correlated with interfaces and discontinuities within the crust, material composition, thickness and heat flow ([8]). Regional differences of Q have been suggested by previous researches but without quantification and systematic approach and mainly focused on the southeastern part of Korea. Recently a study concluded that the Lg Q values do not have same distribution throughout the region based on the Q study by using Reversed Two Station Method ([3]). There were other studies abroad on mapping of lateral variation of Lg wave ([8,9]).

So at the second step, unlike the previous study solely focused on mapping of lateral Q structure, characteristics of quality factor such as anisotropy and lateral variation are comprehensively studied in the aspect of simulating strong ground motion using earthquake data from the Korean seismic networks which are unique in the world and in perfect condition for Q tomographic inversion in that high dynamic range seismic stations are densely populated over the nation.

Theory

The stochastic point-source ground motion model has proven remarkably effective in correlating with a wide range of ground motion observations. The model employed in this study uses an ω-square source model with a single corner frequency and a constant stress parameter ([10]). Random vibration theory is used to relate RMS (root-mean-square) values to peak values of acceleration, and oscillator response computed from the power spectra to expected peak time domain values.

The shape of the acceleration spectral density, s(f), is given by

$$s(f) = C \frac{f^2}{1+(\frac{f}{f_c})^2} M_0 G(R) P(f) A(f) e^{\frac{\pi f R}{\beta Q(f)}} \quad (1)$$

where

M_0 = seismic moment, R = hypocentral distance,

β_0 = shear wave velocity at the source, Q(f) = frequency dependent quality factor ($Q_0 f^{\eta}$),

A(f) = near-surface amplification factors, P(f) = high-frequency truncation filter,

f_c = source corner frequency, $C = \beta_0 (\frac{1}{\rho_0 \beta_0^3}) \cdot (2) \cdot (0.63) \cdot (\frac{1}{\sqrt{2}}) \cdot \pi$

$G(R) = R^{-1}$ *for* $R \le R_0$, $\sqrt{R_0 R}$ *for* $R \ge R_0$

C is a constant which contains source region density (ρ_0) and shear-wave velocity terms and accounts for the free-surface effect (factor of 2), the source radiation pattern averaged over a sphere (0.63), and the partition of energy into two horizontal components ($1/\sqrt{2}$). Source scaling is provided by specifying two independent parameters, the seismic moment (M_0) and the high-frequency stress parameter or stress drop ($\Delta\sigma$). The seismic moment is related to magnitude through the definition of moment magnitude M by the relation

$$\text{Log } M_0 = 1.5\,M + 16.1 \text{ ([11])} \quad (2)$$

The stress parameter ($\Delta\sigma$) is taken to be independent of magnitude throughout the world and relates the corner frequency fc to M_0 through the relation

$$f_c = \beta(\Delta\sigma / 8.44 M_0)^{1/3} \tag{3}$$

The spectral shape of the single-corner-frequency ω-square source model is then described by the two free parameters M_0 and $\Delta\sigma$. The P(f) filter is an attempt to model the observation that acceleration spectral density appears to fall off rapidly beyond some region-dependent maximum frequency. The κ adopted here for P(f) is attributed to attenuation in the very shallow crust directly below the site ([12]). The intrinsic attenuation along this part of the path is not considered to be frequency dependent and is modelled as a frequency independent, but site dependent, constant value of kappa. Geometrical attenuation (G(R)) is divided into two types depending on whether hypocentral distance exceeds the crossover distance, R_0 or not.

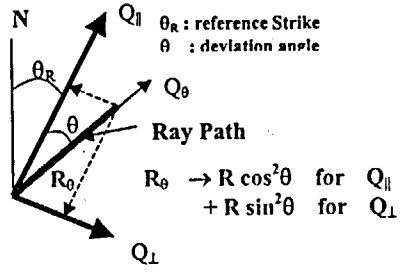

Figure 1. Schematic diagram to illustrate the physical model for Q anisotropy

Characteristics of Q anisotropy is modeled in terms of anisotropy ratio, ε with respect to reference strikes by constructing physical model that anelastic crustal attenuation along a ray path can be constructed by linear combination of directional attenuations along two mutually orthogonal paths with weights determined by a function of angle, which leads to following formula (Figure 1).

$$\frac{R_\theta}{Q_0} = \frac{R_\parallel}{Q_\parallel} + \frac{R_\perp}{Q_\perp} = \frac{R\cdot\cos^2\theta}{Q_\parallel} + \frac{R\cdot\sin^2\theta}{\varepsilon Q_\parallel} \tag{4}$$

where R_θ is the length of path intersecting a block deviating a reference strike with angle θ. $R_\parallel$ and $R_\perp$ is the projection of R_θ into the parallel and orthogonal direction relative to the given strike with the constraint that R_θ equals to the sum of $R_\parallel$ and $R_\perp$ for all deviation angles. $Q_\parallel$ and $Q_\perp$ represent the Q_0 values for the paths parallel and orthogonal to the given strike. Q anisotropy ratio ε is defined here as $Q_\perp / Q_\parallel$.

In addition, if localized Q_{0i} for i-th block is used for Q tomographic inversion instead of regional Q_0, the exponent term of equation (1) can be replaced as follows.

$$\frac{\pi f R}{\beta_0 Q(f)} = \frac{\pi f R}{\beta_0 Q_0 f^\eta} = \frac{\pi f}{\beta_0 f^\eta} \sum_{i=1}^{N} \frac{R_i}{Q_{0i}} \tag{5}$$

where N is the total number of discretized blocks crossing the ray path from hypocenter to the sites and R_i is the length of ray path intersecting i-th block. In this study, depth of ray path intersecting blocks and width of a ray were not explicitly considered. Since the shear wave velocity and η are not so sensitive to local geological features, these values are rightly assumed to be the same for whole region. Even though the localized Q can be modeled using non-parametric form for multiple frequencies, we use a functional form of power-law frequency dependence for quality factor to minimize the site effect expected in high frequencies when using non-parametric forms.

If we denote the natural log of s(f) in equation (1) as $y(x;\vec{a})$ where $\vec{a}$ is a vector of parameters and x is a variable for frequency values, best estimates of model parameters $\vec{a}$ can be found by minimizing the following merit function ([13]).

$$\chi^2(\vec{a}) = \sum_{i=1}^{N} [y_i - y(x_i;\vec{a})]^2 \tag{6}$$

where y_i is observed value at x_i and components of model parameters of $\vec{a}$ depends on the problems to be solved, i.e. in case of inversion for regional parameters

$$\vec{a} = (Q_0,\ \eta,\ R_0,\ M_1, \ldots, M_{N_{eqk}},\ \ln(f_{c1}), \ldots, \ln(f_{cN_{eqk}}),\ \kappa_1, \ldots, \kappa_{N_{sta}}) \tag{7}$$

N_{eqk} = total number of earthquake events, N_{sta} = total number of seismic stations.

For inversion of anisotropy in equation (4), additional parameters Q_0, η, and ε for local regions will be included in model parameters. For Q tomographic inversion, $\ln(Q_{0i})$ in equation (5) will be added. The first and second derivatives of equation (6) with respect to a_k, a component of $\vec{a}$ can be written as equation (8) and (9).

$$\frac{\partial\chi^2(\vec{a})}{\partial a_k} = -2\sum_{i=1}^{N} [y_i - y(x_i;\vec{a})] \frac{\partial y(x_i;\vec{a})}{\partial a_k} \tag{8}$$

$$\frac{\partial\chi^2(\vec{a})}{\partial a_k \partial a_l} = 2\sum_{i=1}^{N} \left[\frac{\partial y(x_i;\vec{a})}{\partial a_k}\frac{\partial y(x_i;\vec{a})}{\partial a_l} - r\cdot[y_i - y(x_i;\vec{a})]\frac{\partial^2 y(x_i;\vec{a})}{\partial a_k \partial a_l}\right] \quad r=1 \tag{9}$$

r in equation (9) is an inserted variable to assign the weight of second derivative terms which has the value between 0 and 1. If we redefine left side of equation (8) and (9) as in equation (10), the increment values of model parameters δa_l for each step of any nonlinear iterative inversion methods can be calculated by matrix inversion of equation (11).

$$\alpha_{kl} = \frac{1}{2}\frac{\partial\chi^2(\vec{a})}{\partial a_k \partial a_l}, \quad \beta_k = -\frac{1}{2}\frac{\partial\chi^2(\vec{a})}{\partial a_k} \tag{10}$$

$$\sum_{l=1}^{N} \alpha_{kl} \delta a_l = \beta_k \tag{11}$$

In conventional Levenberg-Marquardt's (LM) method, the components of Hessian matrix of equation (9) is approximated only in terms of first derivatives (r=0 in equation (9)). There is another point in LM method, in which instead of solving equation (11), a fudge factor λ is involved to stabilize the matrix inversion (see equation (12)). λ, the initial value of which is usually 0.001, is multiplied or divided by 10 according to whether the error in equation (6) increase or decrease, respectively.

$$\sum_{l=1}^{N} \alpha'_{kl} \delta a_l = \beta_k, \ \alpha'_{jj} = \alpha_{jj}(1+\lambda), \ \alpha'_{jj} = \alpha_{jj} \ (j \neq k) \tag{12}$$

Intrigued by the property of λ, we propose here modified LM method that takes into account the second derivatives of the Hessian matrix so as to give robust inversion results. The weight of the second derivative term r in equation (9) is determined by the value of λ in Levenberg-Marquardt's method (13).

$$r(\lambda) = A + B \times \log_{10}(\lambda) \tag{13}$$

In equation (13), constant A and B are determined by putting r=0 at λ_0 and r=1 at λ_1 where λ_0 and λ_1 are the maximum and minimum values of proper range of λ. r is set to 0 for λ greater than λ_0 and r is set to 1 for λ lower than λ_1. As a proper range of λ, λ_0 and λ_1 are given in this study 10^{-3} and 10^{11}, respectively. The essence of the modified LM is to give more weight to the second derivatives of Hessian matrix when the iterative step gets closer to the solution of equation (6).

The modified LM method is applied to the extensive dataset to estimate model parameters which include the moment magnitudes and corner frequencies for the sources, Q_0, R_0, and η for regional crustal attenuation, κ's for each site, and Q anisotropy ratio for major tectonic regions. Especially the southern part of the Korean Peninsula is discretized into many sub blocks and Q_0i s for each block introduced in equation (5) are inverted with η and R_0 assumed to be the same for the entire region. Also some basic model parameters such as β_0, and ρ_0 are fixed to 3.4km/sec and 2.74g/cm^3 respectively and assumed to be the same for the whole region. At the same time, hypocentral distances for all the seismic records are calculated in preparation stage and fixed through the inversion process.

Seismic Data and Processing

There are several seismic networks available for digital earthquake data within and outskirts of the Korean Peninsula. Major seismic networks are operated by Korea Meteorological Agency, Korea Institute of Geology and Mining, Korea Electric Power Research Institute, and Korea Institute of Nuclear Safety. U.S. Air Force also operates array network (KSRS) near the city of Wonju and local universities the others. One IRIS station is located in Incheon and one station in Daejon (moved from Pohang) has been operated by Tokyo University. There are two useful seismic stations in Tsushima of Japan, an island near the southeastern coast of the Korean Peninsula. Some seismic stations in North Korea and northeastern China are temporally deployed. Most of these seismic stations are equipped with high dynamic range recording systems capable of recording high quality ground motion at the distant station even for microearthquakes.

The earthquake dataset used until now comprises 190 earthquakes with 3,400 seismograms mostly since 1996 starting from 1992 and is being updated for renewal of inversion each time earthquake occurs. Most of the data come from the earthquakes of magnitude less than 4.0. The ray paths of the dataset cover entire region of the southern part of the Korean Peninsula. Because the amplitude of Fourier spectrum was concerned the most, quality control of the seismic data was given foremost priority and took most of the time and effort in this study. Since the hypocentral distance is required to be fixed as inputs and critical for the inversion, all of the local public reports of earthquake source parameters are carefully examined. Among these, epicenters and focal depths announced by KIGAM are given the most preference followed by KMA and ISC information resources in the following order. Calibration status of all the seismic stations was checked by all the possible means ([14]). Instrumental correction was rigorously performed in the time domain to enlarge the available frequency band. Mainly acceleration data are used for spectrum calculation, low frequency spectrum supplemented by using velocity data.

The data segment for spectrum evaluation was selected by a time window of varying span depending on the epicenter with the onset time manually picked to include main wave energy packets. The length of the window is designed based upon the crustal velocity structure by S.K. Kim ([14]) to exclude Rayleigh wave components. Fourier spectra for two horizontal components were calculated after cosine tapering with 5% at each end, vector summed and smoothed by averaging the spectrum of 0.4 octave frequency band. Spectrum values are used of frequency range with more than three to four S/N ratio. Since most of the seismic data are recorded with 100 sampling per second after downsampling sharply by a FIR filter, the highest frequency used goes up to 40 Hz which is favorable for detailed Q tomography if site effects are efficiently removed.

Inversions of regional parameters for stochastic point-source ground model are implemented and evaluated under a few case of conditions such as types of source model, frequency dependence of crustal attenuation, and consideration of crustal amplification. Crustal amplification for Korean Peninsula is evaluated based on the crustal model suggested by S.K. Kim ([15]) and by using the program RASCAL ([16]). The crustal amplification is obtained by smoothing the transfer function calculated from the seismic source located at 10km depth to the ground surface with a layer on top of 20m in thickness having shear wave velocity of 1,500m/sec. The resultant crustal amplification gives 1.67 at high frequencies above 5 Hz which is a little higher than the one in central and eastern U.S.A. ([17]). The types of source model considered are ω-square and ω models. ω model is tried according to a study ([18]) that supported ω model for small earthquakes.

For Q anisotropy evaluation, two-step approach was adopted to save time for inversion runs. First, all the ray paths are divided into the ray paths, one passing the region of interest and the rest of the path. By fixing the regional model parameter for the outside region using the estimates obtained for regional area, the model parameters for the region of interest are inverted by floating the anisotropy ratio introduced in equation (4) for strike angles varying from 0 to 90 degree. The strike direction with the lowest fitting error, most of the time corresponding to the largest or lowest anisotropy ratio ε, is determined to be the principal strike. Once the principal strike is found out for every single block, anisotropy ratios for all the blocks are simultaneously inverted for the predetermined principal strikes.

To perform Q tomographic inversion, three phases of inversion were performed (see Figure 2). First, except the ocean, the inland is discretized into evenly spaced grids and inversion is performed to obtain Q tomographic structure. Second, besides the region around the southern part of the Korean

Peninsula is divided into six large blocks, the region in the inland is treated as one major block. This time, the delineation of blocks off the coast are chosen roughly by extrapolating the boundaries identified in the inland based on the preliminary results of the first phase. Inversion is performed for seven major blocks (Figure 2(b)). Lastly while the blocks off the coast remains unchanged, the inland area is divided again into grids and properties for all the grids are simultaneously inverted. But as the final phase of inversion is expected to be unstable, one physical contraint is assigned to Q_{0i} values that the summation of crustal attenuations by many discretized blocks should be the same as the one calculated for the whole area covering the same discretized region in phase two as in equation (14). No other constraints such as spatial smoothness on Q_{0i} values are supposed.

$$\frac{R^{cum}}{Q_0} = \sum_{i=1}^{N_{block}} \frac{R_i^{cum}}{Q_{0i}} \qquad (14)$$

In equation (14) R^{cum} and R_i^{cum} represent the total length of ray path intersecting the whole block and i-th discretized block respectively, both of which are cumulatively summed for all the seismic records. N_{block} is the total number of floated Q_{0i} s.

Regardless of the type of inversion, ray crossing block number, deviation angle relative to a reference angle, and fractional lengths of ray paths crossing the blocks were calculated beforehand for all the seismic records.

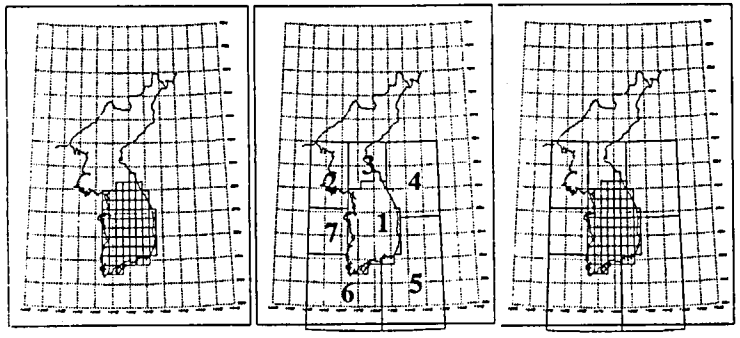

(a) phase 1 (b) phase 2 (c) phase 3

Figure 2. Three phases to stably perform Q tomographic inversion

Results

Regional parameters

Inversion results of regional parameters for stochastic point-source ground motion model are obtained for various cases of conditions by using modified Levenberg-Marquardt's as listed in Table 1. It is to be noted in the Table that different results were obtained for various cases with small differences in the fitting error. However case 1 is determined to be the best results based on the following reasons.

1) Past studies on crustal attenuation (Q) by using coda waves show strong frequency dependence of Q
2) Similar results of Q(f) and R_0 as case 1 is obtained in another study ([19])
3) Inversion results using ω source model show large standard deviation of $\Delta\sigma$ and undesirable strong correlation (correlation coefficient > 0.9) between Q_0 and η

Table 1. Inversion results of regional model parameters under various conditions

case	Median of $\Delta\sigma$	Q_0	η	R_0	κ	STD of κ	Crustal Amp.	γ	mean/ median	χ^2	etc
1	33.7	348	0.53	50	0.019	1.18	1.67	2	1.30	14569	Best estimates
2	69	400	0.47	51	0.017	1.56	1.00	2	1.30	14600	
3	14.6	1436	0	80	0.043	7.7	1.67	2	1.33	15545	
4	large	743	0.2	54.9	0.024	1.15	1.00	1	1.30	14614	Large STD
5	20.4	1465	0	73	0.02	1.18	1.67	1	1.30	14455	
6	36.3	1417	0	70.8	0.018	1.39	1.00	1	1.31	14742	
7	large	613	0.29	56	0.028	1.08	1.67	1	1.3	14223	Large STD

* Shaded area: fixed values for inversions * STD: standard deviation,
* γ: seismic source model; 1 (ω), 2 (ω-square)

Among the model parameters, η is very difficult to determine because it is the value of double exponent in equation (1). Also it has very strong correlation with Q_0. So to determine the best estimate of η, various initial values of η are assumed and by finding the lowest error, the η is selected. Figure 3 shows error distribution in frequency and epicentral distance. From the figure, observed and calculated Fourier spectra have good agreement (about 0.3 lognormal standard deviation) in broad range of frequencies with no bias. Comparison of median levels of observed and simulated data shows no bias, too and good fitting result over the whole epicentral distance range. The distribution of stress drops is shown in Figure 4. The mean level of stress drop is about 20~30bars with about 1.0 lognormal standard deviation. The variation of stress drop is high compared to the values of 0.7 reported in central and eastern North America ([20]). The estimated values of stress drop are based on small-to-moderate earthquakes but have similar level of calculated stress drop (in Figure 4) based on teleseismic seismic records from large earthquakes around the Korean Peninsula ([21]).

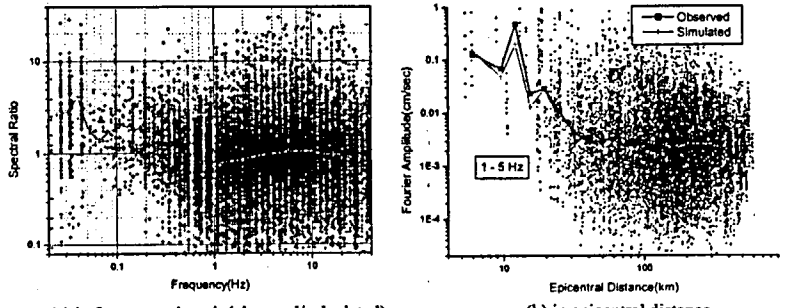

(a) in frequency domain(observed/calculated) (b) in epicentral distance

Figure 3. Error distribution in frequency and epicentral distance resulting from inversion of regional

stochastic point-source ground motion model

Model parameters R_0 and η, which are assumed to be the same for the whole region, were inverted to give the stable values between 50 to 60 km and 0.53 respectively regardless of the inversion runs. The value of R_0 known to be at least twice the crustal thickness ([22]) seems to be reasonable considering the reported Moho depth of about 30-40 km. Since the iterative non-linear inversion method is used, the initial solution should be close enough to the global solution so as not to get diverged or trapped in local minimum. In this sense, the regional values of model parameters were used as initial values throughout the following inversions.

The inversion adopted here involves a simultaneous inversion of M_0 and f_c for source terms which are known to be correlated each other and converting these to moment magnitude and $\Delta\sigma$ by using equation (2) and (3). So as a way of indirectly checking the accuracy of the inversion, the relationship between moment magnitudes obtained by the inversion and the local magnitudes reported by KIGAM was compared with the one in eastern North America ([23]) which has similar crustal attenuation characteristic as Korea. Figure 5 shows a comparison result revealing close match between the two relations even though the range of earthquake magnitude is limited to less than 5.0. This fact implies that the moment magnitude obtained by the inversion is valid. This result also supports the applicability of moment-to-local magnitude converting relation of the eastern North America to the Korean Peninsula for the Probabilistic Seismic Hazard Analysis which requires ground motion attenuation relation with local magnitudes.

Since the localized Q_0 is assumed to be present, it directly interacts with the definition of kappa. The calculated kappa values in Q tomographic inversion were comparable with the one in case where single regional Q value is inverted. But the standard deviation of log of kappa values tends to be lower by about 10%. The localized Q_0 is more of attenuation characteristic below a depth, above which the effect of kappa dominates. The values of kappa are reported to have large differences even for the localized area. However the localized Q_0 defined here has the same value within a designated block. The fitting results for some sites are still poor with the observed spectrum lower than the estimated, which is attributed to low crustal amplification factor for this site or bad calibration of the respective seismic stations.

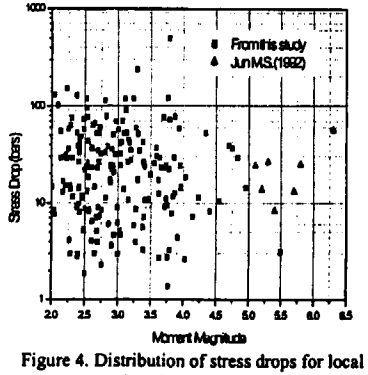

Figure 4. Distribution of stress drops for local earthquakes

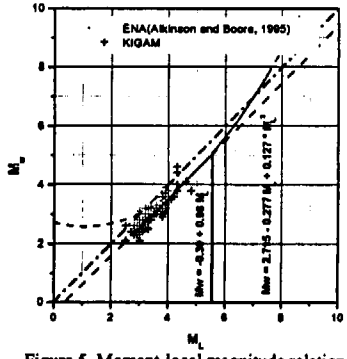

Figure 5. Moment-local magnitude relation

Q Anisotropy

Q anisotropy is evaluated for four major tectonic provinces in the southern part of the Korean Peninsula that are named Gyeonggi Massif, Ogcheon Folded Belt, Sobaegsan Massif, and Gyeongsang Basin (Figure 6). Table 2 shows how Q anisotropy ratio and error decreasing rate are changing according to the reference strike. From the Table 2, there is a reference strike called principal strike (50^0) at which Q anisotropy ratio is maximum (or minimum) and the error is minimum. Following the same procedure exemplified in Table 2, the principal strike and the corresponding Q anisotorpy values are sought for giving the result of Table 3 for four tectonic provinces. The result shows that Sobaegsan Massif has very high anisotropy with Q along ENE-WSW direction having almost two times larger than the other orthogonal direction. The other tectonic provinces have no distinct Q anisotropy except Geongsang Basin. It is to be noticed that the principal orientation of Q anistropy of Geongsan basin (NW-SE) is quite different to the others and also contradict the previous results ([2,6]) that revealed that the quality factor of P wave measured along the ray paths perpendicular to the strike direction NNE-SSW of the major faults appeared to be lower than the one parallel to the fault direction. Even though yet to be fully identified, plausible causes of the strong Q anisotropy are attributed to the heterogeneous Q structure described below, the directional property of the stratified dipping layer in Geongsan basin, the folded belt or the tectonic stress regime. Even though the possibility that the Q anisotropy is a result of assuming the same β_0 is ruled out due to no report of velocity anisotropy as high as 1.4 along different direction, this can be a candidate reason in part. However, overall NE-SW directional property of strong wave propagation is well explained by phenomenal fact observed when modest earthquake at Yeongwol shook the nationwide in 1996.

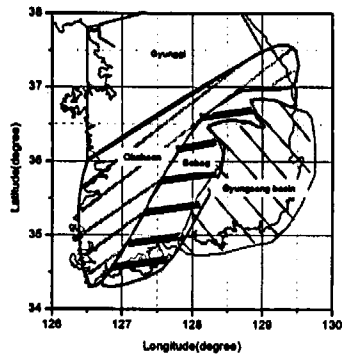

Figure 6. Result of Q_0 anisotropy inversion for major tectonic regions. Direction and width of lines correspond to principal Q_0 anisotropy direction and proportional Q_0 value

Table 2. Example results of inversion of anisoropy ratio for Gyeongsang Basin

Reference Strike (in degree)	Anistropy Ratio	Error Decreasing Ratio
0	0.9668	0.26%
10	1.0372	0.26%
20	1.1299	0.29%
30	1.2412	0.35%
40	1.3321	0.40%
50	1.3343	0.41%
60	1.2639	0.38%
70	1.1787	0.33%
80	1.1046	0.29%

Table 3. Q anisotropy ratio and principal strike for major tectonic regions

Tectonic Province	Q_0 ($\eta = 0.53$)	Principal Strike (in degree)	Anisotropy ratio ($Q_\perp / Q_0$)
Gyeonggi Massif	350	0	0.91
Ogcheon Folded Belt	415	50	0.76
Sobaegsan Massif	659	70	0.57
Gyeongsang Basin	254	50	1.33
South Korea as a wholes	348	30	0.84

Q_0 Tomogrphy

Cumulative length of ray path per a block for tomographic inversion is found to be at least 1,200 km, showing spatially inhomogeneous and nonuniform distribution around the Korea almost proportional to the concentration of seismic stations (Figure 7(b)). The site effect is believed to be insignificant because the direction of ray path is uniform for all angles in the effect of on average canceling site effect on the paths of two opposite direction. But for regions lying just beside the coastline Q_0 values are suspicious of being contaminated by site effects or bad calibration status of seismic stations because the direction is limited toward the inland. Setting the grid, the distribution of the stations is considered. Also the grid size is selected to be as small as possible as long as the inversion is stable. If the grid size decrease, the site effect might more severely interact with the crustal attenuation. The final grid size capable of producing stable inversion result is 0.4 x 0.4 degree.

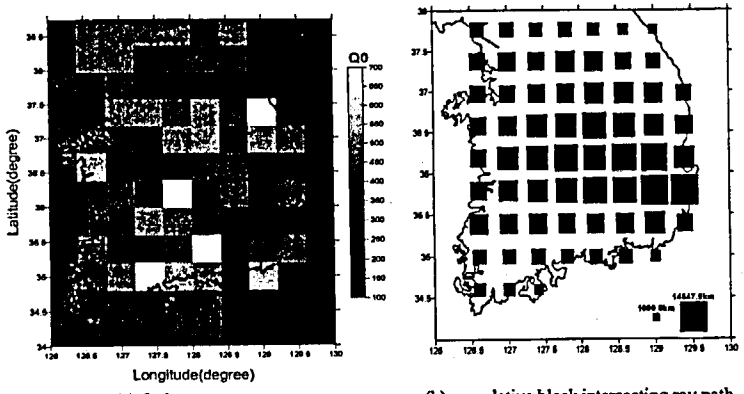

(a) Q_0 image map (b) cumulative block intersecting ray path

Figure 7. Q_0 tomographic inversion result

The resultant fitting error produced by Q tomography is significantly lower than the one from assuming the single regional Q parameters. Even though the ray path coverage off the coast are not concentrated enough to give detailed Q structure, the concentration and quality of seismic networks in the inland of Korean Peninsula were good enough to provide detailed lateral variation of Q structure as a result of inversion (Figure 7(a)). It is found that Q values varies over the regions off the coast as well as in inland, suggesting that seismic source parameters cannot be precisely determined by using single set of model parameters. Since the image in Figure 7(a) is hard to interpret, another image of Q structure was obtained by interpolating the grid values of Q_0 by Kriging method, which is thought to be reasonable considering the smooth variation of Q_0 over the space. The interpolated image of localized Q structure revealed very complicated shape of Q distribution in the southern part of the Korean Peninsula. Belt of high Q value encompassing the Gyungsang Basin is found. The Q_0 value for the Gyungsang Basin is consistent with the coda Q value determined by other authors. The results of image also agree well with the Lg Q value ([3]). The inverted Q values can be said to be representative value of Q structure above the earthquake prone depth. Also considering most of the epicenters are distributed above R_0, the resultant Q tomographic image is likely to much resemble Lg Q structure.

The interpretation of heterogeneous Q value can be linked to the Q anisotropy. Q tomographic image seems to be strongly correlated with the geological map as well as geophysical maps such as geomagnetic anomaly map and geothermal gradient map with less degree. The most remarkable fact is that the location of earthquake is largely limited to the transitional zone of Q_0 value. Uncertainty of Q, which is important in capturing uncertainties in strong ground motion simulation, is found to be about 0.4 lognormal standard deviation, which is very close to the EPRI result ([20]).

Discussion

Conventional Levenberg-Marquardt's nonlinear inversion method is simply modified by taking into account the second derivatives of the Hessian matrix so as to give robust inversion results. The weight of the second derivative terms is determined by the value of so-called λ in Levenberg-Marquardt's method. The proposed inversion method is applied to observed data from small-to-moderate earthquakes to simultaneously evaluate the regional model parameters of the stochastic point-source ground motion model in and around the Korean Peninsula. Best estimates of the regional stochastic model parameters are obtained along with their statistics. However after reviewing the result of crustal attenuation (Q), there is a need for more detailed study on the characteristics of Q.

Therefore, two features of crustal attenuation which are anisotropy and lateral variation were additionally evaluated based on earthquake data recorded in and around the Korean Peninsula. Strong Q anisotropy characteristics, defined here as the ratio of Q_0s between two mutually orthogonal direction, for Sobaegsan Massif and Gyeongsang Basin were revealed. Different Q_0 values were obtained for several blocks off the coast area around the Korean Peninsula and localized Q_0 values for the inland were obtained for evenly spaced grids the size of which is unprecedentedly as small as 0.5 degree by exploiting the high quality and densely deployed seismic recording system. Previously reported Q value matched well the inverted values. The other parameters related to regional, source, and site effect were found to have little change compared to the previous studies regardless of the inversion types. The use of 0.4 lognormal standard deviation for Q_0 is justified for the whole region of the South Korea in simulating strong ground motion and smaller value of lognormal standard deviation of Q_0 is recommended for site-specific strong ground motion prediction.

As a result of this study, the characteristics of crustal attenuation are identified providing scientific bases for developing site specific ground motion. It is believed that more reasonable ground motion attenuation relation can be developed for probabilistic seismic hazards with less variability. Furthermore, it looks promising that as the large amount of earthquake data are accumulating rapidly, we will be able to identify more detailed Q structure of the Korean Peninsula in the near future for the region particularly where seismic networks are densely deployed and crustal attenuation is severe. However for these purposes, several issues should be resolved in advance, some of which are full separation of site effects and crustal attenuation and more precise calibration of seismic sensors. Also

it still remains to validate the inversion results by using numerical modeling, review the limitation of the inversion and its conditions, and perform systematic error and resolution analysis. More in-depth study of geological and geophysical implication of the result may contribute to validating the result. Separation of intrinsic and scattering parts of Q may help to more delicately interpret the geological setting of Korean Peninsula. Comparison with the distribution of felt area of historical earthquakes is another way, helping properly interpret the historical records. Other method capable of imaging lateral variation of Q value can also be conducted and compared, too. Some model parameters assumed to be the same for the entire region such as R_0, η, and β_0 can be floated to improve the inversion result. Finally, particular attenuation should be paid to more qualified use of the earthquake data more than anything else. This might include discarding the data from poorly determined hypocenters and calibrated recording systems.

References

[1] "Inversion of Stochastic Earthquake Model Parameters using the Modified Levenberg-Marquardt's method (in Korean)", Yun Kwan-Hee, Walter Silva, Park, Dong-Hee, and Chang, Chun-Jung, 20-27, Proceedings of Earthquake Engineering Society of Korea Conference-Spring 2002.

[2] "Quality factor structure of the Southeastern Part of the Korean Peninsula (in Korean)", Sung Kyun Kim, Yun Kyung Park and Myng-Soon Jun, Journal of the Geological Society of Korea, 529-544, December 2000.

[3] "Estimation of Q factor and Mapping of Regional Variation (in Korean)", The 3rd Seminar on the Observation and Analysis of Strong Ground Motions, Korea Institute of Nuclear Safety, December 2001.

[4] "Attenuation of High-Frequency P and S Waves in the Crust of Southeastern South Korea", Tae-Woong Chung and Haruo Sato, Bulletin of the Seismological Society of America, 91, 6, pp. 1867-1874, December 2001.

[5] Seismological Study (in Korean) (KR-94(C)1-16), Myung-soon Jun, Heon Cheol Chi, Jeong-soo, In-chul Shin, Korea Institute of Geology, Mining & Materials, 1995.

[6] "Q estimates using the coda waves in the Kyeongsang Basin (in Korean)", Lee, W.S. and Lee, K.H., 1998, Proceedings of EESK Conference - Fall 1998

[7] Attenuation of coda waves from local earthquakes in the Gyeongsang Sedimentary Basin (in Korean), Lee Ji-Min and Baag, C.E., Thesis (masters) of Seoul National University, 1999.

[8] "Q_{Lg} topography in Columbia", Anibal Ojeda and Lars Ottemoller, Physics of the Earth and Planetary Interiors 130, 253-270, 2002.

[9] "Lg coda Q and its relation to the geology and tectonics of the Middle East". Cong, L., and Mitchell, B.J., Pure and Applied Geophysics, Vol. 153, no. 2/3/4, pp. 563-585, 1998.

[10] "Stochastic Simulation of High-Frequency Ground Motions Based on Seismological Models of the Radiated Spectra", Boore, D.M, Bulletin of the Seismological Society of America, 73, 1865-1894, 1983.

[11] "A Moment Magnitude Scale", Hanks and Kanamori, Journal of Geophysical Research, 84, 2348-2350, 1979.

[12] "A Model for the Shape of the Fourier Amplitude Spectrum of Acceleration at High Frequencies", Anderson, J.G. and S.E. Hough, Bulletin of the Seismological Society of America, 74, 1969-1993, 1984.

[13] Numerical Recipes in Fortran 77: The art of scientific computing, Cambridge University Press, 1986.

[14] "Review on Pre-processing of Earthquake Data for KEPRI Seismic Monitoring System (in Korean)", Yun Kwan-Hee, Park Dong-Hee, Choi Weon-Hack, and Chang Chung-Jung, Journal of the Earthquake Engineering Society of Korea, Vol. 6, N0. 2, 39-50. April 2002.

[15] "A study on the crustal structure of the Korean Peninsula (in Korean)", Kim, S.K., Journal of Geological Society of Korea, Vol. 31, pp. 393-403, 1995.

[16] "Software Routine RASCALS, Ver. 5.4 (Manual Revision #3)", Pacific Engineering and Analysis, 1999.

[17] Technical Basis for Revision of Regulatory Guidance on Design Ground Motion: Hazard- and Risk-consistent Ground Motion Spectrum Guidelines (NUREG/CR-6728), U.S. Nuclear Regulatory Commission, October 2001.

[18] "Scaling Law of Earthquake Source Time-Function", K. Aki, Geophys. J. R. Astr. Soc., 31, 3-25, 1972.

[19] "Attenuation of peak spectral amplitude of acceleration in the southern part of the Korean Peninsula (in Korean)", Sung Kyun Kim, Sue Kyung Kim and Heon Cheol Chi, Journal of the Geological Society of Korea, June 2002.

[20] "Guidelines for determining design basis ground motions", Electric Power Research Institute, 1993.

[21] "Source parameters of earthquakes in and around the Korean Peninsula deduced from spectral analysis", M.S. Jun and O. Kulhanek, Physics of the Earth and Planetary Interiors, 65, 255-266, 1991.

[22] "Modelling some empirical vertical component Lg relations", Herrmann, R.B., Kijko, A., Bulletin of the Seismological Society of America, 73, 157-171, 1983.

[23] "Ground motion relations for eastern North America", Atkinson, G. and D. Boore, Bulletin of the Seismological Society of America, 85, 17-30, 1995.

STUDY ON THREE-DIMENSIONAL STRONG GROUND MOTIONS

Keiichi OHTANI, Bunho KOJIKA
National Research Institute for Earth Science and Disaster Prevention, Japan

Abstract

Analysis of three-dimensional strong ground motions along principal axes was carried out based on K-NET records. By applying moving window technique to ground motion records, the time-dependent characteristics of ground motions along principal axes were examined. It is observed that the three rotation angles between conventional coordinates and principal axes are the function of time and the angles keep stable for a short time period after the arrivals of P and S waves, respectively, based on theory and that based on observation data were compared.

We initiated the new research project, which objects are to arrange the database of strong ground motions for using the input waves of E-Defense experiment. The research program is included 3 themes; (1) Prediction of strong ground motions by the statistic method, (2) Prediction of strong ground motions by semi-empirical method and (3) Construction of 3-D strong ground motion database.

Introduction

Shaking table test provides a powerful means to investigate the complicated mechanism of the failure of structures under three-dimensional earthquake loads. However, the ground motion records with large magnitude and short focal distance, which are often required as the input of shaking table, are very limited. As the first step to estimate the three-dimensional ground motion input for shaking table test, the characteristics of the three-dimensional ground motions along principal axes and their relationships with the source mechanism, direction from site to source were examined in this paper.

Table 1 The list of selected earthquakes

No.	Original time	M(JMA)	Depth	Lat., Long.
1	1996/05/23 18:36	5.0	39 km	38.7 , 142.3
2	1996/08/11 03:12	5.9	10 km	38.9 , 140.6
3	1996/09/09 13:34	5.7	20 km	30.5 , 130.9
4	1996/10/19 23:44	6.6	39 km	31.8 , 132.0
5	1996/12/21 10:29	5.4	53 km	36.1 , 139.9
6	1997/02/20 05:22	5.4	90 km	37.4 , 141.2
7	1997/02/20 16:55	5.6	50 km	41.8 , 142.9
8	1997/03/03 23:09	5.0	3 km	35.0 , 139.2
9	1997/03/04 12:51	5.7	2 km	35.0 , 139.2
10	1997/03/16 14:51	5.8	39 km	34.9 , 137.5
11	1997/03/26 17:31	6.3	8 km	32.0 , 130.4
12	1997/04/03 04:33	5.5	9 km	32.0 , 130.3
13	1997/05/12 07:59	5.5	54 km	37.0 , 141.3
14	1997/05/13 14:38	6.2	8 km	32.0 , 130.3
15	1997/05/18 06:25	5.0	10 km	32.4 , 130.6
16	1997/06/15 13:54	5.1	100 km	43.0 , 144.2
17	1997/06/25 18:50	6.1	12 km	34.5 , 131.7
18	1997/09/04 05:16	5.2	6 km	35.3 , 133.4
19	1997/10/11 14:44	5.0	30 km	34.4 , 138.2
20	1997/11/15 16:05	6.1	153 km	43.7 , 145.1
21	1997/12/07 12:50	5.3	83 km	37.7 , 141.8
22	1998/01/03 03:20	5.3	50 km	42.9 , 145.5
23	1998/02/21 09:55	5.0	21 km	37.3 , 138.8
24	1998/04/09 17:45	5.4	93 km	36.9 , 141.0
25	1998/04/22 20:32	5.4	10 km	35.2 , 136.6
26	1998/05/03 11:09	5.7	3 km	35.0 , 139.2
27	1998/05/21 06:54	5.0	84 km	38.6 , 142.1
28	1998/05/23 04:49	5.3	85 km	33.7 , 131.9
29	1998/08/16 03:31	5.4	5 km	36.3 , 137.6
30	1998/08/29 08:46	5.1	67 km	35.6 , 140.1
31	1998/09/03 16:58	6.1	10 km	39.8 , 140.9
32	1998/09/15 16:24	5.0	13 km	38.3 , 140.8
33	1998/11/24 04:48	5.1	82 km	38.0 , 141.6
34	1999/01/24 09:37	5.9	50 km	30.6 , 131.3
35	1999/02/26 14:18	5.1	19 km	39.2 , 139.9
36	1999/03/11 20:06	5.0	40 km	39.6 , 141.9
37	1999/03/16 16:43	5.1	10 km	35.3 , 135.9
38	1999/03/26 08:31	5.1	50 km	36.5 , 140.6
39	1999/04/25 21:27	5.2	50 km	36.5 , 140.5
40	1999/05/13 02:59	6.1	100 km	43.0 , 143.9

According to the recent studies from the strong ground motions of large earthquakes such as 1994 Northridge earthquake and 1995 Kobe earthquake, it becomes clear that the correlation of three-dimensional ground motions have a considerable influence on the failure of structures. The purpose of this paper is to elucidate the correlation between the three-dimensional ground motions through an analysis of strong motion records. The strong ground motions recorded by K-NET (a strong ground motion observation network in Japan with an distance of about 25 km between stations), which can be accessed over Internet, were used here. Forty earthquakes whose magnitude is larger than 5.0 and the maximum acceleration exceeds 100 gal were selected from the K-NET database. The parameters of selected earthquakes are shown in Table 1. For each selected earthquake, at least several tens of observation records are available.

Analysis Method

The three components of ground motion records represent, in general, the accelerations measured along the instrument axes. If ground motions are assumed to be Gaussian stochastic process with zero mean values, the three-dimensional ground motion process can be completely characterized in a probabilistic sense through the covariance matrix

$$c(t,\tau)=\begin{bmatrix} c_{xx} & c_{xy} & c_{xz} \\ c_{yx} & c_{yy} & c_{yz} \\ c_{zx} & c_{zy} & c_{zz} \end{bmatrix} \tag{1}$$

where

$$c_{ij}=c_{ij}(t,\tau)=E\left[a_i(t)a_j(t+\tau)\right], \quad i,j=x,y,z \tag{2}$$

and E denotes the ensemble average. In this case, the influence of coordinate directions in the covariance functions in Equation (1) can be investigated through the approximate relations [Kubo and Penzien, 1979]

$$c_{ij}(t,0)=E\left[a_i(t)a_j(t)\right], \quad i,j=x,y,z \tag{3}$$

The components of motion along orthogonal axes x', y', z' can be simply transformed to components along another orthogonal axes x, y, z by

$$\begin{Bmatrix} a_x(t) \\ a_y(t) \\ a_z(t) \end{Bmatrix} = A \begin{Bmatrix} a_{x'}(t) \\ a_{y'}(t) \\ a_{z'}(t) \end{Bmatrix} \tag{4}$$

where A is a transformation matrix satisfying the condition

$$A^TA=I \text{ (Identity matrix)} \tag{5}$$

Then the covariance matrix for axes x', y', z' is

$$\begin{aligned} c'(t) &= A^{-1}c(t)\left(A^{-1}\right)^T \\ &= A^Tc(t)A \end{aligned} \tag{6}$$

This transformation of three-dimensional ground motion is identical to that of three-dimensional state of stress. Therefore, A set of principal axes exists along which the components of ground motion have maximum, minimum and intermediate values of variance and have zero values of covariance. It can be easily shown that the directions of the principal axes are the eigenvectors derived through the use of the covariance matrix defined be Equation (1) and the principal variances are the corresponding eigen-values, i.e.

$$c_p(t)=P^Tc(t)P$$

or

$$c_p(t)=\begin{bmatrix} c_{11}(t) & 0 & 0 \\ 0 & c_{22}(t) & 0 \\ 0 & 0 & c_{33}(t) \end{bmatrix} \tag{7}$$

where P is an orthogonal matrix which designates the principal transformation matrix.

Since the off-diagonal terms in a covariance matrix indicate quantitatively the correlation between the corresponding components, the components along the principal axes are fully uncorrelated with respect to each other. For Gaussian stochastic processes, they are statistically independent of each other if they are uncorrelated with each other. Therefore, the components directed along principal axes are independent of each other in a statistical sense.

In practical application, the desired properties of stochastic processes can often be estimated by examining individual members from the processes if assuming the process is an ergodic process.

Characteristics of Ground Motions along Principal Axes

Because ground motions are non-stationary, a moving window technique was applied in order to see the time-varying characteristics. The principal axes of ground motion are defined by the three rotation angles of r_x, r_y and r_z to satisfy equation (7). r_x, r_y and r_z are the rotation angles with respect to x, y and z axes, respectively.

From principal axis analysis, some of which are shown in Figures 1 and 2, the findings are summarized as follows:

1. The three rotation angles of r_x, r_y and r_z are time dependent, but they are stable for a short time period after the arrival time (T_P and T_S) of P and S waves, respectively. This indicates that the direct P and S waves have their respective specific input directions.
2. The rotation angles r_x and r_y are nearly zero after S wave arrives. This means the principal axes vary only in horizontal plane after S wave arrives. This can also be shown by comparing it with the rotation angle r_z, which is the transformation function from X and Y coordinates to principal axes in horizontal plane.
3. The directions of the two principal axes in horizontal plane were examined by the mean rotation angles of the stable time period after the arrival of S wave for all of the observation stations. A close relationship between the directions of principal axes and the direction of source was not found.
4. From the spatial distribution of the maximum and intermediate principal axes, their correlation with radiation pattern of SH and SV waves was not found, either.

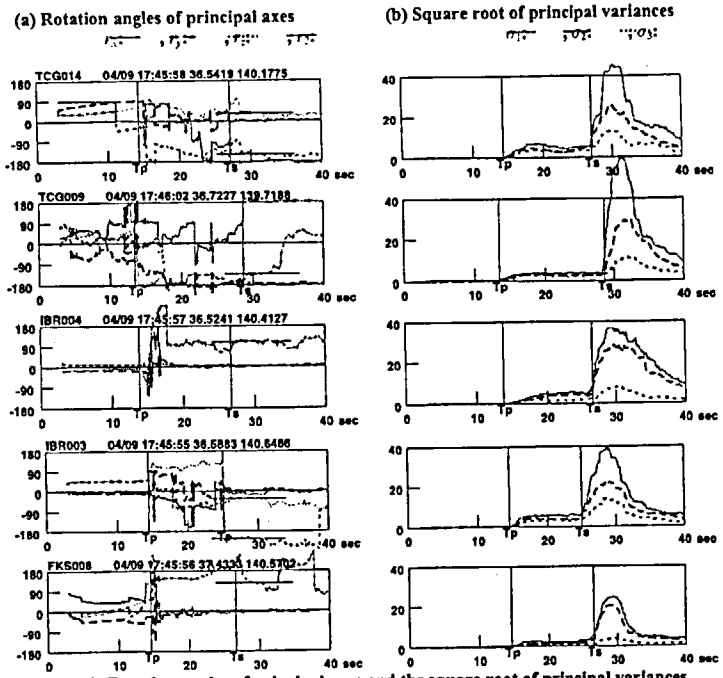

Figure 1: Rotation angles of principal axes and the square root of principal variances. (M5.4, Depth93km, 1998/04/09 17:45)

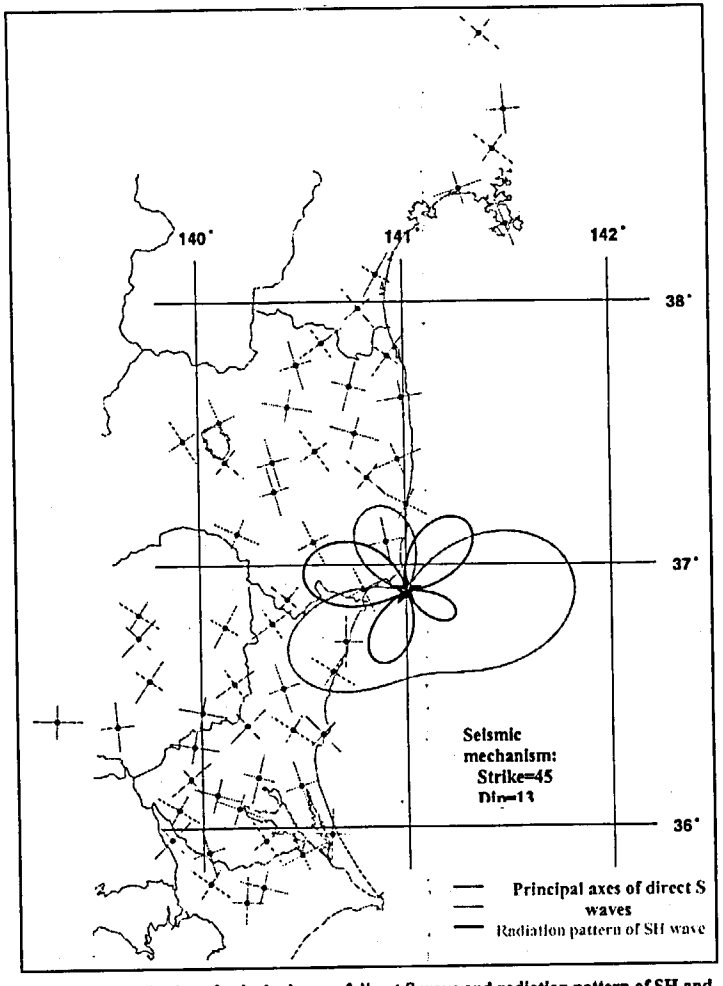

Figure 2: Distribution of principal axes of direct S wave and radiation pattern of SH and SV waves. (M5.4, Depth93km, 1998/04/09 17:45)

Influence of Source Mechnism

When the source mechanism of an earthquake is known, the SH wave and SV wave can be theoretically calculated. The SH and SV waves have the same source spectrum and the same path from source to site. The only difference between them is their radiation pattern. In this regard, SH wave and SV wave should be resemblance to each other and there exists a predominant axis for SH and SV waves. S wave vibrates in the shaft direction of the predominant axis only. The vibration amplitude is zero in the plumb direction. The predominant direction can be determined by the equation

$$c_{m_1 m_2} = \frac{1}{2\pi}\int_{-\infty}^{\infty} F_{m_1}(\omega)F_{m_2}(\omega)d\omega = 0 \tag{8}$$

with coordinates transformation.

$$\begin{aligned} m_1 &= SV \cdot \cos\theta_m + SH \cdot \sin\theta_m \\ m_2 &= -SV \cdot \sin\theta_m + SH \cdot \cos\theta_m \end{aligned} \tag{9}$$

and

$$\begin{aligned} F_{SV}(\omega) &= R_{SV} \cdot S_{source}(\omega) \cdot P_{path}(\omega) \\ F_{SH}(\omega) &= R_{SH} \cdot S_{source}(\omega) \cdot P_{path}(\omega) \end{aligned} \tag{10}$$

where $S_{source}(\omega)$ is source spectrum of S wave, $P_{path}(\omega)$ is path effects and R_{SV} and R_{SH} are radiation patterns of SV and SH waves, respectively. Substitute Equations (9) and (10) into Equation (5), the rotation angle θ_m, from which the predominant axis is determined, can be derived.

$$\theta_m = \frac{1}{2}\tan^{-1}\left(\frac{2R_{SV}R_{SH}}{R_{SV}^2 - R_{SH}^2}\right) \tag{11}$$

The principal axes and amplitudes of S wave from the observed ground motions, the amplitudes of SH and SV waves of the theoretical solution from the source mechanism, and the predominant axis of SH and SV waves are compared in Figure 3. When the difference of the directions of principal axes and predominant axis for a site is less than 10 degrees, it is marked with a red circle. The red-marked sites are about 20% of the total observation sites.

From the theoretical solution of source mechanism, SH wave and SV wave are completely correlated and they can be composed to a vector in the predominant axis. On the other hand, it is found that the vibration along the maximum principal axis is not so larger than that along the minimum principal axis from ground motion records. The principal axis analysis of ground motions in short period range cannot explain the theoretical solutions of SH and SV waves.

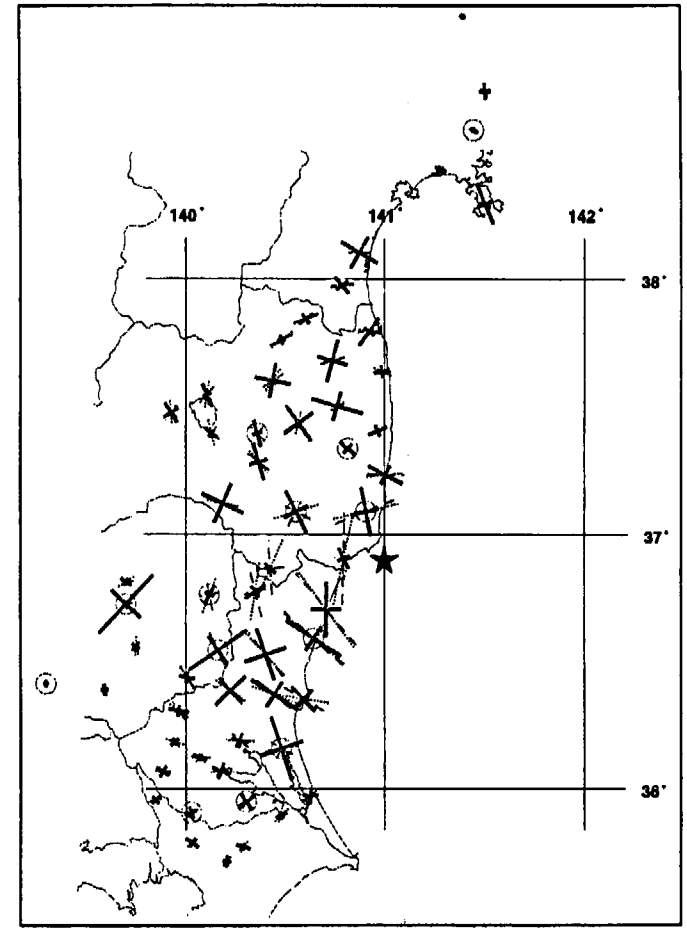

Figure 3: Comparison of the direction and amplitude of principal axes, SH and SV waves, and the predominant axis of SH and SV wave. (M5.4, Depth93km, 1998/04/09 17:45)

Results of Calculation

The principal axes of ground motions were calculated by zeroing the all covariance values of the covariance matrix of the three components of ground motion records. The principal axes are time varying in general, but after arrivals of P and S waves, a respective stable time period of several seconds is observed. This means that the direct P wave and the direct S wave have their respective specific input directions. The principal axes for direct S wave was compared with the theoretical solution of SH and SV waves from source mechanism, the correlation between them is not found.

For theoretical solution, because SH and SV waves share a common source spectrum and have the same path, the different radiation pattern between them results in that SH and SV waves are completely correlated and they can be composed to a vector in ground surface. The S wave of ground motion cannot be composed to a vector in horizontal plane. There are about 20% sites where the difference between the directions of the vector and the principal axes is within 10 degrees. The theoretical solution of SH and SV waves, which is obtained by the horizontal layer assumption, cannot explain the principal axes analysis results of the short period ground motions.

Research Program

Ministry of Education, Culture, Sports, Science and Technology (MEXT), Government of Japan was established the 5 year special project on Seismic Hazard Mitigation in Mega-Cities in the fall of 2002. This project covers wide areas of seismology and earthquake engineering, which are including (1) Survey of crustal structures in the mega-cities, (2) Upgrading the seismic performance of structures based on the shaking table tests, (3) Strategic study of hazard responses and (4) Unification study of seismic hazard mitigation countermeasures. The second theme is directly related to Project "E-Defense (3-D Full-Scale Earthquake testing Facility)".

Within the above mentioned project, we initiated the research programs related the three dimensional strong ground motions. This research program is covered following three items;

1) Prediction of strong ground motion by the statistic approach (PI: Dr. Masayoshi Sato and Bunho Kojika, National Research Institute of Earth Science and Disaster Prevention)
   Based on the records of strong ground motion, characteristics of grond motions, such as maximum acceleration value, amplitude and phase spectrum and so on, are obtained by the statistical approach. The calculation method of the 3-D artificial earthquakes will be developed by the statistic results. And, we will also develop the prediction method of future strong ground motions.
2) Prediction of strong ground motions by the semi-empirical method (PI: Prof. Kojiro Irikura, Disaster Prevention Research Institute, Kyoto University)
   We will develop the prediction method of the 3-D artificial earthquakes by the semi-empirical method, which is the wave composition by using Green function.
3) Construction of 3 dimensional strong ground motion databases (PI: Prof. Kazuyoshi Kudo, Earthquake Research Institute, University of Tokyo)
   Based on the consideration of the database framework on strong ground motions, which is included the characteristics of strong motion observation site and strong motion records from world-wide, we will collect and arrange the installed strong motion records.

Conclusion

In nowadays, the necessity of information on three-dimensional strong ground motions is increasing, because of increasing of 3-dimensional shaking tables and utilization of 3-component analytical calculation mode of structures. Analysis of 3-dimensional strong ground motions was carried out based on K-NET records.

By applying moving window technique to ground motion records, the time-dependent characteristics of ground motions along principal axes were examined. It is observed that the three rotation angles between conventional coordinates and principal axes are the function of time and the angles keep stable for a short time period after the arrivals of P and S waves, respectively. This indicates that t the directly arrived P and S waves have their respective specific input directions. The rotation angle around vertical axis is almost zero after S wave arrives, which means that the principal axes vary only in horizontal plane after S wave arrives. Making use of the mean rotation angle and the maximum variance along principal axes of all observation stations, the spatial distribution characteristics of principal axes was investigated. A clear relationship between the two horizontal principal directions and the direction of source was not found.

On the other hand, although the radiation patterns of SH and SV waves have a simple form of $\sin(2\theta)$ and $\cos(2\theta)$, respectively, in the moment release plane, they become very complicated in horizontal plane for general source mechanism. With the source mechanism of earthquakes, the theoretical solutions of SH and SV waves were obtained. Under the assumption of horizontal layer structure, the vibration directions of SH and SV waves are transverse and radial with respect to source direction, respectively. Because SH and SV waves exists and the principal axes of SH and SV waves can be obtained theoretically.

We initiated the new research programs related to the three dimensional strong ground motions in this fall. We hope that this research programs will be obtained further results and reported in the near future occasion.

References

1. Kubo, T. and J. Penzien (1979), "Analysis of three-dimensional strong ground motions along principal axes, San Fernando earthquake", *Earthquake Engineering and Structure Dynamics*, Vol.7, pp.265-278.
2. Kojika, B, Ohtani, K and Katayama, T. (2000), "Characteristics of Three-Dimensional Strong Ground Motions along Principal Axes", 12WCEE, paper no. 1348.

ON A TEST TO RESOLVE ISSUES RELATED TO EARTHQUAKE RESPONSE OF NUCLEAR STRUCTURES AND THE GROUND MOTIONS USED FOR THE TEST

KITADA Yoshio
NUPEC (Nuclear Power Engineering Corporation), Japan

Abstract

This paper describes new test methodology to obtain the data available to evaluate ultimate seismic behavior of Nuclear Power Plant (NPP) structures. The paper firstly reviews the existing test data of Soil Structure Interaction (SSI). Secondary, the paper points out the issues in the existing data regarding their applicability to the evaluation of behavior of NPP structures when a big earthquake ground motion strikes them. Then the paper proposes new test methodology to evaluate ultimate behavior of NPP structures against a strong earthquake ground motion. The proposed methodology employs ground motions generated in a surface coalmine that has a large acceleration up to 2g. The simulation analysis is carried out by applying an observed large ground motion at the coalmine to a scaled NPP building model. The results are promising and encourage the application of the methodologies to evaluate ultimate earthquake response behavior of the NPP structures.

Introduction

Major Nuclear Power Plant (NPP) structures in Japan have been designed and constructed carefully because Japan is an earthquake prone country and some damage of NPP structures due to an earthquake might a cause an accident involving release of radioactive materials. Nevertheless, after the 1995 Hyogoken Nanbu earthquake (Kobe Earthquake), there arouse many opinions requiring the evaluation of seismic design margins of NPPs in the case that an unexpectedly big earthquake ground motion, exceeding the design levels, strikes an NPP site [1].

The items which governing the earthquake response of an NPP structures during a big earthquake are generally recognized, firstly the magnitude and characteristics of earthquake ground motions at a site, secondly soil-structure interaction (SSI) of the structures at the site, and thirdly nonlinear response of the reinforced concrete (RC) structures during earthquakes. The present status of seismic technologies indicates that the difficulties in handling the items are in the reverse of the above order.

From structural engineering point of view, the most difficult issue of the above, the input motion, is considered as a given design condition, thus the SSI becomes the most difficult issue for predicting structural behavior. In order to accomplish such a difficult evaluation, some extrapolations from the existing data are indispensable. However, the extrapolation itself is a hypothesis, and its adequacy should be confirmed by some test data obtained by applying a large as possible earthquake-like load.

In the following, we describe new test methodologies, which may supply some test data to supplement the extrapolation. The seismic performance of the buildings of an NPP had been proven by various tests. However, these test data are not necessarily directly applicable to evaluating ultimate structural strength as well as seismic margins of structures against earthquakes. The reason is explained that although the ultimate strength of reinforced concrete (RC) structures are gradually unveiled, Soil-Structure Interaction (SSI) under a strong earthquake ground motion remains a difficult issue to evaluate properly.

Nuclear Power Engineering Corporation (NUPEC) planned and performed a feasibility study to improve seismic test methodologies for NPP structures. As the result of the study, the concept of new test methodology has been extracted. The test methodology applies a blasting power in a field of a coalmine. In this test, the ground shaking generated by blasting for mining coal is regarded as artificial earthquake motion. If an NPP building model is constructed closely to the blasting area, huge artificial earthquake ground motion will be applied to the model. This test will supply us an important field test data of the SSI under severe earthquake ground motion. In the paper, prototypical test for structures by applying newly proposed methodology is presented.

Existing Experimental SSI Data

Here existing experimental SSI data of NPP structures are briefly reviewed, paying attention to evaluating their ultimate strength against earthquake ground motions equivalent and/or exceeding design levels. Seismic tests performed for NPP structures are categorized roughly into the RC structure test and the SSI tests.

The RC structure test has been carried out to study non-linear behavior of an RC structure during large earthquake ground motion.

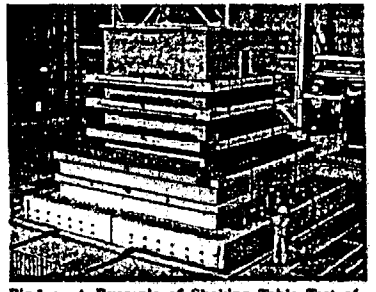

Fig.1 : A Example of Shaking Table Test of NPP Reactor Building. (A 1/12 Scale Model on The Tadotsu Shaking Table)

The test includes static and dynamic tests. The static tests had been carried out by applying static load to an RC structure specimen, using oil-jacks etc., to establish the evaluation methodology of nonlinear characteristics of the RC shear walls up to failure. The dynamic tests had been carried out in general using a shaking table apparatus to confirm whether or not the evaluation methodology of nonlinear characteristics of RC columns and/or RC shear walls obtained by the static test is applicable to that under the dynamic loading condition. Figure 1 shows a typical test example of the dynamic test, the shaking table test of BWR reactor building model. However, the loading capacity and the size of the shaking table are limited, a 1/12 scale is the maximum scale for the whole building model even if the worlds largest Tadotsu Shaking Table is used [2].

In this test, a simulated earthquake ground motion having maximum acceleration of 2.36g was applied to the model. The test brought many fruitful results, however, the phenomena of basemat uplift and rocking motion of the building model were excluded because the test model was fixed to the shaking table.

The SSI test has been carried out to confirm a composite soil-structure system response behavior to earthquake motions as it is described in the theoretical solutions. The test includes field and laboratory tests. The laboratory test applying artificial soil model made of rubber and a building model made of metal i.e., aluminum etc. The test is carried out placing the soil-structure model on a shaking table and applying simulated earthquake ground motions.

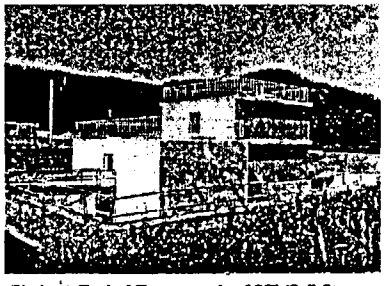

Fig.2 : A Typical Test example of SSI (Soil-Structure Interaction) model test. "Model Test on Dynamic Cross Interaction Effects of Adjacent Structures"

The test is handy because the whole scale of the model is small, i.e., less than 1/250 so that the test is suitable for detailed investigation.
However, the limited scale of the soil model generates some unexpected vibration mode caused by the finite boundary of the soil model, which is not observed in an actual building at actual field where the soil stretches infinitely. Furthermore, in general, the soil model tends to response linearly even to a large acceleration input motion. Therefore the laboratory test is limited for its application to nonlinear SSI test. The field test categorized into two types. One is vibration test of an actual NPP reactor

building using unbalanced-mass rotating shaker, which is performed as an item of pre-operation tests of NPPs [3].

Also, in some of actual NPPs, earthquake observation is carrying out in their safety related important structures. The other is a model test, which is carried out using scaled structure models constructed on a field representing a typical NPP site. Figure 2 shows a SSI field test example of this kind, "Model Test on Dynamic Cross Interaction Effects of Adjacent Structures". The test was carried out by NUPEC to investigate the effect of buildings adjacent to a reactor building on the earthquake response of the reactor building [4]. In the test, vibration tests using a shaker and earthquake observation in the building models were conducted. However, applicable vibration energy is limited in the vibration test, furthermore, observed earthquake motions are also limited in their maximum acceleration, i.e., in general 10-20Gal. and 170Gal. at most. Under those limitations, the SSI phenomena are considered to be within a linear response category.

Figure 3 summarizes seismic test, earthquake experiences and seismic design analyses of NPP structures in Japan. The figure shows the state of arts of the relationship between seismic design analyses and test data as well as the applicability of the data of the seismic tests and earthquake experiences to the evaluation of nonlinear earthquake response and seismic margins of NPP structures. As shown in Fig.3, seismic design analyses have been performed for design earthquakes ranging from 180 to 600Gal. Linear Seismic design analyses have been carried out for the maximum design earthquake. However, nonlinear design response analyses have been introduced for the ultimate design earthquakes. In these nonlinear analyses, nonlinear stress-strain characteristics of RC shear wall and basemat uplift phenomenon have been introduced. Although, a rich data-base of nonlinear behavior of RC shear wall supports the nonlinear analyses, almost no test data supports the basemat uplift analyses.

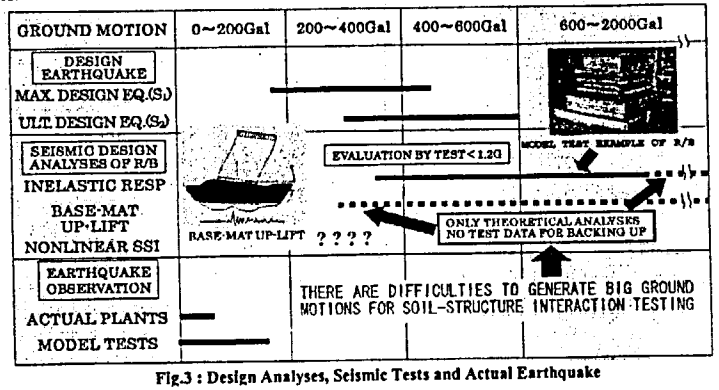

Fig.3 : Design Analyses, Seismic Tests and Actual Earthquake

The situation is mainly caused by the difficulties of catching big earthquake ground motion at the SSI test site and/or NPP plant sites. Our experience of earthquake observation is very limited with regard to the maximum acceleration of earthquake ground motions at free field in SSI test sites and NPP plant sites, a 170Gal. is the maximum for SSI test sites and a 68 Gal. for NPP plant sites. Also there is the difficulty in generating artificial earthquake ground motion resembling actual earthquakes for use in the SSI test. So the analyses had been carried out based on theoretical hypotheses. It is also pointed out that there might be some nonlinear SSI behavior even a rock site for a strong earthquake ground motion. There is information that SSI related natural frequencies tend to decrease with the increment of acceleration magnitude of earthquake ground motion [5]. Because the information is based on the observed acceleration earthquake ground motion of 170Gal. at most, much nonlinear behavior related to of SSI is anticipated for big earthquake ground motion over the design earthquake ground motion.

Thus some SSI-related field test data are needed for big earthquake ground motion equivalent and/or exceeding the acceleration level of typical design earthquake ground motion to confirm adequacy of the current seismic design methodology and to evaluate ultimate seismic strength of NPP structures.

Proposal of New Type Tests

Test Method

Two types of issues are pointed out relating to evaluating the ultimate strength of NPP structures. These are; i) nonlinear characteristics of SSI phenomenon [6], and, ii) nonlinear behavior of an RC structure under three-dimensional loading condition [7]. Naturally, the later issue can be resolved by a shaking table test of structure.

It is pointed out that handling of the scale effect of the specimen on the ultimate strength evaluation of the actual structure is another essential issue for the scaled model test [8]. Thus, for the test, the largest specimen possible and the biggest input motion possible are necessary. Taking into account the above issues, new test methodology, which utilizes artificial earthquake ground motion, is considered desirable if it can be performed at a realistic cost.

With this motivation, the test methodology which applying blasting power as for a big earthquake ground motion has been investigated. The information from a coalmine company in the U.S. indicates that the works performed in the surface coalmine to blast a rock layer covering a coal layer generates a big artificial ground motion, which is similar to earthquake ground motion.

Application of this artificial earthquake ground motion for the SSI test is considered very promising because the blasting work is carried out periodically for mining coal so that we can applied artificial motions generated by the work if we construct a building model at a closed point to the blasting work area.

Vibration Source

Figure 4 shows a picture of the coal mining site. As it can be seen in the figure, sand-rock, coal and mud-rock form strata, and a sand-rock stratum 25-30meters thick covers the coal stratum, so that the sand-rock stratum is removed to mine the coal. The blasting power has been applied to remove the stratum as well as to loosen the coal stratum before mining coal.

A typical blast is being conducted using an underground explosive array (typically, width is a 100meters, length is 1,000meters, and total amount of explosives is 3,000tons). In order to study the ground motions induced by blasting, the ground motion was observed around the underground explosive array area.

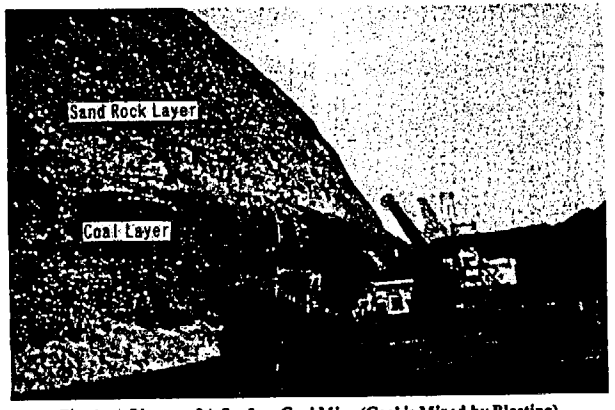

Fig. 4 : A Picture of A Surface Coal Mine (Coal is Mined by Blasting).

Figure 5 shows an outline of the observation arrays of ground motions.
Figure 6 shows acceleration ground motion examples (radial and vertical directional motions) observed at a point 100meters away from the area of explosive array, and their acceleration response spectra of 5% damping. The ground motion induced by the blast has a maximum acceleration of 2.0g and an effective duration of 6.0seconds.

Although the dominant frequency band of the motion are somewhat higher than those of typical design earthquake ground motion, the potential of the motion for future application is promising. If we constructed a building model near the explosive array area, a big ground motion could be applied to the model. In that case, the model should compensate by being scale down for the high frequency dominant characteristics of the ground motion.

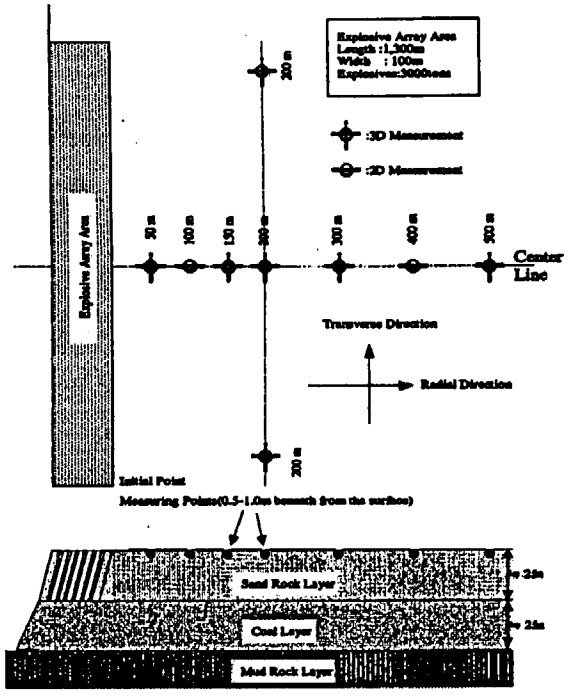

Fig. 5 : Ground Motion Observation Array for Artificial Earthquake Motionby Blasting in A Coal Mine in The U.S.

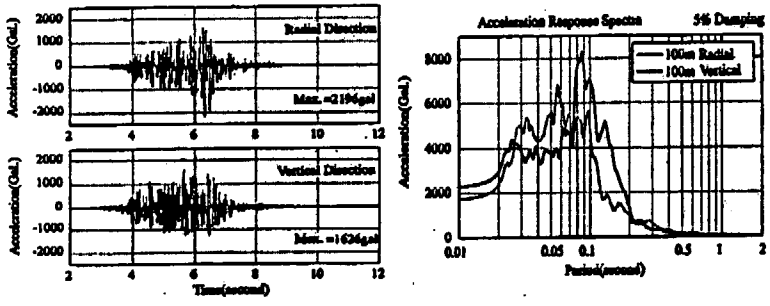

Fig.6 : Observed Acceleration of The Artificial Earthquake Ground Motion and Their Acceleration Response Spectra of 5% Damping.

Figure 7 shows acceleration attenuation characteristics of radial and vertical ground motions. From the figures (Fig.6 and Fig.7), the motion equivalent to design earthquake motion in acceleration magnitude can be observed even from a distance of 300 meters from the explosive array area except that the motion has a lager maximum acceleration in the vertical component than the horizontal component.

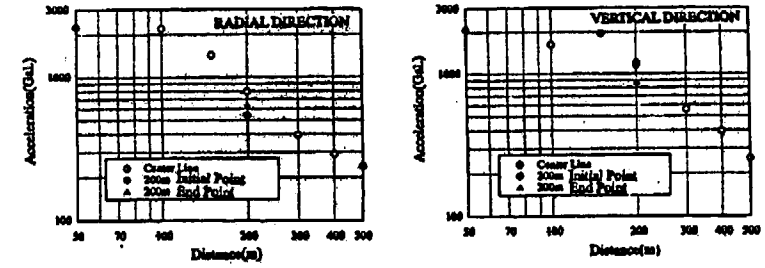

Fig.7 : Acceleration Attenuation of Radial and Vertical Ground Motions.

Response Analysis of Test Model

A simulation analysis of the test was carried out to investigate the applicability of the motion to a seismic test of an NPP structure, which evaluates the ultimate response behavior of the structure, were a big earthquake that exceeds design level to strike an NPP site. The input motion used for the analysis was the ground motion observed at the point of 100 meters distant from the explosive array area. In the analysis, the building model was scaled down to 1/5 to compensation for the difference between the motion generated by blasting and a typical design earthquake ground motion. Figure 8 shows an outline of the simulation model used.

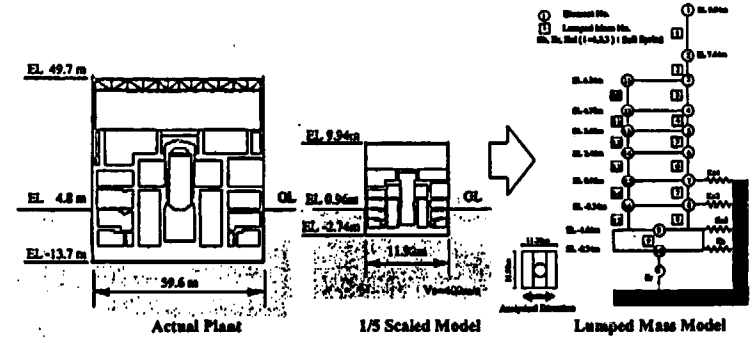

Fig. 8: An Outline of A Typical Analytical Reactor Building Model of 1/5 Scale

The model represents a typical reactor building of an Advanced Boiling Water Reactor (ABWR) [3]. The model is scaled down by 1/5 in length, 1/25 in shear wall thickness, and $1/\sqrt{5}$ in time scale. Meanwhile, the natural frequency of the model becomes $\sqrt{5}$ time larger as compared with the actual building. The other important parameters, i.e., gravity, response acceleration, and generated stress, are kept actual scale.

Figure 9 shows a typical soil profile of the test site. Table 1 shows soil properties used for the simulation analysis. The analytical model includes nonlinear characteristics of base-mat uplift and hysteresis loop of RC shear wall.

The results of the simulation analysis are shown in Fig.10. Figure 10 (a) shows maximum response acceleration and (b) shows maximum response shear strain. It is said from the figure that we can obtain large structural response data by the field test up to ultimatum degree together with SSI data under strong earthquake-like ground motion.

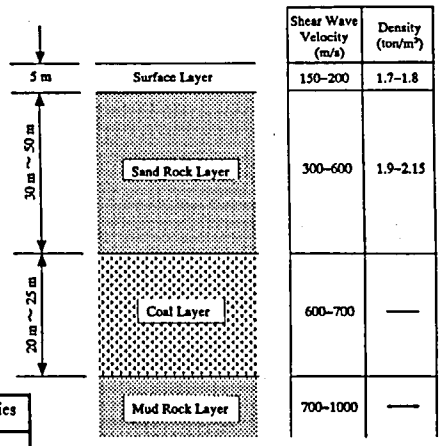

Fig.9: Typical Soil Profile of The Test Site Used for Simulation of The Field Test using Blasting Power.

Table 1: Soil Properties

Item	Pyisical Properties
S-Wave Velocity : Vs	400 m/sec
P-Wave Velocity: Vp	2000 m/sec
Poisson's Ratio: v	0.47
Density : ρ	2.05ton/m^3
Damping Ratio : h	2 %

Design of Proposal Test Model

The building model is designed based on the simulation results for the field test as shown in Fig.11. Some details of the model are shown in Table2. The model is 12.7m in height and 12m square in cross section. Total weight of the model is about 1,600tons including the added mass weight of 653tons, which is used to adjust the natural frequencies of the model to the design values. Thickness of shear walls of the building model is determined as 6.0cm for the lower part and 4.0cm for the upper part and that of the RCCV is determined to be 8cm. The thickness of base-mat is determined to 110cm and that of each floor slab was designed to be 30cm to support the added mass. The added masses are manufactured of steel or lead. The model is embedded by 2.6 meters (two stories) with regard to actual Japanese NPP building construction condition. Figure 12 shows a schematic of the field test. We construct the model beside an explosive array area taking into account the actual coal-mining plan and waited for the major blasting conducted for mining. We are planning to expose the model to artificial earthquake ground motions by mining blasts at least four times, each of which has maximum acceleration ranging from one to five times of that of a typical design earthquake ground motion.

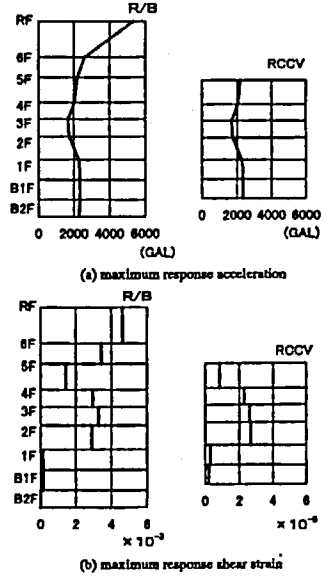

Fig. 10: Results of A Simulation Analysis of the Field Test using Blasting Power.

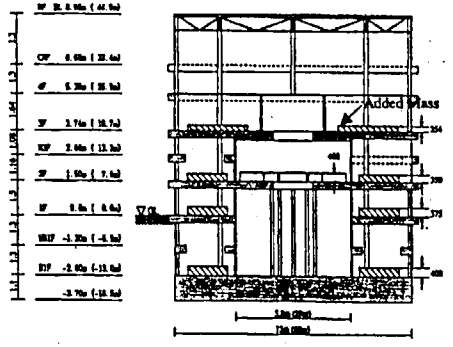

Table 2: Details of the Model

Item	Dimension
Height	12.7 m
Base-mat Size	12 m × 12 m
Thickness of RCCV	8 cm
Shear Wall Thickness	6 cm (For Lower Part) 4 cm (For Upper Part)
Base-mat Thickness	110 cm
Floor Slab Thickness	30 cm
Model Weight	947 ton
Added Mass Weight	653 ton

Fig. 11: The Designed Building Model Based on The Simulation Results for The Field Test.

to artificial earthquake ground motions by mining blasts at least four times, each of which has maximum acceleration ranging from one to five times of that of a typical design earthquake ground motion.

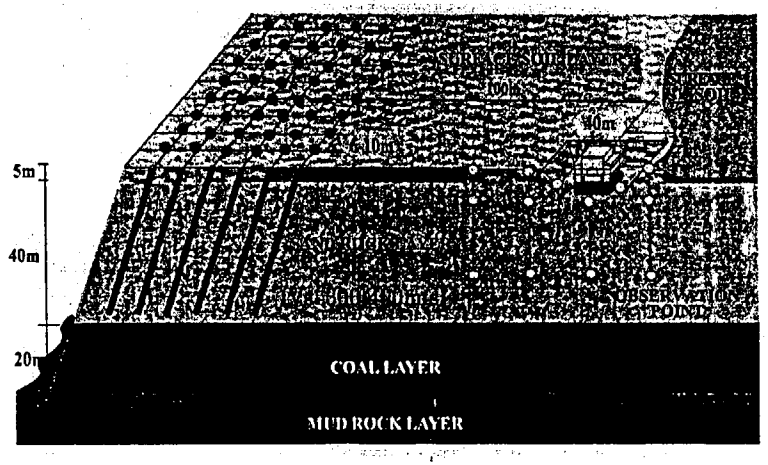

Figure 12: Scheme of Field Test Using Blasting Power of A Coalmine in The U.S.

Purposes of Proposal Test

The major purposes of the field test are to understand (a) basic earthquake response characteristics of an NPP reactor building when a large earthquake strikes the NPP site and (b) nonlinear characteristics of SSI phenomenon during a big earthquake. In order to achieve these purposes, the following items should be studied;

- to study whether or not the natural frequencies related to SSI change with the increment of the magnitude of input motions (and if it changes, to evaluate the degree),
- to evaluate the relationship between soil shear stiffness reduction and the soil strain increase due to increase of the magnitude of input motions, (to compare the field test results with the conventional soil sampling test results)
- to evaluate rocking motion of the building model with regard to increase of input motion magnitude,
- to study how decrease the foundation-ground contact ratio of the building model with increment of input motion magnitude (to comprehend the change of the vertical motion induced by the rocking motions),
- to study vibration amplification characteristics of the building model and its nonlinear behavior,
- to study three dimensional earthquake response behavior of the building model together with its nonlinear characteristics under severe earthquake ground motion exceeding the design earthquake ground motion level.

Concluding Remarks

The test methodology to comprehend ultimate seismic performance of NPP structures against earthquakes was studied to evaluate their seismic safety margin, fragility, and other factors. In the study, we first reviewed the seismic tests of NPP structures and extracted the issues related to our purpose. Then, the need to test large-scale specimens was discovered. In the test, we actuated the specimen together with the surrounding ground with big acceleration motions from deep stratum to confirm the SSI phenomenon under big earthquake conditions. Artificial ground motion generated by the large-scale blasting in a surface coalmine in the U.S. was a promising input motion for the test. Such artificial motion tends to have high frequency band characteristics so that test specimen has to be scaled down to be 1/5 at the maximum. Thus the field test methodology was investigated, which applies the artificial ground motion to a 1/5-scale ABWR reactor building model.
As the results of the study, promising test methodology was proposed for NPP structures, which enables evaluation of their ultimate seismic strength.

Acknowledgment

The study presented herein is commissioned by the Ministry of Economy, Trade and Industry (METI) of Japan. The technical issues herein have been discussed in the "Advisory committee on evaluating NPP seismic design margins", chaired by Prof. T.KUBO, which aims at development of methodologies to evaluate comprehensively ultimate seismic strength of NPPs. The author would like to express his sincere thanks and appreciation to the members of the advisory committee.

References

[1]. Japan Nuclear Safety Commission : "Report on Validity for the Examination Guide of Seismic Design of Nuclear Power Reactor Facilities" (in Japanese), 1995.
[2]. Yano, A. et al. : "Vibration Test of A Model of Nuclear Power Plant using A Large Shaking Table (Part 2 BWR 1/12 Scale Model) , Proc., 9th WCEE, pp.VI-735-740, Tokyo-Kyoto, Japan, 1988.
[3]. Kontani O., et al. : "Forced Vibration Test of ABWR Nuclear Reactor Building", Proc. of 14thSMiRT Conference, vol.K-1, pp.161-168, Lyon, France, Aug., 1997.
[4]. Kitada, Y., et al. : "Model Test on Dynamic Structure-Structure Interaction", Proc.,7th International Symposium on Current Issues Related to Nuclear Power Plant Structures, Equipment and Piping", pp.IV-4-1-15, Raleigh, N.C., U.S.A., Dec.1998.
[5]. Tang, H.T. et al. : "Hualien Soil-Structure Interaction Test", Proc., 7th International Symposium on Current Issues Related to Nuclear Power Plant Structures, Equipment and Piping", pp.VII-3-1-19, Raleigh, N.C., U.S.A., Dec.1998.
[6]. Borja, R.I. et al. : "Nonlinear SSI Analysis", Proc., UJNR Workshop on Soil-Structure Interaction, pp.9-1-12, Menlo Park, C.A., U.S.A..
[7]. Bazant Z. P. : "Modeling of Concrete Behavior : State of the Art", Proc. of 14th SMiRT Conference, vol.0, pp.49-75, Lyon, France, Aug., 1997.
[8]. Mihashi H. : "Influence of Material Structure on Size Effect Law of Concrete Structures", Proc. of 14th SMiRT Conference, vol. H, pp.49-56, Lyon, France, Aug., 1997.

SEISMIC BEHAVIOUR OF MASONRY INFILLED FRAMES LOCAL AND GLOBAL MODELLING FOR THE SEISMIC ASSESSMENT OF EXISTING STRUCTURES

D. Combescure[1], F. Vita[2], P. Sollogoub[1]

[1] EMSI Laboratory, DEN/DM2S/SEMT, CEA Saclay, F-91191 Gif-Sur-Yvette, France
Tel : +33 1 69 08 66 55, Fax : +33 1 69 08 83 31, e-mail : didier.combescure@cea.fr
[2] Universita degli study di Roma La Sapienza, Facolta di Ingegneria, Via Eudossiana 18, I-00184 Roma, Italy

ABSTRACT

The present paper aims at presenting an overview about the effects of the unreinforced masonry infills on the in-plane seismic behaviour of reinforced concrete frames and the global and local non linear models available for the seismic assessment of such type of structures.

INTRODUCTION

In several European countries, the building structures are commonly made by reinforced-concrete frames infilled with unreinforced masonry panels. The infill panels, usually considered as non-structural elements, have a significant effect on the global seismic linear and non-linear responses of R/C frame structure. On one side, they can increase the stiffness and the strength of the frame in a very significant way, for example, by changing the torsional behaviour of the structure or creating a soft storey mechanism. On the other side, they induce supplementary shear or normal forces in the surrounding frame which may conduct to a brittle failure of the reinforced concrete members. This is particularly true for the existing reinforced concrete structures poorly or not designed for a modern seismic action. Furthermore, the design codes penalize such type of structure because of their random behaviour.

The present paper aims at presenting an overview about the effects of the unreinforced masonry infills on the in-plane seismic behaviour of reinforced concrete frames and the non linear models available for the seismic assessment of such type of structures.

Two levels of non linear modelling are used for the analysis of the infilled structures under in-plane loading. At the local level, each constituent has its own constitutive law and geometric finite element support. The main phenomena such as cracking and crushing of concrete and masonry could be reproduced by using the continuous damage and plasticity theories or semi-global models: 2D plasticity model for masonry, joint elements for the interface between masonry and RC frame, non linear fibre type model for the RC frames... Once the constitutive laws validated on elementary tests, this level of modelling allows one to perform predictive calculations on structures with various geometries and material characteristics. The effect of the openings can also be estimated. However the cost of the computations does not allow extensive or dynamic studies and thus the global level -where equivalent diagonal struts and global beam elements with constitutive laws based on empirical rules reproduce respectively the behaviour of the masonry infills and the RC frames- represents the unique strategy for the analysis of complete civil engineering structures under extreme seismic loading. Such a modelling approach has already been validated on experimental results on one bay one storey infilled frames tested under static cyclic loading at LNEC in Lisbon and multistorey structures tested in JRC Ispra [Combescure, 1996 and 2000a]. The paper presents also the results of an extensive parametrical study performed with the refined non linear finite element models in order to identify the main properties of the equivalent diagonal struts -stiffness and strength- and to assess the shear forces induced by the masonry infill in the RC frame. The results of these parametrical studies have been summarized in simple analytical formulae and compared to several classical formulae available in the litterature.

OECD-NEA Workshop on the relations between seismological data and seismic engineering analysis,
Istanbul, 17th and 18th October 2002

GENERAL OVERVIEW

Influence of the masonry infills on the seismic behaviour of buildings

The observations of the damage in the building structures after the past earthquakes have contributed significantly to clarify the impact of the masonry infills on the seismic behaviour of the buildings and the characterization of the damages of the structures. Although they are usually classified as non structural elements, infills - which can be made of masonry bricks, concrete blocks or prefabricated panels – may, on one hand, increase significantly the global stiffness, the global strength and the capacity of energy dissipation of the structures and, on the other hand, create local or global brittle failure mechanisms. The interactions between the RC bearing structure and the infills can also be at the origin of supplementary damage.

The following examples give an idea about the negative impact of the infills on the seismic behaviour of the buildings:

- Soft storey in the lowest storeys of the building due to an irregular vertical arrangement of masonry infills and tendency to concentrate deformation;
- Torsion due to an irregular horizontal arrangement of the infills (Figure 1) ;
- Localized and brittle failure of the bearing elements (columns) due to irregular openings in the infills and lack of anchorage of the panel to the frame ;
- Yielding of the column in tension or shear failure due to the forces induced by the masonry infills ;
- Loss of serviceability of strategic buildings such as hospitals because of the damage in the infills ;
- Out-of-plane failure of the prefabricated panels or the masonry infills due to the insufficient connections with the structure.

Infills can also contribute in a positive way to the seismic behaviour of buildings. Figure 2 shows an example in the area of Sant Angelo dei Lombardi in Italy (Irpinia event) where the good quality of the materials and the homogeneous configuration of the building make this building which was not designed for earthquake loading exhibit no cracking after the Irpinia event.

The modelling of the masonry infill represents then a major interest for the assessment of existing buildings under dynamic loading.

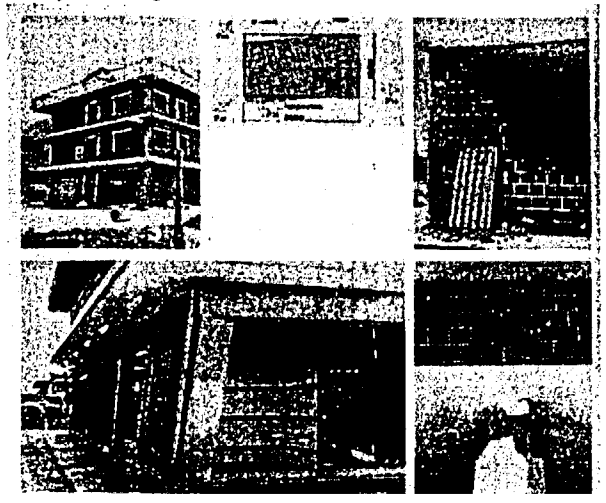

Figure 1: Torsional failure to irregular plan arrangement of infill

Figure 2: Buildings without seismic design and detailing showing no sign of damage after the Irpinia earthquake

Effects on the Code provisions

The recent code takes into account the effect of the masonry infills on the seismic response of the buildings. Let take the example of the Italian code provisions for masonry infills (D.M. 16/1/1996 [Ministero dei lavori pubblici, 1997]). In Part 2 of this document which deals with the interactions between frames and masonry infills, the provisions suggest the use of numerical models of infills made of 2 diagonal struts resisting only in compression. The domain of validity of the model is defined by:

a) The frame is made by reinforced concrete or steel elements well connected between them and in contact with the masonry infills ;
b) The ratio of the length to the height of the panel has to vary between 0.5 and 2 ;
c) The out-of-plane aspect ratio (height divided by thickness) must be lower by 20 in order to have sufficient out-of-plane strength;
d) The infill panel must be without large opening except some openings with surrounding RC.
e) The mechanical characteristics have to be sufficient to sustain the in-plane forces ; for example, masonry with brick with a void ratio higher than 45% can not be considered in the analysis.

The equivalent strut must have the physical thickness of the wall and its width is taken equal to 10% of its length. The strut is connected to the nodes common to the beam and the column. The stiffness of the infill is estimated with this section which means the axial stiffness of the strut is equal to :

$$E_w t_w b_w / d_w = 0.10 E_w t_w$$

The values of Young modulus and masonry strength are determined according the Italian code for structural masonry D.M. 20/11/1987 or by doing experimental material tests performed on masonry wallettes.

Part 2 of the code provisions gives also the failure mechanisms of the infilled frames (Fig. 3) :

- Shear sliding along an horizontal bed joint
- Diagonal tensile failure
- Crushing at the diagonal struts

The verifications have to be performed for the 3 failure mechanisms. The horizontal component of the axial force in the strut is compared to the following formulae:

For shear sliding, $F_w = \tau_w \frac{l_w t_w}{\phi}$ with $\tau_w = f_{w0}\sqrt{1+\frac{F_w}{l_w t_w}\frac{0.8\frac{h_w}{l_w}-0.2}{1.5 f_{w0}}}$

For crushing, $F_w = 0.8\frac{f_{wd}}{\phi}\cos^2\theta_1\sqrt{\frac{E_c I_p h_w t_h}{E_m}}$

For traction, $F_w = f_{wd0}\frac{l_w t_w}{0.6\phi}$

where f_{wd0} is the characteristic shear strength of the masonry without vertical load, f_{wd} the characteristic compressive strength, E_m the masonry Young modulus, t_w the infill thickness, h_w the infill height, E_c the concrete Young modulus and I_p the column inertia. The factor ϕ is a factor equal to 1 or 2

The structural members of the surrounding frame have to be checked:

a) the axial force in the column is computed with the diagonal struts model ;
b) the columns reinforcement is designed in order to avoid a premature shear failure ;
c) the supplementary shear force V_{cd} and bending moment M_{cd} in the column (induced by the masonry infill) are function of the horizontal component of the force transmitted by the masonry infill:
   $V_{cd} \pm F_w$ and $M_{cd} \pm 0.10 h_w \cdot F_w$

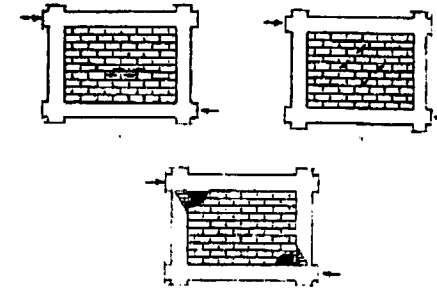

Figure 3: Infills failure mechanisms considered by the Italian design code

THE LOCAL TO GLOBAL MODELLING APPROACH

Definition of the local and global modelling levels

Two modelling approaches, global and local, are classically used to analyse the infilled frame structures under horizontal seismic loading. In the global approach, each masonry panel is often replaced by two trusses with an uniaxial behaviour law [Klingner et at., 1976]. The complexity of the behaviour depends on the various phenomena taken into account by the model (pinching due to crack closure, crushing of masonry at the corners, decrease of stiffness due to cracking, etc...). The frame is modelled by beam and column elements with moment-curvature relationships or fibre type model. This approach allows to perform a large number of computations with dynamic or cyclic loading but the identification of the truss parameters is often based on empirical rules. In case of a modification in the panel characteristics, the limit of validity of the formulae may be reached.

In order to cope with this difficulty, it is proposed to use the refined material models not only to identify the parameters of the panel element but also to highlight the limitation of such a global model by studying, for example, the interaction between different infills in a multi-storey structure [Combescure 1996]. In the local approach, each part (the frame and the infill panels) is discretized. Both materials -masonry and RC concrete- are considered as homogeneous media with an elastic or a non-linear, isotropic or anisotropic behaviour law. In this local modelling, the hypothesis made for the contact between the frame and the infill panels becomes important since the global stiffness is highly dependent on the presence of cracks at this interface. All the computations presented here have been

performed with the Finite Element code CASTEM 2000 developed by CEA-France. Within such an environment, the user can easily compare the two levels of modelling and use them in a complementary way and it becomes easy to identify the parameters of the global models using refined modelling.

Local modelling

R/C frame

2D Timoshenko beam elements supporting a fibre type model have been used for the frame [Guedes, 1997]. Each column has been discretized by 10 elements with 6 concrete fiber and 2 or 3 steel fibers, each fibre having 2 Gauss points. Simplified uniaxial laws have been considered for both concrete and steel: parabolic curve with a perfectly plastic plateau in compression and no strength in tension for concrete (similar to the concrete law of the French BAEL concrete code) and a plastic model with kinematic hardening for steel. Shear behaviour is assumed elastic. Note that such a modelling allows to know the shear forces and the axial forces in the frame and thus to quantify the effect of the presence of the masonry infill onto the surrounding frame.

A masonry plasticity based model

The experimental results and some previous studies have shown that the specimen failure is reached when masonry crushes [Pires, 1993], [Combescure, 1996]. Furthermore, the ultimate strength depends on the number of cycles applied to the specimen. In order to cope with the former property, a plasticity-based model with two yield surfaces and softening behaviour in compression and traction has been developed. Details about this model and its numerical implementation are available in [Combescure, 1996 and 2000a]. As for the classical plasticity-based models, unilateral phenomena due to cracking is not considered. This fact has a minor importance also under cyclic loading since the main cracking is assumed localized at the interface between frame and infill and is modelled by a joint/interface element.

The Young modulus is identified with the results of diagonal test (E=4.G for v=0.2 if G is calculated with the RILEM rules) whereas the compressive strength of the isotropic model of masonry is directly given by the compression tests on wallettes perpendicular to the holes. Note that the identification of the masonry parameters must be realized with tests performed on complete masonry wallettes since masonry has a very complex behaviour due to the difference of Poisson ratio between bricks and mortar.

Contact modelling

The modelling of the interface has a major influence on the failure pattern, the initial stiffness and the global strength. A plasticity-type joint model with a Coulomb yield surface is used [Snyman et al. 1991]. While the sliding behaviour is governed by plasticity rules, the unilateral phenomenon is reproduced in tension: the joint opens without creating plastic strain. Associated or non associated plastic flow and dilatancy phenomenon can be considered. In our case, the dilatancy angle is assumed equal to zero. The considered tensile strength of the joint is equal to 10 percent of the masonry compressive strength. A classical value of 40 degrees taken from the results of the tests described by [Mehrabi et al., 1995] on mortar-brick interfaces is used for defining the Coulomb failure surface.

Global modelling

Simplified modelling of the RC frames

The mesh of the surrounding frame is reduced for the global computation: each column is discretized with one linear Bernoulli beam element with a reduced elastic stiffness ($2/3^{rd}$ of the elastic stiffness) placed between two Timoshenko elements supporting the non linear fibre model. A constant length equal to the column width has been considered for the plastic hinges.

A global model for infill panels

Since the work performed by [Klingner et al., 1976], the non-linear analysis of infilled frames have been usually performed by replacing each individual panel by two -or more- diagonal struts with a uniaxial compressive law. The model introduced in CASTEM 2000 is also supported by a truss element and the behaviour law (Fig. 4) is able to reproduce the classical models by choosing the appropriate parameters. The phenomena reproduced are the stiffness degradation due to cracking -

mainly at the interface between the frame and the panel-, the development of plastic strain and the softening due to crushing, the strength degradation under cyclic loading and the pinching associated with sliding. The strut has no tensile strength and the stress-strain curve under monotonic compressive loading is multilinear and may be identified by using the results given by refined modelling.

Special attention must be brought to the phenomena of compressive strength degradation under cyclic loading which characterizes the masonry components. This effect is not easy to quantify but is taken into account by multiplying the force F_{axial} associated with the plastic strain $d_{plastic}$ by a factor which is a function of the cumulated cyclic plastic displacement (this cumulated cyclic plastic strain is defined as the sum of the increments of plastic strain). A decreasing exponential function is considered. For a constant plastic strain, the force can decrease down to the residual stress $F_{max,res}=\theta.F_{max}$.

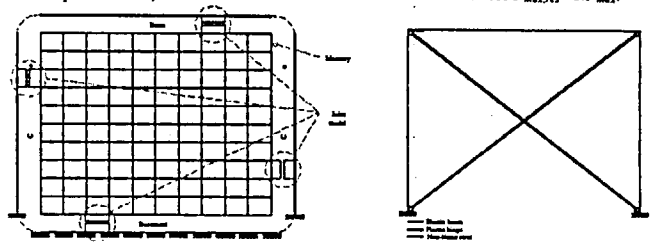

Figure 4: Local and global models of a one bay one storey infilled frame

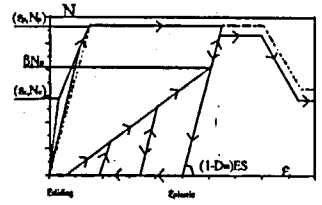

Figure 5: Global axial force-axial strain used for the global model of infill

DESCRIPTION OF THE REFERENCE EXPERIMENTAL RESULTS

A series of 9 one-bay RC frames has been tested under cyclic loading in the framework of the SEISMIR research program supported by the European Commission. The geometric characteristics and the reinforcement details of the models, as well as the applied loads, tried to simulate the real conditions of a reinforced concrete frame located in the ground floor of an ordinary building (Fig. 6). The models had an height of 1.80 m and a length of 2.40 m. The columns and the beams cross sections have, respectively, 0.15 m x 0.15 m and 0.15 m x 0.20 m. The columns were reinforced with 8ø10 longitudinal bars and ø8//0.04 hooks. The beams were reinforced with 6ø8 longitudinal bars and ø6//0.05 stirrups. The infill walls were built with 0.30 m x 0.20 m x 0.15 m horizontally hollow bricks, usual in Portugal, bedded using mortars with the proportions 1:4 in volume (cement: river sand). The materials used in the construction of the frames were a C20/25 concrete and a S400 steel. The models were built on reinforced concrete blocks with a 3.24 m x 0.74 m x 0.35 m volume. These concrete blocks were used to fasten the model to the shaking table.

The models were tested in the platform of a shaking table. The tests consisted basically in the application of a relative horizontal displacement history between the base and the top of the models. A vertical force of 100 kN was applied at the top of the columns. This force was kept approximately constant during the entire tests. Each stage of the tests consisted in the application of 2 complete sine waves of relative horizontal displacement between the base and the top of the models. The maximum

amplitude of the imposed displacement increased from stage to stage of the tests (0.6 mm, 25 mm, 50 mm, 75 mm and 100 mm). The experimental set-up and the main test results are described in details in [LNEC, 1998] and [Pires et al, 1998].

Table 1 shows the maximum strength of the 9 specimens and the increase of initial stiffness due to the presence of the infill panel. Note the great influence of the infill panel for these frames. All the uniformly infilled frames had similar failure patterns: cracking accurs at the interface between the frame and the masonry panel, crushing of masonry in the corners of the wall and some cracking of masonry in the wall itself (Fig. 8). The force-displacement relationship are caracterized by softening and important pinching after the beginning of masonry crushing (Fig 7). Strength degradation under cyclic loading is also visible on the global force-displacement curves: after one cycle, the specimens do not find again the initial strength but a reduced strength.

Specimen	Bare frame		Uniformly infilled frame				Infill frame with window		
	I3	*I4*	*I1*	*I7*	*I8*	*I9*	*I2*	*I5*	*I6*
Max. shear strength	60 kN	64 kN	190 kN	250 kN	181 kN	193 kN	156 kN	123 kN	123 kN
Initial stiffness (kN/mm)	4.8	4.99	206	182.4	155.7	170	50	74.4	75.1
Increase of initial stiffness due to infill *	/	/	x42.9	x38	x32.4	x35.4	x10.4	x15.5	x15.6

**compare to the initial stiffness of the I3 specimen*

Table 1: Increase of strength and stiffness due to the masonry infill panel

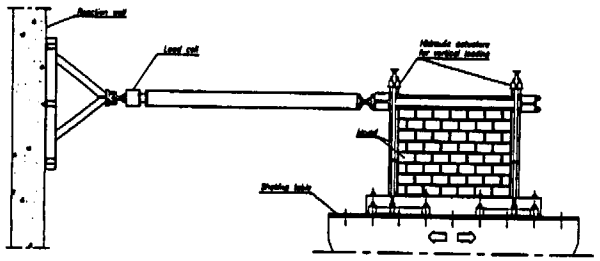

Figure 6: Experimental Set-up

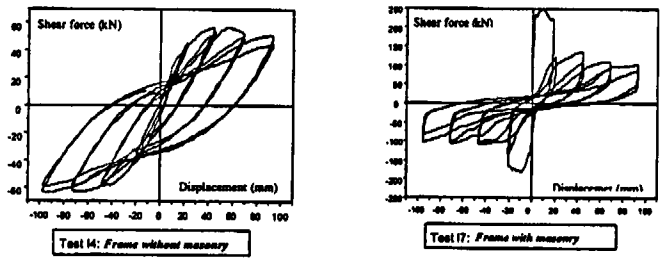

Figure 7: Shear force – top displacement curve (experimental results)

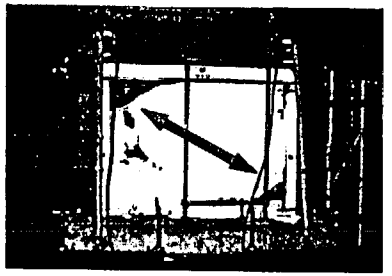

Figure 8: Damage state at the end of the tests showing the crushing of the diagonal strut

REFINED ANALYSIS OF ONE-BAY INFILLED FRAMES

Study of the reference specimen

In the present study, the Young modulus and the compressive strength of masonry has been taken equal to 4000 MPa and 2.2 MPa respectively which correspond to the characteristics determined using compression tests on masonry wallettes. The bricks were horizontally perforated with a void ratio of 60% and have an average compressive strength perpendicular to the holes equal to 4.8 MPa. Let remind the masonry panel has the same thickness than the RC columns (15 cm).

The analysis has been conducted under monotonic loading. The calculation gives the global force-displacement curve of the infilled frame (Fig 9). The curve of the masonry infill is determined by doing the difference between the masonry infilled frame and the bare frame curves. The failure pattern observed during the tests is well captured by the refined modelling: an equivalent diagonal appears between two opposite corners and the maximum strength is reached when masonry begins to crush in the corners (Fig 10). Failure is also characterized by the motion of the diagonal strut down to the base of the windward column.

During past earthquakes, failure of RC frames with limited damage in the infill has been observed for example in case of short columns. It is thus very interesting to know the interaction between the frame and the infill in the refined modelling. For this purpose, the distribution on the height of shear and axial forces and the evolution of their maximum in function of top displacement has been analysed. Fig 11 shows the distribution of shear force for the uniform infilled frame. Note the increase of shear in the parts of the columns at the extremities of the diagonal strut. The maximum values of shear force and axial force are given in Table 2. In the present case, the computed values of shear stress are very high but the columns had sufficient stirrups to avoid brittle shear failure. For axial force, compression is taken as positive. Thus the maximum value is given for the right column which is in compression and the minimum value for the left column which is in tension. These values include the axial force corresponding to the vertical load which is 80.5kN per column.

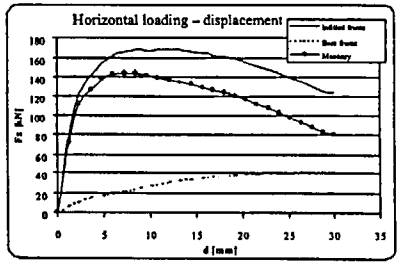

Figure 9: Force-displacement curve for the infilled frame

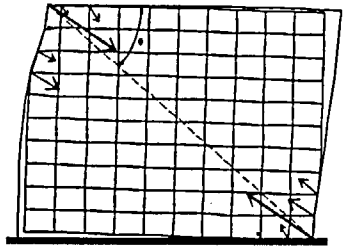

Figure 10: Resulting forces on the masonry

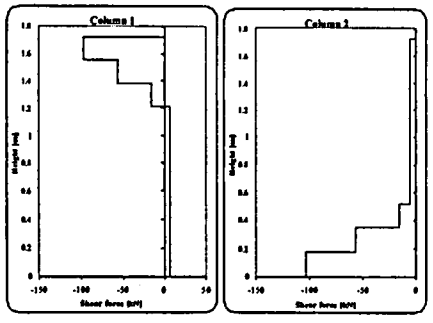

Figure 11: Shear forces distribution in the columns corresponding to the maximum value of shear

	Uniform infill Shear force	Uniform infill Axial force	Infill with window Shear force	Infill with window Axial force
Left column	112 kN (4.98 MPa)	39 kN	78.2 kN (3.47 MPa)	41.3 kN
Right column	123 kN (5.47 MPa)	192 kN	28.2 kN (1.25 MPa)	134.9 kN

Table 2: Maximum values of shear force and axial force in the columns

Parametrical studies

One of the main interests of the non linear model is to allow extensive parametrical studies in order to draw general conclusions and formulae for the identification of the mechanical characteristics of masonry infill with different mechanical and geometrical characteristics.

Due to the large number of parameters of each non linear constitutive law, the present analysis focus only on a couple of parameters which are the compressive strength f_c and the Young modulus E_m. The ratio C between the Young modulus E_m and strength f_c has been taken, in a first stage, equal to the value of the reference model (C=1818) and, in a second stage, equal to 1000 which is a value widely used for masonry. The parameters are both proportional to the same coefficient n:

$E_m = n.4000$ MPa

$f_c = n.2.2$ MPa or $n.4$ MPa

n is equal to n =1/3; 2/3; 1; 1.5; 2; 2.5 or 3.

A variation of the parameter n can also be representative of a variation of other parameters. For example, the variation of Young modulus E_m and of the compression strength f_c, maintaining constant the ratio between them is equivalent to the variation of the infill thickness t_w. Other parameters such as the relative stiffness between the masonry infill and the frame (E_m/E_c) depend also directly on n.

The parametrical analysis have two objectives:

- Predict the characteristics of the equivalent strut whose values can be compared to some reference formulae. The uncracked stiffness and the maximum strength are the 2 characteristics investigated in the present study.
- Assess the shear force induced by the masonry infill in the columns which can be expressed in percentage of the horizontal component of the diagonal compression in the strut (called additional shear force rate).

The force-displacement curve converted to an axial force-axial strain curve is used for the determination of the elastic stiffness, the cracked stiffness and the ultimate strength of the infill (Fig 12). These characteristics are defined in accordance with the multilinear envelop curve of the global model. The elastic stiffness is the result of the difference of the results of the elastic calculations on the infilled and the bare frames. The ultimate strength of the global model is defined as 95% of the maximum strength given by the refined model and is reached for an axial strain for which the axial force given by the refined model is equal to 90% of the maximum strength. This point defines also the cracked stiffness. The elastic stiffness and the ultimate strength can be expressed in term of diagonal width if the infill thickness, the Young modulus and compressive strength of masonry are considered. The diagonal width is given in percentage of the diagonal length D and is noted %D. One may notice the diagonal widths for cracked stiffness and ultimate strength are identical. Table 3 gives an example of determination of the strut characteristics in the case of a linear frame model.

The parametrical study has been conducted with 2 different models for the RC frame which are the non linear model of the frames tested in Lisbon and a linear elastic frame with a reduced Young modulus in order to take into account cracking (2/3 of the elastic Young modulus of the non linear model). Note that the stiffness and the strength of the masonry infill can strongly depend on the characteristics of the frame as illustrated within the following section.

	Relative displacement d [mm]	Base shear force F_x [kN]	Axial strain in the strut ε [%]	Axial force in the strut N [kN]	Strut width %D [%]
Cracking	0.09	18.9	0.003%	23.8	52.6%
Crushing	7.17	179.2	0.20%	225.8	24.1%
Softening	28.25	179.2	0.79%	225.8	24.1%
Ultimate stage	53.59	0.0	1.50%	0.0	24.1%

Table 3: Identification of the parameters of the global model using the model with linear frame

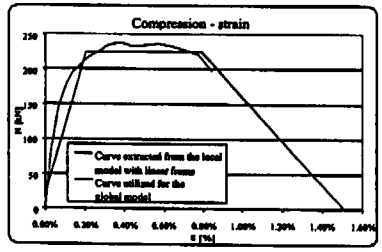

Figure 12: Computation of the axial force-axial strain of the global model with the results of the refined model

Uncracked stiffness

Fig 13 shows the width of the uncracked diagonal strut versus the masonry Young modulus for the 2 models of frame. These numerical results show a very good agreement with the values given by the formulae of Smith [Smith, 1966] and Dawe and Seah [Dawe et al., 1989]. These 2 analytical formulae underestimate only slightly the value of width found by the present parametrical study specially for the lower values of Young modulus Em. In these formulae, the diagonal width w is function of the contact length between the masonry panel and the surrounding frame and so is directly function of the stiffness of the frame.
The classical formulae of Smith is:

$$w=\frac{\pi}{2\lambda}\cos\theta+\frac{\pi}{\lambda}\sin\theta \text{ [Smith, 1966]}$$

with $\lambda_h=\sqrt[4]{\frac{E_m \cdot t_w \cdot \sin 2\theta}{4E_H \cdot I_H \cdot H}}$ and $\lambda_L=\sqrt[4]{\frac{E_m \cdot t_w \cdot \sin 2\theta}{4E_L \cdot I_L \cdot L}}$

with E_m, t_w the Young modulus and the thickness of the masonry infill, E_H, I_H the Young modulus and the inertia of the beam, E_L, I_L the Young modulus and the inertia of the columns, H and L the height and length of the masonry infill and θ the inclination of the diagonal strut.
Dawe and Seah give a very similar expression:

$$w=\frac{\pi}{1.5\lambda}\cos\theta+\frac{\pi}{1.5\lambda}\sin\theta \text{ [Dawe et al., 1989]}$$

Ultimate strength

Fig 13, 14 and 15 show the width of the cracked diagonal strut versus the masonry compressive strength f_c or the Young modulus E_m for the 2 models of frame. At the opposite of the elastic stiffness, the diagonal width depends strongly on the model of frame (linear or non linear).The numerical results have been compared to the values given by the formulae of Mainstone [Mainstone, 1971] and Durrani and Luo [Durrani et al., 1994] which are respectively:

$$w=0.175(\lambda_H H)^{-0.4}\sqrt{H^2+L^2} \text{ [Mainstone, 1971]}$$

$$w=\gamma\sin\theta\sqrt{H^2+L^2} \text{ [Durrani et al., 1994]}$$

with $\gamma=0.32-\sqrt{\sin 2\theta}\left(\frac{H^4 \cdot E_m \cdot t_w}{m \cdot E_H \cdot I_H \cdot H}\right)^{-0.1}$ and $m=6\left(1+\frac{6E_L \cdot I_L \cdot H}{\pi \cdot E_H \cdot I_H \cdot L}\right)$

These 2 formulae give very different estimation of width. The Durrani and Luo formulae which has been calibrated on finite element models gives results similar to the results of the parametrical analysis but the Mainstone formulae seems to underestimate strongly the width and so the strength of the diagonal strut.

Analytical formulae for the non linear and the linear frames

The results of the parametrical studies have been reassumed in simple analytical formulae which can be used directly for the identification of the diagonal struts of the non linear global model.

The maximum axial force found with the non linear model for the RC frame has 2 properties:
a) for the high values of masonry strength, the axial strength tends to an horizontal asymptote: the maximum strength of the masonry infilled frame is limited by the strength of the frame and the yielding of the column in tension. The corresponding value of axial force is equal to:

$N_{max\,0}=\frac{A_s \cdot f_y}{\sin\theta}$ with f_y the steel yield stress and A_s the total section of steel bars in the column section

b) for the low value of masonry strength, the width of the diagonal strut tends to 30% of its length.
The following formula fulfills these 2 conditions:

$$N_{max}(f_c)=N_{max\,0}\left(1-(b \cdot f_c+1)^{-a}\right) \text{ with } b=\frac{0.3 \cdot \sin(2\theta) \cdot D \cdot t_w}{a \cdot N_{max\,0}} \text{ and } a=2.22$$

The value of a has been determined to minimize the difference between the analytical and the numerical results.

For a linear model for the frame, the infill strength is not anymore limited by the capacity of the surrounding frame. On Fig. 15, the section of the cracked diagonal strut $S_f(E_m)$ seems independent on the coefficient C. The strut compression strength N_{max} becomes:

$$N_{max}(E_m)=\frac{E_m}{C}S_f(E_m)$$

In a first approximation, the diagonal width can be taken equal to a value between 20% and 30% of the diagonal length. For the present case, it has been chosen the following analytical formula:

$$N_{max}(E_m)=\frac{d}{C}\left((b \cdot E_m+1)^a-1\right) \text{ with } b=\frac{0.3 \cdot \sin(2\theta) \cdot D \cdot t_w}{a \cdot d}.$$

The error minimization gives a=0.7 and d=355 MN.
The application of the 2 analytical formulae to the infilled frames considered in the present study shows a very good agreement with the results of the parametrical analysis (Fig 14 and 15).

Shear forces induced in the RC frames

The global model based on 2 diagonal struts is not able to catch the additionnal shear forces induced in the infill by the masonry infill since the struts are fixed directly to the nodes common to the beam and the columns. The refined calculations give the total shear force in the columns for both the infilled frame and the bare frame. The additional shear force has been computed by doing the difference with the values found on the bare frame. The additional shear force has been compared to the horizontal projection of the axial force in the strut $N.\cos\theta$. In order to generalize the results of the present study, a dimensionless ratio named additional shear rate has been introduced:

$$\rho=\frac{T_{infill}}{\cos\theta \cdot N_{max}}$$

So one may find the shear induced by the masonry infill in the column to be added to the shear directly given in the columns by the calculation performed with the global model:

$$T_{total}=T_{columns}+T_{infill}$$

A remarkable result has been evidenced by the parametrical studies: for this particular geometry of infill panel, the additional shear rate does not depend on the masonry characteristics and is equal to 64% (Fig 16). This rate is also almost independent of the modelling of the frame (linear or non linear).

CONCLUSIONS

The present paper has presented some generalities about the influence of the masonry infills on the seismic behaviour of RC frames. They can have a major impact –positive or negative- on the seismic response specially in the case of existing buildings with few or no seismic detailing and design. An extensive parametrical analysis has been performed on one-bay one-storey infilled frames with two levels of modelling: the non linear FEM model allows to understand the failure pattern under monotonic loading, to estimate the forces created by the infill panel in the surrounding frame and to identify the properties of the global model of infill while the global model is used for the analysis of complete structures under simplified static loading or dynamic loading. Simple rules are also given for the identification of the diagonal properties and the shear forces into the surrounding RC frame. The

dispersion of the results given by the formulae available in the literature which can be used to characterize both the uncracked and the cracked diagonal struts must be highlighted. The values of diagonal width depend also strongly on the characteristics available for masonry (bricks, mortar or masonry).

These results can be directly used for the assessment of existing structures which requires efficient procedure of calibration of the model parameters. The present paper is limited to the behaviour of infills under in-plane loading which means the out-of-plane behaviour has been checked.

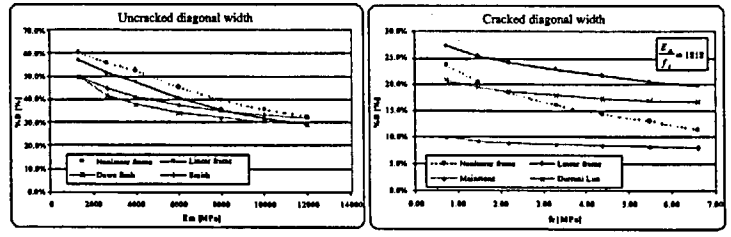

Figure 13: Widths of the uncracked and cracked sections versus the masonry Young modulus and compressive strength

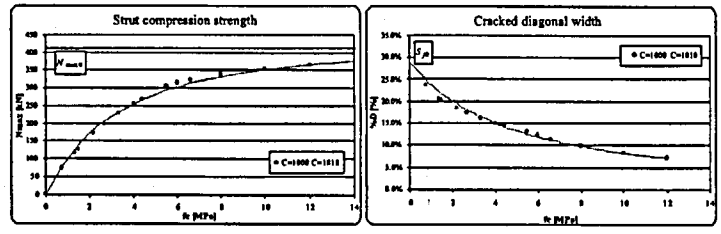

Figure 14: Strut compression strength and width of the cracked diagonal strut versus masonry compression strength (non linear frame)

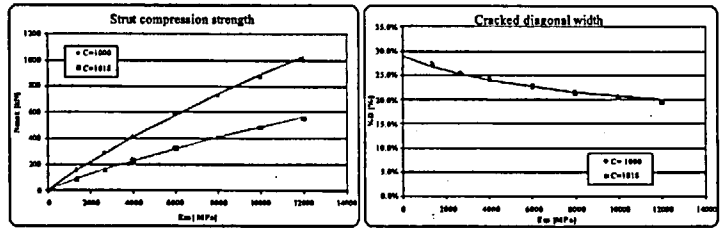

Figure 15: Strut compression strength and width of the cracked diagonal strut versus masonry Young modulus (linear frame)

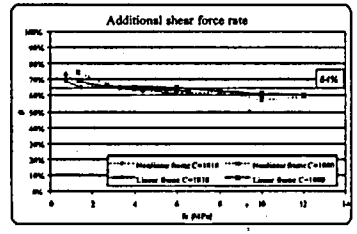

Figure 16: Additional shear force rate versus compressive strength f_c

REFERENCES

Combescure D. [1996], "Modélisation du comportement sous chargement sismique des structures de bâtiment comportant des murs de remplissage en maçonnerie", PhD Thesis prepared at JRC Ispra, Ecole Centrale Paris, France.

Combescure D., Pires F., Cerqueira P., Pegon P. [1996], "Tests on masonry infilled R/C frames and its numerical interpretation", 11th World Conference on Earthquake Engineering, Acapulco, Mexico.

Combescure D., Pegon P. [2000a], "Application of the local-to-global approach to the study of infilled frame structures under seismic loading", Nuclear Engineering and Design 196 Vol.1, 17-40.

Combescure D., Pegon P. [2000b], "Application of the local to global approach to the study of infilled frame structures under seismic loading", 12th World Conference on Earthquake Engineering, Auckland, New Zealand.

Dawe J.L., Seah C.K., [1989], "Analysis of concrete masonry infilled steel frames subjected to in-plane loads", 5th Canadian Masonry Symposium, Vancouver, Canada.

Durrani A.J., Luo Y.H., [1994] "Seismic retrofit of flat slab buildings with masonry infill, NCEER Workshop on Seismic response of masonry infills", San Francisco, USA.

Fardis M.N., Calvi M.G. [1994], "Effects of infills on the global response of reinforced concrete frames" , 10th European Conference on Earthquake Engineering, Vienne, Austria.

Guedes J. [1997], "Seismic behaviour of reinforced concrete bridges. Modelling, numerical analysis and experimental assessment" , PhD Thesis prepared at JRC Ispra, Universidade do Porto, Portugal.

Klingner R.E., Bertero V.V. [1976], "Infilled frames in earthquake resistant construction", Report 76-32, University of California, Berkeley, USA.

LNEC [1998], "Study of the earthquake behaviour of masonry infilled reinforced concrete frames. Tests of model I1 to I9", C3ES Research reports, Laboratorio Nacional de Engenharia Civil, Lisbon, Portugal.

Mainstone R.J. [1971], "On the stiffness and strength of infilled frames", Proc. Inst. Civil Eng., Suppl. IV, Paper 7360S,57-90.

Mehrabi A.B., Shing P.B., Schuller M.P., Noland J.L. [1994], "Performance of masonry infilled R/C frames under in-plane lateral loads", Report CU/SR-94/6, University of Colorado, Boulder, USA.

Ministero dei lavori pubblici [1997], "Circolare 10 Aprile 1997, «Istruzioni per l'applicazione delle norme tecniche per le costruzioni in zone sismiche di cui al decreto ministeriale 16 gennaio 1996 », Supplemento Ordinario alla Gazzetta Ufficiale n. 97, 28 April 1997.

Pires F., Rodrigues J., Campos-Costa A. [1998], "Experimental study of the behaviour under horizontal actions of repaired masonry infilled R/C frames", 11th European Conference on Earthquake Engineering, Paris, France.

Pires F. [1993], "Influencia das paredes de alvenaria no comportamento de estructuiras reticuladas de betao armado sujeitos a accoes horizontaes", PhD Thesis, LNEC Report, Lisbon, Portugal.

Smith B.S. [1966], "Behaviour of square infilled frame", Journal of the Structural Division, Vol. 92, n. ST1, pp.381-403.

THE USE OF SIMPLIFIED MULTI-STORY MODELS IN CHARACTERIZING DAMAGE POTENTIAL OF EARTHQUAKE GROUND MOTIONS

Luis D. Decanini, Fabrizio Mollaioli, Andrea Mura
Dipartimento di Ingegneria Strutturale e Geotecnica - Università di Roma "La Sapienza", Italy
luis.decanini@uniroma1.it, fabrizio.mollaioli@uniroma1.it, andrea.mura@uniroma1.it

Abstract

The characterization of effective damage potential of the earthquakes implies the identification of structural response parameters which reliably represent the most significant features in development of damage in the real structures. For this purpose, models that adequately describe the seismic response of structures must be adopted. As widely recognized, some significant parameters characterizing the cyclic histories of the seismic response can be selected to represent the damaging process of the structures. Obviously, the effects of structural damage reflect also on damaging non-structural elements and technical devices.

The seismic response of multi-story structural systems subjected to severe ground motions should be studied at both global and local levels, as it could be characterized by high demands for inelastic displacement and energy dissipation, often causing concentration of damage in limited zones of the structure. These local effects depend on the type of signal and on the structural characteristics and cannot be predicted by means of SDOF systems. In this research simplified procedures have been adopted for the investigation on the seismic response of multi-story frame structures: inelastic equivalent SDOF systems for the global response of the frame and inelastic equivalent shear-type model for the prediction of local seismic demand in terms of displacements and energy. The results have been also used in estimating the damage imparted to the structures by means of available damage models.

Introduction

The analysis of the seismic behavior of multi-story structural systems subjected to severe ground motions requires the study of the response at global and local levels, as it can be characterized by high demands for inelastic displacement and energy dissipation, often causing concentration of damage in limited zones of the structure, as weak or soft stories. The way these local effects occur depends on the type of ground motions and on the structural characteristics and cannot be completely described by means of SDOF systems, in which the structural response is globally defined, and deformation shape is a simple work hypothesis formulated to obtain response results. Such means of analysis cannot provide any information on the real distribution of drift demand, especially if strong local demand is expected.

In this research two simplified procedures have been adopted for the investigation on the seismic response of multi-story frame structures. The first one consists on the assumption of assigned time-independent global deflection shapes for the lateral displacements of the frame. This simplification allows both the reduction of the response of MDOF systems to the response of equivalent single-degree-of-freedom systems (ESDOF) and an approximate extension of the calculation of parameters characterizing the seismic response, easily obtainable for SDOF systems, to multi-story frame systems. If the significant modes of vibration of the structure are adopted and an approximate modal superposition is executed, this procedure can provide also reliable results for local damage information. The second procedure is based on an equivalent shear-type system, whose lateral stiffness, inertial and strength characteristics approximate those of the frame structure and can vary along the height. With this model, the contribution of all the vibration modes of the structure can be implicitly considered for the evaluation of the inelastic response, and the distribution of displacement and energy dissipation on the height of the structure can be adequately described. Hysteretic models typical of frame force/displacement behavior have been assumed for the local inelastic cyclic response of the system. In order to understand how the response is affected by the characteristics of ground motion, several signals that differ for duration, amplitude and frequency content have been used.

The above mentioned simplified models have been applied in order to quantify the deformation and energy demand parameters that characterize the seismic response of a multi-story frame structure, as dissipated energy and inter-story drift demands. The results have been also used in estimating the damage imparted to the structures by means of available damage functions.

The proposed damage indices can be classified in two different models: in the first one, the level of damage is quantified as a function of maximum deformation and energy dissipation demands, while in the second the number and the amplitude of inelastic cycles are considered, according to low-cycle fatigue hypothesis. Both methods have been adapted to the simplified models analyzed in this research. Damage indices calculated for local level has been used also in the evaluation of global damage and in comparison of results obtained for different hypotheses of behavior.

Equivalent SDOF system

As mentioned in the introduction, the conceptual link between the analysis results obtained or available on SDOF systems, usually resumed in the form of response spectra, and expected response parameters values for MDOF systems, can be identified with the formulation of a calculation procedure in which the MDOF structure is reduced to an equivalent SDOF system (ESDOF). It is useful recalling briefly this concept, because it gives an important means for interpretation of results of MDOF models. The formulation of this simplification is very similar to the first step of a modal analysis for frame structures. In fact a time-independent global deflection shape is assumed for the lateral displacements of the building stories:

$$\mathbf{u}(t) = \Phi\, x(t) \tag{1}$$

where Φ is the vector that defines the deflection shape and $x(t)$ expresses the time-dependent amplitude of motion. This assumption allows to reduce the classic MDOF equations of motion for a frame subjected to a ground acceleration history $\ddot{u}_g(t)$

$$\mathbf{M}\ddot{\mathbf{u}}(t) + \mathbf{C}\dot{\mathbf{u}}(t) + \mathbf{R}(\mathbf{u}(t)) = -\mathbf{M}\,\mathbf{1}\,\ddot{u}_g(t) \tag{2}$$

to the ESDOF equation

$$M_{eq}\ddot{x}(t) + C_{eq}\dot{x}(t) + R_{eq}(x(t)) = -L_{eq}\ddot{u}_g(t) \tag{3}$$

where

$$M_{eq}=\Phi^T\mathbf{M}\Phi;\ C_{eq}=\Phi^T\mathbf{C}\Phi;\ R_{eq}=\Phi^T\mathbf{R}(t);\ L_{eq}=\Phi^T\mathbf{M}\mathbf{1}. \tag{4}$$

The quantity

$$\Gamma = L_{eq} / M_{eq} \tag{5}$$

can be interpreted as a "modal" participation factor, and the assumed displacement shape Φ is seen as a dominant first mode of vibration. The solution $x(t)$ of equation (3) can be derived from the solution $x_S(t)$ of a SDOF motion by means of the relationship

$$x(t) = \Gamma \cdot x_S(t). \tag{6}$$

If a target ductility response analysis is required, one can determine the seismic strength coefficient C_y for the SDOF system and the demanded yielding base shear for the frame structure:

$$V_{by} = \frac{L_{eq}^2}{M_{eq}} C_y g = M_{eff} C_y g \tag{7}$$

where M_{eff} is the effective mass associated with the assigned "modal" shape and g is gravity acceleration.

The energy balance equation for the MDOF system can be written in the usual form

$$E_I(t) = E_k(t) + E_s(t) + E_H(t) + E_D(t) \tag{8}$$

where the energy quantities (associated with unit mass) are respectively absolute input energy, absolute kinetic energy, elastic strain energy, hysteretic energy and damping energy. By means of the ESDOF procedure above resumed, the energy quantities for the MDOF systems can be evaluated multiplying the corresponding SDOF quantities by a factor equal to Γ^2, as can be easily shown introducing the relations (1) and (6) into the MDOF energy expressions, in particular for input energy, hysteretic plus elastic strain energy and damping energy [1]:

$$E_I(t) = \int_t \sum_{i=1}^{N} m_i \ddot{u}_{i,t}(t) du_g \quad ; \qquad E_H(t) + E_s(t) = \int_t \mathbf{R}(t)\, \mathbf{du} \, ; \qquad E_D(t) = \int_t \dot{\mathbf{u}}^T \mathbf{C}\, \mathbf{du} \tag{9}$$

where $\ddot{u}_{i,t}(t)$ is the total (absolute) acceleration of the mass m_i, and the time integration is extended to the duration of ground motion. For the input energy the maximum value during the ground motion is considered in this research. In terms of global energy quantities correlated with the seismic response of a multi-story frame, the above mentioned proportionality relationship means that each of the energy amounts per unit mass of the associated SDOF system must be multiplied by the effective mass (Eq. 7).

In the interpretation of the real response of the MDOF system, if it is admitted to speak in terms of modal contributions also for inelastic behavior, each modal energy per unit mass should be multiplied by a modal effective mass before the ideal operation of modal superposition. The direct relation between the energy parameters of a MDOF structure and the corresponding quantities per unit mass of the SDOF system associated to the fundamental period of vibration of the structure can be empirically maintained by assuming the total mass as an approximate effective mass that includes the contributions of all the modes of vibration.

An analysis based on the equivalent SDOF system can be assumed as a step of seismic design procedure, combined with a pushover analysis that provides local quantities of seismic displacement demand, as story drifts and rotations [2, 3]. The ESDOF method can be use also in the calculation of damage indices for multi-story structures subjected to strong ground motions [4].

Simplified nonlinear dynamic analysis for multi-story frames by means of discrete shear-type model

The choice of using an equivalent shear-type model (ESTM) allows a relatively simple procedure in the integration of the equations of motion: if a shear deformation is assumed to describe the lateral deflection of the frame structure, only translational degrees of freedom are included in the calculation. This simplification can provide a good approximation of the numerical solution if an equivalent lateral shear stiffness is given to the model. In other words, the shear drifts of the stories of the equivalent system may take into account the influence of the flexural deformations of members although the rotational degrees of freedom do not explicitly appear in the dynamic analysis of the structure. The great advantage of this kind of approach is the evaluation of damaging scenarios that is not possible by means of more refined structural modelling. The simplified description of the structural model is ideal in estimation of damage potential of ground motions records on wide classes of multi-story structures.

Bertero, R. and Bertero V.V. [5, 6] have used two uniform models, one defined as an elastic shear beam and the other as an elastic flexural beam, in order to evaluate the maximum drift demand for preliminary design of frame structures of tall buildings. The inelastic behavior has been considered by means of corrective coefficients, estimated in order to predict also inelastic concentration of displacement demand.

Miranda [7] has considered both shear and flexural deformation in an analytical elastic model, used also to find statistical relations between top displacements and inter-story drifts. The same statistical approach has made possible the correlation between inelastic and elastic displacement parameters, by means of empirical coefficients.

Iwan [8] has studied the inter-story drift demand in multi-story buildings by means of an analytical uniform elastic shear-beam model. The approximate code relation between fundamental periods and height of the structure, for steel frame buildings, has allowed the construction of base-level drift spectra, that have shown a strong divergence from SDOF prediction in the long periods range.

Decanini, Mollaioli and Saragoni [9] have studied a continuous shear beam to investigate the response of multi-story frame systems. The inelastic behavior of the structure has been modelled by means of elastic-perfectly plastic model. The global results of the analysis have been compared with the corresponding parameters obtained by means of an equivalent SDOF system. The analysis has shown an approximately parabolic relation between energy and displacements. The shape of the parabola, given by the constant of square proportionality, has shown to be strongly influenced by the type of the signals.

Decanini, Mollaioli and Mura [10] have used the same discrete shear-type model presented in the present paper for a comparison with the results of a push-over analysis. The results have revealed the limitation of the classic pushover analysis, especially in the prediction of inter-story drift and story hysteretic energy demands, when the influence of higher modes is significant. Also in this comparison of results, the tendency to neglect the inelastic concentration effects is shown in the general overestimation of top displacement given by the push-over analysis for high ductilities.

Iwan, Huang and Guyader [11] have related the response of the SDOF system corresponding to the frame structure to capacity spectra affected by equivalent viscous damping; this technique has proved to be not conservative, especially when the maximum response is not caused by structural resonance, but induced by long duration acceleration pulses, as in near-fault ground motions. In order to assess the local deformation parameters values, a push-over analysis with load pattern resembling the first mode shape of the structure has been done, and the results have been compared with those obtained by means of nonlinear analysis of shear-building models characterized by a bilinear story hysteretic model. The Authors have found that local response in terms of story drifts can be much larger than the displacement response obtained by an equivalent static pushover analysis.

The ESTM model considered in this paper first requires a static condensation of the degrees of freedom of an elastic multi-story frame system, made possible by the irrelevance of rotational inertial contributions of the masses to the seismic response of this kind of structure. Once executed the condensation, the equations of motion for the elastic MDOF system subjected to a ground acceleration history $\ddot{u}_g(t)$ assume the form:

$$\tilde{\mathbf{M}}\ddot{\mathbf{u}}(t) + \tilde{\mathbf{C}}\dot{\mathbf{u}}(t) + \tilde{\mathbf{K}}\mathbf{u}(t) = -\tilde{\mathbf{M}}\ \mathbf{1}\ \ddot{u}_g(t) \tag{10}$$

where $\tilde{\mathbf{M}}$, $\tilde{\mathbf{C}}$ and $\tilde{\mathbf{K}}$ are the translational mass matrix, the damping matrix and the elastic condensed stiffness matrix respectively, $\mathbf{1}$ is a unity vector and $\mathbf{u}(t)$ is the vector of the lateral displacements of the stories. It is useful to choose the damping matrix $\tilde{\mathbf{C}}$ according to Rayleigh's formulation, i.e. through a linear combination of the matrices $\tilde{\mathbf{M}}$ and $\tilde{\mathbf{K}}$. This choice allows to obtain reasonable damping effects in all the significant modes of vibration with a relatively simple computational work, e.g. giving the required

nominal damping values to the first two modes. The tri-diagonal form assumed by the matrix $\tilde{C}$ contributes to the computational simplification.

The following step is the individuation of an equivalent shear stiffness matrix, K_s, defined as the tri-diagonal stiffness matrix that produces the same lateral displacements allowed by the stiffness properties of the structure under the action of a prefixed lateral distribution of static forces. Although this definition is conditioned by the choice of the lateral force pattern, slight differences in the terms of the matrix K_s can be found if different reasonable distributions are assumed. In this study an inverted-triangular static force pattern has been used. Adopting this procedure the structural system is completely described by the stiffness and mass properties of the stories.

For the prediction of the inelastic response of a frame structure subjected to a ground motion, a further approximation can be introduced in order to describe the hysteretic behavior of the system by means of simple rules. For inelastic response, the same above described approximate formulation is adopted for initial stiffness. As for the story stiffness, also a story yielding resistance can be roughly defined. This implies to neglect some information on local inelastic deformations and hysteretic dissipations, as plastic curvature and dissipated energy in portions of members, i.e. it means to have limited data for the frame elements damage. The main local displacement response that can be directly obtained by the above described method is the inter-story drift, that can provide some information on the damage of top and bottom ends of the columns of each story but could give only indirect and rough information on damage of joints and beams. This loss of local information is the main limit of the suggested procedure. On the other hand, this great simplification allows to conduct a wide investigation into the inelastic seismic response of multi-story buildings, because the resistance properties of the frames can be described by means of few data and all the constructive details are not directly required. It is useful to remember that also for the strength evaluation a shear-beam model cannot take into account the effects of variations of axial forces in columns, like tensile yielding or compression failure.

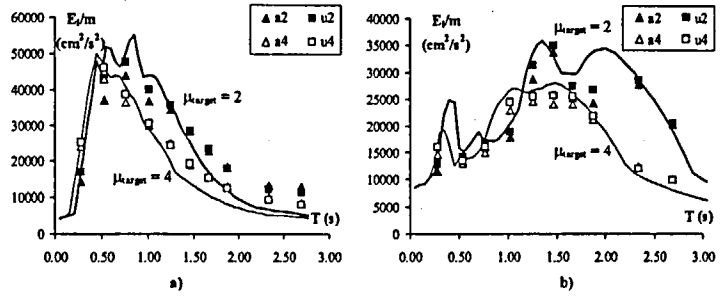

Fig. 1 Input Energy per unit mass. Correlation between spectral SDOF and actual MDOF values. μ_{target} =2 and μ_{target} = 4. a) Kobe JMA; b) Northridge Sylmar 360.

The proposed model is useful in the evaluation of both displacements and energy dissipation demand for generic multi-story frames. Some results of the analysis of ten different R/C two bay-frames is shown in Figures 1 and 2 . Ten different numbers of stories have been chosen, in order to assume information on the seismic response of a wide range of current buildings. For each selected number of stories various different stiffness pattern can been assumed. In this research two different stiffness patterns have been considered: a realistic approximately parabolic distribution (indicated by "a" letter) and a reference uniform pattern (named "u"). The same fundamental period has been selected for the two patterns for each number of stories. The case of stiff foundation structures has been considered by assigning full restraints to the joints at the base of the columns. By means of the ESDOF reduction in terms of yield base strength, global target ductility values have been assigned to the frames when varying the signal. In Figure 1 a comparison between SDOF and MDOF input energy values is shown.

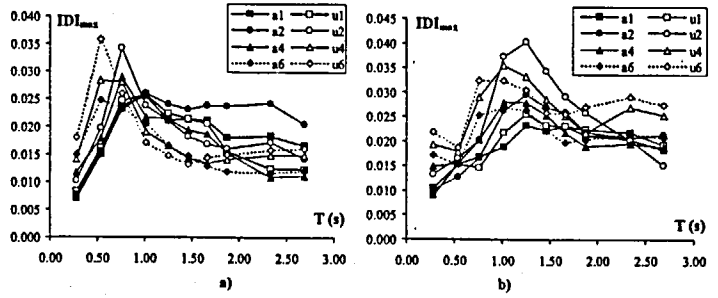

Fig. 2 Maximum inter-story drift spectra. Stiffness patterns "a" and "u", target ductilities 1 (elastic), 2, 4, 6. a) Kobe JMA; b) Northirdge Sylmar 360.

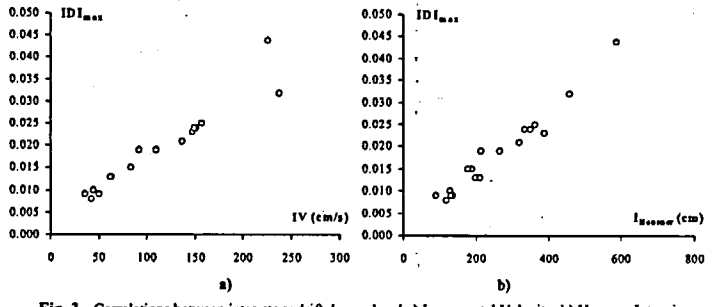

Fig. 3 Correlations between inter-story drift demand and a) Incremental Velocity; b) Housner Intensity.

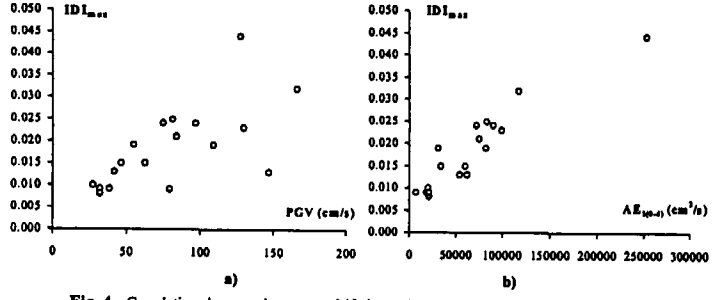

Fig. 4 Correlations between inter-story drift demand and a) Peak Ground Velocity; b) $AE_{I(0-4)}$.

By means of the analysis of the twenty frames modeled by the ESTM, it has been possible to obtain demand spectra of inter-story drift, that has proved to be a very significant measure of failure likelihood for frame structures. In Figure 2 two examples such spectra are presented. The maximum inter-story drift index (IDI_{max}) is the maximum drift demand normalized by story height. The shapes of drift spectra are strongly correlated to the energy demand. This general trend is evident in Figures 1 and 2 for Kobe JMA and Sylmar 360 spectra. The correlation of the spectral shapes is better than the analogue one between energy and SDOF spectral displacement.

In Figures 3 and 4 the good direct correlations between inter-story drift and some meaningful ground motion velocity-based parameters are shown. The $AE_{I(0-4)}$ is the area under input energy spectra in the period range between 0 and 4 s, and represents significant global information on the energy demand potential of the signal.

Damage indices for the characterization of the seismic response

Generally, available damage indices can be mainly classified in two different classes: in the first one, the level of damage is quantified as a combination of maximum deformation and energy dissipation demands, while in the second the number and the amplitude of inelastic cycles are considered, according to low-cycle fatigue hypothesis.

One of the most widely used damage indices belonging to the first class is the Park and Ang index, also modified according to different criteria. The original version of the index, as well known, is

$$DI_{PA} = \frac{\delta_{max}}{\delta_{u,mon}} + \beta \frac{E_H}{F_y \delta_{u,mon}}. \tag{10}$$

The mean value of parameter β, that gives the weight of energy dissipation in damage evaluation, has usually proved to be close to 0.15. In the expression of the index modified by Kunnath et al. [12], in the first term the only plastic component of the deformation is considered, in order to not computing damage value greater than zero for elastic deformation, while Chai and Romstad [13] have modified the energy term, in order to assign the condition of unity value for the index for failure caused by a monotonic loading history. In this case a modified value β^* should be considered. The deformation and energy dissipation terms can be associated to both global and local effects.

The two indices DI_1 and DI_2 recently introduced by Bozorgnia and Bertero [14],

$$DI_1 = \frac{(1-\alpha_1)(\mu-1)}{(\mu_{u,mon}-1)} + \alpha_1 \frac{E_H}{E_{H,mon}}, \tag{11}$$

$$DI_2 = \frac{(1-\alpha_2)(\mu-1)}{(\mu_{u,mon}-1)} + \alpha_2 \left(\frac{E_H}{E_{H,mon}}\right)^{0.5} \tag{12}$$

belong to the same type of damage model. For relatively high ductility levels, the authors have found a good correlation with Park and Ang index for α_1 ranging between 0.25 and 0.3 and α_2 close to 0.3.

For all the formulations above mentioned, the right calibration of weighting coefficients is the fundamental choice, that usually appears strongly influenced by the characteristics of the accelerometric records. The main limitation of this damage indices is in neglecting the effective distribution of energy dissipation in cycles of different amplitude, and so also cycles with small damaging effects are included in the calculation of the damage cumulative process.

The damage indices linked to the concept of low-cycle fatigue are based on Miner's hypothesis rules,

$$DI_{MH} = \sum_{i=1}^{N_{cycles}} \frac{n_i}{N_i}. \tag{13}$$

N_i represents the number of cycles that for every cyclic amplitude value would cause failure. It has been correlated to displacement or cyclic ductility of the cycles [15, 16]. The advantage of this model is the simplicity. The effectiveness of cycles in damaging the structure is weighted by means of the normalization of the actual number n_i by the number N_i causing failure for each cyclic ductility demand μ_{ci}. However, it neglects every effect of the actual time distribution in the sequence of the different cyclic amplitudes reached during the structural response.

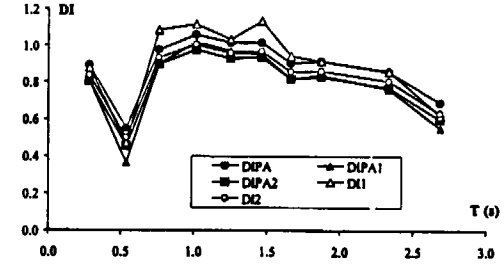

Fig. 5 Sequence of Kocaeli 17/08/99 Duzce E-W and 12/11/99 Duzce E-W records sequence. Maximum story damage indices according to different damage models

Both classes of damage indices can be used for local story damage evaluation, and adapted to simplified models for multi-story frames. The results of damage indices for all the stories can provide also a global evaluation of damage by means of arithmetical or hysteretic energy-weighted averages. Teran-Gilmore & Avila [16] show that, in comparison with the low-cycle damage model, the Park & Ang

criterion tends to underestimate the strength demand of SDOF systems with T approaching the predominant period of the excitation in soft soil conditions. However, it was found that the use of DI_{PA} may lead to a realistic assessment of the damage level also in structures located on soft soil, with the exception of very peculiar cases. For this reason, the discussion of the results will be herein after limited to the case of Park & Ang-based damage functional. In Figure 5 the maximum story damage indices spectra are shown for the E-W component of the sequence of Kocaeli August 17, 1999 (site of Duzce) and Duzce November 12, 1999 records (DI_{PA1} and DI_{PA2} are the variant indices introduced by Kunnath et al. and Chai and Romstad, respectively). In Figure 6 the hysteretic energy-weighted average DI_{PA1} spectrum, calculated for an estimation of global damage, is shown for the two records separately and for the sequence.

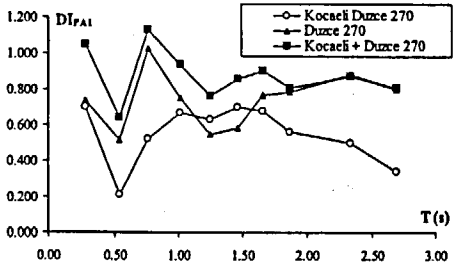

Fig. 6 17/08/99 Kocaeli Duzce E-W and 12/11/99 Duzce E-W records and sequence of the two records. Energy-weighted average DI_{PA1} damage index spectra.

Conclusions

The seismic response of multi-story frame buildings can be usefully studied by means of approximate models, as the discrete shear-type model presented in this study, which provides a simplified approach to prediction of the seismic demand for multi-story frame structures, both for the global response parameters, expressed by energy and displacement quantities, and for the story local response. The model can be used in non-linear time-history analysis or in static pushover procedure, in order to determine global and local energy and inter-story drift demand spectra. While for the global seismic demand, including maximum drift, both analyses lead to reliable results, the study of local effects of the ground shaking on multi-story buildings should be preferably conducted by means of nonlinear dynamic analysis, which can be usefully performed on a simplified equivalent shear-type model. The adoption of this methodology seems necessary when different ground motions are considered due to the large variability of their characteristics (presence of long duration pulses due to directivity effects or basin effects, sequence of the pulses, frequency content, etc.). The simplified method used in this research highlights a great influence of the seismic input energy on the maximum local deformation demand, expressed for the simplified model presented in this paper by means of the inter-story drift. This relationship appears stronger than the analogous one between energy and top displacement. A significant role is assumed by the higher vibration modes of the structure, especially for high ductility levels. The multi-story frame structures, almost insensible to the internal stiffness distribution, but influenced only by the fundamental periods for top displacement response, reveal for inter-story drift a strong dependence on the stiffness pattern when inelastic behavior is considered.

References

1. Uang, C.M. & Bertero, V.V. 1988. Use of energy as a design criterion in earthquake resistant design. *Report no. UCB/EERC-88/18*; Earthquake Engineering Research Center, University of California at Berkeley.
2. Fajfar, P. 2000. A Nonlinear Analysis Method for Performance-Based Seismic Design. *Earthquake Spectra*; 16(3):573-593.
3. Kuramoto, H. & Teshigawara M. 1999. Prediction of Earthquake Response of Buildings Using Equivalent Single-Degree-of-Freedom System. *U.S.-Japan Workshop on Performance-Based Earthquake Engineering Methodology for Reinforced Concrete Building Structures, Maui, Hawaii*, PEER Report 1999/10: 53-67.
4. Rodriguez, M. 1994. A Measure of the Capacity of Earthquake Ground Motions to Damage Structures. *Earthquake Engineering and Structural Dynamics*; 23:627-643.
5. Bertero, R.D. & Bertero V.V. 1992. Tall Reinforced Concrete Buildings: Conceptual Earthquake-Resistant Design Methodology. *Report No. UCB/EERC-92/16*, University of California, Berkeley.
6. Bertero, R.D. & Bertero, V.V. 2002. Performance-based seismic engineering: the need for a reliable conceptual comprehensive approach. *Earthquake Engineering and Structural Dynamics*; 31:627-652.
7. Miranda, E. 1999. Approximate seismic lateral deformation demands in multistory buildings. *ASCE Journal of Structural Engineering*; 125(4):417-425.
8. Iwan, W.D. 1997. Drift spectrum: measure of demand for earthquake ground motions. *ASCE Journal of Structural* Engineering; 123(4):397-404.
9. Decanini, L.D., Mollaioli, F. & Saragoni, R. 2000. Energy and displacement demands imposed by near-source ground motions. *Proceedings of the 12th World Conference on Earthquake Engineering, Auckland, New Zealand*. Paper No. 1136/6/A.
10. Decanini, L., Mollaioli, F. & Mura, A. 2001. Equivalent SDOF systems for the estimation of seismic response of multistory frame structures. *Proceedings of the 3rd International Conference on Earthquake Resistant Engineering Structures, Malaga, Spain*: 101-110.
11. Iwan, W.D., Huang, C.T. & Guyader, A.C. 2000. Important features of the response of inelastic structures to near-field ground motion. *Proceedings of the 12th World Conference on Earthquake Engineering, Auckland, New Zealand*. Paper No. 1740.
12. Kunnath, S.K., Reinhorn, A.M. & Lobo, R.F. 1992. IDARC Version 3.0: A program for the inelastic damage analysis of RC structures. *Technical Report NCEER-92-0022*, National Center for Earthquake Engineering Research, State University of New York, Buffalo NY.
13. Chai, Y.H., Romstad, K.M. & Bird, J.M. 1995. Energy-based linear damage model for high-intensity seismic loading. *ASCE Journal of Structural Engineering*, 121(5):857-864.
14. Bozorgnia, Y. & Bertero, V.V. 2001. Improved shaking and damage parameters for post-earthquake applications. Proceedings, SMIP01 Seminar on Utilization of Strong-Motion Data: 1-22.
15. Chen, Y. & Gong, S. 1986. Double control damage index of structural ductility and dissipated energy during earthquake. *Journal of Building Structure*, pp.35-48.
16. Teran-Gilmore, A. & Avila, E. 2001. Plastic energy as a design parameter. *Proceedings of the 3rd International Conference on Earthquake Resistant Engineering Structures, Malaga, Spain*: 55-64.

NOTES ON GROUND MOTIONS DEFINED BY EUROCODES

Tito Sanò
ANPA, Via Brancati 48, 00144 Roma
sano@anpa.it

ABSTRACT

In this paper the seismic input of the last version of Eurocode 8 (EC8) is briefly described and is compared with the previous version. The paper outlines the strong difference between the ground motion in the last version with literature data valid for high seismic zones. Then it highlights some important features related to soil stability. Numerical analyses, with usual methodologies, show that soft soils type D and some of C and E soils are unstable in an Italian first seismic category under the defined seismic actions. This is consequence of the inelastic shear deformation induced by a strong earthquake. Moreover results show that the ground motions given by the EC8 on soft soils are compatible with that on rigid soil, type A, only in low seismic zones.

1. Introduction

In 1997 four Project Teams have been setting up by CEN/TC250 for conversion of ENV1998 to a final version. The Project Team N. 1 (PT1), charged for modification of seismic actions contained in Part 1 of the code, is supposed to finish his work on June 2002. Modifications on the last version (Draft No 4, 2001) are substantial and refer essentially on a new categorization of soils and on a greater number and new shapes of spectra, specific for each soil type and for two level of seismicity. This report summarizes the main modifications and outlines a few aspects related to the seismic stability of soft soils. As matter of fact, last draft of part 4 of EC8, which regards the foundations, retaining structures and geothecnical aspects, requires that all the analyses should refer to the seismic actions described in Part 1 of the same code. As a consequence the ground motion used as action on the upper structure should be compatible with that in the lower soil. This seams not to be the case of the defined spectra on soft soil in high seismic zones. Spectral shapes, specially those defined on very soft soil, show a great amplification also at high frequencies and are different from both those of the old version of EC8 and those shown in literature (Seed et al., 1946). In order to highlight the evident discrepancy between the new and old shapes and to check the validity of the proposed spectral shapes, a few analyses has been performed with simple computer codes. The case of a first seismic zone in Italy has been taken into consideration also if results can be valid in all seismic countries in the Mediterranean area. Numerical analyses show that the assigned seismic motion on the surface produces high shear deformation in soft soils in a high seismic zone. This means that in many cases the soil itself cannot transmit the assigned motion and the corresponding computed motion on the outcropping rock is not compatible with the spectrum on stiff soil, type A. On the contrary a good compatibility exists in case of low seismicity. This suggests that, in spite of the large number of soil condition and spectra considered by the code, the use of site-specific spectra on soft soil, compatible with that one on rigid soil (subsoil type A), could be explicitly allowed in high seismic zones.

2. Comparison between new and original versions of EC8.

The proposed main changes to EC8 are the following:

1. Seven subsoil classes are described instead of three. The new subsoil classification scheme is introduced as a table (see below) that includes both the stratigraphic descriptions and the ranges of geothecnical parameters. This has been done in order to make the classification as easy as possible and to avoid placing some of this information in an Informative Annex.
The soil classes are characterized not only by shear wave velocity $V_{s,30}$, average value within a dept of 30 m, but also by the blowcount NSPT and the undrained shear strength, cu.
The subclasses S1 and S2 refer to special soft soil, which requires special studies for definition of seismic actions.

TABLE I

Subsoil class	Description of stratigraphic profile	Parameters		
		$V_{s,30}$ (m/s)	N_{SPT} (bl/30cm)	c_u (kPa)
A	Rock or other rock-like geological formation, including at most 5 m of weaker material at the surface	> 800	–	–
B	Deposits of very dense sand, gravel, or very stiff clay, at least several tens of m in thickness, characterised by a gradual increase of mechanical properties with depth	360 – 800	> 50	> 250
C	Deep deposits of dense or medium-dense sand, gravel or stiff clay with thickness from several tens to many hundreds of m	180 – 360	15 - 50	70 - 250
D	Deposits of loose-to-medium cohesionless soil (with or without some soft cohesive layers), or of predominantly soft-to-firm cohesive soil	< 180	< 15	< 70
E	A soil profile consisting of a surface alluvium layer with $V_{s,30}$ values of class C or D and thickness varying between about 5 m and 20 m, underlain by stiffer material with $V_{s,30}$ > 800 m/s			
S_1	Deposits consisting – or containing a layer at least 10 m thick – of soft clays/silts with high plasticity index (PI > 40) and high water content	< 100 indicatively	–	10 - 20
S_2	Deposits of liquefiable soils, of sensitive clays, or any other soil profile not included in classes A –E or S_1			

2. Five response spectra are defined instead of three, one for each classes A to E.
In Fig 1 the spectra of the previous version, while in fig. 2 the new proposal are shown. The curves, shown in fig.1 are also similar to the spectra of the Italian code for isolated structures, issued by the Ministry of Public Works (LL.PP.,1998). Spectra are normalized in respect to the peak ground acceleration in a soil type A, a_g. The definition of the design ground acceleration a_g as the effective peak ground acceleration has been changed to be simply the peak ground acceleration (PGA) and the adjective "effective" has been removed. This change is proposed for two reasons, the first being that there is not universally accepted definition for effective peak acceleration (EPA). The second reason for this change is that by definition the acceleration response spectrum

anchors at the value of PGA for zero period. The shape of spectra is characterized by four parameters.

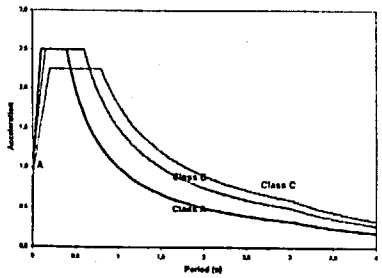

Fig. 1 EC8 spectra in the old version

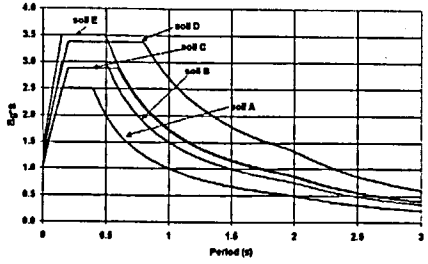

Fig. 2 Proposed spectra

The first is the soil parameter S, which has to be multiplied by a_g to define the zero period acceleration (ZPA). The shapes of spectra change because the width and level of the constant acceleration part (plateau), which always is 2.5 time larger than the ZPA. The plateau is defined by two parameters, the period values Tb and Tc. A forth parameter is the Td period, that defines the period in the spectrum over which the response corresponds to a constant displacement response and it is identified in the figure where the shape changes at high periods. In Table II the over mentioned parameters for high seismic areas are shown.

TABLE II
Spectrum parameters for high seismic areas

Soil classes	S	T_B	T_C	T_D
A	1.0	0.15	0.4	2.0
B	1.2	0.15	0.5	2.0
C	1.15	0.20	0.6	2.0
D	1.35	0.20	0.8	2.0
E	1.4	0.15	0.5	2.0

An importance factor γ_I is introduced which refers to important structures for civil protection or for their social roles, like hospitals. It is related, as in the Italian Guidelines for isolated structures, to the return period, that is the exceedence probability of the seismic event during the structure time life.

3. Type 2 spectra are also defined for low seismic zones.
A second spectral shape (Type 2 Spectrum) is introduced, which has a narrower and higher constant acceleration plateau, for regions only affected by smaller magnitude earthquakes. That will reduce the conservatism that results from using a constant spectral shape. The National Authority must decide which elastic response spectrum, Type 1 or Type 2, to adopt for their national territory or part thereof. The criterion for selecting the Type 1 or Type 2 spectrum is only based on the expected earthquake magnitude, since the spectral shape is comparatively insensitive to distance.
In selecting the appropriate spectrum, consideration should be given to the magnitude of earthquakes that affect the national territory or part thereof. If the largest earthquake that is expected within the national territory has a surface-wave magnitude M_s not greater than 5½, then it is recommended that the Type 2 spectrum should be adopted.

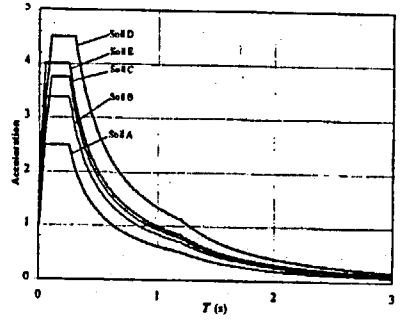

Fig. 3 Type 2 spectra

4. Elastic displacement response spectra are introduced in order to allow the analysis of long period structures.
The elastic displacement response spectrum, $SD_e(T)$, can be obtained by direct transformation of the elastic acceleration spectrum, $S_e(T)$, using the following expression:

$$SD_e(T) = S_e(T)\left[\frac{T}{2\pi}\right]^2$$

This equation shall normally be applied for vibration periods not exceeding 3.0 seconds. For structures with vibration periods greater than 3.0 seconds, a more complete definition of the Type 1 elastic spectrum is presented in an Annex A, derived by the displacement response spectrum.

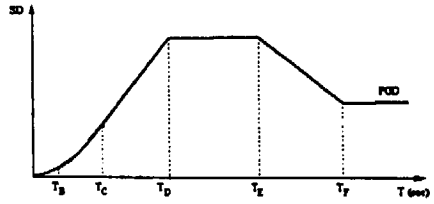

Fig. 4. Elastic displacement response spectrum.

$$T_E \le T \le T_F$$

$$SD_e(T) = a_g.S.T_C.T_D\left[0.4\eta + \left(\frac{T-T_E}{T_F-T_E}\right)(0.025-0.4\eta)\right]$$

$$T \ge T_F$$

$$SD_e(T) = d_g$$

5. New vertical response spectra, one for each response type, are described instead of using modification factors.

6. A new damping correction factor η has been determined:

$$\eta = \sqrt{10/(5+\xi)} \ge 0{,}55$$

instead of $\eta = \sqrt{7/(2+\xi)} \ge 0{,}7$

that is a more conservative formulation, but a greater damping is accepted. The use of elastic displacement spectra in conjunction with a substitute structure to represent the inelastically deformed structure requires equivalent damping values much higher than the 12% of critical permitted in the original EC8. The new, lower limit on η allows response spectra for damping values up to 30% of critical to be constructed

7. The duration of the stationary part of artificial accelerograms is not more depending on the maximum ground acceleration, but it should be not less than10 sec.

8. The kd1 and kd2 coefficient of the exponential decay for long periods of design response spectra are taken equal to those of elastic response spectra. In the previous version they where equal respectively to 2/3 and 5/3, while in the proposed version they are equal to 1 and 2.

It is important to remark that the code is based on a prescriptive approach, with very detailed rules, with no description and explanation of the their rationale. It doesn't accept any alternative definition of the input motion by the designer. It is generally written that a possible variation to the input motion is possible if it is supported by special site classification studies foreseen in the National Annexes.

3. A few notes on ground motion on soft soils in high seismic zones.

The aim is to highlight the difference between spectra on soft soil in the previous and the new version of EC8, particularly on soil type C, which approximately corresponds to the old B, and soil type D,

which corresponds to the old C. In the old version the plateaus were less or equal to that of rigid soil, type A, but larger. In the new version, also if widths are larger in about the same way, the plateaus are higher than that of the rigid soil, type A. This is very different from what it is supposed to be and from what we found in literature on statistics on recorded accelerograms. Seed et al. (1946), who has been referenced in many books, produced results of a statistics on recorded earthquakes and they are shown in diagrams, fig.5.

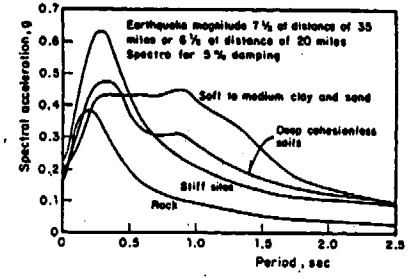

Fig. 5 Mean response spectra on different soil types

The spectra, on fig. 5, are the result of a statistics on Earthquakes magnitude 7.5 at distance of 35 miles or 6.5 at distance of 20 miles. The last case just regards the high seismic zones in Italy. We notice that on soft soils the spectrum become flatter and wider with respect to the rigid one. This corresponds to a physical phenomenon because, in high seismic areas, soil can behave in non-elastic way. High shear deformation causes an increase of the damping, which reduces the response, and a reduction of the stiffness, which can be such that the period range of maximum amplification can drastically change.

4. Stability of soft soils in a first seismic zone of Italy.

In a first seismic zone in Italy, is reasonable to assume a peak ground acceleration equal to 0.35 g. That value has been recorded in the last great earthquakes (Friuli, 1976 and Irpinia, 1980) and has been quoted in the Italian Guidelines for isolated structures (1998). Taking into account the soil parameter S in the new EC8, the zero period acceleration (ZPA) for soft soil is:

Table III

Soil	ZPA (g)
C	0.40
D	0.47
E	0.49

These values should be multiplied by the importance factor, which in Italy can range between 1 and 1.4, so in the last case, the ZPA's are respectively 0.56, 0.66 and 0.69 g. Taking into account such values, analyses were performed with the scope to demonstrate that the ground motions compatible with spectra defined in EC8 Part 1 on soft and very soft soils could cause a soil instability in many high seismic areas in Italy.

At first simple liquefaction analyses then investigations on the level of shear deformation of soft soils were performed.

4.1 Liquefaction analysis.

The procedure of ANNEX B of EC8 part 4 (Nov. 2001) was applied, but results are general and do not depend on a particular used analysis methodology. The main parameters governing the phenomenon, given the appropriate physical characteristics of the soil, like grain size, fine content, saturation, etc, are the maximum acceleration (or ZPA), the magnitude M and the soil characteristic NSPT. The author assumed a Magnitude equal to 6.5, which is similar to that experimented in Italy during the last strong earthquakes of Friuli (1976) and Irpinia (1980), while the other two parameter are given in table I. In fact Eurocode characterizes the soil type D by a NSPT less or equal to 15 for soil D and in the range of 15-50 for soil type C. The simplified method determines the safety factor as the ratio between the resistant cyclic shear stress and that induced by the earthquake. The first depends on physical soil properties and is computed through experimental diagrams, which correlates the cyclic shear stress, known to have caused liquefaction during past earthquakes, to the measured value of NSPT. The second depends on the peak acceleration at the investigated soil depth and on the Magnitude of the event.
The resulting safety factors are less than one in any case for soils type D (ZPA=0.47g) and in many cases for soil type C and E when the NSPT values are near the lower limit of their range or for important structures, $\gamma_I = 1.4$.
In conclusion, from a simplified liquefaction analysis, results that soil type D and large part of soil E and C, in a first Italian seismic category, could be considered exclusion areas for important structures, like hospitals, schools etc and in many cases also for normal buildings. This is important because a lot of villages are built on little alluvial valley, with soft soil type C, D and E, along Apennines Mountains.

4.2 Investigation on soil deformation.

Considering soft soils in an Italian seismic category 1, the shear deformation in the soil, compatible with the ground motion defined by the spectrum shape described in EC8 Part 1 (maximum acceleration= 0.47 g) were computed. The computer code SHAKE (Schnabel et al, 1972), valid for a stratified soil and vertically impinging shear waves on the surface, have been used. The scheme is shown in fig. 6, where the stratified soft soil is shown on the right and the uniform outcropping rock on the left side. The soil non-linearity is accounted for by the use of an equivalent linear analysis using an iterative procedure to obtain, in each iteration, the characteristics of the soil compatible with the effective strain in each layer. The iterations stop when a convergence is obtained on the shear deformation in each layer. The author solved an inverse problem, that is the motion is assigned on the surface of the soft soil, point B in the fig. 6, and results are searched in the lower layers and on the outcropping rock (point A). In order to have generally valid results, I used:

- different shear velocity distributions within 30m depth, with a mean value compatible with the $V_{s,30}$ assigned. I used the upper bound, Vs=180 m/s, for soil type D and the mean value of the assigned $V_{s,30}$ range for soil C and E,
- different artificial and natural accelerograms compatible with the assigned spectrum,
- different realistic soil material laws (G/Go and damping vs shear deformation). They are taken from literature in different sites.(Pergalani et al., 1999; Seed & Idriss, 1970; Seed et al., 1986)

Results are strongly dependent on the shear stiffness distribution on the depth and on the material characteristics: shear modulus and damping versus shear deformation. In case of soil type D, generally the analyses do not converge to a solution because the high level of shear deformation reached in the lower layers. The soil is so deformed that it is not able to transmit the assigned motion on the surface. In few cases the analyses converge to high shear deformations in the lower soil layers and high acceleration on the outcropping rock, point A of fig.6, (greater than 1.0 g). The maximum shear deformation is reached at depth near to 10 m and is greater than 0.2%. Such results do not depend on

the used computer code. A check has been done with other codes, like PHAKE (Sanò and Pugliese, 1991) and SUMDES (Li et al., 1992), and results substantially do not change.

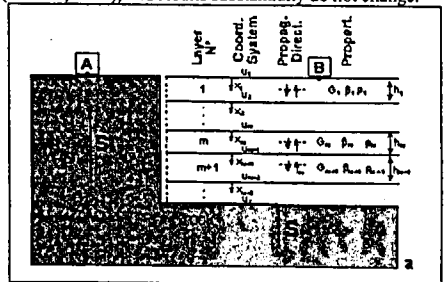

Fig. 6 Scheme of the soil for SHAKE analysis (Schnabel et al. 1972)

In figures 7a and 7b the computed spectra on outcropping rock are shown in two cases: respectively in case of an artificial and a natural accelerogram compatible with the assigned spectrum for a soil type D. The natural accelerogram is that recorded in NS direction at Sturno during the 1980 Irpinia earthquake in Italy. In both cases the levels of the peak acceleration and the spectrum shape on the outcropping rock are different from those of the reference spectrum for soil type A.

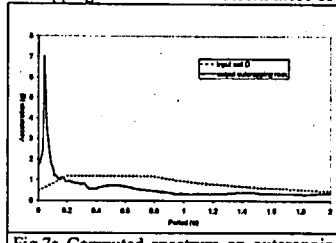

Fig.7a Computed spectrum on outcropping rock compared with that assigned on soil D, case of artificial accelerogram.

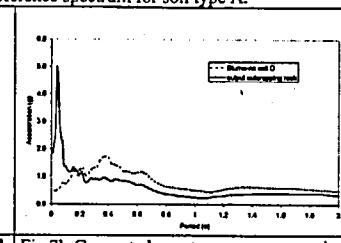

Fig.7b Computed spectrum on outcropping rock compared with that assigned on soil D, case of natural accelerogram.

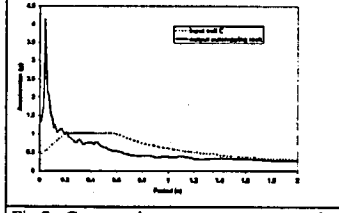

Fig.7c Computed spectrum on outcropping rock compared with that assigned on soil C, case of artificial accelerogram.

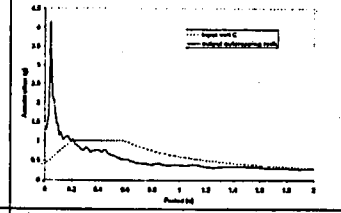

Fig7d Computed spectrum on outcropping rock compared with that assigned on soil C, case of natural accelerogram.

This is a demonstration that spectra of EC8 are not corresponding to the same event at least for high seismic zones.

Similar conclusions hold also for soil type E and C, mainly when their material characteristics, i.e $V_{s,30}$, are at the lower bound of their range of definition (Table I) or in case of important structures, γ_I=1.4 or unfavourable topographic conditions. Results are shown in figures 7c and 7d in case of an input on soil type C (dotted lines) respectively for an artificial and a natural (Sturno-NS) accelerogram and γ_I=1.0.

Checks were made through further analyses. A spectrum on rigid soil type A was assumed as characteristic ground motion of the seismic event, which code want to design for. Then a local amplification analysis was performed facing a direct problem. The ground motion on point A of fig.6 was assigned and the motion on point B on soft soil, type D, was computed, considering a first seismic category in Italy. Finally a comparison of the computed spectrum and that of EC8 on the same soil was made. A few results are shown in fig. 8. The code spectra, for soils type A (a_g=0.35g) and D (a_g=0.35*1.35= 0.472g) are shown as continuous lines while the computed motions on the surface of soil type D, respectively for natural and artificial accelerograms, are shown as dotted lines. The natural Brienza-NS accelerogram refers to that recorded during Irpinia (1980) earthquake.

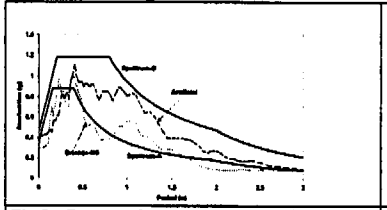

Fig.8 Computed spectrum on soil type D compared with that assigned on soil D and A. Case of a first category seismic zone

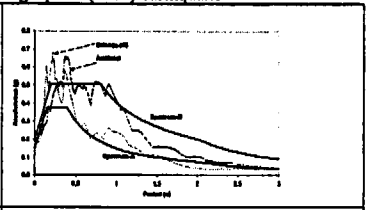

Fig.9 Computed spectrum on soil type D compared with that assigned on soil D and A. Case of a 3rd category seismic zone.

It is important to note that:

- The motion on the surface of soil type D, compared with the A type one, is richer of low frequencies because of the effect of the non-linearity induced by the high intensity of the seismic input. As mater of fact the output spectra are wider in the long period range, but they became not higher than the input one, contrarily to what proposed by the new EC8 code (spectrum D on the figure).
- High frequencies are drastically filtered because the soft soil. It become softer because the reduction of the G modulus caused by the high shear deformation induced by the earthquake. Such filtering explains why in the inverse problem (figures 7) we get high peaks in the high frequency range in the motion on rigid soil A.

The same amplification analysis was performed in a lesser seismic zone, considering an Italian third category and peak ground acceleration equal to 0.15g. Results, shown in fig. 9, are completely different from previous ones. The computed spectra on point B of fig 6, soil type D, are sufficiently comparable to those proposed by the EC8 code. That is because the EC8 spectra on soft soil are suitable for less seismic country than Italy. For it and other high seismic country in the South Europe, the use of site-specific spectra on soft soil, compatible with that one on rigid soil (subsoil type A), could be explicitly allowed.

5. Conclusions:

The seismic ground motions of the last version of Eurocode 8 have been briefly described and their main features have been compared with the previous version. It has been outlined the strong difference between the ground motion on soft soils, defined in the last version, with literature data valid for high

seismic zones. Then some important features have been highlighted in relation to soil stability. Numerical analyses, with usual methodologies, shown that:

- Simplified analyses of soils class D and E, if potentially liquefiable, show that they are likely to liquefy in a first seismic zone in Italy. This is important because a lot of villages are built on little alluvial valley, with soil type C,D and E, along Apennines Mountains.
- The shear deformations of soils type D, E and part of soil C (in case of important structures and/or unfavourable topographic conditions), under input ground motion described by EC8 Part 1, are such that the soil stability cannot be guaranteed in a first seismic zone in Italy.
- Numerical analyses shown that the soil class D cannot transmit waves contained in the ground motion defined by the EC8 in a high seismic area. As a proof, performing a local amplification analysis using as input the ground motion on outcropping rock, compatible with the rigid spectrum (subsoil type A) and peak ground acceleration = 0.35 g, in no case you can find a ground motion, at the surface of the soft soil, compatible with the spectrum of subsoil D and ZPA=0.47g. A compatible motion can be found only in lower seismic areas, in which the soil material behaves in elastic or quasi elastic way. So the spectra described in EC8 Part 1, for subsoil type C, E and D are compatible with low seismic countries like those on the North of Europe, but not in Italy especially in a first seismic zone.
- The use of site-specific spectra on soft soil, compatible with that one on rigid soil (subsoil type A), could be explicitly allowed in high seismic zones.

6. Bibliography

Eurocode 8:Design of structures for earthquake resistance, Part 1: General rules, seismic actions and rules for buildings, Doc CEN/TC250/SC8/N306, Draft No 4, December 2001.

Eurocode 8: Design of structures for earthquake resistance , Part. 5: Foundations, retaining structures and geothecnical aspects, Doc CEN/TC250/SC8/N305, Draft No 4, November 2001.

Li.X.S., Wang L.Z., Shen C.K.,(1992), SUMDES, A Nonlinear Procedure for Response Analysis of Horizontally-Layered Sites Subjected to Multi-Directional Earthquake loading, University of California, Dept of Civil Engineering, Davis.

Linee guida per la progettazione, esecuzione e collaudo di strutture isolate dal siama, Presidenza del Consiglio Superiore dei LL.PP.- Servizio Tecnico Centrale, 1998

Pergalani F., Romeo R., Luzi L., Petrini V., Pugliese, A. & Sanò, T. (1999). Seismic microzoning of the area struck by Umbria-Marche (central Italy) Ms 5.9 earthquake of the 26 September 1997. Soil Dynamic and Earthquake Engineering, Elsevier Science, 18, pp. 279-296

Schnabel P.B., Lysmer J. & Seed H.B. (1972). SHAKE: A computer program for earthquake response analysis of horizontally layered sites. Report No. UCB/EERC-72/12, Earthquake Engineering Research Center, University of California, Berkeley, December, pp. 102

Sanò T., Pugliese A.,(1991), PSHAKE, Analisi probabilistica della propagazione delle onde sismiche, ENEA, RT/DISP/91/03

Seed, H.B. & Idriss, I.M. (1970). Soil moduli and damping factors for dynamic response analysis. Report No. UCB/EERC- 70/10, Earthquake Engineering Research Center, University of California, Berkeley, December, pp. 48

Seed, H.B., Wong, R.T., Idriss, I.M. & Tokimatsu, K. (1986). Moduli and damping factors for dynamic analyses of cohesionless soils. Journal of the Geotechnical Engineering Division, ASCE, Vol. 112, No. GT11, November, pp. 1016-1032.

Seed, H.B., Ugas, H. and Lysmer, J.,(1946), 'Site-Dependent Spectra for Earthquake-Resistant Design', Bull. Seism. Soc. Am., 66, 221-243.

PROOF OF SEISMIC DESIGN CODE
-ROLE OF DAMAGE REPORTS INCLUDING SHAKING TABLE TESTS

Heki Shibata
National Research Institute for Earth Science and Disaster Prevention
1-5-203 Sakurajosui 4 Setagaya, Tokyo 156-0045, JAPAN
Tel. & Fax. +81/3-3303-2591

Memo for Presentation

I have prepared two third of the draft of the manuscript for the proceedings under the title above. However, as the newspapers have been reporting, the degrading of nuclear power plants is the great issue to the related structural engineers in Japan last several weeks. Even recent mornings, September 24 and 26, the newspapers report new facts. Under such a situation, I should rewrite my draft, because the new maintenance criteria has been discussed, and the concept, which I try to discuss, is deeply related to this, that is, the design guideline should be prepared in relation to the maintenance criteria.

The seismic design of mechanical and electrical components should be made as a safety system as well as piping systems. The development of disasters is usually discussed along its scenario. Role of field surveys on damage status and shaking table tests is one of the significant, key subjects in the Workshop, and I try to discuss how to prepare the scenario and what issues are existing in my presentation.

For the meaning of "Scenario", I presented on the paper "Assumption and Analysis on Catastrophic Event by Setting Scenario under Various Uncertainties" in a seminar in the mid-September. The point, which I have been considering for this workshop, was included in the papers of the Seminar in last September. Therefore, temporary, I attach them in the following part of this article.

The figure attached is the key relation of the role of mechanical shaking table, for example, 1,200 ton 3-D shaking table, *E-Defense* in NIED, as well as other large tables like Tadotsu 1,000 ton 2-D shaking table, NUPEC, to establish the seismic safety of nuclear and other critical facilities.

In the papers above, I concluded as follows: Scenario is necessary to make the judgment under existing "uncertainty", and as a result it is "subjective". For planning of tests on the table, we start it based on knowledge of failures which obtained through field surveys. In 1940 ~ 50's, the theory and technique on "Planning of Experiments" had been developed, and it was based on Stochastics, like Monte Carlo Method in the papers above. The menu for testing based on stochastic approach has the same difficulty as Monte Carlo approach. Therefore, a test on a shaking table is usually one specimen test, and how to cover the fluction of test results, I talked at one of the previous workshop[1]. Even though, the one specimen test is taken in usual shaking tests for NPP, and the project which started in this year in NUPEC is the initial project in this field.

To fix a plan of usual one specimen test, we need to assume a kind of the scenario obtained through the results of field survey, and it is subjective. Therefore, in this process, there is a possibility to be biased as well as in the process of data analysis. The paper, which I have been preparing, is discussing the role of scenario, and now we are facing on a certain possibility of such "bias". Newly rewritten papers titled "Proof of Seismic Design Code", and it may be handed at the Workshop.

Reference

[1] SHIBATA, H. and ASADA, H. [1999], Generation of Fragility Curve of Components by Using Shaking Table, *Proc. of OECD/NEA Workshop*, NEA/CSNI/R(99)28, P.299 ~ 326

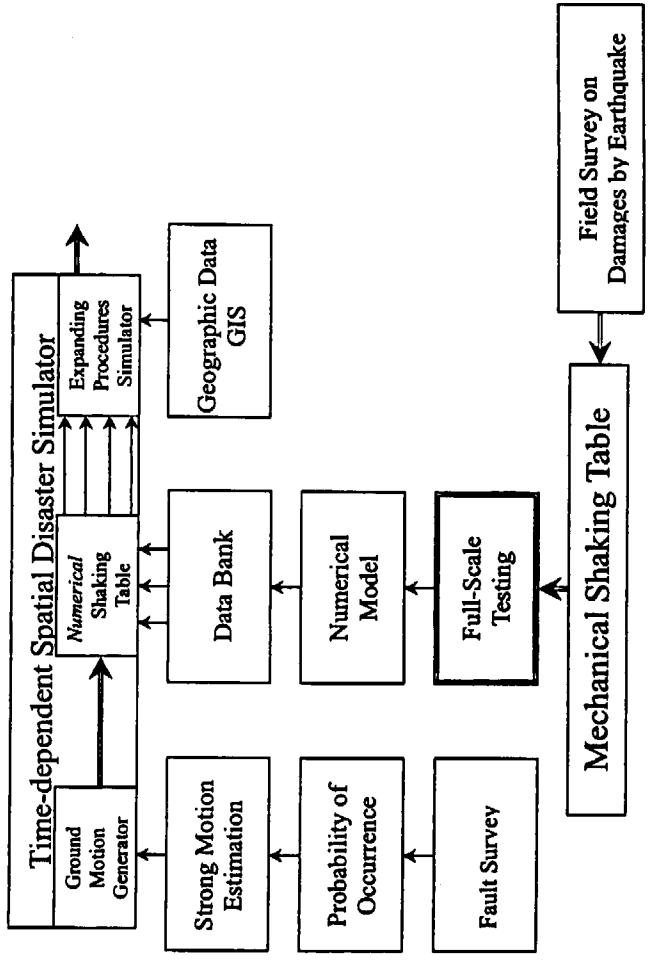

Fig.1 Fundamental Relation of Mechanical Shaking Table to Numerical Model, and Field Survey
Original: Prepared in Okada Rep, 1997

ASSUMPTION AND ANALYSIS ON CATASTROPHIC EVENT BY SETTING SCENARIO UNDER VARIOUS UNCERTAINTIES

Heki Shibata
National Research Institute for Earth Science and Disaster Prevention
1-5-203 Sakurajosui 4 Setagaya, Tokyo 156-0045, JAPAN
Tel. & Fax. +81/3-3303-2591

Abstract

This paper deals with a concept of the worst scenario as an initial condition and boundary conditions to simulate how an event is going to develop mainly related to the safety problem. Some twenty years ago, the worst scenario was decided very subjectively under the limited CPU time of an available computer. The author wants to discuss how to get the worst scenario under uncertainties logically and related matters. Comparison of Fault Tree and Event Tree methods as well as Monte Carlo method has been discussed. And the concept of craziness, that is, fuzziness with fluctuation, is discussed also.

Keywords

scenario, simulation, event, safety, Monte Carlo method, subjective approach, fuzzy

Introduction

It is rather difficult how to assume a scenario of accidental events for the safety analysis. The author has been working for the safety on critical facilities under destructive seismic conditions mainly. And this job has been expanded into disaster preventions of various kind of accidental events induced by a natural phenomenon as well as a man-induced one. Those events are under various degrees of uncertainties. One extreme case is followed surely a certain stochastic distribution, and the other extreme case is, of course, definite one, if we assume that "uncertainty" would be a random process. However, we can obtain a certain scenario from the experienced case of an accidental event in the real world, such as a man-induced air crash to wide urban failures induced by particular ground motions of a strong earthquake like Hyogoken-Nanbu earthquake-1995, so-called Kobe earthquake and so on.

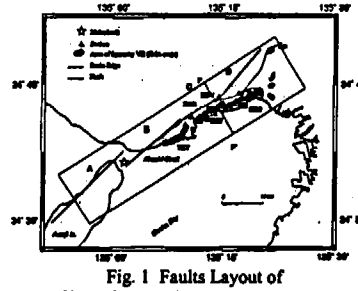

Fig. 1 Faults Layout of
Hyogoken Nanbu Earthquake-1995

It is easy to explain on the scenario of an air traffic accident, but it is rather difficult to explain the scenario of a strong earthquake. If we discuss on a particularity of ground motions in this sense, it comes from the mechanism of an earthquake, that is, a fracture of fault surface, whose size is 20 km

depth x 100 km long or more. How to brake or slip, approximately 1 m to 10 m length, on a fault surface is a scenario in this case. In Fig. 1, Faults for Hyogoken Nanbu, Kobe earthquake – 1995, and also in Fig. 2, its process of failure are shown, and the scenario means this process. The wave form of ground motions is completely depending on this scenario, which is also described by a pattern of sticked areas, so-called "asperity", on a fault surface and its slipping process. Now, we can analyze the pattern of the asperity of the event, which has been occurred. If the fault will move again in a future, will the asperity, that is, the scenario, be the same as before? This question has not been solved yet. But seismologists estimate that it would be almost similar to previous ones, even it might be fluctuated. The author doesn't discuss this subject in detail, but this problem brought the subject in this paper to his mind with it.

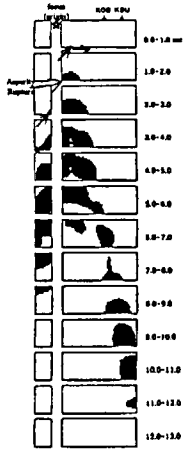

Fig. 2 Asperity Rupture Transmission by Time

Another type of a simulation on an earthquake disaster may be mentioned. We, in Japan, have worked for the simulation how the big fire, induced by a destructive earthquake, will be spread in the urban area like Tokyo. We started this type of the study in late 1960's[1]. For this simulation, the scenario, such as, season of the year, time of the day, wind direction and velocity, is very significant to the result, usually we express it as loss-of-lives. In 1923 earthquakes in Tokyo area, 140,000 lives were lost by such spread fires.

On the other hand, in nuclear engineering we assess the probabilistic risk or safety with fault-tree and event-tree by starting from all probable internal events including man induced ones. In this case, scenarios of all probable events are covered for the assessment, and concluded as one valve, the probability of occurrence of the core damage, CDF. And the expected risk of deaths induced by the leakage of radioactive materials by this core damage is calculated with a scenario of a weather condition and others as described in the latter part of this paper.

The author will try to discuss such various procedures for setting up the "scenario" for the simulation on disasters, both a man-induced event or a natural event more logically than the subjective approach.

Single Scenario for Simulation

Recently, we have more chances to simulate how to develop catastrophic events with various assumptions for estimating and suppressing development of such events. In the assumption, there are many variables as the initial condition and boundary conditions. Some years ago, the CPU time for such a simulation was very limited. Therefore, these initial condition and boundary conditions for the simulation were selected only one set of conditions as already mentioned. We often said that we assume "the worst case". What is the worst case? These variables usually have a stochastic nature, then it is difficult to say that this particular set of variables is the worst for this simulation. If we have some examples in the history, we can find the worst one in the historical document. But, it would be doubtful whether or not this set of variables is the worst one in the stochastic sense. The author has been talking it without actual examples in this article. However, in his mind, the development of spreaded big fires in urban area induced by a destructive earthquake came out at first. Then, the development of crack failure of active earthquake fault came out. The first one might be in the area of disaster prevention engineering, and the second one is in the seismology for deciding input ground motions for the design of critical facilities. As far as spreading the fire, the wind velocity and the humidity are the key parameters. For predicting the ground motions, the length and the amount of its slip or stress drop seem to be key items, but they usually give the total energy of the ground motions, and the detailed time histories are rather depending on its asperity and the initiating point of slipping of the fault, and it is clear that such parameters are very complicated and specialized in each subject.

For simulating a series of time history of events, we need to fix key parameters or variables as initial and boundary conditions. To explain this, we assume that the number of variables is two for the simplicity, and the mapping of key variables is shown in Fig. 3(a). As the result of the simulation, the key variables, for the input to simulate a certain model, transform to the consequent map as shown in Fig. 3(b). The simulation in early period was started from only one point, which was considered as "the worst case", the point "u". We didn't know the figure of over-all results like Fig. 3(b), and only we got one point as "W" in Fig. 3(b), therefore we couldn't judged whether or not that this was actually the worst point. If we can figure out the total scope, "W_{95}" might be said the worst under the condition as discussed later, but the one-point simulation couldn't find such a map. This is the simulation for disaster prevention or other works in early 1980's. It was very subjective to select the condition "u", and actually this "u" was selected with subjective ambiguity rather than uncertainty.

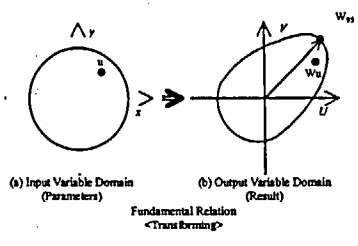

Fig. 3 Fundamental Relation of Parameters and Results

More Chance for Simulations

If the computer runs rapidly, we repeat such simulations for the set of parameters.

The large circle in Fig. 3(a) is defined as 95% confidence of range of parameters in a certain distribution for a simulation, and the result transformed from these parameters is the egg-like curve in Fig. 3(b). A vector from the origin to the curve is considered to be the result, and the vector W_{95} is the worst one under the restriction of parameters in 95% confidence. As an application of Monte Carlo method, we can consider several ways. The first one is to select a set of parameters according to some distribution within a circle of 95% confidence, as point such ×, ●, +, Δ, ∇ and so on in Fig. 4. Another one is to select a set of parameters as uniform distribution like the box-shape distribution between vertical tangents to 95% confidence circle, A and B, and also

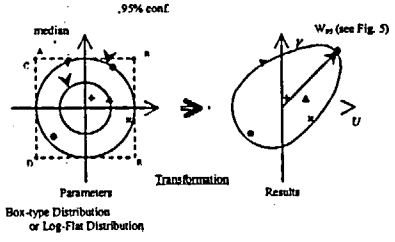

Fig. 4 Monte Carlo Approach for Simulation

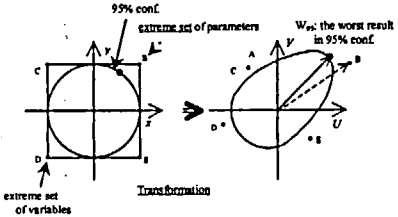

Fig. 5 The Worst Scenario by Extreme Parameter Set

horizontal tangents, C and D in Fig. 5.

More sophisticated example will be discussed on a typical example of stochastic problem. One of the results done by Homma, JAERI was presented in a recent workshop [2]. This simulation was done for "individual risk of radiation fatality at a distance" induced by CDF of a nuclear power plant. And this computation was done for 128 sets of 23 parameters as mostly uniform box-shape distribution by uncertainty which they have. However another group of a boundary condition "weather sequence" is significant for such an analysis. He divided into two sections for his analysis. The author tries to figure out it based on his presentation as Fig. 6. A key issue here, even if the distribution of the sampled set for a scenario meet with the over-all distribution of "weather sequence", the result "individual risk of radiation fatality at a distance" seems not to follow to a certain distribution as shown in Fig. 7. Especially a result of 99% of confidence case extremely deviates, and not smooth as a cumulative curve as we can observe figure on the left hand in Fig. 7. If we would make those distributions much clear, and employ to select sets of parameters, the result might be different. The author will discuss it.

It is possible that such a phenomena comes from the distortion of a "transformation" in Fig. 3. The most of simulation in social science or disaster prevention has this distortion. However, some other reasons might be considered. One is as follows; even the distortion of transforming would give the distortion of the distribution, lack of number of simulation brought such an irregular distribution in Monte Carlo process as observed in Fig. 7. Also, the classifying "weather sequences", and random sampling from each type may curve this distortion on the distribution, because this process of setting parameters works similar to subjective judgment, even all steps were done logically, except the definition of crasters, Type 1 to Type (m) in Fig. 6. It is really an interesting subject how the real distribution is.

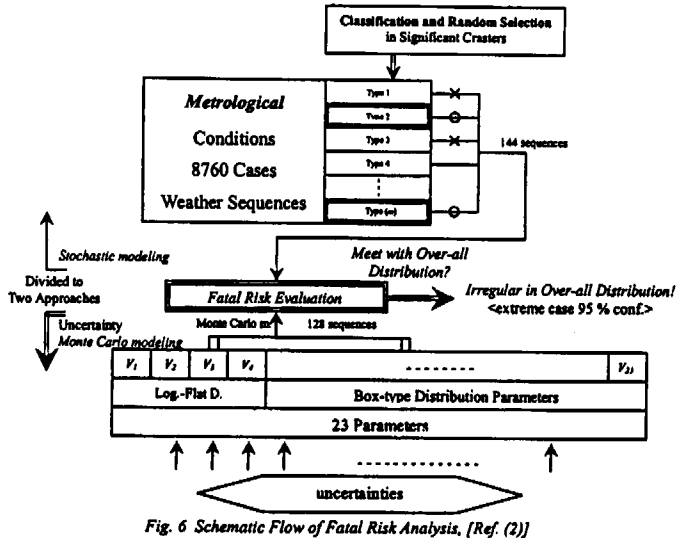

Fig. 6 Schematic Flow of Fatal Risk Analysis, [Ref. (2)]

Prepared by Shibata, based on Homma's Presentation and *Private Communication* [Ref. (2A)]

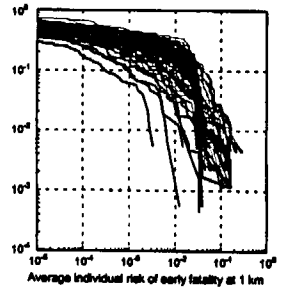

Fig. 7(a) Fatal Risk vs Probability [Ref. (2)]

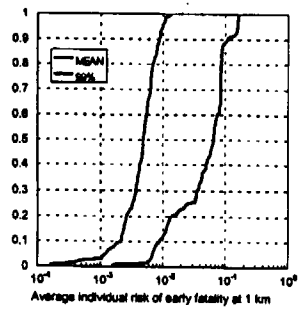

Fig. 7(b) Fatal Risk Cumulative Distribution [Ref. (2)]

As an initial condition and boundary conditions the extreme values of parameters, that is, the corner points A, B, C and D are employed for the simulation. For these results, there is no guarantee to be the worst. Sets should be selected under rules of distribution of each parameter. In this case, required number of "scenario" is numerous based on the concept of Monte Carlo method. If we decide the notations on the nature of "uncertainty" as follows:

R: theoretical randomness.
A: ambiguity origin uncertainty.
U: uncertainty originated from lack of knowledge.
F: fuzzy judgment.
C: crazziness' which will be discussed in the following chapter.

Then, in the transform from Fig. 3(a) to Fig. 3(b), it is theoretically only based on a defined function, therefore deterministic or theoretically random: R. In principle, other uncertainties are in the process of defining initial conditions in Fig. 3(a), however, F and C may be included in the process of transforming to Fig. 3(b).

FT-type analysis

In this Chapter, the author discusses on Fault Tree-type approach. Such a scenario as the initial and boundary conditions mentioned above is only one point which would be possible, and selected as the worst, or a group based on randomly to meet the rule of Monte Carlo approach. The case quoted above, 23 key parameters are contributing to the result, and the simulation was done only in 128 cases. If we select the values of those parameters in two extreme cases as A & B or C & D in Fig. 4, the total number of combinations is 2^{23}, that is approximately 8 x 10^6 cases. The number of 128 cases is only 10^{-4} of that in all combinations of only extreme cases.

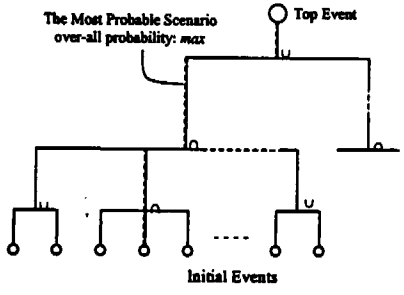

Fig. 8 Fault Tree-type Assessment

To make clear the total scope of the structure of results, we need much number of simulations. To overcome such a difficulty, we can introduce Fault Tree type method as shown in Fig. 8. We assume one top event such as a catastrophic result initiated from initial events at the bottom. If we can find the most probable event with associated other initial (bottom) events, this is the most significant event. Therefore, it is rather easy to find the scenario by a modification of an ordinary Fault Tree analysis method, however, to find the worst one, we need calculate valuesm such as loss, probability or others of each tree, and it is not made in general. Also, it should be recognized, the number of sheets to express a CDF: core damage frequency of a nuclear reactor, may be 5000 sheets, which was drawn in SSMRP, by Lawrence Livermore National Laboratory, in 1980's, it was shown in one sheet drawings, even for the explanation.

The author believes that it is a simple way to establish the complete scenario. Uncertainties, which belong to all roots, may be included the coefficients on each tree. However, he has never implemented this.

Some Examples of FT and ET

Event Tree analysis was used in SSMRP with the result of FT analysis to complete to estimate CDF of a nuclear reactor. Starting from one particular event, such as a loss of external power supply induced by a destructive earthquake, and each branch of a tree will reach to the core melt down or not, that is, fail or success of cooling core. In this example in Fig. 9, the final state is a two value like "success" or "fail" as mentioned above. We can define the probability on each branch, and in final states the most fatal one is only one case with a certain probability of occurrence. And this tree is the scenario for the story. However, during the route to the other end states, some damage would be expected. For example, as an initial event we assume a destructive earthquake, and the second event failure of houses against controlling a quality of residential building by a code, if success, 90% of houses remain to be without collapse, and if fail, 10% of houses remain without collapses. Next step is to start fire, and even a healthy house may start fire in 0.5%, and a collapsed house may start fire in 3 %. Then 0.45% of healthy houses start fire, and 2.7% of collapsed houses start fire. Thus story develops into a big urban fire. In this case, the final result can be expressed by an expected value, or the vector of estimated damage value and the probability of occurrence. In this case, we can define the worst scenario as the maximum expected damage rate as a "value", or the subjected judgment of the vector: probability of occurrence and estimated damage rate as a "value". In general as noted in Fig. 9, the route to the maximum damage value, loss rate is the worst scenario.

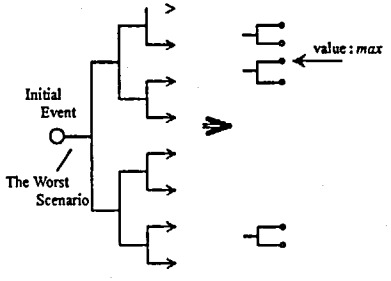

Fig. 9 Event Tree-type Assessment

By the Event Tree analysis, we can find the scenario as an expected value or the maximum loss value as you like, but it will be done with low uncertainty, because uncertainty exists only in probability of branching and estimated value or cost of loss of each success or fail.

Some Examples of FT and ET

In previous two chapters, the author referred to some examples. Here, he tries to discuss on daily events on each approach.

A story on currie mail trouble

The following affair was happened in my, the author's, office:

i) CD-Rom of an annual report to reach to my former office.
ii) My young friend in the office sends the fax to me where shall be remailed it as reaching to me.
iii) I sent the reply to ask to send it to my new office by currie, DHL-type mail by fax on Sunday.
iv) He sent a bottle of whisky as his gift to my home for his appreciation to my gift to congratulate of his marriage almost same time.
v) A package was delivered to my home from my previous office, but all of us were absent in my house at that time.
vi) I asked to resent it to my new office to a currie business office, and they promised to send it tomorrow to my office.
vii) Two days after, it hadn't reached to my office yet.
viii) I phoned to the office of currie near by my office to ask it, and they phoned to the office near by my home, and they found that it was broken. I asked them why CD-Rom was broken, and they said that it was a bottle of whisky and they wanted to replace a new bottle as soon as possible.
ix) The author thought that it was CD-Rom, but it was a bottle of whisky.

The reasons were in the following two points.

- In my previous office, the fax machine was switched off during a weekend, but its responder worked as normally without any message like "Not Received" to the sender. The author, I, forgot it, and believed that my message was reached to the young friend.
- And, when he sent whisky to me, he has not noticed it to me.

Such a type of series of errors can be expressed by FT as certain initial events, and can be evaluated on the probability of occurrence. If we evaluate it by the product of probabilities of each step as mentioned in i) ~ ix) without fault tree approach, the value might be very small like 10^{-10} or so under the assumption that the probability of an error would be 10^{-2}. The typical case of this can be found in TMI Nuclear Power Plant Accident. There were human errors in the process to reach to the final state, core melt down, but some of them were induced by previous steps, therefore, if we would take the number of erroneous steps through the process, the probability of occurrence of this accident might be very, very low. But actually, effective independent essential errors are estimated only 2 steps by the detailed analysis compared to 11 errors which were reported, as that of the former example consist of only two steps based on the author's consideration[3], as the young friend didn't notify on his gift and my belief on his receiving my fax. If we assess such an event, FT assessment is effective to do so, starting from initial events to find the scenario, which are experienced. Of course, after we experience the affair, we can build the ET by knowing the scenario, but FT is more effective to analyses such an event in advance.

Recent accidents of young ladies in Japan

Let's move to another subject. This summer, many young ladies love a mule with high-heels. As a result, they had many chances to injure her ankles. We can analyze this process by simple fore balance problem as Fig. 11. In the case of ordinary shoes with high-heels, they have shells or straps, to fix the shoes and here heels. In the case of mules, no fixing device to fix both legs and mules relation.

Therefore, the safety contact point of a mules in narrower than ordinary shoes. Also more unstable on irregularity of floor flatness, or side force from her legs. For such disturbances, mules are easier to overturn and to have a trouble on her ankles. This process may be analyzed by ET.

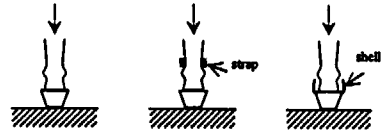

Fig. 10 Mules and Shoes for Young Ladies

Starting from the event to wear shoes with high-heels or mules with high-heels, ETs to reach to have broken ankles both for shoes or mule are almost same, but their critical limit may be different because of the difference of stable zone of loading. This might bring the difference of the worst scenario for each case, even ETs for both cases are not much difference except that of the values of transit probability. Therefore, easy to find the worst scenario by calculating the over-all transit probability.

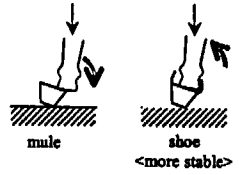

Fig. 11 Dynamics to Injure her Ankle

Fuzziness and Craziness

As far as a judging process, we make our judgment in fuzzy sense sometimes. These fuzzy criteria may be fluctuated time by time. To warm up the room, our feeling would change day by day, and this range of fluctuation also depend on his condition. The author described this in one of his papers [4] approximately 5 years ago. In some sense, we may call this fluctuation as "craziness". In the previous chapter , the author mentioned the final result could be evaluated by a vector like (value, probability). Elements of the vector may be expanded to more such as (value, probability, fuzziness, craziness). Even an example of the previous chapter, the behavior of a lady, way of stepping in her walk is fuzzy and it's fluctuated. Therefore, the occurrence of an accident would be depended to her such a variable behavior associated with conditions of floor, which are randomly distributed. However, in average, an ordinary shoe is safer than mule.

As discussed above, "fuzzy judgment" or "fuzzy selection" may bring uncertainty, but more uncertainty would come from their "craziness", that is, daily fluctuation of them much more. The author tried to measure the individual craziness for the watching and recovery operation in his paper mentioned above, and he found that is quite depended on operator's characteristics person by person. Thus, it is rather difficult to establish the worst scenario definitely, and its uncertainty shall be functions of "fuzziness" and/or "craziness", that means that the worst scenario of even an individuals may not be established, if his craziness is large.

Concluding Remarks

It is very difficult to establish the worst scenario of a particular event. However, in early 1980's, only one scenario was chosen by the subjective way to estimate a future disaster.

The author suggests how to evaluate events by simulation, and the most simple access is the application of Monte Carlo method, however, it is necessary to evaluate on numerous sets of parameters, if the number of parameters, or conditions is not small because of their uncertainty.

Except using Monte Carlo method the author suggests that it is possible to use FT method to evaluate the over-all probability and may be its distribution starting from various initial, bottom, events to its final, top, event without a particular story as the worst scenario. However, if we need the worst scenario for our analysis, we may get it by ET method easier than FT one, because we can obtain of the probabilistic distribution of the final events and its limited confidence.

Each transition of events has a transient probability, but also some parameters coming from its fuzziness, and sometimes the fluctuation of fuzzy judgment or selection, which the author call it as "craziness" in this paper.

Acknowledgement

The author has been thinking on "scenario" since 1960's. Recently he had two chances to develop his thought. One was to estimated the ground motions for "Design Basis Earthquake" for a critical facility near to an active fault. Another chance is writing manuscripts as an Essay on the disaster for a small magazine.

He expresses his gratitude to Professor Irikura, Kyoto University who has been discussing on the estimation of ground motions.

And to Dr. Homma, Japan Atomic Energy Research Institute for his presentation and discussion on OSCAAR as well as Dr. Muramatsu, as the head of their group, which the author has been working as an advisor for some years.

The author doesn't have any intention to implement his concepts. He welcomes for you to use them to any applications.

Reference

[1] Reports from Disaster Prevention Council of Metropolitan Tokyo, 1970 ~ 1990.
[2] HOMMA, T. and others: Uncertainty and Sensitivity Analysis using an Accidental Consequence Assessment Code OSCAAR, Proc. of PSAM6, Puerto Rico, (July 2002).
[2A] Private Communication Related to Ref. (2).
[3] SHIBATA, H.: V-A, Reliability Assessment on Critical Facilities and its Key Issues, Journal of Japan Society of Steel Construction, Vol.17, No.179 (Feb./Mar., 1981) p.98~100 (in Japanese).
[4] SHIBATA, H. and IWASHITA, T.: Evaluation on Ambiguity of Human Factor by Fluctuation of Membership Function, Proc. of FWZZ/IFES'95, IEEE (Mar. 1995)

DESIGN INPUT BASED ON GROUND MOTION ANALYSIS FOR THE TAIWAN HIGH SPEED RAIL PROJECT.

Helmut Wenzel
VCE Vienna Consulting Engineers, Vienna

. Abstract

The design of structures in seismic regions requires careful consideration of near fault effects. This contribution highlights the facts and figures used to make decisions about the design approach to be used for railway bridges crossing and active fault.

The Tuntzuchiao Fault has been classified as a minor active, secondary, right – oblige, strike slip fault. The location of the fault at bedrock is not known sufficiently and its orientation is close to 45° to the longitudinal axis of the bridge. The expression of the fault at the surface is likely to be well defined due to existing site conditions. The fault movement should be expressed over a relatively narrow width. The fault is expected to be able to generate earthquakes with a magnitude of M = 6,5. The expected horizontal fault displacement is a right lateral slip of 150cm. This can be resolved into 106cm along the bridge and 106cm transverse to the bridge axis. The expected vertical fault displacement is a vertical dip of 50cm.

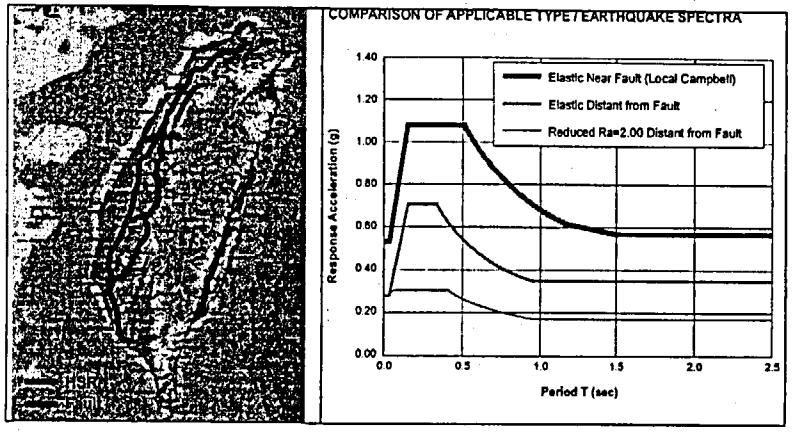

The expected performance objectives are as follows:

- Safeguard against major failures and loss of life under type 1 (severe) earthquakes
- Ensure adequate service performance under type 2 (moderate) earthquakes

When subjected to a type 1 earthquake it is acceptable for the structure to response in the inelastic range, provided the activity demand does not exceed the available ductility. All damage is to be repairable. When subject to a type 2 earthquake no yielding of reinforcement or structural steel is permitted and the displacement of the deck shall be such that trains can break safely to a stop from their full design speed of 350 km/h.

The earthquake characteristics are as follows:

Type 1 earthquake with a 950 year return period, vertical shaking 2/3 of the horizontal shaking.

Type 2 earthquake where the ground acceleration is 1/3 of the type 1 earthquake.

The ground type are layers of conglomerates over 30m thick on mudstone. The site is classified as an ordinary site. The base spectra are provided in the following figures.

1. Introduction

About 15km north of Taichung, the THSR track is crossing the Tuntzuchiao fault. Therefore, a special bridge design has to be developed for the 4 times 30m concrete box girder spans and the steel bridge with 55m span, taking the specific site conditions into consideration. This report is made to enable the development of a specific bridge design for this area. It addresses the relevant items, provides alternative solutions and issues recommendation for the implementation. It is based on the authors experience with seismogene phenomena registered at the Earthquakes of:

- Chi-Chi Earthquake, Taiwan of September 1999
- Kocaeli and Düzge Earthquake, Turkey of August and November 1999
- Kobe Earthquake, Japan of January 1995
- Northridge Earthquake, California of 1994

2. Relevant Fault Characteristic

From the 1999 Earthquakes in Taiwan and Turkey the actual performance of faults at the surface can be studied. For the HSR infrastructure this performance is relevant. Particular the example of the Bolu Viaduct in Turkey, where one of the piers was exactly located on the fault, shows which action has to be expected. In this case the foundation was distorted approximately 15 degrees together with a horizontal and vertical displacement. Never the less no breaking of the pile cap nor a shear failure of any of the piles has been recorded.

The following photos provide information on fault ruptures as experienced in Taiwan and Turkey in 1999. It is clearly visible that the fault rupture is:

- Two dimensional (vertical and horizontal movement)
- Comparatively straight forward
- Effecting only a small strip along the fault

Figure 1 : Chee Lung Pu Fault 1999

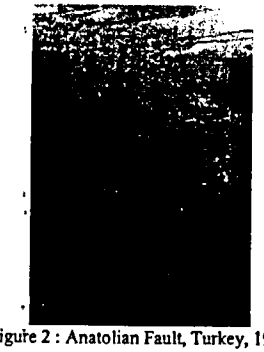

Figure 2 : Anatolian Fault, Turkey, 1999

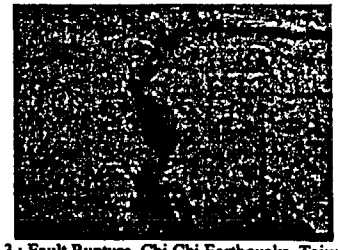

Figure 3 : Fault Rupture, Chi Chi Earthquake, Taiwan 1999

Figure 4 : Fault Crossing Freeway, Turkey

Figure 5 : Typical Fault Appearance, Turkey

Figure 6 : Fault Rupture at Surface, Turkey

Figure 7 : Typical Fault Rupture

This means for the Tuntzuchiao fault that the following has to be accommodated:

- Horizontal and vertical displacement will appear together
- In addition a distortion of the pier in the horizontal plane shall be considered
- A considerable distortion in the vertical plane shall not be expected
- A direct hit will only effect 1 pier in a chain of 35m spans
- The static action by the Earthquake (displacement) will be combined with the dynamic action. Near source effects have to be considered to NCREE recommendations.
- A catastrophic failure of a longer section along the HSR alignment (wedge slip), as experienced in the dam failure in Taiwan, is not to be expected in this case

3. Performance criteria

The following criteria are developed from operational point of view:

a) To prevent loss of span failure

b) To accommodate the potential rupture offset, which has been estimated to 50 cm vertically and up to 150 cm horizontally, as much as possible

c) To allow realignment after a potential rupture offset with a minimum of structural changes

With regard to safety:

d) To guide a derailed train

The discussion of above mentioned criteria provide the following assessment:

a) Can be achieved

b) Can be achieved for the structure, but cannot be achieved for the rail position

c) Can be achieved

d) Can only partly be achieved under the given circumstances. The case of a train being exactly in the position of the rupture or approaching the location rapidly can not be covered by this approach. It is considered that any activity in the fault immediately triggers an emergency breaking of all trains along the line.

4. Specification

The Specification specifies:

- The Tuntzuchiao fault is a fault which would not be able to generate strong motion earthquakes with magnitudes exceeding 6.5
- A maximum magnitude of M = 6.5 shall be taken, which is covered by the zoning factor (Z=0,34)
- As the Tuntzuchiao fault is a secondary slip fault being initiated and probably created in the 1935 earthquake future seismic movement have to be considered.
- The maximum movements to be considered in the HSR infrastructure design shall be takes as natural strike slip = 150 cm and vertical dip slip = 50 cm

5. Items of Consideration

The following items shall be considered in the search for an optimum solution for this case. The first category are the Action driven items:

5.1 Vertical Drop

As indicated earlier a vertical drop of 50cm shall be accommodated. It is assumed that this drop occurs in case of a pier located directly on the fault. It is seen as a differential displacement between the 2 shores of the fault. Anyhow a sharp drop in one location only can not be expected. For the geometric solution (loss of support) the full range shall be considered, whereas for the stress calculations in the structure only 50% as a differential settlement shall be used.

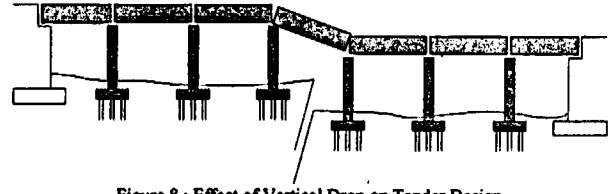

Figure 8 : Effect of Vertical Drop on Tender Design

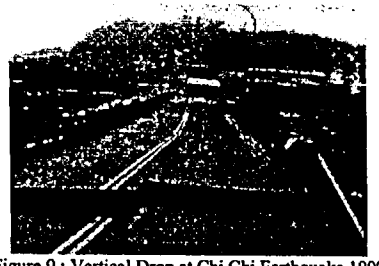

Figure 9 : Vertical Drop at Chi Chi Earthquake 1999

5.2 Loss of Support

In case that a pier is directly located on the fault in a very unfortunate way the complete loss of the support is feasible. Despite the fact that this is most unlikely it should be considered here. Considering the size of the foundation pile cap and the typical characteristic of fault rupture this case is most unlikely.

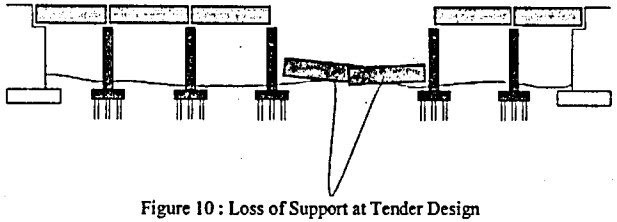

Figure 10 : Loss of Support at Tender Design

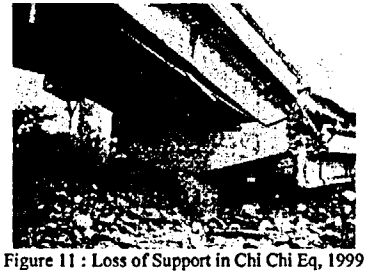

Figure 11 : Loss of Support in Chi Chi Eq, 1999

5.3 Pier Torsion

In case that a pile cap is located directly on the fault it is more likely that a distortion will happen with the pier rather than a shear failure. The horizontal displacement of 150 cm at the fault could result at a pile cap of 12 by 12m in a distortion of 15 degrees approximately. The relevant space shall be allowed at the supporting length. In this case the Bolu Viaduct in Turkey shall be quoted again, where this distortion is clearly visible in the photo.

Figure 12 : Bolu Viaduct, Turkey 1999, Pier Torsion

5.4 Foundation Failure

All piers are founded on piles (8 piles diameter 150 cm) which are covered by a huge pile cap of 12 by 12m. This huge structure is mainly designed to allow for the very small displacement requirements of the train in operation and Therefore shows considerable strength against extraordinary loads such as a fault rupture would bring. It is expected that a fault rupture would rather result in the loss of a couple of piles with a mostly undamaged foundation ready to support the infrastructure loads. Therefore this case shall not be treated as an actual issue of consideration.

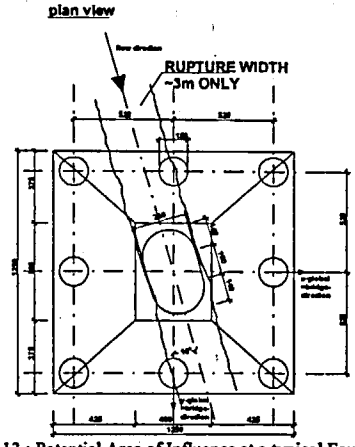

Figure 13 : Potential Area of Influence at a typical Foundation

Figure 14 : Failure of Ground without complete Foundation Failure, Taiwan 1999

5.5 Pile Shear Off

The failure of an individual pile or even a number of piles will not result in a significant problem for structural survival. Anyhow it would effect the operational performance of this structure but could be treated as a midterm repair item.

5.6 Longitudinal Slip

The topographic map shows that the fault crosses the HSR alignment under 45 to 60 degrees. This means that a lateral component of the displacement shall be expected. Rail extension joints shall be provided to accommodate this slip in the rail itself. For the structure the full value of displacement shall be considered in lateral direction for the dimensioning of the support length.

Figure 15 : Failure due to longitudinal Slip, Taiwan 1999

5.7 Transversal Slip

The same facts apply as described under 5.6. The displacement might be fully transversal due to local reasons. No reduction of the displacement value shall be done. In any case vertical and horizontal displacement shall be combined.

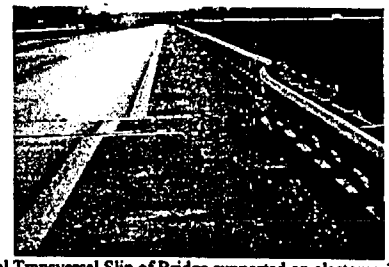

Figure 16 : Typical Transversal Slip of Bridge supported on elastomeric Bearings, Turkey

5.8 Acceleration

All recent earthquakes from Northridge 94 via the 1995 Kobe earthquake to the 1999 Kocaeli and Düzge in Turkey and Chi-Chi in Taiwan earthquakes a trend has been observed in near field action. The recorded acceleration close to faults are in the range of approximately 200% of the given code values. Anyhow the magnitude was always greater than 7, which is not the case here. According to the geological report magnification effects are not to be expected in this case. It might be considered to apply the NCREE recommendations for the directly affected structures, which means only the bridge across the fault. Suitable counter measures to accommodate the increased horizontal forces are proposed in a later chapter.

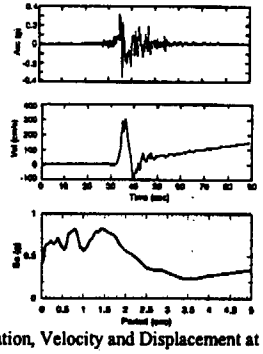

Figure 17 : Acceleration, Velocity and Displacement at Nantou, Taiwan 1999

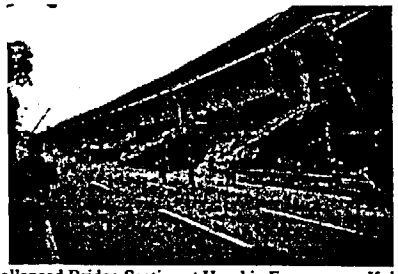

Figure 18 : Collapsed Bridge Section at Hanshin Expressway, Kobe, Japan 1995

5.9 Earthquake Spectra

Considering the spectra of the latest earthquakes it was observed that in Turkey the frequencies between 2 and 4 Hertz particularly exceeded the code values, whereas in Taiwan this region was located between 0,8 and 3 Hz. For this purpose a rather stiff structure could improve the situation considerably. Structures with frequencies above 4 Hz are desirable. This leads to the case "the stiffer the better".

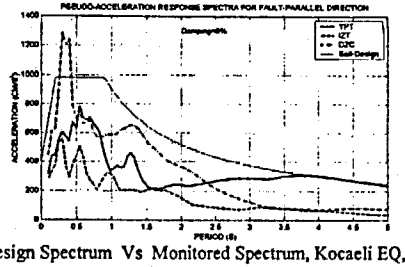

Figure 19 : Design Spectrum Vs Monitored Spectrum, Kocaeli EQ, Turkey 1999

5.10 Multi Support Excitation

The rather short spans of 30 m and 55m suggest that an equal excitation of all piers will occur. Anyhow it is considered that in case of multiple support excitation the structure would rather benefit from this action by unsynchronized out of phase movement which would eliminate part of the action. Therefore this item shall only be considered in case that a large span is chosen finally.

5.11 Train Derailment

In case that a train is located on the fault or directly approaching a fault during an earthquake it will derail. In case of dam the containment earthworks shall make sure that the train is more or less guided in longitudinal direction without crashing completely. In case of a bridge this scenario is much more difficult to achieve. Anyhow a proper guiding system is thinkable, but it would also have effects on the structure itself.

Figure 20 : Track Condition, Taiwan 1999

Figure 21 : Track, Turkey 99

5.12 Track Displacement

The track displacement to be expected is directly related to the interaction between ground – foundation – structure – track. The stiffer the connections between the single elements are the more displacement has to be expected. Anyhow it has to be clearly distinguished between a track performance under usual operational loads and these extraordinary cases. It can not be expected that the tolerances required for operation can be satisfied.

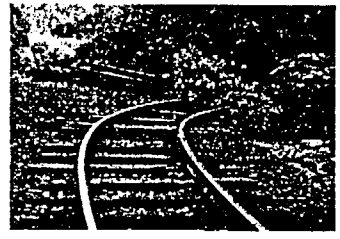

Figure 22 : Taiwan Track Performance 1999

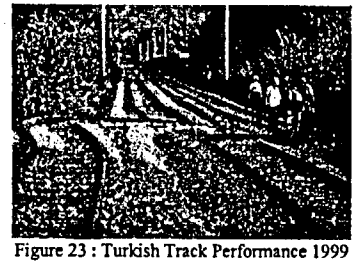

Figure 23 : Turkish Track Performance 1999

5.13 Force Majeur

Any earthquake has the potential of a Force Majeur situation. Anyhow from the geological report the expected magnitude from an earthquake in this fault is 6.4, where the potential for a force majeur situation is small. It shall not be considered in this case.

Figure 24 : Catastrophic Failure of Dam, 9.8m vertical Drop, Taiwan 1999

From operational point of view there are the following circumstances to be taken into consideration:

5.14 Rail Displacement

The limits for rail displacement under normal operation condition are not valid for the earthquake case. The specification does not know any limits for bridges in a near fault situation. Therefore assumptions have to be taken. The rail displacement is a function of the support conditions. In case of a standard bridge the rail displacement would suffer almost the full range of the fault displacement. In case of a base isolation of the bridge structure the rail displacement can be reduced. Anyhow part of the displacement will be retained. This could be seen as a first level of protection. Considering a 2nd isolation, consisting of a slab track on elastic material and a continuos structure below it, this displacement can be further limited. Anyhow it always becomes a function of the effort to be taken by the structure. A comparison will be made in further chapters.

Figure 25 : Tracks across an active Fault, Kocaeli EQ, Turkey 1999

6. Structural Options

The considerations are primarily based on the available single span design.

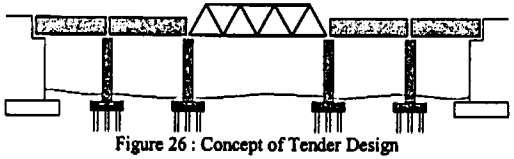

Figure 26 : Concept of Tender Design

The following options are available in the design to accommodate the described phenomena :

6.1 Sufficient Support Length

As indicated earlier a vertical drop of 50cm and a horizontal slip of 150cm shall be accommodated in combination. This results in a minimum pier cap size as shown in the following sketch under the consideration that a minimum of 50% of the bearing size shall be supported.
A reasonable pear head size for this case would be 6,80 x 7,80m which considers that in longitudinal direction the slip consists of 150cm of horizontal displacement by the fault, 47cm displacement by pear torsion and 7cm displacement from the vertical drop. This results in a total margin of 202cm of which the existing margin has been subtracted. In cross direction only the horizontal displacement shall be considered reduced by the existing margin.

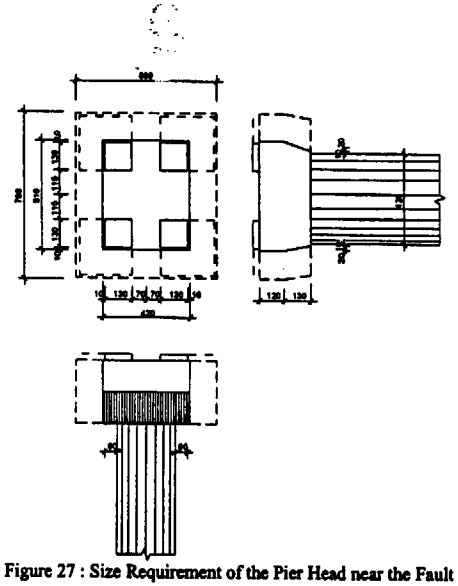

Figure 27 : Size Requirement of the Pier Head near the Fault

Figure 28 : Failure due to Insufficient Support Length, Kobe 1995

6.2 Wider Deck

In principal it should be considered to provide a wider deck structure for this case to allow:

- Movement of the track without falling from the structure
- Realignment of the track after medium earthquakes within very short time
- Space for additional safety measures

Anyhow all this items will require a different design from the single beam standard design. The additional width should be limited to 2/3 of the given 150cm horizontal displacement to both sides, which is in total 2m.

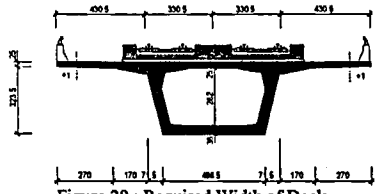

Figure 29 : Required Width of Deck

6.3 Continuous Beam

A continuos beam solution under the given conditions, a chain of 35m spans with a structural height of 3.35m could be designed such that the loss of a complete support could be covered. It has been proven at a case in Austria (Refer to the Annex) that a continuos pre-stressed bridge can survive a settlement of 128cm without major damage and can be repaired to full function. The disadvantage of the continuos beam solution is that single spans can not be exchanged. Anyhow there are cases known, where the complete continuos bridges has been exchanged by parallel movement. From structural point of view the performance of a continuos beam will be much better compared to single spans. Anyhow the decision has to be made also based on the emergency concept.

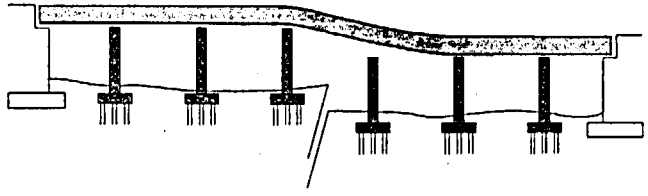

Figure 30 : Performance of the continuous Beam at a typical vertical Drop

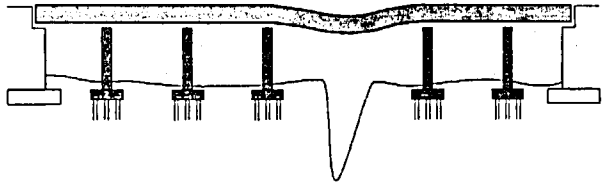

Figure 31 : Performance of the continuous Beam at a typical Loss of Support

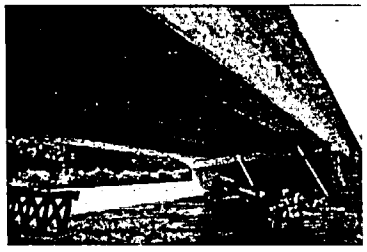

Figure 32 : Settlement of the Kufstein Bridge

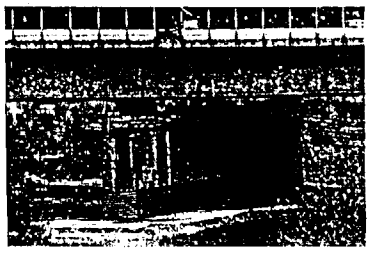

Figure 33:

6.4 Anti Derailing Devices

The distortion of the wheels shall be avoided to keep the direction of the train. This has become standard equipment on tracks of DB (Deutsche Bahn) on all their lines, where derailment is thinkable. It was introduced after the accident of Enschede (Germany). Their function under a huge displacement at a limited distance has to be discussed.

It has to be emphasized that this measure will not be able to avoid a disaster. Anyhow it represents the present state of the art.

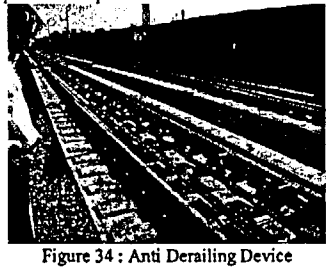

Figure 34 : Anti Derailing Device

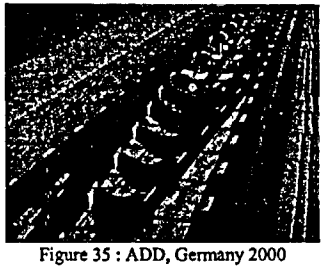

Figure 35 : ADD, Germany 2000

6.5 Rail Expansion Joint

The use of rail expansion joints has to be carefully considered in connection with the safety concept. A whole system approach has to be chosen to decide about location and even application or not of the devices.

Under earthquake loads an elongation of the rail might occur. A rail expansion joints allows an elongation without major resistance. Thus the rails in the adjacent stretches of the line will not be damaged. Anyhow the resistance of the rails might help to keep the alignment of the track in certain cases. But there is the chance of a rail break.

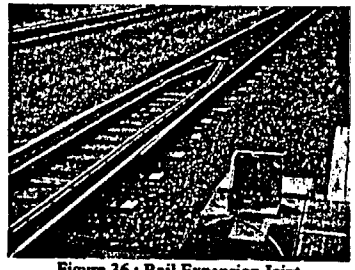

Figure 36 : Rail Expansion Joint

6.6 Guide Walls

The earthwork provided by the dam solution could be replaced by guiding walls on the structure. Anyhow a similar soft impact than at a dam solution can not be guarantied. Regular guiding measures as guardrails and restrainers as used in road bridges, will not be good enough to fulfill the requirement. A special wall solution could be adapted. Nevertheless the function of such a measure is questionable.

The final concept for such a guide wall has to be developed after principal decision have been taken. For that reason the given solution is a standard used on road bridges which has to be adapted for the case.

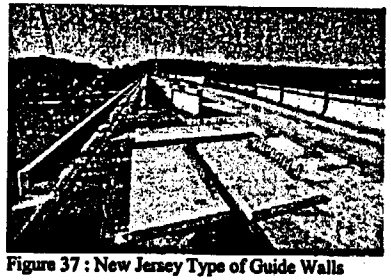

Figure 37 : New Jersey Type of Guide Walls

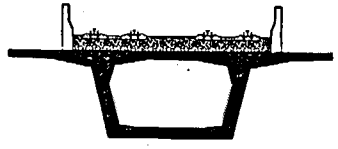

Figure 38 : Cross Section with 1,2m Walls (Ballast)

6.7 Seismic Devices

Seismic devices are of great help in case that displacement and acceleration shall be limited. In case of the Bolu viaduct in Turkey they helped to keep the superstructure in place even an active fault passed directly below the bridge and displaced and distorted a pier. The main function is to reduce the forces coming from ground acceleration to a limit desired by the designer. The dimensioning of such devices is mainly depending on the chosen specification of the fault behavior.

To absorb energy from any earthquake it is highly advisable to install such devices even so they can not provide the perfect solution for the project. It solves part of the near fault amplification effects and problems arriving from large displacement under unfavorable conditions. The costs of such devices might be balanced by the savings in the piers and the substructure, if regulations allow.

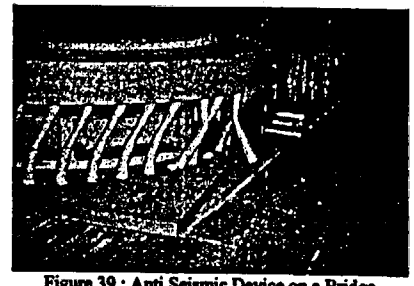

Figure 39 : Anti Seismic Device on a Bridge

6.8 Base Isolation

The concept of base isolation is to take provisions for normal operation, which fulfills all the conditions of the specification and to take a system into operation when excessive acceleration or displacement happens. By this measure the forces on substructures and superstructures can be reduced to the ordinary values of operation, which will not create additional costs from this items. Anyhow the base isolation system itself will eat up most of this benefit. Such system have been used very successfully on road bridges and is under major consideration for railways right now. Tests have been carried out already successfully.

Figure 40 : Base Isolation of a Model (1:6) of the Taiwan HSR Project (HARIS, 1998)

6.9 Isolated Slab Track

In cases where a dominant horizontal displacement is expected and vertical displacement is limited (for example by a continuos beam) an isolated slab track makes sense. In this case it would be desirable to combine both tracks with 1 slab to achieve a huge horizontal rigidity. This slab can be placed on an isolation material with a certain resistance. In case of a major movement of the bridge the track can keep its position as much as possible. This "bridge on a bridge" concept has been used in minor cases but for different conditions. Anyhow such solutions could be to the benefit of the track safety.

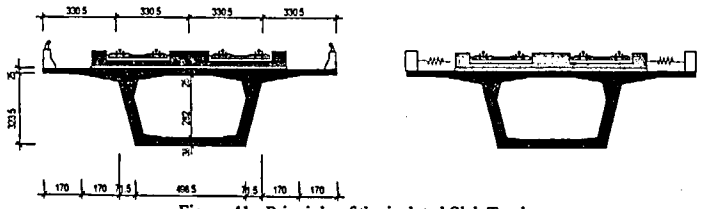

Figure 41 : Principle of the isolated Slab Track

6.10 Structural Control

Today's structural control abilities are good enough to deal with this case. Structural control normally goes hand in hand with base isolation and monitoring. Anyhow there is still resistance against such solutions for railways due to the non existent long time behavior record. Probably structural control systems in connection with a wider deck and an isolated slab track could make sense for this special case. This is discussed in the next chapter.

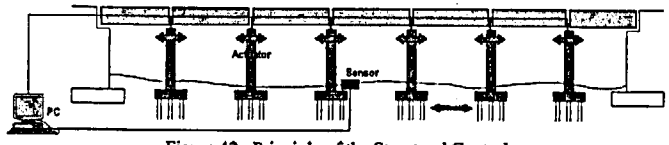

Figure 42 : Principle of the Structural Control

6.11 Track Control

A controlled slab track which is continuos over the length of the bridge might be one of the most attractive solutions for this case. The principle is that the continuos slab with huge horizontal resistance is controlled by hydraulic cylinders which keep its position in case of a movement of the structure. Such a system would not be too difficult and bears a small risk only. In case that it is not in operation during an earthquake the bridge will behave as a normal bridge and not experience disadvantages. The advantage gained by such a system can be huge.

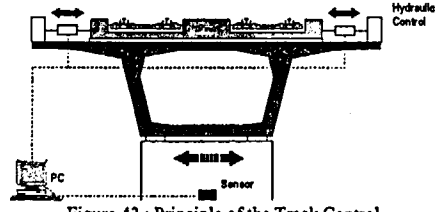

Figure 43 : Principle of the Track Control

6.12 Realignment of HSR Layout

Another option to avoid major problems is a complete realignment of the layout in such way that the fault is crossed with a dam solution as initially intended. Anyhow from the present layout it can be seen that such realignment would bring considerable changes with a variation of consequences.

6.13 Connection of Spans

Considerable unequal behavior of single spans resting on a common pier have been recorded in the Kobe earthquake 1995.

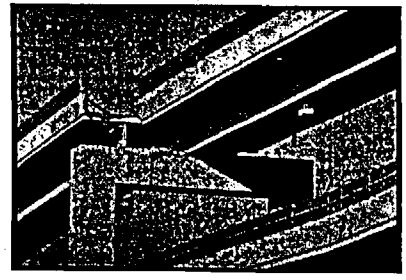
Fig. 44 : Unequally displaced girders in Kobe 1995

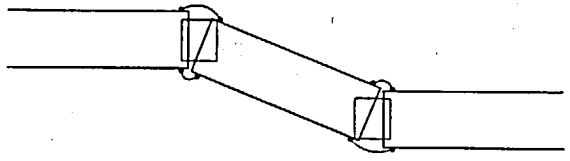
Fig. 45 : Connection principle

7. Assessment

The major items of consideration have been listed in chapter 5 and the structural options are described in chapter 6. In this chapter it shall be tried to assess the cross influence of items of consideration against the options. This has to be repeated in different scenarios which are:
Survival of a displaced superstructure with unusable tracks
Survival of the superstructure with track for emergency use
Survival of the superstructure with limited displacement and provisional use
Complete survival of the system with minor realignment and repair

Szenario :	Survival of a displaced superstructure with unusable tracks													
Options	6.1		6.2	6.3	6.4	6.5	6.6	6.7	6.8	6.9	6.10	6.11	6.12	
Items of Consideration	Tender Design	Support Sufficient Length	Wider Deck	Continuous Beam	Anti Derailing Devices	Rail Expansion Joint	Guide Walls	Seismic Devices	Base Isolation	Isolated Slab Track	Structural Control	Track Control	Realignment of Layout	
Action driven Items														
5.1 Vertical Drop			0		0	0	0	0	0	0	0	0	0	15
5.2 Loss of Support	0	0	0		0	0	0	0	0	0	0	0		10
5.3 Pier Torsion			0		0	0	0	0	0	0	0	0	0	15
5.4 Foundation Failure	0	0	0		0	0	0	0	0	0	0	0		10
5.5 Pile Shear Off		0	0		0	0	0	0	0	0	0	0		15
5.6 Longitudinal Slip	1		0		0	0	0	0	0	0	0	0		16
5.7 Transversal Slip	1		0		0	0	1	0	0	0	0	0	0	12
5.8 Accelleration	4	0	0	4	0	0	0	0	0	0	0	0	0	8
5.9 Earthquake Spectra	4	0	0	4	0	0	0	0	0	0	0	0	0	8
5.10 Multi Support Excitation	3	0	0		0	0	0	0	0	0	0	0	0	8
5.11 Train Derailment	3	0	0	3		0	2	0	0	0	0	0	0	13
5.12 Track Displacement	0	0	3	3	0	0	0	0	0	0	0	0	0	6
5.13 Force Majeur	0	0	0	2	0	0	0	0	0	0	0	0	0	2
Operational Items														
5.14 Rail Displacement	4	0	3	4	3	0	0	0	0	0	0	0	0	14
5.15 Realignment	3	4		4	1	0	0	0	0	0	0	0		22
5.16 Repair of Structures	4	4	2	3	0	0	0	0	0	0	0	0	0	13
5.17 Repair of Substructures	4	4	0	4	0	0	0	0	0	0	0	0	0	12
5.18 Provisional Use	1	3			0	0	0	0	0	0	0	0		24
5.19 Monitoring	4	0	0	4	0	0	0	0	0	0	0	0	0	8
5.20 Emergency Stop	4	0	0	4	0	0	0	0	0	0	0	0	0	8
5.21 Emergency Concept		4	4		4	0	3	0	0	0	0	0		30
	60	39	22	89	18	0	6	0	0	0	0	0	35	

Score
0 not effective
1 very little effective
2 little effective
3 effective
4 very effective
5 solves the problem

Figure 46 : Assessment Scenario 1

Szenario :	Survival of the superstructure with track for emergency use													
	6.1		6.2	6.3	6.4	6.5	6.6	6.7	6.8	6.9	6.10	6.11	6.12	
Items of Consideration / Options	Tender Design	Support Sufficient Length	Wider Deck	Continuous Beam	Anti Derailing Devices	Rail Expansion Joint	Guide Walls	Seismic Devices	Base Isolation	Isolated Slab Track	Structural Control	Track Control	Realignment of Layout	
Action driven Items														
5.1 Vertical Drop	2	4	0		0	0	0	1	0	0	0	0	0	12
5.2 Loss of Support	0	0	0		0	0	0	0	0	0	0	0		10
5.3 Pier Torsion	2		0	4	0	0	0		0	0	0	0	0	16
5.4 Foundation Failure	0	0	0		0	0	0	0	0	0	0	0		10
5.5 Pile Shear Off		0	0		0	0	0	0	0	0	0	0		15
5.6 Longitudinal Slip	1		0		0	0	0		0	0	0	0	5	21
5.7 Transversal Slip	1		4		4	2	1		0	0	0	0	0	27
5.8 Accelleration	3	0	0	4	0	0	1		0	0	0	0	0	13
5.9 Earthquake Spectra	3	0	0	4	0	0	1		0	0	0	0	0	13
5.10 Multi Support Excitation	3	0	0		0	0	1		0	0	0	0	0	14
5.11 Train Derailment	2	0	4	3		0	2	0	0	0	0	0	0	16
5.12 Track Displacement	0	0	3	3	0	0	0	4	0	0	0	0	0	10
5.13 Force Majeur	0	0	0	2	0	0	0	2	0	0	0	0	0	4
Operational Items														
5.14 Rail Displacement	4	0	3	4	3	0	0	4	0	0	0	0	0	18
5.15 Realignment	3	4		4	1	2	0	4	0	0	0	0		28
5.16 Repair of Structures	4	4	2	3	0	0	0	4	0	0	0	0	0	17
5.17 Repair of Substructures	4	4	0	4	0	0	0	4	0	0	0	0	0	16
5.18 Provisional Use	1	3			3	0		0	0	0	0			32
5.19 Monitoring	4	0	0	4	0	0	0	0	0	0	0	0	0	8
5.20 Emergency Stop	4	0	0	4	0	0	0	0	0	0	0	0	0	8
5.21 Emergency Concept	2	4	4		4	3	3		0	0	0	0		35
	48	38	30	88	22	10	9	63	0	0	0	0	35	

Score
0 not effective
1 very little effective
2 little effective
3 effective
4 very effective
5 solves the problem

Figure 47 : Assessment Scenario 2

Szenario : 3		Survival of the superstructure with limited displ., provisional use													
	Items of Consideration / Options	Tender Design	6.1 Support Sufficient Length	6.2 Wider Deck	6.3 Continuous Beam	6.4 Anti Derailing Devices	6.5 Rail Expansion Joint	6.6 Guide Walls	6.7 Seismic Devices	6.8 Base Isolation	6.9 Isolated Slab Track	6.10 Structural Control	6.11 Track Control	6.12 Realignment of Layout	
	Action driven Items														
5.1	Vertical Drop	2	4	0	5	0	0	0	1	2	0	0	0	0	14
5.2	Loss of Support	0	0	0	5	0	0	0	0	0	0	0	0	5	10
5.3	Pier Torsion	2	5	0	4	0	0	0	5	5	0	0	0	0	21
5.4	Foundation Failure	0	0	0	5	0	0	0	0	0	0	0	0	5	10
5.5	Pile Shear Off	5	0	0	5	0	0	0	0	0	0	0	0	5	15
5.6	Longitudinal Slip	1	5	0	5	0	0	0	5	5	0	0	0	5	26
5.7	Transversal Slip	1	5	4	5	4	2	1	5	5	0	0	0	0	32
5.8	Accelleration	3	0	0	4	0	0	1	5	5	0	0	0	0	18
5.9	Earthquake Spectra	3	0	0	4	0	0	1	5	5	0	0	0	0	18
5.10	Multi Support Excitation	3	0	0	5	0	0	1	5	5	0	0	0	0	19
5.11	Train Derailment	2	0	4	3	5	0	2	0	0	0	0	0	0	16
5.12	Track Displacement	0	0	3	3	0	0	0	4	4	0	0	0	0	14
5.13	Force Majeur	0	0	0	2	0	0	0	2	2	0	0	0	0	6
	Operational Items														
5.14	Rail Displacement	4	0	3	4	3	0	0	4	4	0	0	0	0	22
5.15	Realignment	3	4	5	4	1	2	0	4	4	0	0	0	5	32
5.16	Repair of Structures	4	4	2	3	0	0	0	4	4	0	0	0	0	21
5.17	Repair of Substructures	4	4	0	4	0	0	0	4	4	0	0	0	0	20
5.18	Provisional Use	1	3	5	5	5	3	0	5	5	0	0	0	5	37
5.19	Monitoring	4	0	0	4	0	0	0	0	0	0	0	0	0	8
5.20	Emergency Stop	4	0	0	4	0	0	0	0	0	0	0	0	0	8
5.21	Emergency Concept	2	4	4	5	4	3	3	5	5	0	0	0	5	40
		48	38	30	88	22	10	9	63	64	0	0	0	35	

Score
0 not effective
1 very little effective
2 little effective
3 effective
4 very effective
5 solves the problem

Figure 48 : Assessment Scenario 3

Szenario : 4		Complete Survival of the system with minor realignment and repair													
	Items of Consideration / Options	Tender Design	6.1 Support Sufficient Length	6.2 Wider Deck	6.3 Continuous Beam	6.4 Anti Derailing Devices	6.5 Rail Expansion Joint	6.6 Guide Walls	6.7 Seismic Devices	6.8 Base Isolation	6.9 Isolated Slab Track	6.10 Structural Control	6.11 Track Control	6.12 Realignment of Layout	
	Action driven Items														
5.1	Vertical Drop	2	4	0	5	0	0	0	1	2	4	1	2	2	23
5.2	Loss of Support	0	0	0	5	0	0	0	0	0	0	0	0	5	10
5.3	Pier Torsion	2	5	0	4	0	0	0	5	5	5	5	5	5	41
5.4	Foundation Failure	0	0	0	5	0	0	0	0	0	0	0	0	5	10
5.5	Pile Shear Off	5	0	0	5	0	0	0	0	0	0	0	0	5	15
5.6	Longitudinal Slip	1	5	0	5	0	0	0	5	5	5	5	5	5	41
5.7	Transversal Slip	1	5	4	5	4	2	1	5	5	5	5	5	5	52
5.8	Accelleration	3	0	0	4	0	0	1	5	5	4	5	4	0	31
5.9	Earthquake Spectra	3	0	0	4	0	0	1	5	5	4	5	4	0	31
5.10	Multi Support Excitation	3	0	0	5	0	0	1	5	5	4	5	4	0	32
5.11	Train Derailment	2	0	4	3	5	0	2	0	0	0	0	0	0	16
5.12	Track Displacement	0	0	3	3	0	0	0	4	4	5	4	5	3	31
5.13	Force Majeur	0	0	0	2	0	0	0	2	2	0	2	2	0	10
	Operational Items														
5.14	Rail Displacement	4	0	3	4	3	0	0	4	4	4	4	4	0	34
5.15	Realignment	3	4	5	4	1	2	0	4	4	4	4	4	4	43
5.16	Repair of Structures	4	4	2	3	0	0	0	4	4	4	4	4	0	33
5.17	Repair of Substructures	4	4	0	4	0	0	0	4	4	4	4	4	0	32
5.18	Provisional Use	1	3	5	5	5	3	0	5	5	5	5	5	0	47
5.19	Monitoring	4	0	0	4	0	0	0	0	0	0	5	5	0	18
5.20	Emergency Stop	4	0	0	4	0	0	0	0	0	0	5	5	0	18
5.21	Emergency Concept	2	4	4	5	4	3	3	5	5	5	5	5	3	53
		48	38	30	88	22	10	9	63	64	62	73	72	42	

Score
0 not effective
1 very little effective
2 little effective
3 effective
4 very effective
5 solves the problem

Figure 49 : Assessment Scenario 4

Conclusion

From the figures a trend can be derived and the interpretation of the figures can be developed into an assessment of the options. The following conclusions might be drawn :

- A sufficient support length generally contributes to a solution of the problem and has no technical disadvantages.
- Connection cables are a well established mean to ensure equal performance of adjacent single span girders and shall be used here.
- A wider deck has advantages in operational terms only in combination with other measures, but does not create technical disadvantages
- The continuos beam solution appears to be little attractive for the situation because of the span arrangement (4x30m concrete and 55m steel bridge) in the tender design. Reparability is a main focus here.
- Anti derailing devices are essential and state of the art.
- The question of rail expansion joints shall be decided when the final emergency concept is available.
- Guide walls as a substitution of the containment earthworks in case of the dam are very little effective and questionable.
- Seismic devices will provide additional safety in case that a higher level of emergency use is desired and near fault effects shall be considered, but pier sizes shall not be increased.
- Base isolation actually could be of help in case that the concept is changed completely.
- An isolated slab track could be a very attractive solution in case that a high level of safety and emergency use shall be achieved.
- Structural control might be the concept of the future but its readiness for application has yet to be proved.
- Track control might be the simpler version of a structural control and could be taken into consideration.
- A complete realignment of the layout could be a good technical solution but seems to be impossible from organizational point of view considering the progress of the project.

Literature

[1] Juin-Fu CHAI, Chin-Hsiung LOH, Chao-Yu CHEN
Consideration of the Near-Fault Effect on Seismic Design Code for Sites near the Chelungpu Fault
Journal of the Chinese Institute of Engineers, Vol. 23, No. 4, July 2000

[2] Wen-I LIAO, Chin-Hsiung LOH, Shiuan WAN, Wen-Yu JEAN and Juin-Fu CHAI
Dynamic Responses of Bridges subjected to Near-Fault Ground Motions
Journal of the Chinese Institute of Engineers, Vol. 23, No. 4, July 2000

[3] ERDIK, M.
Report on 1999 Kocaeli and Düzce Earthquakes

[4] EERI (1999),
Special Report Learning from Earthquakes (October 1999)

[5] ITU-IAHS (1999)
Proceedings of the Intl. Conf. On Kocaeli EQ, Istanbul Technical University

[6] Kocaeli EQ Online, Bogazici University
http://www.koeri.boun.edu.tr/earthqk/earthqk.html

[7] ITO, M.,
Special Report to IABSE on the Kobe EQ at the 1995 San Franzisco Syposium

SEISMIC INPUT MOTIONS FOR STRUCTURE, PLANT AND EQUIPMENT DESIGN

John H Mills
Babtie Group Ltd.

Abstract

The seismic input motions used in the design of nuclear safety related facilities in the UK were developed in the early 1980's. Although there have been improvements to the methodology used since then, the basic definition remains a peak free field acceleration and piece-wise linear response spectra. The increased computing power available to engineers means that the design process can now accommodate a more fundamental definition of the seismic hazard, whilst the increased availability of strong motion records means that ground motion specialists are perhaps now in a position to meet such requirements. The aim of this paper is to stimulate discussion between design engineers and seismologists about how best to harness these advances in technology to overcome any current problems and to identify the co-operation needed to achieve this.

Introduction

The design engineer's requirement is for a simple deterministic definition of the seismic ground motion hazard suitable for use in an already complex design process. The seismologist's responsibility is to provide ground motion data which properly represent the seismic hazard at the site and which recognise the uncertainty inherent in virtually every input parameter to such data. The regulator's concern is to ensure that the level of conservatism in the totality of the seismic design is sufficient to allow for both the simplifications and uncertainties in the whole process. It is little wonder that the interface between design engineers and ground motion specialists has traditionally been seen as a source of significant, potentially unnecessary, conservatism in the definition of seismic ground motion parameters for the design of safety related nuclear facilities.

This paper is based upon experience in the design of safety related structures, systems and components for nuclear power and nuclear fuel reprocessing facilities in the United Kingdom. In this context, the term design includes the engineering verification of new facilities and the evaluation and re-evaluation of existing facilities. The author is a civil engineer whose principal responsibility is the design of building structures. However, the comments made are also informed by experience as a design manager for nuclear projects. Whilst the author has assisted the UK regulator in the assessment of seismic designs for nuclear facilities, and has in this capacity visited every nuclear facility in the UK, and has close contacts with UK earthquake research facilities, principally Imperial College, the comments and observations in this paper are made essentially from an industrial perspective.

This workshop is a timely opportunity to revisit the way in which the seismic hazard is treated in the design of nuclear facilities, to personally review interaction with ground motion specialists and to gauge the responsiveness of regulators to changes which may be anticipated in the next 5 to 10 years.

Which Parameters to Use?

The UK nuclear industry is regulated by H. M. Nuclear Installations Inspectorate. The industry is regulated through a non-prescriptive, goal-setting regime with the emphasis on the licensee demonstrating to his own satisfaction, and that of the regulator, that the design meets well established principles. In contrast to the US Nuclear Regulatory Commission nothing is prescribed. In the context of external hazards, the principles by which the regulators assess the suitability of the design criteria are shown in Table 1.

The principles do not prescribe how to describe the hazard (peak ground acceleration or other) and do not define in absolute terms the size of the hazard. They do, however, indicate that a degree of caution is required with respect to natural hazards due to the uncertainties inherent in the data and procedures used in the deviation of the design criteria. However, again, the degree of caution or conservatism required is not specified but is left to the licensee depending upon the radiological consequences of the facility.

The UK seismic environment is, by most standards, benign; earthquake loading is not considered in the design of conventional buildings and facilities. Nevertheless, earthquakes do occur and the headline in Figure 1 occurred only last month. Indeed, it was an earthquake of similar magnitude in 1979 which occurred close to Chapelcross nuclear power station in Cumbria that awakened the UK nuclear industry to the need to consider external hazards in general, and seismic hazards in particular, in the design of such facilities

The UK has developed criteria for earthquake resistant design of nuclear safety related facilities based upon.

- peak free field horizontal ground acceleration (pffhga)
- piecewise linear response spectra
- vertical motion = 2/3 horizontal motion

The somewhat tenuous relationship between damage and pffhga has been recognised, particularly for building structures, as has the importance of site specific effects including soil-structure interaction. The aim has been to produce a description of the seismic hazard in a form which can be used in design, remembering that for nuclear facilities the performance of plant and equipment can be critically important to the safety of the facility. Such plant and equipment is subjected to motions which are filtered by the soil at the site, the building structure and intermediate support systems. These interactions are complex and in many cases may be non-linear.

Peak Free Field Horizontal Ground Acceleration

Work in the early 1980's established the geological context of UK seismicity and thoroughly researched the historical archive, which proved to be amazingly rich. Through relationships between magnitude and felt area, established from instrumental data, a magnitude/frequency relationship was developed for the UK as a whole. However, no strong motion data exists for the UK, and the

conversion of the magnitude/frequency relationship into an acceleration/frequency relationship was based upon European and US data and attenuation formulae. The resulting relationship is shown in Figure 2. These analyses also showed that, in terms of risk, the main contribution to the seismic hazard at a UK nuclear facility is from a 'direct hit' by a small earthquake.

The seismologists recognise and understand the uncertainties associated with the derivation of the seismic hazard. No doubt, they believe that the hazard curves eloquently describe these uncertainties so that even an engineer can use the criteria appropriate to his design. The engineer on the other hand is working in an essentially deterministic process. This process is multi-disciplinary with many interfaces between different disciplines and, usually, different companies. Specialist activities, such as dynamic analysis, may be subcontracted. To minimise interactions at these interfaces a linear process is imposed, which together with the inevitable time constraints lead to a requirement for simple, conservative criteria. The uncertainties in the seismic design criteria defined by the seismologist cannot be easily incorporated in this process and for new facilities there has been a tendency to reduce the definition of the hazard to a single value of the peak ground acceleration of 0.25g associated with one set of the piecewise linear response spectra. This has become the de-facto design standard for new UK nuclear facilities, to the extent that the uncertainties inherent in the whole process tend to have been forgotten. There has also been reluctance on the part of the regulator to move away from this definition.

Piecewise Linear Response Spectra

In parallel with the development of the acceleration/frequency relationship sets of piecewise linear response spectra were developed, again based upon European and US data. Three sets of spectra were developed for three different site types, characterised as Hard, Intermediate and Soft.

The development of the UK piecewise linear response spectra followed procedures current in the early 1980s. For each ground type, strong ground motion records were selected using macro-seismic data. These were:

- Complete triaxial set
- Recorded in the free field
- Richter Magnitude between 4.0 and 6.0
- Focal depth between less than 30 km
- Epicentral distance less than 50km
- Duration of strong motion less than 10 seconds
- MMI site intensity ≥ IV
- Peak horizontal acceleration > 0.04g

As noted previously, no strong ground motion records exist for UK earthquakes and the records used were taken from the then relatively small database of US and European records. It is interesting to note that the criteria for duration did not operate in this process. Statistical analysis was carried out of the ratios of v/a and ad/v^2 and median values were obtained. Mean plus one standard deviation amplification factors for acceleration, velocity and displacement were obtained and corner frequencies were chosen. Spectra were plotted for different levels of damping, the Hard Ground spectrum for 5% damping being shown in Figure 3 (note that the spectrum applies to both horizontal and vertical motions). This figure also shows the spectrum of one of the strong motion records used in the analysis, in this case a German record. The actual earthquake spectrum approaches the piecewise

linear spectrum only over a small range of frequencies, each particular earthquake in the dataset challenging the spectrum at a different frequency range.

Figure 4 shows the acceleration time history of the German record. This was a relatively short event with a high peak acceleration but with a limited frequency content. Figure 5 shows a time history generated to match the piecewise linear spectrum using USNRC guidelines. This is much longer and has a much fuller frequency content, altogether a more energetic event. These comparisons show that the input motions defined, whether the piecewise linear spectrum or the spectrum matched time history, input significantly more energy into the structural system than any one particular event. This is particularly important in the analysis of non-linear systems.

The spectra generated in the way described are recognised as having a variable probability of exceedence. More recently, Uniform Risk Spectra (URS) have been generated which have the same probability of exceedence at all frequencies. These are generated using frequency dependent attenuation relationships and derive horizontal and vertical motions separately. To date URS have not been accepted for the design of new facilities. In the evaluation of existing structures URS and piecewise linear spectra are used, although there are concerns about the URS below I Hz.

Analytical Methods

Many of my engineers can carry out the most complex dynamic analyses, including non-linear time history analysis. Only the older engineers can carry out a simple analysis by Equivalent Lateral Force (ELF) methods. I say this to remind myself how far we have moved since the seismic hazard criteria were developed. In the late 1970's and early 1980's ELF methods were used for initial design and relatively simple 'stick' models were used with response spectrum methods for final design verification. Exceptionally, linear time history analysis would be carried out on even simpler models to generate a few in-structure response spectra for design.

Increasing computer power and improved analytical procedures mean that detailed finite element analysis is now the norm. Response spectrum analysis is used primarily in the validation of the model and the main design is based upon time history analysis. For the evaluation of existing facilities non-linear analysis is commonly used. The increased complexity of the analysis itself introduces further uncertainties. For example, in steel frames semi-rigid connections are generally modelled as either fully rigid or pinned. The effect on the overall analysis is small, but locally the stresses calculated are meaningless. The code allowable stresses, against which the results of the analysis are checked are based on simple rules and generally refer to gross stresses on the section. Also most codes were developed before detailed finite element analysis became available. Thus we have a situation where the sophistication of the analysis has out stripped the definition of the input and the treatment of the output. In the context of this workshop the treatment of the output of the analysis is not the issue. But the definition of the input is.

Taking account of the requirements for plant and equipment design can have a fundamental impact on the design of the building structures. Firstly, Soil-Structure-Interaction (SSI) is often beneficial to heavy nuclear structures and for simplicity and conservatism this can often be ignored. For plant and equipment SSI dictates entirely the seismic motions they will be subjected to. Thus SSI must be carried out. Plant-structure-interaction is also often beneficial both to the plant and the structure. However, at the time that the structural analysis is required for building design and the generation of secondary (or floor) response spectra many plant details are not available. Plant-structure-interaction is therefore ignored. Figure 6 shows a typical plant item supported within a structure. Structural analysis will generate floor response spectra at the master nodes marked 'X'.

These will then be used on further detailed models of the plant components. In order to ensure predictable, and easily demonstrated secondary spectra, it is often required to ensure that the building's response is essentially elastic. This seemingly reasonable requirement can completely dictate the building design.

Discussion

The broad band piecewise linear response spectrum was a convenient and concise way of capturing and enveloping the frequency content of the design ground motion, taking account of many of the uncertainties discussed earlier. Coupled with a defined pffhga this simple definition of the seismic hazard allows analysis and design to proceed to acceptable project programmes, albeit at a cost, and has become the 'design standard' for nuclear facilities in the UK.

The recent European Conference on Earthquake Engineering was held in London, and the conference dinner was held in the main hall of the National History Museum. Surrounded by dinosaur bones, such as those shown in Figure 7, seemed to be an appropriate reminder that earthquakes have their genesis in geological ages long gone. And like the palaeontologist who extrapolates an entire skeleton from a single bone, seismologists extrapolate a no less impressive structure for the prediction of seismic hazard from relatively little data. The engineer is the cave man who has to overcome the monster the palaeontologist/seismologist has created!!

Figures 8 and 9 show in a diagrammatical way the change in the seismic criteria and the cost of seismic design in the UK since 1980. The definition of the hazard stepped up sharply in the early 1980's through the work outlined above. Since then, some further data has been recovered, and the science has been refined. The net effect is a small reduction in the 'design standard'. The cost of seismic design has, against this trend, steadily increased, with at times significant step changes. These increases are due to an increased requirement for demonstration of numerical compliance with acceptance criteria, in turn leading to increasing complexity in analysis and design. For new facilities, earthquake resistant design represents a significant design challenge, even at the levels of design event used in the UK. For the evaluation of existing facilities, whose continued operation depends upon demonstrating an acceptable level of earthquake resistance, these methods can become life limiting.

Given the level of analysis now available, is the use of piecewise linear spectrum matched time histories appropriate, particularly for non-linear analysis? If not, what alternatives can the seismologists offer for the definition of the seismic hazard?

Alternative parameters such as Effective Peak Acceleration (EPA) or Arias Intensity may better correlate with earthquake damage for some types of buildings. However, correlation of plant and equipment performance with any seismological parameters is much more complex. Advances in the use of Experience Data have been made, but the possible combinations of plant type, support conditions, performance requirements and possible input motion are so numerous that it is unlikely that anything less than full seismic qualification by analysis will prove satisfactory. Therefore, given that it is now possible to carry out multiple time history analysis on desk top computers relatively quickly, is it possible to replace the piecewise linear response spectra and its matched time histories by a suite of real time histories scaled to an appropriate pffhga? If so, what are the criteria for selecting appropriate the time histories for use in the design of structures, plant and equipment?

P120 For natural hazards, the uncertainty of data may prevent reasonable prediction of events for frequencies less than once in 10 000 years. In these cases, plants should meet the requirements of P25 for a design basis event that conservatively has a predicted frequency of being exceeded no more than once in 10 000 years. Plants which cannot give rise to doses as high as those specified in P25 may be designed against more frequent, i.e. less onerous, events.

P121 It should be shown that there will not be a disproportionate increase in risk from an appropriate range of events which are more severe than the design basis event.

P125 In all cases either site specific or, if this is not appropriate, best available relevant data should be used to determine the magnitude of the hazard.

P128 The seismology and geology of the area around the proposed site and the geology of the site should be evaluated. Information on historical and instrumentally recorded earthquakes which have occurred in the region should be established. The extent of the studies carried out by the licensee should cover all those aspects which could affect the estimation of the seismic hazard at the site.

P129 A design basis earthquake (DBE) should be determined in accordance with Principle P120. This DBE should be defined in terms which will enable buildings, structures and plant in the nuclear installation to be designed to withstand safely the ground motions involved.

Table 1 Safety Principles

THE EARTH MOVES AS QUAKE ROCKS BRITAIN

Figure 1. Newspaper Headline for a Magnitude 4.8 Earthquake in the UK in September 2002

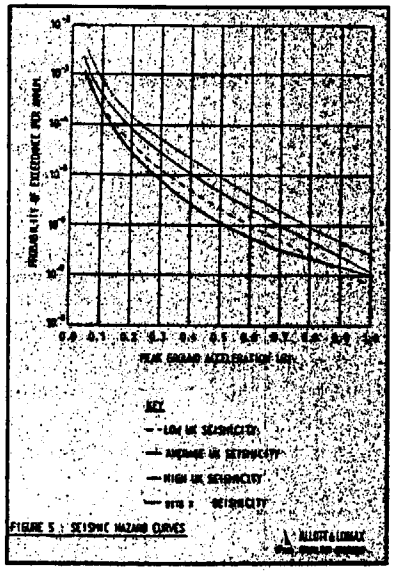

Figure 2. Seismic Hazard Curves

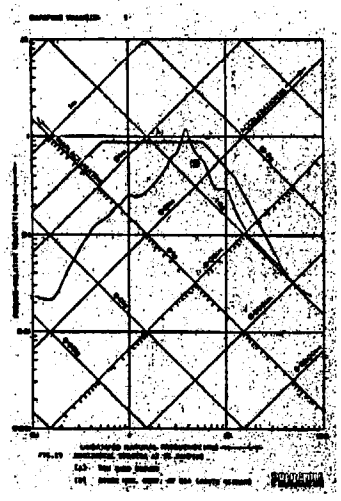

Figure 3. Piecewise Linear Response Spectrum

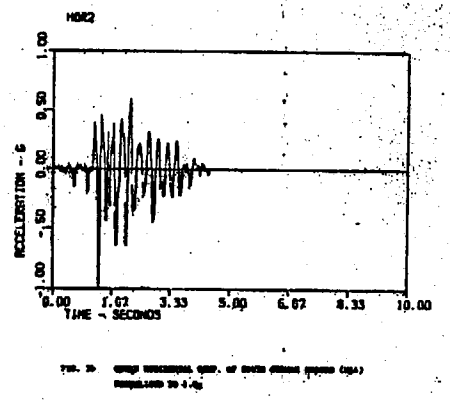

Figure 4. Strong Motion from UK dataset

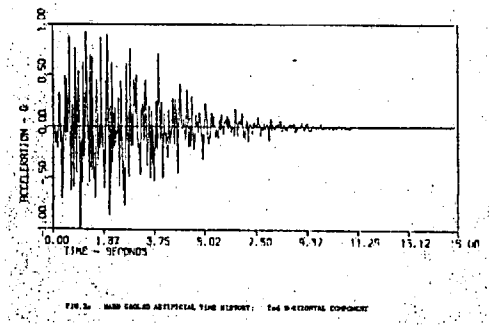

Figure 5. Spectrum Matched Time History

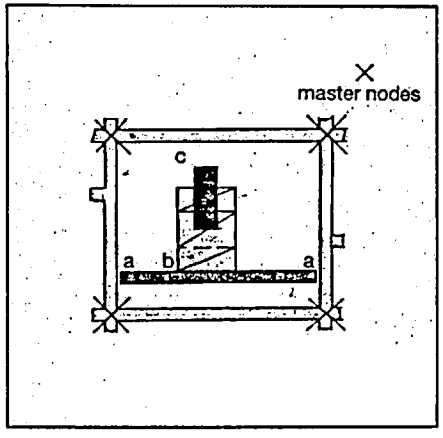

Figure 6. Typical Plant Support System

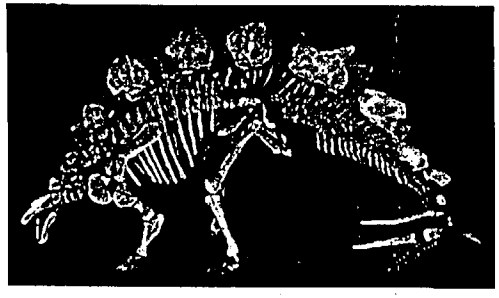

Figure 7. Dinosaur Skeleton

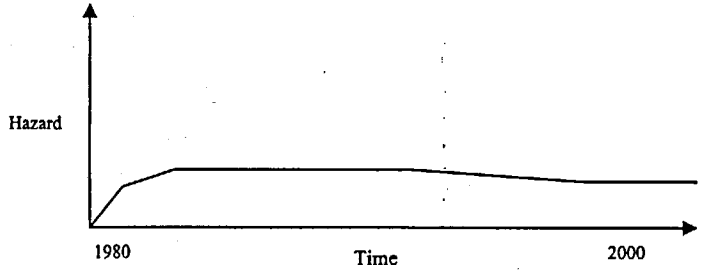

Figure 8. Hazard Development

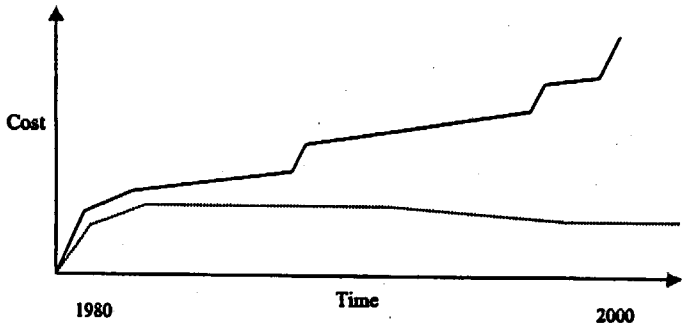

Figure 9. Cost Development

RESPONSE SPECTRA FOR DESIGN PURPOSE OF STIFF STRUCTURES ON ROCK SITES

Shizuo Noda, Kazuhiko Yashiro
Tokyo Electric Power Company, Japan

Katsuya Takahashi, Masayuki Takemura, Susumu Ohno
Kajima Corporation, Japan

Masanobu Tohdo
Toda Corporation, Japan

Takahide Watanabe
Ohsaki Research Institute, Japan

ABSTRACT

For seismic design of nuclear power facilities, we propose an empirical method for evaluating response spectra and time-dependent features of horizontal and vertical earthquake ground motions on free rock surfaces. A response spectrum of horizontal motion on seismic bedrock is given by a control point in the matrix by four magnitudes M and four equivalent hypocentral distances X_{eq}. The response spectra for other M and X_{eq} are determined by interpolation between values in the matrix. The response spectra of the horizontal and vertical motions on the free rock surface are determined by multiplying the horizontal motion on the seismic bedrock by the amplifications of horizontal and vertical motions due to surface layers, which are given as functions of S- and P-wave velocities on the free rock surface, respectively. The proposed evaluation method adequately explains near-source observation records.

Introduction

Earthquake ground motion evaluation methods used for seismic design of structures are roughly classified into empirical, semi-empirical, and theoretical methods [1]. Empirical methods have been widely used as a standard for calculating the response spectrum to be used for seismic design of nuclear power facilities (e.g., Reference 2). This paper discusses and proposes an empirical method for evaluating the response spectra of horizontal and vertical earthquake ground motions on the surfaces of rock mostly composed of Tertiary or older strata, as a reasonable method for establishing a design-basis earthquake ground motion for seismic design of nuclear power facilities.

The earthquake ground motion evaluation method proposed here uses the earthquake magnitude, equivalent hypocentral distance, and elastic wave velocity on the ground at the evaluation point as evaluation parameters. The method is organized so as to reflect, as accurately as possible, actual earthquake ground motion observations. The major features of the method are that (1) it empirically evaluates earthquake ground motion amplification by the surface layers overlaying seismic bedrock using the elastic wave velocity on the ground at an evaluation point, (2) it includes the effect of the extension of the fault on earthquake ground motion so that it can be applied to near-source regions, (3) it can evaluate earthquake ground motion with periods from 0.02 to 5 seconds, which are longer than those in Ref. 2, and (4) it can evaluate both horizontal and vertical motions.

Response Spectra of Earthquake Ground Motion on Free Rock Surface

The response spectra of horizontal and vertical ground motions with periods from 0.02 to 5 seconds on free rock surfaces are evaluated by multiplying the horizontal earthquake ground motion on seismic bedrock by the amplifications of horizontal and vertical motion due to surface layers. Figure 1 shows a schematic flowchart for evaluating the horizontal ground motion.

Horizontal Ground Motion on Seismic Bedrock

The response spectrum S_b (T) of a horizontal earthquake ground motion on seismic bedrock, which is the acceleration response spectrum (cm/s^2) with a damping factor of 5%, is obtained from the pseudo-velocity response spectrum pSv (T) (cm/s) of the period T (s) represented by the control point in Table 1. To determine a control point pSv from an arbitrary magnitude M (the Japan Meteorological Agency Magnitude (JMA) or its equivalent) and an equivalent hypocentral distance X_{eq} that are not directly found in Table 1, $\log pSv$ is interpolated by M first and then by $\log X_{eq}$.

Here, the equivalent hypocentral distance X_{eq} (km) is the distance between an evaluation point and a point source that would produce the same seismic wave energy as the total seismic wave energy that arrives at the evaluation point radiated from the extended fault plane. This is given by [3]

$$X_{eq}^2 = \int e_m X_m^2 ds \Big/ \int e_m ds, \tag{1}$$

where X_m is the distance (km) from the evaluation point to each small segment m in the fault plane, e_m is the relative distribution of seismic wave energy released from each segment m, and ds is the segment area (km^2).

e_m is the distribution of seismic wave intensity released from the fault plane in a period range for response spectrum evaluation. Although it has energy dimensions here, a relative distribution can be used instead. Therefore, the distribution of the square of the slip D_m can substitute for the e_m distribution. Because such a distribution is rarely predicted before an earthquake, calculations can

assume that σ_m is uniformly distributed (i.e., constant) over the fault plane. Figure 2 illustrates the pseudo-velocity response spectrum for each control point in Table 1.

Horizontal Ground Motion on Free Rock Surface

The response spectrum of the horizontal ground motion on the free rock surface at the control point with a specified period is calculated as follows. We multiply the horizontal ground motion spectrum on the seismic bedrock for the control point by the amplification of horizontal motion due to the surface layers. The amplification is a function of both the S-wave velocity at the free rock surface and the dominant period of the surface layers between the seismic bedrock and the free rock surface.

$$S_h(T_i) = S_b(T_i) \circ \alpha_h(T_i) \circ \beta_h(T_i) \tag{2}$$

where $S_h(T_i)$ is the response spectrum (cm/s^2) of horizontal earthquake ground motion on the free rock surface, T_i is the period of control points from A to H in Table 1, $S_b(T_i)$ is the response spectrum (cm/s^2) of horizontal earthquake ground motion on seismic bedrock from Table 1, and $\alpha_h(T_i)$ and $\beta_h(T_i)$ are amplifications of horizontal motion by the surface layers expressed by Eq. (3) below.

The amplifications of seismic waves due to the surface layers overlaying the seismic bedrock depending on the S-wave velocity of the ground and the dominant period are given by the equations below.

$$\alpha_h(T_i) = \begin{cases} (V_s/V_{sb})^{-\delta_h(T_i)} & (T_i \le T_{sl}) \\ (V_s/V_{sb})^{-\delta_h(T_{sl})} & (T_i > T_{sl}) \end{cases}, \quad \beta_h(T_i) = \begin{cases} 1 & (T_i \le T_{sl}) \\ (T_i/T_{sl})^{-\log\{\alpha_h(T_{sl})\}} & (10T_{sl} > T_i > T_{sl}) \\ 10^{-\log\{\alpha_h(T_{sl})\}} & (T_i \ge 10T_{sl}) \end{cases} \tag{3}$$

where V_s is the S-wave velocity (km/s) of the free rock surface, V_{sb} is the S-wave velocity (km/s) of the seismic bedrock, T_{sl} is the dominant period of horizontal ground motion caused by the surface layers overlaying the seismic bedrock, and $\delta_h(T_i)$ is the coefficient given in Table 2.

Vertical Ground Motion on Free Rock Surface

The response spectrum of the vertical ground motion on the free rock surface at the control point with a specified period is calculated as follows. We multiply the horizontal ground motion spectrum at the seismic bedrock for the control point by the amplification of vertical motion due to the surface layers. The amplification is a function of both the P-wave velocity at the free rock surface and the dominant period of the surface layer between the seismic bedrock and the free rock surface.

$$S_v(T_i) = S_b(T_i) \circ \alpha_v(T_i) \circ \beta_v(T_i) \tag{4}$$

where $S_v(T_i)$ is the response spectrum (cm/s^2) of vertical earthquake ground motion on the free rock surface, and $\alpha_v(T_i)$ and $\beta_v(T_i)$ are amplifications of vertical motion by the surface layers expressed by Eq. (5) below.

The amplifications of seismic waves due to the surface layers overlaying the seismic bedrock depending on the P-wave velocity of the ground and the dominant period are given by the equations below.

$$\alpha_v(T_i) = \alpha_{bv}(T_i) \begin{cases} (V_p/V_{pb})^{-\delta_v(T_i)} & (T_i \le T_{pl}) \\ (V_p/V_{pb})^{-\delta_v(T_{pl})} & (T_i > T_{pl}) \end{cases}, \quad \beta_v(T_i) = \begin{cases} 1 & (T_i \le T_{pl}) \\ (T_i/T_{pl})^{-\log\{\alpha_v(T_{pl})/\alpha_{bv}(T_{pl})\}} & (10T_{pl} > T_i > T_{pl}) \\ 10^{-\log\{\alpha_v(T_{pl})/\alpha_{bv}(T_{pl})\}} & (T_i \ge 10T_{pl}) \end{cases} \tag{5}$$

where V_p is the P-wave velocity (km/s) of the free rock surface, V_{pb} is the P-wave velocity (km/s) of the seismic bedrock, T_{pl} is the dominant period of the vertical ground motion caused by the surface layers on the seismic bedrock, $\delta_v(T_i)$ is a coefficient given in Table 2, and $\alpha_{bv}(T_i)$ is the vertical-to-horizontal response spectral ratio on the seismic bedrock given in Table 2.

Table 2 assumes V_{sb} = 2.2 km/s and V_{pb} = 4.2 km/s. When V_s or V_p of the free rock surface exceeds these values, we use instead V_s = 2.2 km/s or V_p = 4.2 km/s, respectively. Figure 3 shows calculation examples of amplification by surface layers of the horizontal and vertical motions. When T_{sl} or T_{pl} does not equal the periods of the control points shown in Table 1, new control points for them are added. From the spectrum obtained above, the response spectrum for a period not equal to the period of the control points is determined by interpolation along a straight line in a diagram where the abscissa is the logarithm of the period and the ordinate is the logarithm of the pseudo-velocity response spectrum.

Time Dependent Features of Earthquake Ground Motion on Free Rock Surface

The amplitude envelope in the time domain $E(t)$ of horizontal and vertical ground motions on the free rock surface is calculated as an envelope with a build-up section from 0 to t_B, a strong-shaking section from t_B to t_C, and a coda section from t_C to t_D as shown in Fig. 4. The envelope function is

$$E(t) = (t/t_B)^2 \ (0 < t \le t_B), \ E(t) = 1 \ (t_B < t \le t_C), \ E(t) = e^{\ln(0.1) \circ (t - t_C)/(t_D - t_C)} \ (t_C < t \le t_D) \tag{6}$$

The duration t_B (s) of the build-up section and the duration $t_C - t_B$ (s) of the strong-shaking section are calculated as functions of the magnitude M. The duration $t_D - t_C$ (s) of the coda section is a function of both the magnitude M and the equivalent hypocentral distance X_{eq}. These durations are expressed by Eq. (7). Figure 4 shows examples of the envelopes.

$$t_B = 10^{0.5M - 2.93}, \ t_C - t_B = 10^{0.3M - 1.0}, \ t_D - t_C = 10^{0.17M + 0.34 \log X_{eq} - 0.6} \tag{7}$$

Response Spectra for Different Damping Factors

When the damping factor is not 5%, the response spectra of the horizontal and vertical ground motions on the free rock surface for the period of the control point are calculated by multiplying the control point's response spectra for the horizontal and vertical ground motions on the free rock surface by a correction coefficient as a function of the damping factor

$$S_h(T_i, h) = S_h(T_i) \circ \eta(T_i, h), \ S_v(T_i, h) = S_v(T_i) \circ \eta(T_i, h) \tag{8}$$

where $S_h(T_i, h)$ and $S_v(T_i, h)$ are the response spectra of the horizontal and vertical ground motions, respectively, on the free rock surface for the damping factor h. $\eta(T_i, h)$ is the correction coefficient of the response spectrum for the damping factor h, which is expressed by Eq. (9). Figure 5 shows examples of the correction coefficient.

$$\eta(T_i, h) = \begin{cases} \left\{1/\left(1 + a \circ (h - 0.05) \circ \exp\left(-b \circ T_i/T_{eq}\right)\right)\right\}^{1/2} & (T_i = T_C, \cdots, T_E) \\ \left\{1/\left(1 + a \circ (h - 0.05) \circ \exp\left(-b \circ T_C/T_{eq}\right)\right)\right\}^{1/2} & (T_i = T_B) \\ 1 & (T_i = T_A) \end{cases} \tag{9}$$

where T_{eq}, which is given by Eq. (10) below, is the duration for which an acceleration wave is assumed to have a constant intensity of the strong-shaking section and its total power equals that of the envelope's acceleration wave. Constants a and b are given by Eq. (11) below.

$$T_{eq} = 10^{0.3M-1.0} + 0.2 \cdot 10^{0.17M+0.54\log X_{eq}-0.6} \quad (10)$$

$$a = 15,\ b = 2.0\ (h < 0.05);\ a = 13,\ b = 5.0\ (h > 0.05) \quad (11)$$

On Application of the Proposed Method

Database

The evaluation method proposed in the above sections is based on an average response spectrum from references 4 and 5 obtained from regression analyses of 107 records (321 components) of 44 earthquakes observed in Tertiary or older strata. The standard error in the regression analysis was nearly independent of period and about 0.23 in common log scale (base 10).

At the above observation points, the S-wave velocity V_s ranged from 0.5 to 2.7 km/s and the P-wave velocity V_p ranged from 1.7 to 5.5 km/s. These values closely correspond to those of the free rock surface (V_s of approximately 0.7 km/s or larger [2]) and the seismic bedrock (with V_s of about 3.0 km/s [6]). This evaluation method is applicable to rock sites with elastic wave velocities within the above range. Its application to rock sites with other elastic wave velocities requires special attention, such as reinvestigation of the amplification by the surface layers. In addition, when many observation records are collected at an evaluation point, the amplification by the surface layers peculiar to the site can be evaluated by comparing the observation records with the estimates on the seismic bedrock by the present evaluation method. However, as a rule, recorded data to be used in this case should be within the range of data used by this evaluation method.

The range of data used in the regression analysis is shown in Table 3. The range of magnitudes for the control points was up to $M = 8.5$, as shown in Table 1, and the control points corresponding to $M > 7.0$ were determined by extrapolation. Nevertheless, it was shown that results obtained from the regression equation agreed closely with records of large earthquakes inside and outside Japan [4,5]. Therefore, the control points at $M = 8.0$ were determined from this regression equation [7]. However, because there were no observation records for comparison, the control points for $M = 8.5$ were extrapolated from those for $M = 8.0$ by a theoretical examination based on a fault model. The time-dependent characteristics and the response spectrum correction coefficient due to damping factor are also based on analysis of earthquake records in the above database.

As all hypocentral depths of the earthquake in the regression data were less than 60 km, and about 80 % of the earthquakes occurred at subduction zones, the proposed method is basically aimed at evaluation of a subduction-zone earthquake. Accordingly, for shallow earthquakes at inland active faults or deep earthquakes within a subducting slab, or for near-source regions at which the long-period pulse become predominant, the following corrections or considerations become necessary.

Evaluation of shallow inland earthquakes

Using the regression data and K-NET data (the K-NET has been widely installed in Japan since the Kobe earthquake of 1995 [8]), we divided these data into two categories: data of subduciotion-zone earthquakes and data of shallow inland earthquakes. We took the spectral ratios between the observations and the estimates by the present method for all categorized data.

The data ranges used for analysis are summarized in Table 3. M-Xeq distributions and the

epicentral map of the data are shown in Fig. 6 and Fig. 7. The stations at which shear-wave velocity within 20m-depth exceeds 0.7 km/s were used. To avoid the effect of soil response by the soft layers shallower than the layer of Vs≥0.7 km/s, the period range longer than twice the soft layer's predominant period were analyzed.

Figure 8 shows the average and the average plus/minus the standard deviation of the spectral ratios. The estimates agree with the observations for the subduction-zone data as the average is close to one, while the estimates for the shallow inland earthquake overestimate the observations. Accordingly, the present method explains the subduction-zone data well, as expected, and corrections become necessary in application to shallow inland earthquakes. As the spectral ratios shown in Fig. 8 are nearly independent of M and X_{eq}, we establish the correction coefficient ζ for the shallow inland earthquakes based on this spectral ratio as

$$\zeta(T_I) = 0.6\ (T_I \le T_E),\ \zeta(T_I) = 10^{\log(0.6)+\log(T_u/T_I)/\log(T_u/T_E)}\ (T_E < T_I). \quad (12)$$

This result means that the amplitudes of the shallow inland earthquake data are smaller than those of the subduction-zone earthquake data. This is probably because (1) the JMA magnitude scale, which is used in this study, tends to be overestimated for shallow inland earthquakes compared with its proper earthquake scale [9], and (2) the radiation strength of the short-period amplitude of shallow earthquakes is smaller than that of deep earthquakes because of the different rigidities of the source media.

Evaluation of Intermediate Depth Earthquakes

Reference 10 reports that the short-period amplitude for an earthquake with a focal depth deeper than 60 km is greater than that for shallower earthquakes, even for the same magnitude and source-to-site distance. It also reports that short-period amplitudes for such intermediate-depth earthquakes have regional variations. Therefore, the evaluation of the response spectrum for an intermediate depth earthquake needs a site-dependent investigation based on the records observed around the evaluation site.

Evaluation of Near-Fault Rupture Directivity (NFRD) Effect

The dominance of the fault-normal component with periods from one to a few seconds has been reported in the near-source records of shallow inland earthquakes such as the 1995 Hyogo-ken Nanbu (Kobe) earthquake, Japan. The reason for this phenomenon is that the horizontal component perpendicular to the fault strike grows larger in the direction of rupture propagation due to the combined effects of rupture propagation and the fault mechanism. Therefore, attention must be paid to such effects in the evaluation of near-fault ground motion. Reference 11 describes the range in which the NFRD effect is dominant and also describes a method for correcting the response spectrum for this effect. For correction of the NFRD effect based on Reference 11, the corrected spectrum can be obtained by multiplying the correction factor λ, where

$$\lambda(T_I) = 1\ (T_I \le T_D),\ \lambda(T_I) = 10^{\log(2.5)+\log(T_I/T_D)/\log(T_u/T_D)}\ (T_D < T_I), \quad (13)$$

by the response spectrum obtained by the evaluation method proposed in this paper.

Figure 9 compares the response spectra of the observation record at Kobe University during the Hyogo-ken Nanbu earthquake of 1995 and the record at Sakarya during the Kocaeli earthquake of 1999 with the estimates by this evaluation method. At Sakarya, the NS (Fault-normal) component was not observed. As both were shallow inland earthquakes, the correction by Eq.(12) was applied in the estimation. In spite of the fact that the stations are located very close to the faults, the proposed

method can explain the observation records well. Still, by the correction of Eq. (13), the correspondence between the estimate and the observation improve for the NS (Fault-normal) component of Kobe Univ.

Conclusions

We proposed a method for empirically evaluating response spectra and time-dependent features of horizontal and vertical earthquake ground motions on a free rock surface, based on analysis of observation records on rock. This method should be useful for calculating design-basis earthquake ground motion used for seismic design of nuclear power facilities. We also showed that the evaluation method could adequately explain observations of near-source regions.

Acknowledgments

This study was jointly funded by ten electric power companies in Japan. Because of their helpful guidance, we also thank the late Emeritus Prof. Syun'itiro Omote of Kyushu Industrial University, former Prof. Makoto Watabe of Keio University, Prof. Motohiko Hakuno of Kogyokusha College of Technology, and Emeritus Prof. Hiroyoshi Kobayashi of Tokyo Institute of Technology.

References

1. The Architectural Institute of Japan, "Earthquake Motion and Ground Conditions," Part III. Prediction of Strong Ground Motion and Its Application to Earthquake Engineering, Chapter 1, Simulation and Prediction of Strong Ground Motion, The Architectural Institute of Japan, 1993.
2. Hisada, T., Ohsaki, Y., Watabe, M. and Ohta, T., "Design Spectra for Stiff Structures on Rock," Proc. of the 2nd International Conference on Microzonation for, Vol. III, pp.1187-1198, 1978.
3. Ohno, S., Ohta, T., Ikeura, T. and Takemura, M., "Revision of Attenuation Formula Considering the Effect of Fault Size to Evaluate Strong Motion Spectra in Near Field," Tectonophysics, Vol. 218, pp.69-81, 1993.
4. Takahashi, K., Takemura, M., Tohdo, M, Watanabe, T. and Noda, S., "Empirical Response Spectral Attenuations on the Rocks with Vs = 0.5 to 3.0 km/s in Japan," Proc. of the 10th Japan Earthquake Engineering Symposium, pp.547-552, 1998 (in Japanese with English Abstract).
5. Kawano, H., Takahashi, K., Takemura, M., Tohdo, M., Watanabe, T. and Noda, S., "Empirical Response Spectral Attenuations on the Rocks with Vs=0.5 to 3.0 km/s in Japan," Proc. of the 12th World Conference on Earthquake Engineering, Reference No. 953, 2000.
6. Kobayashi, H. and Midorikawa, S., "A Semi-Empirical Method for Estimating Response Spectra of Near-Field Ground Motions with regard to Fault Rupture," Proc. of the 7th European Conference on Earthquake Engineering, pp.161-168, 1982.
7. Nishimura, I., Noda, S., Takahashi, K., Takemura, M., Ohno, S., Tohdo, M. and Watanabe, T., , "Response Spectra for Design Purpose of Stiff Structures on Rock Sites," Transactions, SMiRT 16, Paper # 1133, 2001.
8. Kinoshita, S., "Kyoshin Net (K-NET),"Seism. Res. Lett., 69, pp.309-332, 1998.
9. Takemura, M., "Magnitude - Seismic Moment Relations for the Shallow Earthquakes in and around Japan, " Zisin, 2nd Series, 43, pp.257-265, 1990 (in Japanese with English Abstract).
10. Kato, K., Takemura, M., Ikeura, T. and Yashiro, K., "Excitation Strength of High-frequency Seismic Motion due to Intermediate Depth Earthquakes," Proc. of the 10th Japan Earthquake Engineering Symposium, pp.673-678, 1998 (in Japanese with English Abstract).
11. Ohno, S., Takemura, M. and Kobayashi, Y., "Effects of Rupture Directivity on Near-Source Strong Motions," Proc. of the 2nd International Symposium on the Effects of Surface Geology on Seismic Motion, pp. 1163-1170, 1998.

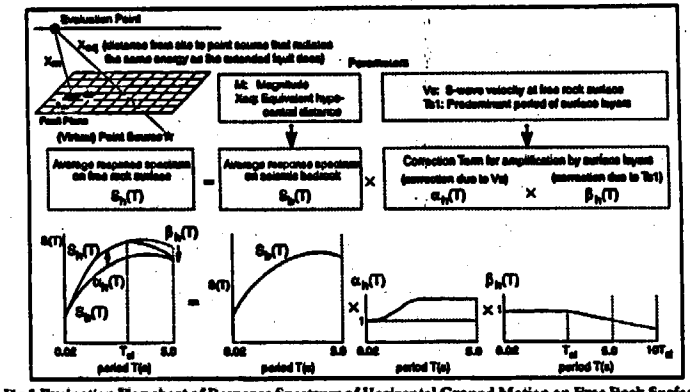

Fig.1 Evaluation Flowchart of Response Spectrum of Horizontal Ground Motion on Free Rock Surface

Table 1. Control Points of Horizontal Earthquake Motion on Seismic Bedrock

Field	M	Xeq (km)	Coordinates of Control Points pSv (cm/s) A TA(s) 0.02	B TB(s) 0.09	C TC(s) 0.13	D TD(s) 0.3	E TE(s) 0.6	F TF(s) 1	G TG(s) 2	H TH(s) 5
Very Near	8.5	40	1.62	18.44	27.32	47.87	68.05	64.66	53.52	40.06
	8	25	1.69	20.05	28.96	48.22	67.80	65.25	52.51	38.35
	7	12	1.40	17.20	24.84	33.86	43.42	38.42	25.15	17.85
	6	6	1.04	12.82	18.51	21.84	23.17	17.41	9.64	3.88
Near	8.5	80	0.73	7.36	11.43	22.92	34.79	32.58	27.80	21.96
	8	50	0.67	7.45	11.17	20.05	28.65	27.06	22.70	17.19
	7	20	0.78	9.44	13.84	19.10	24.83	20.69	14.48	10.37
	6	8	0.77	9.45	13.65	16.23	17.18	12.73	7.16	2.89
Intermediate	8.5	160	0.26	2.22	3.87	9.45	15.17	14.83	13.64	12.26
	8	100	0.32	3.08	4.86	10.27	16.04	14.96	12.73	10.37
	7	50	0.23	2.65	4.01	6.02	7.64	6.68	4.87	3.64
	6	25	0.21	2.49	3.80	4.54	4.84	3.98	2.07	0.86
Far	8.5	200	0.18	1.44	2.43	6.87	11.17	11.17	10.67	10.04
	8	200	0.10	0.80	1.35	3.82	6.21	6.21	5.93	5.58
	7	125	0.046	0.43	0.70	1.34	1.81	1.59	1.28	1.05
	6	78	0.041	0.45	0.65	0.95	1.03	0.80	0.49	0.22

The value of pSv is pseudo-velocity response spectrum with a damping factor of 5%.

Table 2. Coefficients $\delta_h(T)$, $\delta_v(T)$, and $\alpha_{hv}(T)$

	A TA(s) 0.02	B TB(s) 0.09	C TC(s) 0.13	D TD(s) 0.3	E TE(s) 0.6	F TF(s) 1	G TG(s) 2	H TH(s) 5
$\delta_h(T)$	0	0.03	0.05	0.35	0.48	0.61	0.80	0.83
$\delta_v(T)$	0.12	0.28	0.42	0.67	0.90	1.03	1.10	1.09
$\alpha_{hv}(T)$	0.58	0.55	0.52	0.59	0.56	0.60	0.70	0.75

The coefficients are common for all combinations of M and Xeq

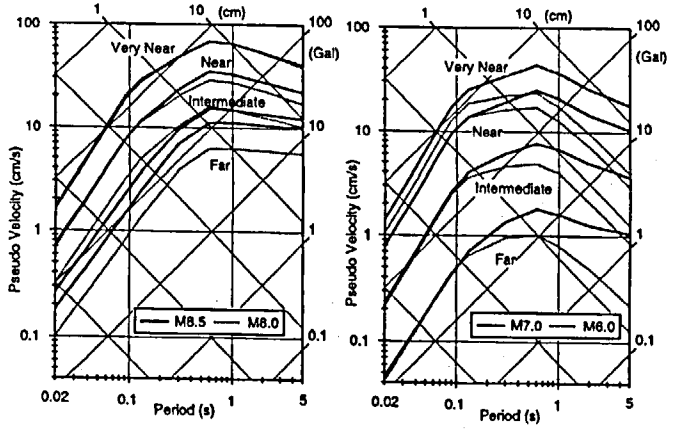

Fig. 2 Response Spectra of Horizontal Earthquake Motions on Seismic Bedrock at the Control Points in Table 1.

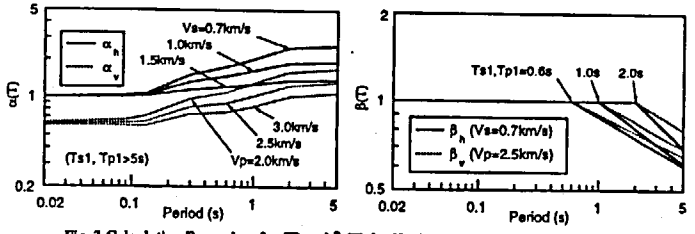

Fig. 3 Calculation Examples of α (T) and β (T) for Horizontal and Vertical Ground Motions

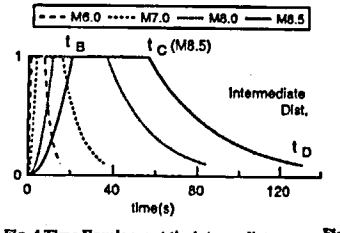

Fig. 4 Time Envelopes at the Intermediate distances of the Control Points in Table 1.

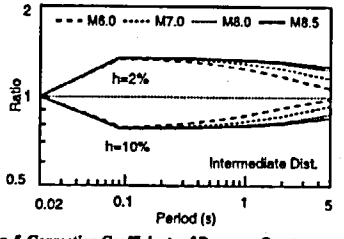

Fig. 5 Correction Coefficients of Response Spectra for Different Damping Factors at the intermediate distances of the Control Points in Table 1.

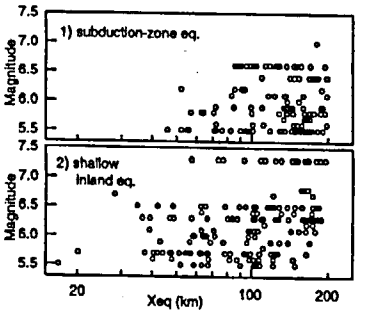

Fig. 6 M-Xeq distribution of the data used for analysis in Fig. 8.

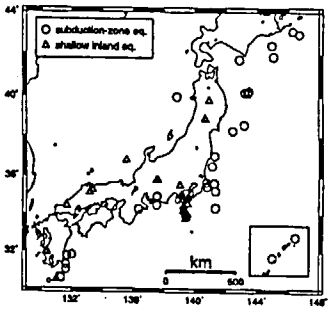

Fig. 7 Epicenter distribution of the earthquakes used for analysis in Fig. 8.

Table 3. Data Range used for analysis

	Data for regression analysis in Ref. 4,5	Data for applicability check in Ref.7	Data used in this paper	
			subduction-zone eq.	shallow inland eq.
Magnitude	5.5 - 7.0	5.4 - 8.1	5.5 - 7.0	5.5 - 7.3
Xeq (km)	28 - 202	14 - 218	46 - 199	17 - 195
Vs (m/s)	≥500	≥550	≥700	≥500
Number of Records	107	37	124	170

All data satisfy 1) Focal depth ≤ 60km, 2) Observation sites belong to stratum of tertiary or older.

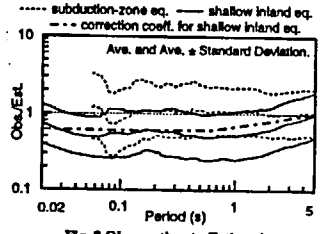

Fig. 8 Observation-to-Estimation Response Spectral Ratios

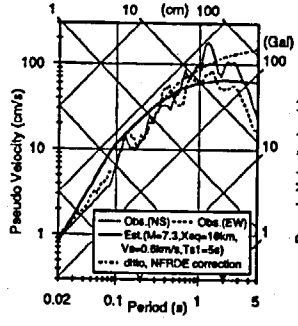

(1) 1995 Hyogo-ken Nanbu (Kobe) Eq., Kobe Univ. station, Japan

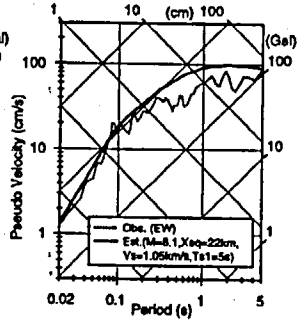

(2) 1999 Kocaeli Eq., Sakarya station, Turkey

Fig. 9 Application Examples of the Evaluation Method to Near-Source Records.

LONG TERM SEISMOLOGICAL HAZARD ASSESSMENT FOR MORSLEBEN SITE: DETERMINISTIC AND PROBABILISTIC APPROACH

Günter Leydecker[1] & Jürgen R. Kopera[2]
[1]Federal Institute for Geosciences and Natural Resources, Germany
[2]Consultant for Engineering Seismology, Germany

Abstract

Existing and planned nuclear waste repositories in the Federal Republic of Germany are situated in areas of low seismicity. Nevertheless, seismic hazard assessment has to be performed for a very long time period in order to prove the facilities of the repositories to withstand seismic induced loads. As an example, the site of the former salt mine Morsleben, which now is a nuclear waste repository, is investigated. A combination of deterministic and probabilistic methods is used to assess the seismic hazard for this site in Northern Germany. The probabilistic evaluation has the advantage of quantifying the seismic hazard. Both methods together are a practical tool for mutual control of the results and to overcome the deficiencies of each approach alone. The combination of both, seismicity and structural geology, provides the basis for a long term seismic hazard assessment with probabilities of exceedance in the order of 10^{-5} per year. The following parameters are derived: site intensity as a function of exceeding probability; site acceleration; strong motion duration; site dependent response.

1. Introduction

An important aspect for the selection of a suitable site for a nuclear waste repository is the seismic activity of the area. The existing repository and potential sites under investigation are situated in Northern Germany, an area of very low seismicity. There is a considerable debate whether or not it is possible to quantify the seismic risk in such an area. An attempt to do this will be presented in this paper. As an example we will use the site of a nuclear waste repository, the former salt mine Morsleben. This site is situated near the southern border of the Northern German Lowlands, about 100 km east of Hannover.

A deterministic and a probabilistic approach will be applied for the seismic hazard assessment of the Morsleben site. The deterministic approach follows the German regulations for nuclear power plants, the "Technical Safety Guide" of the KTA (Nuclear Safety Standard Commission). The probabilistic method is based on the works of Cornell (1968) and McGuire (1976). The comparison of the results of both methods finally should lead to more realistic seismic load assumptions for the selected site.

[1] guenter.leydecker@bgr.de Tel.: +49-511-643-2867; Stilleweg 2, 30655 Hannover / Germany
[2] bis_kopera@hotmail.com Tel.: +49-511-6101 442 ; Seerosenstrasse 10 B, 30916 Isernhagen / Germany

2. Seismic activity in Germany

The distribution of epicenters in Germany is shown in fig. 1. The map contains all registered and felt earthquakes for the time period from 800 to 2001 (Leydecker, 1986; 2002) and it gives an impression of the seismicity of the site area. The epicenters are plotted together with the "seismogeographic regions", the result of the recent regionalisation of Germany (Leydecker & Aichele, 1998). The subdivision of Germany into seismogeographic regions is not only based on the distribution of epicenters, but also on the tectonic structures and the geological development of the area. Therefore, these regions are used in the following investigation as "tectonic units" with respect to the regulation guide KTA 2201.1 (1990) and as "seismotectonic provinces" with respect to the IAEA Earthquake Safety Guide (International Atomic Energy Agency, 1991).

Relatively high seismicity in southern Germany is observed in the Alps, the lake of Constance area and the Swabian Jura, south of Stuttgart. The activity follows the river Rhine through the Upper Rhine Graben from Basel to Frankfurt and north-westward into the Lower Rhine Area. In eastern Germany, Central Saxony and the swarm-quake area of Vogtland near the Czech border are zones of relatively high activity. Isolated events up to the macroseismic epicentral intensity VI MSK (macroseismic scale; s. Sponheuer, 1965) have occurred in the northern parts of Germany, the area of interest. It is covered by thick sedimentary deposits of about 3000 to 4000 m and includes big salt domes and salt structures.

3. Deterministic approach

For nuclear power plants and nuclear installations, the regulations of the technical safety guide (KTA 2201, 1990) are obligatory for Germany. From this we have to estimate the so called "design earthquake". This is the earthquake with the highest intensity at the site which can take place, from a scientific point of view, in an area of about 200 km around the site.

Following the instructions of the deterministic approach in the regulation guide KTA 2201.1 (1990), the tectonic unit in which the site is situated has to be determined. The site Morsleben is located inside the seismogeographic region Altmark. The three strongest events in this area are historical earthquakes in the years 997, 1202 and 1409. They reached intensities up to VI MSK. Taking into account that the maximum possible earthquake has not occurred in our observation time of approximately 1200 years, the maximum epicentral intensity in the Altmark is assumed to be half a unit higher, that is VI-VII MSK. We thus assume that an earthquake of intensity VI ½ MSK will occur at the nearest potential seismogenic structure. This structure has to be identified.

The site Morsleben is situated near the border of the Northern German Basin, a region where subsidence prevailed since Permian time. Therefore sediments of some thousand meters thickness were accumulated over the folded basement (Carboniferous and older). Salt layers (Permian) of more than 1000 m which later formed salt domes and pillows were important for the structural development.

In detail, Morsleben is situated (fig. 2) at the northeastern border of the NW-SE striking Allertal zone. The most important fault nearby is the fault zone of Haldensleben, which is parallel to the Allertal zone to its NE. The shortest distance of the fault zone of Haldensleben to the site is 17 km, but it plunges southwestwards deep into the crust and also under the site. The last main activity phase of the Haldensleben faulted zone was in middle Upper Cretaceous. Smaller creeping movements occurred

0.5 or 2 Ma years ago. The main stress field in Central Europe shows a NW-SE orientation of the principal compressional axis (Ahorner, 1975, 1982; Müller et al. 1992). As the fault is parallel to this direction, a reactivation is very unlikely. Only on parts of the fault with a favorable strike direction, earthquakes with small rupture areas and therefore with moderate magnitude seem possible.

As a consequence the Haldensleben fault has to be assumed as the potential seismogenic structure for the design earthquake. As the Haldensleben fault plunges beneath the Allertal zone, an earthquake at this fault with the epicentral intensity VI-VII MSK will lead to the same intensity at Morsleben.

4. Probabilistic approach

The widely accepted probabilistic approach used in our investigation was developed by Cornell (1968) and was transferred into a numerical algorithm by McGuire (1976). The method is based on a specific probabilistic mathematical model. It assumes that the distribution of the parameter epicentral intensity follows a Poisson process. The Poisson probability distribution can be expressed in the form:

$$P_k(x) = \frac{(\lambda \cdot \Delta T)^k}{k!} \cdot \left[\exp(-\lambda \cdot \Delta T)\right] \qquad (1)$$

which is the probability of k successes of an arbitrary event x in a given unit of time ΔT. λ is defined as the expected number of occurrences of this event and k! means the factorial of k.

In terms of earthquakes: $P_k(x : i_0 \geq I_0)$ is the probability of having k earthquakes with epicentral intensities [3] $i_0 \geq I_0$ during a time interval ΔT. λ is defined as the average rate that an intensity I_0 will be exceeded in a given spatial area and a time interval of normally one year. The Poisson distribution is valid for rare and independent events, therefore pre- and aftershocks as well as nontectonic earthquakes have to be excluded from the data catalogue. From eq. (1), the probability that no event (k=0) will occur during the time interval ΔT is simply

$$P_0(x) = \left[\exp(-\lambda \cdot \Delta T)\right] \qquad (2)$$

Seismic risk (better called "seismic hazard", if we do not consider the consequences of earthquakes for people or structures) is defined as the probability that at least one earthquake (i.e. $k \geq 1$) with epicentral intensity i_0 equal or greater I_0 will take place within the time interval ΔT. As the secure event has the probability P = 1 the seismic hazard can be expressed as

$$P(i_0 \geq I_0) = 1 - \left[\exp(-\lambda \cdot \Delta T)\right] \qquad (3)$$

One of the principles of Cornell's method is that epicenters are not uniformly distributed over the entire area of investigation. The earthquakes are bounded to seismic source regions, the seismotectonic units. The epicenters inside these source areas are assumed to be statistical uniformly distributed. The seismic source areas can then be characterized by the statistic distribution of epicentral intensities. The cumulative number N_e of events with epicentral intensities I_0 within a source area is assumed to obey the following Gutenberg-Richter relation:

$$\log_{10}(N_e) = a - b \cdot I_0 \qquad (4)$$

The cumulative number $N_e^*(I_0) = N_e / T_{obs}$ of events x: $i_0 \geq I_0$ in a region per unit of time, with the observation period T_{obs}, is called the seismic activity rate $\nu(I_0)$ of that region.

[3] Small letters define the stochastic variable of the parameters in capitals.

Taking into account the parameters focal depth H, attenuation coefficient α, lower and upper intensity limits I_{min}, I_{max}, an appropriate attenuation law like Kövesligethy's and further relations (for details see Leydecker & Kopera, 1999), the contributions of all seismic source regions to the site intensity I_S are calculated and their expected values are summed up. The probability of exceedance for a site intensity I_s, caused by the m-th source region, can be represented in the most basic form by the theorem of total probability

$$\lambda_m(i_S \geq I_S) = \int_R \int_{I_{min}}^{I_{max}} P(I_S \mid I_0, R) \cdot f_{I_0}(I_0) \cdot f_R(r)\, dI_0\, dr \qquad (5)$$

where the distribution function $P(i_S \geq I_S | Io, R)$ represents the conditional probability of the random variable i_S reaching or exceeding the value I_S at the site, under the condition that an epicentral intensity I_0 has occurred at an epicentral distance R. Assuming stationary conditions, the seismicity of the source area is characterized by the probability density functions f_{I_0} and f_R. They specify the frequency distribution of epicentral intensities I_0 and the distribution of epicenters with distance R to the site. The average rate per year that an intensity I_s will be exceeded, is obtained by summing up the expected values of all source areas:

$$\lambda(I_S) = \lambda(i_S \geq I_S) = \sum_m \nu_m \cdot \lambda_m(I_S) \quad , \qquad (6)$$

where $\nu_m = \frac{N_e(I_{0\min})}{T_{obs}}$ defines the activity rate of the m-th source region (s. tab. 1).

Finally, to calculate the seismic hazard at the investigated site, $\lambda(I_S)$ is used in the Poisson distribution of eq. (3)

$$P(i_S \geq I_s) = 1 - e^{-\lambda(I_s)} \qquad (7)$$

where $P(i_S \geq I_s)$ gives the annual ($\Delta T = 1$) probability, that the intensity I_s will be reached or exceeded at the investigated site.

5. Seismotectonic models

The three seismogeographic regions, Southern Altmark, Central Saxony and Vogtland, are used to establish seismotectonic models for the investigated site (fig. 1). From all possible models that were tested, only two seem reasonable. In **model 1** only Central Saxony and Vogtland and in **model 2** all three regions are taken as seismic sources, applying the approach of McGuire (1976). The tectonic earthquakes outside these source areas but inside the 200 km radius around the site are considered as seismic background activity. The events of the seismic background are assumed as uniformly distributed over the remaining area. The parameters of the seismotectonic models are summarized in tab. 1.

The low seismicity in the wider vicinity around the site is shown in fig. 1. Only the north-western parts of the active regions Central Saxony and Vogtland, south-east of the site, are within 200 km distance. The different seismicity of the seismotectonic regions and of the seismic background is reflected in the activity rate of intensity (tab. 1). The number of events N_e of Southern Altmark is barely sufficient for a statistical analysis. Therefore model 1 is preferred in which the effects of the active but distant regions Central Saxony and Vogtland are considered, using the remaining earthquakes as background activity.

Table 1: Parameters of seismic source regions and seismic background activity

Seismic source region	begin of selected time interval		focal depth	cumulat. number of events[1]	I_{max} observed	linear regression (intensity interval)[2]		activity rate[3]	
	year	with I_0	km	Nc		a	b	v	for I_0
Southern Altmark (sAM)	997	6.0	6 / 8	9 ($I_k \geq 4$)	6.0	1.903 (4 - 6)	0.239	0.0089	4
Central-Saxony[4] (CS)	823	7.0	8	69 ($I_k \geq 4$)	7.5	3.20 (5 - 8)	0.354	0.0519	4
Vogtland (VG)	868	5.5	10	174 ($I_k \geq 5$)	8.0	5.233 (5 - 8)	0.585	0.1807	5
Background BG_1	997	6.5	8	19 ($I_k \geq 5$)	6.5	4.564 (5 - 7)	0.639	0.00212	5
Background BG_2	1079	5.0	8	14 ($I_k \geq 5$)	6.5	4.053 (5 - 7)	0.573	0.00175	5

BG_1 = Background area, excluding the source regions CS and VG (model 1)
BG_2 = Background area, excluding the source regions sAM, CS and VG (model 2)
For all regions, an absorption coefficient of $\alpha = 0.001$ [km^{-1}] was used for the intensity attenuation.
[1] Half intensity values are accounted to the next higher intensity class I_0, e.g. I_0 = III-IV and I_0 = IV belong to $I_k = 4$. To exclude fore- and aftershocks for the Vogtland region, $I_0 \geq 5$ is used.
[2] The intensity interval for the regression analysis in the frequency distribution eq. (4) was selected individually, depending on the data. The intensity limits are given in parenthesis.
[3] The activity rate for the background is calculated for an area of 200 km around the site and normalized to 10 000 km^2. The areas and activities of source regions within the background are excluded.
[4] The seismotectonic region Central Saxony was modified for this investigation. Its southern boundary was moved northwards, to coincide with the northern boundary of the Erzgebirge. As a consequence, CS is completely included in the 200 km zone around the site.

Applying eq. (7) gives the annual probabilities of exceedance for macroseismic intensities at the site (fig. 3). Curves 1 to 4 are the results of model 2 with three seismic source regions and seismic background, while curve A1 and A2 were calculated for model 1. The numerical upper intensity limit I_{max} in each source area is assumed to be half a unit respectively one intensity unit higher than the maximum observed value. This takes into account, that the observation period was probably too short for the maximum possible earthquake to occur in the area of 200 km around the site, or that historical records of these events are lost.

6. Seismic load assumptions

From the deterministic approach, a site intensity of 6 ½ MSK is estimated: The probabilistic calculations give a site intensity of 5.6 MSK for a probability of exceedance of 10^{-4} per year and 6.4 MSK for 10^{-5} (curve A2 in fig. 3). For nuclear installations a probability level of 10^{-5} per year is widely applied[6]. As mentioned above, the geological development and the tectonics of the area of Morsleben are well known. The latest activity of the nearest fault zone of Haldensleben is probably more than 0.5 Ma ago. We believe that the stable geological conditions of this area over such a time span permits us to extrapolate the probability calculations to a level of 10^{-5} per year.

This can be summarized to:
deterministic approach ⇒ site intensity I_s = 6 ½ MSK
probabilistic approach ⇒ site intensity I_s = 6.4 MSK with $P(I_0 \geq I_s) = 10^{-5}$ per year

Both methods have led to comparable results. A probabilistic evaluation quantifies the hazard assessment, but deterministic and probabilistic approaches together provide a practical tool for mutual control of the results and to overcome the deficiencies of each method alone. A probability of exceedance of 10^{-5} per year is an appropriate level for long term safety aspects.

The maximum horizontal component of acceleration is derived from the high frequency values of the response spectra (Hosser, 1987) in the next chapter (fig. 4). A factor of $\sqrt{2}$ is applied to estimate the resultant maximum horizontal acceleration. The maximum vertical acceleration is assumed as 50 % of the horizontal acceleration (KTA 2201.1). The intensity- and site-specific strong ground motion duration is taken from Hosser (1987). The acceleration inside a mine is commonly expected to be lower than at the surface. However for conservative reasons, the same intensity inside the mine as at the surface is assumed. The response spectrum and the strong motion duration inside the mine are determined for rock conditions. The results are summarized in tab. 2.

Table 2: Seismic load assumptions (design earthquake) for the site of Morsleben at the surface and inside the mine

	at surface	inside mine
site intensity I_s	VI ½ MSK	VI ½ MSK
probability of exceedance	$< 10^{-5}$ / year	$< 10^{-5}$ / year
maximum horizontal acceleration (resultant)	113 cm/s^2	99 cm/s^2
maximum vertical acceleration	57 cm/s^2	50 cm/s^2
strong motion duration	4 s	1.5 s

7. Response spectra

The seismic load assumptions, resulting from the design earthquake, have to be expressed in terms of response spectra. A catalogue of response spectra for three classes of site intensities and for three soil classes was developed on the basis of mostly European strong motion records (Hosser, 1987). In contrast to standard response spectra, which had to be scaled by a single value of horizontal acceleration, site-specific response spectra are preferred here, because they are defined with respect to the site intensity of the design earthquake and the dynamic behavior of the subsoil.

The used site-specific response spectra are 50 % fractile spectra belonging to a design earthquake with a probability of exceedance of 10^{-5} per year. After Hosser (1986) this corresponds with a 84 % fractile response spectra and with the widely used probability of exceedance of 10^{-4} per year. The response spectra of the resultant horizontal acceleration (fig. 4) for the Morsleben site are valid for the

site intensity 6 ½ MSK with a probability of exceedance less than 10^{-5} per year. The local geological conditions of the shallow subsoil, known from several borehole logs, are laterally rapidly changing. Therefore the site had to be classified as a mixture of soft and medium stiff subsoil. Inside the mine, rock conditions must be assumed.

8. Conclusions

The Morsleben mine is situated in an area with very low seismic activity. It is obvious that in such a region seismic hazard assessment is difficult to realize. We have tried to do this by a combination of deterministic and probabilistic methods. In both cases, assumptions had to be made which are not free of subjective weighting. Seismic source areas had to be defined, and in each of them parameters like maximum earthquake, focal depth and absorption coefficient had to be fixed. A transparent presentation of all these parameters is vital for an assessment of the quality of the results.

Because of the required long term stability of a nuclear waste repository, a probability of exceedance of at least 10^{-5} per year for the design earthquake is demanded. The limited German earthquake history covers 1200 years with various completeness over the time. An extrapolation up to a mean recurrence period of 10 000 years appears tenable. This limit of 10 000 years can only be overcome by incorporating detailed information on the tectonic history of the last million years. For Morsleben the last activity of the nearest and most important fault was more than 0.5 Ma ago. This justifies to assign a probability of exceedance of 10^{-5} per year to the design earthquake.

The deterministic approach in an area of low seismicity can be dominated by a single strong shock. This may result in an overestimation of the design earthquake. The probabilistic evaluation has the advantage to quantify the seismic hazard and allows a judgement of the reliability of the deterministically estimated design earthquake. Both methods together form a practical tool for mutual control of the results and to overcome the weakness of each approach alone.

References

Ahorner, L., 1975. Present-day stress field and seismotectonic block movements along major fault zones in Central Europe. Tectonophysics 29, 233-249.

Ahorner, L., 1982. Seismicity and neotectonic structural activity of the Rhine graben system in Central Europe. In: A.R. Ritsema, Gürpinar, A. (Eds.), Seismicity and Seismic Risk in the Offshore North Sea Area. Reidel Publishing Comp., Dordrecht. 101-111.

Baldschuhn, R., Frisch, U. & Kockel, F. (1996): Geotektonischer Atlas von NW-Deutschland 1:300 000. - Teil 17: Strukturübersicht 1 : 500 000. -- Bundesanstalt f. Geowissenschaft. u. Rohstoffe, Hannover, Germany.

Cornell, C.A., 1968. Engineering seismic risk analysis. Bull. Seis. Soc. America, Vol. 58, 5, 1583-1606.

Hosser, D., 1987. Realistische seismische Lastannahmen für Bauwerke. Ergebnisse einer interdisziplinären Forschungsarbeit. Bauingenieur 62, 567-574, Springer Verlag.

IAEA, 1991. Earthquakes and associated topics in relation to nuclear power plant siting. A safety guide. Safety series No. 50-SG-S1 (Rev. 1). International Atomic Energy Agency, Vienna, 60 pp.

KTA 2201, 1990. Sicherheitstechnische Regel des KTA Auslegung von Kernkraftwerken gegen seismische Einwirkungen. Fassung 6/90. Kerntechnischer Ausschuss (KTA). Carl Hauptmanns Verlag, Köln, Berlin.

Leydecker, G., 1986. Erdbebenkatalog für die Bundesrepublik Deutschland mit Randgebieten für die Jahre 1000 - 1981. Geol. Jb., E 36, 3-83, Hannover.

Leydecker, G., 2002. Earthquake catalogue for the Federal Republic of Germany and adjacent areas for the years 800 till 2001. – Datafile http://www.bgr.de/quakecat ; Federal Institute for Geosciences and Natural Resources, Hannover/Germany.

Leydecker, G., Aichele, H., 1998. The Seismogeographical Regionalisation of Germany: The Prime Example for Third-Level Regionalisation. Geol. Jb., E 55, 85-98. Hannover.

Leydecker, G., Kopera, J.R., 1999. Seismological hazard assessment for a site in Northern Germany, an area of low seismicity. – In: Langer, M. & C. Talbot (Eds.): The status quo on nuclear waste isolation. - Engineering Geology 52, 293-304; Elsevier.

McGuire, R.K., 1976. FORTRAN Computer Program for Seismic Risk Analysis. US Department of the Interior, Geological Survey: Open-File Report 76-67. 90 pp.

Müller, B., Zoback, M.L., Fuchs, K., Mastin, L., Gregersen, S., Pavoni, N., Stephansson, O., Ljungreen, C., 1992. Regional patterns of tectonic stress in Europe. J. Geophys. Res. 97, 783-803.

Sponheuer, W., 1965. Bericht über die Weiterentwicklung der seismischen Skala (MSK 1964). Dtsch. Akad. d. Wiss., Veröff. Inst. Geodynamik, Jena, Heft 8, Akademie Verlag, Berlin, 117 pp.

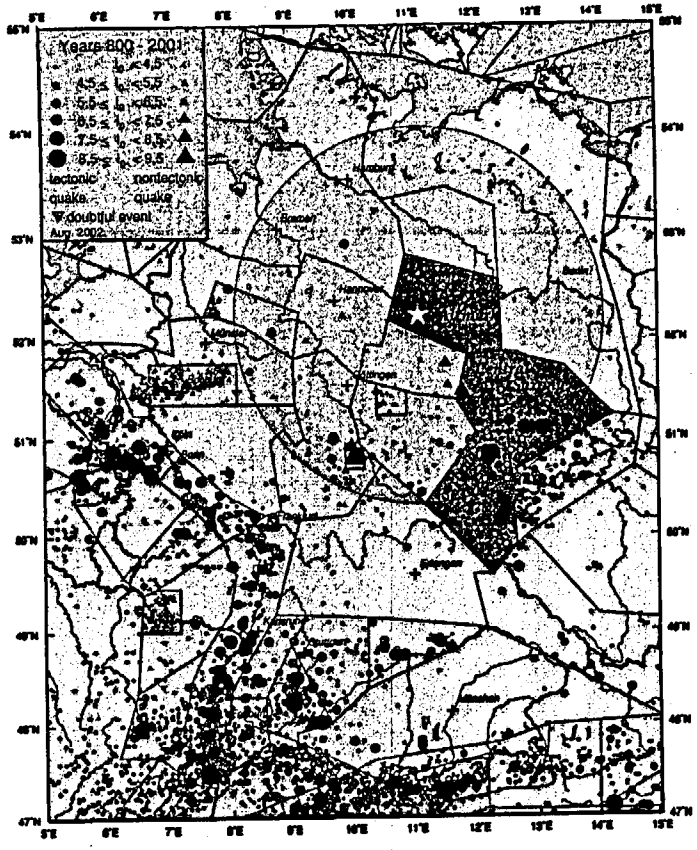

Fig. 1: Earthquake epicenter map for Germany and border regions for the years 800 - 2001 (Leydecker, 1986, 2002) together with the seismogeographic regions (straight line segments) (Leydecker & Aichele, 1998). The size of the earthquake symbols corresponds to the epicentral intensity Io. Io < 4.5 means also non felt events. –
★ Morsleben, radius of circle 200 km, Altmark = southern part of Altmark.

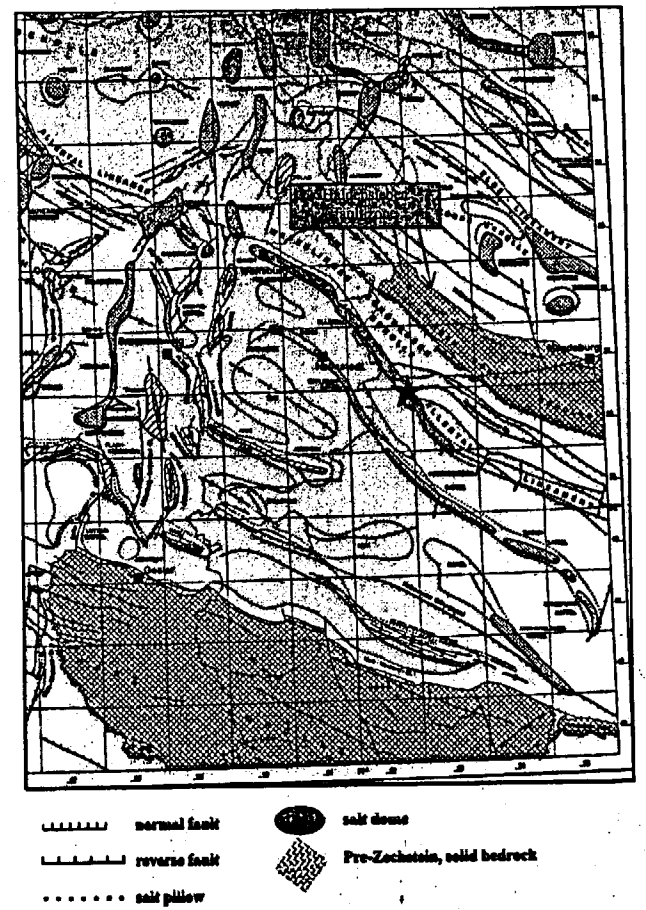

Fig. 2. Structural geology of the Allertal zone (Baldschuhn, Frisch & Kockel 1996)
★ = Morsleben site

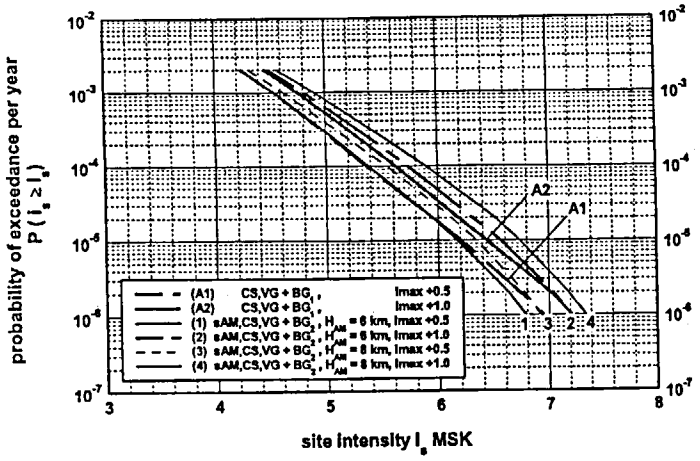

Fig. 3. Annual probability of exceedance for earthquake intensities at Morsleben site. Curve A1 and A2 are the results of model 1 with two sources: Central Saxony and Vogtland and the seismic background BG_1. Curves 1 to 4 are calculated for model 2 with the two sources of model 1 plus Southern Altmark (H_{AM} = focal depth) and the background activity BG_2.

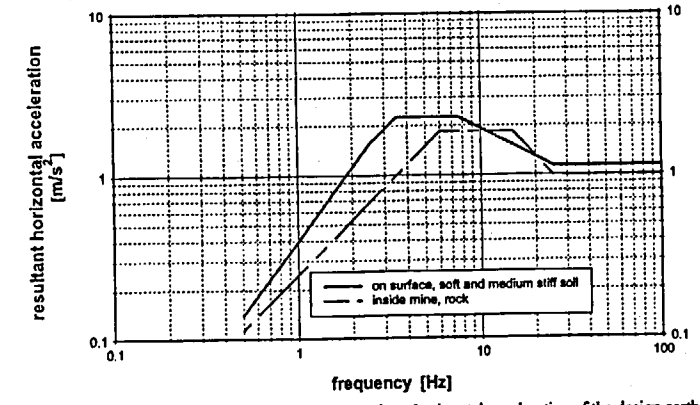

Fig. 4. Response spectra (5 % damping) of the resultant horizontal acceleration of the design earthquake with intensity 6 ½ MSK at Morsleben site. Soil conditions at surface: soft and medium stiff; inside mine: rock.

METHODOLOGY TO PRODUCE HAZARD CONSISTENT FREE-FIELD AND IN-STRUCTURE DESIGN RESPONSE SPECTRA

C. J. Costantino, Professor Emeritus, City University of New York
W. J. Silva, Senior Scientist, Pacific Engineering and Analysis, El Cerrito CA
R. K. McGuire, Risk Engineering, Boulder, CO
R. M. Kennedy, Senior Structural Engineer, USNRC, Washington, DC
A. J. Murphy, Senior Technical Advisor, USNRC, Washington, DC

Abstract

This report summarizes recommendations recently published by the USNRC in NUREG/CR-6728 [9] for development of seismic ground motions to be used in the design and analysis of nuclear facilities. The recommendations for response spectral shapes are developed for western US (WUS) and central/eastern US (CEUS) rock site conditions. Procedures to develop corresponding response spectra at the ground surface for soil sites have also been developed, using as input the recommended rock site spectra. Recommendations for use of these newly developed ground motion estimates in SSI analyses are not as yet complete. Procedures to determine consistent estimates of structural member loads and in-structure response spectra are in the process of development for use in design.

Introduction

Recommendations for prediction of seismic design ground motions for nuclear facilities require a consistency with both the observed strong motion data set and with seismological theory on the characteristics of strong shaking. The recommendations need to capture the potential effects of regional differences in source characteristics and crustal properties to be appropriate for application to various regions of the US. In this study, recommendations for spectral shapes were first developed for WUS rock sites based primarily on characteristics of California strong motion recordings. For the CEUS sites, numerical modeling was used to quantify the differences between WUS and CEUS motions to account for anticipated differences in both seismic source and path properties. A well-validated model was used for prediction of strong motion [17] to quantify the effect of these characteristics. This model was used to adjust the WUS empirical soft-rock spectral shapes to corresponding CEUS hard-rock conditions. The spectral shape recommendations have been made using both 1-corner and 2-corner seismic source models considered appropriate for the CEUS.

The procedure recommended to develop facility design response spectra begins with the development of a probabilistic seismic hazard analysis (PSHA) for rock site conditions. The PSHA is then used to obtain the uniform hazard spectrum (UHS) at the appropriate annual frequency of

exceedance, which is typically set at or near the 10^{-4} level for the design of nuclear facilities. The seismic hazard is then deaggregated at the 1 and 10 Hz structural frequencies to determine dominant magnitudes and distances at the design exceedance level. The spectral shapes incorporated into the attenuation models used in the PSHA need to be consistent with those contained in these recommendations. In the CEUS, both 1- and 2-corner source models need to be considered to obtain weighted spectral shape recommendations. Finally, the spectral shapes associated with the deaggregated events are then scaled to match the UHS amplitudes at appropriate low (1 Hz) and high (10 Hz) structural frequencies.

For design recommendations for structures founded on rock, the UHS is then modified by a Scale Factor to determine a Uniform Reliability Spectrum (URS). The purpose of the Scale Factor is to achieve a relatively consistent annual frequency of plant component failure across the range of plant sites and structural frequencies. It is intended to account for differences in the slope of the seismic hazard curve, which changes with both structural frequency and site location, as well as the fragility curve of plant component equipment. The Scale Factor to convert the UHS to the URS may be either greater or less than unity, depending upon values of these particular parameters.

Historical Perspectives

The development of ground motions, as described by the approaches described in the Standard Review Plan (SRP) [14], attempts to reflect the current state of the uncertainty in ground motion estimation methods, together with limitations of available data. Its objective is to provide reasonable assurance that the ground motion at any site would be conservatively estimated. Recent studies [6] have shown that it is difficult to capture the total uncertainty in ground motion prediction even with the large number of strong motion recordings now available in California.

To develop design spectra, two teams were organized by NRC [10, 12] to separately analyze almost identical data sets. Each team used different normalization schemes to develop spectral shapes. In both studies, amplification or scale factors on peak ground motion parameters were derived from statistical analyses of normalized shapes to construct smooth design spectra for varying fractile and damping levels. In the Blume study, a single normalization parameter, peak ground acceleration (A), forms the basis for the shapes with scaling factors specified at fixed anchor points. In the Mohraz study, spectral amplification factors on peak ground acceleration (A), peak ground velocity (V), and peak ground displacement (D) were developed to construct the design spectrum. The spectral shape, based on A, V, and D, does to some extent accommodate site and magnitude dependencies in terms of the parameters V/A and AD/V^2 ratios.

Based on the two studies, NRC adopted and formalized a slightly modified form of the single parameter shape [12] as a recommendation in RG1.60 [15]. The single parameter scaling results in a spectral shape that is source, path and site independent. A limitation that resulted from the small size of the data set available at the time and the normalization procedure used was that both the fractiles and damping scaling were not well constrained and were not uniform with structural frequency. The RG1.60 horizontal spectral shape was generally considered representative of an 84th fractile from an

event of magnitude about 6.75 occurring at a distance about 20-30 km from a deep soil site. Recommendations for corresponding vertical spectra were reasonable for distances in the 20-40 km range for soil sites and about the 10-20 km range for rock sites. Based on recent empirical data, the appropriateness of these factors at other distances is considered questionable.

More Recent Observations

Recent studies show that the dependence of spectral shapes on source, path, and site conditions is well constrained by both recorded motions and the results of well-validated modeling [17]. In general, shapes broaden and show a shifting of the peak spectral amplification to lower frequencies with increasing magnitude due to a decrease in the earthquake source comer frequency [18, 19]. Site dependencies are reflected in an increase in spectral levels at low frequencies and a decrease in levels at high frequencies as site stiffness decreases due to a combination of site amplification and material damping.

To capture some of these known effects in the development of design ground motions, it was considered necessary in this study to use the theoretical-empirical modeling method to realistically estimate ground motions, particularly for sites in the CEUS. The method [17] uses the empirical data from the relatively large database currently available to constrain results generated from the theoretical model. The approach develops a theoretical estimate of the ground motion spectrum based on parameters of the fault rupture (magnitude, stress drop) and travel path (distance, crustal and surficial rock properties). In regions where only few recordings of strong shaking, are available the parameters are estimated with empirical data from seismograph records. In addition, site-specific geologic and site soil information can be quantitatively incorporated directly into the ground motion estimation at any particular site.

Characteristics of Strong Ground Motions at CEUS AND WUS Rock Sites

Observations of strong ground motion due to small magnitude earthquakes occurring in CEUS, although not causing damage to engineered structures, have shown considerably higher peak accelerations than would have been expected based upon WUS experience. In addition to the relatively higher peak accelerations associated with these CEUS events, response spectral ordinates appear richer in high frequency energy, particularly for frequencies exceeding about 10 Hz. It has been known for some time that ground motion for CEUS attenuate less rapidly with distance than ground motion in WUS for events of similar moment magnitudes and source depths [2, 6]. The difference in attenuation rate has been attributed to the higher absorptive characteristics generally present in the crust and upper mantle beneath WUS as compared to CEUS.

The trends shown in available CEUS data indicate significantly higher spectral content at high frequencies as compared to WUS rock motion of comparable magnitudes and distances [7, 18]. The difference in spectral content can perhaps be most easily seen in spectral amplification (SA/A) computed from recordings from WUS and CEUS rock sites. Figure 1 shows average spectral shapes (SA/A) computed from recordings made on rock at close distances ($\leq$ 25 km) for magnitudes of approximately 6.75 and 5.75 earthquakes in CEUS and WUS tectonic environments. The differences

are significant and indicate that the magnitude of spectral content is higher in CEUS events than that in WUS for frequencies greater than approximately 10 Hz.

The controlling mechanism for the differences in high frequency spectral content (at close distances) between WUS and CEUS ground motions is thought to be due to differences in damping in the shallow (1 to 2 km) part of the crust. The parameter which controls the shallow damping is termed kappa and is defined as the thickness of the zone over which the damping is taking place times the damping and divided by the average velocity over zone of damping or

$$\kappa = H / (V_s Q_s) \text{ and } Q_s = 1/(2\eta_s) \quad (1)$$

where H is the thickness of the shallow crustal damping zone (1 to 2 km), V_s is the average shear-wave velocity over the depth H, Q_s is the average quality factor over depth H, and η_s is the corresponding average hysteretic damping ratio (in decimal terms)

An example of generic crustal models reflecting typical WUS soft rock and CEUS hard rock crustal conditions is shown in Figure 2 for both compression and shear wave velocities. The CEUS model is the midcontinent crustal model [6] and is considered appropriate for strong ground motion propagation in CEUS except for the Gulf Coast region. The Gulf Coast region is typified by a crustal structure somewhat intermediate between those of the CEUS and WUS and is predicted to have correspondingly different wave propagation characteristics. The shallow portion of the WUS crustal model, with $V_s \leq 1$ km/sec, is based on velocities measured at strong motion rock sites. Such sites generally show very low near surface (0 to 30m depth) shear and compression wave velocities.

The differences in the shallow crustal velocities between the WUS and CEUS models is striking, particularly over the top 2 to 3 km, and its effect on strong ground motions is profound. In terms of amplification from source regions below about 5 km to the surface, the differences between hard (CEUS) and soft (WUS) crustal conditions results in a difference of a factor of near 3 in amplification for frequencies exceeding about 5 Hz. All else being equal, WUS high frequency ($f \geq 5$ Hz) ground motions would then be expected to be nearly three times larger than corresponding CEUS motions. However, damping in the shallow crust, parameterized through kappa, is much greater in soft crustal rocks, resulting in a dramatic loss in high frequency energy content as compared to hard rock conditions, counteracting the effects of the lower velocities.

Effects of Source Processes on Model Predictions

Another issue of consideration regarding the differences in spectral composition between WUS and CEUS strong ground motions at rock sites is the probable differences in earthquake source processes. Prior to the occurrence of the 1998 magnitude 5.8 Saguenay earthquake, there was thought to be a difference of about two in stress drop (the difference in stress across the rupture surface before and after an earthquake) between WUS and CEUS sources. Typically, the CEUS was assumed to exhibit larger values of about 100 bars as compared to about 50 bars for WUS sources. These measures of stress drop, termed Brune stress drops, are primarily based on high frequency ground motion levels

assuming a single-corner frequency source model. Apart from the differences in stress drop, overall source processes were thought to be similar in both tectonic regimes. The stochastic single-corner-frequency point-source model [8] provides accurate predictions of WUS strong ground motions using a stress drop of about 50 bars although having a tendency to overpredict low frequency (≤ 1 Hz) motions for large magnitude earthquakes.

For the CEUS, the simple point-source model with a stress drop of about 100 bars, about double that of the WUS, provided good agreement with existing data until the occurrence of the 1988 magnitude 5.8 Saguenay earthquake. Strong ground motions from this earthquake depart significantly from predictions of the simple 100 bar stress drop model. The stress drop required to match high frequency strong ground motions for this earthquake exceed 500 bars, causing intermediate frequency spectral levels to be overestimated by a factor of two or more. In addition, source spectra generated from teleseismic data from large intraplate earthquakes differ in general from the simple single-corner-frequency omega-square model, showing the presence of a second corner frequency. Based on the limited ground motion data in the CEUS as well as inferences on intensity observations, an empirical two-corner source model [3] was developed for CEUS earthquakes. In this model, the high frequency spectral levels are consistent with a Brune stress drop of about 150 bars while the equivalent stress drop for the low frequency spectral levels is about 40 to 50 bars.

This two-corner model currently provides unbiased estimates of recorded CEUS ground motions over the frequency range of the majority of the data, from about 0.1 to 10.0 Hz, while the single-corner-frequency model, with stress drops ranging from about 120 to 150 bars, overpredicts low frequency ground motions in the frequency range of about 0.1 to 1 Hz but is unbiased in the 2 to 10 Hz frequency range. Both the double and single corner source models, with actual or implied stress drops below 200 bars, underpredict the high frequency (≥ 2 Hz) ground motions for the Saguenay earthquake by factors of 2 to 3, suggesting anomalous high frequency levels for this event. While it currently appears that a two-corner source model may be more appropriate for CEUS strong ground motions, it is evident that in predicting strong ground motions for engineering design, significantly more variability needs to be accommodated in applications to the CEUS than to the WUS. This increased variability should accommodate both randomness (aleatory variability) in stress drop above that for the WUS as well as uncertainty (epistemic variability) in the source model.

A model which appears to be more consistent with WUS source spectra inferred from the strong motion data is similar to the CEUS two corner model but with a less pronounced spectral sag at intermediate frequencies. The two-corner nature of WUS source spectra is filled-in by crustal amplification resulting in a comparatively subtle feature in strong ground motions compared to CEUS data [1].

Comparison of WUS and CEUS Spectral Shapes

To characterize the differences in WUS and CEUS ground motion models, a few comparisons are presented in the following discussion. Much more detail is presented in NUREG/CR-6728. Comparisons of WUS to CEUS response spectra are shown in Figures 3 and 4 for shapes and absolute

spectra respectively. Also illustrated in the Figures are the differences between the single and double corner source spectral models. With regard to spectral shapes, Figure 3, the difference in spectral composition between the WUS and CEUS single corner models (solid lines) is clearly illustrated in the maximum spectral amplifications. The spectral peak occurs at about 5 Hz for WUS events and 40 Hz for CEUS. The difference between the single and double corner source models (solid verses dashed lines) is also clearly illustrated. For the WUS, the difference is mainly at low frequency and is not large, about 20% near 0.3 Hz. For the CEUS, the single corner source model significantly exceeds the double corner below about 2 Hz. The largest difference occurs near 0.4 Hz and is a factor of over 3 in 5% damped spectral acceleration. Choices between the two shapes for the CEUS, single or double corner, clearly have major impacts on implied motions.

The corresponding absolute spectra are shown in Figure 4. The WUS and CEUS single corner spectral estimates are nearly the same for frequencies up to about 5 Hz. This is the result of compensating effects previously discussed, higher stress drop for CEUS and larger crustal amplification factors for WUS. Beyond about 5 Hz, the differences in kappa (crustal damping) values (0.04 sec as compared to 0.006 sec) results in the differences in high frequency spectral estimates.

Comparison of Model and Statistical Shapes at Rock Sites

To see how well the simple point-source models (single and double corner frequency) capture the differences in shapes between WUS and CEUS rock motions, Figures 5 and 6 compare model predictions to statistical shapes available for magnitude 6.5 to 7.0 (6.75) bins from 10 to 50 kms. Figure 5 for WUS data compares both the single and double corner model predictions to the statistical shape. Both models capture the overall shape reasonably well but overpredict at low frequency (below 1 to 2 Hz). The double corner model provides a better fit but still shows overprediction in this magnitude range.

Figure 6 presents the corresponding comparison for CEUS data. Unfortunately, there is only one earthquake, 1985 Nahanni, with hard rock site recordings (3 stations) in this distance range. Both spectral models capture the difference in shape between WUS and CEUS equally well with the single corner frequency model showing an overprediction at low frequency (≤ 1 Hz) similar to the WUS. The double corner model shows an underprediction for frequencies below about 2 Hz. However, the lack of data available for CEUS strong ground motions reflects the current state of uncertainty regarding CEUS strong ground motion predictions.

Figures 7 and 8 show similar comparisons for magnitude 5.0 to 5.5 events for WUS and CEUS respectively. For the WUS, Figure 7 shows reasonable model predictions down to about 1 Hz, below which the number of spectra are rapidly dropping out due to increasing noise levels. Figure 8 shows the corresponding plot for CEUS. The models capture the shift in shape to higher frequency but overpredict for frequencies above about 20 Hz. As with the comparisons with the larger magnitude 6.75 bins, the low frequencies are enveloped by the two models. Again, model departures at high frequency for the CEUS bin, reflects the paucity of data available. These comparisons to CEUS statistical shapes point out the quandary in estimating strong ground motions in the CEUS. Sufficient

recordings at close distances (≤ 50 km) for earthquakes of engineering significance are currently not available to unequivocally distinguish between plausible ground motion models.

Based upon the empirical data base and associated attenuation models available for WUS rock sites, a functional form was developed which allows prediction of response spectral shapes given magnitude and distance of any event. For the WUS events, the form of the relationship is not based on a physical model of the ground motion process but is designed to fit the general characteristics of the empirical spectral shapes. For WUS sites, the functional form is given by:

$$\ln (SA/A) = [\, C1/\cosh(C2*f^{C3}] + C4\, [\exp (C5*f)/f^{C6}] \qquad (2)$$

The coefficients C1 through C6 are functions of magnitude and distance and are provided in Table 1. The first term in equation 2 is designed to fit the high frequency portion of the response spectral shape while the second term models the low frequency portion of the curves.

The approach used to develop spectral shapes for CEUS rock site conditions were based on the results from numerical modeling. Scaling relationships were first developed to convert WUS to CEUS spectral shapes. These scaling functions were then applied to the weighted empirical functional forms available for the WUS statistical shapes to develop comparable CEUS spectral shapes. The resulting functional form for response spectral shapes appropriate for CEUS sites is given by:

$$\ln (SA/A) = [\, C1/\cosh(C2*f^{C3}] + C4\, [\, \{\exp (C5*f)/f^{C6}\} + \{\, C7 \exp (C8*f)/f^{C9}\} \,]^{0.5} \qquad (3)$$

The parameters C1 through C9 are again functions of magnitude and distance and are listed in Table 1.

For comparison purposes, the results obtained for the developed spectral shapes are compared with the standard spectral shapes defined by RG1.60 [15] or Newmark-Hall (N-H) 0098 spectra [11]. For the N-H comparisons, average bin values for A, V and D for WUS sites were used to develop median and 1-sigma design spectral shapes. For WUS rock sites, Figure 9 indicates a reasonably good comparison of the predicted bin shapes with the N-H shapes, provided the recommended bin peak velocity is used in the N-H development. If the higher recommended values are used, the comparison of shapes is not as good and the N-H model is not supported by the empirical data. Comparisons with the RG1.60 shape indicate that it is generally conservative, particularly for the smaller magnitude events.

Comparison with similar data for CEUS rock sites is shown in Figure 10, including predictions for both 1- and 2-corner source models. The N-H shapes were generated using the WUS mean bin values since they are not available for CEUS sites. The CEUS shapes are lower at low frequencies than either set of standard spectra. Since CEUS peak accelerations are higher than the corresponding

WUS values, the WUS and CEUS absolute spectra are comparable at low frequency while the CEUS absolute spectra is higher than the WUS data and peaks at much higher frequencies.

Development of Hazard-Consistent Motions at Soil Sites

The approach to developing site-specific soil motions involves convolution analysis, using either equivalent-linear or fully nonlinear characterization of soil properties, and using rock outcrop control motions at the soil/rock transition zone. For "bottomless" profiles the rock control motions may be input at a sufficiently deep location such that soil amplification extends to the lowest frequency of interest. This depth has generally been about 500 ft for motions adequate to a low-frequency limit of about 0.5 Hz [16].

To develop procedures and results appropriate for soil sites at either WUS and CEUS locations, the point source model was first exercised to develop PSHA results for two sites, one in the WUS (site in Southern California) and one in the CEUS (site in South Carolina). Relatively complete hazard information for these sites was available in terms of the suite of magnitudes and distances that contribute to the seismic hazard. Model parameters appropriate for these two locations (source characteristics, rock properties, stress drops, etc.) were used to generate appropriate PSHA data. The rock outcrop UHS for both the WUS and CEUS sites are shown in Figure 11 at the 10^{-4} annual probability of exceedance level. As can be seen, the WUS motions generally exceed the CEUS motions by a factor of five or more for frequencies below about 10 Hz. The deaggregated earthquake spectra at 1 and 10 Hz, scaled back to the UHS, are shown in Figures 12 and 13 respectively. The difference in the hazard environment between WUS and CEUS sites is evident by noting the difference in deaggregated magnitudes dominating the 1 and 10 hz frequencies (1.3 units for the CEUS site and 0.6 units for the WUS site).

The WUS site profile was developed using the Imperial Valley soil configuration extended to a depth of 1,000 feet while the CEUS soil site was developed from the Savannah River site data. The base case shear wave velocity profiles are shown in Figure 14. Strain degradation data for the two sites used in the convolution studies were based on either generic models or site-specific data considered appropriate for the site [9]. In the convolution analyses, uncertainty in dynamic material properties was accommodated through inclusion of parametric variations, using a Monte Carlo approach with the equivalent-linear site response calculation. Uncertainty in shear wave velocities and damping were based on statistical distributions available for the sites. For each input control motion, a number of convolution calculations were performed, with soil properties randomly selected from available site data, to obtain mean estimates of surface response and associated transfer functions.

The various approaches used to develop site-specific soil surface spectra following this procedure are listed below in the order of increasing difficulty: In each approach, the UHS rock outcrop spectra described previously and its deaggregated information at low and high frequency are used as input to the site response problem to varying degrees of completeness.

Approach 1: Use the rock UHS as the rock outcrop control motion.

Approach 2A: Use the deaggregated earthquake spectra at 1 Hz and 10 Hz scaled to the UHS as control motions (R.G. 1.165 approach) or develop transfer function for 1 Hz and 10 Hz rock characteristic earthquakes, using a single control motion. The envelope of the two transfer functions is then used to scale the rock UHS.

Approach 2B: Develop weighted deaggregated earthquake spectra (typically at the 5th, 50th and 95th percentiles) at 1 Hz and 10 Hz as rock outcrop design earthquakes, accommodating magnitude distributions at each frequency. The mean of the soil surface motions for each frequency is then obtained. The envelope of the two mean surface motions is then defined as the soil surface spectrum. Alternatively, the envelope of the two mean transfer functions is used to scale the rock UHS.

Approach 3: Approximations to convolution integrations to obtain the mean transfer functions.

Approach 4: Develop the soil UHS using site-specific soil attenuation relations.

Approach 3 is a simplification to Approach 4 used to obtain the mean transfer functions. In the following, calculations using Approaches 1, 2A, 2B, and 4 are compared to determine the recommended convolution procedure. Approach 1, the simplest calculational model, involves driving the soil column with the broad rock UHS spectrum (rock control motions) and may result in unconservative high frequency motions, particularly in the context of equivalent-linear site response analyses. Approach 2A recognizes that different earthquakes may dominate the high and low frequency range of site response, which generate separate transfer functions for these average events. The use of multiple rock shapes scaled to the UHS at high and low frequencies is consistent with Regulatory Guide 1.165 [13] although not explicitly stated.

In Approach 2B, mean, high and low percentile magnitudes from the rock UHS deaggregations at the 1 Hz and 10 Hz frequencies, scaled to the rock UHS, are used as input to the site response evaluations. The resulting control motions are then used to develop weighted mean transfer functions for each design earthquake. The transfer functions, in turn, are then used to scale the rock UHS to obtain the corresponding soil surface spectrum. The use of a three-point magnitude distribution for each design earthquake better accounts for potential non-linear effects in the site response calculation caused by a wide range of earthquake magnitudes contributing to the hazard as compared to Approach 2A. In Approach 4, a site-specific soil attenuation relation is used in the hazard analysis. This approach assumes that appropriate parametric variations are incorporated in the development of the attenuation relation and that they are also reflected in the uncertainty about the median ground motions.

For the WUS site (Figure 15), the results from the calculations indicates that Approaches 2A and 2B yield very similar results, both of which are generally higher than Approach 1 (the single broad-banded UHS rock outcrop input spectrum). Nonlinear effects in the soil column cause the site to be softened more by the single input than by either of the approaches using the scaled deaggregated spectra. For the CEUS site (Figure 16), Approach 1 again tends to underestimate soil surface spectra as compared to Approach 4 while Approaches 2A and 2B are again similar and conservative above about 10 hz. Strain levels at the CEUS site are generally much lower than those at the WUS site (0.02% as compared to 0.3%) due to its generally stiffer profile and lower ground motion input. These results are typical of the various site response calculations described in NUREG/CR-6728. Approach 1, although often used for site response calculations, generally leads to underprediction of site response.

Approaches For Vertical Motions

Assessment of site specific vertical motions for soil sites to accompany corresponding horizontal motions is a much more issue, particularly if it is desirable to maintain hazard consistency with the horizontal motions. Rarely are separate hazard analyses performed for horizontal and vertical control or rock outcrop motions and there are no widely accepted site response methodologies currently available to accommodate vertical analyses. Commonly, equivalent-linear site response analyses for vertical motions have used strain iterated shear moduli from a horizontal motion analysis to adjust the compression-wave velocities assuming either a strain independent Poisson's ratio or bulk modulus. Some fraction (generally 30% to 100%) of the strain iterated shear-wave damping is used to model the compression-wave damping and a linear analyses is performed for vertically propagating compression waves using the horizontal input control motions scaled by some factor near 2/3.

Alternatively, fully nonlinear analyses can be made using two- or three-component control motions [4, 5, 6]. These nonlinear analyses require two- or three-dimensional soil models, which describe plastic flow and yielding, and the accompanying volume changes as well as coupling between vertical and horizontal motions through linear and inelastic constitutive models. While these analyses are important to examine expected dependencies of computed motions on material, the models are very sophisticated and require specification of many parameters, at least some of which are difficult to measure both in mean or central values as well as their uncertainties.

The equivalent-linear approach implicitly assumes some coupling between horizontal and vertical motions. This is necessitated by the lack of appropriate strain-dependent degradation models for the constrained modulus of the soil and corresponding hysteretic damping data. Ideally, the strain dependency of the constrained modulus should be determined independently of the shear modulus. Also, the conventional approach assumes vertically propagating compression waves and not inclined P-SV waves. More recently, use has been made of V/H ratios for rock computed from empirical attenuation relations. This process accommodates observed trends in magnitude and distance dependencies of vertical motions [6, 17] and results in vertical control motions appropriate for the controlling earthquakes. These are generally based on UHS 1 Hz deaggregation, as this usually results in the definition of the largest dominant earthquakes. Again, it would be more appropriate to use two

design spectra (e.g. at 1 Hz and 10 Hz) or envelop the 1 Hz and 10 Hz (or PGA) V/H ratios to develop a conservative vertical rock outcrop spectrum.

The approach recommended here makes use of generic soil V/H ratios to scale the site specific horizontal soil motions. It is intended to maintain as many site specific attributes as possible through the use of the horizontal soil motions (soil column) and generic soil V/H ratios (controlling magnitudes and distances) while avoiding the currently inherent ambiguity inherent in vertical site response analyses. This is the case for WUS sites where vertical and horizontal component empirical attenuation relations for soil sites are available. For the CEUS, this approach again relies on generic soil V/H ratios based on a validated site response methodology [17]. In this approach, WUS-to-CEUS scale factors are developed and used to scale an empirical WUS deep soil V/H ratio. The scale factors are ratios of WUS and CEUS V/H ratios computed for generic deep soil, representative of deep soils beneath the WUS strong motion recording sites and assumed to occur both in the WUS and CEUS. To compute the V/H ratios, a generic deep soil column is placed on the generic WUS and CEUS crustal models and the stochastic point-source model used to generate motions. Inclined P-SV waves are used as input to model the vertical motions [6, 17].

Impact on SSI Analyses

The effect of these new recommendations for site response evaluation on the computations for soil-structure interaction analyses is significant. The deterministic SSI analysis procedures currently used to develop in-structure design spectra and member design loads are not consistent with these newly recommended probabilistic approaches for developing free-field surface design ground motions. The current procedures typically used in SSI analyses make use of a time history generated to envelope a relatively broad-banded design surface response spectrum. Often the surface spectrum is defined by either a RG1.60 or N-H shaped spectrum controlled by only one or several ground motion parameters as previously described. The structural model and site geometry is specified as indicated schematically in Figure 17.

The site properties are specified in terms of their low strain values of shear wave velocity and hysteretic damping for each soil layer in the soil profile. These parameters are typically defined in terms of their best estimate, lower bound and upper bound values in an effort to capture variability of these properties over the building footprint as well as uncertainty in their specification as well as the SSI process. The broad-banded surface ground motion is then deconvolved to obtain "strain-compatible" parameters. However, since the broad-banded spectrum does not correspond to a single event, the deconvolution process leads to unrealistically high strains in the near-field soil profile and implied ground motions at depth. This problem led to the so-called "60% rule" contained in the SRP to try to prevent placing structures at depth to minimize ground motion input to the foundation.

In the new recommended procedures, surface ground motion design spectra are developed consistently; that is, the surface spectra are already associated with a compatible strain-iterated soil profile. Therefore, deconvolution of the surface ground motion is certainly no longer valid. However, procedures for development of upper and lower bound soil profiles to be used in the SSI analyses still

need to be developed. It is known, for example, that simple scaling of the site properties above and below the best estimate site profile does not necessarily bound response spectra, particularly at frequencies higher than the fundamental frequency of the soil column.

Currently, a process used to specify these bounding profiles involves selecting the ± one-sigma values of strain-iterated velocities and hysteretic damping. The lower bound damping is typically associated with the upper bound velocities and vice versa, although this selection is subjective. It is not clear as yet whether these bounding selections lead to consistent estimates of ± one-sigma values of in-structure spectra or member loads. Studies to confirm these selections are being undertaken and recommendations still need to be developed to ensure conservative estimates of mean structural demand.

References

1. Atkinson, G.M and W.J. Silva (1997). "An empirical study of earthquake source spectra for California earthquakes." Bull. Seism. Soc. Am. 87(1), 97-113.
2. Atkinson, G.M. and D.M. Boore (1995). "Ground motion relations for eastern North America." Bull. Seism. Soc. Am., 85(1), 17-30.
3. Atkinson, G.M. (1993). "Source spectra for earthquakes in eastern North America." Bull. Seism. Soc. Am., 83(6), 1778-1798.
4. Costantino, C. J. (1969), "Two Dimensional Wave Propagation Through Nonlinear Media", Journal, Computational Physics, vol. 4, no. 2, August
5. Costantino, C. J. (1967), "Finite Element Approach to Stress Wave Problems", Journal, Engineering Mechanics Division, ASCE, April
6. Electric Power Research Institute (1993). "Guidelines for determining design basis ground motions." Palo Alto, Calif: Electric Power Research Institute, vol. 1-5, EPRI TR-102293.
7. Fletcher, J.B., (1995). "Source parameters and crustal Q for four earthquakes in South Carolina. Seismological Research Letters, 66(4), 44-58.
8. Hanks, T.C., and McGuire, R.K. (1981). "The character of high-frequency strong ground motion." Bull. Seism. Soc. Am., 71(6), 2071-2095.
9. McGuire, R.K., W. J, Silva and C. J. Costantino. (2001). Technical Basis for Revision of Regulatory Guidance on Design Ground Motions: Hazard and Risk Consistent Ground Motion Spectra Guidelines, NUREG/CR-6728, Risk Engineering Inc. October
10. Mohraz, B., Hall, W.J. and Newmark, N.M. (1972). "A Study of Vertical and Horizontal Earthquake Spectra." Nathan M. Newmark Consulting Engineering Services, Urbana, IL: AEC Report No. WASH- 1255.
11. Newmark, N. M. and W. J. Hall (1978). "Development of Criteria for Seismic Review of Selected Nuclear Power Plants", NUREG/CR-0098
12. Newmark, N.M., J.A. Blume and K.K. Kapur (1973). "Seismic Design Criteria for Nuclear Power Plants." Journal of the Power Division, ASCE 99, 287-303.
13. NRC (1997). "Identification and Characterization of Seismic Sources and Determination of Safe Shutdown Earthquake Ground Motion," Regulatory Guide 1. 165, USNRC, Washington, DC.
14. NRC (1989). Standard Review Plan, USNRC, Washington, DC, NUREG-0800, Rev. 2, August

15. NRC (1973). "Design Response Spectra for Seismic Design of Nuclear Power Plants," Regulatory Guide 1.60, Revision 1, USNRC, Washington, DC.
16. Silva, W. J. R. McGuire, and C. Costantino. (2001). Comparison of Site Specific Soil UHS to Soil Motions Computed with Rock UHS, Proceedings, OECD-NEA Workshop on Engineering Characterization of Seismic Input, Nov., 15-17, 1999, NEA/CSNI/R(2000)2, vol. 2: 397-504.
17. Silva, W.J., N. Abrahamson, G. Toro, C. Costantino (1997). "Description and validation of the stochastic ground motion model." Submitted to Brookhaven National Laboratory, Associated Universities, Inc. Upton, New York.
18. Silva, W.J. and R. Darragh (1995). "Engineering characterization of earthquake strong ground motion recorded at rock sites." Palo Alto, CA, Electric Power Research Institute, TR-102261.
19. Silva, W.J. (1991). "Global characteristics and site geometry." Chapter 6 in Proceedings: NSF/EPRI Workshop on Dynamic Soil Properties and Site Characterization. Palo Alto, Calif.: Electric Power Research Institute, NP-7337.

DISCLAIMER

This paper was prepared in part by an employee of the United States Nuclear Regulatory Commission. It presents information that does not currently represent an agreed-upon staff position. NRC has neither approved or disapproved its technical content.

Table 1
Shape Coefficients for 5% Damped Response Spectra

Coef	WUS	CEUS – 1 Corner	CEUS – 2 Corner
C1	1.8197	0.88657	0.97697
C2	0.30163	exp(-10.411)	exp(-9.4827)
C3	0.47498+0.034356M+ 0.0057204ln(R+1)	2.5099	2.3006
C4	-12.65+2.4796M-0.14732M^2 +0.034605Mln(1+0.040762R)	-7.4408+1.522M-0.088588M^2 +0.0073069Mln(1+0.12639R)	-12.665+2.4869M-0.14562M^2 +0.024477Mln(1+0.041807R)
C5	-0.25746	-0.34965	-0.21002
C6	0.29784+0.010723M- 0.0000133R	-0.31162+0.0019646R	0.74361+0.0000671R
C7	NA	3.7841	exp[-13.476+4.4007M- 0.31651M^2+0.000235MR]
C8	NA	-0.89019	0.95259-0.58275M +0.000166MR
C9	NA	0.39806+0.058832M	-3.3534+0.44094M

M = moment magnitude
R = fault distance (km)

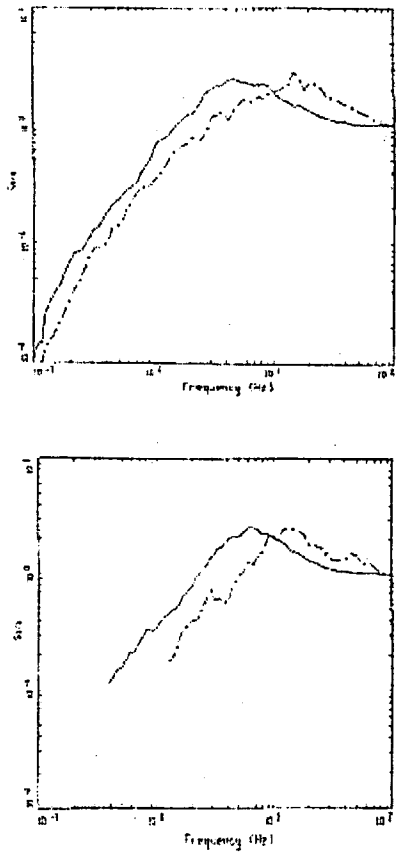

Figure 1 Comparison of Rock Response Spectral Shapes (5% Damping) Between WUS (Solid Lines) and CEUS (Dashed Lines) for Earthquakes Recorded at Rock Sites [M 6.75 (upper figure) and M 5.75 (lower figure)]

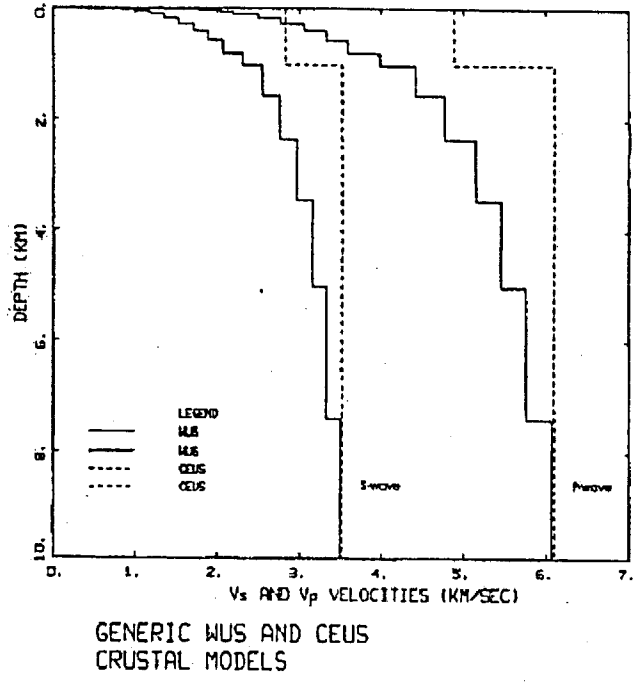

Figure 2. Comparison of Generic Shear and Compression Wave Velocity Profiles for WUS and CEUS Crustal Models

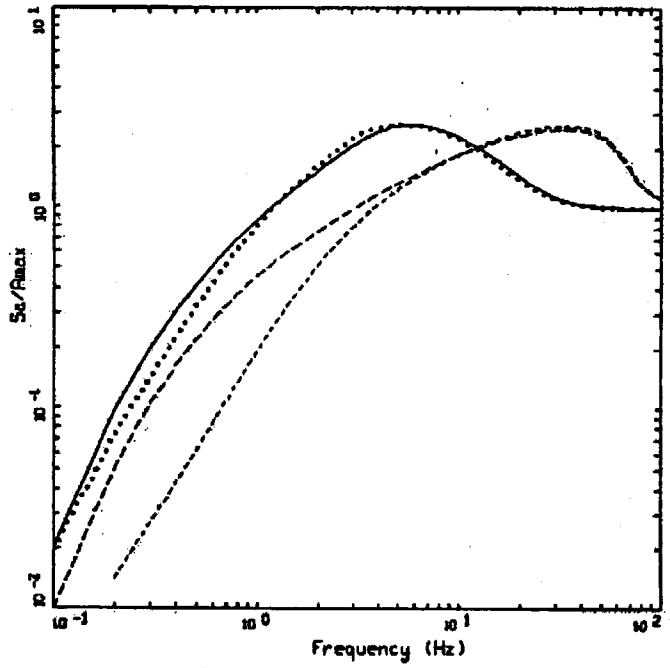

Figure 3. Response Spectral Shapes (5% Damping) for WUS and CEUS Crustal Conditions

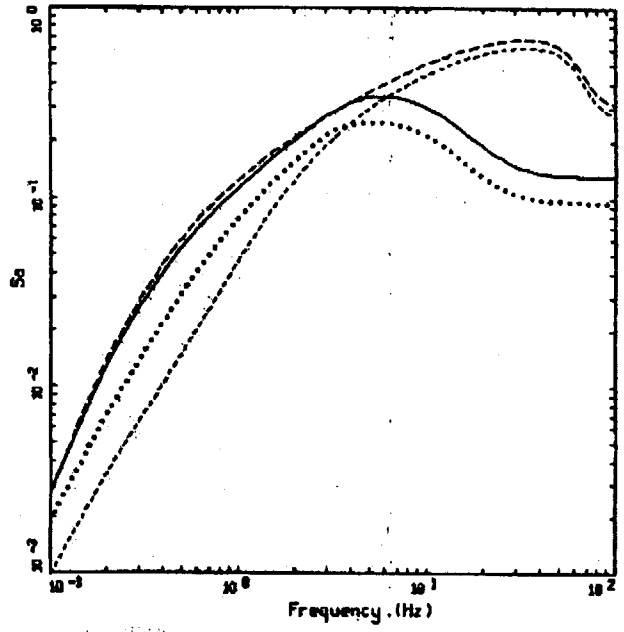

Figure 4. Absolute Response Spectra (5% Damping) for WUS and CEUS Crustal Conditions

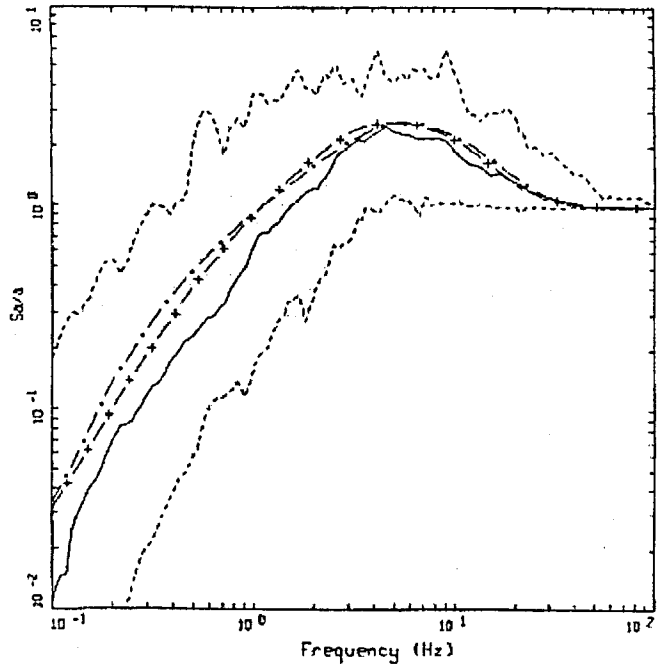

Figure 5. Comparison of 5% Damped Bin Statistical Spectral Shapes with Model Predictions, WUS Recordings, Bin M 6.5 - 7.0, R 10-50 km

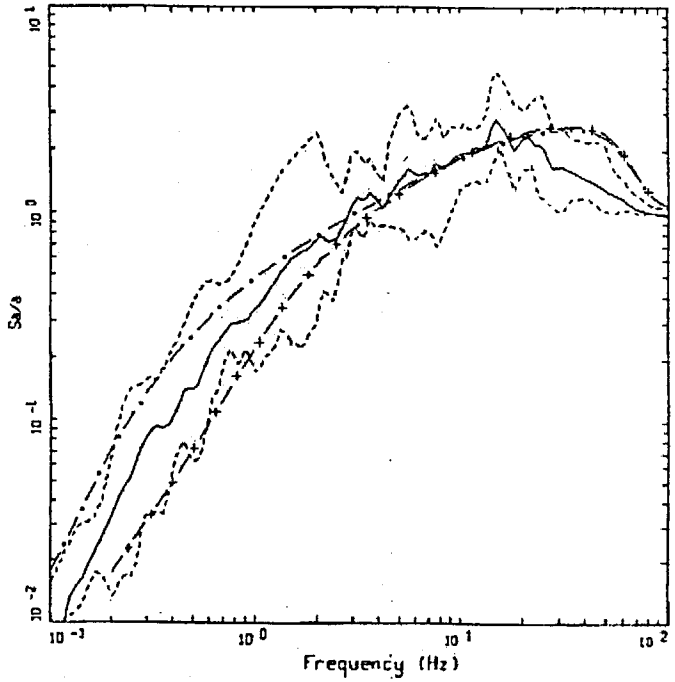

Figure 6. Comparison of 5% Damped Bin Statistical Spectral Shapes with Model Predictions, CEUS Recordings, Bin M 6.5 - 7.0, R 5 – 50 km .

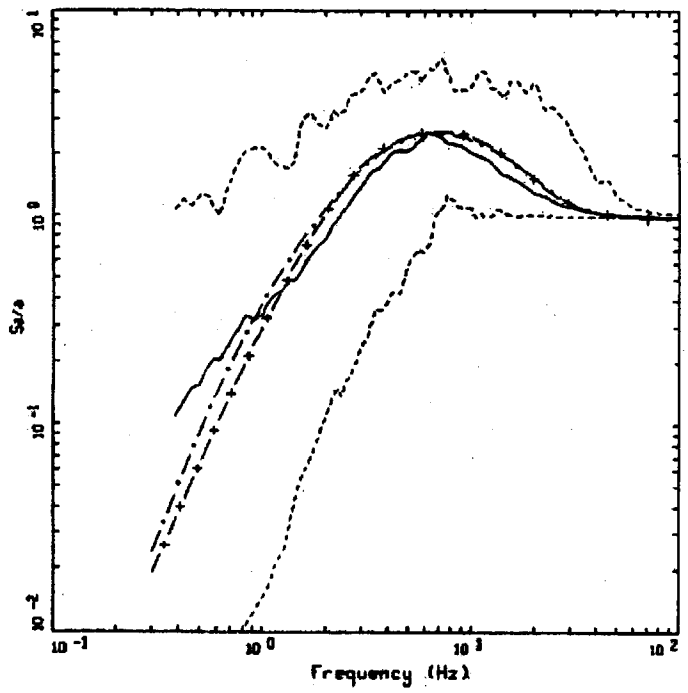

AVERAGE HORIZONTAL SPECTRA, WUS
M=5 1/4 (5.0-5.4), R=0-25 KM, ROCK
AVERAGE M = 5.18, AVERAGE DISTANCE = 13.57 KM

LEGEND
——— 50TH PERCENTILE
- - - - - MINIMUM ENVELOPE
- - - - - MAXIMUM ENVELOPE
— • — WUS SINGLE CORNER MODEL
— + — WUS DOUBLE CORNER MODEL

Figure 7. Comparison of 5% Damped Bin Statistical Spectral Shapes with Model Predictions, WUS Recordings, Bin M 5-5.4, R 0 – 25 km

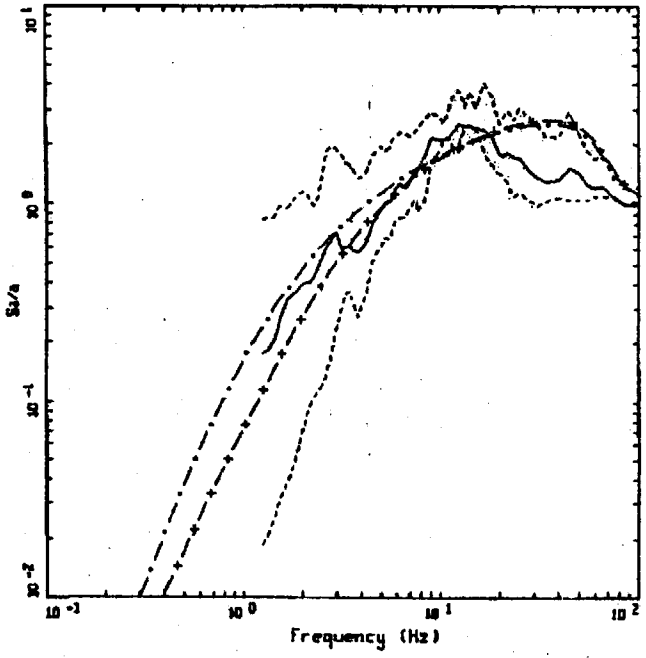

AVERAGE HORIZONTAL SPECTRA, CEUS
M=5 1/4, R=0-25 KM, ROCK

LEGEND
——— 50TH PERCENTILE
- - - - - MINIMUM ENVELOPE
- - - - - MAXIMUM ENVELOPE
— • — CEUS SINGLE CORNER MODEL
— + — CEUS DOUBLE CORNER MODEL

Figure 8. Comparison of 5% Damped Bin Statistical Spectral Shapes with Model Predictions, CEUS Recordings, Bin M 5.0 – 5.5, R 0 - 25 km

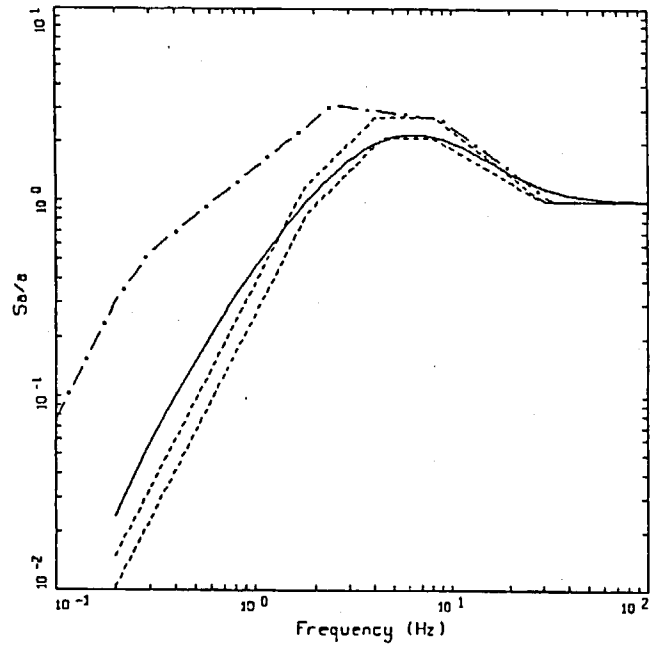

Figure 9. Comparison of WUS Model Prediction (Small Event) with RG 1.60 and Newmark-Hall 0098 Spectral Shapes (5% Damping)

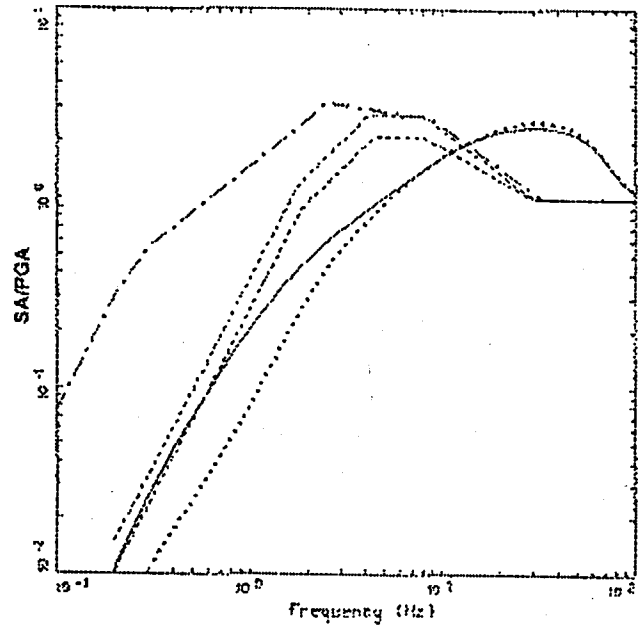

Figure 10. Comparison of CEUS Model Prediction (Small Event) with RG 1.60 and Newmark-Hall 0098 Spectral Shapes (5% Damping)

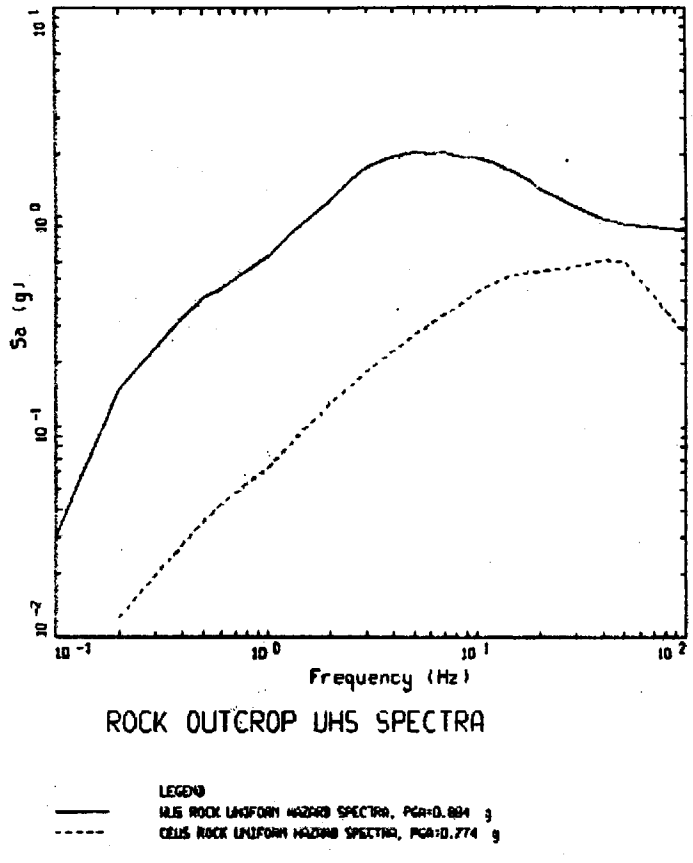

Figure 11 Comparison of 5% Damped Rock Outcrop UHS Spectra for WUS and CEUS Sites at 10^{-4} Probability of Exceedance Level

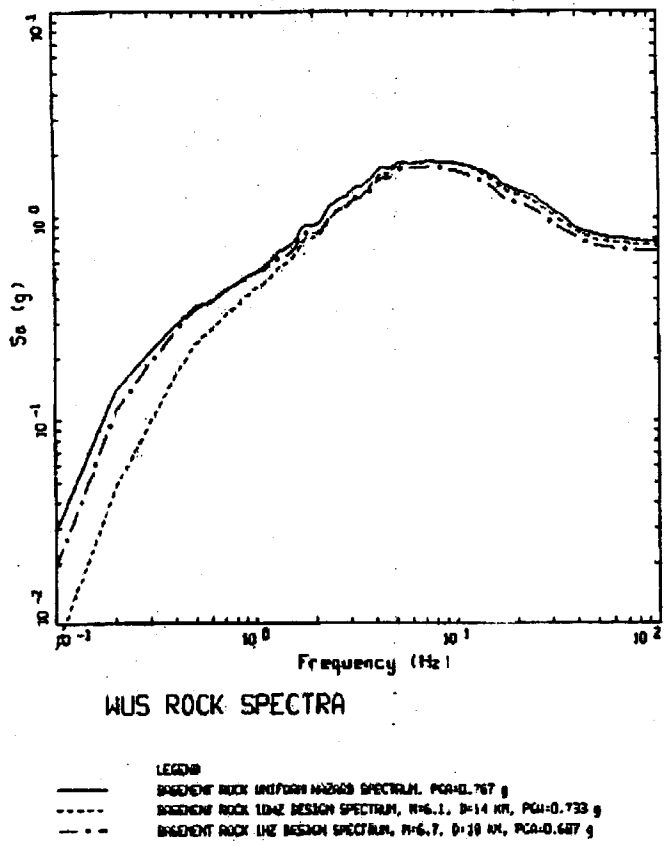

Figure 12. WUS Bedrock UHS and Scaled Deaggregated Spectra At 1 Hz and 10 Hz

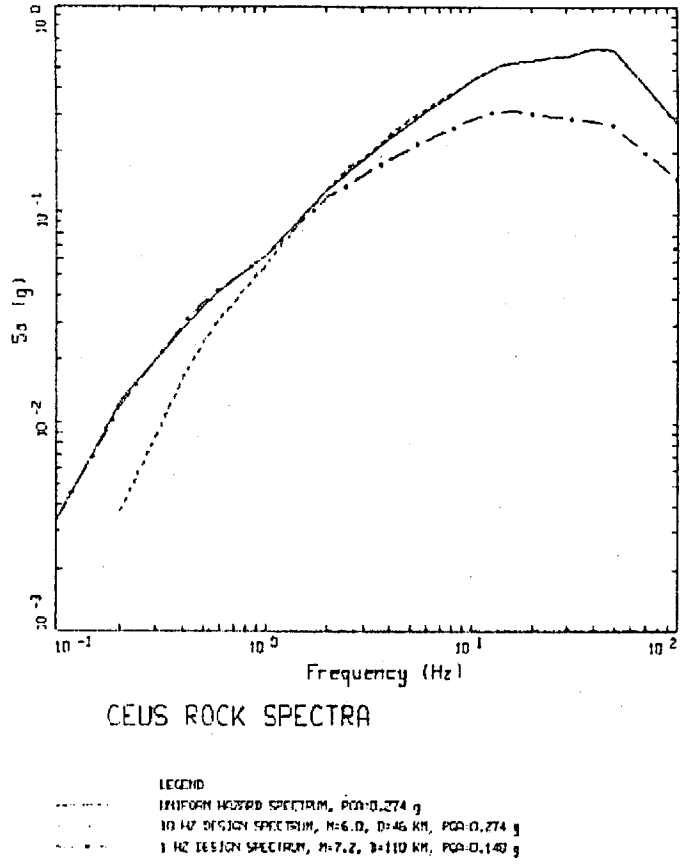

Figure 13. CEUS Bedrock UHS and Scaled Deaggregated Spectra
At 1 Hz and 10 Hz

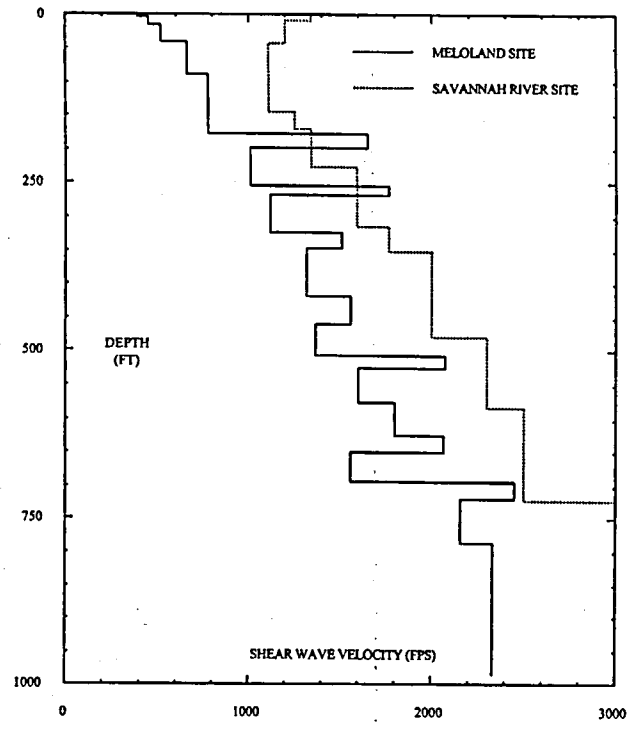

Figure 14. Base Case Shear Wave Velocity Profiles
Meloland and Savannah River Site

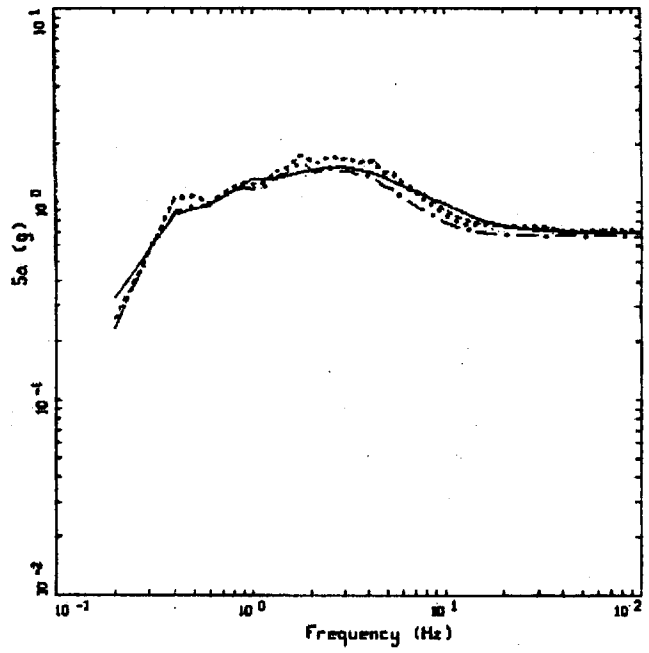

WUS 1DE-4 APPROACH COMPARISON, MELOLAND

LEGEND
APPROACH 4, 1D-4 UHS SOIL UNIFORM HAZARD SPECTRUM; PGA = 0.704 G
APPROACH 2A, 1 HZ AND 10 HZ DESIGN CONTROL MOTIONS, MEAN PGA = 0.721 G
APPROACH 2B, 1 HZ AND 10 HZ DISAGGREGATION CONTROL MOTIONS, MEAN PGA = 0.718 G
APPROACH 1, 1D-4 UHS ROCK CONTROL MOTION, MEAN PGA = 0.670 G

Figure 15. Comparison of Soil Surface Spectra Using Approaches 1, 2A, 2B and 4 For WUS Soil Site Conditions

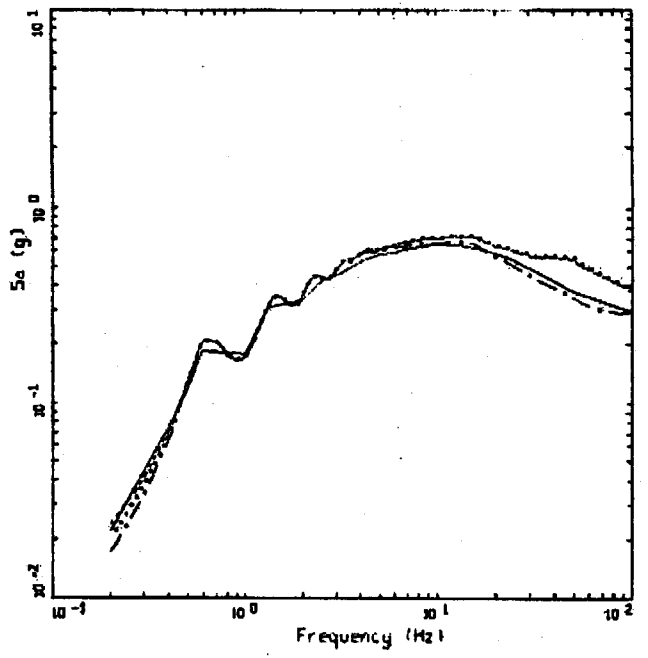

CEUS 1DE-4 APPROACH COMPARISON, SAVANNAH RIVER GENERIC

LEGEND
APPROACH 4, 1D-4 UHS SOIL UNIFORM HAZARD SPECTRUM; PGA = 0.294 G
APPROACH 2A, 1 HZ AND 10 HZ DESIGN CONTROL MOTIONS, MEAN PGA = 0.277 G
APPROACH 2B, 1 HZ AND 10 HZ DISAGGREGATION CONTROL MOTIONS, MEAN PGA = 0.356 G
APPROACH 1, 1D-4 UHS ROCK CONTROL MOTION, MEAN PGA = 0.269 G

Figure 16. Comparison of Soil Surface Spectra Using Approaches 1, 2A, 2B and 4 For CEUS Soil Site Conditions

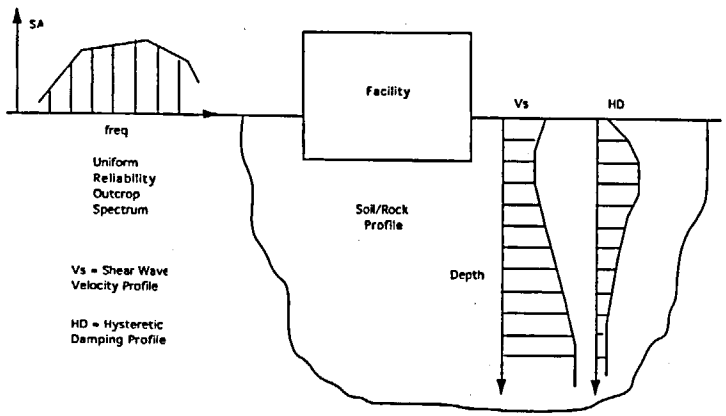

Figure 17. Typical Configuration for SSI Response Analyses

POSTER

SESSION

SEISMIC HAZARD ASSESSMENT OF THE LUCAS HEIGHTS HI-FLUX AUSTRALIAN REACTOR, SYDNEY, AUSTRALIA: SEISMIC HAZARD ASSESSMENT IN A LOW-SEISMICITY REGION

Mark Stirling, Kelvin Berryman, & Graeme McVerry
Institute of Geological & Nuclear Sciences Ltd, P.O. Box 30368, Lower Hutt, New Zealand

Gary Gibson
Seismological Research Centre, Level 3, 20 Council St, Hawthorn East, Victoria 3123, Australia

Norm Abrahamson
Pacific Gas and Electric Company, P.O. Box 770000, B32, San Francisco, CA 94177, USA

Abstract

We present an overview of our probabilistic seismic hazard assessment (PSHA) of the Lucas Heights site in south Sydney, New South Wales, Australia. The study represents the first modern PSHA of its kind ever carried out in Australia, including the full treatment of uncertainty in the input parameters. The study had the considerable challenge of being located in a low seismicity intraplate setting, and was also undertaken without access to any well established attenuation relations for eastern Australia. The peak ground accelerations calculated were in the range of 0.3 to 0.4g for the mean 10,000 year return time, somewhat higher than the estimates from previous studies which did not incorporate the modern methods of PSHA for the siting of nuclear reactors.

Introduction

In this paper we present a brief overview of our probabilistic seismic hazard assessment (PSHA) of the Lucas Heights site in south Sydney, New South Wales, Australia. The study was undertaken for the Department of Industry, Science and Resources in accordance with international best practice in seismic hazard analysis for the siting of nuclear reactors by a multinational team of seismologists, geologists and earthquake engineers (Alliance, 1999; Stirling & Berryman, 2001). The study had the considerable challenge of being located in the intraplate setting of eastern Australia (Fig. 1) where seismicity rates are low and difficult to constrain from the short (approximately 100 year) historical record of earthquakes. An additional difficulty was the lack of a well established attenuation relation for eastern Australia. Furthermore, only limited work had been done to determine the recency of activity on faults in eastern Australia prior to our study.

Methodology

An early step in construction of the PSHA was to define area sources that enclose areas of roughly homogenous seismicity and geology (Fig. 2). Magnitude – frequency distributions and the associated seismicity parameters were then constructed from the historical seismicity for each area source, and parameters were also defined for the Lapstone Structural Complex (the one fault in the region thought to be active; Fig. 2). To address the epistemic (knowledge or model) uncertainty in the earthquake parameters and likely accelerations produced at the site from the resulting earthquakes we constructed logic trees for each area source and also for the Lapstone Structural Complex (Fig. 3). Particular emphasis was placed on incorporating a range of attenuation relationships for intraplate and interplate tectonic settings into the logic trees, acknowledging that the Sydney Basin is not a "classic" intraplate environment (i.e. not within an area of stable continental shield or craton like central Australia or eastern North America). The weightings used in the logic trees were determined by consultation among the Alliance team and by consultation with Australian experts. We ran the PSHA by way of a Monte Carlo method, which involved repeatedly sampling the logic tree and constructing "hazard curves" for each sample (annual frequency of exceedance for a suite of acceleration levels; e.g. the peak ground acceleration example shown in Fig.4). The uniform hazard (probabilistic) spectra for a series of percentile levels and return times were calculated by this method from 1000 samples of the logic trees.

Hazard Estimates

The peak ground accelerations and spectral accelerations (0.1, 0.2, 0.4, and 1 second periods) calculated from the 1000 samples of the logic tree are given in Table 1. The peak ground accelerations are in the range of 0.3 to 0.4g for the mean 10,000 year return time, somewhat higher than the estimates from previous studies which did not incorporate the modern methods of PSHA (i.e. treatment of uncertainty, and other aspects). Throughout the analysis considerable effort went into conducting sensitivity analyses to determine the "robustness" of our results, and in doing so we found no one parameter to strongly influence the hazard above all of the others.

Deaggregations

To aid in providing appropriate information for eventual definition of design earthquakes for the site we conducted deaggregations of a number of samples from the logic trees to determine the dominant (modal) magnitudes and distances that dominate the hazard. The results of the deaggregations were then used to select representative historical earthquakes from global strong motion datasets (for eventual use in earthquake loading analyses at the site) by finding the best match of the individual spectra for these events to the uniform hazard spectra of the site. The analysis showed that the mean 10,000 year return period accelerations given in Table 1 are most likely to come from moderate earthquakes occurring less than 20km from the site.

Conclusions

Our study has utilised the modern methods of PSHA applicable to the siting of nuclear reactors to calculate the levels of peak and spectral acceleration expected at the Lucas Heights site.The peak ground accelerations calculated are in the range of 0.3 to 0.4g for the mean 10,000 year return time, somewhat higher than the estimates from previous studies which did not incorporate the modern methods of PSHA. A deaggregation analysis shows that these accelerations are most likely to come from moderate earthquakes occurring less than 20km from the site.

References

Alliance, 1999. Seismic hazard analysis, Lucas Heights site of the High-Flux Australian reactor. Alliance *Client Report prepared for the Department of Industry, Science and Resources, Australia.*

Stirling, M.W., and Berryman, K.R. 2001. Extension to Lucas Heights Probabilistic seismic hazard assessment. *Institute of Geological and Nuclear Sciences Client Report 2001/85.*

Table 1

Estimates of PGA and 0.1, 0.2, 0.4, and 1 second spectral acceleration (SA) for Lucas Heights, for the 50th percentile, mean and 84th percentile levels, for four return periods (RP).

PGA

RP	10^2	10^3	10^4	10^5
50th	0.05	0.10	0.35	0.75
Mean	0.04	0.12	0.37	0.85
84th	0.05	0.17	0.49	1.25

0.1 Second SA

RP	10^2	10^3	10^4	10^5
50th	0.05	0.21	0.68	1.48
Mean	0.05	0.22	0.70	1.64
84th	0.07	0.29	0.97	2.53

0.2 Second SA

RP	10^2	10^3	10^4	10^5
50th	0.05	0.20	0.66	1.47
Mean	0.05	0.21	0.67	1.57
84th	0.06	0.28	0.92	2.21

0.4 Second SA

RP	10^2	10^3	10^4	10^5
50th	0.05	0.14	0.46	1.07
Mean	0.04	0.14	0.45	0.07
84th	0.05	0.19	0.61	1.45

1.0 Second SA

RP	10^2	10^3	10^4	10^5
50th	0.05	0.06	0.21	0.52
Mean	0.09	0.06	0.20	0.49
84th	0.05	0.09	0.27	0.66

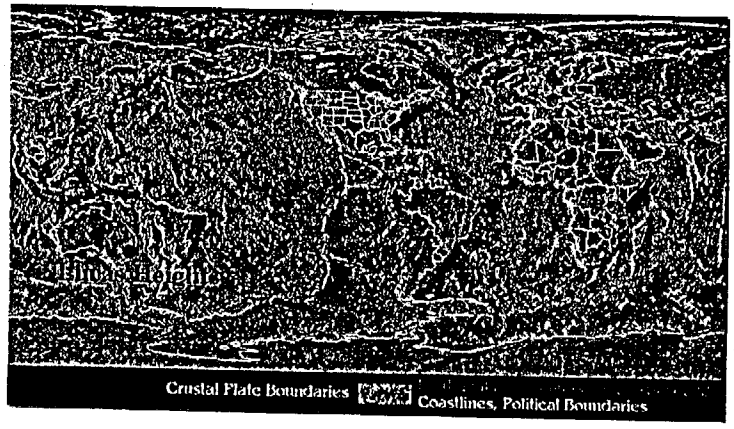

Figure 1
The plate tectonic setting of the Lucas Heights site in the low-seismicity intraplate environment of eastern Australia.

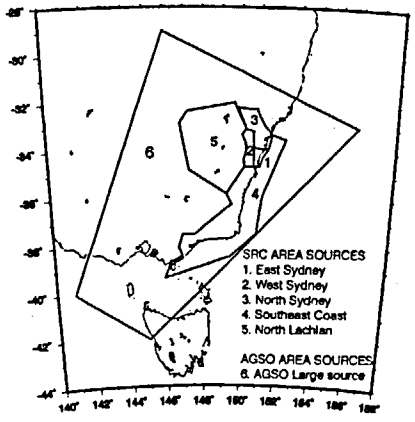

Figure 2. Area sources defined for the study.

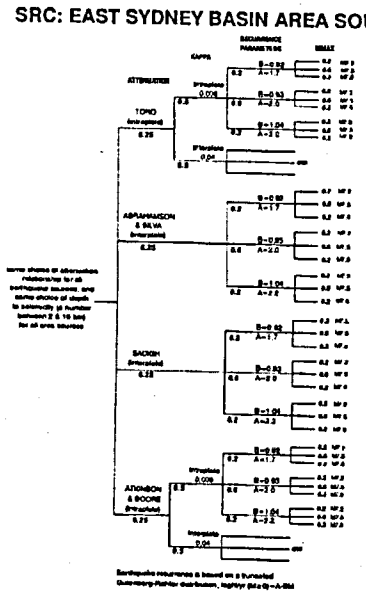

Figure 3.
Logic tree for the East Sydney Basin area source

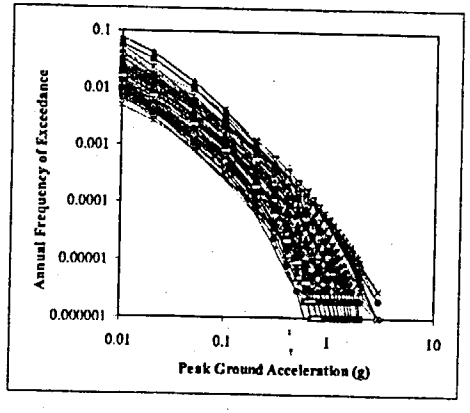

Figure 4.
Hazard curves for peak ground acceleration calculated by way of a Monte Carlo analysis.

SITE RESPONSES IN THE TAIPEI BASIN DURING THE 1999 CHI-CHI, TAIWAN EARTHQUAKE SEQUENCE

Kuo-Liang Wen[1,3], Han-Yih Peng[2], Tao-Ming Chang[3], and Chi-Ling Chang[3]
1. Institute of Applied Geology, National Central University
2. LinkEarth Technology Ltd. Co.
3. Office of the National S&T Program for Hazards Mitigation, National Taiwan University

Abstract

On September 20, 1999 a magnitude M_L 7.3 earthquake struck Taichung and Nantou in central Taiwan. Taipei basin located more than 100 km from the epicenter but also had many buildings damaged during the earthquake. In this study we use the mainshock and aftershocks data of Chi-Chi earthquake to analyze the site effect of Taipei basin. The results show that the dominant low frequency band response is located in the western part of Taipei basin and Songshan area; the main high frequency band response areas are near the edge of basin. Another hand, comparing the results of amplification pattern with the location of damaged buildings found that the tall damaged buildings are located at the high response areas of low frequency band and the low-rise damaged structures are located at the high response areas of higher frequency band. From these results we can find the relationship between the site amplification and damaged structure distribution in the Taipei basin area during earthquakes.

Introduction

Taiwan is located on the Circum-Pacific seismic belt. The seismicity in Taiwan area is very high [1]. Therefore, defense lives and possessions from disaster earthquakes are a major concern of the people in this region. Strong ground shaking primarily causes the damaging effects of earthquakes. To reduce the loss of life and property from strong ground shaking, it requires conscientious application of construction codes and earthquake resistant design, enforcement of adequate land-use policies as well as implementation of appropriate retrofit measures. The implementation of these mitigation measurements must be based in large part on the recordings from large earthquakes at distances from 0 to 100 km. Such data are crucial for designing earthquake resistant structures and understanding the source mechanism of earthquakes and the propagation of seismic waves from source to site, including the local site effects.

Amplification of strong ground motion by alluvial deposits during an earthquake has been documented on a lot of occasions and caused damage in recent large earthquakes, for example, 1985 Michoacan earthquake, 1989 Loma Prieta earthquake, 1994 Northridge earthquake, 1995 Kobe earthquake, and 1999 Chi-Chi, Taiwan earthquake. Many studies shown that the top alluvium layer will play an important role for site amplification effects [2-4]. Therefore, site effects study is very important for mitigating damage during an earthquake. Many methods have been used to characterize the site amplification. The best approach is through direct observation of seismic ground motion, although such observations are limited to high seismicity areas and by high cost. A dense strong motion observation network provides an opportunity to realize the basin effects in the Taipei basin. The preliminary results of the site responses in the Taipei basin had been done before [5-7]. In this study, we used the spectral ratio to analyze the site effect by adopting the data of Chi-Chi earthquake and it's aftershocks for realizing the basin responses during the Chi-Chi earthquake. The spectral ratio contours at some specific frequencies are selected to compare with the geological and velocity structures under the Taipei basin. In the other hand, For the engineering concern, the relationship between the spectral ratio contour and the distribution of damaging building areas are also discussed in this study.

Geological structure of the Taipei basin

The Taipei basin is a triangle-shaped alluvium structure (Figure 1). The ground surface of the Taipei basin is almost flat and tilting gently to the northwest. The total area of the Taipei basin is about 240 square kilometers with an altitude below 20 meters. The Keelung River flows through it in an east-west direction, the Dahang Creek from the south through the basin center and then northwest to the ocean, and the Chingmei Creek from the southeast merge in the Dahang Creek at around the basin center. Because the basin is filled with the unconsolidated sediments, the subsurface geology of the Taipei basin can only be established by the information obtained from boring, electrical, and seismic prospecting [8,9]. Recently, the basement structure in the Taipei basin area had been modified through the work of deep boring by the Central Geological Survey [10] and dense reflection seismic survey by the National Central University [11-13]. The dotted contour lines in Figure 1 indicate the depth to the basement rock in the Taipei Basin, from inner to outer each line shows the depth from 400 to 100 m, respectively.

The geological structure inside the basin is the Quaternary layers above the Tertiary base rock. The stratigraphic formations of the Quaternary layers are, in descending order, surface soil, the Sungshan Formation, the Chingmei Formation, and the Hsinchuang Formation. The Sungshan Formation is composed mainly of alternating beds of silty clay and silty sand, and covers almost the whole Taipei basin. The Chingmei Formation is a fan-shaped body of conglomerate deposits. The Hsinchuang Formation consists of bluish grey, clayey sand with some conglomerate beds [9]. Wen *et al.* [14] calculated the V_p and V_s from surface to the depth of 350 meters through the travel time analysis of seismic waves by using the Wuku downhole records in the western part of Taipei basin. The average P- and S-wave velocity structures of the Taipei basin are shown in Table 1 which were the results from the reflection seismic survey in the whole Taipei basin area [15].

TSMIP network and earthquake data

The Taiwan Strong Motion Instrumentation Program (TSMIP) is executed by the Seismological Observation Center of the Central Weather Bureau, Taiwan, ROC [5,16]. The main purpose of this program is to study the characteristics of the ground motion in different geological conditions and the response of different types of man-made structures. All results can be used to improve the design spectrum and building codes of current use. The program installed up to 600 digital free field strong

motion instruments and 400*3 digital channels of strong motion monitoring systems in nine metropolitan areas. About 100 free field stations are already in operation in Taipei area, and 43 stations are within the Taipei basin. The station interval is about 2 km in average. The distribution of stations is shown in Figure 1 in triangle symbol and the number near each station is the station code. Each station includes one strong motion instrument and a recording room. Strong motion instrument is a force-balance accelerometer. The recorder which has 16 bits' resolution can record the ground motion within ±2g and has pre-event and post-event memory. Each strong ground motion station has the same design. A small fiberglass house covered on a concrete plate. All stations have AC power. When the power system is shutdown by earthquake or other problem, the DC powers of the recording system can still operate about 4 days.

The Chi-Chi earthquake and its 8 aftershocks which magnitude is over 6.0 were recorded by the TSMIP network which is located in the Taipei basin since September 20 to 22 1999. Table 2 shows the source parameters of Chi-Chi earthquake and its aftershocks. All the source parameters in the Table 2 are determined by the local seismic network of the Central Weather Bureau, Taiwan. Figure 2 shows the events location which is listed in the Table 2. In the Figure 2 we can find that, Chi-Chi earthquake and its aftershocks are all located at the south-western direction of Taipei basin and the Taipei basin is located more than 100 km away from the epicenters of these earthquake. In this study, earthquakes list in the Table 2 will be used to make spectral ratio to understand the site response in the Taipei basin during the Chi-Chi earthquake and its aftershocks. Figure 3 shows a typical waveform of Chi-Chi earthquake recorded at station TAP003 which is located at the western part of Taipei basin, and Figure 4 shows the waveform of No. 8 aftershock in Table 2 recorded at the same station of Figure 3.

Site effect analysis

Taipei basin is located in the north of the epicenter and the closed distance to the fault rupture is more than 100 *km* away. Figure 5 plots the waveforms from south to north in the western part of the basin. They indicate that the seismic waves from the south to the north edge of the basin show the amplification effects. If we consider the frequency response (Figure 6), the ground motions change from high frequency to low frequency, as the basin becomes deeper. Toward the north edge, the response turns to higher frequency again. The edge effects [17] seem also play an important role for this event.

In order to understand the soil amplification effects in the frequency domain, the spectral ratios of the soft soil stations were calculated with respect to the TAP043 site that is near the south-western edge of the basin. All the recorded earthquakes are more than 100 km away from Taipei basin in the south directions. The variation of azimuth and incident angle will not be so large. Therefore, selection of TAP043 as reference site will not change the pattern of average spectral ratio very much. The spectral ratios are calculated as follows [18]: (1) a window containing the shear wave is identified; (2) the window is tapered at both ends (at 5% of the length) using a cosine function; (3) the Fourier amplitude spectrum is calculated; (4) the spectrum is smoothed 1 times using a 3-point running Hanning average; (5) two smoothed spectra are divided; (6) the root-mean-square (RMS) spectral ratio is then calculated from the two horizontal ratios of EW and NS components. Figure 7 shows an example of the mean spectral ratio of the TAP003 and TAP043 station pair in Chi-Chin earthquake's aftershocks. The shaded bands represent ±1 standard deviation areas.

For the purpose of the earthquake resistant design, earthquake engineers must consider the site response at a specific period. For example, the structure period of a ten-flour building is at about 1 second. If the input ground motion is dominate at 1 Hz, then the building will has a resonant effect. Which may easily cause big damage to this building. Therefore, in this study, we select 7 periods (4, 3, 2, 1.5, 1, 0.5, and 0.3 sec) to plot out the contour map for understanding the frequency responses in the Taipei basin. Figure 8 shows an example of the mean spectral ratio contour for the period of 2 sec. From these contours, it is obvious that the waves at different frequencies have different amplification patterns in the Taipei basin. For the low frequency responses (period from 4 to 1.5 seconds) in the Taipei basin, the contours show that main amplification effects occurred at the western part of the Taipei basin and the Sungshan area. Nevertheless, the response at the higher frequency band of larger than 1 Hz shows different amplification effects. The high contour areas occur near the basin edges at the north, east, and south basin boundaries. The responses in western part of the Taipei basin and the Sungshan area do not show strong amplification effect anymore. The basement structure (The dotted contours in Figure 1) may explain the high spectral ratio area occurred at the western part of the Taipei basin, which is the deepest area of the Taipei area. But it can not explain the contour high area at the Sungshan area of the low frequency responses. The top alluvium layer in the Taipei basin seems play an important role for site amplifications as mentioned by Anderson et al. (1996). The two deepest areas of the soft Sungshan Formation (Figure 9) can correlate with the two high spectral ratio areas at the lower frequency bands. More research works are needed to clarify the role of this top alluvium layer of the Sungshan Formation.

The damage distribution of the Chi-Chi Earthquake in Taipei basin

Although Taipei basin is located more than 100 km away from the epicenter of Chi-Chi earthquake, there are also three tall buildings collapsing and some low-rise structures damaging during the earthquake. As the spectral ratio method we used above, we chose the Chi-Chi earthquake and it's aftershocks records to analyze the site effect of Taipei basin. The reference site we chose is TAP043. Figure 10 and Figure 11 show the examples of spectral ratio contour of Chi-Chi earthquake for period of 0.5 sec and 2 sec. Figure 12 and Figure 13 show the examples of mean spectral ratio contour of the Chi-Chi aftershocks for period of 0.5sec and 2 sec. These patterns of spectral ratio contour are very consisting with above results. The damages distribution of the Chi-Chi earthquake can compared with the site response in the Taipei basin. The three tall buildings are located in the high response areas of the lower frequency. The low-rise buildings are located near the basin edges where has the higher response in the higher frequency band. This phenomenon also shown in the earthquake of November 15, 1986.

Summary

The dense TSMIP network provides an opportunity for us to realize the site effects in the Taipei basin. In this study, we use the spectral ratio method to calculate the frequency response at each station with respect to a referent site TAP043 that is located at the southern edge of the basin. The spectral ratio contours at some specific periods are selected to compare with the geological structure under the Taipei basin.

From the analysis of Chi-Chi earthquake and its aftershock records of the dense TSMIP network, it is noted that different areas have different local site effects in the Taipei basin. By comparison of the results with the geological structure, we can understand that the low frequency responses on the western part of the Taipei basin and Sungshan area are correlated with the basin structure and the top soft soil layer (Sungshan formation). The high frequency responses are mainly occurred near the edge

of the Taipei basin except the western boundary of a steep structure. The soft soil layer of the Sungshan formation may dominate the site response at the Taipei basin. During the 1986, Hwalien earthquake and 1999, Chi-Chi earthquake, there are some buildings damaged. By comparing between the distribution area of damaging buildings and spectral ratio contours of the Chi-Chi earthquake sequence, we found that the patterns can be correlated. The more accurate relationship between distribution of damaging buildings and earthquake response in Taipei basin needs to do more research works.

Acknowledgements

The authors would like to thank the Seismological Observation Center of the Central Weather Bureau for providing the original TSMIP data. This study was supported by the National Science Council under the grant NSC 89-2116-M-008-017 and NSC 89-2625-Z-002-037.

References

[1]. Hsu, M. T., 1961. "Seismicity of Taiwan (Formosa)," *Bull. Earthq. Res. Inst.*, Univ. of Tokyo, 39, pp. 831-847.

[2]. Boore, D. M., W. B. Joyner, and T. E. Fumal, 1993. "Estimation of response spectra and peak accelerations from western United States earthquakes: an interim report," *U.S. Geol. Surv.* Open-File Rep. 93-509, 72pp.

[3]. Boore, D. M., W. B. Joyner, and T. E. Fumal, 1994. "Estimation of response spectra and peak accelerations from western United States earthquakes: an interim report, Part 2," *U.S. Geol. Surv.* Open-File Rep. 94-127, 40pp.

[4]. Anderson, J. G., Y. Lee, Y. Zeng, and S. Day, 1996. "Control of strong motion by the upper 30 meters," *Bull. Seis. Soc. Am.*, 86, 6, pp. 1749-1759.

[5]. Kuo, K. W., T. C. Shin, and K. L. Wen, 1995. "Taiwan strong motion instrumentation program (TSMIP) and preliminary analysis of site effects in Taipei basin from strong motion data," *in Urban Disaster Mitigation: The Role of Engineering and Technology*, Edited by F. Y. Cheng and M.-S. Sheu, Elsevier Science Ltd., pp. 47-62.

[6]. Wen, K. L., H. Y. Peng, L. F. Liu, and T. C. Shin, 1995. "Basin effects analysis from a dense strong motion observation network," *Earthq. Eng. Struct. Dyn.*, 24, 8, pp. 1069-1083.

[7]. Wen, K. L., and H. Y. Peng, 1998. "Site Effect Analysis in the Taipei Basin: Results from TSMIP Network data," *Ter. Atm. Oce.*, 9, 4, pp. 691-704.

[8]. Wang Lee, C. M., Y. M. Cheng, and Y. Wang, 1978. "Geology of the Taipei basin (in Chinese)", *Taiwan mining*, 30, 4, 350-380.

[9]. Wang Lee, C. M., and T. P. Lin, 1987. "The geology and land subsidence of the Taipei basin", *Memoir Geol. Soc. China*, 9, 447-464.

[10]. Fei, L. Y. and T. C. Lai, 1994. "The preliminary result of an integrated survey of subsurface geology and engineering environment of the Taipei basin", *Proc. of the Joint Symposium on Taiwan Quaternary (5) and on Investigation of Subsurface Geology/Engineering Environment of Taipei Basin*, 121-128.

[11]. Wang, C. Y., W. C. Hsiao, and C. T. Sun, 1994. "Reflection seismic stratigraphy in the Taipei basin (I) - Northwestern Taipei", *J. Geol. Soc. China*, 37, 1, 69-95.

[12]. Wang, C. Y., Y. L. Tsai, M. L. Ger, and H. C. Chang, 1994. "Investigation of Tertiary basement in Taipei basin using shallow reflection seismics", *Proc. of the Joint Symposium on Taiwan Quaternary (5) and on Investigation of Subsurface Geology/Engineering Environment of Taipei Basin*, 169-175.

[13]. Hsieh, C. H., C. M. Lin, and S. H. Hsieh, 1994. "Seismic and well logging surveys in Taipei basin", *Proc. of the Joint Symposium on Taiwan Quaternary (5) and on Investigation of Subsurface Geology/Engineering Environment of Taipei Basin*, 185-191.

[14]. Wen, K. L., L. Y. Fei, H. Y. Peng, and C. C. Liu, 1995. "Site effect analysis from the records of the Wuku downhole array", *Ter. Atm. Oce.*, 6, 2, 285-298.

[15]. Wang, C. Y., Y. H. Lee, and H. C. Chang, 1996. "P- and S-wave velocity structures of the Taipei basin", *Symposium on Taiwan strong motion instrumentation program (II)*, Central Weather Bureau, 171-177.

[16] Shin, T. C., 1993. "Progress summary of the Taiwan Strong Motion Instrumentation Program," *Symposium on Taiwan Strong Motion Instrumentation Program*, pp. 1-10.

[17] Kawase H, 1996. "The cause of the damage belt in Kobe: 'the basin-edge effect', constructive interference of the direct S-wave with the basin-induced diffracted/Rayleigh waves," *Seism. Res. Lett.*, 67, 5, pp.25-34.

[18] Beresnev, I. A., and K. L. Wen, 1996. "The accuracy of soil response estimates using soil-to-rock spectral ratios," *Bull. Seis. Soc. Am.*, 86, 2, pp. 519-523.

Table 1. Velocity structure of Taipei basin [15].

Formation	Depth (m)		V_P(m/sec)	V_S(m/sec)
	Northwest	Southeast		
Sungshan	0-20	0-15	450	170
	20-50	15-35	1500	230
	50-100	35-50	1600	340
Chingmei	100-160	50-100	1800	450
Wuku	160-320	100-200	2000	600
Panchiao	320-400	200-250	2200	650
Besement			3000	1200

Table 2. Events source Parameters used in this Study.

Event No	Origin Time	Epicenter	Depth (km)	M_L
1	1999 9 20 17:47:16	23.85N 120.82E	8.00	7.30
2	1999 9 20 17:57:15	23.91N 121.02E	2.23	6.47
3	1999 9 20 18:03:41	23.79N 120.88E	3.53	6.57
4	1999 9 20 18:05:53	23.95N 120.84E	19.58	6.01
5	1999 9 20 18:11:53	23.85N 121.06E	5.21	6.70
6	1999 9 20 18:16:16	23.84N 121.04E	3.54	6.66
7	1999 9 20 21:46:37	23.60N 120.82E	5.32	6.59
8	1999 9 22 00:14:41	23.83N 121.05E	7.5	6.80
9	1999 9 22 00:49:43	23.76N 121.02E	8.95	6.29

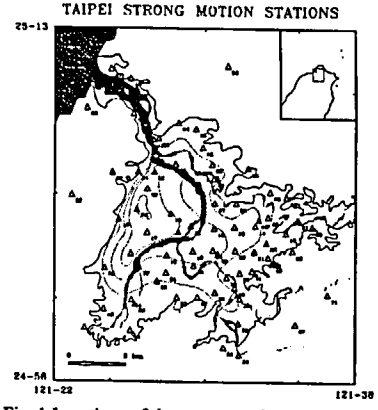

Fig. 1 Locations of the strong motion stations in Taipei area. Numbers indicate the station codes of TSMIP network. The dotted contours indicate the depth in meters to the base rock surface in the Taipei basin, from inner to outer each line shows the depth from 400 to 100 m, respectively. The black triangles indicate the downhole array sites.

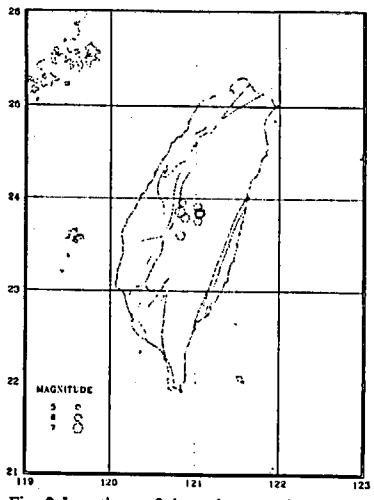

Fig. 2 Locations of the epicenters that used in this study.

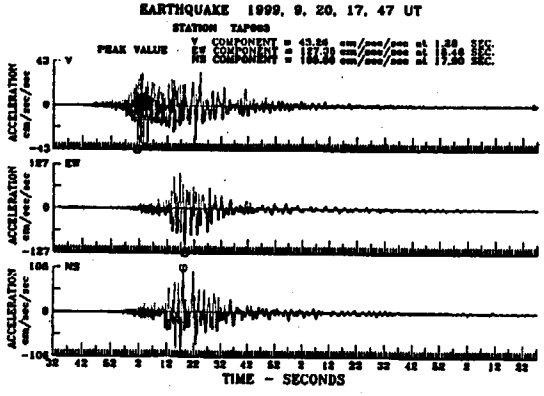

Fig. 3 Accelerograms of the September 20, 1999 Chi-Chi earthquake recorded at station TAP003.

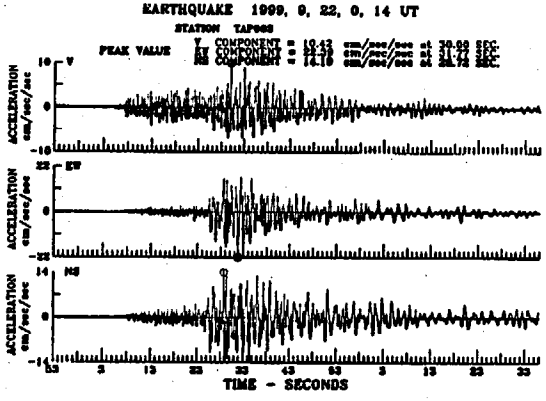

Fig. 4 Accelerograms of the September 22, 1999 earthquake recorded at station TAP003.

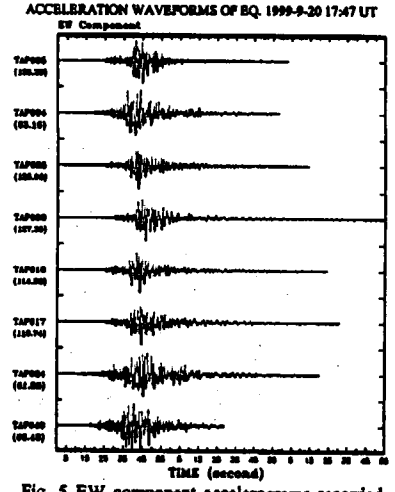

Fig. 5 EW component accelerograms recorded in the Taipei basin area. The stations from bottom to top are located from south to the north direction. Unit in gals.

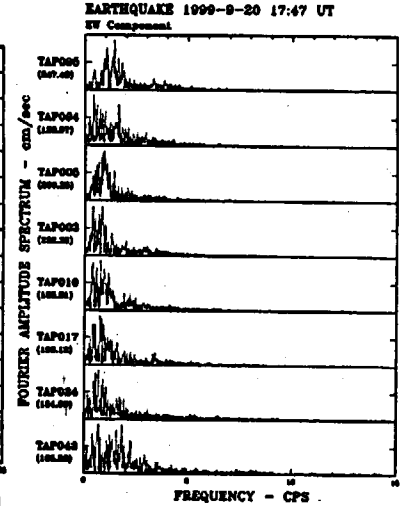

Fig. 6 Fourier amplitude spectra of the EW component accelerograms recorded in the Taipei basin.

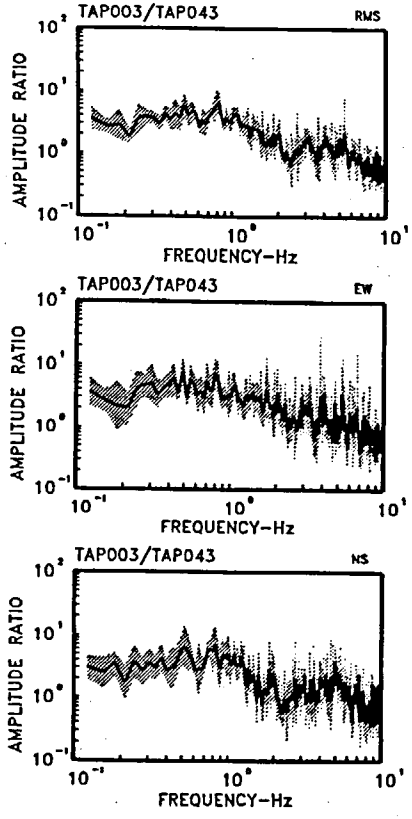

Fig. 7 Mean spectral ratio of 8 aftershocks of Chi-Chi earthquake between TAP003 and TAP043 station pair. Figures include the results of two horizontal components and their RMS value. The shaded band represent ±1 standard deviation areas.

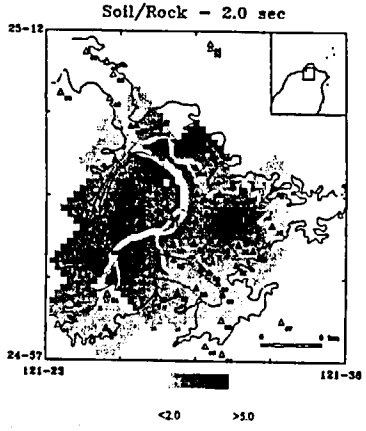

Fig. 8 Contours of the mean spectral ratio at 2 sec in the Taipei basin from the TSMIP records. The triangles and dotted contours are the same as those in Figure 1. The black triangles are stations that used in this analysis.

Fig. 9 Taipei basin Sungshan formation Bottom.

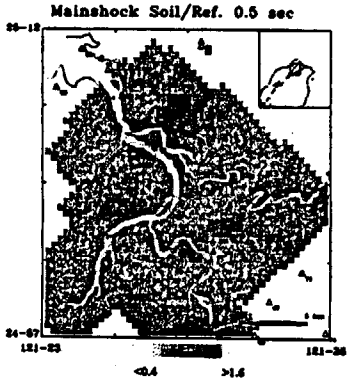

Fig. 10 The spectral ratio contour of Chi-Chi earthquake at 0.5 sec in the Taipei basin from the TSMIP records. The triangles and dotted contours are the same as those in Figure 1. The black triangles are stations that used in this analysis.

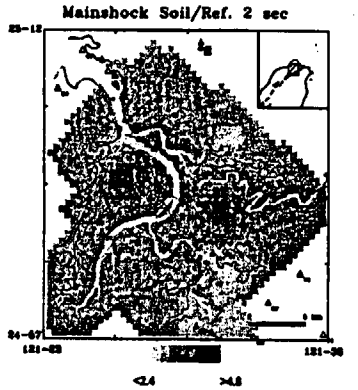

Fig. 11 The spectral ratio contour of Chi-Chi earthquake at 2 sec in the Taipei basin from the TSMIP records. The triangles and dotted contours are the same as those in Figure 1. The black triangles are stations that used in this analysis.

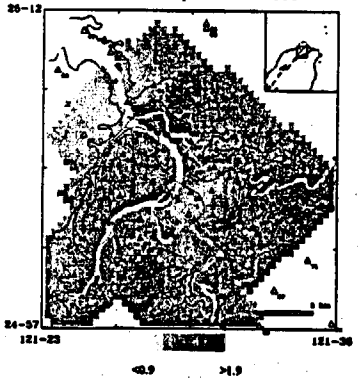

Fig. 12 The mean spectral ratio contour of Chi-Chi earthquake aftershocks at 0.5 sec in the Taipei basin from the TSMIP records. The triangles and dotted contours are the same as those in Figure 1. The black triangles are stations that used in this analysis.

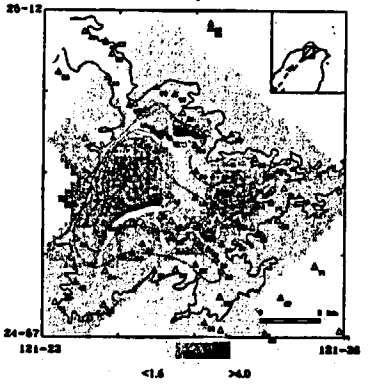

Fig. 13 The mean spectral ratio contour of Chi-Chi earthquake aftershocks at 2 sec in the Taipei basin from the TSMIP records. The triangles and dotted contours are the same as those in Figure 1. The black triangles are stations that used in this analysis.

NUCLEAR POWER PLANTS SEISMIC INSTRUMENTATION: SPANISH PRACTICE.

Jiménez Juan[*], *A., and Sánchez-Cabañero*[*], *J.G.*

Abstract

Seismic instrumentation system of Spanish plants are required to reach the following main goals: first at all to determine the OBE exceedance, and second to obtain site specific data in order to capture or reduce both uncertainties from the site and the structural design (e.g. near field attenuation and site effects models, or structural ageing effects and design models), and to improve the safety re-evaluation analysis. From licensing, the main Spanish NPP's (5 sites) were equipped with the best analogical instrumentation at that time, adequate to record strong earthquakes, but with limited resolution to register on free field low accelerations with reasonably confidence.

In a general way, seismic PRA results addressed new and higher perception on the earthquake occurrence probability in Spain, and a cost/benefit program to improve seismic instrumentation of all plants was planned. Implementing this action requires to get new digital free field instrumentation, and to develop procedures to quickly decide an OBE exceedance, like it is recommended in USNRC regulatory guides 1.12, rev. 2, and 1.166. Plant owners endorsed these guides and proposed a full change of their seismic monitoring system instrumentation, what includes a review of the plant Technical Specifications. Some instrumental improvements like universal time reference or higher resolution than 12 bits are recommended.

Introduction

New earthquake occurrence and developed knowledge on seismic sources, transmission path, and site effects, show a necessity of capture the current uncertainties in order to perform in a more consistent way new seismic designs, or to know plants seismic margin and vulnerabilities through safety re-evaluations analysis.

Far from the seismic margin concept (Ref. 2), Spanish NPP's seismic design is enveloped by two levels: the SSE (Safe Shutdown Earthquake) and the OBE (Operating Basis Earthquake). Both quakes are characterized to design on free field, and OBE input was selected as SSE/2. OBE is assumed that can occur at least one time in the plant life.

If OBE is exceeding, the affected plant is beyond of the established design basis to have a safety operation and does not fulfill the limits and conditions of its Operation Permit. If an OBE or minor earthquake occurs, plant seismic design guarantee an elastic behavior of its structures, systems and components (SSC's); but if the earthquake is larger it's not possible to reject plastic behavior with permanent

[*] Consejo de Seguridad Nuclear. Spain. C/ Justo Dorado, 11, Madrid, 28040, ajj@csn.es, jsc@csn.es

displacements for non seismic class SSC's and, relate to plant safety operation, it will not be consistent to assure SSC's availability.

To detect an OBE instrumental exceedance and to reach aims like reducing uncertainties, it's necessary to compare plant OBE master values in front off *in situ* measured values, through a plant seismic monitoring system capable to record different earthquakes sizes with good quality.

Original status

According with the following licensing process, the Spanish NPP's were obtained an new Operation Permit for ten years (the process is not yet finished for Trillo, and José Cabrera -the oldest one- will must be shutdown on April 2006 before beginning its decommission). Those permits was awarded as result of a Safety Periodic Review process started five years ago, in which some detected items were capable to be improved under low cost and Nuclear Safety benefits criteria. These ones are following:

The oldest Spanish plants (José Cabrera, Stª Mª de Garoña) have been from the beginning non seismic instrumented plants. But the rest of them (Almaraz I-II, Ascó I-II, Cofrentes, Vandellós II, and Trillo) were full equipped according the USNRC R.G. 1.12, Revs. 0 and 1, and had associated procedures to use if an earthquake occurs. Table 1 collects the name of the seven Spanish sites and operating units, beside to reactor type, electric power installed, year of operation starting, and SSE and OBE inputs to each one. Table 1 also includes the Spanish low/medium level radioactive waste repository named El Cabril. Figure 1 shows those eight Spanish nuclear sites overlapped on known seismicity of the Iberian Peninsula till 1999 year.

Site	Reactor type	Power (MWe)	Operation since	SSE (PGA_H)	OBE Characterization	
					PGA_H - PGA_V	Spectra $_{H-V}$
José Cabrera	Westinghouse-PWR	160	1968	0.07g	0.035g – 0.023g	Nureg/Cr-0098
S.M. Garoña	Gen. Electric-BWR	466	1971	0.10g	0.05g	RG-1.60
Almaraz I – II	Westinghouse PWR	974 – 983	1981 - 1983	0.10g	0.05g – 0.033g	Newmark
Ascó I – II	Westinghouse PWR	1028 – 1027	1983 - 1985	0.13g	0.07g – 0.0467g	Newmark
Cofrentes	Gen. Electric-BWR	1025	1984	0.17g	0.085g	RG-1.60
Vandellós II	Westinghouse-PWR	1087	1988	0.20g	0.10g	RG-1.60
Trillo	Siemens/KWU-PWR	1066	1988	0.12g	0.06g**	RG-1.60
El Cabril	L.R. Waste Disposal		1992	0,24g	0.12g**	RG-1.60

Table 1. Characteristics of the Spanish nuclear power plants.

The original seismic monitoring system instrumentation of the plants was, in general, analogical and did not let to quickly analyze seismic records in an automatically way (by the moment any earthquake has been recorded on a nuclear site in Spain). However, one plant (Vandellós II) had tape register adapted to analyze automatically possible records. Available analogical instrumentation was varied and heterogeneous in record performance (a few accelerometers and more seismometers and pick

** Formally it's a level of inspection. This plant must apply a technical procedure addressed to find plant damages if a 0.04g PGA (Peak Ground Acceleration) value is reached in free field conditions.

registers). In the same way, global resolution of the systems measures was limited (it could reach till 0,05g in some plants) if comparing to PGA of Spanish plant OBE (between 0,033g - 0,1g). Also the system had not adequate resolution to compare *in situ* measured values in front of design response spectra values with two decimals.

Free field sensors were sitting outside plant buildings but, in general, were not in free field outside of structures influence, because sensors were anchored to metallic tanks or into 400Kv electric park (relays building non seismic qualified). In the same way plants did not have technical procedures about OBE exceedance, and seismic monitoring systems only can apply criteria to determine spectral values exceedance. These criteria may be too conservative for near field earthquakes with high PGA, but low energy to transfer significant damage.

On the other hand, maintenance, verification and calibration test of seismic monitoring systems required by Technical Specifications (TS), did not have well comparing with new digital instruments, including type and instrument number needed to be tested. After twenty years of operation, availability of elements and components was limited.

Current status

Highlighting from above mentioned RPS results and seismic IPEEE analysis performed in ninety years (Refs 1 and 2), seismic monitoring systems have been full renewed in all Spanish NPP´s, and OBE border conditions have been formally established in a clear way in the licensing documents and technical procedures. This updating process has tried to know potential plant vulnerabilities if an earthquake higher than SSE occurs, and also try to implement some improvements with reasonable cost (economical and radiological) and Nuclear Safety benefits to Spanish NPP´s. These improvements are following:

- Original seismic monitoring system has been full replaced by accelerometers according with USNRC R.G.-1.12, rev. 2.
- OBE exceedance criteria as USNRC R.G.-1.166 have been adopted.
- Seismic monitoring of structures was adapted to sensors number and locations recommended by R.G.-1.12, Rev. 2. Plants with two units -Almaraz, Ascó- only monitor one unit.
- As possible, changing process identified new sites close to free field conditions in order to observe the importance assigned to this sensors by R.G.-1.166.
- All seismic monitoring systems have been synchronized by the universal time.
- In general, seismic monitoring systems with higher resolution than 12 bits were considered.

Seismic monitoring synchronization by universal time makes possible to use free field records in a larger way through future seismic re-evaluations, or future new designs in the same site: That improvement can reduce uncertainties on source location and distance of the recorded earthquake. Constraint these uncertainties is important if near field earthquake occur (in areas with low seismicity like most parts of Spain it's usual to have low seismic monitoring coverage by national network agencies, and the resulting resolution in location can be an order of tens of kilometers.

An improvement in the same way consists of placing seismic monitoring with a global resolution larger than 12 *bits*. This resolution is good enough to analyze strong earthquakes records, but it's limited if small quakes occur, just those of in the same level than OBE in areas with low/moderate seismicity like Spain. Resolution of 12 bits can be also limited to analyze low fore and aftershocks of the main shock. Some plants in Spain (Ascó I-II, Cofrentes, and Vandellós II) have systems with 12 bits, and they are complemented by a seismograph (in the same way El Cabril will install an broad band seismograph). Table 2 inserts decommissed instrumentation and current seismic systems status in Spain.

	Original System	Current System - updated to RG-1.12, rev. 2		
Site	Status	Supplier	Resolution	Accuracy
José Cabrera	None	Geosis	19 bits	4×10^{-6}g
Sta. Mª de Garoña	None	Kinemetrics	18 bits	8×10^{-6}g
Almaraz I – II	Full RG-1.12, rev.0	Kinemetrics	18 bits	8×10^{-6}g
Ascó I – II	Full RG-1.12, rev.1	Syscom	12 bits	5×10^{-4}g
Cofrentes	Full RG-1.12, rev.1	Syscom	12 bits	5×10^{-4}g
Vandellós II	Full RG-1.12, rev.1	Syscom	12 bits	5×10^{-4}g
Trillo	Full RG-1.12, rev.1	Kinemetrics	18 bits	8×10^{-6}g
El Cabril (LRWD)	Free field	Geosis	24 bits	1×10^{-7}g

Table 2. Spanish nuclear power plants seismic instrumentation systems.

Like in the origin, current monitoring systems have seismic qualification adequate to register seismic input of design basis, but in some plants it was not possible to have qualification of routing between new free field sensors and register center. To prevent appropriate actions if an earthquake cut that communication router, it has been developed a procedure to handling extract and analyzes free field records.

Technical Specifications of Spanish NPP's collect a specific Operating Limit Condition if OBE is exceeding, requiring plant shutdown in a safe manner, with the purpose of including accomplish of limits and conditions in a licensing document. Also has been developed technical procedures linked to Emergency Plan of the plants, to enclose OBE exceedance criteria and actions to adopt if an earthquake occurs.

On the other hand, some applicants showed that periodical test of old analogical systems (system and sensors calibrations, and function verification) are obsolete, and they are too hard if comparing with supplier user's guide of new digital instrumentation. The applicants propose to review those periodical test after analyzing during several refuel cycles system behavior.

References

1 Sánchez-Cabañero, J.G.; Jiménez Juan, A. "*Integrated Program on PSA. Seismic categorization of Spanish NPP's sites*". OECD-NEA Workshop on Seismic Risk. Tokyo, Japan, 10 to 12 August 1999.

2 Beltrán, F.; García-Monge, J.; and Sánchez-Cabañero, J.G. "*Seismic margin assessment of Spanish NPP's: A perspective from Industry and regulators*". OECD-NEA Workshop on the Seismic Re-evaluation of all Nuclear Facilities, Ispra Italy, 26 to 27 March 2001.

Figure 1.- Ibero-Magrhebian seismicity from 1320 to 1999. The green dots are earthquakes happened before XX Century, the red ones are shocks instrumentally well located, and the brown ones only are roughly located. The biggest size represents earthquakes with MSK Intensity ≥ VIII